14

TECHNIQUES AND INSTRUMENTATION
IN ANALYTICAL CHEMISTRY

ANALYTICAL APPLICATIONS
OF CIRCULAR DICHROISM

edited by
N. Purdie and H.G. Brittain

ANALYTICAL APPLICATIONS OF CIRCULAR DICHROISM

TECHNIQUES AND INSTRUMENTATION IN ANALYTICAL CHEMISTRY

ANALYTICAL APPLICATIONS OF CIRCULAR DICHROISM

Edited by

N. Purdie
Oklahoma State University, Department of Chemistry,
College of Arts and Sciences, Stillwater, OK 74078-0447, U.S.A.

and

H.G. Brittain
Bristol-Myers Squibb Pharmaceutical Research Institute,
P.O. Box 191, New Brunswick, NJ 08903, U.S.A.

This book is printed on acid-free paper.

Preface

I was first introduced to the science of polarized light spectroscopy as an undergraduate at the University of Glasgow in the late 50's. I had decided that my PhD study would be in the area of physical chemistry and seriously considered working on a problem that dealt with the interactions of chiral transition metal complexes with circularly polarized light, i.e. CD. My adviser would have been Professor S.T.R.S. Mitchell, author of "The Cotton Effect" published in 1933, and considered to be one of the few bright "lights" in the field at that time. Mitchell was a warm, kind gentleman, whose roots were in, what the British would call, "the old school". His initial charm had convinced me to work with him in his laboratory. ST was a short man with a high pitched voice. His eyesight was dreadfully poor and seemed to fade even further every time we conversed. He was the perfect human caricature for a nocturnal mammal. His impaired vision was easily explained. His CD spectrometer was his entire laboratory and he lived and worked inside it ! Night was a constant condition. The custom-built instrumentation was so delicate and so fickle, that it demanded perpetual and precise care. Stealth was mandatory and communicating was done in whispers. With much reluctance, I decided that the claustrophobic conditions were as hazardous as coal mining, and chose to specialize in electrochemistry. Instruments were still custom-made, but the study could be done in relative daylight.

When my interest returned and we began researching the analytical applications of CD in the 70's, I felt I had a head start. But there was so much that was new. A great deal had happened to CD over the years as it matured and expanded to include: the far-UV; the study of optical activity in excited state emissions, and in vibrational and Raman spectroscopy; and the evolution of new empirical models applicable to the interpretation of the structural properties of macromolecules. Most important of all, perhaps, was the arrival of high tech electronics and materials which had brought CD instrumentation out of the dark ages. And now, ironically, almost 35 years after my introduction to CD, my special interest is the exploitation of chiral transition metal complexes as chirality induction reagents in chemical analysis.

A stimulus that is common to all of this progress is the challenge to understand the meanings behind the ultimate chirality, that of life itself. With that as an objective, the continued growth of CD as an analytical method is assured. What we have endeavored to do here is to assemble a group of contributing authors, each a recognized expert in his area of specialty, to substantiate the consensus opinion that CD has a significant role in future research, and in biomedical applications in particular. Contrary to the prevailing general opinion, CD is an intellectual property that is not difficult to understand and apply. This text should provide all of the salient information that makes CD and its applications easy to comprehend. There is room at the inn, and it is our hope that the added stimuli that are permeated throughout this text will be enough encouragement to interest and recruit a host of new investigators.

Neil Purdie,
Stillwater, OK
September 1993.

Preface

An understanding of the spectroscopy of dissymetric molecules has been central to the science of inorganic and organic compounds. It is probably true that modern views of molecular stereochemistry have been determined through the systematic studies of chirality which have been conducted by numerous scientists.

My own introduction to this field came during the course of my graduate studies when my mentor decided that I needed to learn the Jones calculus for treating optical phenomena. The department also possessed a Cary 60 spectrometer system, and in the time between my final oral exam and the beginning of my postdoctoral work I investigated the induction of circular dichroism in several metal complexes of acetylacetone by various chiral agents. Little did I know at the time that this particular work would subconsciously prepare me for the writing of one of the chapters in this book.

During my postdoctoral work, and throughout other aspects of my career, I have been involved (in some way) with the spectroscopy of chiral molecules. A lot of this work has been with the chirality of excited states, and for this reason, Professor Riehl's article is of special interest to me. Most of the time I have worked with homemade instrumentation, although lately I have had the luxury of dealing with a commercially supplied system.

It is my opinion that chiroptical spectroscopy has been under-utilized as of late, but I think that situation will change for the better. Many pharmaceutically active compounds are inherently chiral, and the registration agencies are balking to some degree at the filing of racemic compounds. To register a chiral agent requires considerable skill in the resolution of the appropriate enantiomer (or diastereoisomer), and suitable analytical techniques to verify the enantiomeric purity. Although the reflex action is to invoke a chiral HPLC method for such work, there are many answers which can only be supplied upon the completion of suitable spectroscopic investigations.

In the present volume, Professor Purdie and I have attempted to illustrate the wide range of uses to which CD has been applied. Some of these are investigative, and others applied, but all provide indications as to how the technique could be used to solve intractable problems. The chapter authors have used countless examples to bring home their points, and each example provides further incentive for additional work. The book has been assembled for this reason, and we hope that a re-seeding of the field will bring out a new crop of applications.

Harry G. Brittain
New Brunswick, NJ
September 1993.

LIST OF CONTRIBUTORS

D.R. Bobbitt, Department of Chemistry and Biochemistry, University of Arkansas, Fayetteville, AR 72701, USA

H.G. Brittain, Bristol-Myers Squibb Pharmaceutical Research Institute, P.O. Box 191, New Brunswick, NJ 08903, USA

D. Che, Department of Chemistry, Syracuse University, Syracuse, NY 13244-4100, USA

M. Citra, Department of Chemistry, Syracuse University, Syracuse, NY 13244-4100, USA

M. Diem, Department of Chemistry, City University of New York, Hunter College, 695 Park Avenue, New York, NY 10021, USA

A. Gergely, Department of Pharmaceutical Chemistry, Semmelweis University of Medicine, Hogyes Endre U. 9, H-1092 Budapest, Hungary

D.A. Lightner, Chemistry Department, University of Nevada, Reno, NV 89557-0020, USA

M.C. Manning, School of Pharmacy, Campus Box C238, University of Colorado Health Sciences Center, Denver, CO 80262, USA

L.A. Nafie, Department of Chemistry, Syracuse University, Syracuse, NY 13244-4100, USA

N. Purdie, Chemistry Department, Oklahoma State University, Stillwater, OK 74078-0447, USA

N. Ragunathan, Department of Chemistry, Syracuse University, Syracuse, NY 13244-4100, USA

J.P. Riehl, Department of Chemistry, University of Missouri-St. Louis, St. Louis, MO 63121, USA

J.F. Towell III, Department of Chemistry, Carroll College, Waukesha, WI 53186, USA

G-S Yu, Department of Chemistry, Syracuse University, Syracuse, NY 13244-4100, USA

This Page Intentionally Left Blank

CONTENTS

1

Chapter 1

Introduction to Chiroptical Phenomena

Harry G. Brittain

Bristol-Myers Squibb Pharmaceutical Research Institute,
 P.O. Box 191,
New Brunswick, NJ 08903, USA

Abstract
    The most commonly encountered manifestations of
chiroptical phenomena are circular birefringence (also known
as optical rotation), optical rotatory dispersion (ORD), and
circular dichroism (CD). An explanation as to the nature of
circularly and linearly polarized light is provided, and the
origins of the various chiroptical effects are discussed. In
each instance, a concise summary of the calculations used by
workers in the field to report the results of their
investigations is provided.

    When the mirror images of a compound cannot be
superimposed on each other, that compound is said to be chiral
and the mirror images are denoted as enantiomers. The
phenomenon of enantiomorphism and optically active compounds
has become especially important to pharmaceutics as both
industry and regulatory bodies discover the importance of drug
chirality [1]. The enantiomers of a compound may or may not
exhibit equivalent pharmacokinetic or pharmacologic
properties, and this situation must be determined during the
development of a new drug [2].
    The interaction of polarized light with chiral compounds
is of great interest since chiroptical techniques are
extremely useful as methods of characterization. It is
equally true that although most scientists are aware that
enantiomerically rich solutions will rotate the plane of
linearly polarized light, the origins of this effect are not
as simple as might be imagined. In this first article, the
phenomena of polarimetry and optical rotatory dispersion will
be discussed. A subsequent note will concern the related
phenomenon of circular dichroism.
    E.T. Malus discovered that images of objects viewed
through calcite crystals appeared to become doubled [3]. This
phenomenon of double refraction was ultimately ascribed to
linear birefringence, where the indices of refraction along
the axes of the anisotropic crystal were unequal. A beam of

collimated light passed through a calcite crystal would emerge
as two beams, the electric vectors of which were shown to be
orthogonal. The blockage of one of these beams yields an
optical element known as a linear polarizer. It was
demonstrated that light polarized in this manner would not
pass through a second linear polarizer, whose crystal axis was
rotated by 90° with respect to the original plane of
polarization.

J.-B. Biot and others found that when certain materials
were placed between these crossed polarizers, light could be
transmitted by the second optical element. This medium could
be crystals cut along certain directions (e.g., slabs of
quartz cut perpendicular to the hexagonal axis) or solutions
of some organic compounds (e.g., solutions of camphor or
sugars). It was quickly realized that the initial plane of
polarization appeared to be rotated upon passing through the
"optically active" medium between the polarizers. This
phenomenon led to the development of the polarimeter, where
the amount of optical rotation induced by a given solution was
quantitated. The convention developed by Biot was that
positive optical activity corresponded to a clockwise rotation
of the linearly polarized light. A block diagram describing
the action of a polarimeter is shown in Figure 1.

Light Source   Polarizer   Sample Cell   Analyzer   Detector
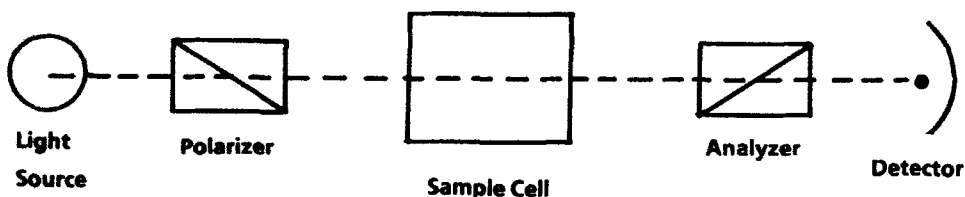
Figure 1. Block diagram of a simple polarimeter.
Monochromatic light from the source is linearly
polarized by the initial polarizer, and then allowed
to pass through the sample medium. The angle of
polarization associated with the light leaving the
medium is determined by rotating the analyzer
polarizer to the new null position. A variety of
photoelectric methods are available which can be
used to automatically determine the observed angle
of rotation.

An explanation for this effect was only possible once
Fresnel applied the new transverse wave theory of light to the
phenomenon of optical activity. He differentiated between
linearly polarized light (light whose electric vector lay
along a single axis as it propagated through space), and
circularly polarized light (light whose electric vector
rotates about the axis perpendicular to its direction of
propagation through space). Right circularly polarized light
represents a clockwise rotation of the electric vector, while
left circularly polarized light represents a counterclockwise
rotation. These relations are illustrated in Figure 2.
Fresnel proved that linearly polarized light is actually the
resultant of two coherent circular components of opposite
sense of rotation.
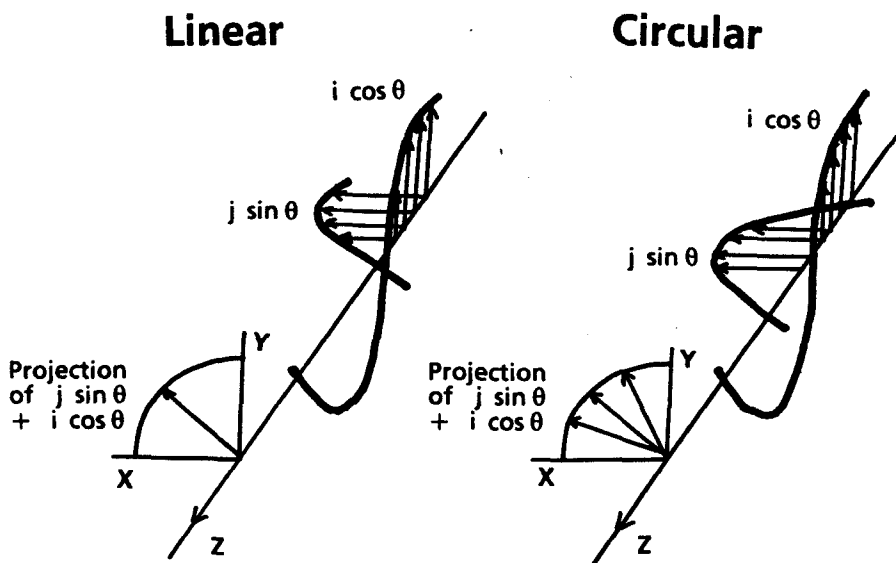
Figure 2. Relationships of the electric vectors associated
with linearly and circularly polarized light as
these are propagated.

The phenomenon of optical activity is determined by the
relative indices of refraction for left- and right-circularly
polarized light in the medium under consideration. In an
optically inactive medium, the refractive indices of left- and
right-circularly polarized light are equal. Since the two
polarization senses would remain in phase at all times during

4

passage through the medium, the resultant vector leaving the
medium would be unchanged with respect to the vector which
entered the medium (see Figure 3a). In an optically active
medium, the refractive indices for left- and right-circularly
polarized light are no longer equal. The components are then
no longer coherent when they leave the medium. When viewed
directly along the direction of the oncoming beam, the
resultant vector appears as a rotation of the initial plane of
polarization (see Figure 3b). Optical activity is therefore a
manifestation of circular birefringence.
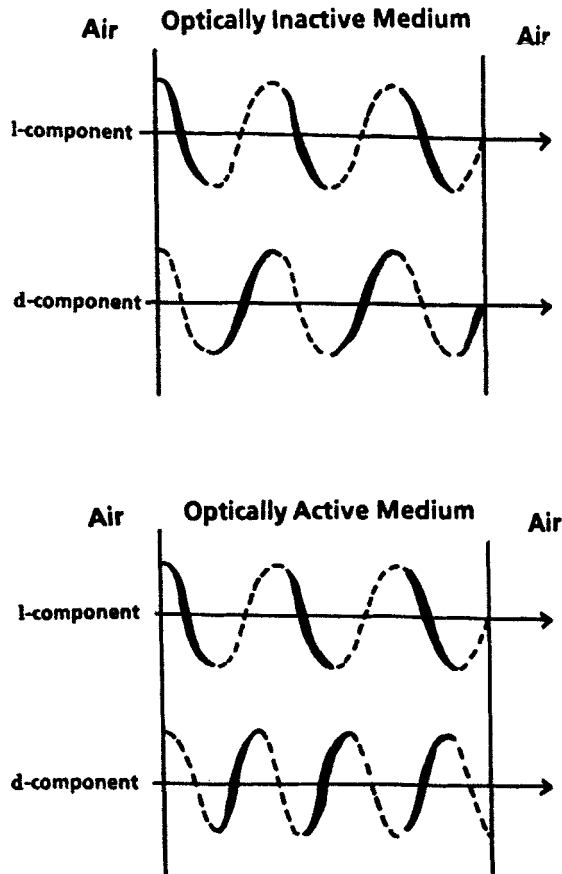
Figure 3. Behavior of the two circularly polarized components
         of linearly polarized light as they pass through (a)
         an optically inactive medium, and (b) an optically
         active medium.

In units of degrees, the observed optical rotation (α) is given by:

$$\alpha = \{ 1800 \, b \, (n_L - n_R) \} \; / \; \lambda_o \tag{1}$$

where b is the pathlength in decimeters, λ_o is the wavelength of light used in the determination, and n_L and n_R are the refractive indices for left- and right circularly polarized light. The specific rotation of a material dissolved in a fluid solution is given by:

$$[\alpha] = 100 \, \alpha \; / \; b \, c \tag{2}$$

if c is the solute concentration in units of grams per 100 milliliters of solution. The molar rotation of a solution is defined as:

$$[M] = FW \, \alpha \; / \; b \, c \tag{3}$$

$$= FW \, [\alpha] \; / \; 100 \tag{4}$$

where FW is the formula weight of the optically active solute. When the solute concentration is given in terms of molarity (M), equation (3) becomes:

$$[M] = 10 \, \alpha \; / \; b \, M \tag{5}$$

Biot also observed that the optical rotation of tartaric acid solutions was a function of the wavelength used for the determination. The wavelength dependence of optical rotation is termed optically rotatory dispersion, or ORD. When measured outside of absorption bands, an ORD spectrum (as illustrated in Figure 4a) will consist either of a plain positive or plain negative dispersion curve. When measured inside of an absorption band, the ORD will exhibit anomalous dispersion, which is referred to as a Cotton effect. A positive Cotton effect consists of positive ORD at long wavelengths, and negative ORD at shorter wavelengths (see Figure 4b). In the simplest measurement of ORD, the fixed wavelength source of Figure 1 is replaced by a tunable source (such as a xenon arc combined with a monochromator).

One of the most intensive studies involving ORD has concerned the $n \rightarrow \pi^*$ transition in the 300 nm spectral region of ketones, where very strong Cotton effects can be observed. The effects were particularly useful to the characterization of steroids, and molecules containing smaller ring systems. Djerassi, Klyne, and others established that the optical activity observable within this band was determined by the location of the ketone group in the molecular ring structure, the absolute configuration of neighboring ring junctions, the nature and configuration of adjacent substituents, and the conformation of the rings making up the molecule [4]. These observations led to the development of the "octant rule", which represented an attempt to generalize the ORD trends in
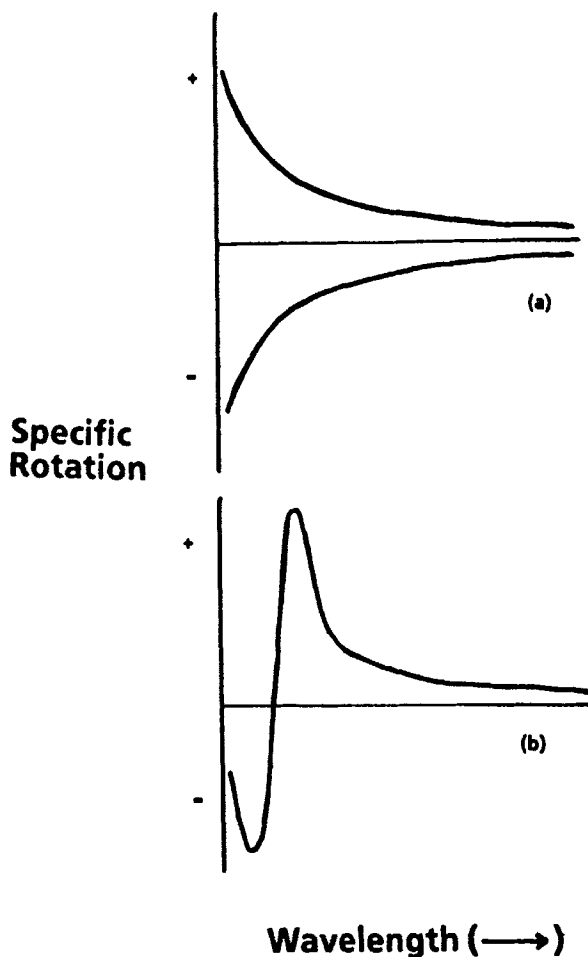
Figure 4. Optical rotatory dispersion curves as would be
obtained in (a) optically inactive media (both plain
positive and negative curves are illustrated), and
(b) optically active media (a positive Cotton effect
has been shown).

light of stereochemical structure [5]. In this system, the
three nodal planes of the n and π^* orbitals of the carbonyl
group are considered to divide the molecular environment into
four front octants and four back octants. A group or atom
situated in the upper left or lower right rear octant
(relative to an observer looking at the molecule parallel to
the C=O axis) induces a positive Cotton effect in the n→π^*

band. A negative Cotton effect would be produced by substitution within the upper right or lower left back octants. Although exceptions to the octant rule have been demonstrated, its utility in predicting molecular stereochemistry on the basis of observed ORD trends has been extremely valuable to synthetic organic chemists.

As discussed, optical rotatory dispersion (ORD) is determined by the unequal indices of refraction for left- and right-circularly polarized light in a chiral medium. Within an absorption band, the ORD spectrum exhibits anomalous dispersion, which is referred to as a Cotton effect. Full understanding of ORD and anomalous dispersion requires a more detailed examination of the properties associated with refractive indices.

The refractive index of a material is actually the sum of a real and an imaginary part:

$$n = n_o + i k \tag{6}$$

where n is the observed refractive index at a given wavelength, n_o is the refractive index at infinite wavelength, and k is the absorption coefficient of the substance. By definition, k will equal zero outside of an absorption band. For an achiral compound, no difference in refractive index exists for left-circularly polarized light as opposed to right-circularly polarized light. For a chiral material, the refractive indices for left-and right-circularly polarized light are no longer equal, and can be expressed as:

$$n_L = n_{o(L)} + i k_L \tag{7}$$

$$n_R = n_{o(R)} + i k_R \tag{8}$$

The criteria for a substance to exhibit either optical rotation or optical rotatory dispersion is that $(n_L - n_R)$ not equal zero. Within an absorption band it can be concluded that if $(n_L - n_R)$ does not equal zero, then $(k_L - k_R)$ will not equal zero either. The quantity $(k_L - k_R)$ is defined as the **circular dichroism** (CD).

Circular dichroism therefore represents the differential absorption of left- and right-circularly polarized light. The effect of this differential absorption is that when the electric vector projections associated with the left- and right-circularly polarized light are recombined after leaving the chiral medium, they describe an ellipse whose major axis lies along the new angle of rotation. The measure of the eccentricity of this ellipse is defined as the ellipticity, or ψ. These relations are illustrated in Figure 5. It is not difficult to show that [6]:

$$\psi = \{ \pi z (k_L - k_R) \} / \lambda \tag{9}$$

where z is the path length in centimeters, and λ is the particular wavelength at which ψ is measured. If C is the
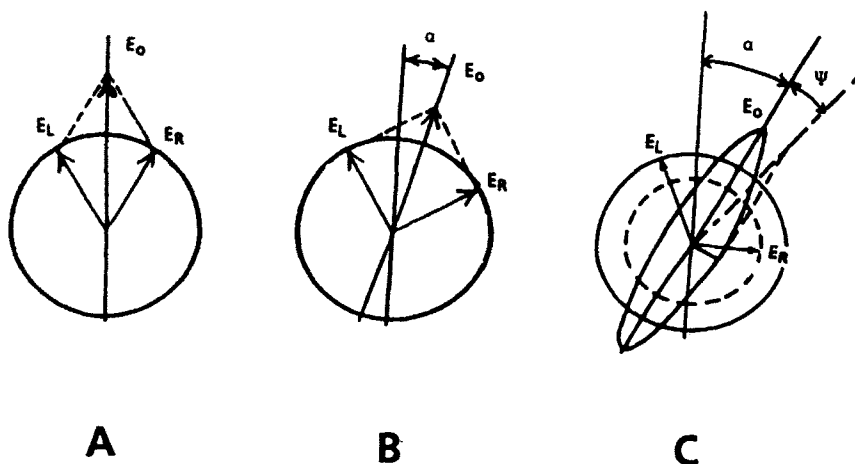
Figure 5. Phase relations associated with the passage of
circularly polarized light through various media.
(A) For optically inactive media, the recombination
of left- (E_L) and right-circularly (E_R) polarized
light yields linearly polarized light whose electric
vector (E_o) is unchanged with respect to the
incident axis. (B) For optically active media
outside of an absorption band, recombination of E_L
and E_R yields a resultant E_o vector rotated from the
incident axis by the angle α. (C) For optically
active media inside of an absorption band,
recombination after differential absorption of E_L
and E_R yields a resultant E_o vector rotated from the
incident axis by the angle α, and describing an
ellipse of ellipticity ψ.

concentration of absorbing chiral solute in moles/liter, then
mean molar absorptivity, a, is derived from the absorption
index by:

$$a = \{ 4 \pi k \} / \{ (2.303) \lambda C \} \tag{10}$$

In that case, the ellipticity (still in units of radians)
becomes:

$$\psi = \{ (2.303) C z (a_L - a_R) \} / 4 \tag{11}$$

The expression of ellipticity in radians is cumbersome, and
consequently this quantity is converted into degrees by the
relation:

$$\theta \;\; = \;\; \psi \;\; (\; 360 \; / \; 2 \; \pi \;) \tag{12}$$

and then:

$$\theta \;\; = \;\; (a_L - a_R) \; C \; z \; (32.90) \tag{13}$$

The molar ellipticity is an intrinsic quantity, and is calculated from:

$$[\theta] \;\; = \;\; \{ \; \theta \; (FW) \; \} \;\; / \;\; \{ \; b \; c' \; (100) \; \} \tag{14}$$

where FW is the formula weight of the solute in question, b is the medium path length in decimeters, and c' is the solute concentration in units of grams/mL. The molar ellipticity is related to the differential absorption by:

$$(a_L - a_R) \;\; = \;\; [\theta] \; / \; 3298 \tag{15}$$

Most instrumentation suitable for measurement of circular dichroism is based on the design of Grosjean and Legrand [7], and a block diagram of their basic design is shown in Figure 6. Linearly polarized light is passed through a dynamic quarter wave plate, which modulates it alternately into left- and right-circularly polarized light. The quarter wave plate is a piece of isotropic material, which is rendered anisotropic through the external application of stress. The device can be a Pockels cell (in which stress is created in a crystal of ammonium dideuterium phosphate through the application of AC high-voltage), or a photoelastic modulator (in which the stress is induced by the piezoelectric effect). The light leaving the cell is detected by a photomultiplier tube, whose current output is converted to voltage and split. One signal consists of an alternating signal proportional to the CD, and is due to the differential absorption of one circularly polarized component over the other. This signal is amplified by means of phase-sensitive detection. The other signal is averaged, and is related to the mean light absorption. The ratio of these signals varies linearly as a function of the CD amplitude, and is the recorded signal of interest. A much more detailed description of CD instrumentation will be provided in a subsequent chapter by Donald Bobbitt.

Drude first proposed that the rotatory power of a dissymmetric substance could be understood if its absorption of light involved the motion of a charged particle along a helical path within the molecule [8]. This type of motion would result in the simultaneous production of an electric dipole from the translatory motion and a magnetic dipole from the rotatory motion. The model requires that the electric and dipole moments have at least some components which are collinear with each other, or else stereospecific interaction with circularly polarized light would not be possible.

The absorption of light is accompanied by the transition from the ground state of the system (ψ_o) to an excited state
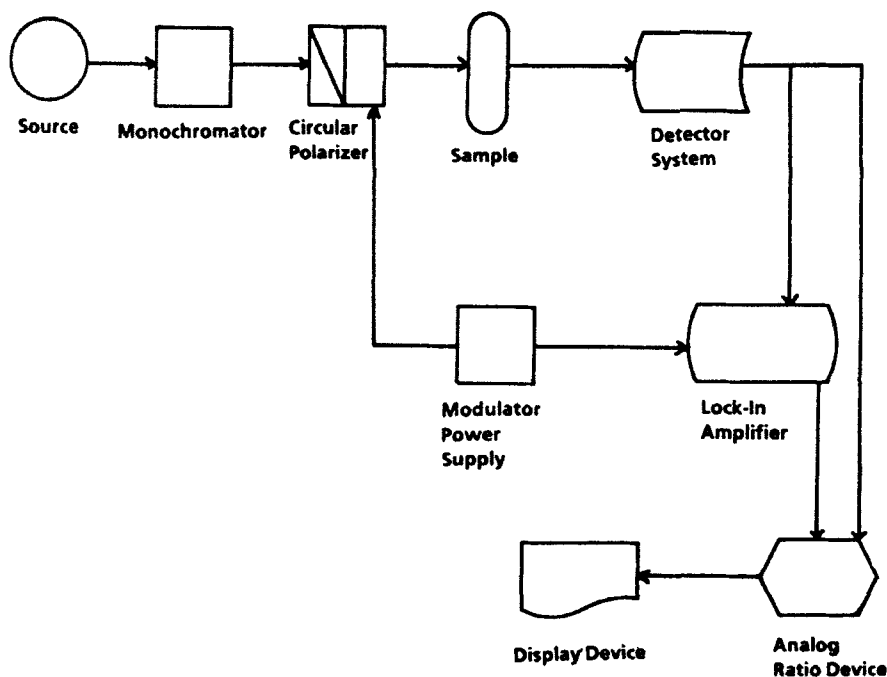
Figure 6. Block diagram of a circular dichroism spectrometer.

(ψ_i). In order for a chiroptical transition to take place, the electric and magnetic transition moments must not be totally orthogonal. If μ is defined as the electric dipole operator and m is the magnetic dipole operator, then the rotational strength of the transition is given by:

$$R \quad = \quad Im \ \langle\psi_o|\mu|\psi_i\rangle \ \langle\psi_o|m|\psi_i\rangle \tag{16}$$

The observed intensity of a given chiroptical transition is directly proportional to the magnitude of the rotational strength.

In group theory, the electric dipole operator transforms according to the operations of translation, and the magnetic dipole operator transforms as a rotation. It is not difficult to show that the individual transition moments are invariably orthogonal as long as the molecular point group contains improper axes of rotation. This rule is often trivialized to

state that an optically active molecule cannot contain either a center of inversion or a mirror reflection plane.

Assuming a model wherein a molecule possesses only two electronically excited states, Schellman has proposed three mechanisms would lead to the observation of optical activity in the electronic transitions among these [9]. The three models may be summarized as:

The One-Electron Mechanism. Both the electric and magnetic dipole transitions reside in the same chromophore. The rest of the dissymmetric molecule acts as a perturbing field which partially breaks down the symmetry of the chromophore, and therefore mixes the two transitions. The one-electron theory is also known as the Condon, Altar, and Eyring theory.

The Dipole-Dipole Coupling Mechanism. In this model, two absorbing groups have a single electronic transition. Owing to their proximity, these are coupled by their dipolar fields to produce a magnetic moment. This has been termed the Kuhn-Kirkwood mechanism, which has been extended to include degeneracy by Moffitt.

The μ-m Mechanism. In this instance, one chromophore contains the electric dipole transition and another contains the magnetic dipole transition. These are coupled in the molecule to produce optical activity in both transitions.

It goes without saying that the highly simplified models described above are only useful toward understanding the complicated nature of the behavior of real dissymmetric molecules. It is highly likely that a given observed chiroptical transition would contain contributions from all three mechanisms, although plausibly one might be dominant. When it can be decided that a given interaction does determine the bulk of a Cotton effect, then a symmetry rule can be developed to interpret the observed results.

CD spectroscopy has played an important role in the characterization of optically active molecules, and will continue to do so as long as chemists are interested in small molecules. HPLC detectors which make use of the CD effect also show great potential as being the chiroptical detectors of choice for work with dissymmetric compounds [10].

CD spectroscopy is not limited to the study of small molecules, and has become extremely important in the characterization of biomolecules. The secondary structure of proteins can be characterized through studies of the CD associated with the amide chromophores. Using a combination of models and calibration spectra, it is possible to deduce the relative contributions to the overall secondary structure made by α-helix, antiparallel ß-sheet, ß-turn, and random coil portions of the polypeptide [11]. With the increasing use being made of such agents in the pharmaceutical industry, it

is not difficult to envision the role which will belong to chiroptical spectroscopy.

In this book, a variety of topics will be presented which are centered upon applications for which chiroptical spectroscopy has played an essential role. Neil Purdie has placed the field into perspective by contributing a comprehensive summary of the analytical applications of CD spectroscopy to forensic, pharmaceutical, clinical, and food science areas, focussing strongly on compounds of natural origin.

A general discussion regarding the instrumentation which can be used for the measurement of CD spectroscopy has been provided by Donald Bobbitt, while the more specialized requirements associated with vibrational optical activity have been discussed by Laurence Nafie. This latter chapter deals with both the methods of vibrational CD spectroscopy as well as raman vibrational optical activity. The use of CD as a detector in liquid chromatography represents an important area of heightened activity, and this has been covered by Andras Gergely.

CD spectroscopy has historically been of extreme importance in the study of small, optically active organic molecules. David Lightner has provided a review of the CD methods used to establish the absolute configuration of dissymmetric centers, covering both the octant rule as well as the exciton chirality rule. The use of difference CD studies in the characterization of steroids has been detailed by Andras Gergely.

As instrumental advances continue and computational methods become more powerful, the frontiers of chiroptical spectroscopy are being continually pushed back. One important area has been in the characterization of biopolymers. Mark Manning and John Towell have contributed a chapter covering the use of ultraviolet-CD in the analysis of protein structure, and Max Diem has described the application of infrared-CD to the study of similar systems. Finally, the range of chiroptical investigations which can be performed on molecules in electronically excited states has been summarized by James Riehl.

These review articles (when viewed as a coherent whole) provide a general overview of the various applications to which CD spectroscopy has been put, and where the technique is headed.

REFERENCES

(1)   W.H. De Camp, *Chirality*, 1 (1989) 2.
(2)   F. Jamali, R. Mehvar, and F.M. Pasutto, *J. Pharm. Sci.*, 78 (1989) 695.
(3)   For an excellent review of the history and principles associated with optical rotation and optical rotatory dispersion, see T.M. Lowry, *Optical Rotatory Power*

(Dover Publications, New York, 1964), pp. 89-148.

(4)   Much of this work in summarized in C. Djerassi, *Optical Rotatory Dispersion: Applications to Organic Chemistry* (McGraw-Hill Book Co., New York, 1960).

(5)   W. Moffitt, R.B. Woodward, A. Moscowitz, W. Klyne, and C. Djerassi, *J. Am. Chem. Soc.*, **83** (1961) 4013.

(6)   E. Charney, *The Molecular Basis of Optical Activity*, John-Wiley & Sons, New York, 1979.

(7)   L. Velluz, M. Legrand, and M. Grosjean, *Optical Circular Dichroism: Principles, Measurements, and Applications*, Verlag Chemie, Weinheim, 1965.

(8)   P. Drude, *Lehrbuch der Optik* (Dover Publications, New York, 1959).

(9)   J.A. Schellman, *Acc. Chem. Res*, **1** (1968) 144.

(10)   N. Purdie, *Prog. Analyt. Spect.*, **10** (1987) 345.

(11)   W.C. Johnson, *Ann. Rev. Biophys. Chem.*, **17** (1988) 145.

This Page Intentionally Left Blank

Chapter 2

Instrumentation for the measurement of circular dichroism; past, present and future developments

Donald R. Bobbitt

Department of Chemistry and Biochemistry, University of Arkansas, Fayetteville, Arkansas 72701

Abstract

   The basic procedures for the measurement of circular dichroism were developed over 100 years ago. Over the past century, measurement advances have occurred in an incremental fashion as improvements have been made in the various instrumental components involved in the measurement process. One significant development has been the use of the photoelastic modulator for polarization modulation of the probing radiation. The PEM's large optical aperture, good stability, and ability to polarize the probing light with excellent purity has transformed the measurement of CD from a difficult experimental technique to a routine tool for the determination of complex structure. This capability has been extended to the time-dependent study of biological reactions through the association of the stopped-flow technique with the CD measurement. Recent advances have introduced the laser as the probe source allowing microvolume sampling and time-dependent CD studies in the nanosecond to picosecond regime. Finally, the introduction of multichannel light detection devices, for example, charge-coupled devices, into the CD experiment may have as dramatic an effect on the measurement of CD as the introduction of electro-optic polarization modulation had 30 years ago. Although several obstacles remain to be solved, preliminary results clearly demonstrate the advantages of this approach and these advantages will serve as an impetus for the future development and application of this technology to the measurement of CD.

OUTLINE

1. Introduction
    1.1. Dynamic Reserve
    1.2. Instrumentation Overview
2. Historical Perspective
3. Transmission-Based CD Instrumentation
    3.1. Light Sources
    3.2. Polarizing Optics
    3.3. Photoelectric and Photoelastic Modulators

16

1. INTRODUCTION

Circular dichroism (CD) is the differential absorption exhibited by a system for left-versus right-circularly polarized light. In order to demonstrate CD activity, a system must contain a dissymmetric center which is coupled in some manner to the chromophore giving rise to the absorption. In the context of the study of biologically active species, the close relationship between structure and function in such systems suggests that CD measurements are extremely important is discerning these subtle associations. The use of CD measurements in a variety of applications, including such structural determinations, will be discussed in detail in subsequent chapters. However, what is not often explicitly stated in treatises on CD applications is that CD measurements are experimentally challenging, and a variety of instrumental anomalies have been identified which can degrade the quality of the CD information available from such a determination. Therefore, the crux of this chapter will be to review the various instrumental approaches employed for the measurement of CD starting from a historical perspective, and then to use this as a basis to understand how the CD measurement process can be improved in order to enable more complicated, and/or difficult problems to be addressed in the future.

CD can be measured by two methods which, although appearing to be different, can be shown mathematically to be equivalent. In the first, the differential absorption exhibited by an optically active system for left- and right-circularly polarized light is obtained directly by measuring the absorption for the two circularly polarized components separately and then taking the difference. In the second method, linearly polarized light, which can be resolved into two oppositely rotating circular components with a specified phase relationship, is introduced into an optically active sample. The differential absorption of the two circular components will result in the elliptical polarization of the probing radiation. The arctangent of the ratio of the minor axis of the ellipse to the major axis is known as the ellipticity (θ), and it is related to the absorption coefficients for the circular components by

$$\theta = \tan^{-1}(\text{minor/major}) = (\pi\Delta\varepsilon)/\lambda \qquad (1)$$

In eq. 1, $\Delta\varepsilon$ is the difference in the molar extinction coefficients for left- and right-circularly polarized light (i.e. $\varepsilon_L - \varepsilon_R$) and λ is the wavelength at which the measurement is made. Thus, a determination of the degree of ellipticity of the emerging radiation can provide a measure of the CD. Similar information can also be obtained using other permutations for the polarizing characteristics of the probing radiation. Although the latter method appears experimentally simpler than the former, intrinsic birefringence can greatly affect the measurement process and most commercial CD instruments are modified absorption spectrophotometers which utilize the first method.

1.1. Dynamic Reserve

Since the CD measurement process requires a differential absorption to be probed, it is implicit in such a measurement that the system under study must absorb. In effect, this characteristic suggests that CD is inherently a background-limited measurement. Specifically, in performing the CD experiment, one must monitor a small absorbance difference ($A_L - A_R$) in the presence of a highly absorbing background. Instrumental dynamic reserve (DR) is a measure of a systems ability to monitor a small signal change in the presence of a constant background response and it is defined as the ratio of the magnitude of the background signal to the smallest change that can be observed in the presence of that background.

For CD measurements, the DR is given as

$$DR = A/\Delta A = a/\Delta a \tag{2}$$

where a is defined as the absorptivity (cm^{-1} $(g/L)^{-1}$). The fact that CD is a background limited technique therefore requires that the instrumentation possess a large dynamic reserve and this characteristic limits the approaches that can be successfully applied to CD measurements.

In general, high quality absorption spectrophotometers possess noise levels, given in absorbance units, of 5×10^{-5} cm^{-1}. The minimum measurable absorbance for these systems is therefore 1×10^{-4} cm^{-1} at a signal-to-noise ratio (SNR) of 2. Further, this level of performance can be maintained in the presence of background absorbances up to approximately 2. This upper limit for the background is a reflection of the fact that at an absorbance of 2, only 1% of the incident light actually reaches the photodetection device. Under such conditions, conventional absorption instruments would be able to provide a DR at the 2×10^4 level which implies that changes of 50 parts per million (ppm) should be measurable.

A relative measure of the degree of CD activity for a material is given as the ratio of the differential absorbance (or a proportional measure of this quantity) of the system for left- versus right-circularly polarized light, to the inherent absorbance at the probing wavelength. To put this value in the context of CD measurements, many CD active chromophores possess $\Delta a/a$ values which range from 2×10^{-4} (e.g. cholesterol derivatives at 300 nm) to 2×10^{-2} for a variety of transition metal complexes (e.g. $Co(en)_3^{3+}$ at 500 nm). Based on the DR determined above, the instrumentation currently available can provide the necessary instrumental performance to operate under the demanding conditions required for CD measurements. However, as will be shown later, this level of performance is achieved by using long measurement time constants to average out the

influence of random noise sources. This precludes the use of these conventional approaches in time-resolved studies of events occurring on the sub-millisecond time scale.

1.2. Instrumentation Overview

A generic transmission-based CD instrument is schematically depicted in Fig. 1 below. Although a number of different approaches for the measurement of CD will be compared in subsequent sections, it is useful to use the arrangement in Fig. 1 as a starting point in a discussion of CD instrumentation.

In Fig. 1, light of a selected wavelength interval is obtained from a polychromatic source and monochromator combination. In general, high power arc lamps are used as light sources in CD instruments as these can provide appreciable output powers over wide spectral ranges. However, laser sources have recently been used in select applications. Randomly polarized light exiting the monochromator is then converted into circularly polarized radiation by the appropriate combination of polarizing optics and/or electro-optic device. This combination can be termed a circular polarizer. One of the most common approaches is the one depicted in Fig. 1 in which a linear polarizer is used to isolate one plane polarized component of the randomly polarized light, and a photoelastic modulator or Pockels cell is then used to create the two circularly polarized components by application of the proper phase retardation. Modulation of the incident light allows one to use ac detection electronics with a concomitant improvement in the SNR. With a properly tuned modulation/detection system, signal can be abstracted from noise and background that may be 10^2 to 10^3 times larger in magnitude. Light detection is usually accomplished using a photomultiplier tube, since, as described above, the large background absorbance assures that only a small portion of the incident light exits the sample.
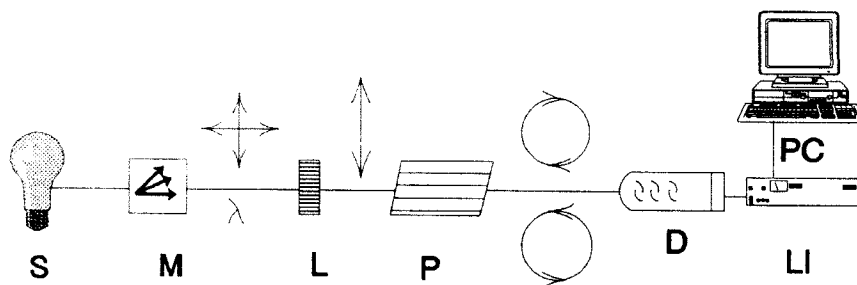
Figure 1. Conventional, transmission-based CD spectrophotometer. S, light source; M, monochromator (wavelength selection); L, polarizer (linear); P, electro-optic circular polarizer; D, light detection (photomultiplier); LI, lock-in amplifier (tuned amplifier); PC, data procurement and display.

With the exception of the polarizing modules, the spectrometer schematically represented in Fig. 1 is identical to any high quality absorption spectrophotometer. This

suggests that the key to the CD experiment is in the manner in which circularly polarized light is produced. Subsequent sections will discuss techniques for the production of circularly polarized light in detail as these techniques have allowed CD to be converted from an experimental technique of substantial difficulty to a routine method for chiral-optical studies. However, these available techniques are limited in their response time and novel methods have recently been developed to allow the CD technique to be applied to time-resolved studies of events occurring on the microsecond to picosecond timescale. Finally, it is appropriate to consider some very recent developments in light detection devices which may hold promise for extension to CD studies. New developments such as the charge coupled device (CCD) may allow multiwavelength CD information to be obtained on the same timescale and at the same SNR as single wavelength determinations are made at the present time. This and other new technologies will be explored more fully with particular emphasis placed on how these technologies may impact upon CD measurements.

2. HISTORICAL PERSPECTIVE

It is useful to consider, from a historical perspective, the development of instrumentation for the measurement of CD. Such an analysis demonstrates clearly that the basic techniques for producing and manipulating polarized light have been known for over 100 years. Thus there are many similarities between these first experimental techniques for the measurement of CD, and the commercial CD systems presently available. However, by considering the limitations of these first instruments, the rationale for the approaches utilized in state-of-the-art commercial systems becomes clear. In general, advances have been incremental, reflecting improved technology in terms of a single component rather than indicating a dramatic new approach to the measurement problem.

One of the earliest and most elegant papers dealing with various instrumental approaches for the measurement of CD was published by Cotton in 1896 [1,2]. Cotton developed two different instruments for CD measurements which demonstrated remarkable performance characteristics given the available technology. In one, the differential absorption was measured via separate determinations of A_L and A_R, and in the other the CD was obtained from an ellipticity measurement. As discussed previously, these methods provide equivalent information.

Fig. 2 schematically represents Cotton's instrumental system for measuring CD, which separately determines the sample absorption coefficients for left- and right-circularly polarized light. In Fig. 2, light from a polychromatic source is split between two distinct paths; one of which includes the sample and one which passes solely through a pair of Nicol polarizing prisms. The combination of the first Nicol prism (linear polarizer) and the Fresnel rhomb (circular polarizer) converts the source light into one sense of circularly polarized light. The Frenel rhomb, unlike most 1/4 λ plates is achromatic. This eliminates the need to change plates for each wavelength at which a CD measurement is made. This point will be discussed in more detail in a following section. Light exiting the sample is then converted back to linear polarized light via a second Fresnel rhomb. Each rhomb imparts a $\pi/4$ phase retardation and these two components therefore rotate the plane of

polarization of the light by an angle of 90° relative to the transmission axis of the first Nicol prism. Thus, in the absence of a circularly dichroic sample, there is a distinct orientation of the second polarizing prism where the two beams are of equivalent intensity. In the presence of a CD active sample, the orientation of the second prism is shifted in order to reestablish this equivalency point reflecting the fact that some of the circularly polarized light incident upon the sample has been absorbed. The angle through which the second prism must be rotated in order to achieve equivalent intensity in the two beams is proportional to the amount of absorption. In similar manner, the rhombs can be rotated to create the oppositely circularly polarized component and its absorption coefficient determined. As is evident by comparison of Cotton's apparatus (Fig. 2) to the generic system in Fig. 1, with the exception of the method for observing intensity differences, and the mechanical-optical versus electro-optical method for producing both forms of the circularly polarized light, Cotton's experimental arrangement is virtually identical to the arrangement used in modern CD instruments.
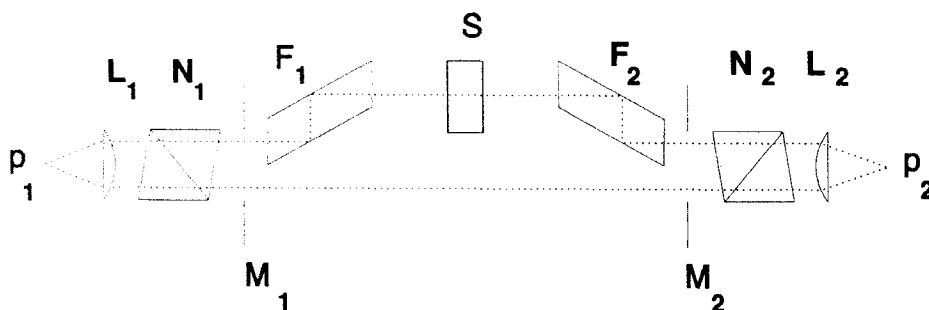
Figure 2. Cotton's experimental apparatus for measuring absorption coefficients for left- and right-circularly polarized light. p_1, incoherent source; L_1, L_2, focusing lenses; N_1, N_2, Nicol polarizing prisms; M_1, M_2, limiting apertures; F_1, F_2, quarter-wave Fresnel rhombs; S, sample cell; p_2, location for light detection (visual). From ref. [2].

Cotton also investigated the use of ellipticity measurements for CD studies. The combination of a linear polarizer and a Fresnel rhomb was used by Cotton to produce polarized light which could vary in its orientation from circular to elliptical. A second linear polarizer was then used to monitor changes in the orientation of the major axis of the ellipse which occurs as a result of the CD. In addition, the apparatus could also be used to measure optical rotation (circular birefringence). The experimental simplicity of this approach relative to his other system allowed more sensitive measurements to be made. This experimental simplicity also served as an impetus for other researchers in the field, and the ellipticity approach dominated the available technology from the time of Cotton's first efforts to the 1960's, when electronically modulated systems were developed.

The intrinsic optical rotation (circular birefringence) exhibited by an optically active sample can experimentally complicate the measurement of CD when the measurement is

made via the ellipticity approach. Changes in rotation due to the optical rotation must be carefully differentiated from orientational changes in the major axis of the ellipse due to the CD. One interesting experimental approach to circumvent this problem was developed by Bruhat in 1915 [3,4]. Bruhat's approach is schematically depicted in Fig. 3 below. From inspection of Fig. 3, it is clear that Bruhat separated the two phenomena by sequentially measuring first the rotation due to the intrinsic circular birefringence of the sample, this rotation was then nulled out and the CD was obtained without interference.
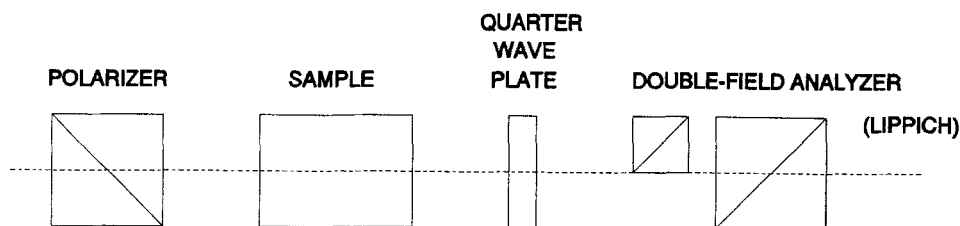
Figure 3. Integrated system of Bruhat for measuring circular dichroism and optical rotation. From ref. [4].

In Bruhat's system, a quarter-wave plate (which will convert linearly polarized light into a specific circularly polarized component) is aligned so that its transmission axis is parallel to the transmission axis of the linear polarizer such that a condition of extinction can be achieved (i.e., minimum light transmission). The quarter-wave plate is then removed and the sample inserted. The optical rotation from the sample is nulled out by rotation of the linear polarizer. The quarter-wave plate (its orientation unaffected by removal and re-insertion) is then placed back into the beam path, again imparting a high degree of circular polarization to the probing light. The CD absorption will then cause this light to become elliptically polarized. Rotation of the linear polarizer to achieve the null condition serves to define the major axis of the ellipse and from the new angular orientation of the linear polarizer the true ellipticity can be obtained. The approach will work even if the quarter-wave device does not impart an exact $\pi/4$ retardation (as long as the exact retardation is known). This is experimentally significant since most quarter-wave plates (but not Fresnel rhombs) only achieve an exact $\pi/4$ phase retardation at a specific wavelength. Therefore, Bruhat required a series of different quarter-wave plates in order to make measurements over an extended spectral range.

Visual detection was replaced by photographic detection by Kuhn and Braun in 1930 [5]. Their approach was also based on an ellipticity measurement which was not significantly different from that of Bruhat, although the photographic detection system allowed CD measurements to be made for the first time in the ultraviolet region. This system, with some minor improvements, served as the state-of-the-art for over two decades through the 1950's.

A new approach for the measurement of CD was described by Grosjean and Legrand in 1960 [6,7]. For the first time, electro-optical modulation of the polarization characteristics of the probing light was used in place of mechanical manipulation of the polarizing optics. This approach has a number of advantages over the other systems described and it has found virtually universal acceptance as the method of choice. Grosjean and Legrand's apparatus is effectively described by Fig. 1. As described previously, a high intensity light source in combination with a monochromator provides the monochromatic source light. This light is then plane polarized by a Rochon polarizer which splits the beam spatially into its two orthogonally polarized linear components. One of these components is blocked from the optical path while the other passes through a Pockels cell and into the sample. A phototube is used to monitor the light levels exiting the sample.

The Pockels cell is designed to provide a variable phase retardation depending upon the applied voltage. An ac high voltage is applied to the optical elements such that the induced axes in the device will make an angle of $\mp 45^\circ$ with the plane of polarization of the non-blocked component from the Rochon prism. This allows alternate production of left- and right-circularly polarized light. Thus, the light exiting the sample will contain both a dc component reflecting the innate transmission of the sample, and an ac component due to the CD. Phase sensitive amplification of the phototube signal provides the CD quantity. Properly optimized, Grosjean and Legrand estimated that absorbance differences of 1×10^{-4} cm^{-1} were measurable over the wavelength range 185 to 600 nm. As will be discussed in subsequent sections, commercial instruments available today utilize the Grosjean/Legrand approach and they differ only in the polarizing optics and devices used to create the circularly polarized light, and in the sophistication of the detection electronics.

3. TRANSMISSION-BASED CD INSTRUMENTATION

3.1. Light Sources

CD measurements, by virtue of the large background absorbance, place severe constraints on the characteristics of the probing light source. For the measurement of CD, the important criteria used in selecting a particular light source include the spectral output of the source (continuum, line, etc.), the usable wavelength region (that is, the wavelength region over which the source can maintain some minimum level of spectral radiance), and the stability of the source. The fact that CD is inherently a background limited measurement sets the minimum level of output radiance. Further, for routine measurements over the range of CD applications cited earlier, source stability must be at the 50 ppm level in order to be able to differentiate the subtle changes indicative of the CD measurement from random fluctuations in the background.

Although a number of incoherent sources are available which meet some of the criteria listed above, only high pressure arc lamps can provide the necessary output radiance. The source most used in commercial CD instruments is the xenon arc lamp, which utilizes an electrical discharge through a high pressure xenon atmosphere to produce a continuum output which spans the spectral range from 200 - 1000 nm. A 75 W arc has an approximate spectral radiance of 0.01 W cm^{-2} nm^{-1} sr^{-1} at 250 nm. Higher wattage lamps are available which provide a concomitant increase in the spectral radiance. This can be a distinct

advantage if output is required in the spectral region below 200 nm. In Xe arc lamps, the discharge is usually confined to a limited spatial region which simplifies the optical arrangement needed to collimate and focus the output radiation.

For operation over a limited spectral region primarily confined to the UV (200 - 350 nm), high wattage deuterium lamps are available and have been used in select applications. The emission region for these lamps is well defined, frequently encompassing approximately 1 mm. However, D_2 lamps provide an output that is severely limited above 350 nm, and for operation at longer wavelengths a second source is necessary. For this reason, most conventional applications utilize a Xe or mercury-xenon arc lamp as the source of choice for CD measurements.

Lasers have received some recent interest as light sources for CD instruments in select applications. Lasers produce coherent light which can provide substantial output radiance at a specified wavelength. Further, the spatial coherence of the output beam allows the radiation to be focused to extremely small dimensions, which has proven beneficial in situations where the sample under study is available in limited quantities or is confined to a limited volume. Such a situation, for example, is encountered when applying CD detection to modern separation techniques. However, laser sources are limited in their available output wavelengths which precludes their use in most CD applications, particularly those which require CD information over wide spectral regions. Even dye lasers only lase over a limited spectral region (approximately 30 - 40 nm) characteristic of the gain curve of the dye in use. However, lasers can be constrained to operate, either through intrinsic or designed processes in a temporal mode, in which all of the output radiation can be confined within a narrow time domain. Thus, depending on the operating mode and characteristics, lasers are available which can provide output pulses that can vary from the femtosecond (10^{-15} s) to the microsecond regime, or longer (although no one laser system can span this entire range). A temporally narrow output is useful in probing transient events, where, for example, nanosecond pulses are required to study events that occur on a similar time scale. This point will be illustrated in subsequent sections.

3.2 Polarizing Optics

A fundamental aspect of the CD measurement is the need to create and manipulate polarized light. Electromagnetic radiation, from a classical view, is stated as being polarized if the vibrations of the electric or magnetic field vector, representing a fixed point in its path, exhibit a long term preference with respect to direction or sense of vibration [2]. Thus, the electric field vector for linear or plane polarized radiation vibrates parallel to a fixed direction. Likewise, light is thought to be circularly polarized if the direction of the electric field vector generates a helical pattern as the beam passes through space. Mathematically, it can be shown that circularly polarized radiation can be resolved into two, orthogonal plane polarized components of equal amplitudes possessing a quarter-wave phase difference. Other polarization states (for example, elliptically polarized light) can be represented as a combination of circular or linearly polarized components by invoking the correct amplitude or phase relationship. A variety of optical elements have been devised to create, purify and convert linear and circularly polarized light, and the topic has been covered in great detail [2,8,9]. For the purposes of CD, the important criteria to consider include the efficiency of the polarizing device (i.e. the purity

of the polarized radiation), the wavelength region over which this efficiency can be maintained, and the geometric constraints of the device. These last criteria include the optical aperture and the acceptance angle over which the device will function. This section will briefly highlight the optical elements currently utilized for these manipulations with particular emphasis on the CD measurement.

Linear polarizers, which create linearly polarized light from unpolarized radiation, can be based on either absorption (linear dichroism), reflection, scattering or linear birefringence (double refraction). Of these four phenomena, only linear dichroism and linear birefringence have obtained wide use in CD measurements. Polarizers based on these effects can provide pure polarized light over wide spectral regions. Since the quality of the CD measurement will be determined by the precision with which the circularly or elliptically polarized light can be defined, the quality of the linear polarizer (which precedes the circular polarizing device) will directly affect the measurement process. Recent advances in thin film coating technology may soon allow new high performance linear polarizers based on reflection to be fabricated. For measurements at wavelengths below 180 nm, a reflection-based linear polarizer may be the most efficient design and this is an area of active investigation.

Of the two polarizer types in general use, linear polarizers based on linear dichroism are decidedly less expensive than those based on birefringent materials, but the polarizing efficiency of these devices is also substantially less. In a linear dichroic device, molecules in a host matrix (usually a plastic sheet) are oriented such that their transition dipole moments are along a specific axis. Light polarized along this axis is then preferentially absorbed, and light polarized perpendicular to the axis is preferentially transmitted. As mentioned earlier, these devices are relatively inexpensive and provide reasonable polarization efficiencies throughout the visible region of the spectrum. In addition, the geometric properties of these devices are excellent.

Uniaxial crystals possess two refractive indices which depend upon whether the propagating light is polarized parallel, or perpendicular to the unique axis of symmetry. In consideration of Snell's law, prisms constructed from such crystals will provide different paths depending on the linear state of polarization of the incoming radiation. A great variety of different prism geometries and combinations have been devised to take advantage of this property. One common design which exhibits superior polarizing characteristics is the Glan-Thompson prism. In this design, two right angle prisms composed of a birefringent material are cemented together at their hypotenuses to form a rectangular shape. In such a configuration, one linearly polarized component will possess a refractive index in the material such that it will be totally internally reflected at the interface between the two prisms, while the other component will be transmitted. The prism thus spatially displaces the one component relative to the other and either polarization state can be obtained in pure form. Other designs use an air space between the two prisms to avoid the prism adhesive, thereby extending the low wavelength operating range. The most common material utilized for such prisms is calcite, which can operate to approximately 215 nm. For work below 200 nm, crystalline quartz has a UV cutoff at 190 nm and MgF_2 can provide reasonable transmission to 150 nm. However, calcite has substantially better polarizing properties than these two materials and is the material of choice for most applications where operation in the far UV region is not required. Although prism polarizers based on birefringence can operate at much shorter

wavelengths than linearly dichroic polarizers, they are much more expensive, have greatly reduced optical apertures and have fairly severe entrance angle limitations.

Circularly polarized light can be produced by introducing a quarter wave retardation between two linearly polarized components of equal amplitude. Devices with this capability are designated as retarders and can function via a number of different mechanisms. One method involves propagation of light through a linearly birefringent material. Birefringent materials possess refractive indices which vary depending upon the polarization state of the incoming radiation and the direction of propagation. When light crosses an interface defined by two materials of differing refractive indices, the propagation velocity of the light is impeded in the material with the larger refractive index. Since the frequency of the light is invariant across the boundary, the phase angle of the light will change more rapidly in the medium with the larger refractive index. Thus for light incident upon a linearly birefringent environment, one linear component will undergo a larger phase change than the other with the total phase difference determined by the properties of the material the light is propagating in and the length of the interaction. The retardation device must therefore be prepared for a specific wavelength since the linear birefringent properties of anisotropic materials are wavelength dependent. Thus one limitation of these devices is their small spectral operating range and multiple devices are necessary to span a reasonable wavelength region.

A quarter-wave retardation can also be imparted by reflection at the appropriate angle, a property utilized in the Fresnel rhomb (Fig. 2). When light is incident upon an interface defined by two isotropic media of differing refractive indices, a portion of the light will be transmitted into the second medium across the interface, and some will be reflected. At a specific angle of incidence, the light will be totally reflected in the denser medium. This process is known as total internal reflection and the phase of the reflected wave can be determined from Fresnel's laws of reflection and the properties of the incident light beam [10]. When the incident light is polarized with its electric field vector at an angle of 45° to the face of the Fresnel rhomb and in the plane of the entrance face, the polarized light can be resolved into two orthogonally polarized components of equivalent amplitude. Upon reflection, a phase **difference**, δ will be imparted to these two components, and, if the phase difference equals exactly one quarter-wave, the light exiting the rhomb will be circularly polarized. In practice, the angle of reflection is chosen such that two reflections occur to cause the quarter-wave retardation. As evident in Fig. 2, the beam is deviated spatially by these reflections which can complicate the optical arrangement. However, the Fresnel rhomb possesses two advantages which make this limitation tractable. At angles of incidence near the point where the retardation is a maximum, the variation of δ with the angle of incidence is small giving a large optical aperture. In addition, δ has a very small wavelength dependence over large spectral ranges thus providing a near achromatic phase retardation. It should be noted that for fused silica, two reflections are not sufficient to induce a quarter-wave retardation in the visible region of the spectrum. This problem can be solved by the use of a three reflection device [2]. This device can provide several advantages over the Fresnel rhomb including the ability to operate from the far UV through the visible, and at the same time the quarter-wave retardation does not require a deviation in the spatial orientation of the beam.

3.3 Photoelectric and Photoelastic Modulators

For optimum performance, CD measurements require a polarization modulated source. In principle, any of the polarization-selective optical devices discussed earlier could be mechanically moved to create the required modulation. However, this approach is problematic in that it is difficult to implement physically, the mechanical movement may introduce noise into the measurement situation, and there are limitations to the rate at which the polarization can be modulated. A preferable approach is to use an electronic device to effect the required phase retardation. Although a number of devices have been used for this purpose (e.g. magneto-optical, Kerr effect, etc.), modern CD instruments rely upon either the Pockels effect, or photoelastic modulation for this function.

When certain crystalline materials are subjected to a strong electric field, the electric field can induce changes in the linear birefringent properties of the material. If the material subjected to the field is illuminated with linearly polarized light, a phase difference will be introduced into the two orthogonal components. The magnitude of the phase difference will be dependent upon the photoelectric medium and the applied voltage. Thus, for a fixed wavelength, a variable retardation can be created by application of the correct voltage. Both transverse (perpendicular to the light beam) and longitudinal Pockels cells are available. The advantage of this approach is that the retardation can be switched very rapidly and Pockels cells are available which can operate at frequencies of 100 MHz, or above. However, in order to achieve a quarter-wave retardation in, for example ammonium dihydrogen phosphate, the applied potential must be approximately 3 kV. Further, due to the expense of the crystals used in these devices, and in order to minimize field inhomogeneities, the interaction region is kept small. Thus Pockels cells have very limited optical apertures.

An alternate approach based on photoelastic modulation has recently been developed and this method has replaced electro-optical modulation in most CD instrumentation [11,12]. Photoelastic modulators take advantage of the birefringence created when isotropic materials are subjected to a pressure induced strain. In a typical photoelastic modulator, a piezoelectric transducer is mounted to the sides of a fused silica block. Application of a voltage to the transducer creates a pressure induced strain in the silica, and the amount of retardation can be varied depending on the voltage supplied to the transducer. The transducer element is usually driven at a resonant frequency of the device and photoelastic modulators therefore require much lower drive voltages than Pockels cells, although they can not be switched as rapidly as photoelectric devices. In addition, these devices provide large spatial apertures and this can improve the signal-to-noise ratio for CD measurements by an order-of-magnitude over applications utilizing Pockels cells.

3.4 Light Detection Devices

For CD measurements, the light detection device must be able to provide a moderate level of sensitivity and possess both low noise and a stable response. The latter two criteria are a consequence of the fact that the absorbance difference being measured will be exceeded by the intrinsic absorbance of the sample by several orders-of-magnitude. For this reason, photomultiplier tubes (PMT) are used in conventional CD instruments for light detection as they can provide a response over a wide spectral region, and they possess both high gain and low noise. However, conventional instruments obtain wavelength dependent CD information on a point-by-point basis in that the CD is measured for each

wavelength of interest in a sequential manner. This approach is time consuming, which limits the application of multiwavelength CD measurements to static systems. Further, it frequently is advantageous to add several spectra together to improve the signal to noise ratio (SNR) thereby highlighting small spectral features. However, for sequential measurements, the grating must be mechanically reset to its original position prior to the start of a subsequent scan. This method can be unreliable unless the data acquisition is electronically tagged, and it will limit the quality of the data obtained using spectral addition techniques with conventional CD instruments.

Multichannel detectors can provide simultaneous detection of a range of wavelengths when the light detection device is placed at the focal plane of the wavelength dispersion system in the spectrometer. This approach can provide spectral information on transient events (i.e. time-resolved information), or for static measurement situations, the same spectral region can be repetitively scanned and spectral addition effected with a concomitant improvement in the measured SNR. For randomly distributed noise in N measurements, the SNR will improve by the factor $N^{1/2}$. There is no fundamental reason why this approach can not be applied to CD measurements and, for many types of studies, for example, in studies of protein folding, time-resolved information will be critical to discerning the subtle features that govern the three dimensional shape of the biologically active entity. This point will be addressed later. However, in spite of the advantages of this approach, the use of high frequency polarization modulation in conventional CD systems and the time characteristics of the available multichannel light detection devices are incompatible. This is a consequence of the time it takes to read out the intensity information in the multichannel device after exposure relative to the modulation frequency of the PEM or Pockels cell (>50 kHz).

As an example, linear arrays of silicon photodiodes (photodiode arrays) are available as a package complete with the necessary circuitry to read out the array following exposure. Arrays are available with up to 2048 elements, and they are read out on an element by element basis. The scanning circuitry can access an element in 10 - 25 μs, which suggests that the entire array can be read out in approximately 20 - 50 ms. Thus modulation frequencies can not exceed 50 Hz. However, as was discussed earlier, PEMs are driven at a resonant frequency which usually varies between 50 and 100 kHz, and this exceeds the readout rate of the photodiode array by three orders-of-magnitude.

Charge coupled devices (CCD) and charge injection devices (CID) are solid state sensors which are fabricated as true two dimensional arrays, as opposed to the one-dimensional arrangement characteristic of the diode array. In addition to these differing spatial characteristics, CCDs and CIDs are more sensitive than conventional diode arrays and are read out by a different mechanism. The CCD and CID utilize a three-phase clocking arrangement in which stored charge is shifted horizontally to a high speed shift register. Although this approach can be faster than the element by element scan of the diode array, it still is not fast enough to allow operation at the modulation frequencies demanded by the PEM. For a CD instrument with a PEM operating at 50 kHz, the multichannel device must be capable of making a measurement at twice this frequency in order to obtain separate intensity information for the absorption of the sample with respect to the two circularly polarized components.

The significant advantages which would result from multichannel CD measurements has led to a number of different approaches designed to incorporate a multichannel

detector into the CD experiment. This goal can be achieved by one of two approaches: either the modulation frequency of the CD system must be lowered to match the capacity of the multichannel detector, or a new technique must be developed in order to allow sampling from the multichannel detector at a rate compatible with the modulation device. Wetzel and coworkers [13] have pursued the first approach and have succeeded in developing a CCD-based CD instrument which is capable of simultaneously measuring CD at all wavelengths over a limited spectral range. To circumvent the limitation imposed by the readout rate of the CCD, an electro-optic modulator (Pockels cell) was used at an operating frequency of 58 Hz. As was pointed out above, the Pockels cell places fairly severe limitations on the spatial characteristics of the light beam to be modulated. In this system, in spite of the fact that a longitudinal arrangement was utilized for the Pockels cell, an acceptance angle of approximately 2° was required. This necessitated the incorporation of an iris before the Pockels cell to limit the cone of light entering the device.

Fig. 4 below schematically depicts the optical arrangement developed by Wetzel and co-workers which was designed to incorporate multichannel detection into the CD experiment.
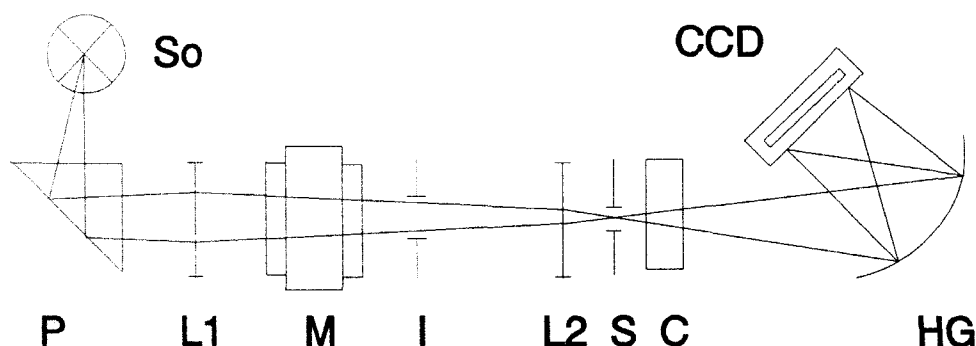
Figure 4. Experimental arrangement for multichannel-detected CD. So, 30 W deuterium lamp source; P, beam steering prism; L_1, L_2, beam focusing, collimating lenses; M, Pockels cell; I, beam limiting iris; S, slit; C, sample cell; HG, holographic grating (polychromator); CCD, charge coupled device (light detection array). All optical elements are constructed from fused silica, or designed to be transparent to 200 nm. From ref. [13].

Comparison of Fig. 1, which depicts a conventional CD system, and Fig. 4 shows the primary difference in the two approaches to be in the type and location of the wavelength dispersion device. For multichannel detection, the monochromator has been replaced by a polychromator which does not possess an exit slit to define a wavelength interval. For multichannel detection, the location (pixel) on the multichannel device defines the wavelength of interest. In conventional approaches, the monochromator is placed after the source in order to limit the UV exposure of the sample. However, in the multichannel arrangement, the polychromator is located after the sample to allow the sample to be

exposed to all wavelengths simultaneously. The CCD can be configured such that a group of elements will define a specific wavelength interval, and exposure data for these elements allows the sample absorption at that wavelength to be determined. In one complete cycle, the CCD will be readout twice, thereby providing sample transmittances at the specified wavelength for both left- and right-circularly polarized light.

The combination of the CCD and polychromator used in this system allowed CD information to be obtained over a wavelength range spanning 80 nm, with a lower wavelength limit of approximately 200 nm [13]. The wavelength range available is a function of the CCD, polychromator and ancillary optics. Excellent agreement was found between CD spectra obtained on this system and spectra obtained on a conventional instrument. The investigators found the main advantages of this approach to be in the elimination of the mechanical movement of the wavelength dispersion device in order to obtain CD spectra. It is suggested that the lack of moving parts will be a significant advantage in CD studies in the far UV (180 - 160 nm) where the system must be evacuated to function. A lower absolute mass detection limit, reflecting the improved SNR available by spectral averaging, was realized with this system, but it is not clear if this will justify the added cost of the CCD detector and electronics over a PMT. Certainly, the advantages in terms of time-resolved studies or spectral addition, when demonstrated will justify these considerations.

As discussed earlier, the PEM is, in many ways, an ideal modulation device for polarization-selective measurements. Thus, the optimum simultaneous multiwavelength CD instrument should incorporate both the PEM and CCD, and at the same time allow the PEM to operate at its resonant frequency. One way to overcome the basic incompatibility of the PEM and CCD is to use an optical demodulation scheme in which the two oppositely polarized components would be directed by a polarizing beamsplitter, to either different areas of the same CCD, or to different CCDs [14]. Since two distinct detector areas would be accessed by the oppositely polarized light, pixel-to-pixel sensitivity variations may be a significant source of noise.

A radical new approach has recently been proposed which is designed to operate the CCD in a mode that is compatible with the modulation constraints imposed by the PEM [15]. In this system, the CCD itself is configured to provide an electronic demodulation of the orthogonally polarized image planes. Fig. 5 illustrates the masking scheme used to provide two temporally separate (as opposed to spatially distinct) image planes in the same CCD. The masking arrangement shown in Fig. 5 is used to create exposed and unexposed regions. In one half-cycle, the region of the CCD defined by the open area of the mask will be exposed to light of a given polarization state and charge will be created in a given pixel depending on the intensity of the light impinging upon it. At the conclusion of the time period defined by the half-cycle modulation period of the PEM, the charge in the exposed regions is then electronically shifted to the pixels in the unexposed section, and the open region is then exposed to light of the opposite polarization. For accumulation cycles after the first exposure, the charge residing in the unexposed pixels, which reflects the total exposure measured for a given polarization state, is shifted to the exposed region for further exposure. At the same time, the charge accumulated during the previous half-cycle is shifted into the unexposed pixels. The electronic switching process is then repeated and each pixel continues to accumulate charge reflecting the total exposure of that pixel within a given polarization cycle. Thus, when one image plane is being

exposed, the other plane resides in an unexposed storage region of the CCD. After a number of such cycles, but before the CCD elements are saturated, the CCD is read out, and the process repeated. This approach eliminates the geometric considerations cited above as limiting for the other method utilizing spatially distinct image planes since the same pixels are illuminated regardless of the polarization state being monitored. This electronic shifting process can be completed in a time domain that is compatible with the PEM resonant frequency.
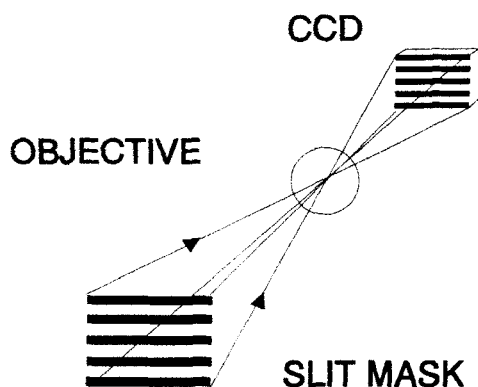
Fig. 5. Imaging of a slit mask onto a CCD. The slits are parallel to the CCD pixel rows and each slit has a width that is 82% of the row width. From ref. [15].

For a given CCD array, one dimension, (such as the vertical plane), could be used to define distinct wavelength regions. Intensity information for a given wavelength interval for the two, oppositely polarized states would then be alternately stored in the exposed and unexposed regions defined by the CCD mask. After readout of the two planes in the CCD array, the CD information could be obtained from the integrated exposure information in the two image planes as accomplished conventionally. At this point, a number of key operating parameters (mask type, element dimension, CCD exposure duration before readout, etc.) have yet to be optimized. However, it is clear from this initial report that this approach will have important implications for simultaneous, multiwavelength CD measurements.

3.5 Vibrational CD Instrumentation

Although the crux of this chapter is devoted to instrumental developments for the measurement of CD in the visible and UV regions, it is appropriate to consider the instrumental modifications necessary to extend CD measurements to the mid-infrared region. The anisotropy ratio, g is given as the ratio of the differential absorbance (or absorptivity) to the parent absorption strength ($g = \Delta A/A$). For vibrational CD, this value can vary from 10^{-3} to 10^{-6}. Given that the strength of a vibrational transition can be 10 to 1000 times smaller than that of an electronic transition in the UV or visible, the circular dichroism of a vibrational transition is therefore exceedingly small and the instrumentation

designed to measure vibrational CD must be capable of providing a high SNR. CD measurements in this region can be obtained on either dispersive or Fourier-transform based instruments. Obviously, for operation in this region, the source and detector must be capable of producing and responding to mid-IR radiation. Thus, dispersive CD instruments for the mid-IR would appear identical schematically to those designed for operation in the visible/UV with the exception of the source and detector. In addition, a slightly different modulation protocol is used to improve the SNR. In this double modulation scheme, a low frequency modulator (e.g. light chopper) is used in combination with a PEM operating at a much higher frequency. Demodulation of the low frequency component allows one to determine the conventional single beam transmission spectrum of the sample. Demodulation of the high frequency component gives the transmittance of the sample with respect to either left- or right circularly polarized light. The differential transmission data is then normalized with respect to the single beam transmission spectrum to minimize the influence of experimental artifacts on the CD measurement [16].

Fourier-transform, vibrational CD instruments have been used extensively and they provide significant advantages over other approaches in the mid-IR region [17]. In a Fourier-transform based system, the Michelson interferometer takes the place of the light chopper. In this approach, the moving mirror in the interferometer encodes each distinct wavelength separately with a Fourier frequency which is given as twice the velocity of the mirror multiplied by the frequency (in wavenumbers) of the infrared light. This is equivalent to the low frequency modulation component in the double modulation scheme. As in the dispersive VCD system, a PEM is used to circularly polarize the source radiation. In both the dispersive and FT systems, a cooled semi-conductor detector is utilized to enhance its response time, reduce noise and allow adequate sampling of the high frequency modulated output of the PEM. The advantages of the FT approach over the dispersive method include improved resolution, enhanced light throughput and an improvement in the experimental SNR by virtue of the multiplex advantage. Thus, Fourier transform-based CD instruments have virtually replaced dispersive instruments in the region from 600 -2000 cm^{-1}. The advantages of the FT-VCD method have changed the VCD experiment from one of substantial challenge to a routine method for studying subtle structural features in chiral molecules.

3.6 Stopped-Flow Circular Dichroism

The capability of CD to discern subtle conformational differences in large, biologically active molecules is well known. However, many biological associations rely upon a conformational change in one, or both of the interacting entities to facilitate the relationship. For example, the study of a ligand binding process may require detailed information as to the **time evolution** of the conformational changes in the entities which will eventually define the structural relationship of the ligand to the binding site. Thus, with this information, one could address the question as to whether the conformational changes occur as a single step, or as a series of sequential interrelated transformations.

With this possibility in mind, the technique of stopped-flow has been combined with CD detection. The stopped-flow technique allows precisely defined quantities of reactants to be rapidly mixed and the reaction initiated within a well defined time interval. CD, as a chiroptical technique, would then allow one to glean information as to the conformational

changes that occur after initiation of the reaction and the time domain of these events. However, in spite of the importance of these problems, the combination of stopped-flow and CD was limited by instrumental considerations related to the low SNR of the CD experiment and the rapid time response required by the stopped-flow mixing technique (10 - 50 ms). Baley and Anson [18,19] combined the two techniques to produce a system that is able to respond to a differential absorbance of 2×10^{-5} cm^{-1} with a time response of 2 ms. Conceptually, their experimental arrangement is similar to the conventional instrument schematically depicted in Fig. 1. However, in order to increase the SNR, they used a stabilized, high intensity light source and they designed the optical system to maximize the light throughput of the system.

The light source utilized for the stopped-flow CD system was a high pressure mercury arc, as it can provide a high spectral radiance over the spectral range 280 - 600 nm. The output of this source contains many lines from atomic mercury superimposed on a xenon continuum background, and the radiance can exceed that of the Xe arc by a factor of 10-20 over its usable range. The limitation to this source is its instability, as intensity fluctuations are usually large and significant. This problem was solved by splitting off a portion of the source light before the polarizing optics with a beamsplitter. This portion was sent to a photodiode to serve as a reference intensity. Thus, each data point reflecting the sample's transmittance for one of the two circularly polarized components was normalized to this reference intensity. Light throughput was improved by replacing the monochromator with an interference filter. The interference filter makes it impossible to obtain CD information at more than one wavelength interval per measurement, however, the time evolution of the CD signal at that wavelength is obtained instead. From these first reports further refinements in the technique of stopped-flow CD have proceeded incrementally. The concepts of source intensity, stability, and throughput to improve the SNR are still the underlying basis for the success of the technique.

Another problem of significant interest concerns studies designed to uncover the rules which govern the kinetics and direction a protein takes when folding into its active conformation. Studies of this nature require CD measurements in the UV where protein polypeptide backbone conformation can be observed. Beychok and Luchins have developed a stopped-flow CD instrument which combines millisecond time resolution with the ability to make measurements down to 200 nm [20]. A stabilized Xe arc was used as the source to take advantage of its appreciable output radiance to 200 nm, and the optical system was designed to maximize light throughput. In addition, the influence of mechanical noise on the CD measurements was minimized by mounting the instrument on a vibration damping apparatus. Through such an instrumental approach, an impressive level of both CD detectability and time resolution is possible.

The tremendous interest in understanding protein folding has served as a significant impetus for commercial CD instrument manufacturers. Many systems available today are designed to encompass the experimental considerations discussed earlier and offer a stopped-flow mixer as a system option. Based on the wealth of information available from such measurements, the technique of stopped-flow CD is now ubiquitous in modern biochemical research.

3.7 CD Detection in Chromatography

Separation resolution can be enhanced by coupling to the separation system a detector that responds to a specific molecular property. This selectivity has served as the rationale which has led to the application of CD as a detection system for gas chromatography (GC) and high performance liquid chromatography (HPLC). An additional advantage of such an approach is in the analysis of enantiomers. Enantiomeric materials present a significant challenge to the analyst and physical separation of an enantiomeric pair through the application of a chiral-selective separation mode is difficult to achieve. For example, chiral-selective HPLC columns are easily fouled, expensive and a given type of column only exhibits selectivity towards a limited group of compounds. Therefore, in the absence of chemical modification to form a diastereomeric entity, the differing ability of a pair of enantiomers to interact with polarized light provides the only simple and direct approach which can be used for differentiation.

CD detection has been used to monitor optically active molecules separated by GC [21]. Although the CD detection system was constructed on a component basis and not derived from a commercially available instrument, it was conventional (i.e. PEM modulation, etc.) with the exception of the source. A 200 W Hg-Xe arc lamp was utilized due to its high radiance and it was operated under conditions designed to maximize output stability. To improve detection, a 6 cm path cell was needed, however, this cell had an internal volume of 1.38 mL. This volume is too large to be compatible with modern, high performance GC columns (e.g. capillary columns). The complete GC-CD system demonstrated a minimum measurable mass in the 10 - 50 μg range, which is several orders-of-magnitude greater than other, commonly used GC detectors. Thus, the only justification for this approach lies in the type of information available. However, the analyte distribution resulting from separation in a modern GC column requires that the detector be able to provide a measurement once every 1-3 seconds. Therefore, using conventional, sequential scanning approaches, the CD information is limited to a single wavelength.

Synchrotron radiation has been used to extend GC-CD measurements to the vacuum UV (VUV) [22]. The synchrotron source provides a high radiance output over the spectral region from 600 - 135 nm. This radiation is inherently plane polarized and is converted to circularly polarized light using a PEM constructed from CaF_2. With the exception of the light source, both the GC and CD systems are conventional. Wavelength selection was accomplished using a grating-based monochromator and a long-path detection cell was used to improve measurement sensitivity. However, as before, the volume of this cell precludes its use with high resolution modes of GC. The various components were either placed in, or attached to a vacuum chamber to remove oxygen and facilitate operation in the VUV. The unique advantage of this system is the extended UV operating range. Conventional arc lamp-based CD systems can not provide reasonable measurement sensitivity in the spectral region below approximately 180 nm. However, for saturated hydrocarbons which are optically active, this is the region where they absorb and where the CD must be monitored. The synchrotron-based CD system demonstrated a mass limit of detection in the nanogram range for optically active hydrocarbons, which is adequate for many important applications. The only limitation to extensive application of this approach for CD measurements in the VUV is the restricted availability of the synchrotron source.

The development of CD HPLC proceeded using a conventional, static mode CD spectrometer [23,24]. The combined system demonstrated a mass detection limit of $3\mu g$ of L-tryptophan. As in the GC examples cited above, only single wavelength CD measurements could be made based on the time domain required for wavelength scanning. Again, justification for such an approach must originate from the uniqueness of the information available from the detection system. Kurosu, et. al. [25], interfaced a conventional CD spectrometer and microvolume flow cell to a HPLC in order to study several model proteins separated by both reverse-phase and hydroxyapatite (HAC) chromatography. The advantage of CD detection was clearly evident in this work as the influence of the stationary phase, various salts and surfactants on the secondary structure of the separated proteins was monitored. These authors suggest that from the CD information, chromatographic conditions could be adjusted to both optimize the separation and, at the same time maximize the structural integrity of the biologically active protein.

As the previous study suggests, specific advantages can be obtained by combining CD detection with HPLC separation. However, with the exception of the source, most attempts to date have approached the problem using either a commercial CD system, or a conventional arrangement for a modular spectrometer. There is one limitation where such an approach cannot be avoided: modern, high resolution separation systems provide analyte distributions which are minimally dispersed. In order to be compatible with these separation systems, the CD sample detection cell must provide an internal volume which is 5 - 10 times smaller than the total analyte peak volume. Thus, 4.6 mm i.d. HPLC columns require detection volumes which are on the order of 20 μL, or smaller. The inherent limitation of using an incoherent source for the CD system is that conventional incoherent sources can not be molded to efficiently fit within the small dimensions required for microvolume detection. Thus, one must either sacrifice light throughput with a concomitant decrease in sensitivity, or one must be prepared to tolerate large detection volumes with a concomitant decrease in chromatographic resolution and efficiency.

Synovec and Yeung [26] used a laser source to facilitate coupling of CD detection to microvolume HPLC. These researchers were interested in applying CD detection to optically active materials separated on 1 mm i.d. microbore HPLC columns. For this separation mode, analyte elution volumes are on the order of 20 μL, which implies that detection volumes need to be approximately 1 μL. For such small detection volumes, a coherent source is required in order to efficiently focus the probing light into such small dimensions. However, many lasers of the type used in these studies possess fairly high levels of amplitude noise (approximately 1%). It has been observed that the magnitude of this noise source varies as the reciprocal of the frequency (1/f). Thus, high frequency polarization modulation and detection (500 - 700 kHz) utilizing a Pockels cell was used to minimize this noise source and provide CD detection at 488 nm. With the exception of the source and modulation frequency, the system is identical to the instrument schematically depicted in Fig. 1. The probing wavelength is limited by the output lines available from the continuous-wave laser source, however, recent developments in these lasers has made available several lines in the UV. These UV lines though exhibit more amplitude noise than the output lines in the visible region. A mass limit of detection of 5.6 ng for $(+)-Co(en)_3^{3+}$ was demonstrated using microbore column separation.

It is clear that CD measurements can provide unique information which can be used to design and optimize the separation of structurally complex, biologically active materials. However, the fact that HPLC is a time dependent experiment, and the time dependence of the analyte distribution is not compatible with the scanning rate of conventional CD instruments currently limits the CD-HPLC measurement to a single wavelength. This problem will be solved if multichannel detection can be effectively coupled to the CD experiment.

4. NEW DEVELOPMENTS IN CD INSTRUMENTATION AND MEASUREMENTS

The previous section clearly demonstrated the need for CD measurements on a time-resolved basis. Both stopped-flow and chromatographic applications require that CD measurements be obtained on the millisecond, or longer time scale. For this time domain, modification of conventional CD systems is appropriate and this approach has met with excellent success. However, there are a number of important applications where CD information is required in the microsecond to picosecond time domain. Certainly this time regime can not be accessed by simple modification of conventional CD detection strategies and new approaches have therefore been devised to extend CD measurements into the microsecond, and below, time domain. The crux of this section will be to consider CD detection strategies which are designed to improve the measurement SNR, and therefore allow extension into new domains such as time-resolved CD studies.

4.1. Fluorescence-Detected CD

Fluorescence detection of CD (FDCD) has been used to extend both the sensitivity and selectivity of the CD experiment [27]. Fluorescence in solution originates from the first excited singlet state of a molecule possessing the appropriate structural characteristics. These specific structural requirements add an additional degree of selectivity to the CD experiment in that most chromophores are not also fluorophores. If one were to alternately probe a fluorophore with left- and right-circularly polarized light, the resulting fluorescence intensity will alternate in magnitude to reflect the differential absorption. Thus, one can obtain similar information from the FDCD experiment as available by a conventional transmission-based measurement. This degree of selectivity has been exploited to measure the CD of a single fluorophore in a complex macromolecule with multiple chiral centers. In addition, the sensitivity advantage of fluorescence, that is, the advantage of being able to obtain a measurement on a theoretically zero background, suggests that FDCD should be an extremely sensitive way to measure CD.

The instrumental arrangement for the FDCD experiment is schematically depicted in Fig. 6. The optical arrangement from the source to the detection cell is identical to that of the transmission-based CD experiment. Thus an arc lamp source and monochromator are used to provide the appropriate wavelength interval for excitation. Circularly polarized light is produced through the combination of a linear polarizer (Glan-Thompson prism) and Pockels cell. However, as in traditional fluorescence measurements, the light detection system is placed at right angles to the exciting beam to minimize the influence of scattered light on the measured fluorescence intensity. An additional wavelength selection device is usually located before the PMT to further reduce the amount of scattered

excitation light measured by the PMT and resolve the fluorescent emission into its spectral components. Wavelength resolution of the fluorescence can add an additional level of selectivity to the measurement and permit identical CD active fluorophores located in different chemical environments to be differentiated.

Warner and co-workers [28] have developed a multidimensional FDCD spectrometer using an intensified diode array as the light detection device. Their system combines the optical arrangement depicted in Fig. 6 for the FDCD experiment, with the polychromator/multichannel light detection arrangement illustrated in Fig. 4. However, instead of using polarization modulation in combination with synchronous amplification, a non-alternating (dc) detection strategy was employed. This was necessitated by the time limitations imposed by the readout rate of the diode array.

In Warner's system, light from a 500 W Xe arc was passed through a monochromator to select the excitation wavelength. This light was then passed through a Glan-Taylor polarizing prism and a Fresnel rhomb appropriately aligned to produce circularly polarized light from the linearly polarized excitation beam entering it. The circularly polarized light then served to excite the sample. To obtain circularly polarized light of the opposite orientation, the Glan-Taylor prism was rotated mechanically by 90°. The multichannel light detection system was oriented at an angle of 90° to the excitation path. The polychromator provided wavelength dispersion of the fluorescent emission, which was subsequently detected by a 512 element, large area intensified diode array. This optical arrangement facilitated the collection of both excitation and emission spectra.
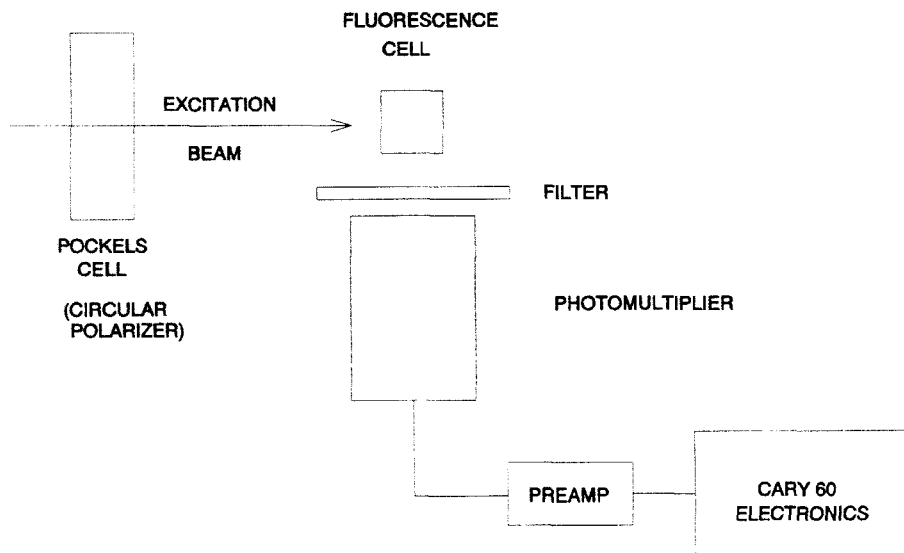

Figure 6. Experimental arrangement for measuring fluorescence-detected CD. From ref. [27].

In order to provide this multidimensional information, for each excitation wavelength, a complete emission spectrum must be obtained for both left-, and right-circularly

polarized light. This was accomplished by mechanical movement of the polarizing prism to vary the linear polarization of the light entering the rhomb by 90°. The measurement sequence followed the order: (1) select excitation wavelength; (2) measure emission spectrum for one circularly polarized component; (3) move Glan-Taylor prism orientation; (4) measure emission spectrum for other circularly polarized component; and (5) move excitation monochromator to select new excitation interval. From this data set, spectra for the different circular polarization states were subtracted to obtain the FDCD signal matrix. Thus, for each excitation interval, a complete FDCD emission profile is collected. Likewise, for each emission wavelength, a complete excitation FDCD profile is available and with this data, a two dimensional FDCD matrix can be obtained. However, in order to extend this level of sophistication to the CD experiment, approximately 30 minutes is required to obtain the data set for each sample.

Warner and co-workers justify the elaborate optical/detection system and the time commitment required per analysis on the basis of the additional sensitivity available using fluorescence detection, and on the multidimensional CD information available. For applications in which two, or more CD active fluorophores may be present, the ability to provide both an excitation and emission FDCD profile for the sample may allow differentiation of the individual components without pre-separation. Replacement of the mechanical mechanism for prism movement with an electro-optical device may improve both the SNR and reduce the time required per sample. These improvements will greatly facilitate general application of this multidimensional approach to FDCD measurements.

FDCD has been utilized as a detection principle in HPLC [29] in order to exploit both the sensitivity and selectivity advantages of the technique. A helium-cadmium (HeCd) laser operating at 325 nm and providing 8 mW of power was used as the excitation source. As demonstrated previously, the laser source facilitates focusing of the excitation light into the microvolume probe region (14 μL) required by the high efficiency separation system. High frequency polarization modulation via a Pockels cell in combination with synchronous amplification was used to reduce laser noise and improve the SNR. Improvements in the detection limit were noted, as compared to the transmission-based high frequency CD HPLC detection system described earlier [26]. This improvement (a minimum measurable quantity of 170 pg of riboflavin) reflects the advantages of fluorescence detection versus transmission-based measurements.

Christensen and Yeung [30] applied this technology to the detection of CD active analytes separated by capillary electrophoresis (CE). CE is a recently developed separation mode which relies upon electromigration for the separation of charged species. Highly efficient separations have been demonstrated in this mode using capillary columns with internal diameters which can vary between 25 and 100 μm. Analyte volumes in such capillaries are on the order of nanoliters, which places severe constraints on the CE detection system. Thus FDCD, with its high selectivity and capability for small volume detection appears to be ideally suited to the detection problem in CE. Physically the instrumental arrangement differs little from the previously described system for FDCD (Fig. 6), and the high frequency, laser-based CD detection system for HPLC. However, microscope objectives were needed to both focus the exciting laser light into the small diameter capillary, and collect the resulting fluorescent signal. The argon ion laser source was polarization modulated by a Pockels cell and the resulting fluorescence was collected at 90° to the excitation path. It is suggested that with this system, FDCD measurements

can be made on volumes as small as 10 picoliters. A detection limit of 0.07 pg of riboflavin, which corresponds to an improvement of three orders-of-magnitude over the FDCD system designed for detection in conventional HPLC, was demonstrated. As configured at the present, detection is limited to a single excitation wavelength determined by the available output lines from the laser source. More general application must await the development of suitable laser sources with stable output lines in the UV and the good beam spatial characteristics needed to facilitate efficient focusing of the excitation radiation into the small probe volume required for detection in CE.

4.2 Lifetime-Resolved Fluorescence-Detected CD

McGown and co-workers have recently described a new instrumental approach for FDCD measurements that is capable of individually resolving multiple chiral fluorophores in complex mixtures [31-33]. As has been pointed out [31], CD measurements, and consequently FDCD measurements provide information about the average chiral characteristics of the sample under study. By introducing lifetime resolution into the FDCD experiment, identical fluorophores residing in different chemical environments can be resolved by measuring the differences in their excited state lifetimes. As has been demonstrated, lifetime analysis is a very powerful tool for probing complex systems and the chemical characteristics which one can differentiate by such an approach can be extremely subtle.

A schematic of the frequency domain lifetime-resolved FDCD spectrometer is given in Fig. 7. The instrument is based upon a conventional phase-modulated fluorescence spectrometer in which fluorescence lifetimes are calculated from the phase-shift and demodulation of the fluorescence signal [34]. In this approach, high frequency intensity modulation produces a time-dependent fluorescence signal. For lifetime-resolved FDCD, the intensity modulation is coupled with a device to produce left- and right-circularly polarized light. Multifrequency excitation with circularly polarized light, in combination with heterogeneity analysis provides the lifetime distributions and fractional intensity contributions of both the individual chiral and achiral components to the total FDCD signal.

The LR-FDCD phase-modulated fluorescence spectrometer is based upon a commercially available instrument which has been modified to incorporate polarization selectivity into the excitation path. The output from a 500 W Hg-Xe arc lamp is passed through a monochromator for selection of the excitation wavelength, and then into a Pockels cell/polarizing cube combination to intensity modulate the excitation source. A portion of this beam is directed by a beam splitter to a reference PMT for phase and ratiometric correlation. The excitation beam is then made circularly polarized by the use of a linear polarizing prism (Glan-Thompson) /Babinet-Soleil compensator combination placed just before the sample cell. Fluorescent emission from the sample is detected at right angles to the excitation path. The fluorescence is passed first through a linear polarizer to correct for photoselection, and then through a second monochromator, or other wavelength dispersion device to wavelength resolve the fluorescent emission. Light detection is accomplished by a second PMT.

As evident from Fig. 7, and the previous instrumental description, the LR-FDCD system appears similar in configuration to a conventional phase-modulated spectrofluorometer with the exception of the Babinet-Soleil compensator (BSC). The BSC

is a variable-wave plate that can be oriented to produce circularly polarized light over an extended wavelength range. It is constructed of two, identical quartz wedges, one of which is attached to a quartz compensator plate to ensure that the quartz is uniform over the optical aperture. The second wedge is moved relative to the first creating a variable thickness of quartz, and therefore a variable retardation. In the latest design of this system, the BSC is mounted in a motorized stage which allows micrometer adjustment of the BSC orientation. This appears to be the most reproducible way to produce circularly polarized light for these measurements. The BSC was chosen as the circular polarizing device due to its large wavelength operating range (as compared to a quarter-wave plate), and its large spatial aperture which can create the desired polarization manipulation without physically displacing the beam (as compared to a Fresnel rhomb). Note from Fig. 7 that the excitation wavelength is fixed and the emission profile is scanned in order to obtain the LR-FDCD measurement. Thus, for each excitation wavelength, a compete emission scan is obtained for each of the two circular polarization states and for modulation frequencies of 1, 2, 3, 5, 10, and 20 MHz.
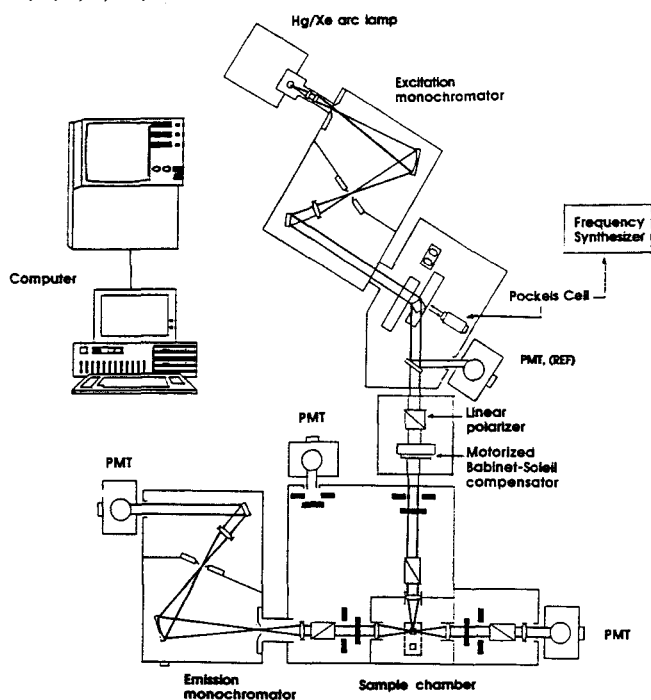

Figure 7. Schematic diagram of modified phase-modified spectrofluorometer for FDCD/LR-FDCD measurements. From ref. [33].

The advantages of this approach in studies involving chiral fluorophores in nonequivalent chemical environments is clear. With this system, steady-state FDCD and lifetime-resolved FDCD measurements can be obtained on a single instrument with a large experimental SNR. Detection limits at the 10 nM level have been demonstrated,

and, more importantly, these early studies suggest that it may be possible to accurately distinguish between different chiral and/or achiral components in a complicated mixture. Additional study is required to assess the influence of instrumental and other artifacts on the quality of the measurement before more extensive application of this approach can proceed.

4.3. Thermal Lens - Detected CD

Thermal lens spectroscopy (TLS) has received much recent interest due to its unique capabilities, particularly in the probing of weakly absorbing systems. A thermal lens is created when the gaussian - distributed intensity profile of a TEM_{00} laser beam is passed through an absorbing sample. The absorbed laser creates an absorption profile in the sample which mirrors the laser profile, and, under conditions where nonradiative processes dominate over radiative ones, this absorption profile manifests itself as a similarly distributed heat profile that can change the density, and therefore the refractive index of the sample in the probed region. This refractive index gradient can then act as a lens, and for materials that expand upon heating, the thermal lens created by such a process will be diverging. Of particular interest is the fact that this thermal lens can either focus or defocus a probing laser, depending upon whether the lens is located before, or after the waist of the probing laser. This point will be explored in more detail in a subsequent section. The change in probe beam spatial characteristics can be monitored by a number of different techniques, the simplest of which is to allow the probe beam to impinge upon an aperture and then use a photodiode to monitor the light intensity passing through it. The processes which lead to the formation of a thermal lens are summarized pictorially in Fig. 8 below.
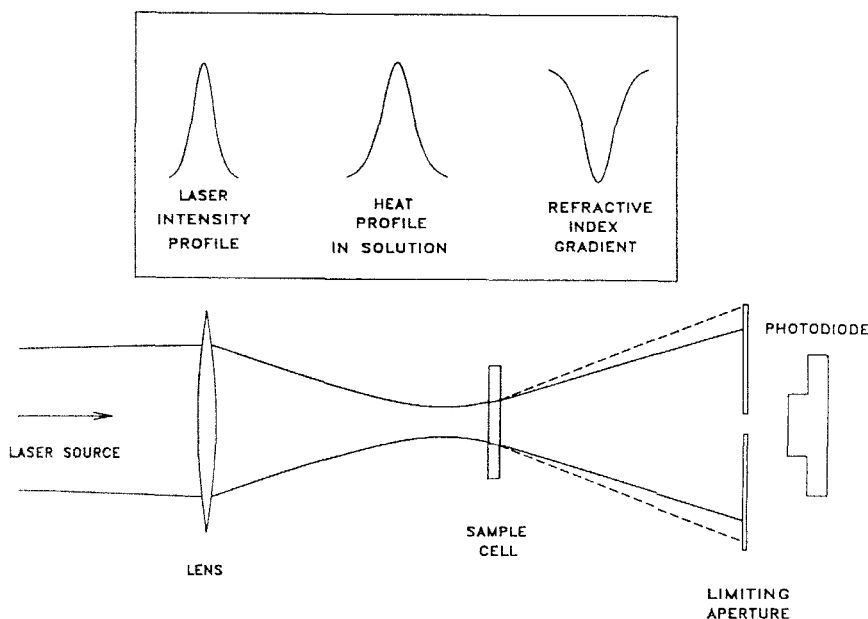

Figure 8. Processes leading to the formation of a thermal lens.

The magnitude of the refractive index gradient is directly proportional to the exciting laser power and the thermo-optical properties of the solvent system or environment surrounding the chromophore. Absorbance detectabilities at the 2×10^{-7} cm^{-1} level have been demonstrated with TLS, which is a substantial improvement over the capabilities of conventional transmission-based techniques. In addition to the detectability advantage, TLS has demonstrated the ability to maintain this level of performance even when a large background signal is present [35]. This high level of measurement dynamic reserve is a significant advantage in the measurement of CD. Both TLS and FDCD would be expected to provide an equivalent level of detectability, however, the TLS approach should be much more widely applicable as many more molecules absorb than fluoresce.

4.3.1. Temporally Modulated, TL - Detected CD

Tran and co-workers [36] have developed a TL-detected CD instrument which is schematically represented in Fig. 9. The overall approach resembles a conventional CD measurement, with the exception that the absorption is probed via the heat deposited in the sample (i.e. the thermal lens) rather than by taking the ratio of two similar intensities, one obtained before, and one after the sample, as is done in transmission-based measurements.
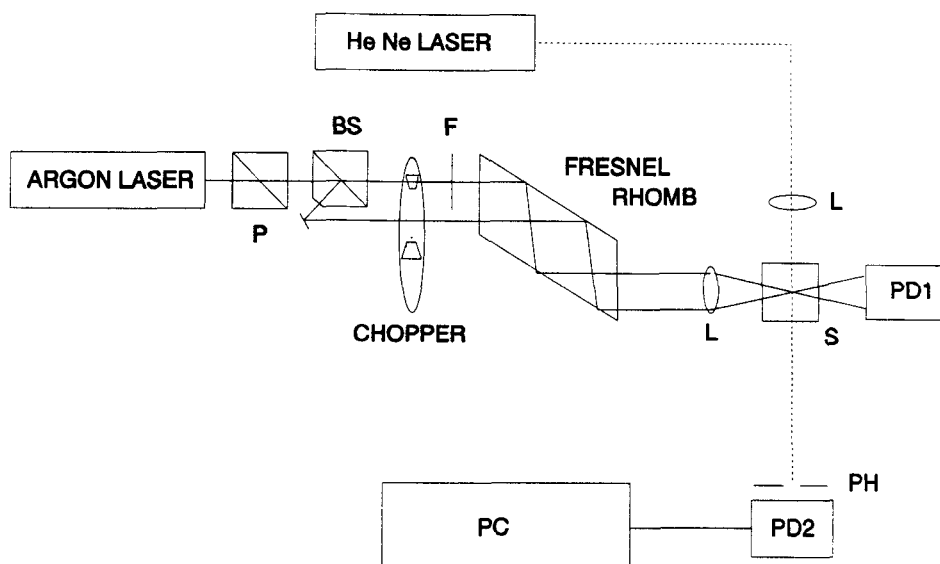

Figure 9. Instrumental arrangement for thermal lens - detected CD. P, Glan-Thompson prism polarizer; BS, polarizing beam splitter; F, filter (for intensity balance); L, lens; S, sample; PD, photodiode; PH, aperture; PC, computer. From ref. [36].

From Fig. 9, it is clear that the CD absorbed laser beam and the probe beam intersect at right angles to each other in the sample. This is an efficient way to probe extremely small volumes, however, it requires a sample cell with two distinct optical paths. The absorbed or pump beam originates from an argon ion laser, the output of which was linearly polarized by a Glan-Thompson prism. The TL pump beam was then split into two components of near equal intensity, but of orthogonal linear polarization, by a polarizing beam splitter. To account for small differences in these two beams, a separate photodiode monitored each pump field and the resulting TL signal was normalized to the intensity of the pump beam for that measurement. Both beams were then passed through a Fresnel rhomb to circularly polarize the linearly polarized components of the pump beam. The two circularly polarized components were then focused into an identical region of the sample which is interrogated by the probe laser. Absorption of the pump field to create a thermal lens altered the focal properties of this probe, and these spatial changes were monitored by an aperture/photodiode combination, as described earlier.

The sequence of events required for the measurement of CD by TLS proceeded as follows: first, the sample was illuminated with one circularly polarized component of the pump field, the pump beam was then blocked, and the sample allowed to relax (heat dissipation). The probe laser experienced both the formation of the thermal lens (pump beam to cell) and the decay of the lens (pump beam blocked) during the two measurement cycles. During the next measurement sequence, the sample was illuminated with the other circularly polarized component, the lens measured as before, and the sample allowed to relax before the measurement cycle was begun again. As evident from Fig. 9, the chopper was designed to incorporate these various steps. In one complete revolution of the chopper, each circularly polarized component was individually passed to the sample while the other was blocked. In between these two measurement cycles, the chopper blocked both beams simultaneously to allow sample relaxation to occur. Based on thermal relaxation rates in water for this system, a modulation frequency of 2.3 Hz was used.

Two disadvantages are evident in this early design. First, the crossed pump/probe arrangement limits the interaction path to the diameter of the pump laser. A collinear optical arrangement would provide a substantial improvement in the interaction length without increasing the sampled volume appreciably. Second, the manner in which the thermal lens was measured is inefficient for CD since a differential measurement is required, rather than the absolute magnitude of the absorbance for either right- or left-circularly polarized light. Thus elimination of the dark periods could allow more measurements per time period with the potential for improved SNR. For dynamic measurement applications of the TL-CD experiment, this decrease in the time required per measurement would be critical.

Recently, Tran [37] has modified the TL-CD system to incorporate changes designed to address the limitations cited above. The chopper/Fresnel rhomb combination has been replaced with a Pockels cell, and a collinear arrangement for the pump and probe beams has been utilized to increase the interaction region. The Pockels cell, as opposed to the chopper, can only produce left- and right-circularly polarized light without providing a dark period in the measurement cycle. With this approach, a thermal lens is always present in the detection cell and only the difference in the magnitude of the lens for the two oppositely polarized components is registered. This reduces the time commitment

required per measurement and has allowed these researchers to apply this TL-CD system as a detector for HPLC. Impressive detectabilities were demonstrated for the enantiomers of $Co(en)_3^{3+}$ separated by ion pair chromatography using a chiral mobile phase ion pairing additive. As discussed previously when considering other laser-based CD detection systems, general application of this approach is limited by the characteristics of the lasers now available commercially. The optimum lasers for use in TLS measurements are those that possess low levels of flicker noise and which provide excellent spatial (i.e. gaussian) beam properties. However, only a few lasers (e.g., argon ion, helium neon, krypton ion) possess these characteristics and, for the most part, these lasers operate at only a few wavelengths in the visible region of the spectrum. This limits application to compounds that absorb in the visible region. In addition, as now configured, the TL-CD experiment is still limited by the time dependence of the thermal lens to applications which require information no faster than on the order of 1 Hz (i.e. seconds). In TL-CD, the absorbance, much like in the conventional transmission approach, is still separately measured for both circularly polarized components and then these values are electronically differenced to obtain the CD quantity. New approaches will be required for TL-CD measurements if conditions of high SNR are to be obtained on the millisecond or below time domain.

4.3.2. Differentially-Arranged, TL-Detected CD

The positional dependence of the thermal lens signal suggests an intriguing way to obtain a differential measurement directly without the need to electronically subtract two large and similar numbers. If one assumes that the thermal lens formed in a given absorbing system is diverging in terms of its focal characteristics, then this lens placed **before** the focus of the probe laser will cause the light rays to converge less rapidly. This effect manifests itself as a decrease in the beam size measured at an aperture located in the far field (a distance much larger than the focal length of the thermal lens). The same thermal lens now located **after** the focus of the probing laser will cause the already diverging rays to diverge more rapidly. This effect will cause the probe beam size to increase at the aperture. Thus, the thermal lens can produce two effects which are equal in magnitude but opposite in sign depending upon where the thermal lens is located relative to the probe focus. To achieve a direct differential measurement, one could place a sample cell before, and one an equivalent distance after the probe focus, and then create a thermal lens in these two cells. Only the **difference** in the magnitude of the two lenses will cause the far field beam size to change. That is, if the absorption in the two cells is equal, the far field beam size will remain unaltered. Thus, for CD measurements, one could introduce left-circularly polarized light into one cell, and right-circularly polarized light into the other and only under the condition where a differential absorption exists (i.e. the sample is CD active) will the spatial properties of the probing beam change. In effect, the differencing procedure required to obtain the CD quantity will have been performed optically rather than electronically under such an arrangement. Specifically, this approach eliminates the need to switch alternately from left- to right-circularly polarized light as these two fields are coincident in time with each other using this experimental approach. In addition, this approach effectively nulls out the large background signal since, as described, only the difference in the absorbance in the two cells is measured.

The optical arrangement for the direct observation of CD via the use of differentially arranged, TLS is given in Fig. 10 [38]. In this experimental configuration, a neodymium-

yttrium aluminum garnet (Nd:YAG) laser is used as the pump source and its output is frequency doubled to produce 532 nm radiation. The pump field is linearly polarized by a polarizing prism. The pump beam then enters a half-wave rhomb which is used to rotate the plane of polarization. This device, in combination with a double-escape polarizing beam splitter is used to create two orthogonally polarized pump fields of equal intensity. The two pump fields are then circularly polarized by Fresnel rhombs, focused and passed into a matched pair of sample cells. The dichroic mirrors are designed to reflect the CD pump beam into the sample cells and transmit the probe beam. By consideration of the polarization properties of the beams in the two arms of the optical system, it can be seen that one cell will be pumped with left-circularly polarized light, and the other cell with the right-circularly polarized component. A helium-neon probe laser operating at 632.8 nm (nonabsorbed) is then focused between the two cells and it serves to monitor the lens strength in the two cells created by the pump fields.
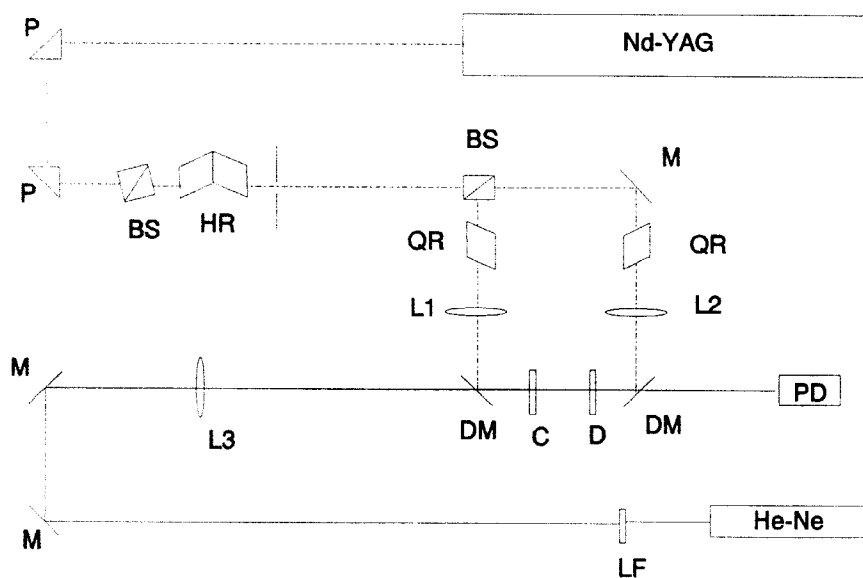

Figure 10. Optical configuration for differentially arranged, thermal lens detected CD. P, beam steering prism; M, beam steering mirror; BS, polarizing beam splitter; HR, half-wave rhomb; QR, quarter-wave rhomb; L, focusing lens; DM, dichroic mirror; C, converging sample cell (before probe focus); D, diverging sample cell (after probe focus); PD, aperture/photodiode combination; LF, line filter (to isolate the probe laser from extraneous pump radiation). Solid line, probe laser optical path; broken line, pump beam path.

Fig. 11 shows CD data acquired for $(+)$-$Co(en)_3^{3+}$ obtained using the differentially arranged TL-CD system. The entry shows the intensity level measured for the probe laser when both pump beams were blocked, the signal obtained when each cell was

independently pumped, and the differential signal measured when both cells were simultaneously pumped by the Nd:YAG laser. From the data obtained with the differential configuration, it is clear that the net lens in the two cells was distinguishable from the probe intensity observed with the pump field blocked. The same experimental protocol was followed for both for the (-) enantiomer, and for a racemic mixture. The net lens observed for (-)-$Co(en)_3^{3+}$ was opposite in sign to that measured for (+)-$Co(en)_3^{3+}$, and clearly distinguishable from the inherent probe level. The differential TL-CD signal observed for the racemic mixture was not distinguishable from the inherent probe level.
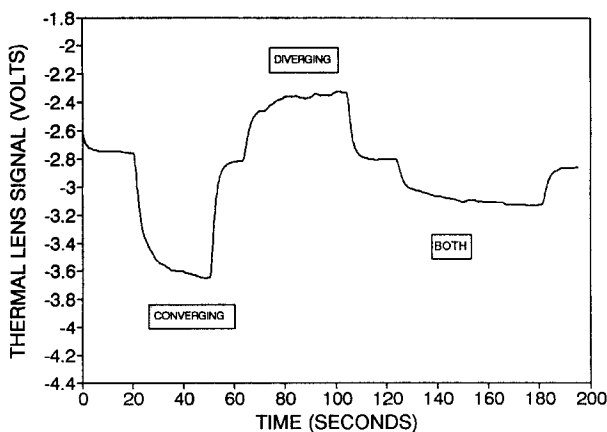
Figure 11. CD signal for (+)-$Co(en)_3^{3+}$ measured at 532 nm using the differentially arranged, TL configuration. Concentration of (+)-$Co(en)_3^{3+}$ is 0.79 mg/mL. Converging, TL signal in cell located before the probe focus; diverging, TL signal in cell located after the probe focus; both, signal with both cells simultaneously exposed to the circularly polarized pump field. The baseline signal measured before the converging signal was obtained with both pump beams blocked and reflects the baseline intensity level of the probe.

The magnitude of the TL-CD signal obtained for various concentrations of the (+), (-) and (+/-) samples of $Co(en)_3^{3+}$ is plotted in Fig. 12. Excellent correlation is observed for the CD signal strength, sample concentration and direction of the differential absorption for the two enantiomers. The racemic mixture, in comparison, produced a signal which was, within experimental error, undistinguishable from the baseline. It should be noted that the inherent absorbance for this racemic mixture is large relative to the differential signals being measured, and this clearly demonstrates the ability of the differential configuration to null out the influence of this background on the observed beam spatial properties. The CD signal obtained with this system also shows a linear dependence on the pump field power, as predicted by previous TLS studies. The detectability of this approach is very good, with results obtained which are at least as good as those obtained using a conventional transmission-based approach. However, it is the possibility that one can obtain the CD quantity by a direct optical differencing procedure that appears most

interesting. The time domain of the pump field used in the studies described above was approximately 7 ns. It is possible, given the above results, that CD information can be obtained in this same time frame, that is, in the domain of a single laser pulse. This approach may therefore have important applications in the study of conformational changes associated with biological reactions. However, more study is needed in order to optimize the differentially arranged TL-CD experimental configuration before challenging studies of this nature can be attempted.
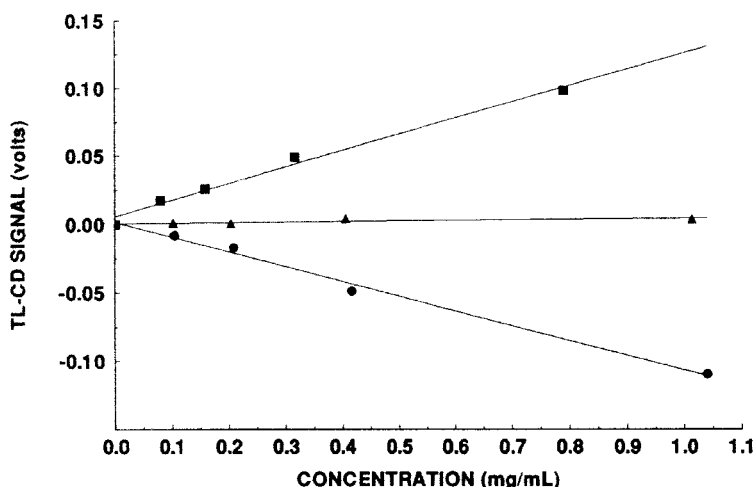
Figure 12. TL-CD signal for ((-), circles), ((+), squares) and ((+/-), triangles) $Co(en)_3^{3+}$ measured at 532 nm using the differentially arranged, TL configuration.

4.4. Time-Resolved CD

The potential to study conformational changes associated with a variety of biological phenomena on a time-resolved basis has served as an important driving force for the development of new instrumental approaches for the measurement of CD. Two recently developed experimental techniques have demonstrated that the capability to obtain CD information on the nanosecond to picosecond time scale is possible.

Kliger and co-workers have developed an elegant approach to the measurement of time-resolved CD [39] which utilizes an ellipticity measurement to improve the experimental SNR and allow extension to short time regimes. Kliger's instrumental arrangement for CD measurements of transient photolysis intermediates is given in Fig. 13. The time-resolved CD system utilizes a Xe flashlamp which produces an $8\mu s$ pulse as the CD probe source. The spectral distribution of the lamp output was limited by an interference filter to minimize the possibility of sample degradation. The source light was then polarized by a Glan-Taylor prism and passed through a variable phase retarder to induce elliptical polarization. After passage through the sample, a second Glan-Taylor prism was used to monitor changes in the ellipticity of the light leaving the sample. A monochromator and PMT is used to wavelength analyze and detect the light which passes

the second analyzing prism. The output from the PMT is sampled by a transient digitizing recorder. A Nd:YAG laser pulse (7 ns FWHM) frequency doubled to 532 nm was used for photoinitiation of the reaction under study.

The key to this approach is the variable retarder used to induce elliptical polarization in the plane polarized source light. The retarder is constructed from a quartz plate which is subjected to a uniaxial strain. The retardation can be varied by rotating the compression axis of the plate ∓ 45° with respect to the plane of polarization of the monitoring beam. The elliptically polarized monitoring beam can be thought of as the superposition of two phase-related beams of left- and right-circularly polarized light with different amplitudes. This difference in amplitudes for the two components will be changed after interaction with a circularly dichroic sample and the change can be monitored by analyzing the ellipticity of the emerging beam using a linear polarizer. As has been pointed out [39], the advantage of this approach is in the fact that for a sample with a $\Delta a/a$ of 1 part in 10^4, the change in the minor axis of the ellipse representing the polarization state of the CD probe light may be as large as 1 part in 10. Thus, an improvement of 10^3 is possible over the precision required in a transmission-based measurement. However, since the measurement SNR is proportional to the square root of the measurement interval, this improvement in the SNR suggests that the measurement time resolution can be extended by 6 orders-of-magnitude using this approach.
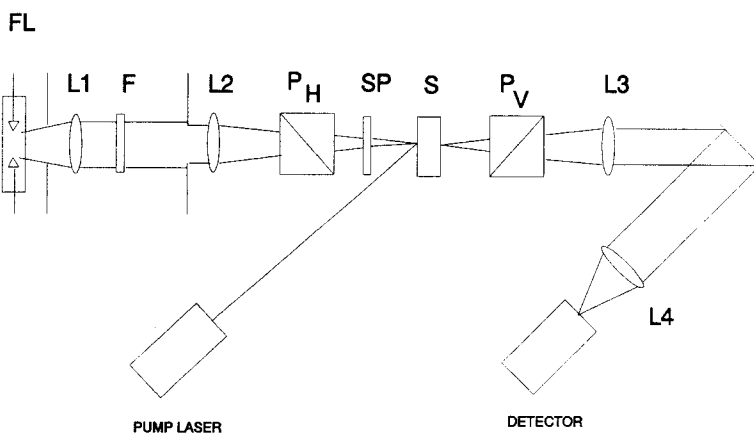

Figure 13. Experimental arrangement for time-resolved CD measurements of photolysis transients based on an ellipticity measurement. FL, flashlamp; L_1, L_2, L_3, L_4, collimating/focusing lenses; F, interference filter; P_H, P_V, Glan-Thompson polarizing prisms oriented orthogonally to each other; SP, strain plate; S, sample cell. From ref. [39].

This approach is potentially limited by photoselective, transient linear birefringence induced in the sample by the actinic field. Kliger [40] has shown that this potential interference can be minimized by circularly polarizing the actinic field. Additionally, it has recently been shown that the monochromator/PMT combination can be replaced by a

polychromator/multichannel detector (CCD) [41]. Multiwavelength CD measurements of transient species can now be obtained using this system.

As has been described, CD is one of the few spectroscopic techniques sensitive to the structural parameters that define and guide the three-dimensional shape of a biologically active entity. This important structural information, obtained on a time-resolved basis in the same time domain as the biological event under study, is an extremely important advance that will have wide application in biophysical studies of proteins, polypeptides and other biologically significant species.

The experimental design of Kliger relies upon an incoherent light source to probe the CD. Within the time domain of the photoinitiated reaction under study, this system requires a sufficient number of photons from the incoherent source to probe the CD at an adequate SNR. As one attempts to narrow the temporal observation window using this approach, the photon flux available during the measurement interval, which is distributed over the $8\mu s$ Xe arc pulse, becomes smaller such that shot noise, and other experimental limitations, become significant. Yet, a large number of important biological phenomena exhibit conformational changes which occur on a time scale shorter than that presently available with the approach of Kliger. Recognizing this, Simon and co-workers have developed a time-resolved CD instrument which can provide time resolution on the picosecond time scale [42].

The experimental configuration for acquiring CD information in the picosecond time domain is given in Fig. 14 below.
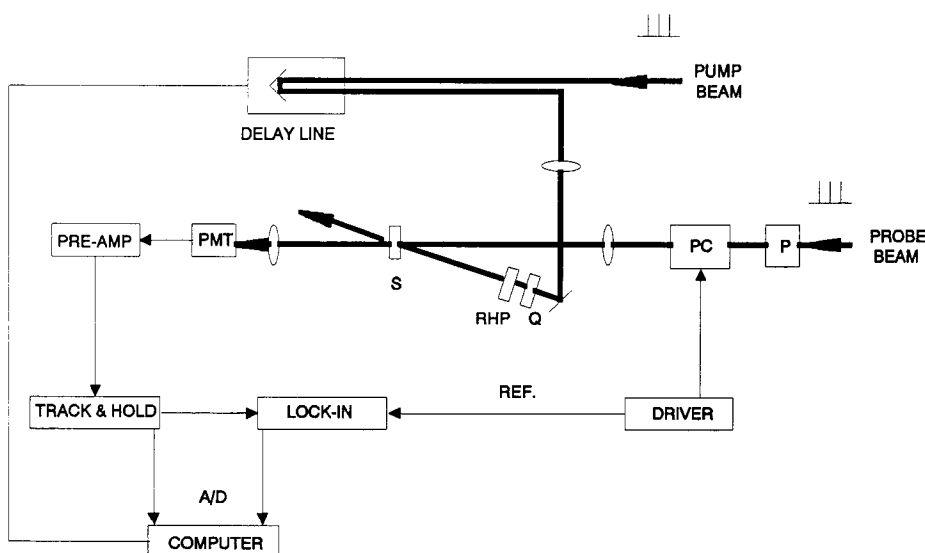

Figure 14. Experimental apparatus for picosecond, time-resolved CD measurements using a mode-locked, Q-switched, cavity dumped pump laser. P, polarizer; PC, Pockels cell; Q, quarter-wave plate; RHP, rotating half-wave plate; S, sample cell; PMT, photomultiplier tube. From ref. [42].

The system is based upon a mode-locked, Q-switched, cavity dumped Nd:YAG laser which can produce light at several specified wavelengths, or this source can be used to synchronously pump a dye laser for operation over an extended wavelength range [43]. The Nd:YAG can provide output at 1.064 μm, and by various nonlinear processes, harmonics of this wavelength can be created. The Nd:YAG laser produces 80 ps pulses at a repetition rate of approximately 1 kHz. This output serves as both the CD probe beam, and the pump light source for photoinitiation of the reaction under study. The computer controlled delay line serves to provide a variable time delay between the pump pulse and the probing CD beam. This is achieved by varying the distance the pump beam is constrained to travel.

Probe pulses are linearly polarized by a polarizing prism, and then converted alternately into left- and right-circularly polarized light by a Pockels cell. The circularly polarized pulses interact with the sample and are then detected by a PMT. The output from the PMT is amplified, and sent to a track and hold amplifier. The signal from the PMT, due to the short duration of the laser pulses it is observing, has an extremely small duty cycle. This output from the PMT is an alternating signal with a half cycle that consists of a signal pulse which is approximately 5 ns (dictated by the minimum time response of the PMT) in duration and modulated at a frequency of 1 kHz. The track and hold amplifier effectively increases the duty cycle of the measurement system by sampling the short duration signal pulse, and then providing a relatively constant equivalent of that signal to the lock in for the remainder of the half-cycle. The lock in amplifier then will respond to differences in the two half-cycles of the measurement which will reflect the differential absorbance (CD) of the sample. 3-10 second time constants can then be used to average out limiting sources of experimental noise. With this approach, an instrumental response function of 80 ps was demonstrated which is equivalent to the time domain of the laser pulses. By fixing the probe wavelength and varying the time delay between the pump and probe event, the time dependence of the conformational changes associated with the photoinitiated reaction can be obtained from the CD signal. Alternately, by fixing the time delay and scanning the probing wavelength, the CD spectra of transient species can be acquired.

As in the ellipticity approach developed by Kliger for time-resolved CD, linear birefringence or linear dichroism can complicate the CD measurement. Simon and coworkers have devised a very effective technique for eliminating these polarization effects. Under ideal conditions, a pure circularly polarized pump field will not cause pump induced linear dichroism or linear birefringence. However, in practice it is extremely difficult to create sufficiently pure circularly polarized light to totally eliminate these effects. Even small deviations from pure circularly polarized light can induce linear polarization effects which will dominate the CD signal. Although it was determined that linear birefringence was negligible under these experimental conditions (i.e. degree of circular purity of the pump field), linear dichroism was found to be a significant interference in the CD measurement. To circumvent this limitation, a second quarter-wave plate was rotated at a frequency of 3.5 Hz in the pump beam path. The rotating wave plate induces a rotation in the polarization ellipse of the pump field which modulates the linear dichroism at twice this frequency , or 7 Hz. Thus, the linear dichroism will be modulated at a frequency which is significantly different than that of the

polarization modulation, and the linear dichroism signal will be effectively suppressed by the lock-in amplifier.

Recent advances, for example, replacement of the Pockels cell with a PEM system, has provided an improvement in the experimental SNR of an order-of-magnitude [44]. Further, the authors suggest that with their experimental approach, the picosecond laser system now in use could be replaced by one operating with femtosecond pulses. If successful, this would allow extension of CD measurements into a time domain where the initial structural changes which determine the outcome of a sequence of complicated events can be probed.

5. CONCLUSIONS

Instrumental approaches for the measurement of CD have evolved in an incremental manner over the past century such that commercially available systems today can provide excellent measurement sensitivity under demanding experimental conditions. The difficulty of the measurement derives from the background limited nature of CD which requires that a small difference between two large numbers be determined. Modern approaches rely upon polarization modulation of the exciting field, in combination with phase-sensitive detection to provide improvements in the experimental SNR of several orders-of-magnitude over nonmodulated measurement approaches. One development which has had a significant impact on conventional CD measurements has been the application of the PEM. The PEM has replaced the Pockels cell under most CD measurement situations due to its large spatial aperture, good stability, and excellent capability to create circularly polarized light. This and the other instrumental advances described in this chapter have allowed the measurement of CD to become a routine tool for conformational studies of the complex structure of biologically active species.

Replacement of the conventional incoherent light source with a laser has allowed CD measurements to be made on extremely small samples, such as those encountered in capillary electrophoresis. In addition, the unique spatial properties of the laser are utilized to advantage in thermal lens spectroscopy. TL detection of CD, either via a single beam, or a differentially configured arrangement, has demonstrated significant improvements in the measurement SNR. Application to HPLC detection, or time-resolved studies, are currently under investigation.

The improvement in the instrumental SNR afforded by the use of polarization modulation has permitted CD detection to be applied to stopped-flow studies of biological reactions. The important information which can be obtained from such an approach has served as an impetus for the development of new instrumental approaches for the measurement of CD. These new approaches have allowed CD measurements to be extended to the time domain below that available with stopped-flow techniques. Presently, nanosecond, and even picosecond CD techniques have been developed, and it seems clear that extension to the sub-picosecond regime will follow.

The application of multichannel light detection devices to the measurement of CD will significantly improve the technique and allow extension into areas not presently accessible by conventional, sequentially scanned CD. For example, multichannel devices will enable SNR improvements via spectral averaging. Alternately, a complete CD spectrum can be obtained on a transient species in the time domain required for a single wavelength

measurement. The obstacle limiting widespread application of this approach remains the incompatibility of the PEM and the CCD. However, several approaches now in development have shown promise in being able to eliminate this incompatibility. Although there are significant problems to solve, the potential advantages of such an approach are significant and will serve as an impetus for further development. Preliminary studies have shown that multichannel-detection may have as significant an impact on CD measurements as was provided by the introduction of polarization modulation by Legrand and Grosjean over 30 years ago.

6. ACKNOWLEDGEMENTS

7. REFERENCES

1. A. M. Cotton, Ann. Chim. Phys. 8 (1896) 347.
2. J. J. Duffield and A. Abu-Shumays, Anal. Chem. 7 (1966) 29A.
3. G. Bruhat, Ann. Phys. (Paris) 3 (1915) 232.
4. G. Bruhat, Bull. Soc. Chim. France 47 (1930) 251.
5. W. Kuhn and E. Braun, Z. Physik Chem., B.8 (1930) 445.
6. M. Grosjean and M. Legrand, Compt. Rend. Acad. Sci. (Paris) 251 (1960) 2150.
7. M. Grosjean and M. Tari, Compt. Rend. Acad. Sci. (Paris) 258 (1964) 2034.
8. D. S. Kliger, J. W. Lewis and C. E. Randall, Polarized Light in Optics and Spectroscopy, Academic Press, Inc.:New York, NY (1990) chapter 3.
9. W. A. Shurcliff, Polarized Light, Harvard Univerity Press: Cambridge, Massachusetts (1962).
10. P. Drude, Theory of Optics, Dover Publishing: New York, NY (1959) 350.
11. K. W. Hipps and G. A. Crosby, J. Phys. Chem. 83 (1979) 555.
12. T. Oakberg, PEM-90 Application Note, Hinds Instruments, Inc., Hillsboro, OR.
13. K. Andert, W. Schalike, B. Nolting, R. Pittelkow, R. Wetzel and G. Snatzke, Rev. Sci. Instrum. 62 (1991) 1912.
14. H. Povel, H. Aebersold and J. O. Stenflo, Appl. Opt. 29 (1990) 1186.
15. J. O. Stenflo and H. Povel, Appl. Opt. 24 (1985) 3893.
16. L. A. Nafie and D. W. Vidrine, in Fourier Transform Infrared Spectroscopy, J. R. Ferraro and L. J. Basile, eds., vol. 3, Academic Press: New York, NY (1982) 83 - 123.
17. L. A. Nafie and T. B. Freeman, Spectroscopy 2 (1987) 24.
18. M. Anson and P. M. Bayley, J. Phys. E: Sci. Instrum. 7 (1974) 481.
19. P. M. Bayley and M. Anson, Biopolymers 13 (1974) 401.
20. J. Luchins and S. Beychok, Science 199 (1978) 425.
21. J. S. Gaffney, E. T. Premuzic, T. Orlando, S. Ellis, P. Snyder, J. Chromatogr. 262 (1983) 321.

22. M. A. Wickramaaratchi, E. T. Premuzic and M. Lin, J. Chromatogr. 390 (1987) 413.
23. A. F. Drake, J. M. Gould and S. F. Mason, J. Chromatogr. 202 (1980) 239.
24. S. A. Westwood, D. E. Games and L. Sheen, J. Chromatogr. 204 (1981) 103.
25. Y. Kurosu, T. Sasaki, T. Takakuwa, N. Sakayanagi, K. Hibi and M. Senda, J. Chromatogr. 515 (1990) 407.
26. R. E. Synovec and E. S. Yeung, Anal. Chem. 57 (1985) 2606.
27. D. H. Turner, I. Tinoco and M. F. Maestre, J. Am. Chem. Soc. 96 (1974) 4340.
28. M. Thomas, G. Patonay and I. Warner, Rev. Sci. Instrum. 57 (1986) 1308.
29. R. E. Synovec and E. S. Yeung, J. Chromatogr. 368 (1986) 85.
30. P. L. Christensen and E. S. Yeung, Anal. Chem. 61 (1989) 1344.
31. K. Wu and L. B. McGown, Appl. Spectrosc. 45 (1991) 1.
32. L. Geng and L. B. McGown, Anal. Chem. 64 (1991) 68.
33. K. Wu and L. B. McGown, Anal. Chem. 66 (1993) in press.
34. J. R. Lakowicz, Principles of Fluoresence Spectroscopy, Plenum Press: New York, NY (1983).
35. S. R. Erskine and D. R. Bobbitt, Appl. Spectrosc. 43 (1989) 668.
36. C. D. Tran and M. Xu, Rev. Sci. Instrum. 60 (1989) 3207.
37. M. Xu and C. D. Tran, Anal. Chem. 62 (1990) 2467.
38. P. D. Rice, J. D. Thorne and D. R. Bobbitt, SPIE: Optical Methods for Ultrasensitive Detection and Analysis-Techniques and Applications 1435 (1991) 104.
39. J. W. Lewis, R. F. Tilton, C. M. Einterz, S. J. Milder, I. D. Kuntz and D. S. Kliger, J. Phys. Chem. 89 (1985) 289.
40. C. M. Einterz, J. W. Lewis, S. J. Milder and D. S. Kliger, J. Phys. Chem. 89 (1985) 3845.
41. D. S. Kliger and J. W. Lewis, Rev. Chem. Intermed. 8 (1987) 367.
42. X. Xie and J. D. Simon, Rev. Sci. Instrum. 60 (1989) 2614.
43. X. Xie and J. D. Simon, Opt. Comm. 69 (1989) 303.
44. X. Xie and J. D. Simon, J. Opt. Soc. Am. B. 7 (1990) 1673.

Chapter 3

Instrumental methods of infrared and Raman vibrational optical activity

Laurence A. Nafie, Mario Citra, N. Ragunathan, Gu-Sheng Yu and Diping Che

Department of Chemistry, Syracuse University, Syracuse, New York, USA, 13244-4100

Abstract

We present the basic concepts and methods for the measurement of infrared and Raman vibrational optical activity (VOA). These two forms of VOA are referred to as infrared vibrational circular dichroism (VCD) and Raman optical activity (ROA), respectively The principal aim of the article is to provide detailed descriptions of the instrumentation and measurement methods associated with VCD and ROA in general, and Fourier transform VCD and multichannel CCD ROA, in particular. Although VCD and ROA are closely related spectroscopic techniques, the instrumentation and measurement techniques differ markedly. These two forms of VOA will be compared and the reasons behinds their differences, now and in the future, will be explored.

Outline

1. Introduction
    1.1 Vibrational optical activity
    1.2 Infrared vibrational circular dichroism
    1.3 Vibrational Raman optical activity
    1.4 Comparison of VCD and ROA instrumentation
2. Fourier Transform Infrared Circular Dichroism
    2.1 Optical and electronic layout
    2.2 Alignment optimization
    2.3 Polarization Modulation Interferometry
3. Multichannel Raman Optical Activity
    3.1 Polarization Modulation Techniques
    3.2 Optical and electronic layout
    3.3 Data acquisition process
    3.4 Comparison of right-angle and backscattering ROA
    3.5 Artifact reduction
4. Conclusions

1. INTRODUCTION

Vibrational optical activity (VOA) is a relatively new area of natural optical activity. It consists of the measurement of optical activity in the spectral regions associated with vibrational transitions in chiral molecules. There are two basic manifestations of VOA. The first is simply the extension of electronic circular dichroism (CD) into the infrared region where fundamental one-photon vibrational transitions are located. This form of VOA is referred to as vibrational circular dichroism (VCD). It was first measured as a property of individual molecules in 1974 [1], and was independently confirmed in 1975 [2]. Within the past twelve years, VCD has been reviewed on a number of occasions from a variety of perspectives [3-15], and two more reviews are currently in press [16,17]. The second form of VOA has no direct analog in classical forms of optical activity. Optical activity in Raman scattering, known simply as Raman optical activity (ROA), was measured successfully for the first time in 1973 [18], and confirmed independently in 1975 [19]. ROA has been described in detail and reviewed several times in the past decade from several points of view [20-24], and two additional reviews [25,26], one with a view toward biological applications [25] and the other from a theoretical perspective [26], are currently in press. In addition, two articles of a pedagogical nature are in press that have been written for a general audience, one on infrared CD [27] and the other on ROA [28].

VOA differs from the classical forms of optical activity, and in particular from electronic CD, in that individual vibrational transitions, instead of electronic or vibronic transitions, are probed. If one is interested in ground electronic state properties of molecules, such as the equilibrium molecular geometry or significantly populated conformations, VOA has a number of significant advantages over classical optical activity. First, the complications of excited electronic states are not present, at least not directly. Second, there are many more vibrational transitions, involving virtually all portions of the molecule, than there are in the accessible electronic region of the spectrum. For example, hydrogen stretching modes provide a route to stereochemical detail in molecules that is unavailable in electronic CD. Third, by combining VCD and ROA in the same region of the spectrum, the same stereochemical sensitivity can be interrogated by two independent, complementary spectroscopies. The principal drawbacks of VOA, at least at this point in time, are the degree of spectral sensitivity and the availability of commercial instrumentation. In many cases, relatively high concentrations of samples in solvents are needed to obtain spectra with adequate signal-to noise ratios. In spite of these difficulties, much progress is being made in VCD and ROA, both experimentally and theoretically, and it is now clear that VOA will eventually find its rightful place among the readily

available techniques for studying important aspects of molecular structure and stereochemistry.

The purpose of this review is to present the fundamental concepts underlying the instrumental methods used in VOA. In this section, we first present the definitions and basic intensity expressions associated with the various forms of VOA. We then describe the most fundamental aspects of the measurement of VCD and ROA, and discuss the reasons behind the distinctly different ways in which these two forms of VOA are measured.

In the two subsequent sections, we provide a more detailed look at two particular classes of VOA instrumentation: 1) instruments that measure VCD using a Fourier transform infrared spectrometer, and 2) instruments that measure ROA using a multichannel CCD detector. Our aim is to provide enough detail to enable the reader to obtain a firm grasp of the measurement method and some of the complexities associated with obtaining high-quality spectra. Where space does not permit, the reader will be guided to previous review articles and original publications for further detail and additional information.

1.1 Vibrational optical activity

As described above, there are two forms of vibrational optical activity, one derived from infrared absorption and the other from Raman scattering. Both forms involve the differential response of a molecule to the modulation of polarization of the interacting radiation between right and left circularly polarized states. In the case of infrared absorption, VCD is defined as the differential absorbance for left minus that for right circularly polarized infrared radiation. This is expressed by the relation:

$$\Delta A = A_L - A_R \tag{1}$$

where A_L and A_R are the decadic absorbances of the sample for left and right circularly polarized radiation, respectively, and where:

$$A = -\log_{10}(I / I_0) = (A_L + A_R) / 2. \tag{2}$$

Here, I and I_0 represent the transmission of the infrared instrument with and without the sample in place, respectively. It is convenient to define the dimensionless ratio of the VCD absorbance to the ordinary absorbance as:

$$g = \Delta A / A \tag{3}$$

where g, referred to as the anisotropy ratio, is a measure of the VCD intensity for unit absorbance and represents the intrinsic strength of a VCD band.

In the case of ROA, the situation is more complex. Because circular polarization modulation can be imposed on either the incident laser radiation, the scattered radiation, or both either in-phase or out-of-phase, there are four distinct forms of circular polarization (CP) ROA. The form in which circular

polarization modulation is present in the incident beam, with the polarization state of the scattered light held fixed in a state α, is called incident circular polarization (ICP) ROA. The normalized circular intensity differential is defined as the ratio of the ROA intensity, $(I_\alpha^R - I_\alpha^L)$, to the parent Raman intensity, $(I_\alpha^R + I_\alpha^L)$, and is expressed as [20,29]:

$$\Delta_\alpha = (I_\alpha^R - I_\alpha^L) / (I_\alpha^R + I_\alpha^L), \tag{4}$$

where superscripts refer to the polarization state of the incident radiation, and subscripts to the polarization state of the scattered radiation. We note that in ROA, the sign convention for intensity is for right minus left circular polarization states, which is the opposite of the that for VCD, or CD in general [30,31]. We also note that the dimensionless quantities g and Δ differ by a factor of two in the ratio of the magnitude of the optical activity to that of the parent intensity, with ROA defined in the smaller way.

The form of ROA with circular polarization discrimination in the scattered beam and the polarization of the incident beam held fixed in a state α was first measured and referred to as scattered circular polarization (SCP) ROA [32], although it was originally identified and called the degree of circular polarization [33]. The corresponding normalized CID for SCP ROA is given by:

$$\Delta^\alpha = (I_R^\alpha - I_L^\alpha) / (I_R^\alpha + I_L^\alpha), \tag{5}$$

where we have used the same convention for superscripts and subscripts as in eq. (4).

If circular polarization modulation is carried out simultaneously, and in-phase, in both the incident and the scattered beam, one obtains the first form of dual circular polarization (DCP$_I$) ROA [34], with a normalized CID given by:

$$\Delta_I = (I_R^R - I_L^L) / (I_R^R + I_L^L), \tag{6}$$

and the corresponding out-of-phase form of dual circular polarization (DCP$_{II}$) ROA is given by:

$$\Delta_{II} = (I_L^R - I_R^L) / (I_L^R + I_R^L). \tag{7}$$

Recently, DCP$_I$ ROA was observed for the first time [35], although successful measurements of DCP$_{II}$ ROA have yet to be reported.

In Figure 1, we present energy-level polarization state diagrams corresponding to the one form of VCD and the four forms of CP ROA. In the case of VCD, only a single photon is involved in the vibrational transition from state g0 to state g1 in the ground electronic state. For ROA, two photons are involved for a transition between the same two vibrational sublevels of the
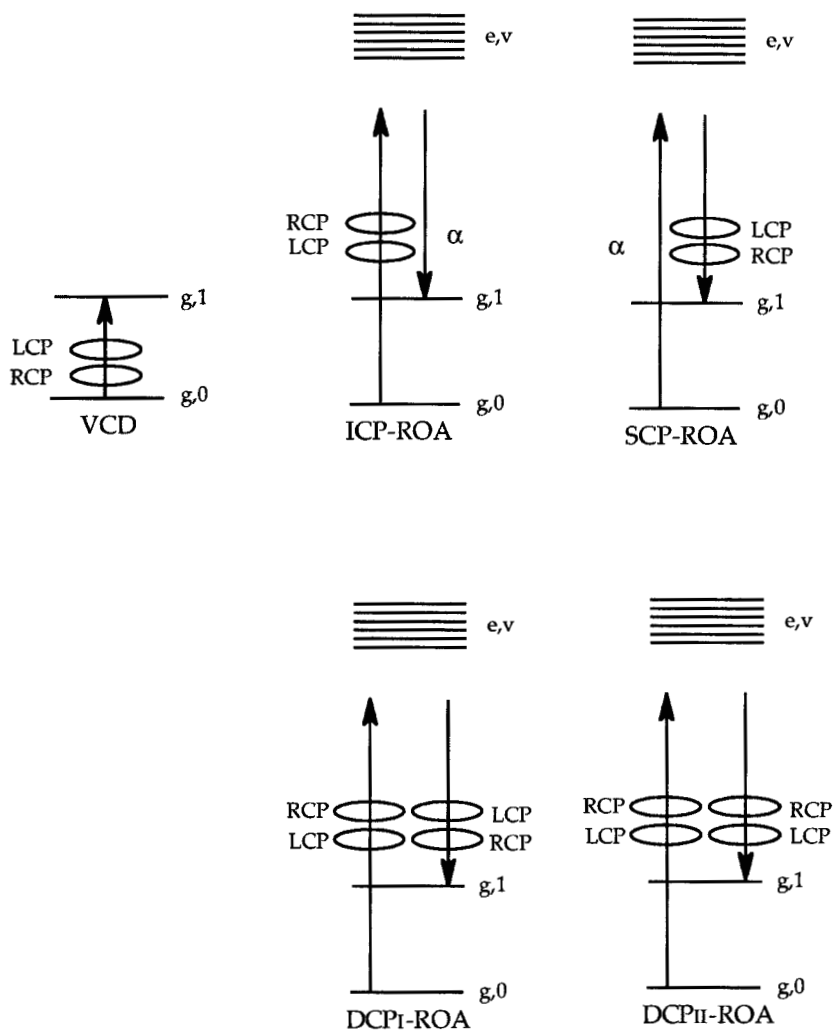
Figure 1. Energy-level polarization diagram for circular forms of vibrational optical activity.

ground electronic state. The Raman photons are potentially in resonance with excited vibronic levels labeled ev, depending on the incident laser frequency and the excited state structure of the molecule.

Other forms of VOA can be considered. Early attempts to measure VOA involved measurements of optical rotatory dispersion (ORD) in the near-infrared region, but no spectra in regions of vibrational transitions were successfully obtained [36]. One could also consider measuring the emission form of VCD; however, fluorescence is intrinsically very weak in the infrared region and no attempts to measure vibrationally-excited, circularly-polarized emission in the infrared have been carried out. A new form of ROA has been identified theoretically in which differences between orthogonal linear polarization states are measured [37]. This form of ROA is referred to as linear polarization (LP) ROA, and as with CP ROA, there are four distinct forms called ILP, SLP, DLP_L, and DLP_{II} ROA. The existence of this kind of linear-polarization difference scattering was noted earlier [38], but it was not identified as a form of natural optical activity and the various ways which it could be measured were not identified [39]. LP ROA has not yet been measured, and it is predicted to arise only in conjunction with resonance Raman scattering.

1.2 Infrared vibrational circular dichroism

The first measurements of VCD were made possible by a number of significant technical advances which today are still needed in the design and construction of a VCD instrument. The most important of these advances involved the development of liquid-nitrogen-cooled semiconductor detectors, stable high-sensitivity lock-in amplifiers, and photoelastic modulators operating in the infrared region [40,41]. The combination of these advances permitted measurement of high-frequency circular polarization modulation intensity in the infrared region.

Photoelastic modulators operate in the tens of kilohertz frequency range by a compression-elongation cycle of an infrared transmissive crystal driven by two piezoelectric quartz crystals. The entire modulator assembly oscillates at its natural longitudinal harmonic frequency. A key development for the observation of VCD was the extension of the operating range of the photoelastic modulator into the infrared, which required new kinds of transmission crystals and increased retardation capabilities to achieve a full measure of modulation between the left and right circular polarization states [40,41]. As the wavelength of the radiation increases, it becomes linearly more difficult to reach the same degree of polarization modulation.

The first manifestation of VCD in the optical train of a spectrometer is the modulation of the *intensity* of the infrared beam in synchronization with the modulation of the polarization as the beam passes through the circular dichroic sample. The phase of the synchronization is opposite for negative and positive VCD bands. More specifically, in reference to the definition of VCD in Eq. (1), there will be a synchronization between larger transmission (smaller absorbance) and right CP radiation for positive VCD bands, and between larger transmission and left CP radiation for negative VCD bands.

In order for a detector to follow the intensity modulation of the sample in the frequency range of 50 kHz, it must have a response time on the order of a few microseconds or less. Standard infrared detectors are thermal detectors which

operate on the basis of some property change in the detector as its temperature changes. The response of such detectors is in the millisecond range at best, and hence they are not suitable for VCD measurements with photoelastic modulators. The advent of semiconductor detectors cooled with liquid nitrogen in the late 1960s paved the way for successful VCD measurements. In such detectors, a small current is created as an infrared photon promotes a valence electron in the semiconductor into the conduction band. This current can be converted to a small voltage and then amplified for subsequent electronic processing. Because the response of these detectors is triggered by individual photons, they typically have response times shorter than one millisecond.

In order to convert the high-frequency voltage oscillation at the detector preamplifier to a VCD spectrum, a stable, high-sensitivity lock-in amplifier is needed. With the development of solid state electronics, again in the 1960s, such amplifiers became available. A lock-in amplifier works on nearly the same basis as an AM radio. It converts intensity (amplitude) modulation riding on a photoelastic modulator (station) frequency to produce a VCD intensity (voice-music) through a demodulation process. All noise present on the detector signal that is not in the narrow bandwidth of the modulation frequency is rejected by the lock-in amplifier. This allows the very small detector signal to be amplified to an observable level without being overwhelmed by noise. A lock-in amplifier is also able to keep track of the electronic phase and sense of the synchronization of the detector modulation signal with respect to a polarization modulation signal. This is achieved by a reference signal obtained directly for the electronics that drives the photoelastic modulator. In the process, the information about the signs of positive and negative VCD bands is preserved.

In Figure 2 we present a simple block diagram representing the basic components of a VCD spectrometer. The source is a high-intensity infrared source, such as a silicon carbide glower, a Nernst glower, a carbon rod or a xenon lamp. Unfortunately, the use of tunable lasers has led to stability problems that have not yet been resolved. With a conventional non-laser source, some form of wavelength discrimination is required to measure a spectrum. VCD instruments have been constructed using either a dispersive grating spectrometer or a Fourier transform infrared spectrometer for this purpose. In the former case, the wavelengths are scanned, and in the latter, the wavelengths are intensity modulated at different Fourier frequencies and measured simultaneously. The radiation emerging from the spectrometer is first polarized, typically with a wire-grid polarizer, and then modulated in polarization by the photoelastic modulator. After the radiation passes through the sample, it is imaged on to the detector where it is converted to an electronic signal. This signal must be processed through at least one lock-in (shown) but additional lock-ins are typically employed, and in the case of a Fourier transform instrument, a Fourier transform algorithm in a computer is needed. Following the final steps of electronic processing, the spectra are sent to a plotter for hard copy display. Figure 2 should be regarded as schematic of the essential components, but in an actual instrument, there is considerable more complexity, as will be illustrated below in the case of a Fourier transform VCD instrument.
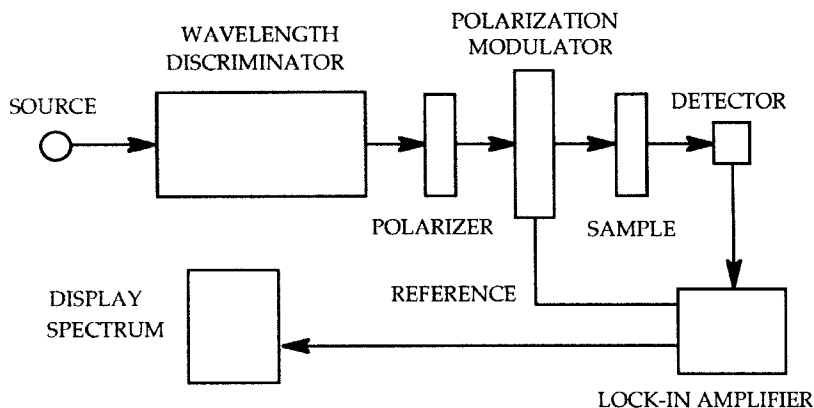
Figure 2. Block diagram of a generic VCD instrument showing the essential components in schematic form.

1.3 Vibrational Raman optical activity

The first measurements of ROA followed by approximately five years the application of commercially available lasers to the measurement of Raman scattering spectra. More than any other technical advance, the laser light source elevated Raman scattering from the status of a curious alternative to infrared absorption to that of a powerful research tool. As will be discussed below, the processing of electronic data in ROA is much simpler than it is for VCD. In Raman scattering and ROA, spectral detection involves the conversion of scattered photons to individual electronic pulses that can be counted and stored. The main complication associated with the detection of ROA is the need to keep track of two separate bins of photon counts, one associated with RCP Raman intensity and the other with the corresponding LCP intensity. When the measurement is complete, the counts in the two bins are added to obtain the parent Raman spectrum and subtracted to obtain the ROA.

In Figure 3, a simple schematic diagram is provided for a generic ROA spectrometer. Following the laser is a device to modulate the polarization of the incident radiation between RCP and LCP in a square wave cycle. In most ROA instruments, this is an electrooptic modulator (EOM), but in the one at Syracuse a zeroth-order quarter waveplate (QWP) is used. It is assumed that the radiation from the laser is pure linearly polarized, otherwise a polarizer is needed before the EOM or QWP in order to establish a single coherent polarization state of the light beam. For ICP and the DCP forms of ROA, the incident beam is first modulated in polarization. It is then focused into the sample cell and the scattered light is collected about the scattering angle ξ. Typically, this angle is
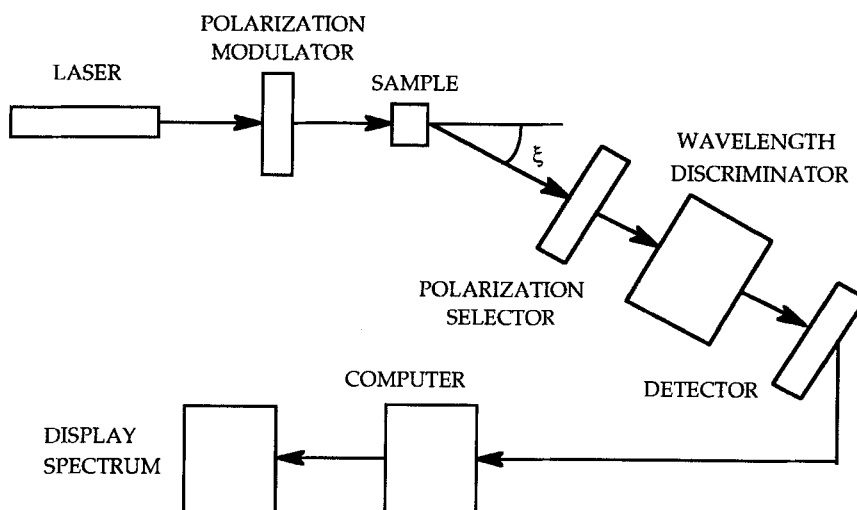
Figure 3. Block diagram of a generic ROA instrument showing only the essential items in schematic form.

$90°$ (right-angle), $0°$ (forward) or $180°$ (backward), and the light is collected in a solid-angle cone about this scattering angle. For SCP and the DCP forms of ROA, the RCP and LCP components of the scattered light need to be selected and measured separately. This is accomplished with a zeroth-order QWP which converts RCP and LCP light over a broad frequency range to orthogonal linear polarization states with a high degree of efficiency (typically above 97 % across the entire Raman spectrum) [32]. A linear polarizer can then effectively select either the RCP or the LCP component of the scattered light. Once the polarizer is set, the QWP can be rotated back and forth by $90°$ to select alternatively RCP and LCP light for a fixed polarizer position. The wavelength discriminator in Figure 3 is a spectrograph, and it is equipped with some form of photon detector, for example a photomultiplier tube in photon counting mode, an intensified diode array, or a charge coupled device (CCD) detector. A computer or digital storage device then keeps track of the counts in two separate channels and provides a plotter with the desired spectra for display.

1.4 Comparison of VCD and ROA instrumentation

From the two preceding sections, it is clear that VCD and ROA are measured in entirely different ways. Most of these differences stem from the way in which the parent vibrational intensity is measured. In the case of ROA, the spectral region is the visible, where it is possible to reach photon-limited background

noise. In other words, detectors in the visible are sensitive enough relative to background noise that the dominant source of noise in the spectrum is the statistics associated with individual photon counts. This noise is proportional to the square root of the photon intensity. ROA spectra are approximately three to four orders of magnitude smaller than the parent Raman intensity, and hence the level of effective total Raman counts needs to be larger than 10^8 in order to observe the ROA features above the noise. Even higher total count levels are needed for high quality ROA spectra. Since the focus in an ROA measurement is on maximizing the number of total photon counts, the electronic processing is set up to keep track of digital counts. The modulation cycle is square wave, and the modulation frequency is of no particular importance since there are no noise considerations that depend on this frequency. If the ROA optical system is stable, the square wave cycle can be as long as one minute (i.e. $1/60$ Hz), which is extremely slow compared to the modulation cycle time in VCD.

The principal source of noise in VCD measurements is detector background noise. In addition, other sources of noise that depend on the modulation frequency of the measurement are also present. The source of the detector background noise is the thermal emission at room temperature of everything that the detector element sees when it is exposed to the infrared beam. For instance, the detector window, the focusing lens and the surfaces of the mirrors used to direct the beam to the detector all emit infrared radiation in a room-temperature near black-body distribution. One cannot observe the isolated effects of individual photon strikes on the detector since they are merged with the constant background noise that leads to an overall detector signal. In order to reduce this large background signal, the desired intensities are modulated at a particular frequency and the amplitude of this modulated signal is measured within a narrow bandwidth of the modulation frequency. Noise in all other frequency regions is then rejected by the detection electronics and does not contribute to the measured intensity.

Background noise can also be reduced by limiting the field of view of the detector element with a surrounding metal cylinder at liquid nitrogen temperature, although this also limits the solid angle of focused light that can be imaged on the detector element. Cold shielding of the detector with an infrared optical filter is also a way to reduce the background noise, although this may lead to certain kinds of optical distortions that interfere with VCD measurements. By an appropriate choice of such optical filtering, it is possible to limit the effective spectral range of the detector to the degree that the background noise falls below the statistical photon count noise. Such conditions are rare, and the range of possible spectral measurements is greatly reduced. However, if one is interested in only a small spectral region, it is possible to achieve very low background noise levels that approach those encountered with photon counting detectors over broad spectral ranges in the visible region.

The selection of the modulation frequency with which to carry out infrared (and VCD) measurements is influenced by the characteristics of the detector used for the measurement. For semiconductor detectors, such as InSb and HgCdTe, the response (relative to the noise level) of the detectors increases with

modulation frequency and finally plateaus above 10 kHz [42]. Such detectors are ideal for VCD measurements carried out at high modulation frequencies with a photoelastic modulator. If low-frequency polarization modulation, say below 10 Hz as in ROA, were employed with a semiconductor detector, or any other infrared detector, the signal-to-noise ratio would be an order of magnitude or more below what is routinely achieved at high frequency.

Although VCD and ROA are presently measured in entirely different ways, future configurations of the two kinds of instruments may draw them into closer correspondence. For instance, measurement of ROA using a Fourier transform infrared spectrometer, with polarization modulation developed within the interferometer, has been proposed as a possible way to measure ROA [43]. Under such circumstances the same instrument might be used to measure both VCD and ROA, albeit with different detectors and beamsplitters. So, even though there are numerous differences between the instrumentation for VCD and ROA measurements, both are very efficient in their own right and the future may bring opportunities for these two forms of VOA to borrow instrumental advantages from one another.

2. FOURIER TRANSFORM INFRARED CIRCULAR DICHROISM

There are three classes of instruments for the measurement of VCD. The first is based on a dispersive grating monochromator as the source of wavelength discrimination. This was the first kind of VCD instrument to be built and this design was used in the discovery of VCD in 1974 [1]. The early versions of these instruments have been described in detail [3,4,44-47]. The low-frequency limit was initially 1900 cm^{-1}, the cut-off of the InSb detector. Using a PbSnTe detector the low-frequency limit was extended to 1550 cm^{-1} [46], and subsequently using HgCdTe detectors the limit was lowered to 1250 cm^{-1}[48] and then 900 cm^{-1} [49], and finally using a Si:As detector it was lowered to 650 cm^{-1} [50]. Dispersive VCD instrumentation has been further refined for the mid-infrared region from 800 to 1800 cm^{-1} [51] and this design was further optimized for the 6μ spectral region between 1600 and 2000 cm^{-1} [52]. Additional discussion of dispersive VCD instrumentation can be found elsewhere in this book [53].

The next class of VCD instruments to be developed was centered around a Fourier transform infrared (FT-IR) spectrometer. The idea was to design the sample compartment to be the same as in a dispersive VCD instrument, including a photoelastic modulator. To measure VCD, the detector signal is first sent to a lock-in amplifier to demodulate the high-frequency polarization modulation. The output of the lock-in is a VCD interferogram which is Fourier transformed in much the same way as the ordinary transmission interferogram. If the detector signal bypasses the lock-in and is Fourier transformed directly, the ordinary transmission is obtained. Since there are two interferograms generated simultaneously by the instrument, this general approach to measurements with a FT-IR spectrometer is called double modulation [5,6,11]. The concept of carrying

out CD measurements in this way [54,55] preceded the first measurements of FT-VCD [56], and it was pointed out at an early stage that the double modulation method could be extended to linear dichroism and other kinds of repetitive, high-frequency modulations of the sample transmission [55]. A number of improvements in double modulation FT-VCD have been published over the past decade [57-65]. They involve improved performance and methodology [57,63], extension of low-frequency coverage to 600 cm^{-1} [58], reduction of artifacts [59,61,64], implementation of Fourier self deconvolution [60], and improved phase correction procedures [62,65].

A third class of VCD instruments also is centered around a FT-IR spectrometer. In this approach, the modulation of the polarization is generated in the interferometer itself by substituting a polarizing wire-grid beamsplitter for an ordinary dielectric one. In such an FT-IR spectrometer, the radiation at various wavelengths is modulated in polarization through successive complete 360 degree cycles. If desired, the polarization modulation at the sample can be converted to intensity modulation by insertion of a linear polarizer just before the sample. This approach to VCD measurement, known as polarization modulation interferometry (PMI), was first proposed in 1981 [66] and subsequently implemented first for infrared linear dichroism measurements [67], then infrared circular dichroism measurements [68], and finally infrared VCD [69,70]. This type of interferometer has also been referred to as a Martin Pupplet interferometer (MPI), named after the originators of this approach to FT-IR [71], but not CD, measurements. The unique aspect of the PMI -FT-VCD instrument is that there is no photoelastic modulator. Measurements of VCD with this instrument represent the only examples of VCD obtained without such a modulator. The principal advantage that this brings is the potential to extend the method into the far infrared region where photoelastic modulators have little chance of being useful for reasons of transmission efficiency and retardation efficiency. Several additional steps toward the achievement of far-infrared PMI-FT-CD measurement have been taken by preliminary work with a far-infrared PMI interferometer. [72-74].

A review of progress in the development of dispersive and Fourier transform VCD methodology has been provided recently by Keiderling [13]. Detailed descriptions of the dispersive and the double modulation FT-VCD instruments in his laboratory are presented. These two approaches to VCD measurement are compared and critiqued, with the relative advantages and disadvantages of each described. In the following subsections, we describe further details related to FT-VCD instrumentation as developed in our laboratory at Syracuse.

2.1. Optical and electronic layout

The optical layout of our FT-IR-VCD instrument is based on a Nicolet 7199 Fourier transform spectrometer. A block diagram of the optical and electronic components of the instrument is shown in Figure 4. The instrument has been described in detail in several previous publications [57,68,75], and some of the more recent changes in the instrument will be indicated below.
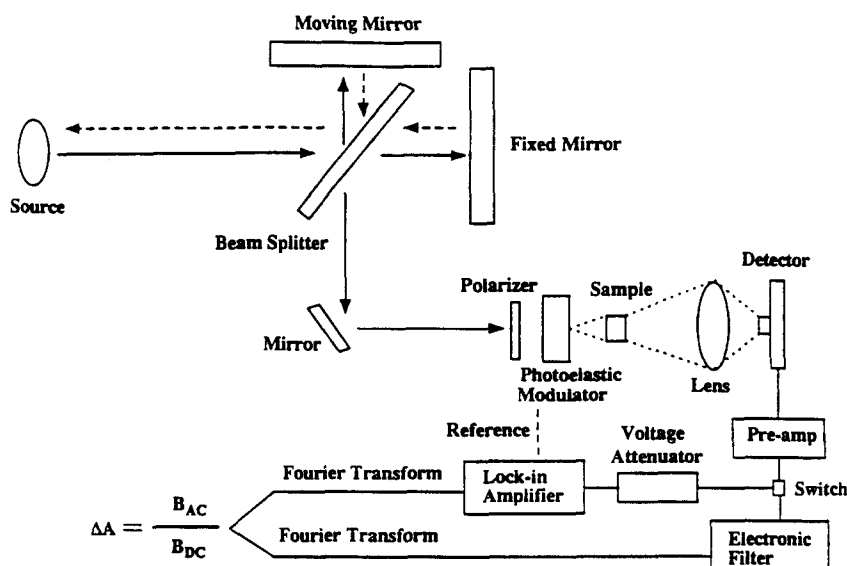
Figure 4. Optical and electronic diagram of the double modulation FT-VCD spectrometer at Syracuse University.

The source is a standard silicon carbide glower. Radiation from the source is collimated and directed to a dielectric beamsplitter. Half of the radiation is sent to a moving mirror and the other half to a fixed mirror. The light recombines at the beamsplitter and the Fourier-modulated, collimated infrared beam is directed out of the main optical bench by a mirror to an auxiliary bench that was originally designed and sold by the Nicolet Instrument Corporation for gas chromatography applications. All of the VCD optics, including the detector, is set up on this auxiliary bench. The beam is focused to the sample through an optical filter, a BaF_2 wire-grid polarizer, and a ZnSe photoelastic modulator (PEM) operating at 37 kHz. The infrared beam is vertically polarized as it enters the PEM where it is converted to sinusoidal polarization modulation. The driving voltage of the PEM is adjusted so that optimum polarization modulation is achieved at roughly the midpoint of the spectral range being measured. The optimum phase retardation for sinusoidal modulation is between approximately +105° and -105° [40,41]. In Figure 5 we present a diagram illustrating the relationship between phase retardation angle and polarization state. The optimum sinusoidal modulation of a PEM corresponds to starting at 0° and vertically polarized radiation and making a swing from that point out to +105°, just beyond RCP, and then back through 0° and out to -105°, just beyond LCP, and then back to 0° again where cycle begins again. The sample is placed immediately after the PEM, without any intervening optics, in order to eliminate distortions of the polarization of the light beam before circular dichroic absorption occurs. The infrared beam is then focused on to a HgCdTe detector by ZnSe lens, although originally we used an off-axis ellipsoidal mirror for this purpose.
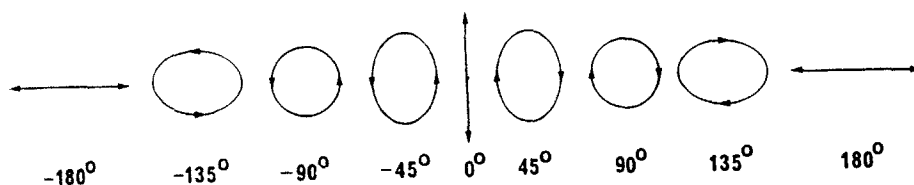
Figure 5. Diagram illustrating the relationship between polarization state and optical phase retardation for a beam of radiation.

The electronic signal from the detector is first amplified by a detector preamplifier and is then sent to a relay switch where it is directed either though a ten-fold attenuator to a lock-in amplifier or to a low-pass electronic filter. The interferogram of the high-frequency polarization modulation signal, the so-called AC-interferogram, emerges from the lock-in, and from there it is sent to a computer for digitization and Fourier transformation. The signal from the low-pass filter, the DC-interferogram, represents the ordinary transmission interferogram (with the high-frequency component removed by the filter). This signal can be sent directly to the computer for digitization and Fourier transformation. The ratio of the AC transmission spectrum, B_{AC}, and the DC transmission spectrum, B_{DC}, is directly proportional to the VCD spectrum ΔA.

VCD spectra are measured by collecting blocks of AC and DC scans. Typically, we collect 12288 AC scans and 1536 DC scans in 48 blocks of 256 AC scans preceded and followed by 32 DC scans. Each block of Fourier transformed AC scans is divided by the average of the Fourier transformed 32 block DC scans that were collected just before and just after the AC block. This minimizes the effect of instrumental drift in taking this ratio since the entire spectral collection process requires approximately 2.5 hours to complete. For most of our measurements with neat liquids, we employ 4 cm^{-1} resolution, although resolution as high as 1 cm^{-1} has been used.

2.2 Alignment optimization

The optical alignment of the FT-VCD instrument is carried out with three principal goals. One is to maximize the throughput, and hence the electronic signal of the detector relative to the background noise. Another is to avoid detector saturation. And a third is to minimize or control optical artifacts. These goals are not independent of one another, and care needs to be exercised in their realization. The general approach is to maximize the size of the transmission interferogram by adjusting the positions of the various optical components. The starting point is a symmetrical alignment with the beam passing though the

center of the optical components. Once the signal has been maximized in the vicinity of the starting point, the spectrum is checked for signs of detector saturation. Saturation is most easily detected by the appearance of negative transmission intensity in regions just outside the spectral coverage of the instrument, where the transmission should be exactly zero. In any case, negative intensity should never appear in an ordinary transmission spectrum, but it may appear if the detector signal becomes saturated at the detector itself or at some point along the electronic pathway. The most productive procedure is to be somewhat conservative in the initial alignment of the instrument until some confidence has been gained in the recording of VCD spectra. To be safe, adjust the throughput of the instrument at 10% below the point where saturation can no longer be detected. Once this has been achieved, proceed to the goal of minimizing VCD artifacts. There are several approaches to this problem [57,59,61], but with further adjustments, the transmission level should be maintained at the level reached just prior to artifact reduction.

The problem of the occurrence of artifacts in VCD spectra is serious, and in the past, it has limited the application of the method to those samples for which both enantiomers are available. Today, this problem is more under control; however, it is still true that the most accurate and reliable spectra are obtained by subtracting the VCD spectra of opposite enantiomers. The essence of the problem is that at the low intensity levels associated with VCD, in the range of four to six orders of magnitude below the ordinary transmission, imperfections and biases in the optical components of the instrument lead to spurious background VCD signals that interfere with the appearance of genuine VCD. In some cases, the artifacts are broad features associated with the overall alignment of the instrument, and in other cases, they are dependent on the spectral location and intensity of sample absorption bands. The exact physical origin of these artifacts has not been demonstrated, but they appear to be related to polarization phase shifts that alter the polarization balance between right and left circular polarization in the modulation cycle and thereby produce modulation between residual, orthogonal linear polarization states. This small linear polarization modulation in turn may produce intensity modulation, that mimics VCD, as the result of differential reflectivity or transmission at optical surfaces and differential response of the detector to certain orthogonal linear polarization states.

Within the past year, we have experimented with the detector focusing optics and the detector. Our goal has been to achieve an optical layout in the vicinity of the sample that possessed cylindrical symmetry. Our standard configuration has been an off-axis ellipsoidal focusing mirror, with 6 to 1 image reduction, and a 1 mm X 1 mm HgCdTe detector element. This arrangement involves a right-angle reflection just prior to the detector focus that produces large background artifacts. More recently, we have used the cylindrical arrangement in Fig. 4 that features a 38 mm-diameter f/1 ZnSe lens from Infrared Optics and 3 mm x 3 mm HgCdTe detector element from Graseby Infrared (formerly Infrared Associates). In order to keep artifacts at low levels and to improve the reliability of focusing

the infrared beam, this detector is equipped with a ZnSe anti-reflection coated window rather than the standard germanium window.

With the new optical arrangement the background artifact levels for VCD measurements are greatly diminished. In fact, the AC interferogram is no longer discernible on the oscilloscope used to monitor individual interferograms. Previously, there was a large artifact background that gave rise to a relatively large AC interferogram, and the Fourier transform of the AC interferogram yielded a broad positive background upon which the positive and negative VCD intensities were superimposed. The true VCD could be obtained by subtracting the corresponding VCD spectrum of the opposite enantiomer or the racemic mixture. The fact that all measured AC transmission intensities were positive, because of the large background, the phase correction could be derived from the interferogram in the usual way using the Mertz method. With this method, if negative transmission intensities are encountered, the Fourier phase is shifted automatically by 180° so that these intensities are positive in the final result. Since the background artifact signal is no longer present with the new optical arrangement, negative VCD intensities may actually be present as negative transmission intensities. In order for VCD spectra to be measured properly, a new phase correction procedure needs to be invoked. Such a procedure has been published previously by McCoy and de Haseth [62], and we have implemented their method.

The effect of the McCoy-de Haseth phase correction method is illustrated in Figure 6. The spectral curve on the right side of the figure is the multiple waveplate calibration spectrum that we employ to determine the VCD intensity scale for our instrument. This spectrum has nearly unit CD intensity and hence the magnitude of the spectrum is comparable to that of an ordinary transmission spectrum. There are negative as well as positive intensities. The phase correction used to Fourier transform this spectrum is that of McCoy and de Haseth. By comparison, the same spectrum with the Mertz phase correction is given in the left side of the figure. It can be seen that all negative intensities have been automatically rectified to positive values and it is no longer possible to distinguish between negative and positive intensities.

We have carried out a comparison of the artifacts present when using the ellipsoidal mirror and the lens focusing optics for samples of α-pinene. On the right-hand side of Figure 7, we present the (+) and (-)- enantiomers of α-pinene above their common transmission spectrum in the midinfrared region between 1400 and 800 or 900 cm^{-1}. Although the VCD spectra of the two enantiomers are not the same, they are also not equal and opposite in sign as expected if there were no artifacts. By comparison, on the left-hand side of the same figure, we present the (+) and (-)- enantiomers of α-pinene, as well as the racemic ($\pm$) mixture of the enantiomers, for the lens focusing optics. Here, the racemic mixture gives a relative smooth featureless spectrum and the two enantiomeric samples yield spectra whose principal features ride on the racemic background and are equal and opposite to nearly the noise limit.

The fact that the VCD content of the spectra on the left- and right-hand sides of this figure are the same is demonstrated in Figure 8 where VCD spectra are
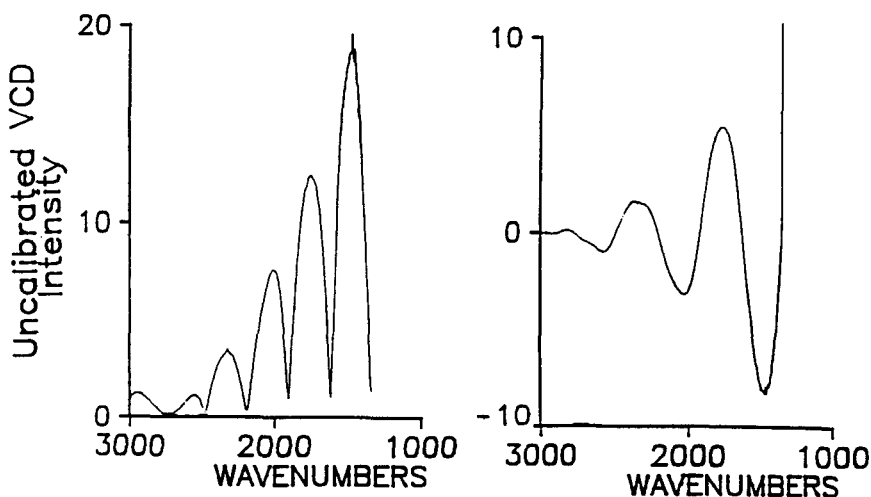
Figure 6. Multiple waveplate calibration curves taken with the McCoy-de Haseth phase correction (right) and the Mertz phase correction (left).
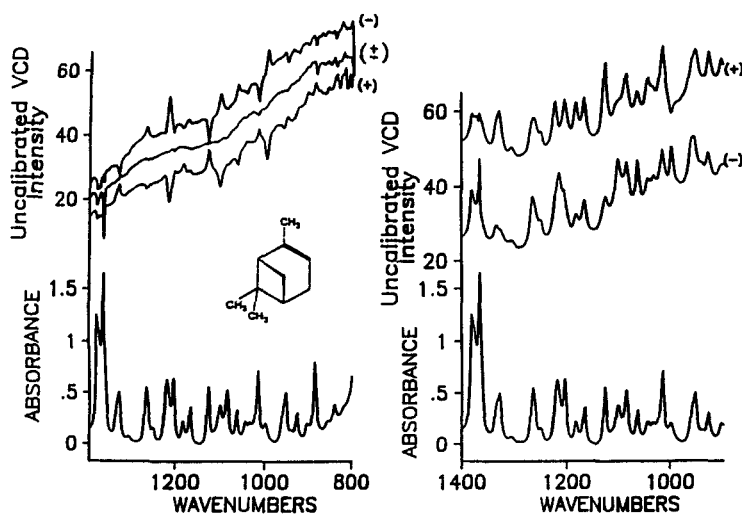

Figure 7. Uncalibrated VCD absorbance curves (upper) and ordinary absorbance (lower) for α-pinene. The signs of the enantiomers and the racemic mixture of α-pinene are indicated. The spectra on the left were take with the lens focusing optics and those on the right with the ellipsoidal mirror focusing optics.

presented that represent the difference between the raw VCD of the (-)- minus the (+)-enantiomers. The VCD spectrum for the lens focusing optics is slightly noisier than that of the mirror focusing optics since the latter has somewhat

higher throughput at the expense of much higher artifact levels. With the aid of additional optical adjustments it is possible to straighten the background (racemic) spectrum to near zero VCD. Then VCD spectra for single enantiomeric species can be measured with a high level of confidence.
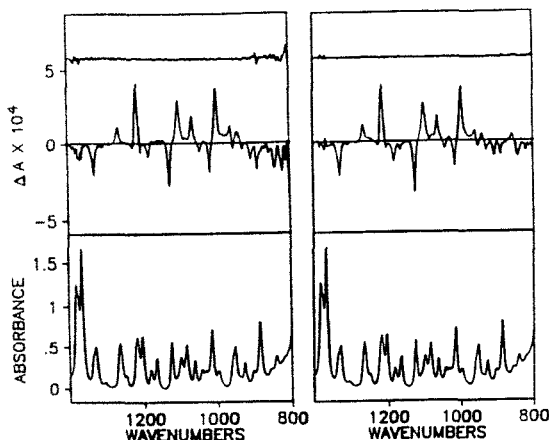
Figure 8. Corrected VCD spectra (middle) obtained by subtraction of the spectra of the enantiomers for the lens focusing optics on the left and the mirror focusing optics on the right. Absorbance spectra (bottom) and noise curves (top) are also given.

2.3 Polarization modulation interferometry

As discussed above at the beginning of this section, PMI-FT-VCD represents an entirely new approach to the measurement of VCD spectra. It is the only successful method for VCD measurement which does not employ a PEM. We present here the basic principles of the method and the VCD spectrum of (+)-limonene as an example of the PMI-FT-VCD method.

The approach we have used at Syracuse is based on a Bomem DA3 FT-IR spectrometer with two overall modifications [68-70]. The first is a special sample chamber fitted with an additional source mounted on the side, and the second is the substitution of a wire-grid polarizing beamsplitter on a BaF_2 substrate in place of the standard midinfrared beamsplitter. Radiation from the additional source is linearly polarized and focused into the sample chamber where it is directed back into the beamsplitter using a small pick-up mirror. At the beamsplitter, the plane of polarization of the beam is at 45° with respect to the polarizing grids of the beamsplitter which divide the beam into two beams with orthogonal linear polarization states traveling at right angles to one another. One beam encounters a fixed mirror and the other a moving mirror after which they both return to the beamsplitter. Because the beams are orthogonally polarized, they cannot interfere with one another, but they are coherent in optical phase. Instead of generating an intensity modulated beam, as in an ordinary Michelson

interferometer, a polarization state modulated beam is generated where all the radiation is returned to the source, i.e. there is no intensity modulation. As in a regular interferometer, each wavelength passes through the modulation cycle at its own Fourier frequency. The optics in the sample chamber is adjusted so that the beam returning from the beamsplitter bypasses the pickup mirror used to direct the polarized beam from the source to the beamsplitter.

In Figure 9 we present a diagram illustrating some of the features of the PMI-FT optical setup. Two optical trains are shown. In each case, a beam is shown entering the diagram from the left with four polarization states, vertical linear, right circular, horizontal linear, and left circular. This represents one complete cycle of polarization modulation in one direction. This corresponds to a polarization cycle in Figure 5 in which the polarization state is always changing toward the right, recognizing that $+180°$ and $-180°$ are the same states. By contrast, the polarization modulation cycle of a PEM corresponds to alternating changes to the right and left in a sinusoidal fashion. In the PMI measurement, all wavelengths experience the full polarization cycle, although at different modulation frequencies, their Fourier frequencies.

In the upper diagram, a polarizer has been placed in the beam ahead of the sample. VLP states pass through the polarizer, HLP states are blocked, and the CP states pass through at half strength. The polarizer serves to convert the polarization modulation of the beam into intensity modulation. In this configuration, the instrument is operating as an ordinary FT-IR spectrometer. Also in this configuration, the point of zero phase retardation for each wavelength is established, and the phase correction can be used in subsequent polarization measurements. The absorption spectrum is recovered from the real part of the interferogram, also referred to as the cosine interferogram.

In the lower portion of Figure 9, two different polarization difference measurements are illustrated. In these cases, the polarizer used for the absorption measurement and the phase correction is removed. If the sample contains linear dichroism (LD) with respect to VLP and HLP radiation, then the LD spectrum can be recovered from the real part of the complex Fourier interferogram. If the sample is circularly dichroic, then CD can be recovered from the imaginary part of the complex interferogram. As illustrated, once the point of zero phase has been established, using the vertical polarizer, the cosine (real part) transform is sensitive to intensity differences at the $0°$ and $180°$ phase points, while the sine (imaginary part) transform is sensitive to differences at the $90°$ and $270°$ points. The definitions for LD and CD are also given in the diagram.

The PMI-FT-VCD spectrum of (+)-limonene in the mid-infrared region is presented in Figure 10 [70]. This spectrum compares favorably with previous double modulation (DM) FT-VCD spectra of this sample. In general, we have found that the PMI-FT-VCD method yields spectra that are within a factor of two of the noise levels of the corresponding DM-FT-VCD spectra; however, in the PMI case we also encounter some degree intensity instability that has an undetermined origin. The effects of the instabilities can be removed if a sufficient number of spectral runs are averaged together. For the spectrum of
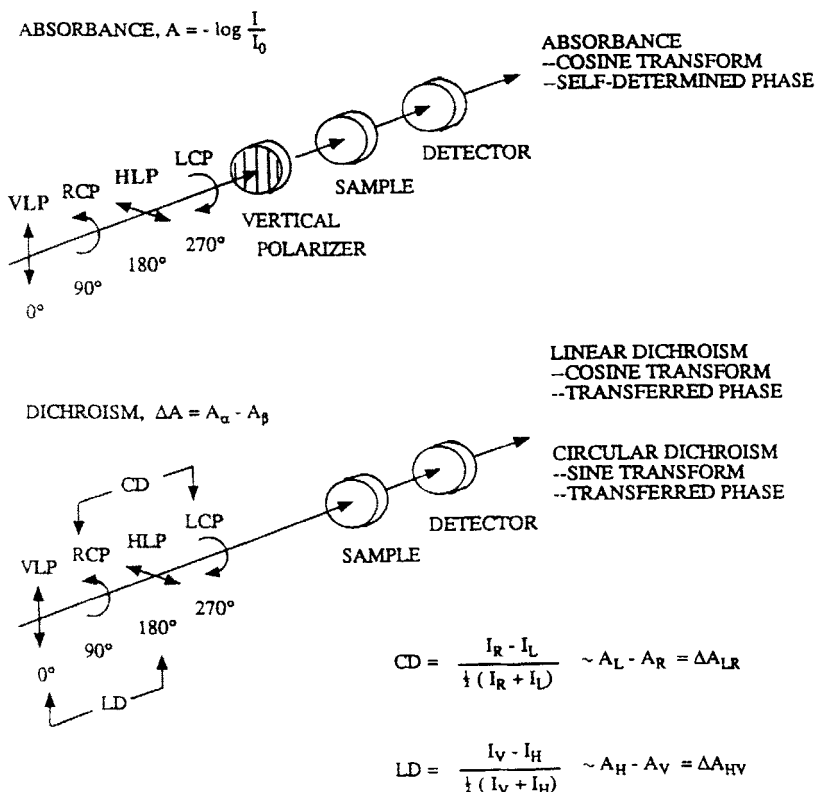
ABSORBANCE, $A = -\log \frac{I}{I_0}$

ABSORBANCE
--COSINE TRANSFORM
--SELF-DETERMINED PHASE

DETECTOR

LCP
HLP
RCP
VLP

SAMPLE

VERTICAL
POLARIZER

270°
180°
90°
0°

LINEAR DICHROISM
--COSINE TRANSFORM
--TRANSFERRED PHASE

DICHROISM, $\Delta A = A_\alpha - A_\beta$

CIRCULAR DICHROISM
--SINE TRANSFORM
--TRANSFERRED PHASE

CD

LCP

DETECTOR

HLP
RCP
VLP

SAMPLE

270°
180°
90°
0°

LD

$$CD = \frac{I_R - I_L}{\frac{1}{2}(I_R + I_L)} \sim A_L - A_R = \Delta A_{LR}$$

$$LD = \frac{I_V - I_H}{\frac{1}{2}(I_V + I_H)} \sim A_H - A_V = \Delta A_{HV}$$

Figure 9. Diagram illustrating the principal modes of operation of a PMI FTIR spectrometer.

limonene, a total of 30,000 VCD scans were block averaged and transformed using the same approach [69,70] described above for DM-FT-VCD measurements. As a result of the instability problem, the PMI approach has not been employed in our laboratory for routine applications of VCD.

3. MULTICHANNEL RAMAN OPTICAL ACTIVITY

As with VCD, the first ROA instruments were built around single-channel scanning dispersive spectrometers [18,19,76,77]. Photomultipliers with dual-channel photon-counting electronics were used to record the spectra. Scanning rates were no faster than 1 cm^{-1} per minute because of the requirement to accumulate at least 10^7 counts per spectral location, and preferably 10^8. Applications with these instruments were limited to samples with favorable Raman scattering and the goals of these early studies were simply to explore the nature of ROA spectra and to improve measurement techniques. Several reviews
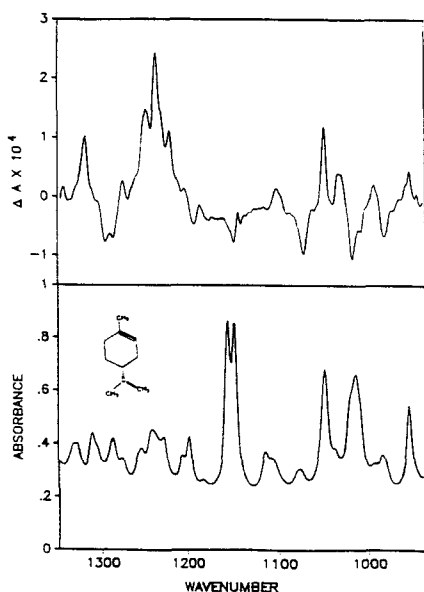
Figure 10. VCD and absorbance spectrum for (+)-limonene measured with a PMI FT-VCD spectrometer.

of the work from this period are available [33,78-80], two of which also cover early advances in VCD [79,80].

The next significant advance in the measurement of ROA was the introduction of multichannel detectors. The first employed vidicon technology which had the draw back of relatively long persistence times for the channel readings [76,81]. Shortly thereafter, Hug introduced diode array detection with which he was able to measure ROA spectra with very high signal quality [82]. In subsequent years, several other groups were able to develop diode array ROA instruments [83-85]. Although these instruments represented a significant advance over their single-channel predecessors, applications were still limited to neat liquids or non-aqueous solutions in high concentrations. The principal drawbacks of the diode array detector are small size of the diode elements and a low level of photon efficiency, typically 10% or less.

The most recent advance in ROA instrumentation is the use of charge coupled device (CCD) detectors [86,87]. These detectors have extremely low background noise, large areas, and very high quantum efficiency (in the range of 25 to 80%). The use of these detectors in ROA measurements has given rise to a renaissance in this field. Applications that were previously impossible due to low signal quality have now become almost routine.

Advances in two other areas have been introduced in the past five years. One is the use of the backscattering experimental geometry [35,88]. From a theoretical standpoint, backscattering ICP ROA offers approximately eight times higher ROA intensities compared to the standard depolarized right angle measurement.

Hug first pointed out the virtues of backscattering over ten years ago [89], but unfortunately, he was only able to carry out a few preliminary measurements before his instrument was destroyed by fire. The other area of recent advance, as discussed above, was the introduction of alternative polarization modulation schemes. SCP ROA was measured for the first time with a diode array detector [32], and the first measurements of DCP_1 ROA coincided with our first measurements of backscattering ROA [35]

Presently, there are three ROA instruments equipped with CCD detectors that are capable of making advanced measurements of ROA. Two of these are at the University of Glasgow in the laboratory of Laurence Barron. One is a backscattering unpolarized ICP ROA instrument that can be easily configured for forward scattering measurements [90] if desired. The instrument has been designed with the aim of carrying out measurements of biological samples [25,91,92] such as amino acids [93-95], peptides [96], proteins [96,97], cyclodextrins [98] carbohydrates [99] and nucleosides [25,91]. The performance of this instrument and the applications for which it has been used have been described recently in depth [91]. The second ROA instrument at Glasgow has just been completed [100]. It is configured to carry out polarized and depolarized right-angle ICP ROA measurements. It serves as a complement to the backscattering ROA instrument since it is able to make very low frequency measurements, below 100 cm^{-1}, as well as polarized and depolarized measurements. Its importance lies primarily in the area of providing experimental data for comparison with results of *ab initio* theoretical calculations of ROA intensity [100,101].

The ROA instrument at Syracuse has been described in detail for its use in right-angle SCP ROA measurements [32]. Upgrades of its performance for backscattering DCP measurements [35], comparison of ICP and SCP forms of right-angle ROA [102], and isolation of ROA invariants using right-angle and backscattering geometries [103] have been published. In addition, general descriptions of its current and potential capabilities have been provided in overviews of advances in ROA [28,104-106]. This instrument has also been used for applications of ROA to molecules of biological interest, including amino acids, peptides, proteins, carbohydrates, and ephedrine molecules [104-107]. The backscattering ROA instruments at Glasgow and Syracuse have been compared in a recent review [26].

A complete theory of circular polarization ROA, including all known scattering geometries and polarization modulation schemes, has been presented recently [108], and this theory, combined with linear polarization ROA, has been formulated in a unified way [26,109,110] using the Stokes-Mueller formalism. In addition, progress in the theoretical description and experimental measurement of ROA invariants has been reviewed recently [26].

3.1 Polarization modulation techniques

The first successful ROA measurements were achieved with the use of an electro-optic modulator (EOM) operating in a square-wave modulation cycle. For well over the next decade, this was the only method employed for

modulating the polarization in ROA experiments. The alignment of an EOM requires considerable care, since the resulting polarization modulation of the beam depends on the spatial and angular positioning of the EOM, on the positive and negative control voltages, and on the temperature of the device. EOMs have only been used to measure ICP ROA. Here, the laser beam can affect the temperature of the EOM, and hence some form of thermostat control is necessary for reliable operation.

In an attempt to reduce the number of degrees of freedom associated with the alignment of an EOM, in 1986 we undertook a different approach to ICP ROA measurements [85]. This effort led to successful ICP ROA measurements using a Soleil-Babinet compensator [85]. This device allows very high sensitivity control of polarization states using a fine mechanical adjustment. Although alignment of the compensator was simpler than that of an EOM, we still encountered some difficulties associated with laser heating.

Following this work, we investigated the possibility of polarization state control with a simple quarter waveplate (QWP). We were interested to determine whether a QWP could be employed in the scattered light beam to measure the SCP form of ROA. In this position there would be no thermal effects due to laser heating. Further, the QWP is a relatively thin object which probably would suffer only small thermal effects even if it were placed in the laser beam. We found that if the QWP were zeroth order, a $0+\lambda/4$ plate rather than an $n+\lambda/4$ plate where n is some integer, typically 30 or 40, representing the number of full wave retardations, the SCP form of ROA could be successfully measured [32].

The concept behind the SCP ROA measurement is the reverse of generating circularly polarized radiation from linear polarized radiation with a QWP. Circularly polarized light is converted to linear polarized light by the QWP. The opposite sense of circularly polarized light is converted to the orthogonal linear polarization state. Hence RCP and LCP can be selectively measured by using a QWP followed by a polarizer. One can either rotate the polarizer or the QWP by 90° to switch between RCP and LCP measurement. We prefer to rotate the QWP in order to maintain the same polarization state for the scattered radiation entering the spectrograph for analysis.

Subsequently, we found that a zeroth-order QWP could be employed successfully in the laser beam for ICP measurements, and from that point it was relatively straightforward to carry out DCP ROA measurements [35]. If desired, linear polarization modulation can be set up by using half waveplates in place of the QWPs. In the following sections we provide details associated with present operation of our dual QWP ROA spectrometer.

3.2 Optical and electronic layout

The ROA instrument designed for right angle scattering at Syracuse University [87] is shown on the block diagram in Figure 11 which includes both the optical and electronic layout. The plane of the linearly polarized laser beam emitted from a Spectra Physics argon ion laser is first oriented by a Fresnel rhomb and then sent to a beam expander. It passes through a quarter waveplate
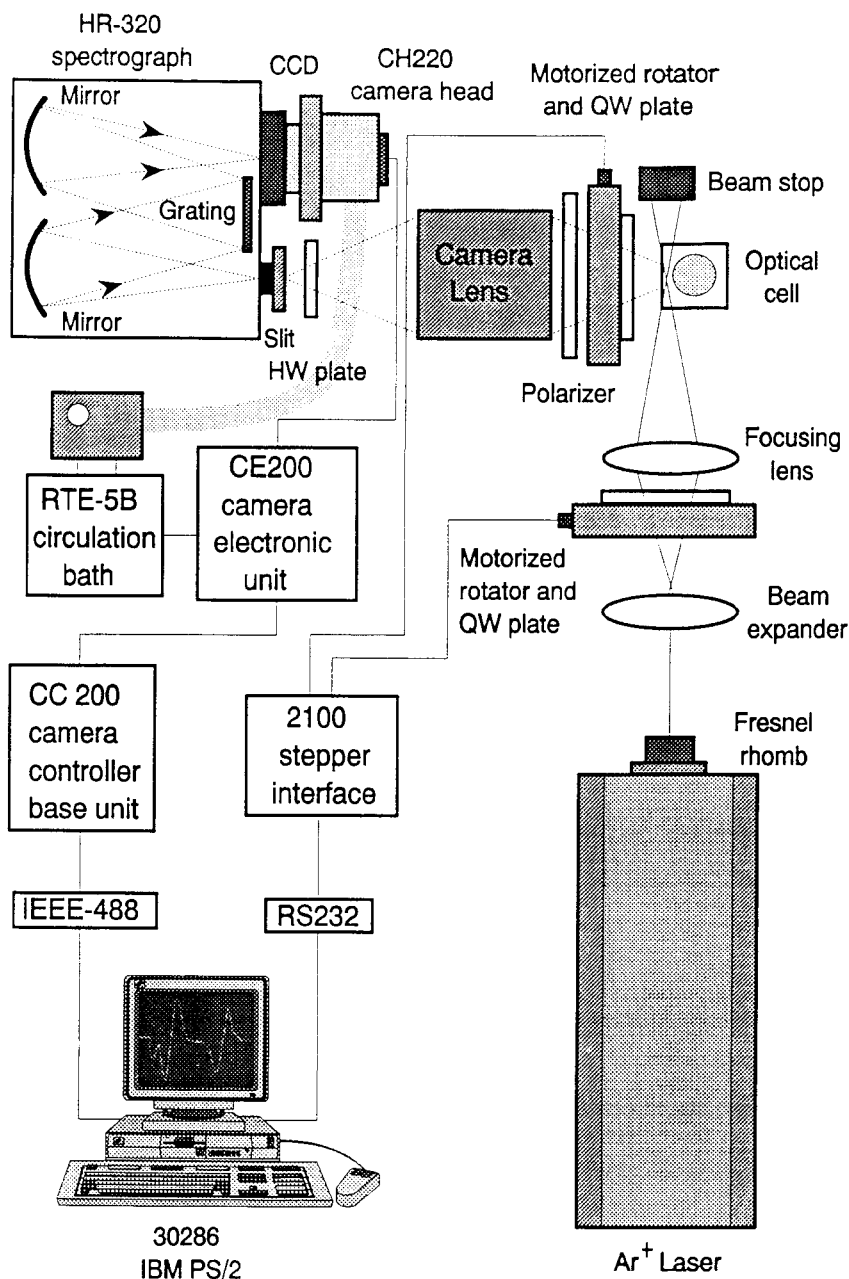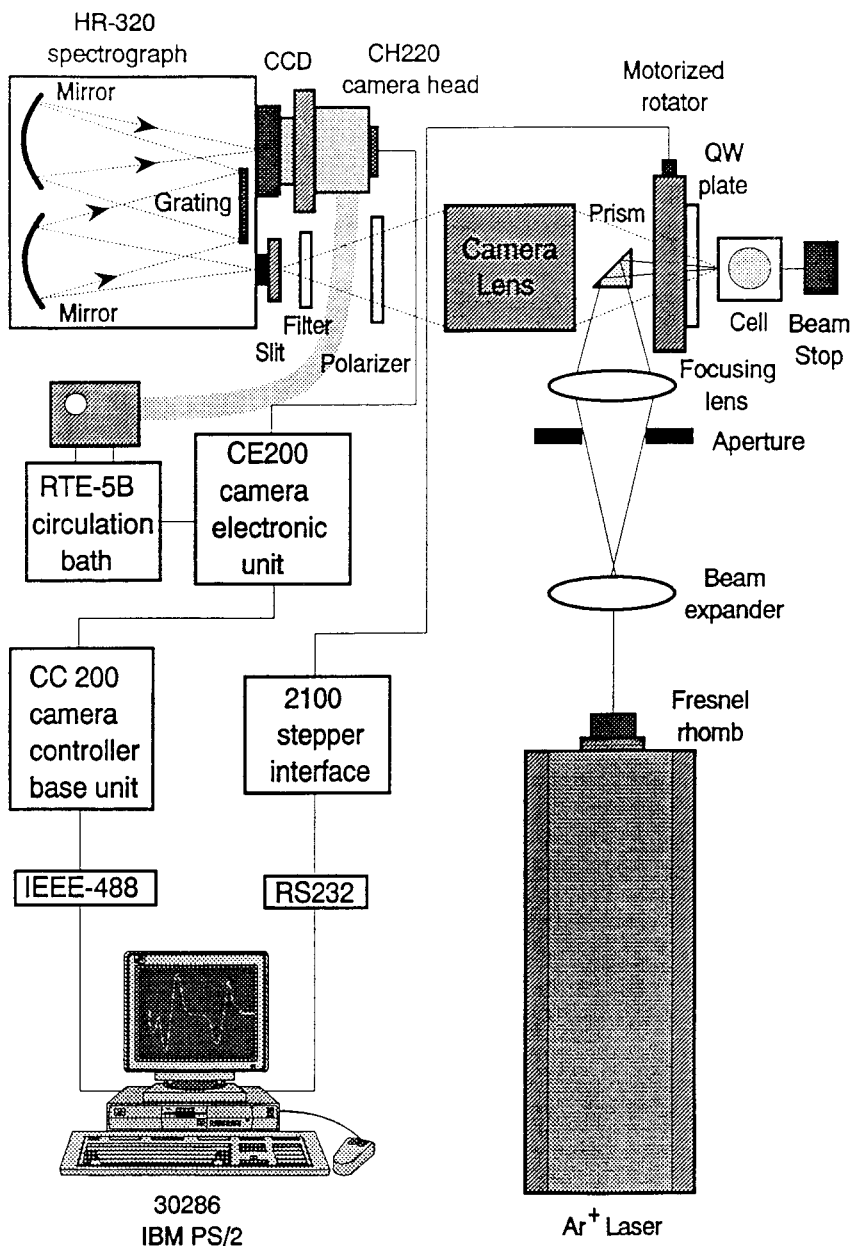
Figure 11. Optical and electronic layout for the right-angle scattering mode of operation of the ROA spectrometer at Syracuse University.

(QWP) mounted in a computer-controlled motorized rotator and is focused to the optical cell, which contains the sample, and is absorbed by a beam stop.

The scattered light from the sample cell passes through another QWP in a motorized mount and a polarizer, and is collected and focused via a half waveplate (HWP) to a slit on an HR-320 spectrograph by a Canon 85 mm $f/1.2$ camera lens. The HWP is used to orient the plane of polarized scattered light to the angle of maximum efficiency of the spectrograph. Within the spectrograph, there are two collimating mirrors. One collimates the scattered light from slit to the grating, and the other refocuses the scattered light from the grating to the CCD detector. The CCD detector is mounted on a CH220 camera head and is cooled by an RTE-5B circulation bath which is powered by a CE200 camera electronic unit. The signal from the CCD detector is transferred to the camera controller base unit via the camera electronic unit for digitization and temporary storage. The camera controller communicates with a IBM PS/2 computer through an IEEE-488 interfaced board. Further data manipulation is carried out in the computer using a program written in Array Basic supplied by Spectra Calc software. The computerized QWP rotators are controlled with an RS232 board and a 2100 stepper interface with a rotational precision of 0.05°. The ICP and SCP depolarized, polarized or unpolarized, and DCP experiments using a right angle scattering geometry, can be easily performed with this system by selecting the location of the fast or slow axes of both QWPs and the transmitting axis of the linear polarizer with respect to the scattering plane.

The backward scattering ROA experiment is executed with the same equipment, but with a slightly modified setup, as shown in Figure 12. A 5 mm prism is used to turn the laser beam by 90° away from its initial propagation direction and then to the optical cell. A QWP is positioned between prism and sample cell to modulate the polarization states of both the incident and scattered light. The camera lens is moved close to the laser beam to obtain the correct focusing distance. The linear polarizer is repositioned after camera lens because of space limitations before this lens, and a holographic edge filter is used to reduce the Rayleigh background. With the combination of the modulation of the polarization of the incident beam and scattered light, unpolarized ICP and (depolarized) DCP$_I$ and (polarized) DCP$_{II}$ can be implemented with this setup. The SCP experiment can be carried out by positioning the QWP between the prism and camera lens. We have observed no adverse optical effects associated with positioning polarization selection optics (QWP or polarizer) after the camera lens, although, in principle, these optical elements should be placed before the cameral lens to avoid possible polarization distortions.

3.3 Data acquisition process

The process of measuring the difference between the two Raman parent spectra (right and left) is shown on the flow chart of the ROA data acquisition program in Figure 13. This program is written in Array Basic supported in Spectra Calc software. First, three spectral memory banks are created for the current, Raman parent and ROA spectra. Then several coadded spectra at four different quarter-wave plate positions are taken to complete one QWP cycle. The

HR-320
spectrograph

CCD

CH220
camera head

Motorized
rotator

Mirror

QW
plate

Grating

Prism

Camera
Lens

Mirror

Cell   Beam
Stop

Filter

Focusing
lens

Slit   Polarizer

Aperture

RTE-5B
circulation
bath

CE200
camera
electronic
unit

Beam
expander

CC 200
camera
controller
base unit

2100
stepper
interface

Fresnel
rhomb

IEEE-488

RS232

30286
IBM PS/2

Ar$^+$ Laser

Figure 12.   Optical and electronic layout for the backscattering mode of
operation of the ROA spectrometer at Syracuse University.
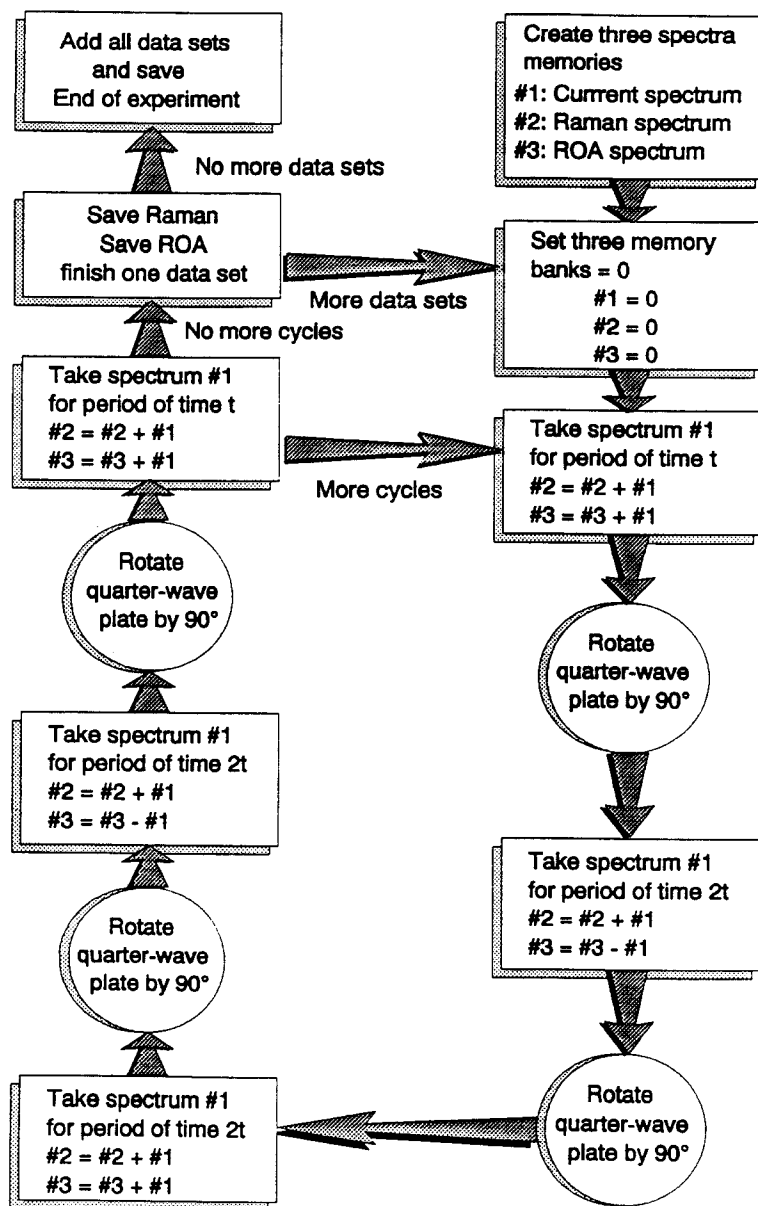
Figure 13. Diagram illustrating the data acquisition method for the computer-controlled measurement of Raman and ROA spectra at Syracuse University.

Raman parent spectrum is obtained simply by adding all the spectra together. However, the ROA spectrum is obtained by either adding or subtracting from the current coadded spectrum depending on the position of quarter-wave plate. After several cycles, the Raman and ROA spectra are saved on the hard disk as one data set. After several data sets, all the data are added and saved into either the Raman parent spectrum or the ROA raw data spectrum and stored for the data manipulation. Occasionally, the raw data contains parental bias or first derivative contributions due to the fluctuation of the laser intensity or the quality of the optics, and these are reduced or removed digitally.

In Figures 14 and 15 we provide examples of two ROA spectra measured recently with our instrument at Syracuse. In Figure 14, the depolarized right-angle SCP-ROA for (-)-α-pinene as a neat liquid is shown. This spectrum was obtained with 488 nm incident laser radiation at a resolution of approximately 15 cm^{-1} as a single enantiomer with a spectral collection time of approximately 8.7 hours. In Figure 15 we present the backscattering DCP_I ROA spectrum for 1R-(-)-nopol. This spectrum was obtained using 514 nm incident laser radiation at the same resolution with a 4.6 hour exposure time.

3.4 Comparison of right-angle and backscattering ROA

In this section, we compare briefly the two most widely used scattering geometries for ROA measurements, right-angle scattering and backscattering. Before the advent of backscattering, the most common form of ROA measurement was depolarized right-angle ICP ROA. Occasionally, the results of polarized right-angle ICP ROA [82, 111-113] or magic angle right-angle ICP ROA [114] have been reported, but these measurements are much more difficult owing to a strong tendency toward larger artifacts [110, 115-118]. The circular intensity difference (CID) and circular intensity sum (CIS) associated with right-angle depolarized ICP ROA are given in the far-from-resonance approximation by [20,25,104]:

$$I_z^R(90^\circ) - I_z^L(90^\circ) = 8\frac{K}{c}\left[3\beta(G')^2 - \beta(A)^2\right] \tag{8}$$

$$I_z^R(90^\circ) + I_z^L(90^\circ) = 4K[3\beta(\alpha)^2], \tag{9}$$

and the CID and CIS for the right-angle polarized ICP ROA are given by:

$$I_x^R(90^\circ) - I_x^L(90^\circ) = 4\frac{K}{c}\left[45\alpha G' + 7\beta(G')^2 + \beta(A)^2\right] \tag{10}$$

$$I_x^R(90^\circ) + I_x^L(90^\circ) = 2K\left[45\alpha^2 + 7\beta(\alpha)^2\right], \tag{11}$$

where the subscript z refers to the orientation of the polarizer in the scattered beam as being in the plane of the scattering, while the x subscript refers to the

WAVENUMBERS (cm⁻¹)
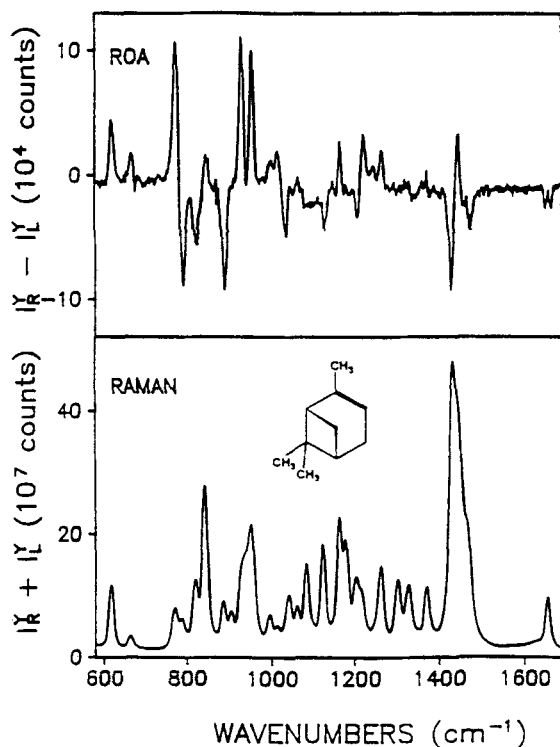
RAMAN AND ROA SPECTRA OF (−)—α—PINENE

Figure 14. Right-angle depolarized SCP ROA and Raman spectra of (-)-α-pinene.

orientation of this polarizer perpendicular to the scattering plane. In these expressions α^2 and $\beta(\alpha)^2$ are the standard Raman isotropic and anisotropic invariants, respectively, for the electric dipole polarizability, and $\alpha G'$, $\beta(G')^2$ and $\beta(A)^2$ are the isotropic magnetic dipole optical activity invariant and the anisotropic magnetic dipole and electric quadrupole optical activity invariants, respectively, for ROA [20,26].

The introduction of backscattering ROA brought two additional principal modes of measurement which bear some similarities to the two right-angle measurements just described. One of these is backscattering DCP_I ROA [35]. The CID and CIS expressions for this form of ROA are [26,35,103]:

$$I_R^R(180°) - I_L^L(180°) = 32\frac{K}{c}\left[3\beta(G')^2 + \beta(A)^2\right] \tag{12}$$

$$I_R^R(180°) + I_L^L(180°) = 8K[3\beta(\alpha)^2]. \tag{13}$$
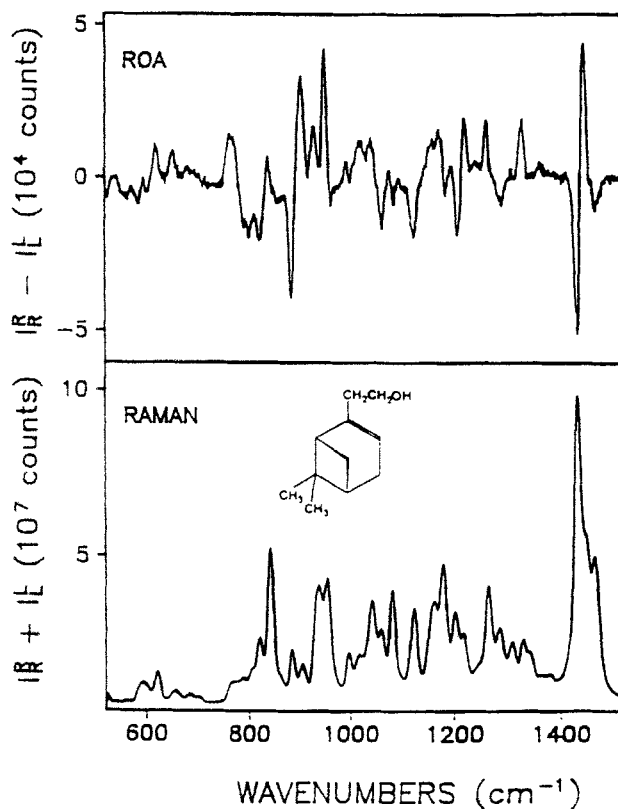
RAMAN AND ROA SPECTRA OF 1R(−)NOPOL

Figure 15. Backscattering DCP$_I$ ROA and Raman spectra for 1R-(-)-nopol.

The other is unpolarized backscattering ICP ROA and the corresponding intensities are [20,26,35,88,103]:

$$I_u^R(180°) - I_u^L(180°) = 32\frac{K}{c}\left[3\beta(G')^2 + \beta(A)^2\right] \tag{14}$$

$$I_u^R(180°) + I_u^L(180°) = 4K\left[45\alpha^2 + 7\beta(\alpha)^2\right]. \tag{15}$$

Inspection of these intensity expressions reveals that the CIS for backscattering DCP$_I$ Raman is the same as that for right-angle depolarized ICP ROA except that the backscattering measurement is twice as intense. The corresponding two ROA invariants appear with four times the strength in backscattering, and they combine with a positive sign in backscattering and with

a negative sign in right-angle scattering. These enhanced intensities are the main reasons why backscattering ROA enjoys a significant advantage over right-angle scattering.

If the polarizer is removed from the scattering arm of a backscattering DCP$_I$ setup, one then measures unpolarized ICP intensities. In this case the CIS is the same as the right-angle polarized ICP CIS, although twice as intense, but the CID is identical to the DCP$_I$ CID. By removing the polarizer, one allows additional Raman intensity to reach the detector, but the additional ROA is simply that associated with DCP$_{II}$ ROA, and this is zero in the far-from-resonance approximation. The equality of backscattering DCP$_I$ and unpolarized ICP ROA has been demonstrated experimentally [35]. The relationships among the intensities given in eq. (8-15) have been utilized to propose a method for isolating the three far-from-resonance ROA invariants [103], and the method has been executed in the case of the two anisotropic ROA invariants [103]. A slight improvement of the overall method has been described more recently [26]. A modification of the method required in the case of sufficiently large collection angles has also been provided [119].

In practice, the theoretical advantages of backscattering ROA over right-angle scattering are not fully realized. The reason is due to the imaging of the Raman scattering volume onto the entrance slit of the spectrograph. For right-angle scattering, the focal region of the laser beam in the sample cell appears approximately to be a line, the full extent of which is nearly equidistant from the spectrograph. This line can be imaged sharply on the slit of the spectrograph, which may be set at a narrow width without loss of throughput. This permits higher resolution provided a narrow focal region is illuminated by the laser. For backscattering, the line of laser focus is moving away from the spectrograph, the ends of which are in front of and beyond the focal depth of the collection lens. Hence, a more limited focal region is imaged sharply on the entrance slit. Some of this light can be recovered by opening the entrance slit, but this lowers the resolution and exposes the spectrometer to higher levels of background Rayleigh scattering. Background scattering and fluorescence are serious problems when measuring ROA in biological samples. On the other hand, high resolution is not needed for these applications and the higher levels of ROA relative to the parent Raman scattering more than compensate for the reduced spectral collection efficiency. We have determined the relative collection efficiencies for right-angle scattering and backward scattering to be about a factor of two in favor of right-angle scattering for our instrument at Syracuse. The overall efficiency for ROA measurement favors backscattering by a factor of approximately four.

3.5 Artifact reduction

Artifacts in our instrument can arise from a variety of sources [110,118]. Consequently, before ROA measurements are carried out, a careful alignment of the scattering geometry and optical path is essential. Further reduction of artifacts is achieved by adjustment of the polarization states, the position of the beam expander, the focusing lens and the two QWPs. The beam expander reduces the likelihood that small, local imperfections in optical components will

lead to large artifacts. The alignment of the incident arm is carried out using the laser beam as a reference to check the location and orientation of the optics. The alignment of the scattering arm, however, requires a small He-Ne laser as a reference.

The alignment of the polarization of our ROA instrument for right-angle scattering is carried out by first removing both QWPs, the polarizer and the HWP. The Fresnel rhomb is adjusted to obtain a depolarized Raman spectrum of (-)-α-pinene, which is used as a standard sample for the alignment. From the observation of the strongest polarized band at 667 cm^{-1}, the deviation of the polarization state of the laser beam is adjusted to within 0.5° using the reading of the Fresnel rhomb. Then a QWP is placed in the incident beam and rotated to maximize the strongest polarized band to within a deviation of less than 0.2° based on the reading of the rotator. Following the alignment of the QWP, the linear polarizer is put back in the scattering arm to reduce the intensity of the strongest polarized band. Then the second QWP is placed in the scattered beam, again to minimize the strongest polarized band. Finally, the HWP is placed right before the slit and adjusted to maximize the overall Raman intensity. This specific configuration is now set up for depolarized ICP measurements. Polarized or unpolarized ICP measurements for this geometry can be carried out by rotating the polarizer by 90° or removing it, respectively. For the depolarized SCP measurement, both QWPs need to be rotated by 45° from this setup. For the polarized SCP measurement, both the Fresnel rhomb and the polarizer need to be rotated by 90°, and for the unpolarized SCP one only needs to rotate the QWP in the incident arm by 45°. DCP measurements can be performed with this setup by rotating both QWPs simultaneously. Usually, further reduction of artifacts is necessary after the above alignment procedure. Slightly adjusting either the QWPs or polarizer is very effective in reducing artifacts further. Sometimes, small adjustments of the positions of the camera lens, the CCD detector or the focusing lens can be helpful to further reduce monosignate artifacts or first derivative artifacts [110,118].

The alignment of the backward scattering is similar to that for right-angle scattering. However, the alignment of the prism in the incident beam requires considerable care. For the alignment of the polarization, first the polarizer and QWP are removed from the beam. The Fresnel rhomb is rotated to maximize the strongest polarized band in the α-pinene sample. Then the QWP is put back in the beam and rotated to maximize the polarized band. This serves to locate the fast or slow axes of the QWP. The QWP is then rotated by 45° for the modulation of the polarization of the light between circularly polarized states. Finally, the polarizer is replaced to minimize the intensity of the polarized band. This is now the configuration for the (depolarized) DCP$_I$ experiment. The DCP$_{II}$ ROA setup can be easily obtained by rotating the polarizer by 90° or the plane of polarization of the radiation leaving the laser by 90° (using the Fresnel rhomb). Unpolarized ICP ROA can be carried out by removing the polarizer from the scattered light beam. The unpolarized SCP experiment is more complicated and requires two QWPs. One is used to generate a circularly polarized incident beam, and the

other is to select the circularly polarized scattered light. However, unlike right-angle scattering, slight adjustments of the Fresnel rhomb and polarizer are more effective for reducing further monosignate artifacts. On certain occasions, monosignate and first derivative artifacts, as well as parental bias, may be reduced by adjustment of the fast or slow axes of the QWP, the tilt angle of the edge filter, the position of the camera lens or the location of the CCD detector.

4. CONCLUSIONS

Within the past decade, dramatic technical improvements in the measurement of both VCD and ROA have occurred. Initially during this period, VCD gained an advantage in signal quality and ease of application, and this form of VOA has been used for a variety of applications, mostly of biological molecules [16]. However, within the past two or three years, ROA has advanced to a stage that is nearly equal to that enjoyed by VCD, and routine applications of ROA to a wide variety of molecules of biological significance are now possible [25, 104, 105].

VCD and ROA possess a number of complementary advantages which preclude the superiority of one over the other for a broad range of applications. VCD is limited to vibrational modes above 600 cm^{-1} and more practically above 800 cm^{-1}. ROA is readily measured in the low frequency to within 100 cm^{-1} of the Rayleigh line. VCD is strong and informative in the hydrogen stretching regions, whereas ROA is small and not readily measured for these modes. Water is a favorable solvent for ROA, but not for VCD. Artifacts are more difficult to control for ROA, but once a good alignment is achieved, ROA spectra of single enantiomers are readily obtained. VCD is nearing this capability, although typically some form of baseline correction is needed. To date ROA spectra have evidenced a higher degree of variation of intensity with small changes in molecular structure, whereas VCD spectra tend to vary in a more systematic manner. Strong VCD intensities can be interpreted in terms of simple theoretical or empirical models, and ROA spectra appear to be more complex and sensitive to subtle effects.

The coming years will see the publication of increasing numbers of applications of both VCD and ROA to biological molecules as both forms of VOA develop into widely recognized probes of chiral molecular structure and conformation.

5. ACKNOWLEDGMENTS

6. REFERENCES

1   G. Holzwarth, E.C. Hsu, H.S. Mosher, T.R. Faulkner and A. Moscowitz, J. Am. Chem. Soc., 96 (1974) 251.

2   L.A. Nafie, J.C. Cheng and P.J. Stephens, J. Am. Chem. Soc. 97 (1975) 3842.

3   T.A. Keiderling, Appl. Spectrosc. Rev. 17 (1981) 189.

4   L.A. Nafie, in Vibrational Spectra and Structure, Vol. 10, J.R. Durig (ed.), Elsevier, Amsterdam, 1981, p. 153.

5   L.A. Nafie and D.W. Vidrine, in Fourier Transform Infrared Spectroscopy, Vol. 3, J.R. Ferraro and L.J. Basile (eds.), Academic Press, New York, 1982, p. 83.

6   L.A. Nafie, in Advances in Infrared and Raman Spectroscopy, Vol. 11, R.J.H. Clark and R.E. Hester (eds.) Wiley-Heyden, Chichester, 1983, p. 49.

7   P.L. Polarvarapu, in Vibrational Spectra and Structure, Vol. 13, J.R. Durig (ed.), Elsevier, Amsterdam, 1984, p. 103.

8   P.L. Polavarapu, in Fourier Transform Infrared Spectroscopy, Vol. 4, J.R. Ferraro and L.J. Basile (eds.), Academic Press, New York, 1985, p. 61.

9   P.J. Stephens, Ann. Rev. Phys. Chem. 36 (1985) 213.

10   T.B. Freedman and L.A. Nafie in Topics in Stereochemistry, Vol. 17, E.L. Eliel and S.H. Wilen (eds.), Wiley, New York, 1987, p. 113.

11   L.A. Nafie in Advances in Applied Fourier Transform Infrared Spectroscopy, M.W. Mackenzie (ed.), Wiley, Chichester, 1988, p.67.

12   P.L. Polavarapu, in Vibrational Spectra and Structure, Vol. 17B, H.D. Bist, J.R. Durig and J.F. Sullivan (eds.), Elsevier, Amsterdam, 1989, p. 319.

13   T.A. Keiderling, in Practical Fourier Transform Infrared Spectroscopy, J.R. Ferraro and K. Krishnan (eds.), Academic Press, San Diego, 1990, 203.

14   A. Rauk, in New Developments in Molecular Chirality, P.G. Mezey (ed.), Kluwer Academic Publishers, Dordrecht, The Netherlands, 1991, p.57.

15   M. Diem, in Vibrational Spectra and Structure, Vol. 19, J.R. Durig (ed.), Elsevier, Amsterdam, 1991, p.1

16   T.A. Keiderling and P. Pancoska, in Advances in Spectroscopy, Vol. 20, R.E. Hester and R.J.H. Clark (eds.), Wiley-Heyden, Chichester, 1993, in press.

17   T.B. Freedman and L.A. Nafie, in Advances in Chemical Physics, Vol. 85B, M. Evans and S. Kielich (eds.), Wiley, New York, 1993, in press.

18   L.D. Barron , M.P. Bogaard and A.D. Buckingham, J. Am. Chem. Soc. 95 (1973) 603.

19   W. Hug, S. Kint, G.F. Bailey and J.R. Scherer, J. Am. Chem. Soc. 97 (1975) 5589.

20   L.D. Barron, Molecular Light Scattering and Optical Activity, Cambridge Univ. Press, Cambridge, 1982.

21   L.D. Barron and J.Vrbancich, Topics in Current Chemistry, 123 (1984) 151.

22   L.D. Barron, in Laser Scattering Spectroscopy of Biological Objects, J. Stepanek, P. Anzenbacher and B. Sedlacek (eds.) Elsevier, Amsterdam, 1987, p. 27.

23   L.A. Nafie and C.G. Zimba, in Biological Applications of Raman Spectroscopy, Vol. 1, T.G. Spiro (ed.) Wiley, New York, 1987 p. 307.

24   L.D. Barron, in Vibrational Spectra and Structure, Vol. 17B, H.D. Bist, J.R. Durig and J.F. Sullivan (eds.) Elsevier, Amsterdam, 1989 p. 343.

25   L.D. Barron and L. Hecht, in Advances in Spectroscopy, Vol. 20, R.E. Hester and R.J.H. Clark (eds.), Wiley-Heyden, Chichester, 1993, in press.

26   L.A. Nafie and D. Che, in Advances in Chemical Physics, Vol. 85B, M. Evans
     and S. Kielich (eds.) Wiley, New York, 1993, in press.
27   T.B. Freedman and L.A. Nafie, in Metallochemistry, Methods in
     Enzymology, Part C, J.F. Riordan and B.L. Vallee (eds.), Academic Press,
     Orlando, 1993 (in press).
28   L.A. Nafie and T.B. Freedman, in Metallochemistry, Methods in
     Enzymology, Part C, J.F. Riordan and B.L. Vallee (eds.), Academic Press,
     Orlando, 1993 (in press).
29   L.D. Barron and A.D. Buckingham, Mol. Phs. 20,(1971) 1111
30   L.D. Barron and J.F. Torrance, Chem. Phys. Lett. 102 (1983) 285.
31   L.A. Nafie, Chem. Phys. Lett. 102 (1983) 287.
32   K.M. Spencer, T.B. Freedman and L.A. Nafie, Chem. Phys. Lett. 149 (1988)
     367.
33   L.D. Barron and A.D. Buckingham, Ann. Rev. Phys. Chem. 26 (1975) 381.
34   L.A. Nafie and T.B. Freedman, Chem. Phys. Lett. 154 (1989) 260.
35   D. Che, L. Hecht and L.A. Nafie, Chem. Phys. Lett. 180 (1991) 182.
36   Y.N. Chirgadze, S.Y. Venyaminov, and V.M. Lobachev, Biopolymers 10
     (1971) 809.
37   L. Hecht and L.A. Nafie, Chem. Phys. Lett. 174 (1990) 575.
38   R.A. Harris and W.M. McClain, Chem. Phys. Lett. 195 (1992) 633 .
39   L. Hecht and L.A. Nafie, Chem. Phys. Lett. 195 (1992) 637.
40   J.C. Kemp J. Opt. Soc. Amer. 59 (1969) 661.
41   J.C. Cheng, L.A. Nafie, S.D. Allen and A.I. Braunstein, Appl. Opt. 15 (1976)
     1960.
42   P.R. Griffiths and J.A. de Haseth, Fourier Transform Infrared Spectroscopy,
     Wiley, New York, 1986, p.216.
43   P.L. Polavarapu, Chem. Phys. Lett. 148 (1988) 21.
44   I. Chabay and G. Holzwarth, Appl. Opt. 14 (1975) 454
45   L.A. Nafie, T.A. Keiderling and P.J. Stephens, J. Am. Chem. Soc. 98 (1976)
     2715.
46   P.J. Stephens and R. Clark, in Optical Activity and Chiral Discrimination,
     S.F. Mason (ed.), Reidel, Dordrecht, 1979, p.263.
47   S.F. Mason, in Advances in Infrared and Raman Spectroscopy, Vol. 8, R.J.H.
     Clark and R.E. Hester (eds.), Heyden, London, 1980, p.283.
48   C.N. Su, V.J. Heintz and T.A. Keiderling, Chem. Phys. Lett. 73 (1980) 157.
49   C.N. Su, Ph.D. Thesis, University of Illinois, Chicago Circle (1981).
50   F. Devlin and P.J. Stephens, Appl. Spectrosc. 41 (1987) 1142.
51   M. Diem, G.M. Roberts, O. Lee and A. Barlow, Appl. Spectrosc. 42 (1988) 20.
52   O. Lee and M. Diem, Anal. Instr. 20 (1992) 23.
53   M. Diem, This book - Chapter XX.
54   M.F. Russel, M. Billardon and J.P. Badoz, Appl. Opt. 11 (1973) 2375.
55   L.A. Nafie and M. Diem, Appl. Spectrosc. 33 (1979) 130.
56   L.A. Nafie, M. Diem and D.W. Vidrine, J. Am. Chem. Soc. 101 (1979) 496.
57   E.D. Lipp and L.A. Nafie, Appl. Spectrosc. 38 (1984) 20.
58   P.L. Polavarapu, Appl. Spectrosc. 38 (1984) 26.

88

59 P.L. Polavarapu, D.F. Michalska and D.M. Back, Appl. Spectrosc. 38 (1984) 438.
60 E.D. Lipp and L.A. Nafie, Appl. Spectrosc. 38 (1984) 774.
61 P. Malon and T.A. Keiderling, Appl. Spectrosc. 42 (1988) 32.
62 C.A. McCoy and J.A. de Haseth, Appl. Spectrosc. 42 (1988) 336.
63 P.L. Polavarapu, Appl. Spectrosc. 43 (1989) 1295.
64 R.A. Shaw, N. Ibrahim and H. Wieser. J. Phys. Chem. 94 (1990) 125.
65 R.K. Yoo, P.V. Croatto, B. Wang and T.A. Keiderling, Appl. Spectrosc. 45 (1991) 231.
66 M.J. Dignam and M.D. Baker, Appl. Spectrosc. 35 (1981) 186.
67 H. Ishida, Y. Ishimo, H. Buijs, C. Tripp and M.J. Dignam, Appl. Spectrosc. 41 (1987) 1288.
68 L.A. Nafie, N.S. Lee, M.G. Paterlini and T.B. Freedman, Mikrochim. Acta [Wein] 1987 III (1987) 93.
69 N. Raguanathan, N.S. Lee, T.B. Freedman, L.A. Nafie, C.Tripp and H. Buijs, Appl. Spectrosc. 44 (1990) 5.
70 N. Ragunathan, Ph.D. Thesis, Syracuse University, 1991.
71 D.H. Martin and E. Puplett, Infrared Physics, 10 (1969) 105.
72 P.L. Polavarapu, Infrared Physics, 28 (1988) 109.
73 P.L. Polavarapu, in Polarization Considerations for Optical Systems II, SPIE 1166 (1989) 472.
74 S. Weibel and P.L. Polavarapu, Appl. Spectrosc. 44 (1990) 1369.
75 E.D. Lipp, C.G. Zimba and L.A. Nafie, Chem. Phys. Lett. 90 (1982) 1.
76 H. Boucher, T.R. Brocki, M. Moskovits and B. Bosnich, J. Am. Chem. Soc. 99 (1977) 6870
77 P.L. Polavarapu, M. Diem, and L.A. Nafie, J. Am. Chem. Soc. 102 (1980) 5449.
78 L.D. Barron, in Advances in Infrared and Raman Spectroscopy, Vol. 4, R.J.H. Clark and R.E. Hester (eds.), Heyden, London, 1978, p. 271.
79 L. A. Nafie and M. Diem, Acc. Chem. Res. 12 (1979) 296.
80 L.A. Nafie, in Vibrational Spectra and Structure, Vol. 10, J.R. Durig (ed.), Elsevier, Amsterdam, 1981, p. 153.
81 T. Brocki, M. Moskowits and B. Bosnich, J. Am. Chem. Soc. 102 (1980) 495.
82 W. Hug and H. Surbeck, Chem. Phys. Lett. 60 (1979) 186.
83 M.R. Oboodi, M.A. Davies, U. Gunnia, M.B. Blackburn and M. Diem, J. Raman Spectrosc. 16 (1985) 366.
84 L.D. Barron, J.F. Torrance and D.J. Cutler, J.Raman Spectrosc. 18 (1987) 281.
85 C.G. Zimba, T.B. Freedman, K.M. Spencer, X.-M. Hu, and L.A. Nafie, Chem. Phys. Lett. 134 (1987) 233.
86 L.D. Barron, L. Hecht, W. Hug and M.J. MacIntosh, J. Am. Chem. Soc. 111 (1989) 8731.
87 L. Hecht, D. Che and L.A. Nafie, Appl. Spectrosc. 45 (1991) 18.
88 L. Hecht, L.D. Barron and W. Hug, Chem. Phys. Lett. 158 (1989) 341.
89 W. Hug, in Raman Spectroscopy, J. Lascombe and P.V. Huong (eds.), Wiley-Heyden, New York, 1982, p.1.
90 L.D. Barron, L. Hecht, A.R. Gargaro and W. Hug, J. Raman Spectrosc. 21 (1990) 375.

91 L.D. Barron, A.R. Gargaro, L. Hecht, Z. Q. Wen, and W. Hug, in Laser Applications in the Life Sciences, S.A. Akhmanov, M.Y. Poroshino, N.I. Koroteev and B.N. Toleutaev, eds., SPIE Vol. **1403**, 66 (1991)

92 L. Hecht, L.D. Barron, A.R. Gargaro, Z.Q. Wen and W. Hug, J. Raman Spectrosc. 23 (1992) 401.

93 L.D. Barron, A.R. Gargaro and L.Hecht in Proceedings of the 12th International Conference on Raman Spectroscopy, J.R. Durig andJ.F. Sullivan, (eds.) Wiley, New York, 1990, p.834.

94 L.D. Barron, A.R. Gargaro, L.Hecht and P.L. Polavarapu, Spectrochim. Acta 47A (1991) 1001.

95 L.D. Barron, A.R. Gargaro, L.Hecht and P.L. Polavarapu, Spectrochim. Acta 48A (1992) 261.

96 L.D. Barron, A.R. Gargaro and Z.Q. Wen, J. Chem. Soc. Chem. Comm. 1034 (1990).

97 L.D. Barron, Z.Q. Wen and L. Hecht, J. Am. Chem. Soc., 114 (1992) 784.

98 L.D. Barron, A.R. Gargaro, Z.Q. Wen, D.D. MacNicol and C. Butters, Tetrahedron: Asymmetry 1 (1990) 513.

99 L.D. Barron, A.R. Gargaro, Z.Q. Wen, Carb. Res. 210 (1991) 39.

100 L.D. Barron, L.Hecht and P.L. Polavarapu, Spectrochim. Acta 48A (1992) 1193.

101 P.L. Polavarapu, J. Phys. Chem. 94 (1990) 8106.

102 L. Hecht, D. Che and L.A. Nafie, J. Phys. Chem. 96 (1992) 4266.

103 D. Che and L.A. Nafie, Chem. Phys. Lett. 189 (1992) 35.

104 L.A. Nafie, D. Che, G.-S. Yu and T.B. Freedman in Biomolecular Spectroscopy II, R.R. Birge and L.A. Nafie, (eds.), SPIE 1432 (1991) 37.

105 L.A. Nafie in Lectures and Posters of the Fourth International Conference on Circular Dichroism, Bochum, Germany, H. Klein and G. Snatzke, (eds.), Ruhrgebiet, Essen, 1991 p. 101.

106 L.A. Nafie in Optically Based Methods for Process Analysis, J.M. Lerner, (ed.), SPIE 1681 (1992) in press.

107 G.-S. Yu, D. Che, T.B. Freedman and L.A. Nafie, Tetrahedron Asymm. 4 (1993) 511.

108 L. Hecht and L.A. Nafie, Molec. Phys. 72 (1991) 441.

109 L. Hecht, unpublished results.

110 D. Che, Ph.D. Thesis, Syracuse University, 1992

111 L.D. Barron, J.R. Escribano and J.F. Torrance, Mol. Phys. 57 (1986) 653.

112 L.D. Barron and J.R. Escribano, Chem. Phys. Lett. 126 (1986) 461.

113 L. D. Barron, L. Hecht and S.M. Blyth, Spectrochimica Acta 45A (1989) 375.

114 L.D. Barron and L. Hecht, Spectrochimica Acta 45A (1989) 671

115 W. Hug, Appl. Spectrosc. 35 (1981) 115.

116 L.D. Barron and J. Vrbancich, J. Raman Spectrosc. 15 (1984) 47.

117 L. Hecht and L.D. Barron, Appl. Spectrosc. 44 (1990) 483.

118 D. Che and L.A. Nafie, Appl. Spectrosc. (in press).

119 L. Hecht, Chem. Phys. Lett. 195 (1992) 518.

This Page Intentionally Left Blank

Chapter 4

Application of infrared CD to the analysis of the solution conformation of biological molecules

Max Diem

Department of Chemistry, City University of New York, Hunter College
695 Park Avenue, New York, NY 10021

Abstract
     This article presents the application of a novel technique, which combines the structural sensitivity of vibrational spectroscopy with the conformational sensitivity of chiroptical methods to study the solution conformation of biological molecules. Instrumental aspects, computational methods and spectral results for peptides and nucleic acids will be discussed.

Outline

1. INTRODUCTION

Over the past decade, a new spectroscopic technique called infrared or vibrational circular dichroism (VCD) has been applied to study the molecular conformation of biomolecules. Observation of VCD had been attempted for some years because of the conformational information which was predicted on theoretical grounds. However, all experimental efforts prior to 1974 failed due to the small magnitude of the effect. Even since its first experimental verification nearly simultaneously by Holzwarth and coworkers [1] and Stephens and coworkers [2], it took over a decade until results on large biomolecules in aqueous solution were reported [3]. In this article, a broad review of experimental results obtained for biological molecules will be presented, along with a discussion of experimental aspects and computational methods applicable to biological systems. The experimental results to be discussed will deal with peptides and nucleic acids. In both cases, results for small model systems, large homo-oligomers with regular structures, as well as some naturally occurring molecules will be presented, and methods to extract conformational information will be discussed.

1.1. Phenomenological Description and Basic Equations

Conceptually, one may view VCD as an extension of the principles of electronic circular dichroism (CD), normally observed in the ultraviolet spectral region (UV-CD), into the realm of vibrational transitions in the infrared spectral region. CD itself is one manifestation of natural optical activity and is mathematically related to Optical Rotatory Dispersion (ORD), or the rotation of plane polarized light by an optically active medium. Optical activity, which is a property exhibited by enantiomerically pure, chiral molecules, is one of the most fascinating spectroscopic phenomena. Chiroptical techniques, one of which is CD, are specialized spectroscopic methods to determine the chirality of molecules. They measure differential interaction of left and right circularly polarized light with chiral molecules. Most of the time, these interactions are monitored *via* absorption methods, although differential interactions have been observed in emission spectroscopy as well, *via* fluorescence (fluorescence detected circular dichroism) and (vibrational) Raman scattering, Raman Optical Activity (ROA).

Optical activity is created through the interference of molecular electronic (μ) and magnetic (m) dipole transition moments:

$$R_{01} = \text{Im} \left[\langle 0 \mid \mu \mid 1 \rangle \cdot \langle 1 \mid m \mid 0 \rangle \right] \tag{1}$$

The quantity R_{01} is called the *Rotatory Strength*, in analogy to the dipole strength of a transition:

$$D_{01} = \langle 0 \mid \mu \mid 1 \rangle^2 \tag{2}$$

where 0 and 1 denote ground and excited state wave functions of the system. Since most optical activity was originally observed as optical rotation, the optical activity created *via* equation 1 was always associated with the ability of a transition to rotate the plane of light, which explains the name given to R.

Electronic CD (ECD), observed most commonly between 180 and 300 nm and also referred to as UV-CD, is a measure of the differential molar absorptivities a of the sample toward left and right circularly polarized light:

$$\Delta a = a_L - a_R \tag{3}$$

Since the differential molar absorptivity, Δa can be related to the theoretically relevant quantity, R,

$$R_{01} = \int (\Delta a / \nu) \, d\nu \tag{4}$$

it is most appropriate to express the observed CD in terms of this differential absorptivity, which may be converted easily, *via* path length and concentration, to the actually observed differential absorption,

$$\Delta A = A_L - A_R \tag{5}$$

For ECD, the wave functions referred to in equations 1 and 2 are, of course, electronic wave functions, and the differential absorption may be 1 to 0.1 % of the absorption. Differential signals of this magnitude are easily accessible experimentally, since the extinction coefficients for electronic transitions are large, and since efficient spectrometers can be constructed in this spectral range of high energy photons.

In VCD, the differential absorption of left and right circularly polarized infrared radiation by a vibrational transition of a chiral molecule is observed. Equations (1 - 5) hold equally well for electronic and vibrational transitions, but in all transition moments, the electronic wave functions need to be replaced by vibrational (or vibronic) wave functions. In vibrational CD, the ratio of differential absorption to the infrared absorption, defined as

$$\Delta A / A = 4 R_{01} / D_{01} \tag{6}$$

is about 10^{-5}, or about two orders of magnitude smaller than in ECD. This much smaller magnitude, coupled with the less efficient light sources and detectors in the infrared region, makes VCD a difficult experiment to perform, and accounts for the fact that VCD was not verified experimentally until 1974.

Through the diligent efforts of a few research groups in the field, VCD has now become a generally applicable spectroscopic technique. However, it is necessary, at this point, to clarify why it is important to pursue a spectroscopic technique which is so experimentally challenging. In the following section, a short assessment of the utility of VCD will be presented, comparing it to other spectroscopic techniques for the determination of the solution conformation of biological molecules.

1.2. Comparison of spectroscopic techniques for the determination of the solution conformation of biomolecules

The present understanding of processes in modern biology and medicine has resulted from a detailed knowledge of the structure of biomolecules and the structural changes accompanying interactions of biomolecules. To date, X-ray crystallography has probably revealed more structural information of biomolecules than all other physical

techniques combined. The results of these structural studies have revolutionized biology, although crystallographic results strictly apply to solid crystalline phases only. However, deductions about solution phase structures have been made from the structures in the solid phase, and compared with solution structures obtained spectroscopically or *via* other techniques.

Since biomolecular interactions and recognition occur in solution phase in biological systems, physical methods to determine the solution phase structures directly are of prime importance in modern biophysical research. Among all the spectroscopic techniques available, nuclear magnetic resonance (NMR) spectroscopy has clearly emerged as the most powerful solution structural tool. NMR often yields as detailed structural information as crystallography for biological molecules, such as peptides of up to about 150 amino acids. The activity in this field of research is so high that it is impossible to review it here, and the reader is referred to a number of excellent reviews [4,5].

However, one of the interesting aspects of NMR structural results is that they often suggest no discernible solution structure for small systems, such as a tri- or tetrapeptides. This is due to the flexibility and structural variance displayed by these sample systems. However, the lack of interactions between parts of the molecule, which normally are detected *via* Nuclear Overhauser enhancements and refined into molecular structures during NMR structural determinations, should not be interpreted as a lack of a solution structure. It is the slow time scale of NMR, coupled with the rapidly interconverting conformations, which weakens these effects to the point where they can no longer be detected with certainty, and structural techniques which operate on a much faster time scale (*e.g.*, UV-CD spectroscopy, or forms of vibrational spectroscopy) demonstrate that there is a preferred class of solution conformers even in small peptide systems.

Thus, it is sensible to supplement the available resonance spectroscopic methods with other methods, which sample molecular conformation *via* different interactions, and at different spatial and temporal resolution. By virtue of their origin, chiroptical techniques have played an enormously important role in the derivation and establishment of solution structures. ECD has been used very successfully to establish solution conformation of nucleic acids and peptides. In a macromolecule with a fixed structure, such as a helix, repeating units which incorporate an electronic transition are arranged in fixed geometric patterns. The coupling of these transitions yields CD features which not only allow a qualitative identification of a secondary structure, but also reveal quantitative information about the angles between the interacting transitions. In the exciton model, to be discussed in more detail in Section 3 of this article, the rotational strength created by the coupling of interacting transitions depends on expressions of the form:

$$R \propto [T_{ij} \cdot \mu_i \times \mu_j] \tag{7}$$

where μ_i and μ_j are the interacting dipole transition moments, and T_{ij} are the distances between these dipoles. The conformational sensitivity of CD (and VCD) results from the vector cross product in equation 7, as will be discussed later in Section 3.

Thus, CD spectroscopy is a very sensitive tool to monitor conformational changes between well-defined solution structures. However, the interpretation of UV-CD spectra is often complicated by the broadness and overlap of the peaks. This is

particularly true in the case of nucleotides, where the electronic transitions of the bases are superimposed, and where the exact nature and direction of the dipole transition moments, the coupling of which give rise to the observed CD spectra, are not well established. In peptides, two transitions ($\pi^* \leftarrow n$ and $\pi^* \leftarrow \pi$) occur and overlap in the region where the exciton CD is observed, thus, complicating the spectral interpretation. Furthermore, electronic transitions are often not sensitive toward small chemical changes in molecules, unless the chemical modification involves the electronic chromophore, and lack the structural sensitivity of other spectroscopic techniques.

Vibrational spectroscopy *per se* is not a very good quantitative probe of molecular conformation either, although it has been used quite successfully as a qualitative probe. To date, most of these efforts have utilized the frequency shift of certain vibrations, such as the peptide amide I and III vibrations, and certain B or Z-form specific Raman bands in nucleic acids, as markers for secondary structure. These methods are feasible because normal modes of vibrations are sensitive to subtle changes in the surroundings of the probe groups. Best results are obtained for large, well defined secondary structures. Yet, in both Raman and IR techniques, the use of frequency shifts alone to monitor secondary conformation is somewhat ambiguous and will not yield conformational angles directly and quantitatively.

The combination of the principles of vibrational spectroscopy with those of optical activity leads to new spectroscopic techniques, collectively referred as vibrational optical activity (VOA). There are two techniques in VOA, infrared CD (VCD) and Raman optical activity (ROA), just as there are two techniques in conventional vibrational spectroscopy. In VOA, the enormous sensitivity of chiroptical techniques towards the relative orientation of interacting groups is coupled with the advantages of vibrational spectroscopy, namely transitions, which are narrow, well resolved and reasonably sensitive to structural variations (the vibrational "fingerprints"). Therefore, VOA was viewed for a long time as an ideal new tool for conformation investigations of biological molecules, and the observation of optical activity in vibrational transitions was first attempted (unsuccessfully) over five decades ago. Theoretical predictions were published about the magnitudes and conformational sensitivity of vibrational optical activity even before its experimental verification.

Among the two techniques of VOA, VCD was the first to be utilized to solve problems of real biophysical and biostructural significance. Mostly due to insufficient instrumental sensitivity, these studies were not possible until the mid- to late 1980's, when VCD was first applied to study the conformation of homo-polyamino acids in aqueous and non-aqueous media.

The conformational sensitivity of VCD in the amide I region of peptides can be thought of as being due to the dipolar coupling of the $C = O$ stretching vibrations of the peptide linkages according to equation 7. The coupling of these transitions produces distinct VCD and infrared absorption spectra, to be discussed later in detail: the VCD patterns are known as positive and negative couplets, and the infrared spectra show multiplet structures. These spectral features will permit a quantitative determination of dihedral angles between the coupled oscillators. This point was, in fact, recognized prior to the experimental verification of VCD: signs and intensities of coupled oscillator VCD were calculated for poly-amino acids, and the amide A and I VCD was predicted [6].

Similarly, the $C = O$ stretching dipole transition moments of the bases in helical DNA and RNA couple, and give rise to distinct, conformation dependent VCD signals

between 1550 and 1750 cm^{-1}. Since these modes are localized on groups which are achiral, the VCD is nearly entirely due to the dissymmetric coupling of these transitions according to equation 7, which is sensitive to the geometry between the groups. Since VCD is a form of vibrational spectroscopy, it probes DNA and peptide structures at a very fast time scale, and with a conformational specificity that is unavailable by any other experimental means.

The vibrations discussed so far occur in the 6 μm spectral region in the mid-infrared; however, most vibrational modes in a molecule will exhibit VCD, and other vibrations in the 12 μm, as well as the 3.5 to 2.5 μm range, have shown interesting VCD results. In this article, only the 6 μm region (the C=O stretching vibration) will be discussed. To observe VCD in this spectral region, a chiroptical instrument with infrared optics (with materials such as CaF$_2$) needs to be constructed.

In the remainder of this article, some instrumental aspects for the measurement of VCD will be introduced, followed by a discussion of the existing methods to compute VCD for model biological molecules. The last two Sections deal with results obtained by the author, and other research groups, for peptides and nucleic acids.

2. INSTRUMENTAL ASPECTS

Although VCD was first reported nearly two decades ago in 1974 [1,2], progress in the field has been slow, and observation of VCD in the mid-infrared region (5 to 10 μm, or 2000 to 1000 cm^{-1}) in aqueous solutions was not possible until the mid 1980's. VCD is now at a stage where it can reveal solution structural information on biological molecule which is not available from any other technique.

In the past, VCD has been observed *via* one of two experimental approaches: dispersive and Fourier transform (FT) instrumentation. For biological samples, where there are normally no enantiomeric samples available to check for the accuracy of the measurement, dispersive instruments have been used nearly exclusively. These instruments will be described in detail in Section 2.2, and FT-VCD instrumentation in Section 2.3.

2.1. Theory and Principles of the Measurement of VCD

As pointed out above, the differential absorbance ΔA observed in VCD is very small, typically on the order of 5×10^{-4} to 5×10^{-5} of the infrared absorption A. In order to observe effects of this magnitude, sophisticated modulation techniques need to be employed, and instruments with very high light throughput and the most sensitive available detectors need to be constructed. This is particularly true for the study of biological molecules *via* VCD, since water is a necessary solvent for these studies, and the transmission of H$_2$O or D$_2$O is low in the infrared spectral region.

For the measurement of differential absorption spectra in the visible and ultraviolet spectral region, a light modulation technique was introduced over two decades ago [7]. The principle of this measurement also governs the measurement of infrared VCD. This technique involves the high frequency modulation of the exciting beam between left and right circular polarization states *via* a photoelastic modulator, and measuring the differential absorption with a lock-in amplifier tuned to the modulation frequency.

For VCD measurement, the actual differential signal, at constant CD of the sample, will vary with the light level transmitted at a given wavelength. Denoting the signal at the modulator frequency as $I_{AC}(\nu)$, and the overall transmission of the instrument and sample as $I_{DC}(\nu)$, it can be shown from an analysis of the radiant energy at the detector that

$$I_{AC}(\nu) / I_{DC}(\nu) = \tanh (1.15 \, \Delta A) \sin \alpha \tag{8}$$

Here, α denotes the retardation between two linearly polarized components of light used for the production of circularly polarized light (*vide infra*), and equation 8 demonstrates that the ratio $I_{AC}(\nu) / I_{DC}(\nu)$ is proportional to ΔA. The term $\sin \alpha$ itself varies sinusoidally with time, since the retardation α may be written as

$$\alpha = \alpha_0 \sin (\omega_M t) \tag{9}$$

where ω_M is the oscillation frequency of the modulator. The sine of a sine function may be expressed in terms of the Bessel function, $J_1(\alpha)$. Thus,

$$I_{AC}(\nu)/I_{DC}(\nu) = \tanh(1.15 \, \Delta A) \, J_1(\alpha_o) \sin(\omega_M t) \tag{10}$$

Inspection of equation 10 yields that for the observation of ΔA, a signal in phase with ω_M must be monitored *via* a lock-in amplifier and continuously divided by the DC signal.

At the heart of all chiroptical instruments is the device that produces alternating left and right circularly polarized light, the photoelastic modulator (PEM). This device uses the phenomenon of stress birefringence to introduce a phase difference between two orthogonally polarized components of light incident on the modulator. The PEM crystal consists of a uniaxial piece of material which is transparent in the spectral range of interest and is aligned with its unique axis (the z axis) along the propagation direction of the light. Under the influence of a mechanical stress or strain, applied perpendicularly to the propagation direction of the light, and along the crystals x or y axes, the refractive indices along these axes, n_x and n_y become unequal, causing light waves polarized along the x and y directions to travel with different velocities through the crystal. At the exit face of the crystal, circularly polarized light is produced if the retardation between the two orthogonal components of light is $\lambda/4$.

The alternating strain/stress is produced by squeezing the modulator crystal between two piezoelectric drivers. An AC voltage is applied to the piezoelectric crystals, and the amplitude of this voltage determines the stress/strain and therewith, the retardation. Commercial modulators are available for the infrared region, using CaF_2 above 1200 cm^{-1}, and ZnSe down to about 600 cm^{-1} as stress optical materials. The retardation of a PEM varies sinusoidally at the modulator frequency ω_M, which is determined by the crystal material, and its size, and the retardation level depends on the voltage applied to the piezoelectric drivers.

Other methods of phase modulation exist, for example using an electro-optic modulator (EOM), where the birefringence is produced by applying a voltage across an electro-optic crystal. PEM's have several advantages over EOM's, among them a better thermal stability, larger angle of acceptance, and stable frequency modulation. In addition, EOM's for the infrared region are difficult to construct.

2.2. Dispersive VCD Instrumentation

The optical and electronic design of a typical dispersive VCD unit (for example, one of two operating spectrometers at Hunter College [8-10]) is summarized in Figure 1. The light source utilized is a small (1.8 mm diameter, 12 mm useful length) Nernst glower which is heated by an AC current of *ca.* 1.6 amp at 80 volt to about 2400 K. It is chemically sufficiently inert that it may be operated without a protective atmosphere, and its major advantage is its small size: if the light is collected at f/4 and imaged 1:1 into an f/4 monochromator, a slit width of only 1.8 mm is needed to transmit the entire image. Depending on the wavelength range being studied, this mechanical slit width produces a spectral resolution of between 5 and 8 cm⁻¹. The light from the source may also be collected at f/2 and imaged into the monochromator at f/4 with an image magnification of 2. Even at 3.5 mm slits, the resolution is adequate in the region below 1200 cm⁻¹ with the monochromator utilized.

The light collection mirrors of the instrument, as well as the optical elements within the monochromator (including the grating) are gold coated for enhanced reflectivity. The light from the source is modulated at 79.5 Hz by a mechanical chopper, and focused into a high aperture Czerny-Turner monochromator of appropriate focal length, and equipped with a suitable grating, to produce the desired dispersion. Typically, one wishes to operate at a slit width of a few millimeters to transmit the entire image of the source, and still produce acceptable resolution of a few wavenumbers. Details of such designs may be found in the literature [9,10].
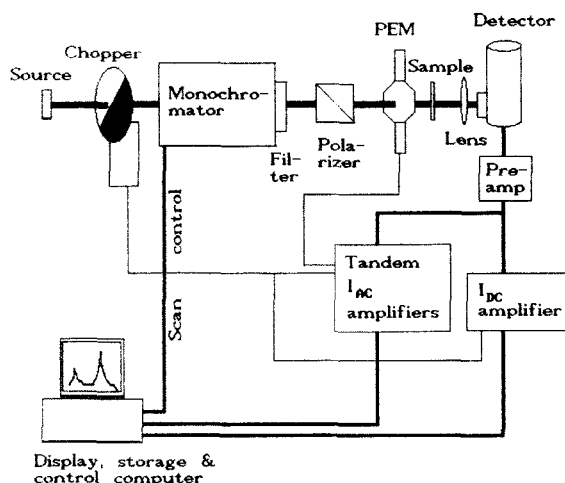
Figure 1. Schematic of a dispersive VCD spectrometer. Heavy lines denote the light path, medium lines the signal path, and thin lines the reference signals.

Upon leaving the monochromator, the light passes through an appropriate band pass filter to remove higher order diffractions, and is recollected and passes through a gold grid polarizer into the PEM. The major stress axis of the PEM is at 45° with respect to the plane of polarization transmitted by the polarizer. The sample is mounted directly behind the PEM in a standard, demountable and temperature controlled IR

cell. Sample volumes as low as 20 μL are used routinely.

The light emerging from the sample is recollected by a single CaF_2 or BaF_2 lens and focussed onto the detector. It is essential that as few optical elements as possible are used between the sample and the detector, and that these elements are as free of optical stress as possible, since stress birefringence at this stage may induce artifacts. In addition, reflective optics should be avoided.

Liquid nitrogen cooled, photoconductive HgCdTe detectors with peak sensitivities between 7 and 12 μm, and detectivities D^* between 5×10^{10} to 9×10^{10} [cm $Hz^{1/2}$ W^{-1}] are suitable. For operation at 6 μm, the instrument needs to be purged with dry air to reduce atmospheric water vib-rotational absorptions.

Electronically, the dispersive instrument operates as follows. The signal from the detector is split into two paths (cf. Figure 1). One of them leads into a low-cost lock-in amplifier which monitors the total signal at 79.5 Hz (I_{DC}). Its output is read directly by the instrument control computer via an A/D board. The other signal path is used to measure I_{AC}. Here, the signal is first demodulated at the PEM frequency (31.2 kHz) by a lock-in amplifier operating in bandpass mode with Q of 50, high-dynamic reserve, and minimum time constant at 12 dB/oct. The gain of this lock-in amplifier, which is defined by the ratio of full-scale DC output voltage (10V) to the input sensitivity, is usually between 10^3 and 10^4; i.e., input sensitivity ranges between 10 and 1 mV full scale are used. The output of this amplifier is further demodulated by a lock-in amplifier (Princeton Applied Research, Model 5207) tuned to 79.5 Hz (cf. Figure 1). This unit is a sophisticated, heterodyning amplifier, all functions of which can be monitored or serviced by an external computer. This is a very important factor, since it allows the measurement of output values with 3.5 digit accuracy over the entire full-scale sensitivity range of the unit, which is from 100 nV to 5V. In this fashion, we circumvent the major problem which persisted with the analog (auto)-normalization technique used previously [11], namely the restriction in dynamic range.

During VCD data acquisition, I_{DC} and I_{AC} are read by a computer at each data point, and the value of ΔA is computed and displayed vs. wavenumber in real time. Also on screen is an absorption spectrum of the sample, collected during the prescan. This "prescan" (forward without sample, reverse with sample) produces the infrared spectrum in absorbance units. The prescan is also employed to test for insufficient light levels at the detector in case of too high sample concentration or too long path length. This prescan is collected via the lock-in amplifier which monitors I_{DC} during the VCD acquisition.

Although a Czerny-Turner monochromator scans linearly in wavelength units, VCD data are collected linearly in wavenumber increments. This is accomplished by computing the next monochromator wavelength from the linear wavenumber increment and scanning the monochromator to this wavelength. The wavelength increments are, of course, not constant over a VCD scan. The retardation level of the PEM is synchronized to the wavelength of the monochromator in order to modulate at $\lambda/4$ at every wavelength during a scan. This synchronization is accomplished by issuing a voltage which controls the PEM modulation amplitude from a D/A converter to the retardation level input of the PEM. This voltage is recalculated at each wavenumber increment.

The control of the monochromator stepping motor, the PEM retardation level, and the lock-in amplifiers, are carried out by a standard IBM-compatible personal computer. It communicates with the PAR lock-in amplifier via a 1200 baud serial link,

and with the remainder of the electronics *via* a 24 bit parallel bus. The software operating the VCD instrument is completely menu driven, and makes instrument operation as easy and reliable as data collection from a standard computerized infrared spectrometer. Off-line data manipulation software, including smoothing, deconvolution, coaddition, integration, *etc.* routines, has been developed in-house specifically for application in VCD.

2.3. FT-VCD Instrumentation

As early as 1978, the possibility of observing VCD *via* Fourier Transform (FT) interferometric methods was investigated [12], mostly with the goal to improve the signal/noise of the measurement and to reduce data acquisition time. Unfortunately, the advantage of FT-VCD over dispersive VCD has been much smaller than the advantage between FT-IR and dispersive IR absorption spectroscopy.

FT-VCD is currently not being carried out in the author's laboratory, although he was involved in the early experiments in this field [12,13]. FT-VCD is commonly observed using a PEM after a standard Michelson interferometer, and both a DC and an AC interferogram are collected in different data acquisitions [14]. Both interferograms are transformed, and division yields the VCD spectrum. Certain well documented initial difficulties have been overcome [15]. However, the improvement (measured in a decrease in acquisition time) of FT-VCD over dispersive instrumentation is negligible for aqueous solutions of biological molecules, where only relatively narrow spectral windows are accessible due to solvent interference. The situation definitely turns in favor of FT-VCD in the case of gaseous or neat liquid samples, where the multiplexing advantage allows large portions of spectral data to be acquired simultaneously.

One of the major advantages of the dispersive instrument is the possibility of computer adjusting the electronics at any spectral point such that the signal can be processed under optimum conditions. This is possible because the signal varies slowly with time, and because the data are not multiplexed. Furthermore, synchronization of the PEM retardation with the wavelength transmitted by the monochromator can be achieved, which results in maximum circular polarization at each wavelength, and therefore, an automatically calibrated signal at optimum amplitude.

One of the major disadvantages of the dispersive system is the fact that the bandpass, and consequently the optical resolution, of the instrument changes with wavelength [9,10], whereas it is constant over a spectral region in FT-VCD. Furthermore, higher resolution will seriously degrade the signal-to-noise ratio in dispersive VCD, and the data acquisition time increases with the spectral range over which data are collected. Thus, the collection of a large spectral range at high resolution is costly in terms of data acquisition time.

3. COMPUTATIONAL METHODS

Tinoco [16] pointed out in 1963 that "once the wave functions for a molecule have been obtained, it is obvious that any optical properties of the system can be computed", including, of course, any optical activity exhibited by a biological polymer. Reality, however, appears somewhat less optimistic, due to the enormous size of the

molecules occurring in biological systems. *Ab initio* quantum mechanical calculations of VOA intensities have been carried out recently by a number of researchers; however, the methods are too time consuming to be applicable to systems of more than ten atoms or so. Thus, approximate methods need to be employed. One of these is the exciton model for optical activity, to be discussed in the next section.

3.1. The Exciton Model for VCD Intensities

One of the dominant mechanisms, which gives rise to VCD (and CD) intensities of polymers, is the coupling of many identical or near identical polar transitions such as the $C=O$ stretching vibrations of the purine or pyrimidine, or the peptide amide I (carbonyl stretching) vibrations, which are arranged in a fixed geometry. If one vibrational quantum is absorbed by these degenerate oscillators, the resulting vibrationally excited state is best described by a sum over all possible one-quantum excitations. This implies that the excitation is no longer localized on one of the oscillators, but is delocalized over the entire array of identical oscillators. This delocalized excitation is referred to as an "exciton" [17]. The dipolar coupling between the transitions lifts their degeneracy; consequently, one observes as many discrete exciton energy levels as there are interacting dipoles.

In the "degenerate extended coupled oscillator" (DECO) description of the optical activity of n interacting dipoles, the rotational strength R, and hence the VCD intensities, is given by [18]:

$$R_k = -(\pi \bar{\nu}_0/c) \sum_{i=1}^{n} \sum_{j>i}^{n} c_{ik} c_{jk} [T_{ij} \cdot \mu_i \times \mu_j] \tag{11}$$

where c is the velocity of light, and the c_{ij} are the eigenvector components of the (dipole- dipole) interaction matrix:

$$V_{ij} = \frac{\mu_i \cdot \mu_j}{|T_{ij}|^3} - \frac{3(\mu_i \cdot T_{ij})(\mu_j \cdot T_{ij})}{|T_{ij}|^5} \tag{12}$$

Here, T_{ij} is the distance vector between dipoles μ_i and μ_j, $\bar{\nu}_0$ is the center frequency (in wavenumbers) of the unperturbed transition, and the subscript k refers to the k'th exciton component ($1 < k < n$). The infrared absorption intensities can be obtained from the dipole strengths D, defined by

$$D_k = \sum_{i=1}^{n} \sum_{j>i}^{n} c_{ik} c_{jk} (\mu_i \cdot \mu_j) \tag{13}$$

In the dimeric case, the coupled oscillator equation predicts the rotational strengths R for the symmetric $| + \rangle$ and antisymmetric $| - \rangle$ combination states of two interacting vibrations according to

$$R^{\pm} = \mp (\pi \bar{\nu}_0 /2c) T_{12} \cdot \mu_1 \times \mu_2 \tag{14}$$

which is the well-known coupled oscillator equation derived independently by Holzwarth and Chabay [20], and by Tinoco [16].

For near-degenerate vibrational transitions, such as certain $C=O$ and $C=N$ stretching vibrations in nucleic acid bases, equation 12 needs to be modified as follows:

$$R_k = -(\pi/c) \sum_{i=1}^{n} \sum_{j>i}^{n} c_{ik} c_{jk} [(\bar{\nu}_j X_j - \bar{\nu}_i X_i) \cdot \mu_i \times \mu_j] \tag{15}$$

In this "non-degenerate extended coupled oscillator (NECO)" equation [25], the X are the coordinates of the center of mass of an oscillator. If $\bar{\nu}_i = \bar{\nu}_j$, equation 15 simplifies to the DECO expression presented in equation 11.

The computations of dipole and rotational strengths for the polymers are carried out using Cartesian coordinates of the C and O atoms of the various carbonyl groups on the purine and pyrimidine bases or the peptide linkages. Furthermore, the transition frequency $\bar{\nu}_0$ of an unperturbed carbonyl transition is needed, and its monomeric dipole strength D, which is proportional to μ^2. For the conversion between rotational (or dipole) strengths (in esu cm)^2 and the extinction coefficients (in Lmol^{-1}cm^{-1}) the approximations

$$D \approx 9.2 \times 10^{-39} \, \pi \, \epsilon_{max} \, w / \bar{\nu}_0 \tag{16}$$

and

$$R \approx 2.3 \times 10^{-39} \, \pi \, \Delta\epsilon_{max} \, w / \bar{\nu}_0 \tag{17}$$

were used [19]. Here, w denotes the width of the observed VCD or absorption band. Equations 16 and 17 hold for Lorenzian band shapes; for Gaussian bands, the factor π needs to be replaced by $\sqrt{\pi}$.

Once the geometry of the dipole transition moments is defined, the interaction energies of all dipoles with each other is calculated according to equation 12, and the interaction matrix is diagonalized numerically. The eigenvalues of V_{ij} are the frequency displacements for each of the exciton components from $\bar{\nu}_0$, and the eigenvector components are used, according to equations 12 and 13, to compute the rotational and dipole strengths of the exciton components. Subsequently, Gaussian, Lorenzian or mixed band shapes are used to simulate the observed spectra. These calculations are carried out using a program written in FORTRAN 77 in our laboratory. Atomic coordinates of the carbonyl groups can be derived from crystallographic data, or from any of a number of molecular graphics program such as MacroModel [21], which uses generalized canonical structures to generate the coordinates of any particular DNA or peptide sequence. The VCD intensity computations are very fast and require about one second execution time on a fast personal computer for 20 interacting dipoles.

In the following examples, a few model calculations will be presented. In addition, calculations of a few "real" systems for which observed data were also available, are introduced here. However, they will be discussed in detail with the experimental data in Sections 4 and 5.

3.2. Computational Results
3.2.1. "Spiral Staircase" Computations

The DECO formalism was first applied to a simple, hypothetical molecule in order to test the equations and the computational procedures for correctness, and to convey a feeling of signal magnitudes to be expected from these computations. In particular, the magnitude of the exciton splitting, the sign pattern in VCD and the distribution of IR intensities within the exciton manifold were obtained from these calculations.

These original calculations utilized a single stranded, hypothetical, helical polymer model as shown in Figure 2. It consists of dipoles arranged in a "spiral staircase" geometry; *i.e.*, all positive ends of the dipoles lie along the z-axis of a right handed coordinate system, and the negative ends describe a right handed helix about the positive z-axis. The dipole transition moment, μ, was taken to be that of a C=O stretching vibration found for the carbonyl groups in guanosine (ϵ = 1000 L/mol cm; D = 2.8 x 10^{-37} [esu cm]^2; μ = .52 Debye). The vertical spacing and the dihedral angles between the dipoles, 0.32 nm and 36°, respectively, closely resemble the values found in a DNA helix. The unperturbed frequency, $\bar{\nu}_o$, of the transition was assumed to occur at 1640 cm^{-1}.

The VCD calculated for this model polymer is shown in Figure 3, and resembles that observed for the decamer sequence d(CG)$_5$, both in overall spectral appearance and signal magnitude (*cf.* Section 5). Thus, the simplistic "spiral staircase" model appears to be a good starting point for the qualitative interpretation of the experimental data.

The influence of the polymer length on the computed spectra was studied for this model as well. It was found that for a transition dipole moment of between about 0.3 and 0.5 Debye (corresponding approximately to an amide I and a guanine C=O stretching vibration, respectively), the computed VCD spectra are more or less inde-
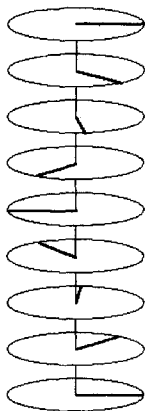
Figure 2. The "Spiral Staircase" geometry used in the original DECO test calculations

pendent of the number of interacting dipoles after one complete turn of the helix. This implies that the dipolar coupling does not extend much further than perhaps the closest four or five neighboring dipoles.

The major components of the absorption spectrum fall close to one value, about 50 cm^{-1} higher than the monomeric frequency, and appear, due to the superposition of many transitions, as a distorted Lorenzian. Similarly, most of the major VCD contributions occur as a positive/negative couplet centered directly under the absorption band (*cf.* Figure 3), *i.e.*, the zero crossing of the VCD trace occurs nearly exactly at the absorption peak. This agrees very well with the observed data.

For increasing chain lengths, low frequency exciton components between 1630 and 1640 cm^{-1}, gain in intensity in the calculated absorption strengths. For the "spiral staircase" geometry, the computed VCD intensities of the low frequency exciton components cancel.
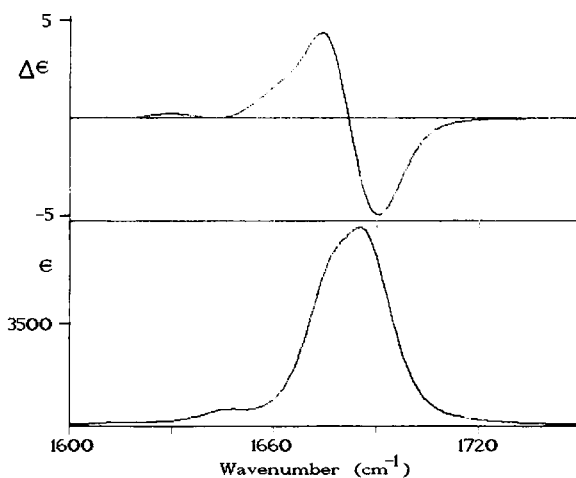
Figure 3. VCD (top) and infrared absorption (bottom) spectra calculated for the "spiral staircase" geometry

3.2.2. Calculations for d(CG)$_5$•d(CG)$_5$

DECO calculations were carried out next for a double stranded polymer, using canonical B-form carbonyl geometries created by program MacroModel [21]. Without any adjustable parameters, the agreement between observed and computed spectral features was outstanding. Details of these results will be discussed along with the experimental data in Section 5.

Using the correct geometries of G-C base pairs in an alternating polymer, we also investigated the computed VCD spectra for even smaller (G-C) polymers. The simplest model system used was a single GC base pair. Since the two carbonyl groups in a GC base pair are virtually coplanar, there is very little chirality induced by their coupling. Furthermore, the coupling energy is relatively small, since the distance of the centers of masses of the two oscillators is large (about 6 Å). Thus, a single GC base pair will not produce any observable VCD.

Next, the interaction of four carbonyl groups in the following two double stranded dimers was considered:

dG - dC   dC - dG

  :   :   :   :

dC - dG   dG - dC

  d(CG)   d(GC)

In these two segments, the orientation of the four carbonyl groups differs drastically, and consequently, entirely different VCD patterns are expected. In double stranded 5'd(CG)3', the four carbonyl groups are virtually all parallel, albeit in different planes. Thus, the induced chirality is low, but the coupling is large, as manifested by the large splitting in the IR absorption spectra. In double stranded d(GC), on the other hand, the second set of carbonyl groups are twisted nearly 90° with respect to the first (lower) set of dipoles. This arrangement results in large induced chirality with a sign pattern similar to the one observed in poly(dG-dC) • poly(dG-dC) and $d(CG)_s$, cf. Section 5.

The arrangement of dipoles found in d(CG) and d(GC) is prototypical for B-type double helixes consisting of CG bases: there will be, between consecutive base pairs, either the "near parallel" alignment of dipoles, or the "near 90° twist" between them. Thus, the segment

dC - dG - dC

  :   :   :

dG - dC - dG

  d(GCG) • d(CGC)
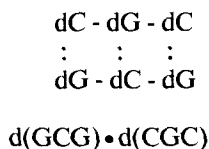
contains both these motives, and its calculated VCD resembles that observed and calculated for alternating GC sequences [22]. However, at these short polymer lengths, the calculated spectra still depend greatly on the number of interaction dipoles, and also on the exact sequence: both experimental and computed VCD results for the tetramers 5'd(GCGC)3', 5'd(CGCG)3', 5'd(GGCC)3'and 5'd(CCGG)3' are quite different, but show certain characteristics associated with right handed helicity (cf. Section 5).

3.2.3. Calculations for (L-Ala)$_3$

In the examples discussed so far, structural data were used to calculate VCD spectra, using the DECO model, and the computed spectra were compared to the observed ones. In the following example, the opposite procedure was followed, and an actual structure was determined from the VCD spectra [23]. This is the first peptide for which an approximate solution structure was determined by VCD spectroscopy. Although the method is still in its infancy, it is obvious that VCD can provide a handle to the determination of solution structures where other techniques fail.

In (L-Ala)$_3$, there are only two peptide linkages. Consequently, according to equation 14, one expects a positive/negative or negative/positive VCD couplet, depending on the geometry, and an absorption spectrum consisting of two peaks. This is exactly what was observed experimentally [23]. Subsequently, we set out to use all the

spectral information available (the rotational strengths, the ratio of dipole strengths and the dipolar splitting) to determine a peptide conformation which would reproduce all observed data. To this end, the peptide geometry was defined for a rigid model using standard bond lengths and angles, with only two degrees of freedom, namely the peptide conformational angles Φ and Ψ. The entire conformational space was then searched for a fit between observed and computed spectral data. The results of this calculations, and the implication for a postulated solution conformation, are discussed in Section 4.

3.2.4. Model Calculation for Helical Peptides

The VCD features for a number of larger peptide models have been calculated in the course of our efforts to define their solution conformation. These calculations proceeded exactly in the same manner as the ones described for small oligonucleotides. Cartesian coordinates from X-ray experiments, or from the program MacroModel [21], were used, along with a vibrational frequency for an unperturbed, single amide I or amide I' vibration. The dipole transition moment for the amide I vibration was taken somewhat lower than that of the nucleotide base carbonyl stretching vibration, in agreement with observed data and literature values. Details of these calculations will also be provided in Section 4.

3.3. Improvements to Computational Procedures

The agreement produced with the simple DECO calculations was surprisingly good for some model systems, but needed refinement in others. There are two major areas where DECO computations can be improved significantly. One of these is the situation when the oscillators which interact are not perfectly degenerate [24]. The situation of non-degenerate, extended coupled oscillators (NECO, equation 15) has recently been applied to some RNA polymers [25]. The NECO calculations reproduced a number of polymers significantly better, and permitted for the first time to obtain good agreement between experimental and computed VCD for A-T (or U) base pairs. T (or U) contains two nondegenerate carbonyl groups which interact very strongly and affect the computed VCD enormously. In addition, semi-empirical quantum mechanical calculations needed to be carried out to better establish the direction of the dipole moment of some of the ring vibrations coupling to the $C=O$ stretching modes.

The other area where the simple DECO model may be improved is the inclusion of vibrational coupling in addition to strict dipole-dipole coupling. All peptide VCD calculations reported here exhibited low VCD intensities, which we attributed to insufficient splitting of the exciton components, and subsequent cancellation of positive and negative VCD intensities. Since $C=O$ groups are only three bonds apart in a peptide, it is likely that some interaction of $C=O$ stretching motions occurs through vibrational coupling. Indeed, preliminary computations in our laboratory have shown that, in the absence of dipole-dipole coupling, the splitting between adjacent carbonyl groups can be as high as five wavenumbers, although there are no stretch-stretch interaction constants used which extend over this distance. Thus, this interaction is strictly through kinetic energy terms in the total energy matrix. Including these kinetic energy terms, along with the dipolar interactions, may significantly improve the VCD intensity calculations.

4. PEPTIDE VCD STUDIES

Within five years of the verification of VCD in solutions, first attempts were made to apply the technique to study biomolecular solution conformation in aqueous solution. The first samples studied as solutions in D_2O were simple amino acids and di- and tripeptides [26]. However, due to instrumental limitations, VCD was collected only in the C-H and N-H stretching region (2.5 to 3.5 μm). Although these early studies were necessary for the development of the experimental technique, it was not until experimental advances allowed the detection of VCD in the 6 μm region that the full potential of VCD was realized for peptide structural investigations.

The results which paved the way for conformational studies of peptides were the observation of VCD signals in the amide I (or I') spectral region by Singh and Keiderling [27], and by Lal and Nafie [28]. The mid 1980's were characterized by several pioneering papers, mostly by Keiderling's group, establishing the sensitivity of VCD to overall secondary structure [3,29,30], and a detailed correlation between VCD spectral features and peptide conformation was obtained. Some of these early studies of peptide models were carried out in non-aqueous solutions, and first data for peptide amide I' vibrations from aqueous solutions appeared in 1986 [3].

Amide III VCD from aqueous solution was published in 1987 [31], and normal coordinate analyses of simple peptides and a number of isotopomers were carried out to define the exact nature of the amide III vibration [32]. Recently, we have reported a detailed comparison of computational and experimental VCD results in the amide I region [33]. Keiderling has pushed the frontiers toward collecting VCD data on a number of proteins, and interpreting the data, *via* factor analysis, in terms of percentages of the common secondary structures [34,35]. A number of excellent reviews, summarizing the progress in peptide VCD in the 1985-1991 time span, have appeared [36,37].

The remainder of this chapter will deal exclusively with amide I VCD, since it is amenable to interpretation *via* the model developed previously. The material that follows will be organized as follows. First, the VCD spectra observed for well-established secondary peptide structures will be discussed qualitatively and quantitatively, where possible. Second, the VCD of a number of small, linear and cyclic peptides will be presented, and the implication of the observed VCD on the solution conformation will be elaborated upon. Finally, a short review of Keiderling's work on much larger peptides and proteins will be presented.

4.1 Prototypical Spectra of Homo-polyamino acids

The development of VCD as a peptide conformational probe proceeded in a manner similar to the one followed earlier by researchers in CD spectroscopy [38]. Homo-polyamino acids, such as poly-L-Tyr or poly-L-Lys, for which the secondary structure is well known and can be varied as a function of solvent acidity, were studied *via* VCD, and distinct results for the established conformations were observed. These results are summarized in Figures 4 and 5. In poly-L-Tyr [41], for example, the α-helical conformation exhibits a distinct, sharp and near-conservative positive / negative couplet in the amide I region. In the context of this discussion, "conservative couplet" implies equal positive and negative VCD intensities, and a description of positive / negative couplet always implies low to high wavenumber. The α-helical conformation is assumed by poly-L-Tyr in acidified DMSO solution (80% : 20% by volume of DMSO
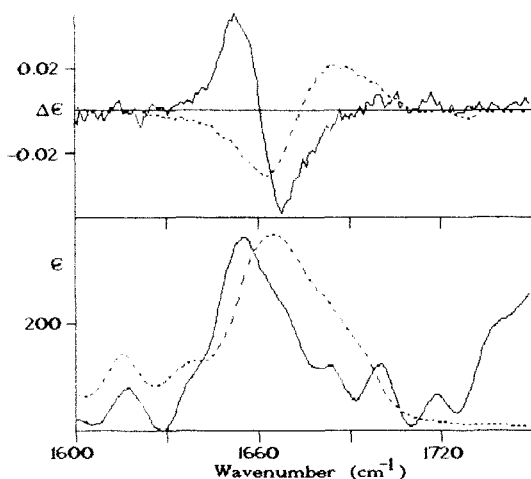
Figure 4. Infrared CD (top) and absorption Spectra (bottom) of α-helical (solid trace) and 'random coil' (dashed trace) poly-L-Tyr

and trifluoroacetic acid). In neutral DMSO, an opposite couplet is observed, which was referred to as a "random coil" conformation in analogy to the CD discussions (*vide infra*).

Poly-L-Lys, in aqueous solution, exhibits a wider variety of conformations. The "random coil", at high pH or pD, shows VCD features similar to those observed for "random coil" poly-L-Tyr, *cf.* Figure 5. The amide I' (the prime denoting a deuterated peptide linkage) VCD of the α-helical conformer contains an additional negative peak at low frequency, and thus, appears as a negative-positive-negative couplet. This pattern is not yet understood. Poly-L-Lys can also be transformed into a pleated ß-sheet conformation, which was first reported by Yasui and Keiderling [3] and by Paterlini *et al.* [30]. This conformation appears to produce all negative VCD, with a main peak at *ca.* 1640 cm^{-1}, and a sharp second peak at 1690 cm^{-1}. However, we believe that these spectra are partially due to precipitated samples, since we were unable to maintain clear solutions at the conditions described in the literature. At lower concentrations, we see a VCD and absorption spectra which are similar to the reported ones, but devoid of the 1690 cm^{-1} feature.

We have carried out a computational and experimental study on the "random coil" conformation of poly-L-Tyr to answer the question about the local order in the "random coil" conformation which had been addressed before by researchers in a number of fields [39,40]. This study was made possible by our successful application of the DECO model (*cf.* Section 3) to interpret VCD spectra of model compounds. Our efforts to deduce a structure for the "random coil" conformation of (homo)-polyamino acids was prompted by the observation by us and others [41] that the "random coil" in systems (such as poly-L-Tyr) produces VCD features which are nearly equal in magnitude, and opposite in sign, to those produced by the α-helical conformation (*cf.* Figure
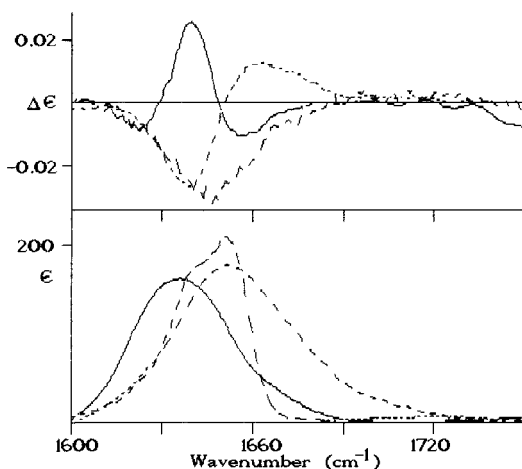
Figure 5. Infrared CD (top) and absorption Spectra (bottom) of α-helical (solid trace), "random coil" (short dashes) and ß-pleated poly-L-Lys (long dashes)

6). In addition, the results by Nafie's group [30] suggested that a truly denatured poly-amino acid shows virtually no VCD in the amide I (or I') region. Thus, we set out to interpret the observed VCD spectra of "random coil" poly-L-Tyr in terms of a more accurate description.

We approached the problem of establishing a structure of the "random coil" conformation by first establishing the limits of the present computational model for a known polymeric structure, the α-helix. Coordinates, created by program MacroModel [22] for the carbonyl groups of α-helical oligomers were used, along with published and experimental dipole transition moments, to compute the VCD and absorption spectra of the α-helical conformer. We found that VCD spectra, independent of chain length, can be calculated for octamers, and that the choice of side chain residues is immaterial for the computed spectra. Both calculated and experimental data were normalized to one residue, to permit a comparison between computed and observed spectra.

The observed and calculated data are shown in Figure 6. The agreement between experimental and theoretical data was within a factor of two for an α-helical structure, with the experimental data being larger than the computed ones. We attribute this discrepancy to the underestimation of the splitting between the exciton components, and consequently, cancellation of positive and negative computed VCD intensity. This is in line with our earlier finding in alanine tripeptide (*vide infra*), and methods to remedy this shortcoming are underway. The previously published calculated data for the α-helix *over*estimated the magnitude of the VCD by a factor of five [6].

Next, we calculated the carbonyl coordinates of a number of left-handed octa-peptides, and computed their VCD features. We found that both a left-handed α-helix, and an extended helix produced an inverted VCD spectrum similar to the one observed for the "random coil". Both these structures exhibit VCD features of approximately the
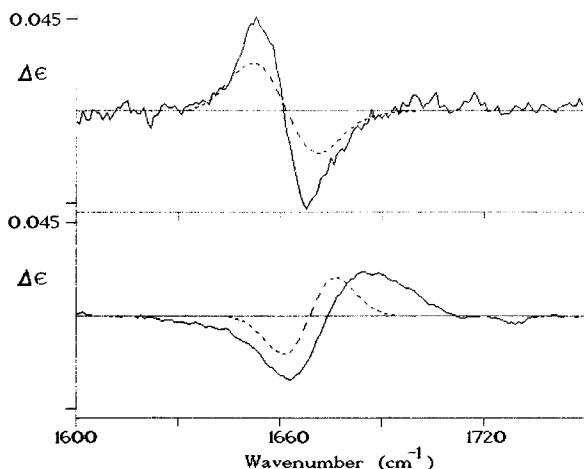
Figure 6. Observed (solid traces) and calculated (dashed traces) VCD features of α-helical (top) and extended helical (bottom) poly-L-Tyr.

correct amplitude, and with a zero crossing shifted toward higher wavenumber. Both calculated spectra fit the observed data so well that one cannot select one structure over the other structure on spectroscopic grounds alone. However, a number of arguments can be made in favor of the extended helix structure to be responsible for the observed spectra. First, the hydrogen bonding patterns of a left- and a right-handed α-helix are sufficiently similar that it would be energetically and entropically unlikely for the polymer to switch from on helical state to the other when the acidity of the solvent is varied. Second, a left-handed structure, known as the extended helix, had been postulated previously by Krimm and coworkers [42,43] on the basis of vibrational data alone. This structure is intriguing, since it occurs in the broad energy minimum of the Ramachandran map of pleated sheet structures, and may be visualized as a "sheet-with-a-twist", and conformational angles $\Phi = -110°$ and $\Psi = 120°$. The helicity we found with our approach is very low, with 2.2 residues per turn, whereas Krimm suggested 2.5 residues per turn. 2 residues correspond to a non-helical, fully extended sheet, and 3.6 residue to the α-helix. Further evidence for the extended helical structure is the fact that a slight increase in temperature produces VCD spectra typical of a ß-sheet [44].

Finally, the shift toward higher wavenumbers of the zero crossing of the negative-positive VCD spectrum is better reproduced by the extended helix than the left-handed α-helix. Thus, we favor the interpretation that the observed spectra of the "random coil" conformation can best be described by an extended helical structure, and that a truly random coil peptide will exhibit virtually no VCD. Dukor and Keiderling [39] reached very similar conclusions about the nature of the "random coil" conformation of homo-polyamino acids based on an extensive study of a number of left- and right handed helical segments, and fully supports the conclusion reached earlier by Krimm [42,43] about the extended helix discussed above. All evidence points to the fact

that in this "random coil" conformation, short pieces of highly ordered, left-handed segments alternate with less ordered pieces, and that VCD is sensitive to the short segments of high order.

Thus, we feel that the α-helical and the extended helical structure are well established in VCD, and that there exists a simple method for the interpretation of the data. The VCD features of the ß-pleated sheet structure appear reasonably well established, too, although its interpretation is much more difficult. Since the data are mono-signate, the DECO model is not appropriate (it always predicts conservative couplets). Nafie and coworkers explained such monosignate VCD in terms of a model similar to one described earlier by Schellman [24], with nearly co-linear (and antiparallel) electric and magnetic dipole transition moments [30].

In 1986, Keiderling and coworkers also published the first VCD spectra of the 3_{10} helix [45], observed for peptides of the form Z-(Aib)$_n$-Leu-(Aib)$_2$-OMe, n = 0 to 5, in chloroform. In this sequence, Z is a common protection group, benzyloxycarbonyl, and Aib is α-amino isobutyric acid, a non-chiral amino acid which is known to induce 3_{10}-helix formation. In the amide I region, this helix was found to exhibit a positive-negative couplet (with the same sense as the α-helix) which is slightly positively biased, whereas the couplet due to the α-helix is slightly negatively biased (cf. Figure 5). This 3_{10} structure is formed even for the case of the tetrapeptide (n = 1) with only one chiral amino acid. This report also delineated methods to distinguish α-helices and 3_{10}-helices by their $\Delta\epsilon$ values, and sounded a strong warning about using infrared frequency shifts alone as an indicator of secondary structures.

The additional negative peak observed for the deuterated peptide linkage at the low frequency side of the amide I' vibration in α-helical peptides is not fully understood. It was thought originally that a triple-peaked amide I (observed by some researchers), and the amide I' might be due to the parallel and tangential, as well as the helical contribution of the transition moment [21], as predicted by Moffit [17]. However, it is now established that the amide I VCD of the α-helix is a simple couplet, and only for the deuterated amide linkage the third peak is observed. We believe that coupling with other vibrations may be responsible for this extra peak, and detailed NECO calculations, including vibrational interactions, are underway.

4.2. Small Peptides

One of the first VCD studies we undertook in 1988 was work on the tripeptide L-Ala-L-Ala-L-Ala [23]. This molecule, in neutral aqueous (D$_2$O) solution, exhibits a distinct, near-conservative VCD spectrum in the amide I' region, shown in Figure 7. The infrared absorption shows two overlapping peaks in the amide I' region, at 1650 and 1675 cm^{-1}. Raman depolarization ratios indicated that the high frequency component is the symmetric stretching combination.

These spectral data were interpreted via a straightforward coupled oscillator model, and calculations were carried out to find a molecular conformation in Φ and Ψ space around the center alanine residue which best reproduces the observed spectral data. The computational methods employed were discussed above (cf. Section 3) and detailed arguments are given in the original report [23]. A similar, yet not as detailed, effort had been published before for peptide models in non-aqueous solution [46].

This analysis of the VCD results on L-Ala-L-Ala-L-Ala suggested a left-handed, twisted conformation, shown in Figure 8 with Φ and Ψ angles (120 and -25°, respectiv-
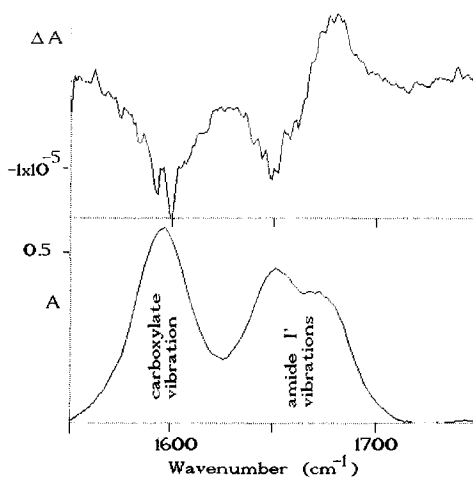
Figure 7. Infrared CD (top) and absorption spectra (bottom) of L-Ala-L-Ala-L-Ala in aqueous solution
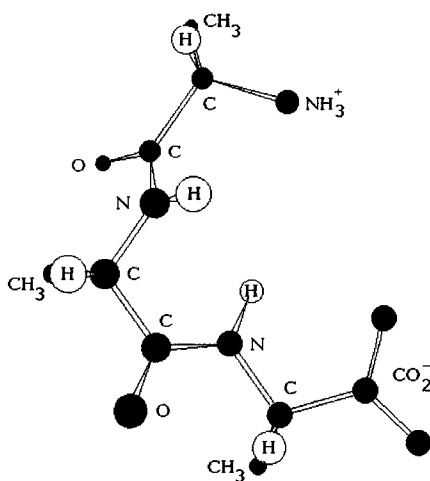
Figure 8. Conformation deduced from VCD data for L-Ala-L-Ala-L-Ala in aqueous solution

ly), which are not common in a typical Ramachandran map. We postulated that the structure of L-Ala-L-Ala-L-Ala is stabilized by a zwitterionic interaction, because of the proximity of the $-ND_3^+$ and the $-CO_2^-$ groups in this structure, and because of the fact that the VCD features disappear in solutions of low and high pH values, which do not support a zwitterion. Further evidence for the role of the zwitter-ionic interaction as a stabilizing factor came from the observation that N-acetyl-alanine-N'-methyl amide (AAMA) does not exhibit coupled oscillator VCD features. AAMA incorporates two amide linkages around a central alanine residue just as L-Ala-L-Ala-L-Ala, but has no zwitterionic end groups, and hence, lacks the ability to form a distinct solution structure.

The conformational angles derived in this study are unusual values in the Ramachandran map because these maps are based on conformational energy calculations for molecules as N-acetyl-alanine-N'-methyl amide, which do not incorporate charged groups and thus will reproduce an uncharged peptide fragment better than an aqueous solution of a zwitterionic peptide.

During this study, we found that the exciton model underestimates the splitting between the coupled states by about a factor of four, indicating that interactions other than dipole-dipole coupling act between adjacent carbonyl groups. These interactions are most likely straightforward vibrational coupling terms, as discussed at the end of Section 3.

At the time the work on the alanine tripeptide was published, it was considered nearly an act of heresy to postulate a solution structure for peptides with less than 25 amino acids. This was because techniques for monitoring solution conformation of peptides of this size often were unable to detect a preferred structure, and consequently, the notion developed that small peptides **had no solution structure**. In this work, we postulated that peptides as small as a tripeptide may exist in a set of preferred structures on the time scale of molecular vibrational transitions. This contention has been further confirmed by us *via* VCD studies on other alanine peptides, and by the VCD results on small proline-containing peptides [39,47], and more recently by NMR studies [4]. These results will be discussed next.

Figure 9 shows a comparison of the infrared absorption and VCD spectra of $(L-Ala)_n$, n = 3 - 5. The spectra are normalized for equal absorption intensity at 1595 cm^{-1}, which is the frequency of the carboxylate anion antisymmetric stretching mode. The data show that the amide I' intensity increases roughly linearly with the number of peptide linkages in the molecule, and that the VCD intensity increases similarly. However, the positions of the infrared absorption maxima are shifted from about 1654 cm^{-1} in the trimer to 1648 cm^{-1} in the pentamer. Similarly, the VCD zero crossing in the trimer occurs at 10 cm^{-1} higher frequency than in the tetramer and pentamer. We have interpreted these results [48] in terms of different solution conformations of the peptides: the trimer seems to be stabilized by zwitterionic interactions, as discussed before, whereas formation of extended helices seems to occur at the level of the tetramer.

The tripeptide L-Pro-L-Pro-L-Pro in aqueous solution was studied by Keiderling and coworkers [47], and exhibits VCD spectra similar to those observed for L-Ala-L-Ala-L-Ala, although the couplet is more negatively biased. Similarly, the protected (L-Pro)$_3$ shows a very similar VCD spectrum [39]. No analysis of these results in terms of a solution conformation based on the coupled oscillator model was carried out. However, there is clear evidence that in aqueous and non-aqueous solutions, distinct solution conformation is reached at the level of the tripeptide, and persists similarly up
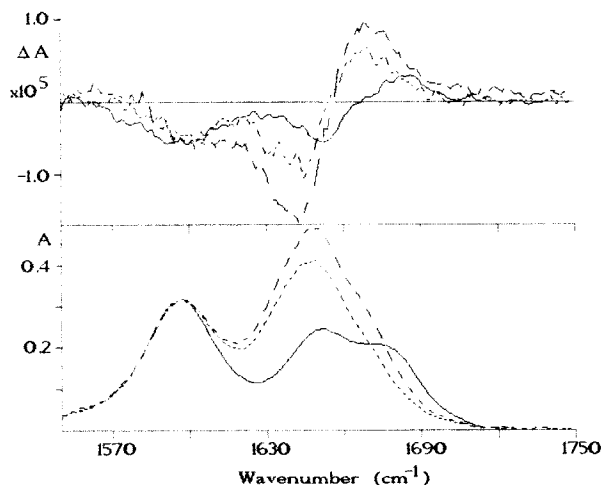
Figure 9. Infrared CD (top) and absorption spectra (bottom) of L-Ala-L-Ala-L-Ala in aqueous solution

to dodecamers. Whether or not the $(L\text{-Pro})_3$ assumes the same solution conformation as does $(L\text{-Ala})_3$ is not clear at this point, and one needs to keep in mind that the proline residues are significantly less flexible than alanine. However, their VCD spectra are certainly similar.

Recently, we have published [49] the first observation of a VCD signal which appears to be due to a ß-turn in a model peptide, *cyclo*-(-Gly-Pro-Gly-D-Ala-Pro-), which is known from NMR and X-ray studies to contain a Type II ß-turn [50,51]. This molecule exhibits in solution a very distinct negative-positive-positive-negative VCD spectrum (*cf.* Figure 10) unlike any other peptide conformation.

In Figure 10, the VCD intensity patterns, calculated using the DECO formalism for the structures derived from X-ray crystallography and from NMR spectroscopy are shown, superimposed on the observed VCD data. The X-ray structure yields a computed VCD spectrum which reproduces the VCD and IR intensities well (*cf.* Figure 10a), and predicts an intensity pattern for the VCD spectrum which is similar to the observed one. Yet, the splitting between the calculated exciton components is only about 30 cm^{-1}, whereas the observed amide I VCD features cover nearly 80 cm^{-1}.

The NMR structure reproduces the splitting between the observed exciton components much better (*cf.* Figure 10b) and produces an IR absorption intensity pattern which is very close to the observed one. However, the calculated VCD spectrum reproduces only the low frequency region of the amide I manifold, and predicts a positive VCD intensity in the highest frequency peak, which disagrees with the observation.

The calculated frequency separation of the amide I exciton components are much larger for the NMR structure than for the X-ray structure, although in both cases identical values for the unperturbed amide I frequency (1665 cm^{-1}), and for the transition dipole moment were used. Further, and it was assumed for computational simplici-
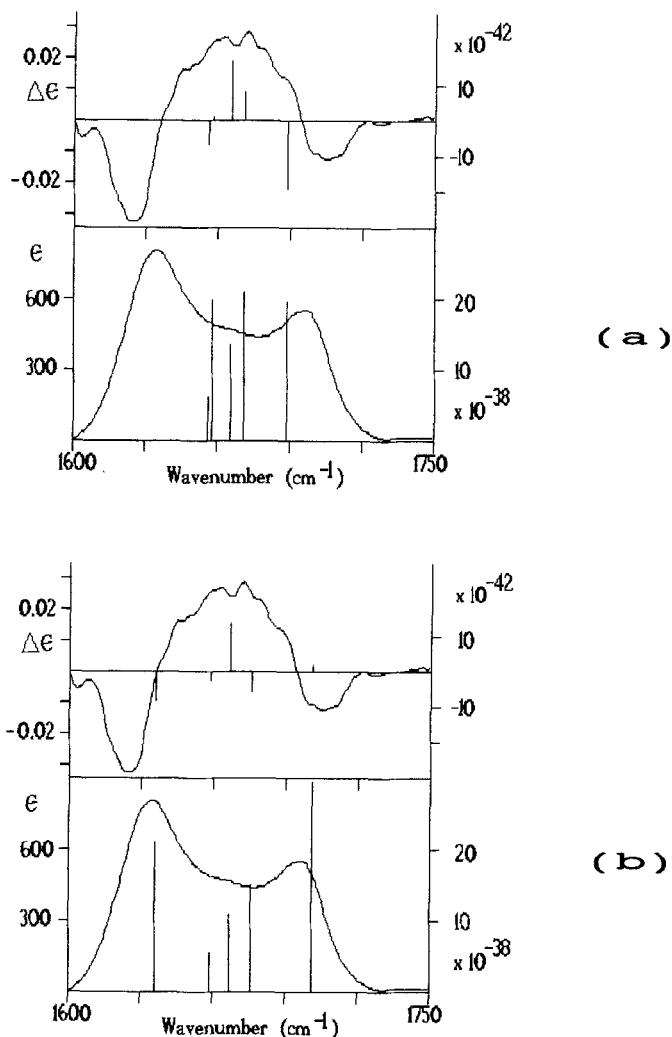
Figure 10. Observed (solid traces) and computed (bar graphs) VCD and infrared absorption spectra for cyclo-(-Gly-Pro-Gly-D-Ala-Pro-), using X-ray (a) and NMR (b) structures

ty that all peptide C=O groups have degenerate frequencies. Thus, the differences computed for the two structures are entirely due to differences in the geometry.

The differences in the calculated VCD and infrared absorption spectra may seem disappointing at a first glance. However, a close inspection of the two structural parameters used to calculate the VCD spectra shows substantial differences in these structures. The NMR solution conformational angles Φ and Ψ listed in reference [51]

are approximate and do not produce an exact ring structure, but leave the C-N bond distance between the C atom of Pro[5] and the N atom of Gly[1] at about 20 % longer than expected. The largest discrepancies between the solution-phase NMR structure and the solid-phase structure occurs at Gly[1]: the computed VCD spectrum of the fragment Pro[2]-Gly[3]-D-Ala[4]-Pro[5], based on the NMR structure yields a VCD spectrum which reproduces both the observed VCD pattern, and resembles the VCD spectra computed from the X-ray geometry. Thus, it is tempting to assume that the differences in the calculated VCD features for the NMR and X-ray structures are due to the uncertainty in the conformational angles of Gly[1].

The observed negative-positive-positive-negative VCD pattern has not been found in any other prototypical peptide conformation. However, a number of the trial structures used to compute VCD features reproduced this characteristic pattern, among them the X-ray structure, the Pro[2]-Gly[3]-D-Ala[4]-Pro[5] fragment derived from the NMR solution conformation of the pentapeptide (*vide supra*), and the Gly[1]-Pro[2]-Gly[3] fragment derived from the solution conformation. In the partial peptide sequences discussed here, the sequence starts with the amide N atom, and extends to the carbonyl group of the last residue. Thus, the sequence Gly[1]-Pro[2]-Gly[3] includes three interacting carbonyl transitions.

All other possible tripeptide sequences derived from the original *cyclo*-(-Gly-Pro-Gly-D-Ala-Pro-), however, gave either very small, or conservative (positive-negative or negative positive) VCD couplets. Thus, we conclude that four amide groups are necessary to reproduce the distinct negative-positive-negative pattern which was observed experimentally. This statement could imply that all four amino acids involved in a 4 → 1 turn, or ß-turn, are required to produce the characteristic VCD spectra. This is particularly interesting since the amino acid residues 1 through 4 (-Gly[1]-Pro[2]-Gly[3]-D-Ala[4]-) are involved in the ß-turn, yet the observed VCD spectra seem to be determined by residues 2 through 5 (-Pro[2]-Gly[3]-D-Ala[4]-Pro[5]-).

The different VCD spectra calculated for the NMR and X-ray structures demonstrate just how sensitive VCD is toward structural changes. It is premature, at this stage, to attempt to use VCD as a tool to distinguish or even judge the quality of either of the previously obtained structures. However, further computational efforts may well establish VCD as a complementary tool to NMR for the determination of solution conformation. VCD will certainly not challenge NMR in large molecules, where the superior resolution allows detailed structures to be derived. However, the much faster time frame of vibrational spectroscopy over nuclear magnetic resonance techniques allows distinct structures to be discerned when NMR measurements perceive little structure.

Among the most recent results from this laboratory are the VCD data of a number of linear and cyclic analogues of the yeast mating factor [52], Trp-His-Trp-Leu-Gln-Leu-Lys-Pro-Gly-Gln-Pro-Met-Tyr, including several analogues where a ß-turn was induced in the peptide by substituting Lys[7] and Gln[10] by two Cys residues, and subsequent ring closure *via* -S-S- bridges. Residues 8 and 9 in the turn were either Pro-Ala or Pro-D-Ala, resulting in Type I and II ß-turns, respectively. The cyclic as well as a linear analog showed similar VCD spectra, which are dominated by negative VCD intensity at *ca.* 1640 cm^{-1}.

The observation of distinct and relatively strong VCD intensity for a small, linear peptide is, as pointed out above, a remarkable result by itself, since it points to the fact that the peptide exists in solution in a number of conformers which are suffi-

ciently similar that their VCD contributions do not cancel. However, the interconversion between these conformers is faster than the NMR time scale. The non-cyclic peptide analogs gave no indication of a stable solution conformation in the NMR experiments. The fact that the linear and cyclized peptides exhibit similar VCD spectra suggests that the linear peptide incorporates a turn, and assumes somewhat of a hairpin structure with a longer and a shorter chain loosely interacting. This problem was further addressed by investigating a cyclic peptide where the Pro-Ala residues in the cyclic portions were substituted by a -CH_2-CH_2-CH_2-CH_2-CH_2-NH- (5-amino pentanoic acid) chain. In this analog, the VCD is due to the side chains, since there is only one C=O stretching vibration in the loop. This peptide also exhibits VCD which is dominated by a strong, negative VCD signal at $ca.$ 1640 cm^{-1}, indicating that the two short peptide chains are able to assume a sheet-like conformation.

4.3. Proteins

The first VCD spectra of proteins were published by Keiderling's group in 1986 [35,36]. The sensitivity of the instrumentation was sufficient at this point to observe these data from solutions in D_2O. A large number of proteins has been studied since, with all work being done at Keiderling's laboratory. These proteins have included myoglobin, hemoglobin, chymotrypsin, papain, lysozyme, ribonuclease, and others. A number of major conclusions can be drawn from these studies. First, the secondary structures apparent from a cursory comparison of UV-CD and VCD spectra may be very different for some proteins. In particular, myoglobin, cytochrome, lysozyme and chymotrypsin all exhibit UV-CD spectra which one would classify as mostly α-helical, but their VCD spectra are distinctly non-helical, with the exception of myoglobin.

Secondly, a quantitative interpretation of the amide I' VCD region is possible. Using factor analysis methodology, reliable percentage of α-helical, ß-sheet and other contributions have been obtained, using prototypical peptide VCD spectra as basis sets. The factor analytical data appear to agree well with solid phase X-ray structures, and to a somewhat lesser extent with UV-CD data. Thus, it appears that the instrumental and computational methods are available to utilize VCD as a novel spectroscopic technique for structural studies on peptides and proteins.

5. NUCLEIC ACID VCD STUDIES

Once the observation of VCD features in the carbonyl stretching region was possible for peptides in aqueous solution, the stage was set for the observation of VCD in nucleic acids. The C=O stretching vibrations of the nucleotide bases occur at approximately the same frequency where the amide I' vibration occurs in peptides. Thus, D_2O was judged to be a suitable solvent for DNA and RNA VCD studies. Since the nucleic acids need to be buffered, and since the buffer solution could not have any strong absorptions in the 6 μm region, sodium cacodylate in deuteroxide emerged as the most suitable solvent system for these studies.

The VCD of helical, single and double stranded ribonucleic acid (RNA) polymers was first reported by Keiderling's group in vibrations associated with double bond stretching vibrations of the bases in RNA [53]. The optical activity was found to be due to the coupling of the virtually achiral stretching vibrations which are arranged in a

dissymmetric, helical pattern. Thus, the origin of the optical activity is similar to the mechanism giving rise to ECD in DNA models, which has been explained using the exciton formalism.

The first observation of VCD in small model DNA molecules, and in large deoxynucleic acid models, was reported by us in 1989 [18]. The VCD signals in the 1550 to 1750 cm^{-1} spectral region were found to be similar to those observed for the RNA reported earlier. In addition, our first report on DNA models also contained the observation of B and Z form DNA, along with the DECO equations and model calculations of the helical polymers. Subsequently, VCD was reported for poly(dG-dC)•poly(dG-dC), poly(dG)•poly(dC), poly(dA-dT)•poly(dA-dT) and poly(dA)•poly(dT) in the B-conformation in buffered, aqueous solution [22]. Differences were observed for DNA models, depending on the base composition and sequence, and the observed results were *quantitatively* interpreted in terms of the exciton model for coupled carbonyl stretching vibrational states.

Keiderling reported the VCD spectra of triple helices in ribonucleic acids by investigating the temperature dependent VCD features of a mixture of poly(rA) and poly(rU) [54]. The spectra of the triple helix are more complicated than those of a double strand, as expected. We have reported the VCD of a number of oligo deoxynucleotides with between four and twelve base pairs. These studies will be elaborated upon after a detailed discussion of the VCD features of polymeric DNA and RNA samples, for which the solution structures are well established.

5.1. VCD Spectra of prototypical nucleic acid structures
5.1.1 *Single stranded nucleic acids*

Single stranded ribonucleic acids, such as poly(rU), poly(rG), *etc.*, exhibit a slightly positively biased, positive - negative VCD couplet in the carbonyl stretching vibration of the bases [53]. This VCD signal was attributed to extensive coupling of the C=O stretching vibrations in these base-stacked polymers. Poly(rA), which does not contain any carbonyl groups, exhibits a similar, but somewhat smaller VCD signal at lower frequency. This signal was attributed to other double bond stretching vibrations, which similarly interact with each other as the C=O stretching vibrations do. Thus, VCD of nucleic acids may be observed in the absence of hydrogen bonding between complimentary strands, and sufficient order exists even in single stranded polymers for dipolar coupling to occur and to produce exciton-type VCD features.

5.1.2 *A-form RNA*

Poly(rC)•poly(rG), which forms a solution conformation of the A-family, exhibits a positive-negative couplet with an additional small low frequency feature (*cf.* Figure 11). The observed spectra are somewhat different from those observed for B-form poly(dG)•poly(dC), *cf.* Figure 12 b. Thus, it appears that A and B-form polymers can be distinguished *via* VCD [55]. The main features of poly(rC)•poly(rG) are three absorptions at 1621, 1649 and 1690 cm^{-1}, accompanied by three VCD couplets: a weak positive-negative one at 1617 cm^{-1}, a weak negative-positive one at 1636 cm^{-1}, and the main positive-negative signal at 1691 cm^{-1}.

The calculated VCD spectra were obtained using the NECO formalism (equation 15), and C=O stretching vibrations for the guanine (1655 cm^{-1}) and cytosine (1650 cm^{-1}) groups, and an independent C=C-C stretching mode on cytosine (1612 cm^{-1}). The directions of the transition moments were calculated semi-empirically [25].
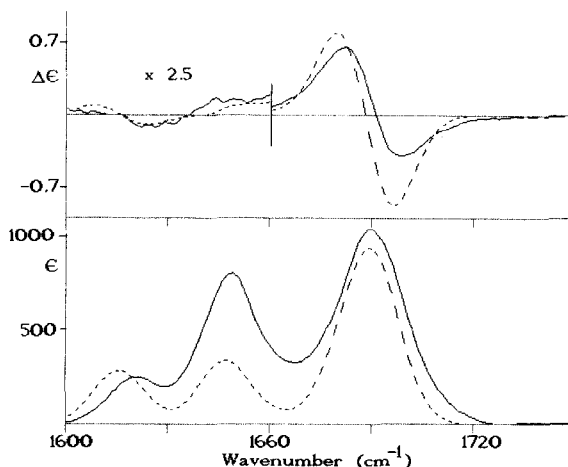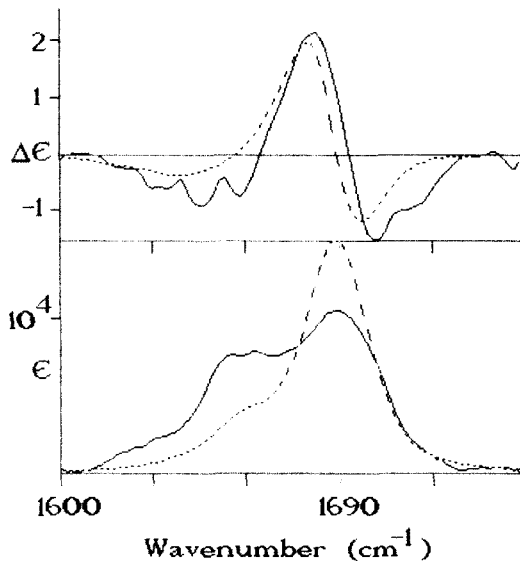
Figure 11. Observed (solid traces) and calculated (dashed traces) VCD (top) and infrared absorption (bottom) spectra of (A-form) poly(rG)• poly(rC).

5.1.3. B-form DNA

In 1989, we reported the first observations of VCD in a double-stranded DNA model, poly(dG-dC)•poly(dG-dC) [18], shown in Figure 12. Slightly different spectral features, both in VCD and infrared absorption, have been observed under identical sample conditions depending on the batch of the sample, and we attribute the differences to the occurrence of small amounts of unordered polymer [57] possibly caused by large variations in polymer lengths.

However, we believe that the B-form may be described by negative VCD at 1700 cm^{-1}, a positive peak at 1682 cm^{-1} and a negative shoulder at 1660 cm^{-1}. The corresponding absorption peaks are at 1690, 1655 and 1625 cm^{-1}. The VCD of other B-form polymers, poly(dG)•poly(dC), poly(dA-dT)•poly(dA-dT) and poly(dA)• poly(dT), are also shown in Figures 12 [22]. The most significant observation about the VCD spectra of the four polymers is the fact that they all differ significantly. Further inspection of Figure 12 reveals that the two G-C polymers are similar to each other, but very different from those of the A-T polymers. Thus, it is clear that VCD distinguishes the base composition and the composition of a strand in the simple DNA models discussed here.

Both G-C polymers, poly(dG-dC)•poly(dG-dC) and poly(dG)• poly(dC) show VCD spectra which are dominated by a large negative-positive couplet. The zero crossing of the VCD trace in the main couplet occurs nearly exactly under the maximum of the absorption spectrum. This absorption spectrum is very different than that of a mixture of the mononucleotides CMP/GMP, indicating that dipolar coupling occurs between the C=O stretching modes, giving rise to the observed VCD and absorption features. Furthermore, the C=C and C=N stretching vibrations, which are strong in the monomeric solution, are barely observed in the polymer.
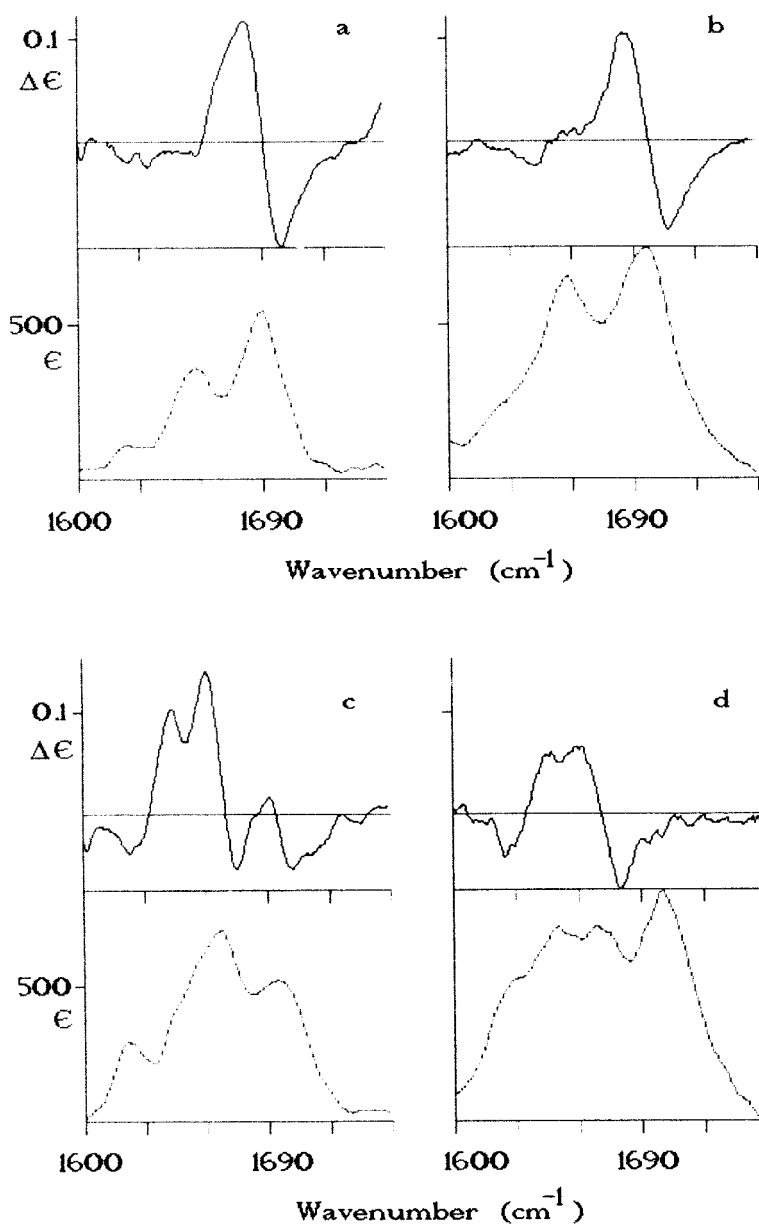
Figures 12. VCD (top) and infrared absorption (bottom) spectra of
a) poly(dG-dC)•poly(dG-dC), b) poly(dG)•poly(dC), c) poly(dA-dT)•poly(dA-dT)
and d) poly(dA)•poly(dT)

The spectra of poly(dA-dT)•poly(dA-dT) and poly(dA)•poly(dT) show more complex VCD patterns than do the G-C polymers. In poly(dA)•poly(dT), the highest frequency absorption peak exhibits no VCD intensity, and a large negative-positive couplet (1675/1650 cm^{-1}) is followed by a positive-negative couplet (1640/1625 cm^{-1}). In poly(dA-dT)•poly(dA-dT), there is an additional negative - positive VCD couplet at about 1700 cm^{-1} under the absorption peak which shows no signal in poly(dA)• poly(dT). The absorption spectra of the A-T polymers appear to be poorly resolved.

Model calculations were carried out to aid in the interpretation of the polymer spectra. These calculations were performed for small DNA segments to avoid the computational difficulties associated with macromolecules. Consequently, the computational results will be discussed below in the section dealing with oligomers.

5.1.4. Z-form DNA

High ionic strength solutions, *e.g.*, aqueous solutions containing high concentration of salt, are known to induce a phase transition to a left handed helical form in ..CGCG.. sequences. The left handed helical form basically shows an inversion of the UV-CD spectral features between the B and the Z forms.

VCD, in fact, shows a similar reversal of the VCD couplets. The VCD spectrum of the Z-form of poly(dG-dC)•poly(dG-dC) in 3M NaCl, shown in Figure 13, exhibits a positive peak at 1677 cm^{-1} followed by a broad negative peak with minima at 1658 and 1643 cm^{-1}. The corresponding IR absorption peaks occur at approximately 1690 and 1650 cm^{-1} [18], and the VCD spectral features of the Z-form appear positively biased. The reversal of the VCD features is expected for a transition from a right to a left-handed helix.
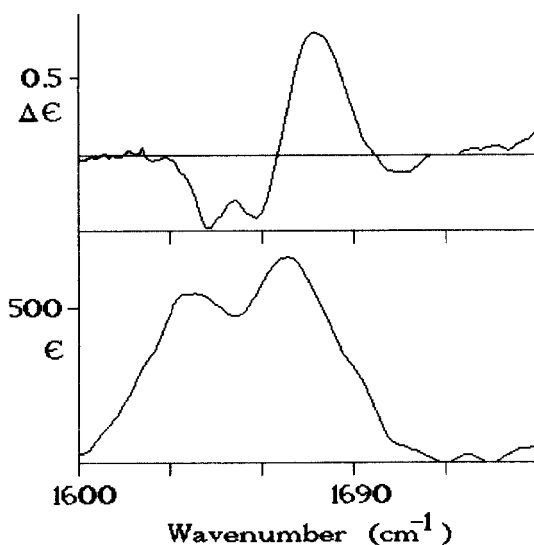
Figure 13. VCD (top) and infrared absorption spectra (bottom) of poly(dG-dC)• poly(dG-dC) in high salt (NaCl) solution (Z-form DNA)

The observed Z-form spectra depend on the choice of the counterion used to induce the B→Z transition, with Mg^{2+} causing larger VCD intensities and shifts to lower frequency. It is not clear, at this point, whether or not the spectral differences between the Na^+ and Mg^{2+} induced Z-forms are due to slightly different structures, or to different interactions of the metal ions with the carbonyl groups.

5.1.5. *Triple helix*

Triple stranded RNA, incorporating Hoogstein base pairs, can be formed by poly(rA)•poly(rU)•poly(rU) at low temperature. Keiderling [54] reported for these polymers an overall VCD signal similar to that observed for double stranded poly(dA)•poly(dT), namely a large negative-positive-positive-negative couplet with an additional, positive low frequency band. The spectrum of the triple helix was also observed when poly(rA)•poly(rU) was slowly heated, and unwinding of two double helices into a triple and a single strand polymer occurred [54]. This study nicely demonstrated the conformational sensitivity of VCD at the phase transition.

5.2. Oligomers

In the following discussion, the VCD of a number of small oligodeoxy nucleotides will be introduced. In some of these studies, a direct comparison between observed and calculated VCD spectra was possible. As pointed out before, the observed and calculated results for the double stranded decamer $d(CG)_5 \cdot d(CG)_5$, henceforth referred to simply as $d(CG)_5$, were a major stepping stone in our efforts to interpret the observed VCD spectra of poly(dG-dC)•poly(dG-dC). Thus, these results, displayed in Figure 14, will be discussed in detail.

Figure 14. Observed (solid traces) and calculated (dashed traces) VCD (top) and infrared absorption (bottom) spectra of $d(CG)_5$

The observed VCD spectra of the decamer (Figure 14) and the polymer (Figure 12) are very similar. This indicates that the structures of the decamer and the polymer are the same within the interaction (coupling) distance at which VCD probes molecular structure. Thus, it appears that the decamer may serve as an excellent model system for the interpretation of the polymer. The agreement between the calculated and observed VCD of d(CG)$_5$ is excellent, both in reproducing the observed VCD patterns and their magnitudes.

For these calculations, the carbonyl transition frequency and intensity were taken from a 1:1 CMP/GMP mixture in D_2O (ν_0 = 1650 cm^{-1}; ϵ_{max} = 950 Lmol^{-1}cm^{-1}). Carbonyl coordinates, created by program MacroModel [21] for a canonical, B-form, alternating CG polymer, were used without geometry optimization. Band shapes were employed that are 50:50 mixtures of Lorenzian and Gaussian contours, since it was found that such a mixed composition provides the best fit between observed and computed spectra, although pure Gaussian or pure Lorenzian band shapes give satis-factory results as well.

A number of conclusions may be drawn from the excellent agreement of computed and experimental data displayed in Figure 14. First, it appears that the DECO formalism is applicable to the simple B-form polymers containing G and C residues. Second, we conclude that the canonical B-form coordinates apply equally well to d(CG)$_5$ and poly(dG-dC)•poly(dG-dC), since they reproduce both the spectral features observed for the decamer and polymer. Third, we find that at the decamer level, end effects (such as fraying) play a relatively minor role, since the observed spectra of the polymer are very similar to those of the decamer. Finally, we wish to point out that the interpretation of infrared absorption data, found in the literature, referring to some of the infrared peaks as guanosine and others as cytosine carbonyls, is most likely incorrect. Our calculations suggest that all the bands observed in the 1640 to 1690 cm^{-1} region are exciton-split carbonyl stretching vibrations, which are indistin-guishable and are located on both C and G residues.

Calculations were also carried out for d(G)$_{10}$•d(C)$_{10}$, and the corresponding A and T containing polymers. The calculations were able to reproduce the VCD spectra of C and G containing oligo nucleotides very well [22], but less satisfactory agreement was achieved for the A and T containing polymers. This is due to the fact that T con-tains two carbonyl groups, and A none. The details of the coupling patterns which give rise to the VCD features of these latter polymers are just now being understood [25].

We have synthesized the double stranded, self-complementary dodecamer CGCGAATTCGCG, which is of special interest since it contains the binding site of the restriction enzyme EcoR I. Crystallographic, NMR and molecular dynamics studies have indicated that the junction between C-G and A-T rich regions may either produce a static kink, or provide a linkage at which large amplitude helix bending vibrations occur. A number of theorists have associated these structural perturbations with the high affinity and specificity of the restriction enzyme EcoR I [56].

The VCD spectra of this oligomer appear, at a first glance, as a superposition of the spectra of poly(dG-dC)•poly(dG-dC) and poly(dA)•poly(dT), and are similar to those of native DNA. Spectra of better signal-to-noise ratio need to be collected before VCD can be used to probe the CG - AT junction; however, the sensitivity of VCD toward he alignment of the bases may be sufficient to shed new light on the conforma-tional aspects at GC - AT junctions.
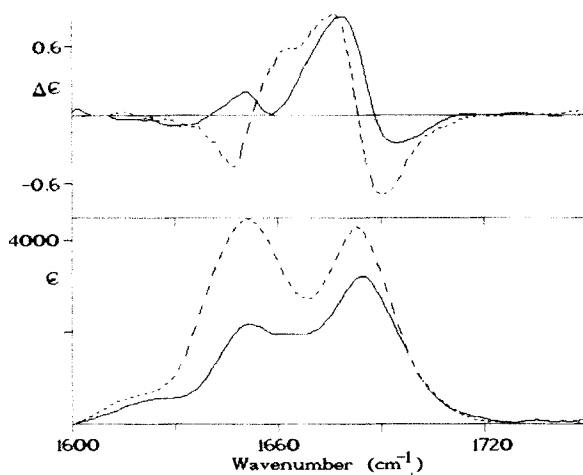
Figure 15. VCD (top) and infrared absorption (bottom) spectra of 5'd(CGCG)3'(solid trace) and 5'd(GCGC)3' (dashed trace) in low salt solution
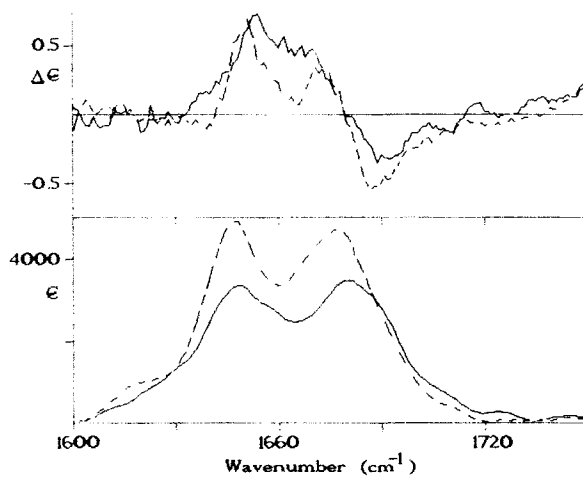
Figure 16. VCD (top) and infrared absorption (bottom) spectra of 5'd(CCGG)3'(solid trace) and 5'd(GGCC)3' (dashed trace) in low salt solution

Next, the VCD spectra of the self-complementary tetramers, 5'd(CGCG)3', 5'd(GCGC)3', 5'd(CCGG)3' and 5'd(GGCC)3' will be discussed. The motivation for this work was twofold: first, we wanted to demonstrate the sensitivity of VCD toward the different structural features of these four tetramers [57], and toward conformational changes brought on by variation of temperature and the ionic strengths of the solvent. Second, we wish to discuss the seemingly different structural information which is revealed by VCD and previously employed methods, such as ECD, Raman and NMR spectroscopies.

ECD spectra of GCGC and CGCG were reported to be similar to those spectra observed for poly(dG-dC)•poly(dG-dC), whereas the CD data for the two non-alternating tetramers, GGCC and CCGG, were found to differ significantly from those of the polymer [58]. The Raman spectra of the two alternating tetradeoxy nucleotides indicated that at low NaCl concentrations, both tetranucleotides maintain a B-form structure, while at high NaCl concentrations only CGCG assumes a double helical Z-form [59-61].

NMR data were interpreted in terms of right handed helicity, but the exact form is not quite clear for these small oligo-nucleotides. A-forms were eliminated as likely structures, based on the calculated chemical shifts of the non-exchangeable ring protons. The temperature dependence coefficients of certain chemical shifts, and the observed hydrogen - deuterium exchange rates, indicate that significant end fraying occurs in some of these tetramers [62-64]. Thus, most solution phase spectral results published to date for these tetramers were interpreted in terms of an overall B-form, which agrees with our VCD results. However, the observed VCD spectra of all four tetramers differ significantly from those of the polymers, and we believe that VCD has a unique ability to sample the conformation of such small biomolecules.

The infrared absorption spectra and VCD spectra of the alternating tetramers CGCG and GCGC are shown in Figure 15. The VCD spectrum of CGCG exhibits a negative - positive couplet (1694 / 1679 cm^{-1}) which resembles that of B-form poly (dG-dC)•poly(dG-dC). In CGCG, this couplet is followed by a VCD minimum at 1658 and a positive peak at 1650 cm^{-1}, which do not appear in the polymer, and thus, indicate a deviation from the canonical B-form. The VCD spectrum of GCGC, on the other hand, exhibits a negative (1690) - positive (1676 and 1662) - negative (1647 cm^{-1}) couplet. In overall appearance, this spectrum is very similar to the one observed for B-form poly(dA)•poly(dT) [22].

The observed data on the non-alternating tetramers are shown in Figure 16. Among the four tetramers studied, CCGG exhibits the simplest VCD spectrum, consisting basically of a weak negative (1690 cm^{-1}) positive (1667 and 1654 cm^{-1}) couplet. The most complex VCD patterns are observed for GGCC: a negative/positive couplet (1688/1672 cm^{-1}) is followed by a minimum at 1665 cm^{-1} and a strong positive peak at 1650 cm^{-1}. The couplets are nearly conservative. According to previous studies, GGCC was found to be in a conformation similar to the B-form, whereas CCGG was found to least B-like. Our studies disagree on this point, since CCGG showed VCD of a normal right-handed form, whereas GGCC shows very unusual spectral features.

The next part of the discussion seeks to consolidate the previously obtained spectral information into one picture. The original CD studies in the 220 - 280 nm range indicated that at low ionic strengths, CGCG and GCGC exists in right handed structures [65] very similar to that of poly(dG-dC)•poly(dG-dC), whereas CCGG and GGCC exhibit different CD features. The latter of these two, GGCC, showed CD

which was consistent with model calculations, and it was concluded that this structure was not unusual, although the observed CD did not appear to be a standard B-form. The CD reported by Kastrup, *et al.* [64] for CCGG at low temperature and relatively high concentrations (50 μM), however, exhibited all features which are now associated with Z-form DNA.

In the Raman studies by Peticolas and coworkers [59-61], the structures of the tetramers were elucidated by a comparison of their Raman spectra to reference spectra of poly(dG-dC) • poly(dG-dC) in the standard B- and Z-forms. The Raman results indicate that CGCG, GCGC and GGCC are in a right handed conformation similar to that of poly(dG-dC) • poly(dG-dC), and that only CCGG is markedly different from a standard B-form. CCGG, however, did not show Raman marker bands typical of the A-form.

All of the previous discussed studies agree that the four tetramers exist in a right handed conformation in low ionic strength solutions, although the exact nature of the conformation is not clear. The Raman data (except for CCGG) are consistent with a canonical B-form structure. CD data suggest that the alternating tetramers are in a B-type conformation, and that the GGCC exists in a similar form, although its CD spectrum is unusual.

The VCD data obtained for the four tetramers are sufficiently different from those of d(CG)$_5$ or poly(dG-dC) • poly(dG-dC) to suggest a significant perturbation of the canonical B-form conformation. In addition, the VCD spectra of the four tetramers differ markedly among themselves, whereas the CD spectra were similar within the alternating and the non-alternating series.

The differences between the VCD spectra of the four tetramers can be explained relatively easily. The most dominant interactions giving rise to VCD intensities are those between adjacent base pairs in a double strand. In CGCG, the VCD is determined by two "parallel interactions" and one "90° interaction" (*cf.* Section 3.2.2), whereas it is determined by two "90° interactions" and one "parallel interaction" in GCGC. Thus, it is not surprising that the observed and computed VCD of 5'd(CGCG)3' and 5d(GCGC)3' are different. Similar arguments can be made for the non-alternating tetramers.

We have used the DECO formalism, and energy minimized solution structures for the four tetramers, to reproduce the observed VCD spectra. In doing so, we found that VCD based on canonical B-form geometries does not reproduce the observed data well. Furthermore, structures in which the C=O groups are displaced further away from the helix axes, and which are less tightly wound, reproduce the observed results much better. A-family structures, for examples, gave a much better agreement between observed and computed spectra. At this point, we wish to emphasize that we do not imply that the tetramers do exist in an A-form structure, but that the VCD is better reproduced for the less tightly wound geometry. These changes in structure could be static or dynamic: VCD cannot differentiate whether or not there is a fast dynamic equilibration between A-, B- or any other geometries, or whether the true geometry is static and corresponds to structural parameters in between those of the extreme A- and B-form geometries.

Contradictory structural information derived from various techniques can be due to a number of reasons. NMR and VCD, for example, sample molecular conformations at vastly different time scales. In some cases, the conformational variations of a molecule may be slower than the time scale of molecular vibrations but faster than the

NMR time scale. In such instances, it is clear that the two techniques are subject to different averaging processes. In the nucleotides discussed here, the difference in time scales between NMR and VCD are less important, since the tetramers are thought to exist as relatively stable, hydrogen-bonded double helices. Dynamic and static end fraying occurs most likely in all the tetramers to a varying degree, but these effects yielded similar results in both NMR and VCD, namely that significant deviation from canonical B-form structure exists. NMR data suggest that end fraying is less prevalent in CGCG [62,64] than in GCGC, and that it retains more of a base-paired and base-stacked structure. Fraying will mainly alters the conformation of the external base pairs and reduces their dipolar coupling, and will leave the central (GC) duplex in the case of the 5'd(CGCG)3' and a central (CG) duplex in 5'd(GCGC)3'. In the latter case, with strong end fraying effects, the spectrum should be primarily determined by the central (CG) pair, for which VCD data have been calculated [22]. The sign pattern of the calculated data agrees with the observed spectrum of 5'd(GCGC)3'. In 5'd(CGCG)3', on the other hand, significant coupling between the center and the end pairs occurs, and the spectra appear more like those of the polymer.

The discrepancy between Raman and VCD derived conformations must be sought in terms of the different regions of the molecules sampled by the two techniques, rather than their time scales. Most Raman interpretations are based on the vibrations of a certain moiety of the oligomer or polymer. When a polymer undergoes a B → Z transition, every other (deoxy-) ribose groups will change from the C2'- endo furanose to the exo conformation. However, the presence of the marker band due to the C2' - endo furanose in the tetramers does not imply necessarily that the **overall** conformation is unchanged. It merely implies that the furanose conformation is unchanged, and that a slight unwinding or opening of the duplex could have happened undetected. Chiroptical techniques, such as CD and VCD, are less sensitive than Raman spectroscopy to local group conformation, as discussed above, but much more sensitive to overall alignment of the transitions which give rise to CD or VCD. Thus, the results from Raman and VCD data are not necessarily in contradiction, but rather supplementing each other. The Raman data suggest that the tetramers, with the exception of CCGG, have many local features consistent with B-form conformation. The VCD data, however, suggest that some unwinding, opening and end-fraying has distorted the canonical structures.

In terms of this discussion, the disagreement between ECD and VCD results for the non-alternating tetramers needs to be investigated further. It appears that for the alternating tetramers, the overall agreement between ECD, VCD and Raman spectral results is good. However, contradictions occur in CCGG and GGCC between ECD and VCD results: ECD results indicated that CCGG was an exception, and that GGCC had an unusual spectrum. Discrepancies between VCD and ECD derived structural information have been documented in peptides and proteins and were interpreted in terms of the different interaction distances by Keiderling and coworkers [35].

The VCD results indicate that at low salt concentration and low temperature, the four tetramers exist in a right handed conformation which is more unwound than the canonical B-form, and may approach distances and dihedral angles between the C=O transition similar to those found in the A-form. However, Raman data suggest that the backbone conformations still resembles most closely that of the B-form. In high ionic strength solution, only CGCG assumes a left handed conformation according to the VCD results, which is in agreement with previous studies. At increasing temper-

ature, all tetramers melt reversibly, which is indicated in the VCD spectra by a loss of detail until only a broad feature is left, and an increase in the integrated infrared absorption intensity. The denaturation point is reached at 40 °C for low and about 25 °C for high ionic strength solution.

6. CONCLUSIONS

In this review, a summary of the developments in the application of VCD to analyze biomolecular structure was given. Although the experimental technique can certainly still be improved upon, instruments have been constructed which permit the fast (< 2 hours) and reliable acquisition of VCD data from biological samples. Preliminary models for the interpretation of VCD spectra have been developed and used successfully for a number of sample systems.

In the case of peptides, VCD may be particularly useful in establishing the solution conformation of small peptides which cannot be analyzed *via* NMR spectroscopy. In fact, there appears to be contradictory information available from these two techniques, which is due to the different time scales at which VCD and NMR transitions occur. In VCD, one samples many billions of snapshots of molecular conformation *via* vibrational transitions, which occur on the femtosecond time scale. The conformational information is probed along the molecular backbone, since the probe groups (C=O) are directly attached to the backbone chain. The coupling distance is relatively short, due to the low dipole transition moment of a carbonyl stretching vibration. In NMR, on the other hand, interactions of amino acids in a peptide are sampled, which may be very far apart along the molecular backbone, but interact due to the particular secondary structure of the molecule. In order for such an interaction to occur, the molecule must be in a well-defined conformation, which will most likely be found in a large peptide. In small peptides, the rapid interconversion of structures can lead to a weakening of the NMR interactions to a point that they are no longer observable.

The small DNA models studied so far do not display as much structural flexibility as do small peptides, and exhibit a conformation which is stable on the NMR time scale. Thus, the conformational information obtained *via* VCD and NMR will be less contradictory than in the case of small peptides. However, VCD can also provide novel conformational information for DNA models as well, since the positions of the nucleotide carbonyl groups are sampled by VCD and a detailed picture of the alignment of the bases can be obtained.

7. ACKNOWLEDGEMENTS

8. REFERENCES

1   a) Holzwarth, G., Hsu, E.C., Mosher, H.S., Faulkner, T.R. and Moscowitz, A., J.Amer.Chem.Soc., 96 (1974) 251.
b) Faulkner, T.R., Moscowitz, A., Holzwarth, G., Hsu, E.C. and Mosher, H., J.Amer.Chem.Soc., 96 (1974) 252.

2   Nafie, L.A., Cheng, J.C. and Stephens, P.J., J.Amer.Chem.Soc., 97 (1975) 3842.

3   Yasui, S.C. and Keiderling, T.A., J.Amer.Chem.Soc., 108 (1986) 5576.

4   Dyson, H.J. and Wright, P.E., Annu.Rev.Biophys.Biophys.Chem., 20 (1991) 519.

5   Wütherich, K., NMR of Proteins and Nucleic Acids, Wiley Interscience, New York (1986)

6   Snir, J., Frankel, R.A. and Schellman, J.A., Biopolymers, 14 (1975) 173.

7   Velluz, L., Legrand, M. and Grosjean, M., Optical Circular Dichroism: Principles, Measurements and Aplications, Verlag Chemie - Academic Press New York (1965)

8   Diem, M., in "Vibrational Spectra and Structure", J.Durig, Editor, Elsevier Science Publishers, Amsterdam, The Netherlands, Vol. 19 (1991) 1 - 54.

9   Diem, M., Roberts, G.M., Lee, O. and Barlow, A., Appl.Spectrosc. 42 (1988) 20.

10   Lee, O. and Diem, M., Analytical Instrumentation, 20 (1992) 23.

11   Nafie, L.A., Keiderling, T.A. and Stephens, P.J., J.Amer.Chem.Soc., 98 (1976) 2715.

12   Nafie, L.A. and Diem, M., Appl. Spectrosc., 33 (1979) 130.

13   Nafie, L.A., Diem, M. and Vidrine, D.W., J.Amer.Chem.Soc., 101 (1979) 496.

14   Lipp, E.D. and Nafie, L.A., Appl. Spectrosc., 38 (1984) 20.

15   Malon, P. and Keiderling, T.A., Appl.Spectrosc., 42 (1988) 32.

16   Tinoco, I., Radiation Research, 20 (1963) 133.

17   Moffit, W., J.Chem.Phys., 25 (1956) 467.

18   Gulotta, M., Goss, D.J. and Diem, M., Biopolymers, 28 (1989) 2047.

19   Faulkner, T. R., PhD Dissertation, University of Minnesota (1976)

20   Holzwarth, G. and Chabay, I., J.Chem.Phys., 57 (1972) 1632.

21   Still, C., MacroModel, Columbia University, New York, NY, Version 2.5, (1989)

22   Zhong, W., Gulotta, M., Goss, D. J. and Diem, M., Biochemistry, 29 (1990) 7485.

23   Lee, O., Roberts, G.M. and Diem, M., Biopolymers, 29 (1989) 1759.

24   Schellman, J., Accounts Chem.Res., 1 (1968) 144.

25   Xiang, T., Goss, D.J. and Diem, M., Biophysical Journal, submitted (1993)

26   Diem, M., Gotkin, P.J., Kupfer, J.M and Nafie, L.A., J.Amer.Chem.Soc., 100 (1978) 5644.

27   Singh, R.D. and Keiderling, T.A., Biopolymers, 20 (1981) 237.

28   Lal, B.B and Nafie, L.A., Biopolymers, 21 (1982) 2161.

29   Sen, A.C. and Keiderling, T.A., Biopolymers, 23 (1984) 1519.

30   Paterlini, G.M., Freedman, T.B. and Nafie, L.A., Biopolymers, 25 (1986) 1751.

31   Roberts, G.M., Lee, O., Calienni, J. and Diem, M., J.Am.Chem. Soc., 110 (1988) 1749.

32   Diem, M., Lee, O. and Roberts, G.M., J.Phys.Chem., 96 (1992) 548.

33   Birke, S.S., Agbaje, I. and Diem, M., Biochemistry, 31 (1992) 450.

34   Pancoska, P. and Keiderling, T.A., Biochemistry, 30 (1991) 6885.

35   Pancoska, P., Yasui, S.C., and Keiderling, T.A., Biochemistry, 28 (1989) 5917.
36   Keiderling, T.A. in "FT-IR Spectroscopy in Industrial and Laboratory
       Analyses", Ferraro,J.R. & Krishnan,K., Eds, (1990) 203.
37   Freedman, T.B. and Nafie, L.A., in Topics in Stereochemistry', Eliel, E.L., and
       Wilen, S.H., Editors, J.Wiley and Sons, New York, Vol. 17, (1987) 114.
38   Greenfield, N.J and Fasman, G.D., Biochemistry, 8 (1969) 4108.
39   Dukor, R.K. and Keiderling, T.A., Biopolymers, in press.
40   Woody, R.W., Ad.Biophys.Chem. (Bush, C.A., Ed.), JAI Press, Greenwich, CT
       2 (1991) in press.
41   Yasui, S.C. and Keiderling, T.A., Biopolymers, 25 (1986) 5.
42   Tiffany, M. L. and Krimm, S., Biopolymers, 6 (1968) 1379.
43   Sengupta, P.K. and Krimm, S., Biopolymers, 26 (1987) S99.
44   Birke, S.S., Farrell, C., Lee, O., Agbaje, I., Roberts, G. and Diem, M., in
       "Spectroscopy of Biological Molecules", R.E.Hester and R.B.Girling, Editors,
       The Royal Society of Chemistry, Cambridge, UK (1991) 131.
45   Yasui, S.C., Keiderling, T.A., Formaggio, F., Bonora, G.M. and Toniolo, C.,
       J.Amer.Chem.Soc., 108 (1986) 4988.
46   Chernovitz, A.C., Freedman, T.B. and Nafie, L.A., Biopolymers, 26 (1987) 1879.
47   Dukor, R.K., Keiderling, T.A. and Gut, V., J.Pept.Prot.Research, in press
48   Diem, M., Barlow, A. and Luque, R., Biopolymers, submitted (1993)
49   Wyssbrod, H. and Diem, M., Biopolymers, 31 (1992) 1237.
50   Karle, I., J.Amer.Chem.Soc., 100 (1978) 1286.
51   Pease, L.G. and Watson, C., J.Amer.Chem.Soc., 100 (1978) 1279.
52   Barlow, A., Gounarides, J.S., Diem, M., Xue, X.B. and Naider, F., Biopolymers
       submitted
53   Annamalai, A. and Keiderling, T.A., J.Amer.Chem.Soc., 109 (1987) 3125.
54   Yang, L. and Keiderling, T.A., Biopolymers, in press
55   Wang, L. and Keiderling, T.A., Biochemistry, 31, (1992) 10265.
56   Swaminathan, S., Ravishanker, G. and Beveridge, D.L., J.Amer.Chem.Soc.,
       113 (1991) 5027.
57   S.S. Birke, M. Moses, B. Kagalovsky, D. Jano, M. Gulotta and M. Diem, Bio
       physical Journal, submitted for publication
58   Quadrifoglio, F., Manzini, G., Vasser, M., Dinkespield, K. and Crea, R.,
       Nucleic Acid Res., 9, (1981) 2195.
59   Thomas, G.A. and Peticolas W.I., Biopolymers, 28 (1989) 1625.
60   Thomas, G.A. and Peticolas W.I., Biochemistry, 23 (1984) 3202.
61   Thomas, G.A. and Peticolas W.I., J.Amer.Chem.Soc., 105 (1983) 986.
62   Patel, D.J., Biopolymers, 15 (1976) 533.
63   Patel, D.J., Biopolymers, 16 (1977) 1635.
64   Patel, D.J., Biopolymers, 18 (1979) 553.
65   Kastrup, R.V., Young, M.A., and Krugh, T.R., Biochemistry, 17 (1978) 4855.

Chapter 5

Determination of absolute configuration by CD. Applications of the Octant Rule and the Exciton Chirality Rule

D. A. Lightner[a]

[a]Chemistry Department, University of Nevada, Reno, Nevada 89557-0020

1. INTRODUCTION
    1.1.   Ordinary absorption of light by chromophores
    1.2.   Circular dichroism (CD)

2. APPLICATIONS OF THE OCTANT RULE
    2.1.   Optical activity of chromophores
    2.2.   The Octant Rule
    2.3.   Stereochemistry and conformational analysis of saturated alkyl ketones
            2.3.1. Monocyclic ketones
            2.3.2. Bicyclic ketones
            2.3.3. Polycyclic ketones
            2.3.4. Isotopically perturbed ketones
    2.4.   Stereochemistry of unsaturated ketones
            2.4.1. α,β-Unsaturated ketones
            2.4.2. The extended octant rule for β,γ-unsaturated ketones

3. APPLICATIONS OF EXCITON CHIRALITY CD
    3.1.   Interaction of chromophores
    3.2.   Origins of exciton coupling
    3.3.   The Exciton Chirality Rule
    3.4.   Bichromophoric systems and the absolute configuration of diols
    3.5.   Examples of determination of absolute configuration

4. CONCLUSIONS

5. REFERENCES AND NOTES

1. INTRODUCTION

1.1. Ordinary absorption of light

Organic molecules typically absorb light in the UV-visible region of the electromagnetic spectrum, from the far UV (below 200 nm) to the near IR, (800-1000 nm). Recording the absorption of light in this spectral region, called electronic absorption or UV-visible spectroscopy, measures both the energy and the probability of exciting a molecule from its ground electronic state to an electronically excited state, a process which involves promotion of an electron from an occupied molecular orbital to an unoccupied molecular orbital (Figure 1). Typically, the absorption phenomenon can be said to originate from within a particular component or group in a molecule, called a chromophore. Although many different electronic excitations are possible, in principle, in a large organic molecule, those of greatest importance for use in structure determination typically involve promotion of an electron from one of the higher occupied bonding or nonbonding orbitals to the lowest unoccupied molecular orbital (Figure 1). The process is measured in UV-visible spectroscopy by plotting the absorption of light vs its energy and is typically displayed (Figure 2) with a horizontal energy axis (excitation wavelength, λ (nm)) vs intensity of absorption (Absorbance, A) or the probability of electronic excitation on the vertical axis. The absorbance scale may be represented in normalized form plotted as ϵ, the molar extinction coefficient, M^{-1} cm^{-1}, which also varies with changing λ. The terms A and ϵ are related by Beer's Law, $A = \epsilon \cdot \ell \cdot C$, where ℓ is sample thickness or cuvette pathlength (cm), and C is the molar concentration. λ is related to energy (E) by Planck's Law, $E = hc/\lambda$, where h is Planck's constant and c is the speed of light.
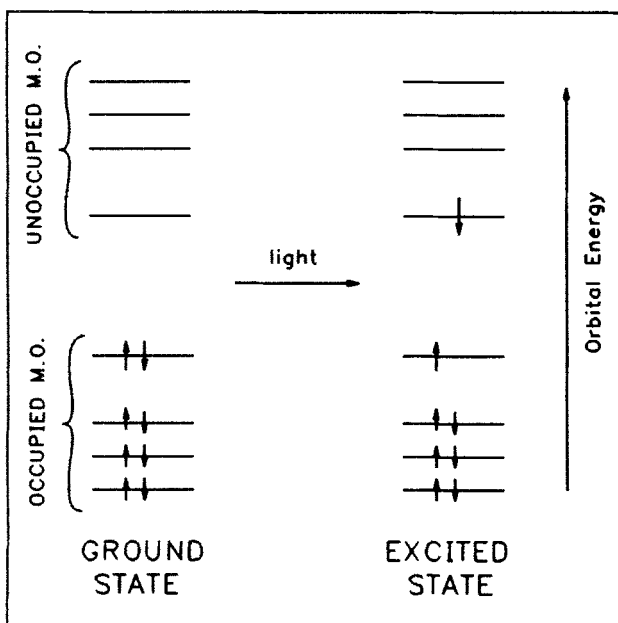
Figure 1. Electronic excitation from the highest occupied molecular orbital to the lowest unoccupied molecular orbital. The absorption of UV-visible light promotes a molecule from its ground electronic state to an excited state. The excited state shown is a singlet excited state where all electron spins are paired.
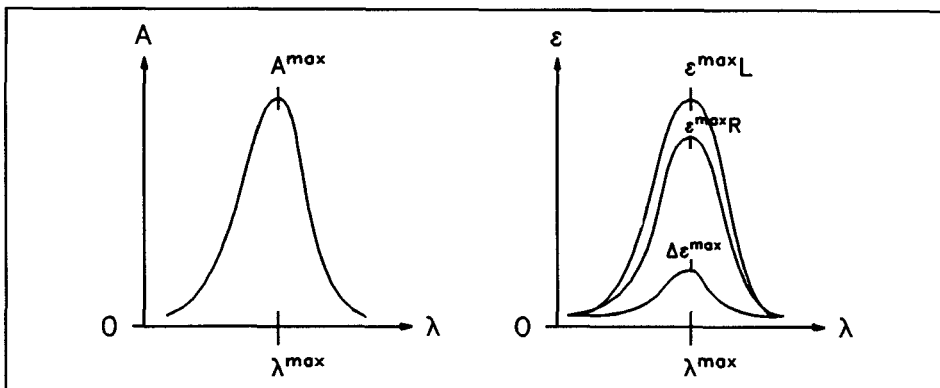
Figure 2. (Left) UV-visible absorption spectrum in the region of an electronic transition. Absorption of light is shown by plotting absorbance (A) on the vertical axis vs wavelength (λ) on the horizontal axis. The plot could just as well have been presented in ϵ vs λ since Beer's Law relates A to ϵ. (Right) UV-visible absorption spectra in the region of an electronic transition for the absorption of left (L) and right (R) circularly polarized light by a chiral compound. In this example, left circularly polarized light is absorbed to a greater extent than right circularly polarized light, $\epsilon_L > \epsilon_R$, so the difference curve $\Delta\epsilon$ vs λ (where $\Delta\epsilon = \epsilon_L - \epsilon_R$ in the standard convention) is positive ($\Delta\epsilon > 0$) and is called a positive circular dichroism (CD) Cotton effect. When right circularly polarized light is absorbed to a greater extent than left circularly polarized light ($\epsilon_R > \epsilon_L$), a plot of $\Delta\epsilon$ vs λ gives a negative CD curve ($\Delta\epsilon < 0$) called a negative Cotton effect. When $\Delta\epsilon > 0$ or $\Delta\epsilon < 0$, the compound exhibits circular dichroism, and a plot of $\Delta\epsilon$ vs λ constitutes its CD spectrum.

1.2. Circular dichroism (CD)

When linearly polarized light is resolved into its two circularly polarized components (left and right circularly polarized light, Figure 3), and the absorption of each component is separately measured in the UV-visible spectral region, the absorption of left circularly polarized light will not always be identical to the absorption of right , $\epsilon_L \neq \epsilon_R$ (Figure 2). The special circumstances for unequal absorption (called circular dichroism, CD) of left and right circularly polarized light result when the compound being measured is optically active, i.e., the component molecules are chiral with one handedness predominating, as in (1R)-2-norbornanone. On the other hand, for an achiral molecule, such as 7-norbornanone, or for equal mixtures of enantiomers, as in racemic 2-norbornanone, left circularly polarized light is absorbed to the same extent as right circularly polarized light ($\epsilon_L = \epsilon_R$), and no CD ($\Delta\epsilon = 0$) is exhibited over the entire spectral range (Figure 4). CD is thus a unique property of chiral molecules, and both UV-visible absorption spectroscopy and CD spectroscopy arise from the same photophysical process: transition of a molecule from its ground state to an electronically excited state. For a ketone carbonyl, the lowest energy singlet excitation involves the transition from a nonbonding orbital (n) to an antibonding π^* orbital.
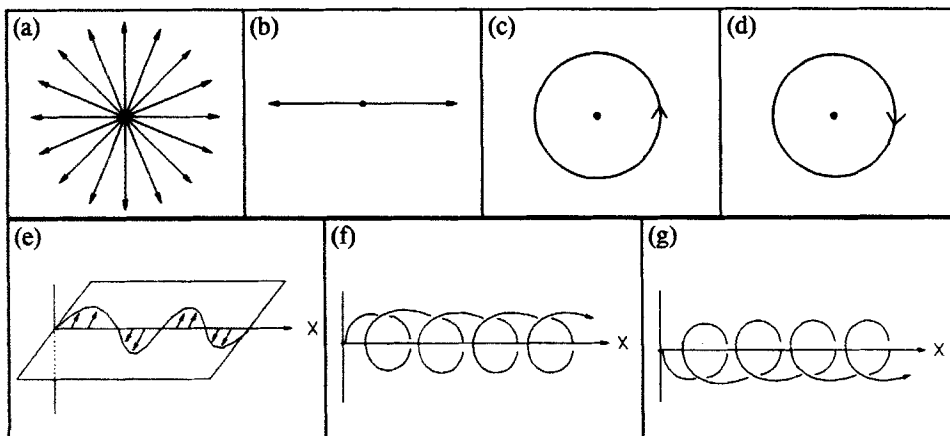
Figure 3. Schematic of (a) unpolarized light, (b) linearly polarized light, (c) left circularly polarized light and (d) right circularly polarized light as viewed with the light travelling toward the observer's eye. Schematic side view of (e) linearly polarized, (f) left circularly polarized and (g) right circularly polarized light propagated in the X direction. Linearly polarized light (b) is only one of the many vectors (directions) comprising unpolarized light and travels in the horizontal plane (e) shown. Left circularly polarized light (c) travels along a left-handed helix (f); and right circularly polarized light (D) travels along a right handed helix (g).
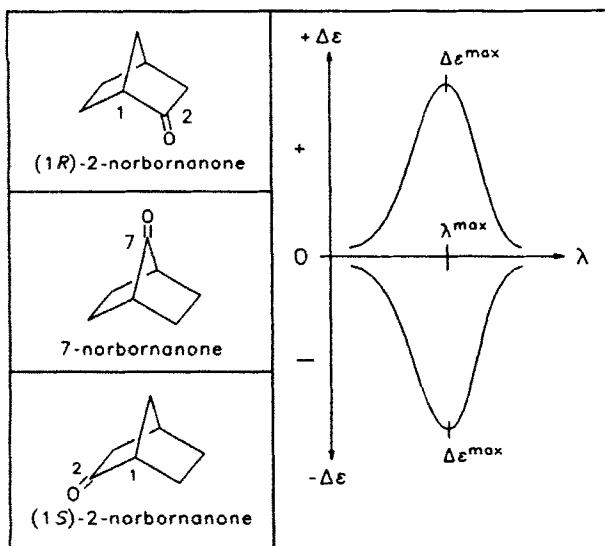
Figure 4. (Left) Structures of norbornanones. (Right) CD curves (plots of $\Delta\epsilon$ vs λ) for the enantiomeric 2-norbornanones. For the carbonyl n $\rightarrow$ π^* transition, the $+\Delta\epsilon$ curve is associated with the (1R) enantiomer and the $-\Delta\epsilon$ curve with the (1S) isomer. An equal mixture of the enantiomers (racemic mixture), or the achiral isomer, 7-norbornanone, would have $\Delta\epsilon=0$ over the range of λ.

In the following sections, we show how circular dichroism (CD) in the UV-visible spectral region can be used to determine the absolute configuration of chiral molecules and to extract conformational information. In the first part we describe the Octant Rule [1] and show how the absolute configuration and/or conformation of ketones can be assigned from their n → π^* CD spectra. In the second part we describe the Exciton Chirality Rule [2] and show how absolute configurations can be assigned from CD spectra which have their origin in the interaction of two (or more) chromophores through exciton coupling.

2. APPLICATIONS OF THE OCTANT RULE

2.1. Optical activity of chromophores

Although chiral molecules may exhibit optical activity as detected by circular dichroism (CD), the focus of understanding is typically the light absorbing unit (chromophore) in the molecule. A chromophore is said to be optically active if it exhibits CD in the region of its UV-visible absorption bands. Any chromophore in a chiral molecule can be expected to exhibit Cotton effects (Figure 2). In some chiral molecules, the chromophore itself is chiral, as in the classic case of hexahelicene and in a nonplanar diene, such as 5-methyl-1,3-cyclohexadiene. In other chiral molecules, the chromophore is achiral, as in the case of the ketone carbonyl of (3S)-methylcyclohexanone and the phenyl group of (2S)-phenylbutane (Figure 5). The distinction between these two limiting types of chromophores, inherently chiral (dissymmetric) and inherently achiral (symmetric), was proposed first by Moffitt and Moscowitz [3] and later by Djerassi, Mislow, Moscowitz [4] and co-workers as a useful classification to account for the origin of the Cotton effects.

Thus, whereas the CD from an inherently chiral chromophore has its origins within the dissymmetry of the chromophore itself, an inherently achiral chromophore cannot exhibit CD without the intervention of extrachromophoric perturbation. Typically, the magnitude ($\Delta\epsilon$) of the Cotton effects of the former are larger than those from the latter by one or two orders of magnitude. For example, the carbonyl chromophore, which is one of the most studied by CD spectroscopy, | $\Delta\epsilon$ | values for the n → π^* transition are typically ~1; in (3R)-methylcyclohexanone $\Delta\epsilon \simeq$ +0.6 at 290 nm, but in M-hexahelicene the long wavelength π-π^* transition near 330 nm has $\Delta\epsilon \simeq$ -200. Because optical activity of the carbonyl chromophore originates from chiral perturbers within the molecule (but lying distant from the chromophore), it can be a very sensitive chiroptical probe. As such, it represents a window for detecting extrachromophoric stereochemistry, as described by the Octant Rule.
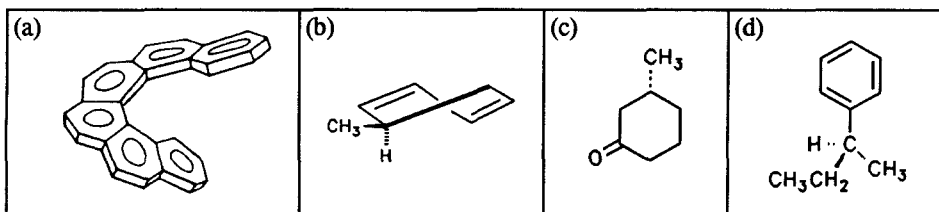
Figure 5. Stereochemical drawings showing the absolute configuration of (a) M-hexahelicene, (b) (5R)-cyclohexa-1,3-diene, (c) (3R)-methylcyclohexanone and (d) (2S)-phenylbutane.

2.2. The Octant Rule

The Octant Rule was one of the first, and probably the most successful, of many different chirality sector rules relating Cotton effects (CE's) to organic stereochemistry. It is certainly the best known and most widely used. On the basis of considerable optical rotatory dispersion data for the n $\rightarrow$ π^* CE's of steroidal ketones and from theoretical considerations, Djerassi, Moscowitz, Woodward, Moffitt and Klyne [1] proposed the Octant Rule for chiral saturated alkyl ketones.[5] Over the more than 30 years since its formulation it has become one of the most important chirality rules for extracting stereochemical and conformational information from optically active ketones. The Octant Rule is derived from the symmetry of the carbonyl n and π^* orbitals of the n $\rightarrow$ π^* transition (Figure 6). In its simplest form, the rule states that all space surrounding the carbonyl chromophore is divided into eight regions (octants) by the two (C_{2v}) local symmetry planes (XZ and YZ, Figure 7) of the isolated C=O chromophore, and a third, non-symmetry-derived surface approximated by a plane (A, in Figures 6 and 7) orthogonal to the other two. This nodal surface separates back octants from front octants. In typical ketones, most of the molecule lies in back octant regions, behind the carbonyl carbon.
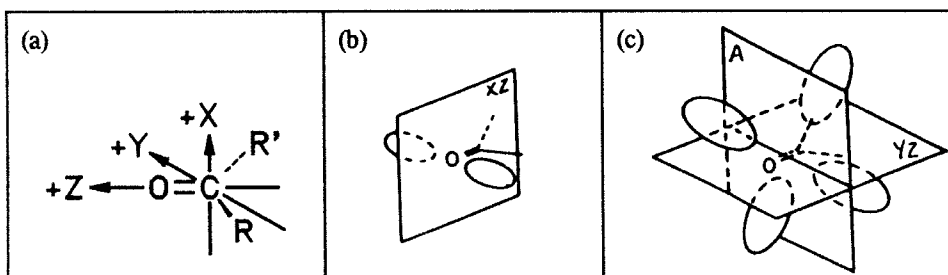
Figure 6. Coordinate system (a) and nodal surfaces (b) and (c) for a saturated ketone R—CO—R'. The nodal plane (XZ) of the n orbital (b) bisects the R—C—R' angle and is perpendicular to the plane of the ketone. The nodal surfaces of the π^* orbital (c) where the plane of the carbonyl group is a nodal plane (YZ, horizontal) and there is another nodal surface (A, vertical), not necessarily a plane, perpendicular to the C=O axis and intersecting it between the carbon and oxygen atoms. [(b) and (c) Redrawn and modified from J.B. Lambert, H.F. Shurvell, D. Lightner and R.G. Cooks, *Introduction to Organic Spectroscopy*, Macmillan, New York, 1987.]

However, some ketones, such as 1-keto and 11-keto steroids have some molecular components lying in front of the carbonyl carbon (even in front of its oxygen), or in front octant regions. Clarification of the boundary between front octants and back octants was the subject of intensive theoretical and experimental studies,[6-11] which led to a clarification on the shape of the third nodal surface as convex (B, Figure 7). For most applications of the Octant Rule it is sufficient to consider only the back octants, and the special circumstances which require consideration of front octants will be obvious from the structure of the ketone. In practical applications of the Octant Rule, the octant diagrams are used to
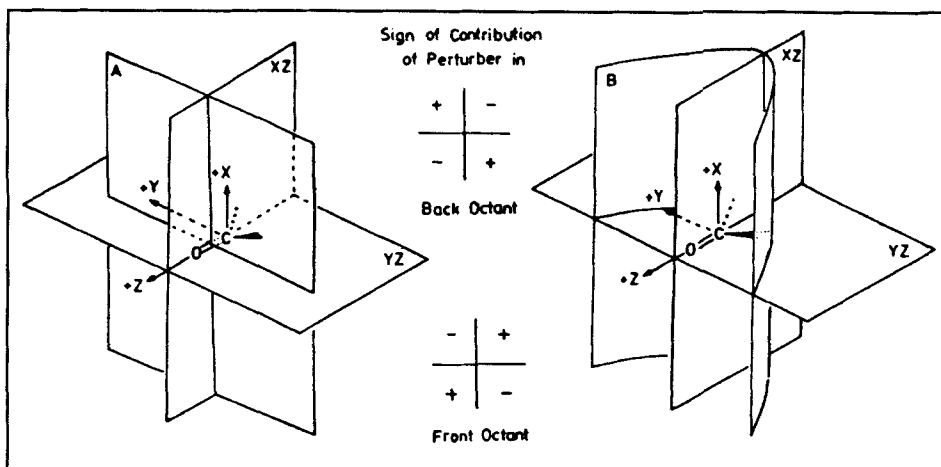
Figure 7. (Left) Classical octant rule diagram (ref 1) for the ketone carbonyl n → π* transition. Local symmetry-derived, orthogonal octant planes XZ and YZ divide all space into quadrants, and a non-symmetry-derived third nodal surface (A) is approximated by an orthogonal plane bisecting the C=O bond. "Front" octants are those nearer an observer along the +Z axis, while "back" octants lie towards -Z. (Middle) Octant contribution signs that perturbers make in back and front octants. (Right) Revised octant rule [6] with octant planes XZ and YZ unchanged and the third nodal surface defined theoretically as a concave surface (B). [Reprinted with permission from ref. 7. Copyright © 1986 American Chemical Society.]

assess the signed contributions made by each main atom or group to the net n → π* CE of the ketone. Contributions from different substituents are assumed to be additive, and the middle part of Figure 7 shows the signed contributions due to perturbers in the various octants. Atoms having counterparts symmetrically placed across the carbonyl symmetry planes (XZ, YZ) and atoms lying in symmetry planes are assumed to make no contribution to the CD. The magnitudes of the contributions vary according to the nature of the perturber, but fall off rapidly with increasing distance from the carbonyl group or closeness to the nodal surfaces. Substituents falling in upper left or lower right back octants make a positive contribution to the CE. The octant signs change with each reflection across a nodal surface.

In order to apply the Octant Rule to the determination of the absolute configuration of a ketone, its conformation must be known. In the case of cyclohexanones, we will assume predominance of the chair conformation and position the cyclohexanone on the octant diagram of Figure 7 so that the local symmetry planes of the cyclohexanone carbonyl are coincident with those shown (as illustrated in Figure 8(a)). A planar projection octant diagram of the carbon atoms of chair cyclohexanone is shown in Figure 8(b), where the (+) and (-) signs shown are the signed contributions made by perturbers lying in octants. In the case of cyclohexanone, which is symmetric and achiral, carbons 1, 2, 4 and 6 lie in

symmetry planes and thus make no contributions. Carbons 3 and 5 lie in upper left (+) and upper right (-) back octants, equally disposed across the XZ symmetry plane and thus make no net contribution (or one cancels the contribution of the other). In (3R)-methylcyclohexanone, however, in which the preferred chair conformation has an equatorial methyl (Figure 9(a)), an octant diagram places the methyl group in an upper left (+) back octant (Figure 9(c)) (or a lower right, and (+) back octant). The net contribution for this conformer is *positive* since all other carbon atoms lie in a carbonyl symmetry plane or are cancelling. Strictly speaking, one weighs the contribution of the equatorial methyl carbon and its 3 hydrogens in the upper left (+) back octant vs an equatorial hydrogen in an upper right (-) back octant. More "weight" is given to the larger group, and hence a net *positive* CD Cotton effect (CE) is predicted. The *observed* CD has a positive CE, $\Delta\epsilon \simeq +0.6$.
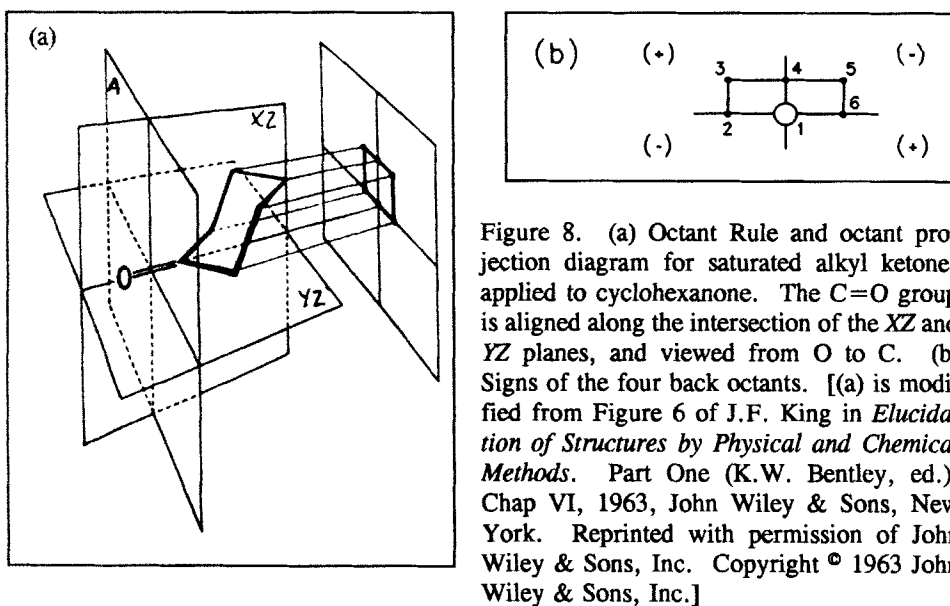
Figure 8. (a) Octant Rule and octant projection diagram for saturated alkyl ketones applied to cyclohexanone. The C=O group is aligned along the intersection of the XZ and YZ planes, and viewed from O to C. (b) Signs of the four back octants. [(a) is modified from Figure 6 of J.F. King in *Elucidation of Structures by Physical and Chemical Methods*. Part One (K.W. Bentley, ed.), Chap VI, 1963, John Wiley & Sons, New York. Reprinted with permission of John Wiley & Sons, Inc. Copyright © 1963 John Wiley & Sons, Inc.]

When the cyclohexanone chair is frozen, as in the adamantanone of Figure 10, one finds a nearly identical CD to that of (3R)-methylcyclohexanone. Thus its counterpart, (1S,3R)-4(e)-methyladamantan-2-one, has $\Delta\epsilon^{max} = +0.67$ (295 nm) and (3R)-methylcyclohexanone has $\Delta\epsilon^{max} = +0.57$ (294 nm) in ethyl ether-isopentane-ethanol (5:5:2, v/v/v) at room temperature.[7] Replacing the methyl perturber with larger alkyl substituents, as with ethyl, isopropyl, *tert*-butyl or neohexyl causes very little change in the adamantanone spectra (Figure 11); so the major contribution must be made by the first carbon in the chain, and the magnitude of the octant contributions falls off rapidly with distance. A rather different CD is found for the corresponding set of 4(a)-alkyladamantanone (Figure 12), attributed to the alkyl perturbers lying in front octants, as noted below.
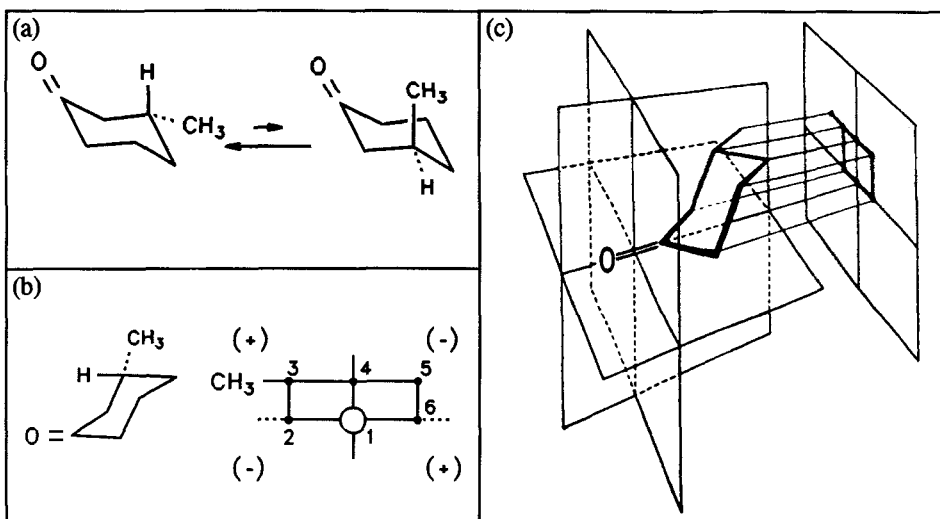
Figure 9. (a) Interconverting chair conformers of (3R)-methylcyclohexanone with equatorial (left) and axial (right) methyls. (b) Orientation of the equatorial methyl conformer for viewing its octant projection diagram. (c) Octant Rule applied to and octant projection diagram for (3R)-methylcyclohexanone with an equatorial methyl configuration. [(c) is reproduced with permission of John Wiley & Sons, Inc. from J.F. King in *Elucidation of Structures by Physical and Chemical Methods*. Part One (K.W. Bentley, ed.), Chap VI, 1963, John Wiley & Sons, New York. Reprinted with permission of John Wiley & Sons, Inc. Copyright © 1963 John Wiley & Sons, Inc.]
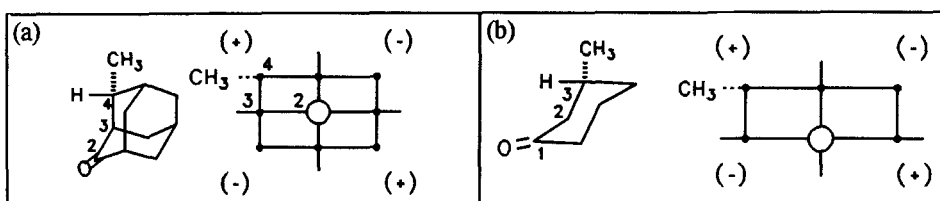
Figure 10. (a) (1S,3R)-4(e)-Methyladamantan-2-one and its octant projection diagram. (b) (3R)-Methylcyclohexanone and its octant projection diagram.

In general octant contributions fall off with increasing distance from the C=O locus, as one might expect. Thus, in methylcyclohexanones (Figure 13), an α-axial methyl (a) makes a much larger contribution than a β-equatorial methyl (b).[12] In these examples, the methyl groups lie far away from octant nodal planes (Figures 7-9). However, when the methyl perturber lies close to an octant symmetry plane, as in α-equatorial (c), even if it also lies close to the C=O the magnitude of the contribution is significantly diminished.
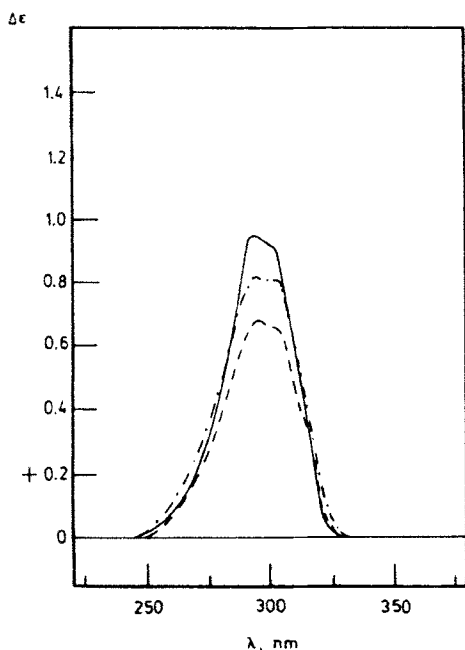
Figure 11. Circular dichroism spectra of 10^{-3} M $(1S,3R)$-4(e)-substituted adamantan-2-ones in EPA (ether-isopentane-ethanol, 5:5:2, v/v/v) run at 25°C and corrected to 100% e.e. The equatorial substituents are methyl (- - - - -), $\Delta\epsilon_{295}^{max}=$ +0.67; ethyl (- · - ·), $\Delta\epsilon_{295}^{max}=$ +0.81; isopropyl (approx. - · - · -), $\Delta\epsilon_{295}^{max}=$ +0.80; tert-butyl (approx. · - · -), $\Delta\epsilon_{295}^{max}=$ +0.771; neohexyl (----), $\Delta\epsilon_{295}^{max}=$ +0.92. [Reprinted with permission from ref. 7. Copyright © American Chemical Society.]
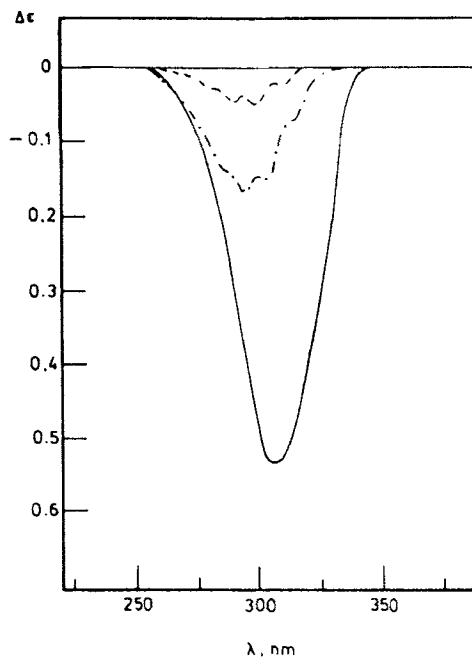
Figure 12. Circular dichroism spectra of 10^{-3} M $(1S,3R)$-4(a)-substituted adamantan-2-ones in EPA (ether-isopentane-ethanol, 5:5:2, v/v/v) run at 25°C and corrected to 100% e.e. The axial substituents are methyl (- - - - -), $\Delta\epsilon_{306}^{max}=$ -0.046; ethyl (approx. - · - · - · -), $\Delta\epsilon_{296}^{max}=$ -0.15; isopropyl (- · - · - · -), $\Delta\epsilon_{297}^{max}=$ +0.17; tert-butyl (-----), $\Delta\epsilon_{296}^{max}=$ -0.54; neohexyl (- · - · - · -), $\Delta\epsilon_{296}^{max}=$ -0.17. [Reprinted with permission from ref. 7. Copyright © American Chemical Society.]

One of the more surprising octant contributions was discovered for a β-axial methyl perturber, which was weak and anti-octant.[13] This finding led to a reinvestigation of the octant rule that resulted in a clarification of the third nodal surface (Figure 7).[6]

The adamantane skeleton locks cyclohexanone units in the chair conformation and thus provides a convenient way to assess the octant contributions of a β-axial ethyl group, which is usually the less stable conformer in cyclohexanone (Figure 14). An octant diagram would predict a (+) CD, but what is actually observed is a very weak *negative* CD (Figure 12), which becomes increasingly negative as the methyl perturber is replaced by larger and

longer alkyl groups. These perturbers are thought to lie very close to, or just *in front of* the convex third nodal surface (B, Figure 7), thus becoming *front octant perturbers*. When perturbers obey the classical Octant Rule (A, Figure 7) for back octants, they are said to make a *consignate* octant contribution; when they make oppositely signed contributions, they are said to make *dissignate* contributions.[11]

(a) α-axial	(b) β-equatorial	(c) α-equatorial	(d) β-axial
Δε ≃ +1.4	Δε ≃ +0.6	Δε ≃ +0.3	Δε ≃ -0.1
(e)	(f)	(g)	(h)

Figure 13. (a)-(d). Chair conformation (upper), approximate Δε (middle), and octant projection diagrams (lower) for α and β-methylcyclohexanones. The Δε values are from refs 6-8, 1 and 12. (e)-(h). (3R)-Methylcyclohexanone with CH_3 in an axial configuration (e); (1S,3R)-4(a)-methyladamantan-2-one (f) and octant diagrams for back octants (g) and front octants (h).

Interest in an experimental verification of front octants and in understanding other dissignate octant effects has been evident from the very beginning of the Octant Rule. The existence of *front octants* was confirmed experimentally in molecules designed to place a methyl perturber in front of the carbonyl oxygen and thus well into a front octant (Figures 14 and 15).[10,14] These studies confirmed *octant* rule behavior, giving further credence to the existence and location of the third nodal surface (Figure 7). They also support the belief that the 3β-axial methyl group of methylcyclohexanone lies in a front octant.

142
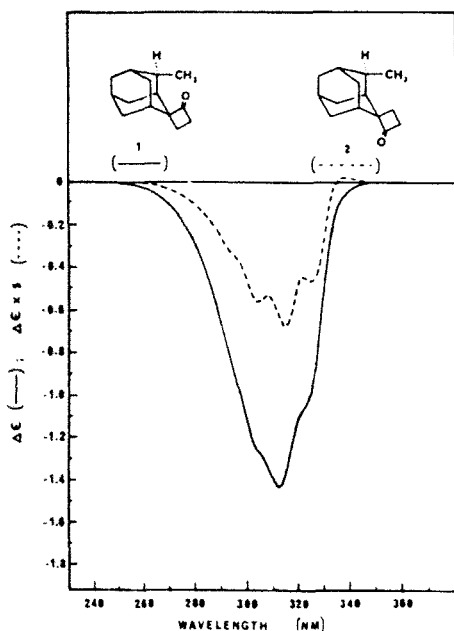
Figure 14. Circular dichroism spectra of *syn*-(1'*R*)-spiro[cyclobutan-2-one-1,2'-(4'(a)methyl-adamantane)] (1) (——) *anti*-(1'*R*)-spiro[cyclobutan-2-one-1,2'-(4'(a)-methyl-adamantane (2) (- - -) in isopentane at 20°. Corrections are made to 100% optical purity. [Reprinted with permission from ref. 14a. Copyright © 1974 American Chemical Society.]
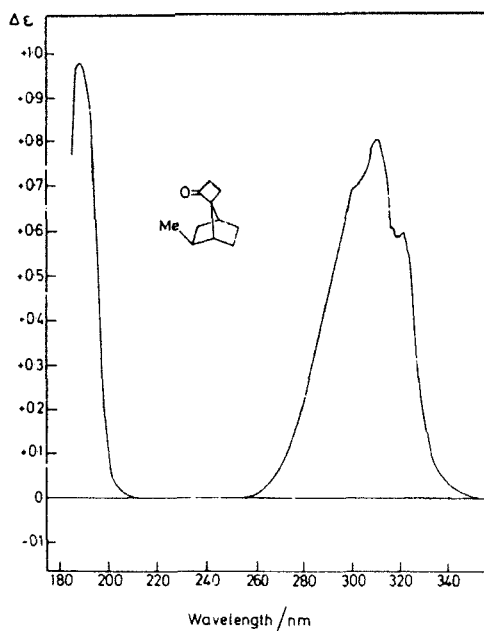
Figure 15. Circular dichroism spectra of *syn*-(1'*R*)-spiro[cyclobutan-2-one-1,7'-(2'-*exo*-methylnorbornane)] in isopentane at 20°. Corrections are made to 100% optical purity. [Reprinted with permission from ref. 14b. Copyright © 1974 The Royal Society of Chemistry.]

2.3. Stereochemistry and conformational analysis of saturated alkyl ketones

2.3.1. Monocyclic ketones. Attempts have been made to assign the magnitudes of contributions to octant perturbers, especially alkyl perturbers (*e.g.*, the contributions of an α-axial methyl or a β-equatorial methyl).[11,12,15] However, these attempts have been incompletely successful due to the lack of suitable conformationally rigid models. It is now known that apparently slight symmetric distortions of the cyclohexanone ring can change the relative orientation of an α-substituent to the C=O group, and hence the magnitude of its octant contribution. For example (Figure 16), the axial methyl of *trans*-2(a)-methyl-4-*tert*-butylcyclohexanone makes an octant contribution $\Delta\epsilon \simeq +1.4$ [12b] but the axial methyl of the corresponding 2(a)-methylbicyclo[3.2.1]octan-3-one contributes only $\Delta\epsilon \simeq +0.89$.[8] Yet the torsion angles between the methyl and carbonyl groups
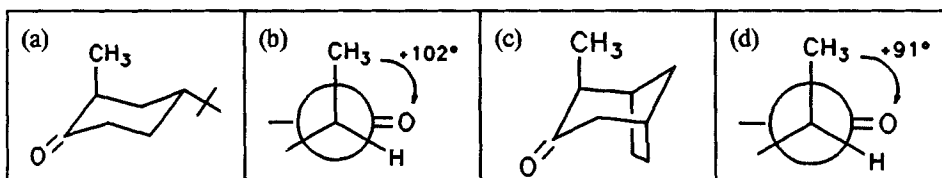
Figure 16. Chair conformations of *trans*-(α-axial)-methyl-4-*tert*-butylcyclohexanone (a) and (α-axial)-methylbicyclo[3.2.1]octanone (c). Newman projections showing relative orientations of methyl and C=O groups (b) and (d), with torsion angles indicated.
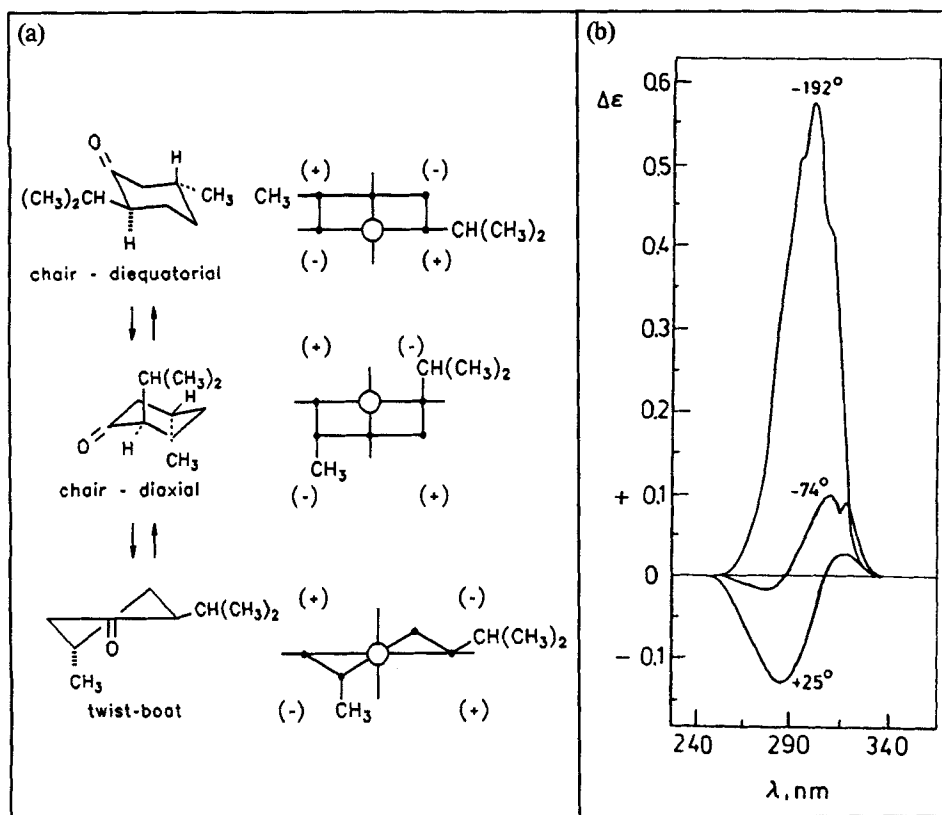
Figure 17. (a) Conformers of (-)-menthone and then octant projection diagrams. (b) Variable temperature CD spectra of (-)-menthone in hydrocarbon solvents: +25° and -74° (decalin); -192° (isopentane-methylcyclohexane).

differ by only ~10°, with the bicyclic ketone being slightly flatter in the vicinity of the C=O due to the anti-reflex action of the two-carbon bridge connecting the β,β' carbons of

144

the cyclohexanone moiety. A possible non-symmetric deformation of the cyclohexanone ring has been considered for trans-2(a)-methyl-4-tert-butylcyclohexanone,[12b] but this is not detected by NMR analyses or molecular mechanics calculations.[8] In addition, CD measurements at 77°K reveal no change in the spectrum, consistent with the postulate that the conformation indicated (Figure 16) is the most stable conformation.

Low temperature CD measurements have been used to extract conformational information when the absolute configuration was already known. Although a wide variety of ketones have been investigated, two classical examples are worthy of note. The most stable conformation of (-)-menthone is almost certainly one where both the α-isopropyl and β-methyl groups are equatorial (Figure 17). The diaxial conformer might relax into a lower energy twist boat conformation, but that would still be a higher energy state. The observed CD spectrum [16] in hydrocarbon solvent at 25°C consists of a mainly negative CD with a weak positive component. As the temperature is lowered, the positive CE predominates, indicating that the lowest energy conformer has a strong positive CD ($[\phi] \simeq 1900$ or $\Delta\epsilon \simeq +0.6$). The diequatorial conformer is predicted to have a moderate (+) CD; whereas, the diaxial and twist boat conformers are predicted to exhibit strong (-) CEs. At room temperature a small population of either the diaxial or twist-boat conformers might thus overwhelm the (+) CD due to the major diequatorial conformer. However, as the temperature is lowered and the population is shifted more toward the more stable conformer, the (+) CE becomes dominant.[16-18]

A second example is that of (+)-1-trans-6-chloro-3-methylcyclohexanone, which can adopt the diequatorial or diaxial chair cyclohexanone conformations, or a twist-boat conformation (as above for (-)-menthone). In isooctane solvent a negative n → π^* CD Cotton effect is observed, but in methanol, the CE is positive (Figure 18).[17-19] Octant projection diagrams for the two chair conformations predict a moderate-to-weak CE for the diequatorial isomer and a strong negative CE for the diaxial isomer. One observes a (+) CE in methanol, suggesting a preponderance of the diequatorial isomer. But in isooctane a (-) CE is seen, corresponding to a significant percent of the diaxial isomer. The red-shifted CD spectrum is consistent with an α-axial chlorine,[17] indicating that the twist-boat conformer is not important in this solvent.

Application of the Octant Rule to 2-oxo-p-menthanol (Figure 19) predicts a (+) CE for the equatorial isopropyl isomer and a (-) CE for the axial isopropyl isomer. Interestingly, a (+) CE is observed in methanol solvent; whereas, a (-) CE is observed in isopentane-methylcyclohexane cosolvent.[20] These results suggest that the axial isopropyl isomer, stabilized apparently by intramolecular hydrogen bonding between the α-equatorial OH and the C=O, is present to a much greater extent in the hydrocarbon solvent than in methanol solvent. This destabilizes the intramolecular hydrogen bonding and in which the equatorial isopropyl isomer is the major species present.

2.3.2. Bicyclic ketones. Application of the Octant Rule to the determination of absolute configurations of decalones illustrates its usefulness.[11,18,21] For (5S)-trans-1-decalone (a) of Table I, a (-) CD CE is predicted, while a (+) CD CE would be predicted for its mirror image. Since a (-) CE is observed, the absolute configuration can be assigned as drawn in Table I. The octant projection diagram indicates that carbons 1, 2, 8, 9 and 10 all lie on a carbonyl symmetry plane; carbon 4 lies on an orthogonal symmetry plane. Carbons 3 and 5 lie equally disposed across a symmetry plane. According to the Octant
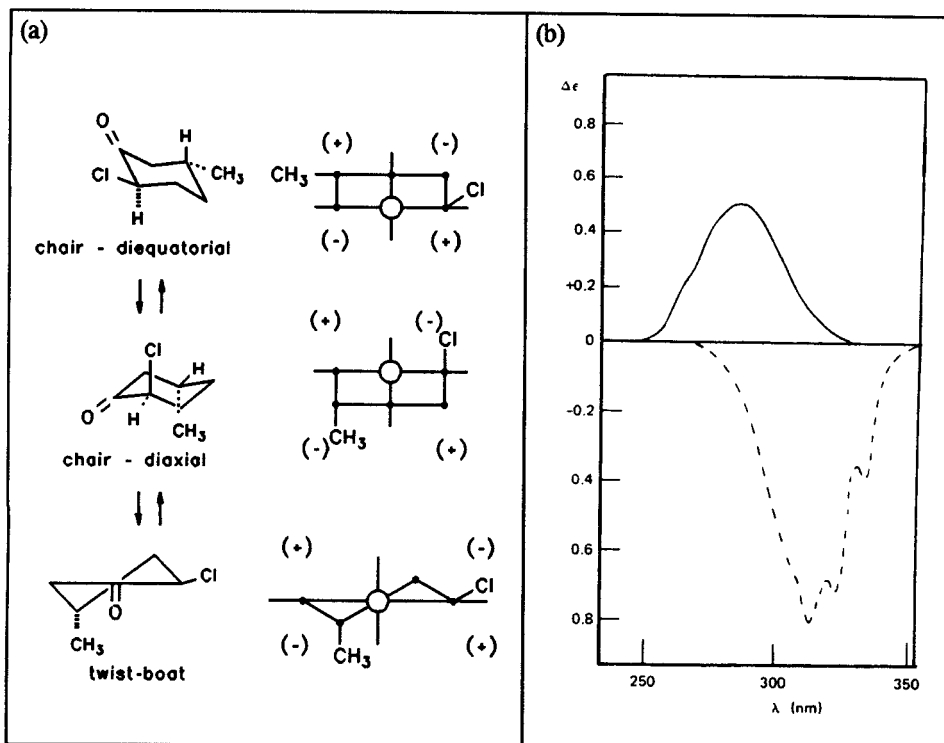
Figure 18. (a) Conformers of (+)-*trans*-6-chloro-3-methylcyclohexanone and their octant projection diagrams. (b) CD spectra in methanol (———) and isooctane (- - - - -).

Conformation	Octant Diagram	Predicted CE	Observed CD
		(+)	$\Delta\epsilon$ + 1.76 (CH$_3$OH)
		(-)	$\Delta\epsilon$ = -1.36 (isopentane-methylcyclo-hexane 5:1)

Figure 19. Chair conformational isomers of 2-oxo-*p*-menthanol, corresponding octant projection diagrams, predicted and observed n → π^* Cotton effects. From reference 20.

Rule, these atoms make no contribution to the CE, and thus the major contributions are drawn from atoms 6 and 7, which both lie in an upper right (or lower left) negative octant. Consequently, one would predict a negative CE for this decalone. The observed negative CE, with $\Delta\epsilon \simeq -1.0$, is similar in magnitude to that seen for 3-methylcyclohexanone or for 4(e)-ethyladamantan-2-one. The influence of an angular methyl at C-10 on the CD of (a) can be seen in (b). For the same absolute configuration, the observed CE is now inverted. Since the ring atoms of (b) make the same contribution as in (a), the angular methyl group causes the sign reversal. This angular methyl is actually quite close to the carbonyl group, much closer than carbons 6 or 7, and it therefore can be expected to act as a stronger octant perturber (since the octant perturbation effects by alkyl groups fall off with distance). In terms of contribution toward $\Delta\epsilon$, an α-axial methyl group on cyclohexanone probably contributes $|\Delta\epsilon| \simeq 1.7$, or $+1.7$ when the α-axial methyl lies in a (+) octant, as is the case in (b). This compares favorably with the value ($|\Delta\epsilon| \simeq 1.4$) from *trans*-2(a)-methyl-4-*tert*-butylcyclohexanone.

The ring carbons of the *trans*-4-ketodecalin (e) lie in the same back octants as the *trans*-1-decalone (a), so these perturbers should sum to a (-) contribution to the CD. The only difference between (e) and (a) is the β-axial methyl in the former, which is known from earlier work on adamantanones (see preceding section) to be a weak dissignate perturber (in this case a weak (+) contributor). The observed negative CE of (e) is only slightly smaller than that of (a).

Octant projection diagrams for the 2 and 3-keto decalins, (c) and (d), are very similar. The octant locations of the ring atoms are identical, with carbons 7, 8 and 9 in (c) and carbons 6, 7 and 8 in (d) lying in a (+) back octant. Since the other ring atoms lie on octant planes, or have counterparts across an octant plane, they make no contribution to the CE. One would therefore expect a net positive n $\rightarrow$ π^* CD coming from each carbocyclic skeleton. The methyl perturbers either lie in an octant plane, *e.g.*, the angular methyl of (d); or they lie (barely) in a front octant, *e.g.*, the angular methyl of (c); or they lie distant from the C=O but still in a (+) back octant, *e.g.*, the C-9 methyl of (c). The net CE's of (c) and (d) are thus both positive and nearly identical in magnitude.

If one needed to distinguish between (c) and (d) on the basis of CD spectroscopy, one might do so by running the spectra in acidified methanol, in which the hemiketal equilibrium is achieved (Figure 20). Hemiketal or ketal formation is discouraged by introducing a 1,3-diaxial interaction with the angular methyl. This interaction is absent in (d), and thus hemiketal or ketal formation would be evident. Since hemiketal or ketal formation effectively reduces the percent of ketone, it can thus be expected to cause a drop in the n $\rightarrow$ π^* CD intensity, with (d) suffering a much greater drop than (c). This technique has been used to distinguish 2-keto and 3-keto steroids.[17,22]

Changing from a *trans* to *cis* ring fusion causes a reorientation of octant perturbers, as is illustrated in (f) and (g). This *cis* geometry is further complicated by the possibility of two different conformations: the steroid (f) and nonsteroid (g) conformers. Octant projection diagrams for (e) predict a strong (-) CE, whereas, for (f) a strong (-) CE is predicted, and for (g) a strong (+) CE is predicted. In (f), assuming chair conformations, nearly all of the ring atoms lie in octant symmetry planes (carbons 1, 2, 4, 7, 10 and the angular methyl) or have counterparts across the octant planes (carbons 3 and 5, 6 and 8), leaving only carbon 9 to contribute like an α-axial methyl(ene) in a (-) octant. In the nonsteroid conformer (g), again most of the ring atom effects are cancelling. Carbons 1, 2, 4, 9 and

Table I. (Also continued on next page) Decalones and their conformational representations, Octant Projection Diagrams, predicted and observed n → π* CD Cotton effects.

Decalone[a]	Conformation	Octant Projection Diagram[b]	CE Pred.	CE Obs.
(a)		(+) ... (-) / 3 4 5 6 7 / 2 10 9 8 / (-) ... (+)	—	-1.0
(b)		(+) ... (-) / (-) ... (+)	+	+0.7
(c)		(+) ... (-) / (-) ... (+)	+	+1.3
(d)		(+) ... (-) / (-) ... (+)	+	+1.2
(e)		(+) ... (-) / (-) ... (+)	—	-0.8
(f)		(+) ... (-) / 6 5 4 3 / 7 10 2 / 8 9 / (-) ... (+)	—	+1.3

| (g) | | (+) | | (-) | + | +1.3 |
| | | (-) | | (+) | | |

^{a} Steroid numbering system. ^{b} Looking down C=O group, from O to C. Back octant contributors are denoted by filled circles (●), front octant contributors or suspected front octant contributors are denoted by open circles (○).
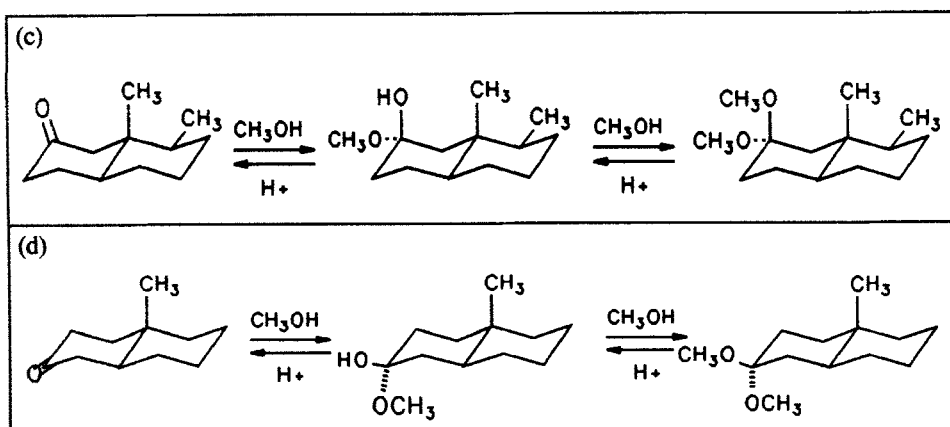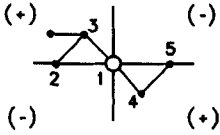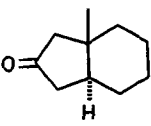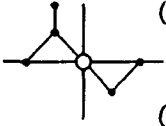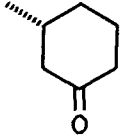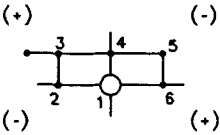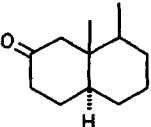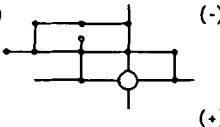
Figure 20. Ketone ⇄ hemiketal ⇄ ketal equilibrium in acidified methanol.

10 lie in an octant plane; carbons 3 and 5 lie equally disposed across an octant plane and thus cancel. The angular methyl lies close to the C=O, as an α-axial methyl in a (+) octant; whereas carbons 6, 7 and 8 lie distant. Carbon 6 lies in a (+) front octant position similar to that of a β-axial methyl on 3-methylcyclohexanone. Less is known about carbons 7 and 8, but their contributions are probably weak. The net predicted CE for (g) is thus (+). Since a strong (+) CE is observed, the *cis*-decalone must adopt conformation (g).

Cyclopentanone CD intensities tend to be much larger than in comparable cyclohexanones (Table II).[11] This is due to the reinforcement (cyclopentanone systems) rather than the cancellation (cyclohexanone systems) of ring atoms lying off the octant planes, *cf*, carbons 3 and 4 of cyclopentanone and carbons 3 and 5 of cyclohexanone. The methyl group makes the dominant contribution in the latter, but in the former ring atoms 3 and 4 make the largest contribution. The octant contributions from perturbers lying close to the C=O thus tend to be greater in cyclopentanones, and the net CE are thus larger. The situation is the same in bicyclic ketones, where the CE magnitudes of fused cyclopentanones are seen to be much larger than in the fused cyclohexanones.

Table II. Comparison of octant projection diagrams, predicted and observed n → π* Cotton effects for 5-ring and 6-ring ketones. Data from references 18 and 23.

5-Ring Ketone	Octant Projection Diagram	Cotton Effect	
		Predicted	Obs. Δε
	(+) (-) / (-) (+)	(+)	+2.1
	(+) (-) / (-) (+)	(+)	+5.4

6-Ring Ketone	Octant Projection Diagram	Cotton Effect	
		Predicted	Obs. Δε
	(+) (-) / (-) (+)	(+)	+0.6
	(+) (-) / (-) (+)	(+)	+1.3

2.3.3. Polycyclic Ketones

The octant rule has been applied successfully to a wide variety of steroids, diterpenes and triterpenes.[11] Crabbé compiled a list of ORD amplitudes [18] for steroid n → π* CE's. These data have been converted to Δε values and are presented in Table III along with the octant projection diagrams. As might be expected for the ring A 5α (A/B trans) steroid ketones, the predicted CE's are the same as for the corresponding decalones (Table I). The larger magnitudes of the 2-keto and the 4-keto steroids are due to the larger number of octant perturbers in the steroids. However, a larger number of perturbers does not always increase the magnitude of the parent decalone CE, as seen in the 3-keto steroid, and may even lead to a sign inversion, as in the 1-keto steroid.

Rings A and B have the same octant perturbers as the corresponding decalone (Table I, entry (b)), but (-) *front octant* contribution rings C and D, together with (-) back octant

Table III. (Also continued on next page) Predicted and observed n → π* Cotton effects for steroid ketones from circular dichroism and optical rotatory dispersion spectroscopy[a]
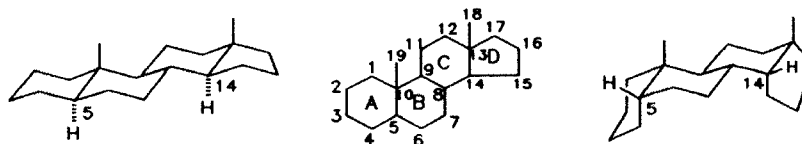
C=O	5α or 14α Stereochemistry			5β or 14β Stereochemistry		
	Octant Projection Diagram	Cotton Effect		Octant Projection Diagram	Cotton Effect	
Position		Predicted	Obs. $\Delta\epsilon$		Predicted	Obs. $\Delta\epsilon$
1		(±)	-0.36		(-)	-3.4
2		(+)	+3.0		(-)	-0.85
3		(+)	+1.3		(-)	-0.45
4		(-)	-2.3		(±)	-0.076

6		(-)	-1.4		(-)	-4.2
7		(-)	-0.67		(+)	+0.73
11		(+)	+0.33		(+)	+0.37
12		(+)	+1.0		(+)	+0.58
15		(+)	+3.3		(-)	-2.5
16		(-)	-5.8		(+)	+3.4
17		(+)	+3.5		(±)	+1.1

contributions from ring B, are sufficient to overcome the strong (+) contribution from the α-axial C-19 angular methyl. The net result is a weak (-) CE, but application of the octant rule without some knowledge of the magnitude that each octant contributor makes leads to an uncertainty in predicting the sign.

The Octant Rule applied to corresponding A/B *cis* (5β) ring A ketones easily predicts the observed CEs. It is interesting to note the weak (-) CE for the 4-keto-5β-steroid is probably due to an accumulation of front octant contributions (mainly from C-7, C-8 and C-9) overcoming the (+) octant contribution of the C-19 angular methyl. Here, as with the 5α-1-ketosteroid, it would have been difficult to predict the CE sign from the octant diagram.
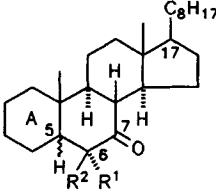
The Octant Rule adequately predicts the signs of the ring B 6 and 7-keto steroids and the ring C 11 and 12-keto steroids. The 6, 7 and 12-keto steroid octant projection diagrams are uncomplicated by front octant contributions. In the 11-keto steroid, however, front octant contributions are made from the C-19 angular methyl and carbons 1 and 2. Since most of the carbons (4, 5, 9, 10, 12, 14) lie on octant planes or are cancelling (8 and 13, 7 and 17), only a few carbons (1, 2, 3, 4, 15, 16, 17, 18, 19) remain as contributors to the n → π^* CE, and their contributions are probably weak, given their remoteness from C=O group. Carbons 3, 15, 16, 17 and 18 lie in (+) back octants; carbon 19 lies in a (+) front octant; carbon 6 lies in a C-1 back octant; carbons 1 and 2 lie in negative front octants. The rough summation would predict a weak (+) CE.

The D ring ketones, all cyclopentanones, would be predicted to have generally more intense CE's than those in rings A, B or C (*cf.* Table II), and larger Δε values are reported, except for the 17-keto-14β-steroid, where the strong (-) octant contributions from the twisted cyclopentanone ring β-carbons are canceled somewhat by the (+) octant contributions from most of the carbons of rings A, B and C.

The sensitivity of the ketone n → π^* CE to alkylation, especially at the α-carbon, is illustrated with the data of Table IV for 7-keto steroids. Comparing Δε for the parent 5α-cholestan-7-one and its 6α-methyl analog, which lies close to an octant nodal plane, the presence of an α-equatorial methyl, contributes very little to the overall CE, as expected. However, introduction of an α-axial methyl at C-6 causes a complete sign reversal. It lies close to the C=O group and in a (+) back octant and apparently outweighs the net negative octant contributions from the steroid skeleton (Table III).

When the A/B ring fusion is inverted from *trans* (5α) to *cis* (5β), the CE of the 6,6-dimethyl-7-ketone inverts. This is surprising because in the octant diagram (Table III) for the all-chair 5β-isomer, a 6-axial methyl is still present at C-6 and lies in a (+) back octant. For this conformation one would predict an even stronger (+) CE than in the 6,6-dimethyl-5α isomer, given the (+) CE in the parent of the former and the (-) CE in the parent of the latter (Table III). In both the 5β and 5α all-chair isomers, introduction of the 6β-methyl introduces a destabilizing 1,3-diaxial non-bonded steric interaction. In the 5α-isomer, ring B is locked into a chair conformation, but allowing ring A to adopt a high energy boat or twist-boat conformation might relieve the 1,3-diaxial CH_3/CH_3 interaction. There seems to be little to be gained energetically from this, as a twist boat cyclohexane lies 5.5 kcal/mole higher in energy than the chair. However, in the A/B *cis* 5β-series, the B-ring cyclohexanone can adopt a boat conformation in which the 1,3-diaxial CH_3/CH_3 interaction is relieved. Since a twist boat cyclohexanone lies only 2.7 kcal/mole higher in energy than chair cyclohexanone, a twist boat ring B seems likely. An octant diagram for

Table IV. Cotton effects for the n →π^* carbonyl transition of 7-keto steroids and their 6-methylated derivatives.

7-Keto Steroid	Config.	Substituents	n → π^* CD
	5α	$R^1=R^2=H$	$\Delta\epsilon = -0.67$
	5α	$R^1=CH_3, R^2=H$	$\Delta\epsilon = -0.70$
	5α	$R-R^2=CH_3$	$\Delta\epsilon = +1.9$
	5β	$R^1=R^2=CH_3{}^a$	$\Delta\epsilon = -1.1$
	5β	$R^1=R^2=H^b$	$\Delta\epsilon = +0.73$

^{a} $3\beta,17\beta$-diacetate. ^{b} 3α-hydroxy-17-(4-pentanoic acid methyl ester).

this conformation (Figure 21) places carbons 4, 6, 7, 8, 9, 11 and 18 on the horizontal octant plane and carbons 1, 10 and 19 on or nearly on the vertical octant plane. Carbons 2, 3, 5, 12 and 14 lie remote in (+) back octants, the C-6 α-methyl lies near to the C=O in a (-) back octant in an α-axial-like position octant. The remaining carbons lie in (-) front octants. Thus, the major, sign-determining octant contribution would appear to be dominated by the strong negative octant contribution of the 6α-methyl perturber. These results are important for they show how CD spectroscopy and application of the Octant Rule can be used to detect conformational perturbation in large polycyclic molecules.

Octant contributions are in principle additive, except when the chromophores interact. In diketones where the two C=O groups do not interact electronically, e.g., as in 1,2-diketones, it can be seen from a few representative diketones (Table V) that the CE of the diketone is usually the sum of the CEs of the component monoketones. However, at present there are too few examples to warrant a more comprehensive analysis.
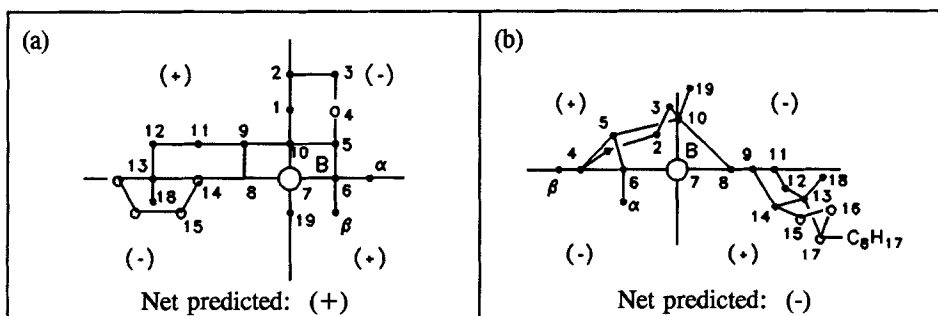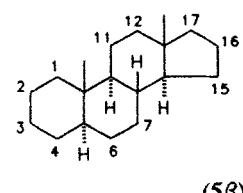
Figure 21. Octant projection diagrams for 5β-cholestan-7-one with ring B in the chair conformation (a) and ring B in the twist-boat conformation (b).

Table V. Diketone and component monoketone n → π^* CD Cotton effects.
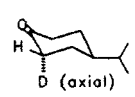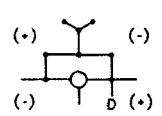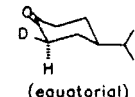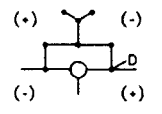
Steroid	Diketone		Monoketone Parent				
	C=O at	Δε	C=O at	Δε	C=O at	Δε	Σ
(5β)	3,17	+4.3	3	+1.3	17	+3.3	+4.6
	3,6	-0.29	3	+1.3	6	-1.4	-0.1
	3,11	+0.27	3	-0.45	11	+0.37	-0.1

2.3.4. Isotopically perturbed ketones

In the 1970s and 1980s intensive efforts were made toward measuring and understanding the CD of isotopic perturbers such as deuterium (D) and carbon-13 (^{13}C).[24] The majority of the studies focussed on the octant contributions of deuterium and conformational analysis (e.g., the conformational stability of an equatorial vs an axial deuterium on chair cyclohexanone). Studies on α-axial and α-equatorial deuterio-4-isopropylcyclohexanones (Table VI) indicate that an equatorial D is a consignate octant perturber and an axial D is a dissignate perturber, but that both are very weak perturbers. The magnitude of the contribution from an α-axial deuterium is an order of magnitude larger than that of α-equatorial, as expected.

Deuterium at a β-equatorial (as well as a β-axial) site on chair cyclohexanone also makes an octant dissignate contribution, as indicated in Table VII for structurally rigid adamantanones.[7,25] The results from adamantanones were confirmed in endo and exo-deuterio-7-norbornanones [26] (Table VII), where the endo and exo-deuteriums lie in octant positions very similar to β-equatorial and axial deuteriums, respectively. The results for the β-equatorial deuterium were confirmed in 4-tert-butylcyclohexanones, but in this system a β-axial deuterium behaved as a weak consignate octant perturber.[27] A β-equatorial (endo) deuterium gave a much larger octant contribution than β-axial (exo), and the dissignate contributions were explained on the basis of a theoretical model.[26]

Table VI. Chair conformations, octant projection diagrams and CD Cotton effects of (2R,4R) and (2S,4R)-2-deuterio-4-isopropylcyclohexanone, upper and lower, respectively.

Ketone	Octant Projection Diagram	Observed n→π^* Cotton Effect
D (axial)		Δε ≃ -0.090
(equatorial)		Δε ≃ -0.0091

In a β,β'-diequatorialmethylcyclohexanone, deuterium again was found to be a dissignate octant perturber.[28] The CD data for $^{13}CH_3$ β,β'-diequatorialmethylcyclohexanone [28] and β-^{13}C-adamantanone [29] lend support to a generalization that the heavier isotope (relative to the lighter isotope) makes a dissignate octant contribution (Table VIII).

Table VII. Structures, octant diagrams and observed n → π^* CD Cotton effects for β-deuterioadamantanones and 2-deuterio-7-norbornanones.

Ketone	Octant Projection Diagram	Observed n → π^* Cotton Effect
		$\Delta\epsilon \simeq +0.11$
		$\Delta\epsilon \simeq +0.01$
		$\Delta\epsilon \simeq +0.13$
		$\Delta\epsilon \simeq +0.03$

Table VIII. Conformations, octant projection diagrams and observed CD Cotton effects for isotopically substituted ketones.

Ketone	Octant Projection Diagram	Observed n → π^* Cotton Effect
		$\Delta\epsilon \simeq -0.02$
		$\Delta\epsilon \simeq -0.003$
		$\Delta\epsilon \simeq -0.005$

156

2.4. Absolute stereochemistry of unsaturated ketones

When two inherently symmetric chromophores are brought into close proximity, as in α,β and β,γ-unsaturated ketones, an inherently dissymmetric extended chromophore is created if the two chromophores are dissymmetrically disposed.[4] The coupling is expressed through coulombic mixing of the local states of the separated chromophores and through interchromophoric charge transfer states. The relative importance of charge transfer diminishes with increasing distance. Consequently, whereas coulombic and charge transfer interactions are both important for coupling between C=O and C=C chromophores in α,β-unsaturated ketones, charge transfer is generally of small importance in β,γ-unsaturated ketones. In dissymmetric α,β and β,γ-unsaturated ketones the Octant Rule, whose derivation rests on the concept of an inherently symmetric (C=O) chromophore, does not apply in general and may be insufficient to explain observed n → π^* Cotton effects.

2.4.1. α,β-Unsaturated ketones
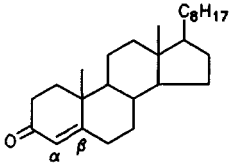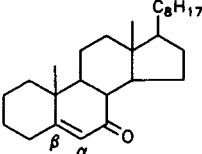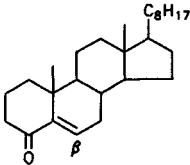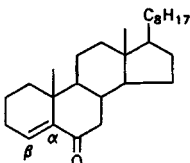
Snatzke [31] proposed a sector rule for the n → π^* transition of planar α,β-unsaturated ketones, with a sign pattern opposite to that of the Octant Rule. However, α,β-unsaturated ketones are often non-coplanar and thus dissymmetric. For these cases, a helicity rule has been proposed for correlating the sign of the O=C-C$_\alpha$=C$_\beta$ torsion angle with the n → π^* CE: for cis-enones a (-) torsion angle correlates with a (-) CE; for trans-enones it correlates with a (+) CE.[30] Examples of application of the helicity rule to the n → π^* CE's of trans and cis steroid ketones may be found in Table IX. In principle, a better correlation between CD and stereochemistry might be found for the π → π^* type transitions of α,β-unsaturated ketones.[4] However, Gawroński has analyzed three bands in the 185-260 nm (π → π^*) region and found that the CE's are variously influenced by the presence of axial allylic substituents, α' or β' axial alkyl groups as well as the enone dissymmetry.[30]

2.4.2. The extended octant rule for β,γ-unsaturated ketones

In β,γ-unsaturated ketones, a chirality rule (The Extended Octant Rule, which is really not an octant rule) has been suggested to correlate with the sign of the n → π^* CE (Figure 23). In this chirality rule, the intersection of the two planes containing the two chromophores, C=O and C=C, has a dihedral angle (θ). When $|\theta| > 90°$, the predicted CE signs are (-) for $-\theta$ and (+) for $+\theta$.[4,32] This chirality rule was extended to other geometries of β,γ-unsaturated ketones, including smaller and larger angles about the α-carbon, encompassing a range of cisoid (Figure 22 a and b) and transoid (Figure 23 c) dissymmetric orientations, all with dihedral angles, $|\theta| > 90°$. However, the rule may appear to break down when the $\Delta\epsilon$ values are not large, such as when ordinary Octant Rule perturbations are of the same magnitude as those from the coupling of locally excited C=O n → π^* and C=C π → π^* transitions.[33]

More recently, a good correlation was found between the cosine of the angle between the O=C and C$_\beta$=C$_\gamma$ bonds (cos ξ), defined in Table X, and sign of the n → π^* CE. For $-90° < \xi < 90°$ (or when cos ξ is positive) a (+) CE is predicted; for $90° < \xi < 270°$ (or when cos ξ is negative) a (-) CE is predicted. Schippers and Dekkers [34] thus formulated a new chirality rule for β,γ-unsaturated ketones: cos θ = -(sign xy) · (cos ξ), as outlined in Table X, where cos θ is the angle between the electric and magnetic transition moments of the erstwhile n → π^* transition, and ξ is the angle of intersection of axes drawn

Table IX. Correlation of predicted and observed n → π^* Cotton effects with the sign of the α,β-unsaturated ketone torsion angle[a]

α,β-Unsaturated Steroid Ketone	$O=C-C_\alpha=C_\beta$ Torsion Angle Sign	Predicted n → π^* Cotton Effect	Observed n → π^* Cotton Effect
	(+) *trans*	(-)	$\Delta\epsilon = -1.31$
	(-) *trans*	(+)	$\Delta\epsilon = +1.35$
	(+) *cis*	(+)	$\Delta\epsilon = +1.43$
	(-) *cis*	(-)	$\Delta\epsilon = -1.2$

[a] Data from reference 30.

(a) (+) Cotton effect   (b) (-) Cotton effect   (c)
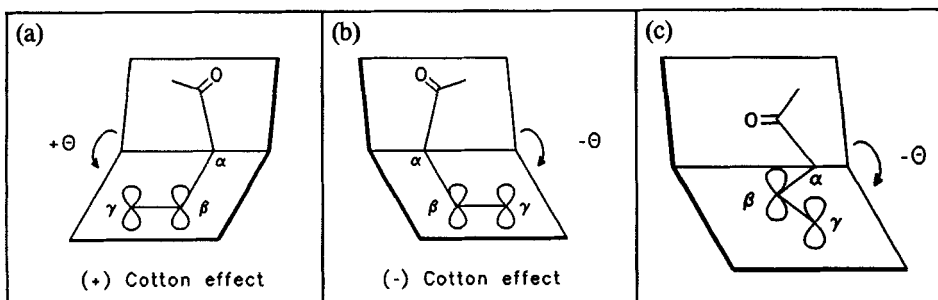
Figure 22. Enantiomeric dissymmetric orientations of β,γ-unsaturated ketone chromophores predicted to give (+), (a), and (-), (b) Cotton effects when the absolute value of the dihedral angle θ is >90°. (c) Transoid arrangement of β,γ-unsaturated ketone. Here the $\Delta\epsilon$ values are often quite small (refs. 32 and 33).

Table X. Relationship between cos ξ, cos θ and n → π^* CD Cotton effects in β,γ-unsaturated ketones. The angle ξ is the angle of intersection of the Z and Z' axes (below), which travel along the C=O and C=C bonds, respectively. Angle θ is the angle between the C=O axis and $\vec{r}$, the electric dipole moment associated with the n → π^* transition.
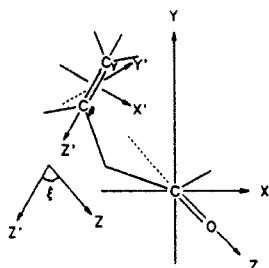
(Left) Reference frame for carbonyl group (x, y, z) and ethylenic group (x', y', z') in β,γ-enones. The C_α atom connecting the moieties lies in the xz plane; the y' axis is perpendicular to the plane of the ethylenic group. ξ denotes the angle between z and z' axes. A more general formulation of the chirality rule is thus: cos θ = -(sign xy)·(cos ξ).

Ketone	ξ	cos ξ	Obs. $\Delta\epsilon$	θ	cos θ
	55°	+0.57	+18.8	48°	+0.67
	60°	+0.50	+12.0	55°	+0.57
	70°	+0.34	+5.69	74°	+0.28
	75°	+0.26	+4.71	76°	+0.24
	90°	0	+2.55	83°	+0.13
	90°	0	+5.4	82°	+0.14
	105°	-0.26	-3.14	101°	-0.19

along and through the C=O and C=C bonds. The correlation for the available examples[34] is quite good, although only one example has been reported for a negative value of cos ξ. Additional experimental support of the chirality rule has been published recently,[35] and a detailed theoretical treatment of 2-norbornenone supported the concept but not all of the assumptions, while clearly showing the importance of extrachromophoric perturbers.[36]

3. APPLICATIONS OF EXCITON CHIRALITY CD

Changes in the distribution of electron density are associated with UV-visible absorption (Figures 1 and 2), consisting of transitions from a high-lying occupied ground state molecular orbital to a low-lying unoccupied molecular orbital. The movement of electron density in going from the ground electronic state to an excited state creates a momentary dipole, called an electric transition dipole. (This was touched upon briefly in the preceding section on β,γ-unsaturated ketones.) Thus associated with each electric transition is a polarization, (electric transition dipole) which has both a direction and an intensity that vary according to the nature of the chromophore and the particular excitation. When two or more chromophores are brought into proximity, their electric transition dipoles may interact through dipole-dipole (or exciton) coupling. The subject of this part is how to use these exciton coupling interactions to extract stereochemical information through the Exciton Chirality Rule.[2]

3.1. The interaction of chromophores

Considerations of exciton coupling and, especially, applications of the Exciton Chirality Rule have begun to play an increasingly prominent role in determining molecular absolute configuration and orientation of proximal molecules.[2,37] Exciton coupling arises from the interaction of two (or more) chromophores through their (locally) excited states. These excited state dipole-dipole interactions, which lie at the heart of exciton coupling, are most effective when the electric dipole transitions are strongly allowed (as in π-π^*-type UV-visible transitions, e.g., the 310 nm transition of the p-dimethylaminobenzoate chromophore with $\epsilon \simeq 30,000$ cm M^{-1}). Exciton coupling leads to shifted and broadened, if not split, UV-visible spectra of the composite molecule.[38] For a chiral orientation of two chromophores, exciton coupling can be seen very clearly in two oppositely-signed circular dichroism Cotton effects flanking the relevant UV-visible absorption band(s) (Figure 23). The signed order of the circular dichroism transitions is correlated with the relative orientation of the relevant electric dipole transition moment from each chromophore, hence the absolute configuration of the composite molecule (Exciton Chirality Rule).

Applications of the Exciton Chirality Rule have become numerous during the past ten years and claim an extraordinarily high degree of success. In most applications of exciton chirality to the determination of absolute configuration, the molecule under study is derivatized with a suitable chromophore, e.g., p-dimethylaminobenzoate, and its circular dichroism spectra are measured and analyzed. The success of this method has led to a search for new and better chromophores, especially those which absorb intensely in the visible spectrum.[39,40] These derivatives can be detected visually, for convenience in laboratory manipulations, and their molecular weights tend to be substantially higher than the underiv-

atized parent. Successful application of the rule depends on knowing which chromophores are interacting, on accurately knowing the orientations of the component chromophore electric dipole transition moment, and carefully considering factors affecting their relative orientation.[2,41] Some typical chromophores for derivatizing diols (or polyols) and di-amines are shown in Figure 24.
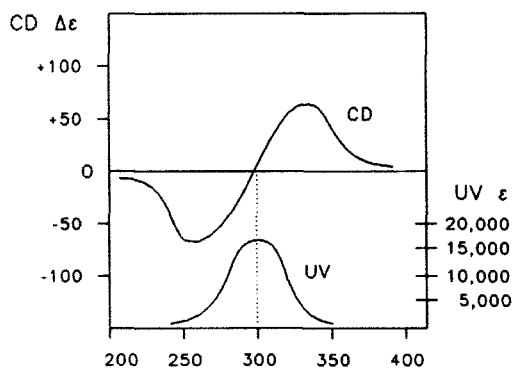

Figure 23. Typical bisignate exciton coupling CD (upper) and bell-shaped UV (lower) spectra for chromo-phores with electronic transitions near 300 nm. The shape of the observed CD curve is due to over-lapping, oppositely-signed (+) and (-) CD curves associated with elec-tronic excitation into the two exciton states (Figure 25).

Figure 24. Structures and long axis polarizations of the intense short wavelength UV tran-sitions of benzoate (a) and p-substituted benzoates (b) and (c) showing the influence of sub-stitution on the intensity (ϵ) and wavelength (λ^{max}). (d) p-Dimethylaminocinnamate.

3.2. The origin of exciton coupling

When two chromophores are brought into close proximity, where orbital overlap and electron exchange are negligible, they may interact through dipole-dipole coupling of their locally excited states to produce a delocalized excitation (exciton) and a splitting (exciton splitting) of the locally excited states (Figure 25).[2,37] The UV-visible and circular dichroism spectra of the composite system thus derive from the UV-visible spectral proper-ties of the component chromophores, and they depend as well on interchromophoric dis-tance, mutual orientation and geometry. Evidence of exciton interaction in bichromophoric

or polychromophoric systems often consists of spectral shifts (which can be to the blue or red) and splittings.[38] Such spectral shifts and splitting magnitudes can be correlated with the intensity and the relative orientation of the electric transition dipole moments associated with the particular UV-visible absorption band of each chromophore (Figure 26). Since excitons arise from electric transition dipole coupling, strongly allowed electronic transitions with large dipoles are intrinsically more effective than are weakly allowed transitions. This arises since dipole-dipole interaction falls off with the inverse cube of the separation distance. Consequently, the most useful chromophores for examining exciton coupling phenomena over short and especially over long distances are those with accessible, electric dipole allowed UV-visible transitions, typically π-π^*, such as aromatic chromophores and polyenes. From a practical standpoint, the stronger the absorption of the parent chromophore, the more sensitive it becomes for detecting exciton coupling and exciton chirality at extremely low concentration levels.
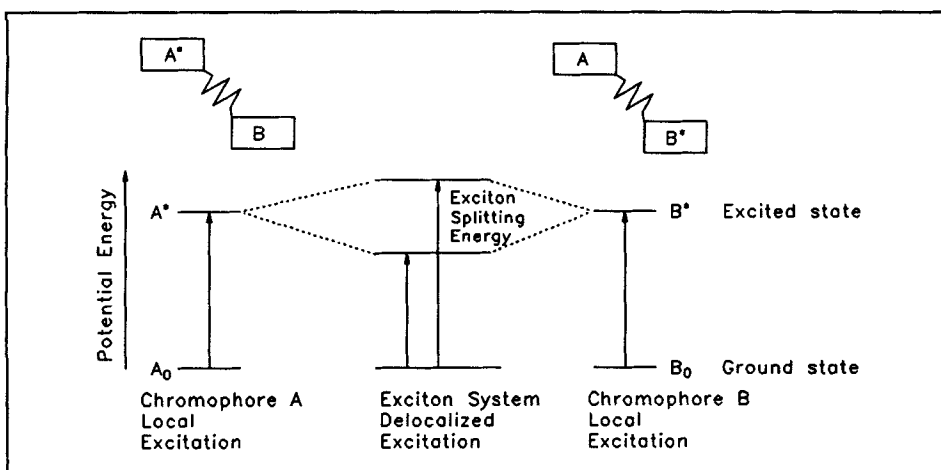
Figure 25. Diagrammatic representation for a system with two chromophores (A and B) held together by covalent bonding or weak intermolecular forces. Local excitations are shown (left and right) for the chromophores in their locally excited (A* or B*) monomer states. In the composite molecule or system (center), excitation is delocalized between the two chromophores and the excited state (exciton) is split by resonance interaction of the local excitations. Exciton coupling may take place between identical chromophores (A=B) or non-identical chromophores (A≠B) but is less effective when the excitation energies are very different, i.e. when the relevant UV-visible bands do not overlap.

A particularly good example of a chromophore for exciton coupling is anthracene, with several π-π^* transitions, including a short axis-polarized UV absorption near 360 nm (ϵ ~ 7,500), ^1L_a, and a long axis polarized intense UV absorption near 250 nm (ϵ ~ 200,000), ^1B_b (Figure 27). The associated electric transition dipole strengths are 2.7×10^{36} and 88×10^{36} (cgs units), respectively.[1] In composite systems, where two anthracenes are fused to bicyclo[2.2.2]octane (Figure 27), the intense long axis-polarized transition dipoles are

oriented neither parallel nor in-line, but intersect at an obtuse angle and lie one in each of two intersecting planes (dihedral angle of ~ 120°). The UV-visible spectrum of the composite molecule (Figure 27) clearly resembles that of the component anthracene chromophores, yet differs in two significant ways. The spectrum is not simply the sum of two *independent* anthracene transitions, as it would be if the chromophores did not interact; rather, it is due to two overlapping *exciton* transitions (Figure 27, case c), which can be seen clearly by a broadening and bathochromic shift of the ^1B_b transition(s) from 252 nm band to 267 nm. The broadening is due to unresolved exciton splitting, and the bathochromic shift is due to alignment of the ^1B_b transition dipoles at a 151° intersection angle.
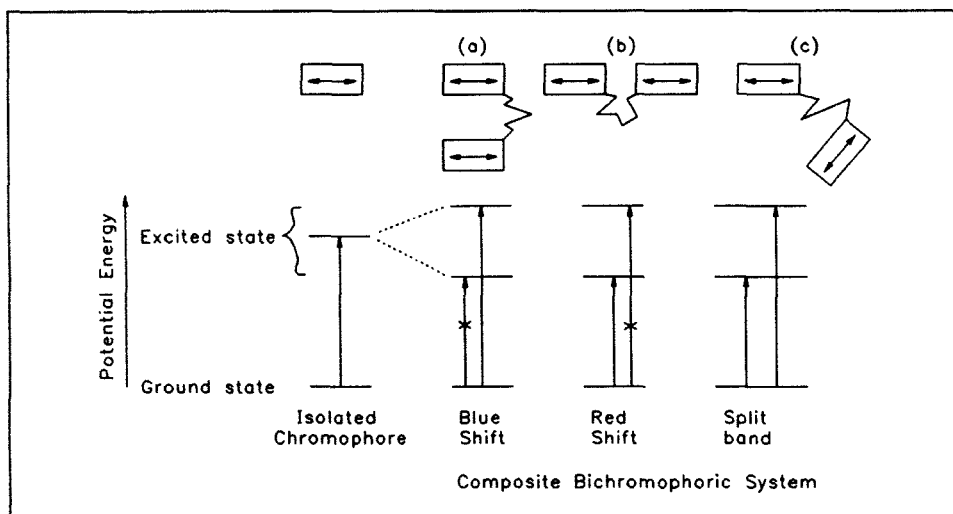
Figure 26. Diagram for the origin of UV-visible spectral shifts and splittings due to exciton interaction of two chromophores' (□) dipoles (◄——►). In two limiting orientations: (a) only excitation into the higher lying exciton state is allowed for the parallel orientation (resulting in a blue shift) and (b) only excitation into the lower lying exciton state is allowed for the in-line orientation (resulting in a red-shift) — relative to the isolated chromophore. For orientations lying between these two limiting cases, (c), a split or broadened band is typically observed.

3.3. The Exciton Chirality Rule

Although exciton coupling leads to shifted and broadened, if not split, UV-visible spectra of the composite molecule, when the chromophores are held in a chiral orientation, exciton coupling can be detected even more clearly in the CD spectrum as two oppositely-signed CE's typically corresponding to the relevant UV-visible absorption band(s). The signed order of the CD transitions correlates with the relative orientation of the relevant electric dipole transition moments, one from each chromophore, and hence the absolute configuration of the composite molecule (Exciton Chirality Rule.)[2] For the bis-anthra-

cene, the CD spectrum (Figure 28) corresponding to the UV spectrum of Figure 27 shows an exciton splitting very clearly as two oppositely-signed, very intense CE's near 267 nm. In fact, the intensity ($\Delta\epsilon$) far exceeds any seen in the previous part (Octant Rule) where the Cotton effects ($|\Delta\epsilon|$ ~1) are attributable to dissymmetric vicinal action. One key to recognizing an exciton is a very intense bisignate CD Cotton effect. The signed order of the Cotton effects can be correlated with the relative orientation of the ^1B_b transition moments from the two anthracenes. In the example shown (Figure 28), the extraordinarily intense exciton couplet has a positive band at 268 nm and negative at 250 nm, corresponding to a (+) helical orientation [(+) chirality] of the transition dipoles.
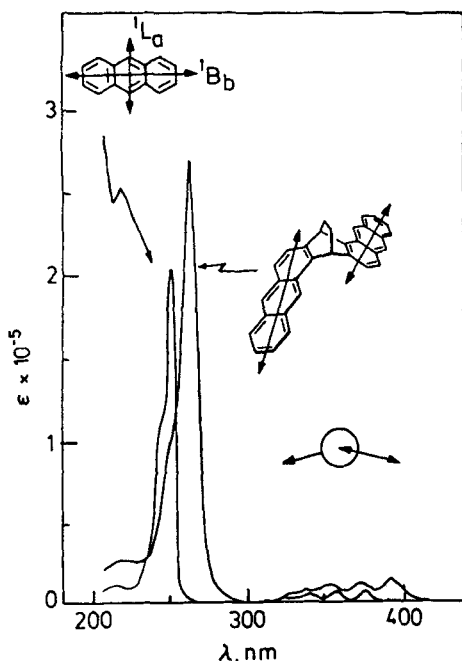
Figure 27. UV spectra of anthracene and the ring fused bis-anthracene (ref. 2). On the anthracene structure are shown the in-plane orientations of the electric dipole transition moment vectors associated with the intense short wavelength UV bands (^1B_b) near 250 nm and the weak long wavelength bands (^1L_a) near 360 nm. The λ^{max} for the exciton bands of bis-anthracene are red shifted from the corresponding bands in the parent, as the vectors intersect at >90°.
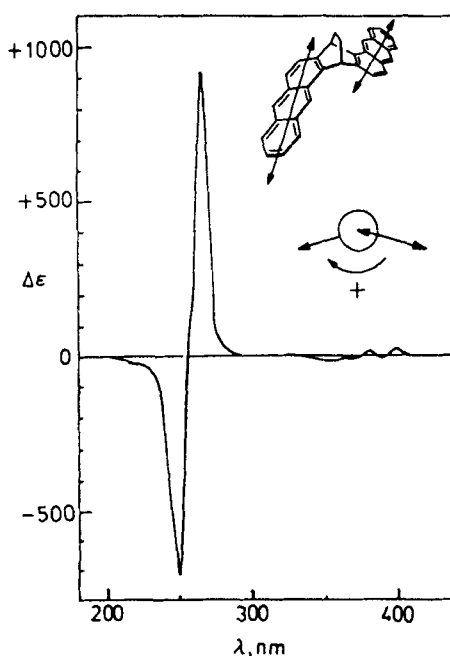
Figure 28. CD spectrum of the chiral ring fused bis-anthracene. The ~250 nm electric transition dipoles (←——→) of each chromophore intersect at a (+) torsion angle of ~151°. The signed order of the Cotton effects of the 250 nm exciton couplet confirms a (+) helicity and thus the absolute configuration shown. (From ref. 2)

According to the Exciton Chirality Rule,[2] when the relevant transition moments are oriented in a (+) chirality, the long wavelength component of the associated exciton couplet can be expected to exhibit a (+) Cotton effect (Figure 29). When they are oriented in a (-) chirality, the long wavelength Cotton effect is negative. Thus, from the CD, one can determine the helical orientation of the transition moments and therefore the absolute configuration of the molecule.

Negative Exciton Chirality
(-)

(+) short wavelength Cotton Effect

Δε
+
0
λ

(-) long wavelength Cotton Effect

Positive Exciton Chirality
(+)

(+) long wavelength Cotton Effect

Δε
+
0
λ

(-) short wavelength Cotton Effect
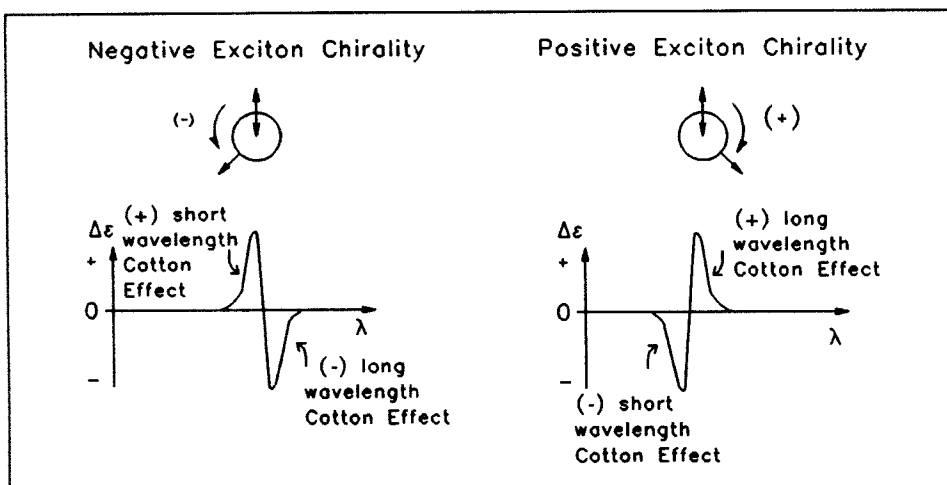
Figure 29. Basic elements of the Exciton Chirality Rule relating the torsion angle or helicity of two electric dipole transition moments (←——→) (upper) to the signed order of the circular dichroism Cotton effects (lower).

3.4. Bichromophoric systems and the absolute configuration of diols

In most examples of application of the exciton chirality rule, a chiral molecule is derivatized to introduce suitable chromophores.[2] In many of these studies, hydroxyl is the typical resident functional group, which is derivatized with appropriate acids containing chromophores suitable for exciton coupling. The ideal chromophore would have a very intense UV-visible transition, located in a convenient spectral window, and with the orientation of its electric transition moment being well-defined relative to alcohol R-OH bond. One of the most successful is p-dimethylaminobenzoate, which has an intense (ϵ ~ 30,000) transition in an easily accessible, generally non-interfering, region (near 310 nm). The associated electric dipole transition moment is oriented along the long axis of the molecule, from nitrogen to carboxyl (Figure 24). Although the chromophore might adopt a large number of different conformations (relative to its point of attachment on the chiral molecule) by rotating about the ester bonds, one conformation (S-cis) apparently predominates, and the relevant transition dipoles are thus aligned parallel to the ester R-O bond (Figure 30). With this in mind, one can determine the (+) or (-) relative helicity of the transition dipoles by inspection and thus the assignment of absolute configuration from the CD spectrum. Chromophores with electric dipole transitions not aligned parallel to the

ester R-O ester bond, such as 2-naphthoic or 2-anthroic acid, are less satisfactory, but other acids with transitions oriented *perpendicular* to the R-O ester bond have been used satisfactorily (*e.g.*, 9-anthroates).[38] A good derivatizing agent is thus a symmetric acid in which the alignment of strongly allowed electric dipole transition moment(s) is known with a high degree of certainty. Other carboxylic acid chromophores such as *p*-dimethylaminocinnamate (ϵ_{362}^{max} 44,000) and *p*-methoxycinnamate (ϵ_{306}^{max} 24,000) [37,42] have proven quite useful, but 6-dimethylamino-2-naphthoate has been found to be much less useful.[40]
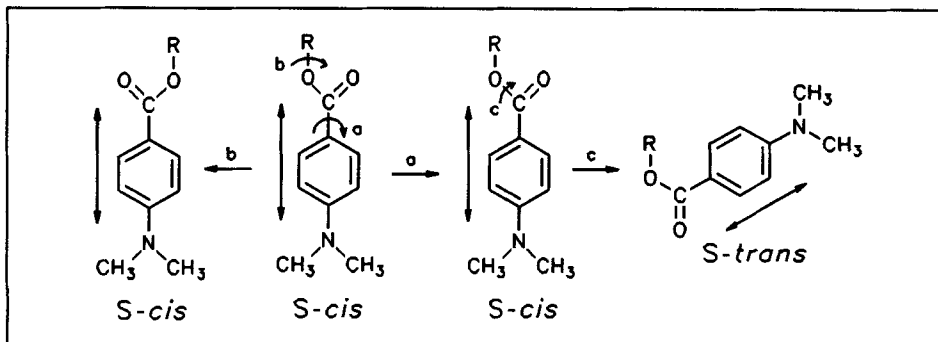
Figure 30. Reorientation of the *p*-dimethylaminobenzoate long wavelength electric transition dipole (⟷) following rotations about the (a) C—C=O, (c) O—C=O and (b) R—O single bonds (rotate the larger group). Only rotation about c re-orients dipole, shown here from vertical to inclined. The transition dipole (⟷) passes through the chromophore, from N to C=O, but is shown offset for clarity.

Table XI. Conformational structures (a and b) and Newman projection diagrams (c and d) of (1*S*,2*S*) and (1*R*,2*R*)-cyclohexane diol (a) and their bis-*p*-dimethylaminobenzoate derivatives (b). CD data for the bisignate Cotton effects of the latter are shown below.

Data in CH_3OH solvent from reference 40.

In *trans*-1,2-cyclohexanediol (Table XI), where the cyclohexane ring adopts the stable chair conformation, the diequatorial configuration is preferred.   The two enantiomers exhibit oppositely signed O-C-C-O torsion angles. And for the reasons cited above, when the diols are derivatized as their bis-*p*-dimethylaminobenzoates, or other suitable chromophores, the electric transition moments lie parallel to the alcohol C-O bonds. Thus, the relative orientation (helicity) of the two transition dipoles correlates with the signs of the torsion angles. According to the Exciton Chirality Rule, a (+) exciton chirality would be predicted for the (1*S*,2*S*) enantiomer (Figure 31) and a (-) exciton chirality for the (1*R*,2*R*) enantiomer (Figure 32). This is in complete agreement with the observed bisignate CE's for the intense ~ 310 nm electronic transition(s) of the bis-*p*-dimethylaminobenzoates. The CE's of the corresponding mono-derivatives are monosignate and very weak because there is but one (inherently symmetric) chromophore being perturbed by dissymmetric vicinal action (Figure 31). The contrasting CD spectra of the mono and diesters are fully evident (Figure 32). The diester CD is not simply the sum of two mono ester CD curves; its marked difference implies a different origin consistent with exciton coupling. The signed order of the CE's is consistent with the predictions of the Exciton Chirality Rule.
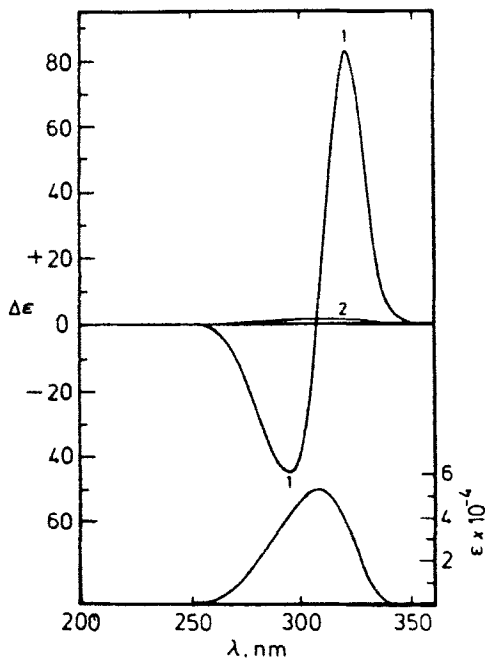
Figure 31. CD (upper) and UV (lower) spectra of (1*S*,2*S*)-cyclohexanediol bis-*p*-dimethylaminobenzoate (1) and mono-*p*-dimethylaminobenzoate (2) in CH$_3$OH solvent at 22°C.
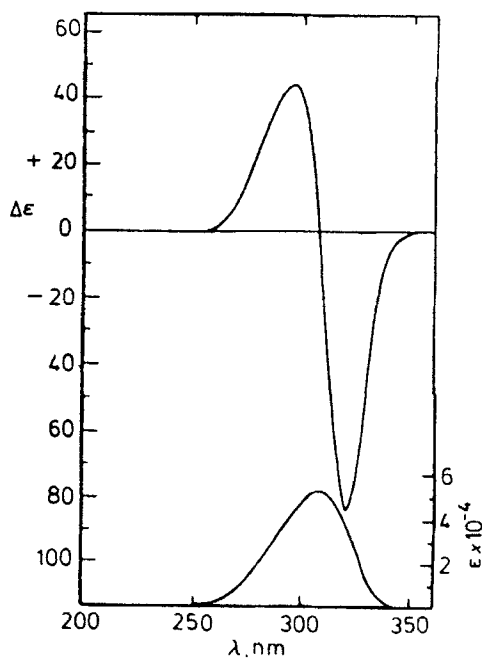
Figure 32. CD (upper) and UV (lower) spectra of the bis-*p*-dimethylaminobenzoates of (1*R*,2*R*)-cyclohexanediol and 5α-cholestan-2α,3β-diol are nearly the same (CH$_3$OH, 22°C).

Orientation, proximity and chromophore are paramount considerations in the Exciton Chirality Rule. Extrachromophoric considerations are relatively unimportant. Thus the CD spectra of bis-p-dimethylaminobenzoates of 5α-cholestan-2α,3β-diol and (2R,2R)-cyclohexanediol (both diequatorial diols of the same absolute configuration) are essentially identical (Figure 32). Other steroid diols, whether with vicinal hydroxyls or very distant hydroxyls, give bisignate CE's originating from exciton coupling and with a signed order consistent with the Exciton Chirality Rule (Table XII).

In most of the examples of Table XII, the relative orientations of the electric dipole transition moments fall into well-defined stereochemical arrangements, and the absolute configuration predicted by the Exciton Chirality Rule is fully realized. Although the magnitudes of the CE's tend to decrease with increasing distance between the chromophores (even in the 3,15-diol where the chromophores are >13Å apart), the Δε values are still larger than those typically seen in Octant Rule ketones. In a few cases, the transition moments lie in the same plane [(2β, 3α) and (3β, 7β)]. In these orientations the Exciton Chirality Rule predicts no CD. Yet, for reasons not fully understood, weak bisignate CD spectra are observed.[2] Relative orientations such as these warrant further study in order to place the Exciton Chirality Rule on a firmer empirical footing.

3.5. Examples of determinations of absolute configuration from exciton chirality

Enzymatic dihydroxylation of toluene by *Pseudomonas putida* affords (+)-*cis*-1,2-dihydroxy-3-methyl-3,5-cyclohexadiene) (Figure 33). The relative stereochemistry was determined to be *cis*, but the absolute configuration was unknown, until determined by Ziffer *et al.*[43] Catalytic reduction of the diene gave a stereochemically well-resolved cyclohexane diol suitable for introducing the benzoate chromophore. The dibenzoate gave a (-) exciton chirality CD, and thus the organism produces the diene-diol shown in Figure 33(a).
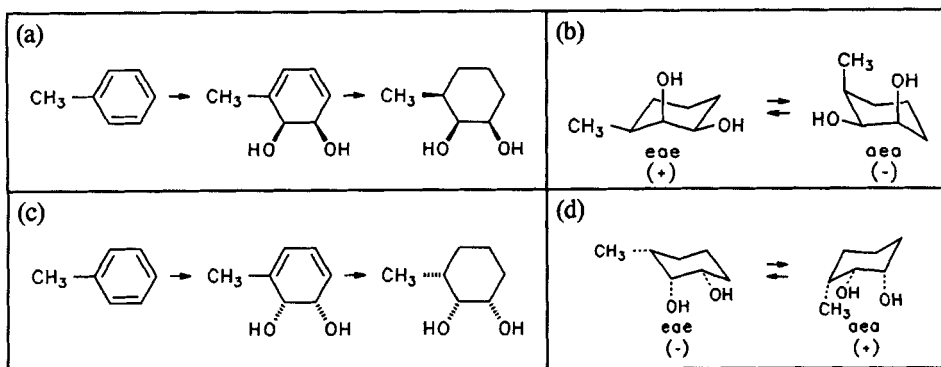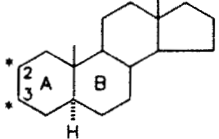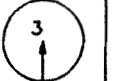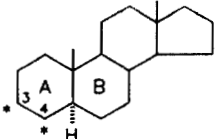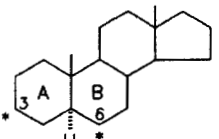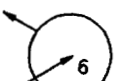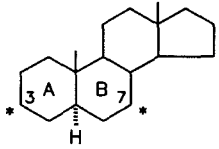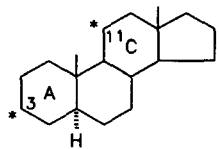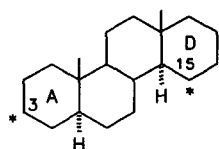

Figure 33. (a) and (c) cis-dihydroxylation of toluene to give enantiomeric diene-diols, and catalytic reduction to the corresponding cyclohexane-1,2-diols. (b) and (c) chair cyclohexane conformers. The *eae* conformers are expected to be more stable than the aea, and the predicted exciton chirality for the *eae* conformers is given: (+) in (b); (-) in (d).

Table XII. (Also continued on next page) Exciton chirality of steroid diol bis-*p*-dimethylaminobenzoates.[a]

STEROID DIOL	OH at	EXCITON CD CE's		EXPECTED EXCITON CHIRALITY SIGN, (+) or (−)
		$\Delta\epsilon(\lambda)$	$\Delta\epsilon(\lambda)$	
	$2\alpha,3\beta$ $2\beta,3\beta$ $2\beta,3\alpha$ $2\alpha,3\alpha$	−27(295) −33(295) − 6(297) − 9(222)[e]	+61(321) +62(320) +12(321) +20(238)[e]	 (−) (2α,3β) (+) (2β,3β) (+) (2α,3α) (w+) (2β,3α)
	$3\beta,4\alpha$ $3\alpha,4\alpha$	− 53(297) +25(296)	+91(322) − 68(321)	 (+) (3β,4α) (−) (3β,4β)
	$3\beta,6\beta$ $3\beta,6\alpha$	+19(295) − 30(294)	− 38(320) +59(319)	 (−) (3β,6β) (+) (3β,6α)

STEROID DIOL	OH at	EXCITON CD CE's		EXPECTED EXCITON CHIRALITY SIGN, (+) OR (-)
		$\Delta\epsilon(\lambda)$	$\Delta\epsilon(\lambda)$	
	$3\beta,7\alpha$ $3\beta,7\beta$	$-11(295)$ $+4(300)$	$+29(320)$ $-3(321)$	
	$3\beta,11\beta$ $3\beta,11\alpha$	$-9(294)$ $+18(295)$	$+18(320)$ $-35(320)$	
	$3\beta,15\beta$	$+6(291)$	$-20(319)$	

[a] The predicted exciton chirality correlates well with the observed CD. In cases where the electric dipole vectors lie in the same plane 180° apart (2β, 3α), or 0° apart (3β, 7β), weak (+) and (-) chirality bisignate exciton chirality CD spectra are observed, respectively. It is unclear whether the very weak Cotton effects are altered, *e.g.*, sign inverted, by changes in solvent, but it is clear that the relevant electric dipole transition vectors cannot strictly be in the same plane. The conformational factors which distort the alignments shown above are not understood completely. [b] From relative orientations of ^1B_b electric transition dipoles of bis-*p*-dimethylaminobenzoates. Epimers not shown have not been studied. [c] Dibenzoate.

The absolute configuration of *trans*-7,8-dihydroxy-7,8-dihydrobenzo[a]pyrene, a carcino-genic metabolite of benzo[a]pyrene, was determined by the exciton chirality method as applied to its bis-*p*-dimethylaminobenzoate.[44] Hydroxylation was determined to yield the *trans* stereochemistry (Figure 34), but there are two mirror image *trans*-diols. The stereo-chemistry of the flexible dihydroxylated ring was determined from the vicinal coupling constant of the hydrogens at C-7 and C-8 ($J_{7,8} = 8$ Hz). With the conformation of the ring known, and the CD spectrum of the diol bis-*p*-dimethylaminobenzoate showing a (-) exciton chirality, the absolute configuration was assigned (7*R*,8*R*).

CD studies of pyranosides derivatized as tribenzoates have shown that the pairwise couplings are additive. For example in the 2,3,4-tris-*p*-chlorobenzoate of methyl-α-D-manno-pyranoside there are three pairwise couplings: (2,3), (3,4) and (2,4).[2] As shown in Figure 35, each of the three is predicted to exhibit a (-) exciton chirality, and thus (assuming additivity) the net CD is expected to correspond to a (-) exciton chirality. This is, in fact, observed. In other sugars, where some of the individual couplets may have a (+) exciton chirality, and others a (-) exciton chirality, the net predicted exciton CD would be determined by the magnitudes and signs of each of the component couplet CEs. Nakanishi *et al* have shown this approach to be exceptionally reliable.[37]
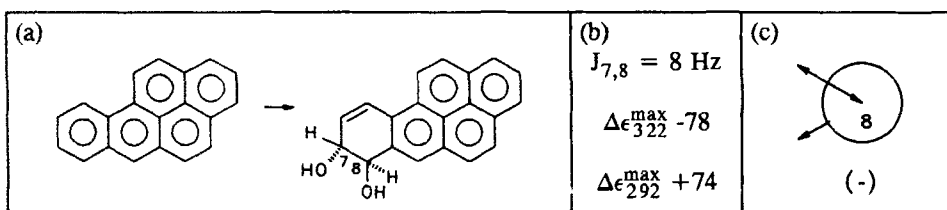

Figure 34. (a) Dihydroxylation of benzo[a]pyrene. (b) Coupling constant and exciton chirality CD CEs of the bis-*p*-dimethylaminobenzoate. (c) (-) Exciton chirality and relative orientation of the transition moment vectors, hence the absolute configuration of the diol.
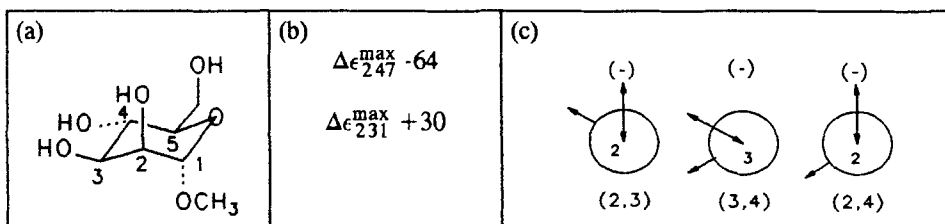

Figure 35. (a) Stable chair conformation of methyl α-D-mannopyranoside and (b) exciton coupling CD Cotton effects of its 2,3,4-tris-*p*-chlorobenzoate. (c) Pairwise couplings of the 2,3,4-tri-*p*-chlorobenzoate with (-) chiralities noted for each.

In some cases, the absolute configuration of a molecule would be quite tedious to deter-mine without the Exciton Chirality Rule. For example, the absolute configuration of opti-cally active binaphthyls and bianthryls may be determined from their exciton chirality CD

spectra (Figure 36).[2] In the 1,1'-bianthryl shown, the ethano bridge fixes the interplanar angle of the two anthracene planes at $\sim 30°$. The CD corresponding to the ~ 250 nm ^1B_b transition is extraordinarily strong. When a (-) CD chirality is observed, the molecule has the P-helicity or (R) absolute configuration (Figure 36). The absolute configuration of (-)-2,2'-bis(bromomethyl)-1,1'-binaphthyl shown in Figure 36 was determined by the anomalous diffraction X-ray method on a crystal of the resolved (-)-binaphthyl. The exciton coupling CD for the ~ 225 nm ^1B_b transition correlates with a (+) chirality, in accord with the X-ray results. The Exciton Chirality Rule is thus confirmed by an independent method, but the CD determination is usually faster.

The absolute configuration of (-)-spiro[4.4]nonane-1,6-dione was determined by application of Horeau's method of optical rotations.[45] In support of the assignment, and with greater certainty, the Exciton Chirality Rule was applied to the bis-p-dimethylamino-benzoate of the $cis,trans$-diol obtained following reduction of the diketone. The $cis,trans$-diol is readily distinguished by NMR from the C_2-symmetry cis,cis and $trans,trans$-diols. Since the $cis,trans$-diol dibenzoate from the (-)-dione exhibits a (-) exciton chirality CD, it follows that the absolute configuration of the dione is that shown in Figure 37. The absolute stereochemistry is easily determined by CD.

(a) $\Delta\epsilon_{267}^{max}$ -1100, $\Delta\epsilon_{248}^{max}$ +1100

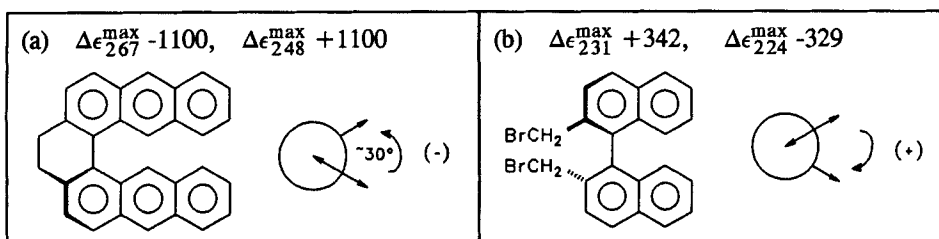(b) $\Delta\epsilon_{231}^{max}$ +342, $\Delta\epsilon_{224}^{max}$ -329

Figure 36. (a) Absolute configuration and exciton chirality of an ethano-bridged 1,1'-bianthryl. (b) Absolute configuration and exciton chirality of (-)-2,2'-bis-(bromomethyl)-1,1'-binaphthyl.
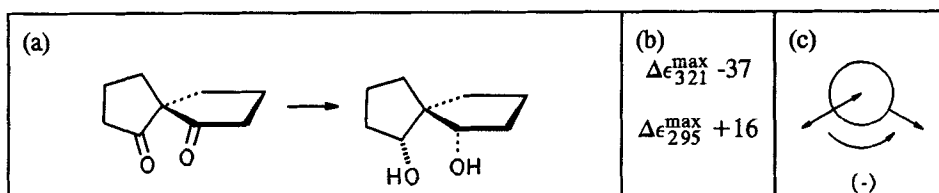

(b) $\Delta\epsilon_{321}^{max}$ -37 $\Delta\epsilon_{295}^{max}$ +16

Figure 37. (a) Formation of the $cis,trans$-diol of (-)-spiro[4.4]nonane-1,6-dione. (b) Observed CD of the bis-p-dimethylaminobenzoate of the $cis,trans$-diol. (c) Exciton chirality.

Tryptycenes can be chiral, but how can one determine the absolute configuration? The CD of (+)-dimethyl 5,12-dihydro-5,12[1',2']benzonaphthacene-1,15-dicarboxylate shows an intense (+) chirality exciton couplet ($\Delta\epsilon_{243}^{max}$ +151, $\Delta\epsilon_{220}^{max}$ -178) for the intense (ϵ^{max} $\sim 84,000$) 233 nm transition. As with the pyranosides, the binary couplets must be

examined, then summed. In the case of the benzotryptycene, the coupling between the two methyl benzoate chromophores is expected to be small because the relevant electric transition moments are parallel. However, the couplings between each methyl benzoate chromophore and the naphthalene chromophore are expected to be large, given the ~90° angle between the transition moment vectors (Figure 38). An examination of the structure would predict a (+) chirality for each of the two couplings, for a net (+) exciton chirality for the enantiomer shown (Figure 38). Determination of absolute configuration by other means would be much more difficult for this substance than by using CD spectroscopy and the Exciton Chirality Rule.
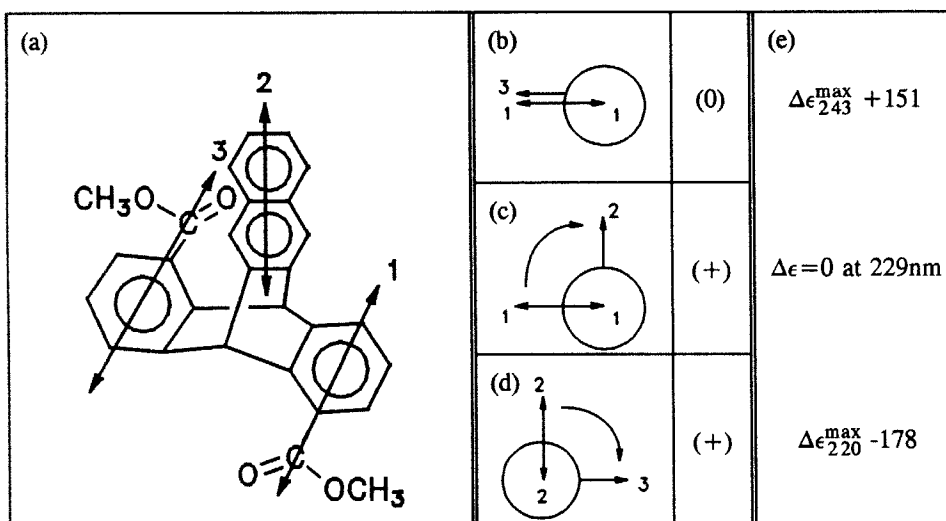
Figure 38. (a) Absolute configuration of (5S,12S)-(+)-dimethyl-5,12-dihydro-5,12[1′,2′]-benzonaphthacene-1,15-dicarboxylate (b), (c) and (d) orientations of pairs of electric transition dipole moments from the chromophores: 1 and 3 from the methylbenzoate chromophores; 2 from the naphthalene. The helicities are shown to the right. The 1,3 couplet is predicted to be zero since the dipoles are parallel. The 1,2 and 2,3 couplets have (+) chirality. The net chirality is predicted to be (+). (e) CD Cotton effects for the intense 233 nm transition of the benzotryptycene showing a (+) exciton chirality.

4. CONCLUSIONS

The origins of two chirality rules, the Octant Rule for ketones and the Exciton Chirality Rule, have been explained, and it has been shown how the rules can be applied to the determination of molecular absolute configuration. In applications of the Octant Rule, when the absolute configuration of a ketone is known, the rule may be used to determine its conformation. Applications of the Exciton Chirality Rule to determine the absolute configuration of diols follows from the derivatization with strongly UV-visible absorbing chromophores.

REFERENCES AND NOTES

1. W. Moffitt, W.B. Woodward, A. Moscowitz, W. Klyne and C. Djerassi, *J. Am. Chem. Soc.*, *63* (1961) 4013-4018.
2. N. Harada and K. Nakanishi, Circular Dichroic Spectroscopy — Exciton Coupling in *Organic Stereochemistry*, University Science Books, Mill Valley, CA, 1983.
3. W. Moffitt and A. Moscowitz, *J. Chem. Phys.*, *30* (1959) 648-660.
4. For leading references see, C.W. Deutsche, D.A. Lightner, R.W. Woody and A. Moscowitz, *Ann. Rev. Phys. Chem.*, *20* (1969) 407-448.
5. The Octant Rule followed as a generalization of the axial haloketone rule and was presented, along with many examples, in C. Djerassi *Optical Rotatory Dispersion and its Applications to Organic Chemistry*, McGraw Hill, New York, 1960.
6. T.D. Bouman and D.A. Lightner, *J. Am. Chem. Soc.*, *98* (1976) 3145-3154.
7. D.A. Lightner, T.D. Bouman, W.M.D. Wijekoon and Aa.E. Hansen, *J. Am. Chem. Soc.*, *108* (1986) 4484-4497.
8. D.A. Lightner, T.D. Bouman, B.V. Crist, S.L. Rodgers, M.A. Knobeloch and A.M. Jones, *J. Am. Chem. Soc.*, *109* (1987) 6248-6259.
9. D.A. Lightner, B.V. Crist, N. Kalyanam, L.M. May and D.E. Jackman, *J. Org. Chem.*, *50* (1985) 3867-3878.
10. D.A. Lightner, T.C. Chang, D.T. Hefelfinger, D.E. Jackman, W.M.D. Wijekoon and J.W. Givens, III, *J. Am. Chem. Soc.*, *107* (1985) 7499-7508.
11. D.N. Kirk, *Tetrahedron*, *42* (1986) 777-818. Also A. Rodger and M.G. Moloney, *J. Chem. Soc. Perkin Trans. II* (1991) 919-925.
12. (a) C. Beard, C. Djerassi, J. Sicher, F. F. Šipoš and M. Tichý, *Tetrahedron, 19* (1963) 919-928. (b) See also J.P. Konopelski, P. Sundararaman, G. Barth and C. Djerassi, *J. Am. Chem. Soc.*, *102* (1980) 2737-2745.
13. (a) G. Snatzke and G. Eckhardt, *Tetrahedron, 24* (1968) 4543-4556. (b) G. Snatzke, B. Ehrig and H. Klein, *Tetrahedron, 25* (1969) 5601-5609.
14. (a) D.A. Lightner and T.C. Chang, *J. Am. Chem. Soc.*, *96* (1974) 3015-3016.
    (b) D.E. Jackman and D.A. Lightner, *J. Chem. Soc. [D]* (1974) 344.
15. H. Ripperger, *Z. Chem.*, *17* (1977) 250-258.
16. K.M. Wellman, P.H.A. Laur, W.S. Briggs, A. Moscowitz and C. Djerassi, *J. Am. Chem. Soc.*, *87* (1965) 66-72.
17. J.B. Lambert, H.F. Shurvell, D.A. Lightner and R.G. Cooks, *Introduction to Spectroscopy*, Macmillan Publishing Co., New York, 1987, chaps. 9 and 10.
18. P. Crabbé, *Applications de la Dispersion Rotatoire Optique et du Dichroisme Circulaire Optique en Chemie Organique*, Gauthier-Villars, Paris, 1968.
19. A. Moscowitz, K.M. Wellman and C. Djerassi, *J. Am. Chem. Soc.*, *85* (1963) 3515-3516.
20. K. Wellman, W. Briggs and C. Djerassi, *J. Am. Chem. Soc.*, *87* (1965) 73-81.
21. (a) D.N. Kirk, *J. Chem. Soc. Perkin Trans. I* (1976) 2171-2177.
    (b) D.N. Kirk and W. Klyne, *J. Chem. Soc. Perkin Trans. I* (1974) 1076-1103.
22. L.H. Zalkow, R. Hale, K. French and P. Crabbé, *Tetrahedron, 26* (1970) 4947-4952.
23. C. Djerassi and J.E. Gurst, *J. Am. Chem. Soc.*, *86* (1964) 1755-1761.

24. For leading references see G. Barth and C. Djerassi, *Tetrahedron, 37* (1981) 4123-4142.

25. H. Numan and H. Wynberg, *J. Org. Chem., 43* (1978) 2232-2236.

26. D.A. Lightner, J.K. Gawroński and T.D. Bouman, *J. Am. Chem. Soc., 102* (1980) 1983-1990.

27. P. Sundararaman and C. Djerassi, *Tetrahedron Lett.* (1978) 2457-2460; errata: *ibid* (1979) 4120. P. Sundararaman, G. Barth and C. Djerassi, *J. Org. Chem., 45* (1980) 5231-5236.

28. C.S. Pak and C. Djerassi, *Tetrahedron Lett.* (1978) 4377-4378.

29. Y.L. Sing, H. Numan, H. Wynberg and C. Djerassi, *J. Am. Chem. Soc., 101* (1979) 5155-5158; errata, *ibid* (1979) 7439.

30. For leading references see J.K. Gawroński, *Tetrahedron, 38* (1982) 3-26.

31. G. Snatzke, *Angew. Chem. Intl. Ed., 18* (1979) 363-376.

32. A. Moscowitz, K. Mislow, M.A.W. Glass and C. Djerassi, *J. Am. Chem. Soc., 84* (1962) 1945-1955.

33. D.A. Lightner, D.E. Jackman and G.D. Christiansen, *Tetrahedron Lett.* (1978) 4467-4470.

34. P.H. Schippers and H.P.J.M. Dekkers, *J. Am. Chem. Soc., 105* (1983) 79-84.

35. A. Lettieri, P.-A. Carrupt and P. Vogel, *Chimia, 42* (1988) 27-28.

36. T.D. Bouman and Aa.E. Hansen, *Croat. Chem. Acta, 62* (1989) 227-243.

37. (a) K. Nakanishi and N. Berova, "Natural Products and the Exciton Chirality Method—Part I. Brief Summary and Recent Results with Cyclic Compounds" in *Abstracts of the 4th International Conference on CD Spectroscopy*, Bochum, FRG, 1991, 115-131. (b) P. Zhou, W.T. Wiester, Y. Chen, N. Berova and K. Nakanishi, "Natural Products and the Exciton Chirality Method—Part II. Bichromophoric Approach to Acyclic Polyols and Aminopolyols" in *Abstracts of the 4th International Conference on CD Spectroscopy*, Bochum, FRG, 1991, 1-16.

38. M. Kasha, H.R. Rawls and M.A. El-Bayoumi, *Pure Appl. Chem., 11* (1965) 371-392.

39. C. Gargiulo, F. Derguini, N. Berova, K. Nakanishi and N. Harada, *J. Am. Chem. Soc., 113* (1991) 7047-7048.

40. (a) Y.S. Byun and D.A. Lightner, *J. Org. Chem., 56* (1991) 6027-6033. (b) Y.S. Byun and D.A. Lightner, *Tetrahedron, 47* (1991) 9759-9772.

41. Aa.E. Hansen and T.D. Bouman, *Adv. Chem. Phys., 44* (1980) 545-644.

42. W.T. Wiester, J.T. Vázquez and K. Nakanishi, *J. Am. Chem. Soc., 109* (1987) 5586-5592.

43. H. Ziffer, D.M. Jerina, D.T. Gibson and V.M. Kobal, *J. Am. Chem. Soc., 95* (1973) 4048-4049.

44. K. Nakanishi, H. Kasai, H. Cho, R.G. Harvey, A.M. Jeffrey, K.W. Jennette and I.B. Weinstein, *J. Am. Chem. Soc., 99* (1977) 258-260.

45. H. Gerlach, *Helv. Chim. Acta, 51* (1968) 1587-1593.

46. H. Harada, N. Ochiai, K. Takada and H. Uda, *J. Chem. Soc. Chem. Commun.* (1977) 495-497.

Chapter 6

Analysis of protein structure by circular dichroism spectroscopy

John F. Towell III[a] and Mark C. Manning[b]

[a]Department of Chemistry, Carroll College, Waukesha, WI 53186

[b]School of Pharmacy, Campus Box C238, University of Colorado Health Sciences Center, Denver, CO 80262

Abstract
    Circular dichroism (CD) spectroscopy is a sensitive analytical tool for assessing protein structure. It can detect changes in both the secondary and tertiary structure of proteins, as well as provide information regarding prosthetic groups, bound ligands and co-factors. The origin of circular dichroism in proteins is described and various applications of CD spectroscopy to the study of protein structure, function, and folding is discussed.

OUTLINE

1. INTRODUCTION

The advent of recombinant DNA technology has led to an increased interest in the structural characterization of proteins by spectroscopic methods. Few spectroscopic techniques can provide the amount of information regarding protein secondary and tertiary structure which can be obtained from circular dichroism (CD) spectroscopy. In this chapter we describe the capabilities of CD spectroscopy to provide details on the globular structure of proteins. In addition, we will provide an overview of quantitative secondary structure estimates via CD spectroscopy and of specialized CD methods for studying proteins in contact with membranes and other biomolecules. Certain aspects of protein CD spectroscopy have been previously reviewed [1-19] .

Most CD spectra of proteins are reported in terms of mean residue ellipticity, which is the molar ellipticity of the protein divided by the number of residues. This allows the CD spectra of proteins to be reported on a normalized scale. Infrequently, the reader may find the spectra reported in terms of differences in molar absorptivity (Δa). Recall that molar ellipticity can be obtained by multiplying Δa by 3298. Conversions between other units of optical activity can be found in a review article by Woody [14].

In general, two spectral regions are of interest for the study of proteins by CD. The far ultraviolet (UV) ($\lambda = 175\text{-}250$ nm) is dominated by contributions from the polypeptide backbone, and typically reflects the secondary structure of the protein. Conversely, many side chain chromophores exhibit CD signals in the near UV ($\lambda = 240\text{-}320$ nm) region. These include aromatic groups (Tyr, Trp, and Phe) as well as disulfides. While all display transitions in the near UV, they also give rise to bands in the far UV as well. Changes in the near UV CD spectra of proteins are usually interpreted as indicating changes in tertiary structure.

Sample requirements for obtaining CD spectra of proteins are minimal. Since the bands in the far UV are much more intense than in the near UV, the amount of material needed to produce an adequate signal is much less. Typically, the concentrations employed range from 0.1 to 5.0 mg/mL. The sample volumes vary from 0.01 to 1.0 mL, so the total amount needed ranges from 5 µg to 5 mg. It should be noted that CD is a nondestructive technique, so all the material can be recovered. However, adsorption of the analyte to the surface of the cells can be a problem, especially at low concentrations [20]. Various kinds of commercial instrumentation is available and this aspect of CD spectroscopy has been discussed elsewhere [21, 22].

A circular dichrograph alternately sends left- and right-handed circularly polarized light (LCPL and RCPL) through a sample. If this sample differentially absorbs these two forms of

light, the sample is optically active and the magnitude of this differential absorption, $\Delta a = a_L - a_R$, when plotted versus wavelength is a Cotton effect (CE) [23]. The area under the curve of such a CE is, to a good approximation proportional to the rotational strength, $R = \text{Im} \{\mu \bullet m\}$, where μ and m represent the electric- and magnetic-transition dipole moments, respectively. Thus, to have optical activity it is necessary that the transition have non-perpendicular electric and magnetic transition dipoles. The transition is characterized as having both axial and linear displacement of charge. Axial and linear charge displacement sum to give a helical charge displacement; the left- or right-handedness depending on the chirality of the molecule. When a chiral molecule interacts with a chiral electromagnetic field, one of the components of the light beam, LCPL or RCPL, is more likely to induce a transition in the molecule because of the helical nature of the transition's charge displacement. Therefore, LCPL and RCPL are differentially absorbed and a CE observed. The models which explain optical activity in molecules must therefore explain the sources of non-perpendicular electric and magnetic transition dipole moments. Typically, transitions are either electrically or magnetically allowed (but not both), or if they are both allowed, they are usually perpendicular [24]. Most contemporary discussions of the theory of optical activity are contained within the boundaries of the following three theories: the one-electron theory [25], the coupled-oscillator theory [26], and the inherently dissymmetric chromophore [27]. The classic example of the inherently dissymmetric chromophore is hexahelicene [27]. The chromophore is a dissymmetric conjugated π system and includes the whole molecule. The structure itself creates the helical electronic motions necessary for optical activity. Other examples of inherently dissymmetric chromophores are skewed dienes and twisted biphenyl systems.

The coupled-oscillator model can be applied to molecules that can effectively be considered as two or more separate chromophores or to molecules that are positioned close to each other. This model considers the effects of coulombic coupling between the transition dipole moments of neighboring chromophores. The magnitude of the coupling between transition moments is dependent on the energies and orientations of the two transition moments, and the distance between them [26]. This coupling can induce magnetic moments in the electrically allowed transitions and thus create helical charge displacement and optical activity. Coupling can also occur between the electric moment of a chromophore and the magnetic moment of a neighboring chromophore to produce optical activity [28-30]. The coupled-oscillator model is a dynamic model because the interaction between separate electronic motions induces the optical activity.

Static effects can also produce optical activity. It has been shown that an anisotropic three dimensional harmonic oscillator is not inherently optically active because the electrically allowed transitions were magnetically forbidden and vice versa [25]. However, when the oscillator is placed in an asymmetric electrostatic field, the perturbation on the wavefunctions of the oscillator causes a mixing of states. This mixing of states causes electrically allowed transitions to gain small magnetic components and the magnetically allowed transitions gain small electric components. These transitions are then optically active due to the presence of an asymmetric electrostatic field. In the one-electron theory, the presence of this perturbation, the asymmetric electrostatic field, causes a loss in purity of the orbitals, resulting in perturbed orbitals that are mixtures of the pure orbitals which were present before the electrostatic field. Before perturbing the system, the transition may have been electrically allowed and magnetically forbidden, but after the perturbation, it may be a hybrid of several orbitals.

One-electron theory is typically applied to molecules in which the chromophore is only part of the whole molecule. This chromophoric part is locally symmetric, but the entire molecule is dissymmetric. It is the dissymmetric perturbation of the locally symmetric chromophore by the rest of the molecule that induces the optically active absorption bands. An example of such a molecule is (+)-3-methylcyclohexanone, in which the lowest energy transition is the n-π^* transition which is centered on the carbonyl group [31]. Locally, this carbonyl group is symmetric, and without the perturbing effects of the rest of the molecule, it would be optically inactive like formaldehyde. However, the coulombic field of the methyl group statically perturbs the carbonyl group and the subsequent mixing causes the transition to become

optically active. The sign of the CD band depends on the chirality of the 3-position and sector rules have been developed [32, 33] that correlate the position of the chiral substituent in the space surrounding the carbonyl group with the sign of CD bands.

2. CD SPECTRA OF PROTEIN SECONDARY STRUCTURES

Fortunately, CD spectroscopy is sensitive not only to the local chirality of the peptide unit, but it also reflects global chirality, that is, the way the chiral units are arranged in space. Therefore, CD can detect different secondary structures within the polypeptide chain. There are four main classes of secondary structures for proteins: the α helix, the β sheet, the β turn, and the random coil. In addition, there are also other helix and turn variants which will be discussed.

2.1. α Helices. Of all the secondary structure types, the α helix is the most frequently observed in globular proteins [34]. It is a regular structure, in that each monomeric unit adopts approximately the same ϕ and ψ angles ($\phi \sim -55°$ and $\psi \sim -50°$) [34-36]. The α helix produces the most intense and distinctive far UV CD spectrum of any secondary structure (see Figure 1). Note that there are two negative maxima, one near 222 nm and a second near 208 nm. While these are the canonical values for the α helix, some variation is observed depending on the length of the helix and its exact ϕ and ψ angles. At approximately 200 nm the spectrum crosses over from negative to positive and displays a strong positive band near 192 nm. The position of this feature is more variable than for the negative bands. The intensity of the negative bands is approximately equal ($\sim -35,000$ deg cm^2 dmol^{-1}), while the intensity of the positive band is nearly double that ($70,000-80,000$ deg cm^2 dmol^{-1}).

The range of ϕ and ψ values which define an α helix is relatively small, yet helices with different average angles appear to display different properties. Blundell et al. [36] describe helices as either hydrophilic or hydrophobic depending on the average backbone dihedral angle. In addition, systematic variation can produce bent helices [36]. Although it is very difficult to characterize the dependence of CD spectra on ϕ and ψ angles, theoretical studies predict that decreasing the hydrophobicity of an α helix (i.e., decreasing ϕ and increasing ψ) should produce a weaker 222 nm band and red-shifted extrema [37, 38].

Many theoretical studies have predicted a significant dependence of α helix CD spectra upon chain length [37-40] which is supported by experimental investigations [41, 42]. Other calculations have found little or no dependence [43,44]. In particular, it is important to delineate two aspects of chain length dependence. First, it is of interest to know the minimal number of residues in an α-helical conformation which would produce an α helix-like CD spectrum. Second, it would be of importance to know the length of an α helix which would approximate an infinite polypeptide chain.

2.2. β Sheets. The other major class of regular secondary structures are the β sheets, where each residue has similar conformational properties ($\phi \sim -150°$ and $\psi \sim -150°$). The variation in the dihedral angles is greater than for α helices [35]. Also known as the extended conformation, the β conformation can exist as a single strand, parallel or antiparallel β sheets, as well as barrels [34, 45-48].

The CD spectra of β sheets are less intense than those of α helices (see Figure 2). They display a single negative band near 217 nm, although the position can vary by up to 5 nm. The cross-over wavelength (from negative to positive) is red-shifted relative to the α helix as is the positive band, which typically occurs near 200 nm. Theoretical studies indicate that the CD spectra of β sheet structures are sensitive to the number of strands and the number of residues per strand [37, 49]. Even more, the CD is sensitive to the twisting of each individual strand. In globular protein structures, β sheets are highly twisted [45], sometimes by as much as 45° per residue from the idealized Pauling and Corey structure [50].
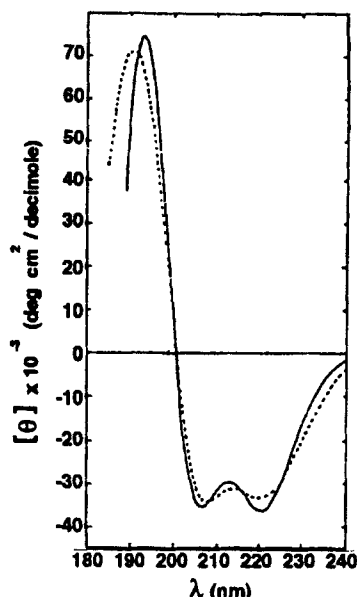
Figure 1.   Far UV CD spectra of homopolymers which adopt an α-helical conformation: poly(Glu-OMe) in hexafluoroisopropanol, —— ; poly(Lys), ···· . (From refs. 14 and 87)

There has been some discussion as to whether CD can distinguish parallel from antiparallel β sheets. As stable, well-defined model compounds are lacking, the spectra available have been derived from secondary structure deconvolutions (see below). Overall, the ability of CD to provide adequate estimates of both parallel and antiparallel β sheet contents is still an ongoing question. Johnson and co-workers were the first to derive basis spectra which corresponded to both parallel and antiparallel β sheet structures in globular proteins using the singular value deconvolution method [11, 12, 51-53]. However, the basis spectra were significantly different from spectra reported for model sheet structures. Recently, Perczel et al. [54] employed another approach, convex curve analysis, to obtain improved β sheet basis spectra. The major improvement was to include more β sheet proteins into the data base.

2.3. β Turn Structures. The term turn refers to a diverse class of structures in which the polypeptide chain reverses direction. In particular, β turns are those in which the *ith* residue hydrogen bonds to the *i+3rd* residue of the turn. Tighter turns (γ turns and δ turns) are also known, although they occur with markedly lesser frequency than β turns [34, 55].

One difficulty in characterizing the CD for a typical β turn has been the lack of well characterized model compounds and the variability of the β turn structure in terms of allowable backbone dihedral angles. Early classification schemes described three general classes of β turns, termed types I, II, and III (see Table I). Type III turns resemble a single turn of a 3_{10} helix (see below), while types I and II are the most common structures for chain reversal found in globular proteins. Types I' and II' have also been identified, with the prime symbols indicating an approximate 180° rotation of the peptide group of the *i+1th* residue.

Woody [56] classified representative CD spectra for β turns based upon theoretical determinations. For types I and II, CD spectra similar to β sheets, but with red-shifted extrema, were predicted. These were referred to as class B spectra, with the standard β sheet spectrum termed as class A. Class C spectra resembled the CD pattern of an α helix, and were predicted to arise for type II' turns. Since then, numerous β turn models have been examined and most experimental results agree with the theoretical studies [14]. Notable exceptions include type I turns which exhibit class C spectra rather than the class B predicted for such structures. Gierasch et al. [57] have suggested that the discrepancy may arise from the presence of a cis'-proline residue (ψ ~ -50°), and that it is the cis'-proline residue which produces the C-type spectrum regardless of the turn type.
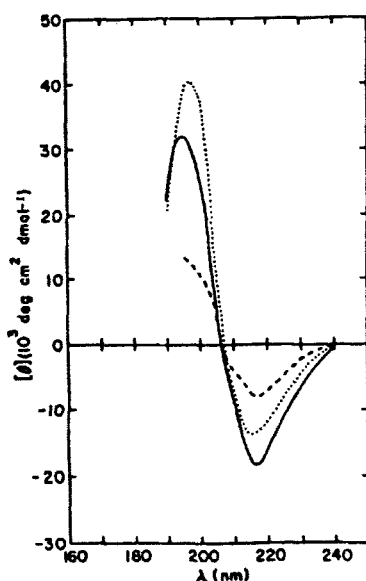

Figure 2.   Far UV CD spectra of homopolymers which adopt a β-sheet conformation: poly(Lys), pH 11.1 after heating, —— ; poly(Lys), in 1% sodium dodecyl sulfate, ---; poly(Lys-Leu) in 0.1 M NaF, pH 7, ···· . (From ref. 14)

Recently, attempts have been made to derive CD spectra of various β turns using deconvolution procedures (see below). Employing an approach termed convex constraint analysis, Perczel, Fasman, and others [58-61] have derived CD spectra for both types I and II turns. Three basis spectra were extracted for a data base of fourteen peptides which displayed either types I or II β turns. One basis spectrum for type I turns resembled a class C spectrum and the other a variation of a class B. The type II turn is said to display a classic class B spectrum [59-61].

2.4. Random Coil Structures. The term "random coil" may be a misnomer. When proteins are unfolded, it is still unclear whether the structure of the denatured protein is truly random. Terms such as 'unordered' or 'other', are often used to refer to the random coil state. The CD of denatured proteins or small peptides displays one dominant feature, a strong

negative band near 200 nm ($[\theta] \sim -40,000$ deg cm^2 dmol^{-1}). Depending on the particular system, there may be a weak positive band near 220-230 nm. It is also worth noting that the CD and absorption bands for the unordered forms of poly(Glu) and poly(Lys) do not coincide [62], again suggesting that the unordered form may not be random.

Table I. Dihedral angles for the central residues of β turns.

Type	i+1th Residue		i+2th Residue	
	ϕ	ψ	ϕ	ψ
I	$-60° \pm 30°$	$-30° \pm 30°$	$-90° \pm 30°$	$0° \pm 30°$
II	$-60° \pm 30°$	$+120° \pm 30°$	$+80° \pm 30°$	$0° \pm 30°$
III	$-60° \pm 30°$	$-60° \pm 30°$	$-60° \pm 30°$	$-60° \pm 30°$

Significant negative CD at 200 nm has prompted a number of workers to propose that in the random coil state, the polymer actually adopts a semi-regular structure (i.e., a restricted conformation). This viewpoint was based on a number of observations. For amino acids larger than alanine, Ramachandran and co-workers concluded that only 23% of conformational space was even partially allowed [35]. Kauzmann estimated that the optical rotation of the random coil was approximately an order of magnitude too large for a truly random structure [63]. Schellman and Schellman postulated that the random coil actually adopts a collagen type of structure, which is also known to display a strong negative band near 200 nm [64]. Despite this body of evidence, Tiffany and Krimm [65, 66] were the first to propose that the random coil was actually an ordered structure, adopting an extended left-handed helical conformation, similar to the threefold helix of poly(Pro) II. Their argument was built around the behavior of poly(Pro) II in concentrated CaCl$_2$ solutions. While this has proved to be a solid starting hypothesis, it has since been shown that under these conditions, the peptide groups of poly(Pro) rearrange to form a significant amount of the *cis* amide isomers. Therefore, this may be a poor model for the random coil state.

Numerous attempts have been made to calculate the CD spectrum of the random coil state, with mixed success [65-69]. Certainly, any ensemble which produces a CD spectrum which is indicative of a random coil structure must have a significant population in the collagen fold region of ϕ, ψ space, the only well defined structure which displays a strong negative band near 200 nm. Theoretical studies indicate that there is an optical node near this region of ϕ, ψ space, that is, the sign of the CD band can change with small deviations in dihedral angles [70]. Therefore, it is difficult to accurately calculate the CD of collagen types of structures, as small variations from the crystal structure may produce significantly different CD patterns.

2.5. Poly Proline Helices. Poly proline (PP) displays some unusual structural properties as it is the only naturally occuring tertiary amide found in polypeptides. The inability of this residue to act as a hydrogen-bond donor leads to two types of extended helical structures, neither of which resembles the α helix. The first, called PP I, is a right-handed helix which possesses *cis* amide bonds (ω = 0°). The other, PP II, is a left-handed helix with *trans* amide bonds (ω = 180°). Both occupy a fairly limited region of ϕ,ψ space. The two forms interconvert slowly over time.

Both PP I and PP II display unusual CD curves. The spectrum for PP II is distinctly nonconservative, with a weak positive band at 230 nm and a strong negative band at 200-205

nm. The presence of a strong negative band at this wavelength has prompted some to propose threefold left-handed helical structures as models for the random coil (see above).

Some description of the chain length dependence of PP helices has been reported [71, 72]. It appears that short helices of PP are sufficient to produce a similar spectrum to that of an extended polymer. Theoretical studies support these results [38, 73], finding that helices as short as three residues in length can produce a PP II-like CD spectrum.

2.6. 3_{10} Helices. A structure which is similar to the α helix is termed the 3_{10} helix. It contains three residues per turn (compared to 3.6 per turn for the α helix) and one less residue per hydrogen bond. Few examples have been found in globular proteins, but it is quite common in antibiotic and pore-forming peptides, especially those which contain Aib (α-aminoisobutyric acid). The ϕ and ψ angles for 3_{10} helices are similar to those for α helices, ranging from $\phi = -60°$, $\psi = -30°$ [35] to $\phi = -44°$, $\psi = -33°$ [74]. Experimentally, 3_{10} helices display a far UV CD pattern similar to that of the α helix, although it has been proposed that the two might be distinguished based upon the ratio of the intensities of the 222 and 208 nm bands [14, 75]. This has been difficult to verify, although theoretical studies do predict that 3_{10} helices should possess a lower 222 nm intensity relative to the 208 nm band due to reduced $n\pi^*$ rotational strengths [38].

2.7. Alternate Helical Structures. Since Pauling and Corey's description of the α helix [76], many other helical structures for polypeptides have been proposed and described. However, most of them are rare or found only in homopolymeric systems. These include the ω helix, the π helix, and the α_{II} helix.

2.7.1 ω Helix. The ω helix possesses a fourfold axis of symmetry, while retaining the i to $i+4$ hydrogen bonding scheme [77, 78]. Therefore, it is 'looser' helical structure than the α helix, and has been identified in forms of poly (L-Phe) [79] and poly (benzyl-L-Asp) [80]. The canonical ϕ and ψ angles are $-38°$ and $-78°$, respectively. No experimental CD spectra have been reported, but a theoretical CD has been computed [38].

2.7.2. π Helix. The π helix is even rarer, having 4.4 residues per turn and an i to $i+5$ hydrogen bonding scheme [81, 82]. Theoretically, it is predicted to have a CD spectrum resembling that of a β sheet [38].

2.7.3. α_{II} Helix. Possibly, the most important and interesting of alternate helical structures is the so-called α_{II} helix. While, it possesses the same rise per residue and number of residues per turn, its backbone angles ($\phi = -70.5°$, $\psi = -35.8°$) are significantly different than that of an α helix [83]. In general, it is an extreme example of a hydrophilic α helix, meaning its carbonyl groups are tilted outwards to optimize hydrogen bonding with the solvent. It has been proposed that the α_{II} helix occurs in the transmembrane helices of bacteriorhodopsin [84], where the relatively high number of Ser and Thr residues may hydrogen bond to the backbone to increase the overall hydrophobicity of the helix. This may account for some of the discrepancies in the CD spectrum of this protein (see Membrane Proteins below). The α_{II} helix has also been proposed to exist for poly (Ala) dissolved in strong hydrogen bond donor solvents, such as hexafluoroisopropanol [85]. Calculations suggest that the α_{II} helix should exhibit red-shifted extrema and a very weak $n\pi^*$ band relative to the α helix [38].

3. SECONDARY STRUCTURE ESTIMATES USING CD SPECTROSCOPY

While qualitative comparisons of CD for proteins of unknown structure using the spectra of individual secondary structures described above can provide insight into secondary structure composition, it would be of greater utility to be able to quantitatively assess the amounts of each secondary structural type. Numerous attempts have been made to develop these capabilities and have been widely reviewed [6, 10-12, 17, 18, 86]. The reader is encouraged to refer to these works for more detailed information.

Early attempts used data obtained from homopolypeptides, such as poly(Lys), for their basis spectra [87, 88]. In the past fifteen years, approaches using data from globular proteins have emerged [18, 89-101]. Basically, a data base comprised of proteins with known secondary structure compositions is assembled and far UV CD spectra recorded. The choice of the proteins to be included is critical and various combinations have been examined. Mathematical matrix methods can be used to extract basis spectra which represent the contributions from the various secondary structures. Typically, four or five basis spectra can be obtained (corresponding to α helices, β sheets, β turns, and random coil structures). In some approaches, such as those developed by Johnson and co-workers [11, 12, 51, 52, 102], separate basis spectra can be obtained for parallel and antiparallel β sheets. These basis spectra are then linearly combined to reconstruct the CD spectrum of the protein of interest. The proportion of the basis spectra used to provide the best fit to the spectrum corresponds to the percentage of that secondary structure in the protein of interest. Complete details of the mathematical algorithms that have been employed can be found elsewhere [10, 12, 17, 89, 103].

While these methods often provide accurate and useful estimates of secondary structure composition, it should be noted that they do involve a number of assumptions, independent of the choice of proteins for the basis set. Briefly, there are four major assumptions made to accomplish the deconvolution of protein CD spectra. They are:

1. The solution conformation and the crystal structure are identical.

2. A single basis spectrum can adequately describe the CD arising from all variations of the secondary structure it represents.

3. Secondary structure units do not interact, i.e., tertiary structure effects can be ignored.

4. Only peptide chromophores contribute to the far UV region of the CD spectra of proteins.

While most protein systems do not significantly violate these assumptions, examples have been found which do. These have been summarized and discussed in detail elsewhere [17].

While earlier basis sets employed CD spectra of model homopolypeptides such as poly(Lys) [87, 88], more developed approaches use CD spectra of proteins with known secondary structure composition. These data sets attempt to span the range of protein types (α, β, α+β, and α/β). The approaches also differ in the algorithm used to reconstruct the experimental CD spectrum in question [10, 12, 103]. Johnson and co-workers even developed methods for systematically eliminating unlike proteins from the basis set to achieve an improved fit [10, 12, 102].

4. NEAR UV CD SPECTRA OF PROTEINS

While the far UV region has received the most attention in the study of protein CD, there are intrinsic chromophores in proteins which give rise to signals in the near UV ($\lambda = 250$-350 nm). These include the side chains of aromatic amino acids (tryptophan, Trp, tyrosine, Tyr, and phenylalanine, Phe) and the disulfide moiety of cystine. The exact position of these bands depends on the extent of exposure to the solvent, the solvent polarity and pH, and their proximity to other groups. The analysis of the near UV CD spectra of proteins has been reviewed [7, 8].

Not only do these two regions possess information on different aspects of the globular structure of a protein, they also differ in the intensities of the signals. Typically, the signals in the near UV are one to three orders of magnitude weaker than those in the far UV. As a result,

the pathlengths and concentrations used for work in the near UV must be significantly greater. Usually, pathlengths of 5 to 10 mm must be used with protein concentrations in the range of 1 to 5 mg/mL. The sample volumes are between 600 μL and 3000 μL. In order to obtain reasonable far UV CD spectra, the demands are more modest, with pathlengths ranging from 0.1 mm to 1 mm and concentrations typically between 0.05 and 0.50 mg/mL with sample volumes of 100 μL to 1.5 μL. It should be noted that at very low protein concentrations, adsorption to the cell may cause diminished CD intensity [20]. Still, coupled with its high sensitivity and its nondestructive nature, its minimal sample requirements have been among the primary reasons for CD spectroscopy being the method of choice in the study of protein structure and stability.

4.1. Aromatic Side Chains. The usual dogma is that while far UV CD spectra of proteins reflect the secondary structure of proteins, the near UV CD spectra indicate changes in tertiary structure. This viewpoint arises from the fact that near UV CD spectra arise from aromatic groups in a fixed geometry relative to the peptide backbone and surrounding chromophores. Loss of tertiary structure would disrupt this ordering and lead to a diminished or altered near UV CD spectrum.

4.1.1.Spectral Properties of Aromatic Side Chains. The CD of proteins arises from signals from aromatic side chains (Phe, Tyr, and Trp) as well as disulfides. As the CD of each of these groups is dependent on the local environment, this leads to the view that perturbation of the near UV indicates disruption of the localized folding pattern. The CD and absorption bands display maxima near 280-290 nm for Trp, near 275-280 nm, and around 250-260 nm for Phe [7, 8].

4.1.2. Use of Near UV CD Spectra to Probe the Globular Structure of Proteins. Along the proper folding pathway for proteins, it has been suggested that there are folding intermediates which adopt a compact globular structure, but are not native-like. These types of structures can be generated during the refolding of acid- or base-denatured proteins [104, 105]. These 'molten globule' states display far UV CD spectra which indicate significant secondary structure, but the near UV CD spectra are featureless, suggesting a lack of tertiary structure. Consequently, these forms are presumed to be similar to early folding intermediates, which have organized secondary structure but have not folded into the proper tertiary structure.

Some studies have been reported where individual aromatic groups of a protein have been systematically replaced using site-directed mutagenesis, allowing the contributions of the individual chomophores to be determined. Craig et al. [106] have systematically relaced all the Trp moieties in interleukin-1β (IL-1β). Earlier work of Elwell and Schellman [107] replaced the tryptophan in T4 lysozyme with tyrosine.

It has been demonstrated that aromatic groups can alter the shape of the far UV CD of proteins so that accurate estimation of secondary structure is difficult. The lowest excited states in both Tyr and Phe are known to couple to the peptide backbone in bovine pancreatic trypsin inhibitor (BPTI) to produce an unusual far UV spectrum [108]. Recently, we have begun an examination of the individual contributions of each aromatic group to the CD of BPTI [109]. Figure 3 shows the CD of wild type BPTI and two mutants where the aromatic residue has been replaced by leucine, another hydrophobic amino acid. In the case of F22L (Phe^{22} -> Leu), the phenylalanine ring lies near the center of a cluster of aromatic side chains, and its removal significantly decreases the intensity of the near UV CD spectrum. On the other hand, replacement of Phe^{33} (which is on the surface of the protein) with leucine does little to change the CD of BPTI. It should be noted that changes are also detected in the far UV CD as well.

4.1.3. Use of Near UV CD Spectra to Probe Aggregation in Polypeptides. Near UV CD spectroscopy can be employed to monitor the aggregation of a polypeptide species. Upon association, the aromatic groups will be in different environments than in the isolated monomers and the CD may change dramatically, especially in small peptides. This can be seen for insulin, where the near UV CD intensity of a monomeric form is only $[\theta] \sim -150$ deg cm^2 dmol^{-1}. Yet, the hexameric form displays a signal nearly twice as intense [110-112].
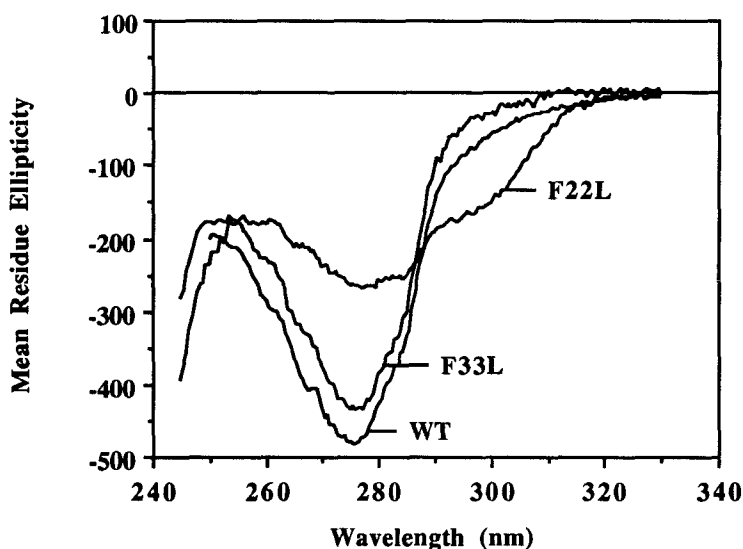
Figure 3. Near UV CD spectra of wild type BPTI and two mutants, F22L and F33L.

Recently, we have shown that the aggregation of leuprolide acetate (LPA), a nonapeptide hormone, can be detected by monitoring the near UV CD spectrum at various concentrations [113]. Figure 4 shows the concentration dependence of LPA in 4:1 ethanol-water mixtures at 5° C. At concentrations below 2 mg/ml, the spectrum is unremarkable, displaying a single negative band at 275 nm ($[\theta] \sim -300$ deg cm^2 dmol^{-1}). However, at concentrations near 4 mg/mL, the spectrum begins to alter, exhibiting two features at 268 nm and 289 nm, which become quite distinct at a concentration of 5.45 mg/mL. Similar behavior is observed at 25° C, but higher concentrations are required to achieve aggregation.

4.2. Disulfides. Relative to the aromatic chromophores in proteins, the CD spectra of disulfides in proteins has received little attention. This is due to a number of reasons. First, the signals from the disulfides are typically weaker than those arising from aromatic groups. Second, the nature of higher energy excited states in disulfides is poorly understood. Third, little data is available on their electronic structure, either from theoretical treatments [114-116] or from experimental studies [117].

5. USE OF CIRCULAR DICHROISM TO DETERMINE PROTEIN STABILITY

One of the primary mechanisms of protein degradation is the loss of globular structure [118, 119]. This process, termed denaturation, leads to a partially or completely unfolded species which usually lacks any of the biological activity of the native protein. A variety of methods have been employed to monitor the denaturation of proteins, including fluorescence, infrared, nuclear magnetic resonance (NMR), and CD spectroscopy. As CD is very sensitive to changes in both secondary and tertiary structure, its application to the study of protein folding

and unfolding has been widespread. A review of the use of CD in assessing protein stability has recently appeared [120].
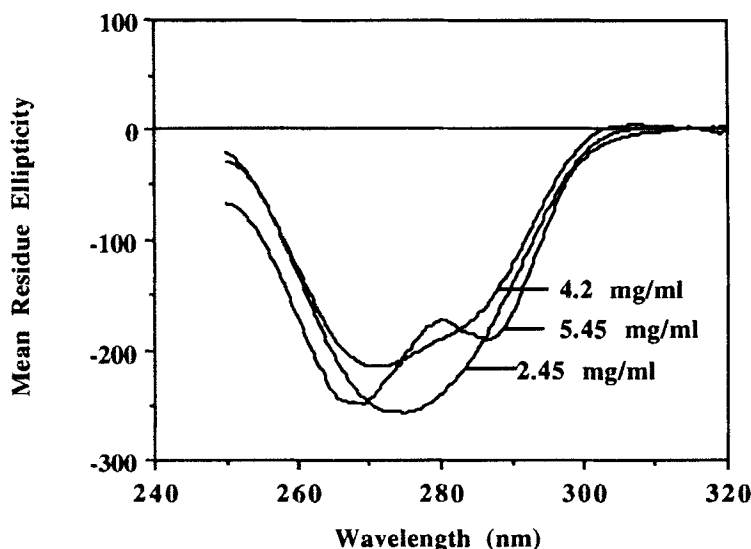

Figure 4. Concentration dependence of the near UV CD spectra of leuprolide acetate dissolved in a 4:1 ethanol/water (v/v) mixture.

Denaturation of a protein can be induced by numerous conditions, including subjecting the protein to extremes in pH, increasing or decreasing the temperature, or by the addition of salts, organic solvents, chelating agents, or denaturants (such as guanidinium hydrochloride, GnHCl, or urea). One advantage of CD spectroscopy is that these changes in solvent composition are essentially transparent to the CD experiment.

Thermal denaturation of proteins is one of the most common determinations of protein stability. By monitoring the change in CD intensity at a particular wavelength, one can determine the degree of unfolding as a function of temperature. For example, it has been shown that there exists a correlation between α-helix content of a protein and its molar ellipticity at 222 nm [99]. A plot of the CD signal as a function of temperature provides the raw data for construction of a denaturation curve. In the vicinity of the melting temperature, T_m, (defined as the temperature where half of the protein is unfolded), there is a rapid, cooperative transition from a relatively rigid, folded structure to a flexible unfolded conformation. This transition may involve denaturation of the entire protein, of a single domain, or even of just a small, independent section. An increase in the T_m value is taken to indicate an increase in protein stability [119, 121-126].

Analysis of a thermal melting curve can provide thermodynamic information regarding the unfolding process [123-126]. From the relative fractions of folded and unfolded protein at a given temperature near T_m, one can determine an equilibrium constant and, thus, a free energy of unfolding (ΔG_u) at that temperature. A plot of ΔG_u versus temperature provides an estimate (from the slope) of the entropy of denaturation. The enthalpy of unfolding can then be calculated from the Gibbs-Helmholz equation.

Lowering the temperature can also cause a protein to unfold in a process termed 'cold' denaturation [127, 128]. This arises primarily from the positive entropic component of the hydrophobic interactions which lead to globular protein structures [119, 129]. A number of examples of this phenomenon have been described [127, 128] and have been detected using CD spectroscopy. Frequently, because many proteins only cold denature below the freezing point of water, nonaqueous solvents and solvent mixtures must be employed to maintain fluidity of the solution [128]. In the case of staphylococcal nuclease [127], the unfolding was measured in an aqueous solution containing 2 M urea. Spectra taken at -7° C indicated a greater degree of unfolding than for heat denatured material at 55° C.

Another common indication of protein stability is the concentration of either urea or GnHCl required to unfold half of the protein available. This concentration, given the symbol $[D]_{1/2}$, is analogous to the T_m value from thermal denaturation curves. Increase or decrease in $[D]_{1/2}$ is presumed to indicate a corresponding increase or decrease in protein stability, respectively. Analysis of these curves can also provide thermodynamic information [123-126]. As these experiments can be done at any temperature, they are more useful in that they can provide information regarding stability at or near room temperature.

Denaturation resulting from either heating the sample or the addition of a denaturant can be followed observing changes in either the near or far UV region of the spectrum. In the near UV, the signals arise from aromatic groups and, to a lesser extent, disulfides. Typically, changes in this region are thought to reflect an alteration of the tertiary structure [7, 8]. Conversely, changes in the far UV represent changes in secondary structure, although contributions from side chains and prosthetic groups may not be negligible at these wavelengths [17].

6. THEORETICAL ASPECTS OF PROTEIN CIRCULAR DICHROISM

6.1. Historical Background. An important effort in the area of the CD of proteins and other biopolymers is the development of accurate and reliable theoretical models. Numerous studies have been reported on the attempts to calculate CD spectra of proteins given a particular structure, using data derived from molecular orbital calculations or empirical data [1, 14, 30, 38, 130-133]. Among the most successful of these have been the exciton method, which assumes each chromophore is a separate, non-overlapping unit. Bayley et al. [132] developed a procedure for calculating CD spectra in the exciton approximation termed the matrix method. A brief description of it is given below. Other methods include polarizability approaches, as developed by Applequist and co-workers [43, 44, 134-140] and modifications of MO schemes, such as the random phase approximation (RPA) method [141].

6.2. Theory of Spectral Calculations. The problem of calculating rotational strengths for polymeric systems has been a long standing one. Initially, the problem was solved using perturbation theory [1]. However, Bayley et al. [132] developed a simpler approach termed the matrix method. This approach avoided the difficulties of first-order perturbation theory and provided a compact and efficient method for calculating rotational strengths. In addition, it is able to account for all of the primary mechanisms of obtaining rotational strength (coupled oscillator, one-electron, and μ-m coupling).

For polymers, a major challenge is to describe the rotational strength of the entire molecule in terms of its constituent identical chromophores (taken to be N in number). In order to accomplish this, some basic assumptions must be made. First, each monomeric unit must be assumed to be an independent chromophore which can be perturbed via interactions with the other groups. In other words, electron exchange or charge transfer between groups is ignored. Also, these groups must not possess some dissymmetry. The inability of the matrix method to account for charge transfer excited states is most likely not problematic in its description of near and far UV CD spectra, but this shortcoming may render it inadequate to describe higher energy states in the vacuum UV. Another assumption is that the energy range of the excited

states under consideration is limited. Polarizability approaches circumvent this difficulty by combining all of the very high energy states into a single polarizable unit, which can interact with lower energy states. Matrix methods rely on accurate descriptions of each individual state. Finally, matrix methods are limited to singly excited configurations. Inclusion of doubly excited states have been shown to increase the accuracy of semi-empirical MO calculations.

Provided these limitations and assumptions are understood, the computations can now be performed. As denoted in its name, initially, a matrix is constructed. On the diagonal of this matrix, the energies of the unperturbed excited states are placed. The off-diagonal elements describe the extent of interaction between the excited states, both within a chromophore and between different groups. Within a given group, the mixing is accomplished by an asymmetric electric field (i.e., the proximity of a chiral center). This is the one-electron mechanism discussed in **section 1**, and is the predominant mechanism by which the n-π^* transition gains its rotational strength. Mixing between excited states on separate chromophores can be via either the coupled oscillator mechanism [32] or the Kuhn μ-m [29] mechanism, which couples electrically allowed transitions with those which are magnetically allowed.

In most studies using the matrix method, the excited states and the ground state are defined as a series of point charges (monopoles). Each collection of charges is placed in such a way to accurately represent the magnitude and direction of the dipole moment (for a more detailed description of the method, see Bayley et al. [132] and Manning and Woody [38]). The extent to which one state interacts with another is calculated using the Coulomb equation which describes the interaction of point charges with each other in a dielectric medium.

Once the off-diagonal elements are computed and the interaction matrix is constructed, the matrix is diagonalized. The resulting eigenvalues are the energies of the individual exciton states after considering interaction with all other excited states. In many early calculations, the interaction with other chromophores was assumed to be zero if they were separated by a distance of more than 10-20 Å in order to limit computer time. The eigenvectors are then used to determine the extent of mixing between any two excited states. This leads to borrowing either magnetic dipole or electric dipole intensity from other transitions, and coupled with the intrinsic dipole moment of the excited state, produces non-zero rotational strength. Recently, Manning and Woody (1991) have extended the matrix method to include four transitions on each peptide group (NV_1, NV_2, $n\pi^*$, and $n'\pi^*$). Each excited state as well as the ground state charges are described in the monopole approximation.

6.3. Calculations of the CD of Polypeptides.
Woody and co-workers have published numerous studies regarding the use of theoretical methods to determine the CD of various secondary structures, primarily helices [37, 38, 142]. All of these investigations employed modifications of the matrix method. The primary improvement was the incorporation of a number of electronic states on each chromophore. Previously, only the $n\pi^*$ and the NV_1 transition were considered. This has now been extended to include NV_2 and the $n'\pi^*$ transitions, as well as aromatic side chain contributions [108]. Conversely, Applequist and co-workers have pioneered the use of polarizability methods for calculating the CD of secondary structures [43, 44, 134-140]. In some cases, the description of the CD behavior for a particlar system is different, but together, they provide a great deal of insight into the physical basis of the rotational strength for a given structure and the ability of CD to characterize protein conformation.

6.4. Contributions of Aromatic Side Chains to the Far UV CD of Proteins.
Numerous theoretical studies of the effects of aromatic groups on both the far and near UV CD spectra of proteins have been conducted by Hooker and co-workers [143-154]. While the calculations on larger proteins were limited in scope, they do provide the only comprehensive attempt to include these chromophores into CD calculations (see below). Other researchers have attempted coupled-oscillator calculations on proteins such as insulin [155, 156], to assess the effects of tertiary structure on near UV CD spectra. More recent work by Woody and co-workers expanded the matrix method to include more elaborate descriptions of

both the ground and excited state structure of both the polypeptide chain and aromatic groups [70, 108]. These have been shown to be effective in describing both the near and far UV CD of BPTI [108].

6.5. Future Development and Applications of CD Spectral Calculations.
More work needs to be done to develop increasingly accurate representations of the electronic states of peptides and various side chain chromophores. Once this is completed, the models are in place to examine interactions between these states for a given protein conformation. An accurate and flexible model which can calculate CD spectra of a variety of protein structures would be invaluable in the study of protein folding, stability, and structure.

7. CD SPECTRA OF PROTEINS CONTAINING PROSTHETIC GROUPS OR COMPLEXED TO OTHER BIOMOLECULES

All proteins have CD spectra in the ultraviolet region due to the transitions of the peptide backbone and side-chain residues. The CD bands due to the protein itself are called *intrinsic* Cotton effects. However, many proteins have CD bands at wavelengths that do not overlap with the intrinsic Cotton effects. These bands are due to enzyme-bound chromophores such as coenzymes, prosthetic groups, metal ions, substrates, inhibitors, etc. and are called *extrinsic* Cotton effects.

Extrinsic Cotton effects are due to the inherent dissymmetry of the enzyme-bound chromophore (an *inherent* effect) and/or to the interactions of the chromophore with the encompassing dissymmetric environment (*interactive effects*). The inherent effects are those which the free chromophore would exhibit if its conformation were identical with that of the enzyme-bound form. The interactive effects result from protein-ligand interactions or ligand-ligand interactions. The main problem in interpretation of the CD of enzyme-bound chromophores is distinguishing between the inherent and the interactive effects.

7.1. Heme Proteins.
Interpretation of the optical activity of protein-bound molecules has not been undertaken extensively. Hsu and Woody [157] analyzed theoretically the sources of optical activity in the bound heme of hemoglobin. When unbound, the heme is optically inactive due to the symmetry properties of the porphyrin. The induced optical activity when bound to the protein is due solely to interactions with the protein environment. The one-electron contribution was not considered in their treatment because the optical activity resulting from perturbations of a highly symmetric chromophore is weaker for a given charge distribution [33]. Also, because the heme is surrounded by many charged side-chains, the net one-electron effects were assumed to be negligible due to mutual cancellations. The inherently dissymetric chromophore was also assumed to be inapplicable even though the iron was known to be out of the plane of the porphyrin ring in myoglobin [158]. Studies by Ruckpaul et al. [159] had shown that complexes between iron-free porphyrins and globin possess CD spectra qualitatively similar to those of native hemoglobin. Thus effects due to the non-planar iron were considered negligible. Therefore, it follows that their studies focussed on the coupled-oscillator mechanism.

Coupled-oscillator calculations indicate that coupling between the heme and aromatic side-chains can account for the observed Soret rotational strengths [157]. Interaction of the heme with π-π^* or n-π^* transitions of amide groups or with σ-σ^* transitions of alkyl groups gave rotational strengths which were negligible by comparison. These results differed from those of Volkenstein et al. [160], who showed that the one-electron mechanism can give comparable rotational strengths when a single point charge perturbs the porphyrin, but their calculations relied on the effect of the d-d transition of the metal ion. Hsu and Woody [157] pointed out that comparable Soret rotational strengths are observed in globin complexes of metal-free porphyrins and thus dismissed the one-electron mechanism as a source of significant rotational strength. Therefore, the coupled-oscillator mechanism appears to be the main source of Soret Cotton effects in myoglobin, hemoglobin, and other heme proteins. Note that

calculations of this type require detailed X-ray data on the three-dimensional protein structure because the exact position and orientation of the chromophore and protein groups must be known.

More recently La Mar and coworkers [161] have shown that native and newly reconstituted myoglobin differ in the orientation of the heme. This results in a 50:50 mixture of two heme orientations which differ by a 180° rotation about the α–γ axis. At neutral pH heme reorientation is very slow with a half-life of greater than 8 hours. Although the absorption properties of the two forms are indistinguishable, the reconstituted form exhibits approximately half the Soret rotational strength [162-164]. Since the reconstituted form is a 50:50 mixture of the two heme orientations then the Soret rotational strength of the rotated heme is nearly zero. Rotating the heme 180° about the α–γ axis causes reorientation of the Soret band transition moments which couple with the surrounding protein aromatic side-chains to yield nearly zero rotational strength. Also, alterations in the position of the heme in the heme pocket must be made to accommodate the exchanges in the position of the methyl groups at heme positions 1 and 3 and the vinyl groups at heme positions 2 and 4.

7.2. Glycoproteins. Glycosylation of a protein is a post-translational modification which can significantly alter the metabolism and biological activity of a protein. However, little is known regarding the effect of glycosylation on the secondary structure of proteins and peptides. Work on model peptides indicates that glycosylation disrupts α–helical structure, presumably due to steric hindrance [165]. However, in globular proteins, the effects of glycosylation seem to be less pronounced. Comparisons between native and recombinant versions of the same protein using CD suggest that they usually exhibit similar structures, as has been seen for interferons [166-169], insulin-like growth factor I [170], and colony stimulating factors [171]. The structural consequences of nonenzymatic glycosylation has also been investigated for α–crystallin, and found to change some tertiary structural features [172, 173].

7.3. Enzyme/Co-Factor Complexes. While studying extrinsic CEs in complexes of creatine phosphokinase (CPK) with adenine coenzymes, Kägi et al. [174] proposed that the observed induced CEs in these complexes can be accounted for by the coupled-oscillator mechanism. Because the interaction of adenine coenzymes with CPK is accompanied by quenching of protein tryptophan fluorescence, Kägi et al. [174] calculated the rotational strength to be expected from optimal interaction of the 260 nm transition of the adenine group with the transitions of a tryptophan side-chain. Ultraviolet difference spectroscopy studies further supported a possible tryptophan role in coenzyme binding. However, these calculations can be taken only as an indication of the potential that the coupled-oscillator model can account for the observed rotational strengths since no detailed X-ray diffraction data was available.

The induced CD of flavodoxin from *Desulfovibrio vulgaris*, was studied theoretically by Woody [175], while CD spectra and X-ray diffraction patterns of the *Desulfovibrio* flavodoxin have been reported by D'Anna and Tollin [176] and Watenpaugh et al. [177], respectively. The flavin is positioned between a tyrosine and a tryptophan side chain and, thus, calculations of the coupled-oscillator interactions between the flavin and the two adjacent aromatic side-chains were performed. The results showed poor agreement with the observed rotational strengths at the 450, 375 and 305 nm absorption bands of the flavodoxin. Woody noted that several other possibilities existed as sources of optical activity. These were inclusion of the effects of n-π^* transitions of the flavin, effects due to possible charge transfer interactions between the flavin and the aromatic residues, and coupling with more distant aromatics and the peptide groups. Innis et al. ([178] used the induced CD at 450 nm to study riboflavin binding by human plasma.

Wicken and Woody [179] observed changes in the CD bands of alcohol dehydrogenase (ADH)-bound auramine O when NAD^+ or NADH were added to form ternary complexes. These CD changes were not observed when AMP, ADP, or ADPR were added to ADH-

auramine O solutions. X-ray diffraction studies [180] indicate that a conformational change occurs in ADH upon binding NAD^+ or NADH but not upon binding the coenzyme fragments. Fluorescence studies by Heitz and Brand [181] also indicated that the nicotinamide portion of the coenzyme is necessary to alter the fluorescence of the enzyme-bound dye when forming the ternary complexes mentioned above. These studies suggest that indeed an ADH conformational change is being monitored through the changes in the induced CD bands of the ADH-bound dye.

Towell and Woody [182] reported that the positive CD band at 345 nm in the binary complex between bovine heart lactate dehydrogenase (H_4-LDH) and NADH is shifted to 322 nm and intensified upon binding the substrate analog, oxamate, to form an abortive ternary complex H_4 LDH-NADH-oxamate. Similar results for porcine H_4-LDH were reported by Gurevich et al. [183]. X-ray diffraction studies have revealed that H_4-LDH undergoes conformational changes after the binding of both coenzyme and substrate. The larger change occurs upon substrate binding, with one residue undergoing a 23 Å displacement [184]. Thus, it was suggested that the large changes in the spectral properties of H_4-LDH-bound NADH upon forming a ternary complex with substrate (or substrate analog) reflect these enzyme conformational changes [185].

In a theoretical analysis of the spectral properties of complexes of dihydrofolate reductase (DHFR) with methotrexate and NADPH, Woody [186] assessed the effects of the electrostatic environment surrounding the enzyme-bound drug and coenzyme. From these considerations, "crystal field shifts" in transition energies, which are due to the difference in charge distribution between ground and excited states, were calculated. Mixing of excited states due to the static field (one-electron effect) were also predicted. These static field considerations account for the large red shift observed in the π-π^* transition following binding of methotrexate to DHFR and the red shift accompanying the binding of dihydronicotinamide to the ternary complex. The calculated CD spectra indicated that, in the DHFR-methotrexate complex, the dominant contribution to the observed CD arises from coupled oscillator interactions between the pteridinium chromophore and the p-amino-benzamide group. In the ternary complex, coupling between the pteridinium chromophore and the dihydronicotinamide chromophore accounted for the observed CD bands.

7.4. Protein-DNA Complexes. Circular dichroism has been used to characterize protein secondary structure in many kinds of nucleic acid-binding proteins, their mutants, and derivatives. Similarly, CD has been employed to characterize the structural changes which occur in the nucleic acids as well, but these are beyond the scope of the present work. Our discussion here will center on a few examples of the use of CD for characterizing structural changes which occur in DNA-binding proteins.

The effects of site-directed mutagenesis on secondary structure of bacteriophage T4 gene 32 protein, which binds preferentially and cooperatively to single-stranded nucleic acids, was characterized with the use of CD [187, 188]. In studies of SP1, a transcription factor from HeLa cells which contains zinc-finger DNA-binding domains, Kuwahara and Coleman [189] cloned the SP1 DNA-binding subdomain and used CD to characterize the protein conformation in the presence and absence of Zn (II) and Cd (II), but did not include studies of protein conformation in the presence of nucleic acids. These results are typical, as zinc fingers cannot adopt any regular structure (and thereby recognize and bind DNA) without the presence of a metal ion. In a similar study, ZFY, a putative transcription factor encoded by the human Y chromosome, contains a distinctive zinc-finger repeating motif with odd-numbered and even-numbered metal-binding motifs exhibiting systematic alternations in sequence pattern. Weiss et al. [190] studied synthesized peptides that were portions of ZFY and used CD to show systematic differences in metal-dependent folding of the even- and odd-numbered domains.

Often, DNA-binding proteins must associate to become active. For example, CD was used to study the concentration-dependent unfolding of bacteriophage P22 Arc repressor, which is associated with a monomer-dimer equilibrium [191]. One major class of DNA-

binding proteins which must associate to be able to become active is the dimeric coiled-coil structure known as the "leucine zipper". It contains sequences in which leucine residues are repeated in such a manner that upon dimerization, they form a hydrophobic face to the coiled-coil α-helical structure. Usually, a portion rich in basic amino acids immediately preceding the leucine zipper is also necessary for activity. This basic region is approximately 25 residues in length and is essential for interaction with DNA base pairs. Using CD, it was found that the leucine zipper forms a two-stranded coiled-coil of parallel α-helices [192, 193]. These structures have since been corroborated by NMR and X-ray diffraction studies [194-196].

GCN4, a yeast transcriptional activator, contains a leucine zipper motif which has been extensively characterized by CD. The DNA-binding portions of GCN4 have been shown to exhibit a concentration-dependent α-helical transition similar to the dimerization properties of isolated leuzine-zipper peptides [190, 197]. In the presence of DNA, the α-helix content of GCN4 fragments increases dramatically, as indicated by large negative increases in $[\theta]_{222}$. The same is true for intact native GCN4 [198], as well as the nuclear oncoproteins Jun and Fos [199], and a fusion protein Lex A-JunZip, where Lex A represents residues 1-87 of an $E.$ $coli$ repressor and JunZip represents residues 280-312 of Jun which contain AP-1 binding sites [200]. Other studies indicate that the α-helical conformation of the basic region is sufficient for sequence specific binding [197, 201]. More recent studies of the transcription factor, MyoD and MyoDrec (a bacterially expressed peptide containing residues 102 to 166 of MyoD), displayed properties similar to those of leucine zipper proteins. Again, large increases in the α-helix content upon binding DNA were demonstrated with the use of CD [202].

Not all DNA-binding proteins show increases in α-helix content following the introduction of nucleic acids. CD studies of fd and Ike gene 5 proteins, which bind strongly and cooperatively to single-stranded nucleic acids, revealed 80% β-structure with no α-helix. There were no significant changes in the CD bands of either protein upon binding to poly (rA) [203].

7.5. Membrane-Bound Proteins. Many proteins exist in intimate contact with phospholipids in cell membranes. In this environment, the protein may display modified physicochemical properties, including an altered CD spectrum. Removal of the protein from the membrane may disrupt the native structure. On the other hand, obtaining CD spectra of membrane fragments may lead to artifacts arising from scattering and birefringence. In addition, optical flattening may produce inaccurate CD intensities.

The chromophore, 11-cis retinal, a vertebrate and invertebrate rod pigment, is now thought to be covalently bound to opsin through the formation of a Schiff-base linkage between the carbonyl of the retinal and the ε-amino group of a lysine in the protein [204]. When free in solution 11-cis retinal is not optically active due to the presence of at least six different optical isomeric forms [205, 206]. When bonded to opsin, a chromophore is formed, retinylidene, which is optically active [207]. The inherently dissymmetric chromophore mechanism has been used in molecular orbital calculations on model systems [208] in an attempt to predict the conformation of the retinylidene chromophore. However, the tacit assumption in such molecular orbital studies is that the inherent dissymmetry of the chromophore will dominate the CD spectrum. Burke et al. [208] were well aware of this and noted that Waggoner and Stryer [209] had pointed out that coupling between the prosthetic group and protein side-chains could induce rotational strengths of the observed order of magnitude. Johnston and Zand [210] have also made a similar proposal. However, because there are no accurate structural data available, calculations of the type employed by Hsu and Woody [157] are not possible.

Bacteriorhodopsin (bR) and rhodopsin both contain a single molecule of retinal covalently bound to the protein. In studies of bR from the purple membrane (PM) of *Halobacterium halobium*, Heyn et al. [211] have shown strong evidence for exciton coupling between chromophores of neighboring bR molecules. The CE of the longest-wavelength visible transition in the bR is split (exciton splitting) into a couplet which disappears when the membrane is solubilized with detergent or when the bR chromophores are mobilized within the

membrane matrix by organic solvents, such as dimethylsulfoxide, ethyl ether, and volatile anesthetics. The protein molecules must be closely packed with restricted mobility for the exciton coupling to occur. Thus, the aggregation state of bR can be quickly assessed by the CD signal. In disk membranes, rhodopsin molecules are highly mobile [212] and, thus, no exciton splitting is observed. Other results indicate that the long-wavelength couplet is due to the superposition of the CD spectra having opposite signs of more than one type of BR rather than due to exciton coupling [213, 214].

The membranes of *Halobacterium halobium* also have a retinal-linked chloride pump. Halorhodopsin (hR), which has a CD spectrum similar to that of BR in the 300-700 nm region, loses its long wavelength couplet in the presence of detergents. With the use of a Gaussian curve-fitting analysis, a trimer was predicted for bR with an interchromophore distance of approximately 31 Å, which is closer to the distances predicted by electron and neutron diffraction studies than previous theoretical studies [215]. The hR data could be fit to either a dimer or trimer model, although the CD spectrum of the dimer was predicted to be more sensitive to conformational changes. Perhaps, the hR structure is more sensitive to changes in ionic strength and pH. Inter-chromophoric distances in the dimer model were close to those of bR.

The CD properties of SR-I, the retinal-linked phototaxis receptor of *Halobacterium halobium*, have been investigated [215]. In contrast to bR and hR, no evidence of exciton coupling was found, which suggests that the chromophores are present in native membranes as monomers or that the interactions between chromophores are weak due to inter-chromophore distances and orientations.

To determine the secondary structure of proteins within aggregates, such as membranes, one must compensate for differential absorption flattening and differential light scattering. As a result of earlier theoretical treatments, it was believed that light scattering artifacts were minimal and compensation for them required small adjustments in the observed circular dichroism spectrum. However, further studies of systems such as bR in PM, where the secondary structure had been determined by diffraction methods [216], indicated gross underestimations of the α-helix content based on CD spectra of PM sheets and vesicles. The size of the particle and the distribution of the chromophores within the particle will determine the magnitude of the differential scattering as well as its angular dependence as determined by varying the acceptance angle of the detector [217, 218].

The model that has received the most attention for the overall structure of bR in the purple membrane of *Halobacterium halobium* is based upon electron diffraction studies [216]. These data suggested that there were seven transmembrane α helices, meaning bR contained an alpha-helix content of approximately 80%. With the use of fluorescence-detected circular dichroism (FDCD), the extent of differential light scattering can be assessed [219, 220], although it was found to play an insignificant role in the CD of purple membrane [221]. In PM particles and dimyristoylphosphatidyl choline vesicles, bR appeared to possess α-helix compositions substantially less than 80% [222]. However, when the bR molecules were dispersed into small unilamellar vesicles, the CD spectra were comparable to that expected of a protein which has 80% of its residues in α-helical conformations. This reduction in absorption flattening is attributed to an equal distribution of the bR molecules within the lipid lattice, as opposed to the close packing in discrete areas which is formed in the native state [222]. These results were contended by Glaeser and Jap [223] who argued that the renormalization procedure used by Mao and Wallace was an inappropriate option to more accurate measurements of the concentration of the membrane proteins. Further work, where more accurate protein concentration determinations were made, resulted in results similar to those obtained by Mao and Wallace and stressed the importance of non-random distribution of chromophores on absorption flattening effects [224]. Hence, it is still not known whether the secondary structure of bR changes upon transfer to detergent micelles and vesicles. Nevertheless, studies with proteolytic fragments and mutants of bR indicate that the tertiary structure is remarkably stable and its refolding capacity is exceptional [225, 226].

Muccio and Cassim [227] studied films of bR in PM and found that, in thin films, the long wavelength couplet was missing, leaving only a positive band due to interactions between the bR chromophore and the protein environment. The disappearance of this feature is strong evidence for the veracity of exciton theory in describing the CD of α helices. For oriented samples, where the CD is being measured normal to the plane, the loss of the exciton band arises from a dependence of the intensity on r_i - r_j, where this difference is measured along the axis of propagation [1]. For the bR trimer in the membrane this value is essentially zero.

An extension of the qualitative analysis of Muccio and Cassim was used to predict the orientation of the transmembrane α helices of cytochrome oxidase in oriented films [228]. This orientation was defined by ϕ_α, the average angle between the helix axis and the normal to the film. The decrease in rotational strength of α helices oriented parallel to the excitation beam axis is due to the polarization of the π-π^* transition component at 208 nm along the helix axis. Therefore, it is not interactive with the electric component of the excitation beam which is perpendicular to the helix axis [39, 229-232; see ref. 13 for detailed discussion of oriented systems). Likewise, in studies of film-oriented β sheets of poly(Leu-Lys), Bazzi et al. [233] showed that in the π-π^* region of the CD spectrum, the exciton couplet is significantly decreased relative to the solution spectrum. Again, as with bR, this is due to the value of r_i -r_j being essentially zero for CD spectra taken normal to the plane.

8. ANALYSIS OF PROTEIN STRUCTURE BY CD USING EXTRINSIC CHROMOPHORES

The mechanisms for inducing optical activity in a protein-bound molecule are the coupled-oscillator and one-electron mechanisms described in the introduction, except that interactions with the protein environment must now be included in the analysis. Inherently dissymmetric chromophores possess a mechanism by which they may gain rotational strength [1]. It is important to note that the protein may preferentially bind one particular conformational or configurational state of a molecule and serve as a mold in which the molecule would be held. A molecule bound in the interior of a protein can be asymmetrically perturbed by the electrostatic field of nearby amino acid side chains and peptide groups, or its transitions can couple with those of nearby aromatic side chains, the peptide backbone itself, or possibly, with the transitions of another neighboring ligand. CD bands which arise from isolated chiral molecules are referred to as intrinsic CEs. Extrinsic CEs are due to interactions of transitions in bound ligands with the surrounding protein. These ligands may be of any type, i.e., coenzymes, prosthetic groups, hemes, substrates, inhibitors, dyes, etc. Extrinsic CEs which lead to CD bands in the visible region ($\lambda > 300$ nm) are the subject of the following discussion.

8.1.Drugs and other Extrinsic Chromophores. Serum albumin is a ubiquitous blood protein which is known to specifically bind a number of substances. Blauer and Wagnière [234] have predicted the conformations of bilirubin and biliverdin bound to human serum albumin (HSA) using molecular orbital calculations. They assumed the optical activity of the bound pigments was dominated by the inherent chirality of the chromophore. Their studies also described a change in chirality of the chromophores, causing an inversion in the sign of their Cotton effects when the pH increases from 4 to 10, suggesting that the protein undergoes large conformational changes with changes in pH. Leonard and Foster [235], using optical rotation measurements, first discovered a conformational change in HSA in the pH range of 7-9. At approximately pH 7.4, HSA undergoes a conformational change now referred to as the N-B transition. Lightner et al. [236] used exciton theory to predict the predominance of the so-called B enantiomer of bilirubin bound to BSA at pH 7.3, while Knudsen et al. [237] characterized bilirubin-HSA complexes using CD spectroscopy. Honore and Frandsen [238] monitored the induced CD of bilirubin to probe conformational changes which occur in the bilirubin-HSA complex at pH ranges of 11-12.

The CD of bilirubin-complexes with serum albumin from a variety of species are very different under identical conditions. In several complexes, the observed CD spectrum is far more complicated than what is observed in the case of HSA. Other rotational strength mechanisms, such as coupling with protein groups, were suggested as additional sources of optical activity [239].

Several investigators have demonstrated that there are at least three relatively specific high-affinity binding sites present on the albumin molecule. These sites are commonly called the warfarin-, the diazepam-, and the digitoxin-binding sites, and are also denoted as Site I, Site II, and Site III, respectively. Albumin is composed of three contiguous domains, each domain containing three loops., which can act more or less independently of each other. Site I is apparently in the second domain. Site II is probably in the third domain, and the location of Site III is unknown. Bos et al. [240] studied the induced CD of diazepam complexes with HSA and two fragments of albumin, P46 and T45 which were produced by peptic and tryptic digests, respectively. The P46 fragment consisted of domains one and two whereas T45 consisted of domains two and three. The binding properties of T45 exhibited a 4-7 fold decrease in affinity relative to albumin, while those of the P46 fragment were nearly two orders of magnitude lower. Because the induced CD of diazepam complexes with albumin and T45 were similar it was concluded that the T45 fragment contained the primary benzodiazepine-binding site, and further suggested that the primary benzodiazepine-binding site is located in domain three of the albumin structure. The induced CD of the P46-diazepam complex was qualitatively different from the diazepam complexes with albumin and T45.

The N-B transition can affect a number of drug-HSA interactions. This was observed in the induced CD of warfarin-HSA complexes [241] and in HSA-bound sulfa drugs [242]. In these studies, both pH- and small ion-induced conformational changes (i.e., the N-B transition) were detected by CD and used to obtain binding information. Vansterkenberg et al. [243] investigated the induced CD of suramin-HSA complexes to study the N-B transition. Suramin has been used since 1920 for treatment for trypanosomiasis and is also a potent inhibitor of reverse transcriptase from a number of animal retroviruses. Matsayama et al. monitored changes in the induced CD of HSA-tolmetin complexes due to pH induced changes in the geometry of the binding site following the N-B transition [244]. Finally, it has been observed that the conformation of albumin influences warfarin binding, and that its effect is entirely opposite to its influence on suramin binding. Warfarin preferentially binds to the B-conformation of albumin, and not to the N state.

In general, detection of extrinsic or induced CD signals are convenient probes to follow not only the binding of various substances to HSA, but also the conformational state of HSA itself under a variety of conditions. For example, Honore et al. examined the conformational changes induced in HSA upon binding laurate by following the induced CD [245]. Similarly, the chaotropic salt, NaSCN, disrupts HSA structure and the process can be monitored by observing the induced CD [246]. Induced CD has been employed as a qualitative conformational probe to study the HSA binding sites of two anthranilic acid derivatives, glafenic acid and floctafenic acid, both of which have analgesic pharmacological properties [247]. Mohanakrishnan and Chignell [248] used difference CD to study interactions in ternary complexes of D-penicillamine, HSA, and various metals, such as copper and zinc.

Maliwal et al. used the induced CD of gossypol-bovine serum albumin (BSA) complexes to study the binding properties [249]. Although the gossypol absorption spectrum was not shown, the induced CD of the gossypol-BSA complex showed a negative couplet in the visible region. Since gossypol is a polyhydroxy binapthalene, it is reasonable to predict that the couplet represents an exciton interaction between the two naphthalene chromophores. Thus, based on exciton theory and with the assumption that the inherent dissymmetry of the BSA-bound gossypol dominates the long wavelength CD couplet, it can be predicted that the conformation of the BSA-bound gossypol exists such that the transition dipoles of the two naphthalene chromophores constitute a counter-clockwise twist.

Trifluoperazine (TFP) is an antipsychotic phenothiazine drug which is bound strongly to brain calmodulin and is a potent calmodulin antagonist. TFP is believed to be bound to

calmodulin in the same way as calmodulin-dependent enzymes and thus is believed to be a good model for studying calmodulin structure-function relationships. The induced CD of trifluoperazine complexes with calmodulin and other S100 proteins have been used to monitor changes in the microenvironment caused by changes in pH and the binding of various mono- and di-valent ions [250, 251].

Other circulating proteins bind drugs as well, the other major drug binding component being α_1-acid glycoprotein. While serum albumin tends to bind cationic drugs, α_1-acid glycoprotein binds anionic substances. Otagiri et al. have described a study which combines the use of fluorescence with induced CD to demonstrate large differences in the warfarin binding site on human α_1-acid glycoprotein and on HSA [252].

8.2. Polypeptide-Dye Interactions. The use of induced CEs in the visible transitions of dyes interacting with polypeptides to discern peptide conformational states was first noted by Stryer and Blout who demonstrated that acridine orange and other cationic dyes were optically active when in solution with the α-helical form of poly-L-glutamic acid (PLGA), but were not when the PLGA was in its random form [253]. They suggested that the observed couplet could be the result of exciton interactions between peptide-bound dyes and thus could potentially provide the means to estimate the geometry of these peptide-dye complexes. These ideas were quantified by Tinoco et al., who incorporated Davydov exciton theory into considerations of helical peptide structures and acridine orange bound to PLGA, polyadenylic acid and DNA [254]. Harada et al. incorporated these techniques into extensive studies of a series of steroidal glycol bis(p-dimethylaminobenzoates), and established the exciton chirality method as a means to determine absolute configuration in systems with interacting identical chromophores [255]. The equation derived by Harada et al . is shown below as equation (1)

$$\Delta\varepsilon\,(\sigma) = \frac{2\sqrt{\pi}\ \sigma_0^2}{2.296\ \times\ 10^{-39}\ \Delta\sigma^2}\ \left(\frac{\sigma_0 - \sigma}{\Delta\sigma}\right)\exp\left\{-\left(\frac{\sigma_0 - \sigma}{\Delta\sigma}\right)^2\right\}$$

$$X\ R_{ij}\cdot(\mu_{ioa}\ X\ \mu_{joa})\ V_{ij}$$

(1)

where R_{ij} is the interchromophoric distance vector from i to j, V_{ij} is the transition dipole interaction energy between i and j, and μ_{ioa} and μ_{joa} represent the electric transition dipole moments for the groups i and j, respectively. σ_0 and $\Delta\sigma$ are obtainable from the electronic spectrum of the corresponding chromophore. This equation has been incorporated extensively to predict helical sense in subsequent CD studies of dye-polypeptide interactions such as in poly(Arg) [256, 257] and in poly(Lys) interactions with azo dyes [258].

However, most studies which examine the induced CD of polypeptide-bound dyes use it as a qualitative conformational probe, although when a characteristic CD couplet is observed, it is generally recognized as being due to exciton interactions. Yamamoto studied the effects of side chain length on the induced CD of poly(Lys) homologues interacting with azo dyes [259]. The induced CD of acridine orange and methyl orange complexes with poly(Arg) and poly(Lys) was used to study changes in the structure of a twisted smectic mesophase formed between Tween 80 and water in the presence of an electric field [260].

Sato and Woody found a preference for binding left-handed conformers of ANS to the beta form of poly(Lys) and suggested that the dyes are bound to the polypeptide in regions of low polarity due to the increase in fluorescence quantum yield and the blue shift in the emission spectrum [261].

8.3. Enzyme-Dye Interactions. Edwards and Woody studied the extrinsic Cotton effects of dyes binding to the dinucleotide fold of dehydrogenase enzymes [262]. Cibacron Blue, the chromophore of blue dextran, has been used to purify several enzymes due to a purported affinity for the dinucleotide fold. The CD spectra resulting from the binding of Cibacron Blue to five dehydrogenases show no particular pattern although a similar pattern was found between bovine H_4 and M_4 lactate deydrogenase. This lack of similarity was attributed to localization of the visible electronic transitions on the anthraquinone portion of the molecules. However, in their studies of induced CD in Congo Red-dehydrogenase complexes, a similarity in patterns was found. The visible transitions of Congo Red are delocalized over the entire molecule and the induced CD is approximately an order of magnitude larger than those of the Cibacron Blue complexes (Figure 5). In a subsequent theoretical study Edwards and Woody showed that coupled oscillator interactions between an indole chromophore and Congo Red could produce rotational strengths only 33% of those exhibited by the Congo Red-dehydrogenase complexes [263]. On the basis of the similarities found between the dehydrogenases, the large rotational strengths and the delocalized visible transitions, Congo Red was recommended over Cibacron Blue as a CD probe of the dinucleotide fold.
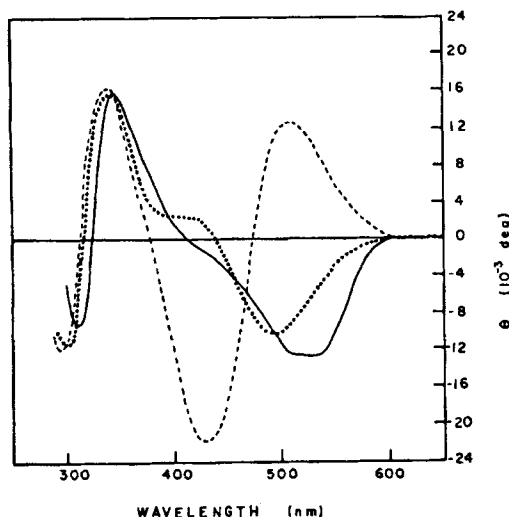
Figure 5. CD spectrum of the bovine lactate dehydrogenase-Congo Red complex (full line). Dashed lines indicate calculated spectra for Congo Red at different conformations [263].

Smith and Woody [264] performed molecular orbital calculations on the N-phenylnapthylamine dyes which have attracted much attention as fluorescence probes [265]. Very large increases in fluorescence intensity and shifts in emission maxima occur when ANS (1,8-anilinonapthalene sulfonate) or TNS (2,6-toluidinonaphthalene-sulfonate) bind to a large number of proteins [266-272]. One purpose of their theoretical study was to determine if the ANS and TNS dyes possessed large enough rotational strengths, due to inherent dissymmetry, to be used as CD probes of protein active-sites. Their results indicated that these dyes do not possess large enough rotational strengths in the wavelength regions outside of the protein absorption bands, to be used effectively as CD probes. These low rotational strengths would not allow the effects due to interaction with the protein environment to be neglected, thus preventing quantitative description of the conformation of the bound dye. These considerations

were incorporated by Era et al. in their interpretations of the induced CD of ANS complexes with bovine plasma albumin during acid-induced isomerizations [273].

Auramine O is a cationic diphenylmethane dye that binds to two independent sites on horse liver alcohol dehydrogenase (ADH) with a dissociation constant of about 10^{-5} M [274]. Kinetic studies [275] and studies of ternary complexes of ADH: auramine O with NAD^+, NADH, 5'-AMP, ADP, and ADPR [181] suggest that the dye overlaps the ADH substrate-site. Because of steric hindrance between the hydrogens substituted ortho to the central carbon atom, auramine is forced into a twisted, propeller-like conformation which is inherently dissymmetric. Wicken and Woody proposed that ADH may preferentially bind a particular conformation of auramine O and that the inherent dissymmetry of the bound dye may dominate the sign of the longest-wavelength transition [179]. The longest-wavelength transition is furthest in energy from the transitions of the protein side-chains and thus the rotational strength of the dye is less likely to be overwhelmed by coupling effects. Molecular orbital calculations were performed and their results indicated that auramine O is probably bound in a left-handed sense of twist with twist angles of approximately 30 degrees.

In studies of the extrinsic Cotton effects induced in complexes of the propellor-like sulfonephthalein dye bromphenol blue with bovine heart lactate dehydrogenase, Towell and Woody suggested the tightest binding site, located at the adenosine portion of the coenzyme binding site, preferred dye molecules with a right-handed conformation [182]. This was based on the assumption that the inherent chirality of the enzyme-bound dye would produce the dominant Cotton effect for the lowest energy visible transition. Application of the C2 rule of Geiger and Wagnière and molecular orbital calculations predicted a positive low energy CD band associated with a molecule with a right-handed conformation. Further studies with a stereochemically-fixed analog of bromphenol blue supported this assignment [185].

8.4. Chemically Modified Proteins. Eosin 5-isothiocyanate (EITC), an inhibitor of the anion transport system in the human erythrocyte, also exhibits an induced CD spectrum when incubated with erythrocyte ghosts. It has been found to bind to band 3 protein which is a major integral membrane protein of the erythrocyte. Band 3 protein, MW ≈ 95 KDa, exists as a dimer and/or tetramer under physiological conditions and controls chloride-bicarbonate exchange. Sulfate, phosphate, and organic anions of low molecular weight plus halide are also transported by band 3 protein. Because of the pH dependence of the anion transport properties it was postulated that a positively charged group in the anion binding site is either arginine or histidine [276]. Preincubation of band 3 protein with histidine- or arginine-specific reagents resulted in repressions of the induced CD of EITC with the histidine-specific reagents causing a greater reduction of the EITC Cotton effects. These results suggested that the histidine residues participate in the anion-transport system of human erythrocytes [277]. Chiba et al. [278] utilized eosin-5-maleimide (EMI), also an anion exchange inhibitor in human erythrocyte, to assess the role of specific amino acids in the relationship between band 3 protein and anion transport function. They found that the induced CD found after EMI was incubated with erythrocyte ghosts was decreased following preincubation with N-ethylmaleimide, a cysteine modifier. CD couplets were proposed due to exciton interactions between stacked chromophores although the authors acknowledged the difficulty in interpreting such a complex system.

9. SUMMARY

Proteins and polypeptides comprise an essential class of biopolymers Their structures are diverse and complex, and provide the basis for their activity, stability, and functon. CD spectroscopy is an effective tool for characterizing these structures, whether in solution or in films or micelles. The sample requirements are minimal and CD can be used to assess structural changes in any type of protein. Therefore, CD is becoming an important method in the determinination of the stability of proteins.

10. REFERENCES

1. I. Tinoco, Jr., Adv. Chem. Phys. 4 (1962) 113.
2. D.W. Sears and S. Beychok, in Physical Principles and Techniques of Protein Chemistry, Part C (Leach, S.J., Ed.), 445 (1973).
3. P.M. Bayley, Prog. Biophys. Mol. Biol. 27 (1973) 3.
4. P.M. Bayley, Prog. Biophys. Mol. Biol. 37 (1981) 149.
5. H. Rosenkranz, Z. Klin. Chem. Klin. Biochem. 12 (1974) 415.
6. W.H. Bannister and J.V. Bannister, Int. J. Biochem. 5 (1974) 673.
7. E.H. Strickland, CRC Crit. Rev. Biochem. 2 (1974) 113.
8. P.C. Kahn, Methods Enzymol. 61 (1978) 339-378.
9. T.A. Bewley, Recent Prog. Hormone Res. 35 (1979) 155.
10. W.C. Johnson, Jr., Photochem. Photobiol. 44 (1986) 307.
11. W.C. Johnson, Jr., Ann. Rev. Biophys. Biophys. Chem. 17 (1988) 145.
12. W.C. Johnson, Jr., Proteins: Structure, Function, Genetics 7 (1990) 205.
13. R.W. Woody, J. Polymer Sci.: Macromol. Rev. 12 (1977) 181.
14. R.W. Woody, in The Peptides: Analysis, Synthesis, Biology. Hruby, V.J., Ed., Orlando, Florida: Academic Press 7 (1985) 16.
15. M. Hatano, Stud. Phys. 36 (1985) 181-204.
16. M.P. Heyn, Methods Enzymol. 172 (1989) 575.
17. M.C. Manning, J. Pharm. Biomed. Anal. 7 (1989) 1103.
18. J.T. Yang, C.-S.C. Wu, and H. Martinez, Meth. Enzymol. 130 (1986) 208.
19. G. Chi Chen and J.P. Kane, Meth. Enzymol. 128 (1986) 519.
20. C.-S.C. Wu and G.C. Chen, Anal. Biochem. 177 (1989) 178.
21. E.S. Stevens, Meth. Enzymol. 49 (1977) 214.
22. W.C. Johnson, Jr., Ann. Rev. Phys. Chem. 29 (1978) 93.
23. A. Cotton, Compte. Rend. 120 (1895) 989 and 1044.
24. D.J. Caldwell and H. Eyring, The Theory of Optical Activity, John Wiley and Sons, New York, 1971.
25. E.U. Condon, W. Altar, and H. Eyring, J. Chem. Phys. 5 (1937) 753.
26. J.G. Kirkwood, J. Chem Phys. 5 (1937) 479.
27. A. Moscowitz, Tetrahedron 13 (1961) 48.
28. W. Kuhn, Trans. Faraday Soc. 46 (1930) 293.
29. W. Kuhn, Ann. Rev. Phys. Chem. 9 (1958) 417.
30. J.A. Schellman, Acc. Chem. Res. 1 (1968) 144.
31. R.S. Mulliken, J. Chem. Phys. 30 (1959) 648.
32. W. Moffitt, R.B. Woodward, A. Moscowitz, W. Klyne, and C. Djerassi, J. Am. Chem. Soc. 83 (1961) 4013.
33. J.A. Schellman, J. Chem. Phys. 44 (1966) 55.
34. J.S. Richardson, Adv. Protein Chem. 34 (1981) 167.
35. G.N. Ramachandran and V. Sasisekharan, Adv. Protein Chem. 23 (1968) 283.
36. T.L. Blundell, D. Barlow, N. Borkakorti, and J.M. Thornton, Nature 306 (1983) 281.
37. M.C. Manning, M. Illangasekare, and R.W. Woody, Biophys. Chem. 31 (1988) 77.
38. M.C. Manning and R.W. Woody, Bipolymers 31 (1991) 569.
39. R.W. Woody and I. Tinoco Jr., J. Chem. Phys. 46 (1967) 4927.
40. V. Madison and J.A. Schellman, Biopolymers 11 (1972) 1041.

41. M. Goodman, A.S. Verdini, C. Toniolo, W.D. Phillips, and F.A. Bovey, Proc. Natl. Acad. Sci. USA 64 (1969) 444.
42. J.M. Becker and F. Naider, Biopolymers 13 (1974) 1747.
43. J. Applequist, J. Chem. Phys. 71 (1979) 4332.
44. J. Applequist, Biopolymers 20 (1981) 287.
45. C. Chothia, J. Mol. Biol. 163 (1981) 107.
46. F.R. Salemme, J. Mol. Biol. 146 (1981) 143.
47. F.R. Salemme and D.W. Weatherford, J. Mol. Biol. 146 (1981) 101.
48. F.R. Salemme and D.W. Weatherford, J. Mol. Biol. 146 (1981) 119.
49. K. Rosenheck and B. Sommer, J. Chem. Phys. 46 (1967) 532-536.
50. L. Pauling, R.B. Corey, and H.R. Branson, Proc. Natl. Acad. Sci. USA 37 (1951) 729.
51. J.P. Hennesey, Jr. and W.C. Johnson, Jr., Biochemistry 20 (1981) 1085.
52. J.P. Hennesey, Jr. and W.C. Johnson, Jr., Anal. Biochem. 125 (1982) 177.
53. L.A. Compton and W.C. Johnson, Jr., Anal. Chem. 155 (1986) 155.
54. A. Perczel, K. Park, and G.D. Fasman, Proteins: Structure, Function, Genetics 13 (1992) 57.
55. B.L. Sibanda and J.M. Thornton, Nature 316 (1985) 170.
56. R.W. Woody, in Peptides, Polypeptides, and Proteins. E.R. Blout, F.A. Bovey, M. Goodman, and N. Lotan, Eds., New York: Wiley (1974) 338.
57. L.M. Gierasch, C.M. Deber, V. Madison, C.-H. Niu, and E.R. Blout, Biochemistry 20 (1981) 4730.
58. A. Perczel, G. Tusnády, M. Hollósi, and G.D. Fasman, Croat. Chem. Acta 62 (1989) 189.
59. A. Perczel, M. Hollósi, B.M. Foxman, and G.D. Fasman, J. Am. Chem. Soc. 112 (1991) 9772.
60. A. Perczel, G. Tusnády, M. Hollósi, and G.D. Fasman, Protein Eng. 4 (1991) 669.
61. A. Perczel and G.D. Fasman, Protein Sci. 1 (1992) 378-395.
62. R.W. Woody, in The Proceedings of F.E.C.S. Second International Conf. on Circular Dichroism. Kajtár, M., Ed., Hungarian Academy of Sciences, Budapest, Hungary (1987) 38.
63. W. Kauzmann, Quantum Chemistry, Academic Press, New York (1957).
64. J.A. Schellman and C.G. Schellman, in The Proteins, 2nd Ed., Vol. 2, (Neurath, H., Ed.), p. 1, Academic Press, N.Y., 1964.
65. M.L. Tiffany and S. Krimm, Biopolymers 6 (1968) 1379.
66. M.L. Tiffany and S. Krimm, Biopolymers 6 (1968) 1767.
67. V.A. Zubkov, T.M. Birshtein, and I.S. Milevskaya, Biopolymers 10 (1971) 2051.
68. E.W. Ronish and S. Krimm, Biopolymers 11 (1972) 1919.
69. E.W. Ronish and S. Krimm, Biopolymers 13 (1974) 1635.
70. N. Sreerama, M.C. Manning, and R.W.Woody, unpublished results.
71. H. Okabayashi, T. Isemura, and S. Sakakibara, Biopolymers 6 (1968) 323.
72. N. Helbecque and M.H. Loucheux-Lefebvre, Int. J. Peptide Protein Res. 19 (1982) 94.
73. L. Tterlikkis, F.M. Loxsom, and W. Rhodes, Biopolymers 12 (1973) 675-684.
74. B.R. Malcolm and M.D. Walkinshaw, Biopolymers 25 (1986) 607.
75. T.S. Sudha, E.K.S. Vijayakumar, and P. Balaram, Int. J. Peptide Protein Res. 22 (1983) 464.
76. L. Pauling and R.B. Corey, Proc. Natl. Acad. Sci. USA 37 (1951) 205.
77. J. Donohue, Proc. Natl. Acad. Sci. USA 39 (1953) 470.
78. G.Nemethy, D.C. Phillips, S.J. Leach, and H.A. Scheraga, Nature 214 (1967) 363.
79. T. Komoto, M. Kodaka, and T. Kawai, Makromol. Chem. 180 (1979) 818.
80. E.M. Bradbury, L. Brown, A.R. Downie, A. Elliot, R.D.B. Fraser, and W.E. Hanby, J. Mol. Biol. 5 (1962) 230.
81. B.W. Low and R.B. Baybutt, J. Am. Chem. Soc. 74 (1952) 5806.
82. B.W. Low and H.J. Grenville-Wells, Proc. Natl. Acad. Sci. USA 38 (1953) 785.

83. S. Krimm, Biopolymers 22 (1983) 217.
84. S. Krimm and A.M. Dwivedi, Science 216 (1982) 407.
85. J. R. Parrish and E.R. Blout, Biopolymers 10 (1971) 1491.
86. S. Brahms and J. Brahms, J. Mol. Biol. 138 (1980) 149.
87. N. Greenfield and G.D. Fasman, Biochemistry 8 (1969) 4108.
88. H. Rosenkranz and W. Scholtan, Hoppe-Seyler's Zeit. Physiol. Chem. 352 (1971) 896.
89. S.W. Provencher, Comp. Phys. Commun. 27 (1982) 229.
90. S.W. Provencher and J. Glöckner, Biochemistry 20 (1981) 33.
91. Y.I. Ramm, V.P. Gorenburg, A.B. Klionskii, and Y.Y. Smirnova, Biofizika 25 (1980) 559.
92. Y.I. Ramm, V.P. Gorenburg, A.B. Klionskii, and Y.Y. Smirnova, Biofizika 25 (1980) 561.
93. I.A. Bolotina, V.O. Chekhov, and V.Yu. Lugauskas, Int. J. Quantum Chem. 16 (1979) 819.
94. I.A. Bolotina, V.O. Chekhov, V.Yu. Lugauskas, A.V. Finkel'stein, O.B. Ptitsyn, Mol. Biol. 14 (1980) 891.
95. I.A. Bolotina, V.O. Chekhov, V.Yu. Lugauskas, and O.B. Ptitsyn, Mol. Biol. 14 (1980) 902.
96. I.A. Bolotina, V.O. Chekhov, V.Yu. Logauskas, and O.B. Ptitsyn, Mol. Biol. 15 (1981) 167.
97. I.A. Bolotina, V.O. Chekhov, and V.Yu. Lugauskas, Int. J. Peptide Protein Res. 20 (1982) 218.
98. I.A. Bolotina and V.Y. Lugauskas, Mol. Biol. 19 (1985) 1409.
99. Y.-H. Chen, J.T. Yang, and H.M. Martinez, Biochemistry 11 (1972) 4120.
100. Y.-H. Chen, J.T. Yang, and K.H. Chau, Biochemistry 13 (1974) 3350.
101. Y.-H. Chen and J.T. Yang, Anal. Lett. 10 (1977) 1195.
102. P. Manavalan and W.C. Johnson Jr., Anal. Biochem. 167 (1987) 76.
103. I.H.M. van Stokkum, H.J.W. Spoelder, M. Bloemendal, R. van Grondelle, and F.C.A. Groen, F.C.A. Anal. Biochem. 191 (1990) 110.
104. Y. Goto and A.L. Fink, Biochemistry 28 (1989) 945.
105. J. Baum, C.M. Dobson, P.A. Evans, and C. Hanley, Biochemistry 28 (1989) 7.
106. S. Craig, R.H. Pain, U. Schmeissner, R. Virden, and P.T. Wingfield, Int. J. Peptide Protein Res. 33 (1989) 256.
107. M.L. Elwell and J.A. Schellman, Biochim. Biophys. Acta 494 (1977) 367.
108. M.C. Manning and R.W. Woody, Biochemistry 28 (1989) 8607.
109. D. Goldenberg and M.C. Manning, unpublished results.
110. J.W.S. Morris, D.A. Mercola, and E.R. Arquilla, Biochim. Biophys. Acta 160 (1968) 145.
111. Y. Pocker and S.B. Biswas, Biochemistry 19 (1980) 5043.
112. J. Goldman and F.H. Carpenter, Biochemistry 13 (1974) 4566.
113. M.E. Powers, A. Adjei, and M.C. Manning, submitted for publication.
114. D. Boyd, J. Am. Chem. Soc. 94 (1972) 8800.
115. D.B. Boyd, J. Phys. Chem. 78 (1974) 1554.
116. R.W. Woody, Tetrahedron 29 (1973) 1273.
117. A. Rauk, J. Am. Chem. Soc. 106 (1984) 6517.
118. M.C. Manning, K. Patel, and R.T. Borchardt, Pharm. Res. 6 (1989) 903.
119. C. Tanford, Adv. Protein Chem. 23 (1968) 121.
120. M.C. Manning, ACS Symp. Ser. 516 (1992) 26-42.
121. M.H. Hecht, K.M. Hehir, H.C.M. Nelson, and J.M. Sturtevant, J. Cell. Biochem. 29 (1985) 217.
122. M.H. Hecht, J.M. Sturtevant, and R.T. Sauer, Proteins: Structure, Function, Genetics 1 (1986) 43.
123. J.A. Schellman, Ann. Rev. Biophys. Biophys. Chem. 16 (1987) 115.

124. W.J. Becktel and J.A. Schellman, Biopolymers 26 (1987) 1859.
125. C.N. Pace, Trends Biochem. Sci. 15 (1990) 14.
126. C.N. Pace, Methods Enzymol. 131 (1986) 266.
127. Y.V. Griko, P.L. Privalov, J.M. Sturtevant, and S.Y. Venyaminov, Proc. Natl. Acad. Sci. USA 85 (1988) 3343.
128. A.L. Fink, W.D. Anderson, J.E. Hattersley, and B.S. Lustig, FEBS Lett. 236 (1988) 190.
129. P.L. Privalov and S.J. Gill, Adv. Protein Chem. 39 (1988) 191-238.
130. J.A. Schellman and P. Oriel, J. Chem. Phys. 37 (1962) 2114.
131. J.A. Schellman and W.J. Becktel, Biopolymers 22 (1983) 171.
132. P.M. Bayley, E.B. Nielsen, and J.A. Schellman, J. Phys. Chem. 73 (1969) 228.
133. J.A. Schellman, Chem. Phys. 75 (1975) 323.
134. J. Applequist, K.R. Sundberg, M.L. Olson, and L.C. Weiss, J. Chem. Phys. 70 (1979) 1240.
135. J. Applequist, Biopolymers 20 (1981) 2311.
136. J. Applequist, Biopolymers 21 (1982) 703.
137. J.W. Caldwell and J. Applequist, Biopolymers 23 (1984) 1891.
138. B.K. Sathyanarayana and J. Applequist, Int. J. Peptide Protein Res. 26 (1985) 518.
139. B.K. Sathyanarayana and J. Applequist, Int. J. Peptide Protein Res. 27 (1986) 86.
140. K.A. Thomasson and J. Applequist, Biopolymers 31 (1991) 529.
141. E.S. Pysh, Biopolymers 13 (1974) 1563.
142. T.M. Cooper and R.W. Woody, Biopolymers 30 (1990) 657.
143. W.J. Goux, D.B. Cooke, R.E. Rodriguez, and T.M. Hooker, Jr., Biopolymers 13 (1974) 2315.
144. W.J. Goux and T.M. Hooker, Jr., J. Am. Chem.Soc. 97 (1975) 1605.
145. W.J. Goux, T.R. Kadesch, T.M. Hooker, Jr., Biopolymers 15 (1976) 977.
146. W.J. Goux and T.M. Hooker, Jr., J. Am. Chem.Soc. 102 (1980) 7080.
147. W.J. Goux and T.M. Hooker, Jr., Biopolymers 19 (1980) 2191.
148. P.E. Grebow and T.M. Hooker, Jr., Biopolymers 14 (1975) 871.
149. P.E. Grebow and T.M. Hooker, Jr., Biopolymers 14 (1975) 1863.
150. T.M. Hooker, Jr. and J.A. Schellman, Biopolymers 9 (1970) 1319.
151. J.W. Snow and T.M. Hooker, Jr., J. Am. Chem. Soc. 96 (1974) 7800.
152. J.W. Snow and T.M. Hooker, Jr., J. Am. Chem. Soc. 97 (1975) 3506.
153. J.W. Snow, T.M. Hooker, Jr., and J.A. Schellman, Biopolymers 16 (1977) 121.
154. R.W. Snyder and T.M. Hooker, Jr., Biopolymers 21 (1982) 547.
155. E.H. Strickland and D. Mercola, Biochemistry 15 (1976) 3875.
156. A. Wollmer, J. Fleischhauer, W. Strassburger, H. Thiele, D. Brandenburg, G. Dodson, and D. Mercola, Biophys. J. 20 (1977) 233.
157. M.-C. Hsu and R.W. Woody, J. Am. Chem. Soc. 93 (1971) 3515.
158. J.C. Kendrew, Brookhaven Symp. Biol. 15 (1962) 216.
159. K. Ruckpaul, H. Rein, and F. Jung, Naturwissenschaften 57 (1970) 131.
160. M.V. Volkenstein, L.T. Metyaev, and I.S. Milevskaya, Mol. Biol. 3 (1969) 190.
161. G.N. La Mar, H.Toi, and R. Kirshnamoorthi, J. Am. Chem. Soc. 106 (1984) 6395.
162. W.R. Light, R.J. Rohlfs, G. Palmer, and J.S. Olson, J. Biol. Chem. 262 (1987) 46.
163. H.S. Aojula, M.T. Wilson, and A. Drake, Biochem. J. 237 (1986) 613.
164. A. Bellelli, R. Foon, F. Ascoli, and M. Brunori, Biochem. J. 246 (1987) 787.
165. L. Otvos, Jr., J. Thurin, E. Kollat, L. Urge, H.H. Mantsch, and M. Hollosi, Int. J. Peptide Protein Res. 38 (1991) 476.
166. T. Arakawa, Y.R. Hsu, D. Chang, N. Stebbing, and B. Altrock, J. Interferon Res. 6 (1986) 687.
167. J. Utsumi, S. Yamazaki, K. Hosoi, H. Shimizu, K. Kawaguchi,and F. Inagaki, J. Biochem. 99 (1986) 1533.
168. J. Utsumi, Y. Mizuno, K. Hosoi, K. Okano, R. Sawada, M. Kajitani, I. Sakai, M. Naruto, and H. Shimizu, Eur. J. Biochem. 181 (1989) 545.

169. M. Boublik, J.A. Moschera, C. Wei, and H.F. Kung, J. Interferon Res. 10 (1990) 213.
170. S. Elliot, K.D. Fagin, L.O. Nahri, J.A. Miller, M. Jones, R. Koski, M. Peters, P. Hsieh, R. Sachdev, and R.D. Rosenfeld, J. Protein Chem. 9 (1990) 95.
171. N. Kubota, T. Orita, K. Hattori, M. Oh-eda, N. Ochi, and T. Yamazaki, J. Biochem. 107 (1990) 486.
172. J.N. Liang and L.T. Chylack, Jr., Biochem. Biophys. Res. Commun. 123 (1984) 899.
173. J.N. Liang and L.T. Chylack, Jr., Invest. Ophthalmol. Vis. Sci. 28 (1987) 790.
174. J.H.R. Kagi, T.K. Li, and B.L. Vallee, Biochemistry 10 (1971) 1007.
175. R.W. Woody, in Protein-Ligand Interactions, H. Sund and G. Blauer, Eds., Walter de Greyter and Co., Berlin, 1975.
176. J.A. D'Anna, Jr. and G. Tollin, Biochemistry 11 (1972) 1073.
177. K.D. Watenpaugh, L.C. Sieker, and L.H. Jensen, Proc. Natl. Acad. Sci. USA 70 (1973) 3857.
178. W.S. Innis, D.B. McCormick, and A. H. Merrill, Biochem. Med. 34 (1985) 151.
179. J.S. Wicken and R.W. Woody, Biochemistry 12 (1973) 3459.
180. E. Zeppezauer, B.-O. Söderberg, C.-I. Brandén, A. Åkeson, and H. Theorell, Acta Chem. Scand. 21 (1967) 1099.
181. J.R. Heitz and L. Brand, Biochemistry 10 (1971) 2695.
182. J.F. Towell and R.W. Woody, Biochemistry 19 (1980) 4231.
183. V.M. Gurevich, B.I. Kurganov, N.P. Sugrobava, and V.A. Yakolev, Biokhimiya 37 (1972) 1023.
184. M.J. Adams, M. Buchner, K. Chandrasekhar, G.C. Ford, W.S. Allison, M.L. Hackert, A. Liljas, M.G. Rossman, I.E. Smiley, J. Everse, N.O. Kaplan, and S.S. Taylor, Proc. Natl. Acad Sci. USA 70 (1973) 1968.
185. J.F. Towell, Ph.D. Dissertation, Colorado State University (1977).
186. R.W. Woody, Fed. Proc. 42 (1983) 2103.
187. D.P. Giedroc, H. Qiu, R. Khan, G.C. King, and K. Chen, Biochemistry 31 (1992) 765.
188. Y. Shamoo, L.R. Ghosaini, K.M. Keating, K.R. Williams, J.M. Sturtevant, and W.H. Konigsberg, Biochemistry 28 (1989) 7409.
189. J. Kuwahara and J.E. Coleman, Biochemistry 29 (1990) 8627.
190. M.A. Weiss, K.A. Mason, C.E. Dahl and H.T. Keutman, Biochemistry 29 (1990) 5660.
191. J.U. Bowie and R.T. Sauer, Biochemistry 28 (1989) 7139.
192. E.K. O'Shea, R. Rutkowski, and P.S. Kim, Science 243 (1989) 538.
193. E.K. O'Shea, R. Rutkowski, W.F. Stafford and P.S. Kim, Science 245 (1989) 646.
194. V. Saudek, T. Gibson, Gausepohl, R. Frank, and A. Pastore, Biochemistry 30 (1991) 1310.
195. T.G. Oas, L.P. McIntosh, E.K. O'Shea, F.W. Dahlquist, and P.S. Kim, Biochemistry 29 (1990) 2891.
196. R. Rasmussen, D. Benvegnu, E.K. O'Shea, P.S. Kim, and T. Alber, Proc. Natl. Acad. Sci.. USA 88 (1991) 561.
197. K.T. O'Neil, R.H. Hoess, and W.F. DeGrado, Science 249 (1990) 774.
198. K.T. O'Neil, J.D. Shuman, C. Ampe, and W.F. DeGrado, Biochemistry 30 (1991) 9030.
199. L.Patel, C. Abate, and T. Curran, Nature 347 (1990) 572.
200. T. Schmidt-Dorr, P. Oertel-Buchheit, C. Pernelle, L. Bracco, M. Schnarr, and M. Granger-Schnarr, Biochemistry 30 (1991) 9657.
201. R.V. Talanian, C.J. McKnight, and P.S. Kim, Science 249 (1990) 769.
202. S.J. Anthony-Cahill, P.A. Benfield, R. Fairman, Z.R. Wasser,an, S.L. Brenner, W.F. Stafford, C. Altenbach, W.L. Hubbell, and W.F. DeGrado, Science 255 (1992) 979.
203. B.C. Sang and D.M. Gray, Biochemistry 28 (1989) 9502.
204. E.W. Abrahamson and R.S. Fager, Curr. Top. Bioenerg. 5 (1973) 125.

204

205. W. Mommaerts, in The Retina, B.R. Straatsma, Ed., Univ. of Cal. Press, Los Angeles, California. (1969).
206. B. Honig and T. Ebrey, Biochemistry 12 (1973) 1637.
207. T.G. Ebrey and T. Yoshizawa, Exp. Eye Res. 17 (1973) 545.
208. M. Burke, D. Pratt, T. Faulkner, and A. Moskowitz, Exp. Eye Res. 17 (1973) 557.
209. A.S. Waggoner and L. Stryer, Biochemistry 10 (1956) 3250.
210. E. Johnston and R. Zand, Biochem. Biophys. Res. Commun. 47 (1972) 712.
211. M.P. Heyn, P.-J. Bauer, and N.A. Dencher, Biochem. Biophys. Res. Commun. 67 (1975) 897.
212. M. Poo and R.A. Cone, Nature 247 (1974) 438.
213. J.J. Du, M.A. El-Sayed, L.J. Stern, T. Mogi, and H.G. Khorana, FEBS Lett. 262 (1990) 155.
214. M.A. El-Sayed, C.T. Lin, and W.R. Mason, Proc. Natl. Acad. Sci., U.S.A. 86 (1989) 5376.
215. C.A. Hasselbacher, J.L. Spudich, and T.G. Dewey, Biochemistry 27 (1988) 2540.
216. R. Henderson, Ann. Rev. Biophys. Bioeng. 6 (1977) 87.
217. C. Bustamante, I. Tinoco, and M. Maestre, Proc. Natl. Acad. Sci. USA 80 (1983) 3568.
218. L. Finzi, L. Ulibarri, and C. Bustamante, Biophys J. 59 (1991) 1183.
219. C. Reich, M.F. Maestre, S. Edmondson, and D.M. Gray, Biochemistry 19 (1980) 5208.
220. I. Tinoco, Jr., M.F. Maestre, and C. Bustamante, Trends Biochem. Sci. 8 (1983) 41.
221. B.K. Jap, M.F. Maestre, S.B. Hayward, and R.M. Glaeser, Biophys. J. 43 (1983) 81.
222. D. Mao and B.A. Wallace, Biochemistry 23 (1984) 2667.
223. R.M. Glaeser and B.K. Jap, Biochemistry 24 (1985) 6398.
224. B.A. Wallace and C.L. Teeters, Biochemistry 26 (1987) 65.
225. H. Sigrist, R.H. Wenger, E. Kislig, and M. Wuthrich, Eur. J. Biochem. 177 (1988) 125.
226. M.A. Gilles-Gonzales, D.M. Engelman, and H.G. Khorana, J. Biol. Chem.266 (1991) 8545.
227. D.D. Muccio and J.Y. Cassim, Biophys. J. 26 (1979) 427.
228. M.D. Bazzi and R.W. Woody, Biophys. J. 48 (1985) 957.
229. I. Tinoco, Jr., J. Am. Chem. Soc. 81 (1959) 1540.
230. S.J. Hoffman and R. Ullman, J. Polymer Sci. 31C (1970) 205.
231. R. Mandel and G. Holtzworth, Biopolymers 12 (1973) 655.
232. Y. Wu, H.W. Huang, and G.A. Olah, Biophys. J. 57 (1990) 797.
233. M.D. Bazzi, R.W. Woody, and A. Black, Biopolymers 26 (1987) 1115.
234. G. Blauer and G. Wagnière, J. Am. Chem. Soc. 97 (1975) 1949.
235. J.W. Leonard and J.W.F. Foster, J. Biol. Chem. 236 (1961) 2662.
236. D.A. Lightner, M. Reisinger, and G.L. Landen, J. Biol. Chem. 261 (1986) 6034.
237. A. Knudsen, A.D. Pederson, and R. Brodersen, Arch. Biochem. Biophys. 244 (1986) 273.
238. B. Honore and P.C. Frandsen, Biochem. J. 236 (1986) 365.
239. D. Harmatz and G. Blauer, Archiv. Biochem. Biophys. 170 (1975) 375.
240. O.J. Bos, M.J. Fisher, J. Wilting, and L.H. Janssen, Biochim. Biophys. Acta 953 (1988) 37.
241. J. Wilting, W.F. van der Geisen, L.H.M. Janssen, M.M. Weideman, M. Otagiri, and J.H. Perrin, J. Biol. Chem. 255 (1980) 3032.
242. M. Otagiri, H. Nakamura, U. Imamura, J. Fleitman, and J. Perrin, Chem. Pharm. Bull. 37 (1989) 1401.
243. E.L. Vansterkenberg, J. Wilting, and L.H. Janssen, Biochem. Pharmacol. 38 (1989) 3029.
244. K. Matsuyama, A.C. Sen, and J.H. Perrin, J. Pharm. Pharmacol. 39 (1987) 190.
245. B. Honore, H. Sato, and R. Broderson, Arch. Biochem. Biophys. 266 (1988) 189.
246. S. Watanabe, J. Steroid Biochem. 23 (1985) 177.

247. E. Albengres, S. Urien, P. Riant, G.A. Marcel, and J.P. Tillement, Mol. Pharmacol. 31 (1987) 294.
248. P. Mohanakrishnan and C.F. Chignell, Biochem. Pharmacol. 34 (1985) 675.
249. B.P. Maliwal, A.G.A. Rao, and M.S.N. Rao, Int. J. Peptide Protein Res. 25 (1985) 382.
250. T. Shimuzu and M. Hatano, Biochemistry 23 (1984) 6403.
251. Y. Ogama, T. Shimuzu, H. Kobayashi, T. Fujii, A. Hachimori, Y. Kondo, and M. Hatano, Biochim. Biophys. Acta 997 (1989) 188.
252. M. Otagiri, T. Maruyama, T. Imai, A. Suenga, and Y.A. Imamura, J. Pharm. Pharmacol. 31 (1987) 416.
253. L. Stryer and E.R. Blout, J. Am. Chem. Soc. 83 (1960) 1411.
254. I. Tinoco, Jr., R.W. Woody, and D.F. Bradley, J. Chem. Phys. 38 (1963) 1317.
255. N. Harada, S.L. Chen, and K. Nakanishi, J. Am. Chem. Soc. 97 (1975) 5345.
256. H. Yamamoto and A. Nakazawa, Bull. Chem. Soc. Jap. 56 (1983) 2535.
257. H. Yamamoto and A. Nakazawa, Biopolymers 23 (1984) 1367.
258. P.V. Scaria, M. Atreyi, and M.V.R. Rao, Int. J. Biol. Macromol. 10 (1988) 60.
259. H. Yamamoto, Int. J. Biol. Macromol. 8 (1986) 130.
260. Y. Sato and M. Hatano, Makromol. Chem. 183 (1982) 997.
261. Y. Sato and R.W. Woody, Biopolymers 19 (1980) 2021.
262. R.A. Edwards and R.W. Woody, Biochem. Biophys. Res. Commun. 79 (1977) 470.
263. R.A. Edwards and R.W. Woody, J. Phys. Chem. 87 (1983) 1329.
264. J.C. Smith and R.W. Woody, J. Phys. Chem. 80 (1976) 1094.
265. G.K. Radda and J. Vanderkooi, Biochim Biophys Acta 265 (1972) 509.
266. G. Weber and D.J.R. Lawrence, Biochem. J. 53 (1954) 31.
267. L. Stryer, J. Mol. Biol. 13 (1965) 482.
268. E. Daniel and G. Weber, Biochemistry 5 (1966) 1893.
269. W.O. McClure and G.M. Edelman, Biochemistry 6 (1967) 559.
270. L. Brand, J.R. Gohlke, and D.S. Rao, Biochemistry 6 (1967) 3510.
271. N. Cittanova and A. Alfsen, Eur. J. Biochem. 13 (1970) 539.
272. N.K. Nagradova, R.A. Asyrants, and M.V. Ivanov, Experentia 27 (1971) 1169.
273. S. Era, K. Kuwata, K. Kida, M. Sogami, and A. Yoshida, Int. J. Peptide Protein Res. 26 (1985) 575.
274. R.H. Conrad, J.R. Heitz, and L. Brand, Biochemistry 9 (1970) 1540.
275. D.S. Sigman and A.N. Glazer, J. Biol. Chem. 247 (1972) 334.
276. T. Chiba, Y. Sato, and Y. Suzuki (1987) Biochim. Biophys. Acta 897 (1987) 14.
277. T. Chiba, Y. Sato, and Y. Suzuki (1986) Biochim. Biophys. Acta 858 (1986) 107.
278. T. Chiba, Y. Sato, and Y. Suzuki, Biochim. Biophys. Acta 1025 (1990) 199.

This Page Intentionally Left Blank

Chapter 7

Chiroptical studies of molecules in electronically excited states

James P. Riehl

Department of Chemistry, University of Missouri-St. Louis, St. Louis, Missouri, 63121, USA

Abstract
There are two chiroptical spectroscopic techniques designed to probe molecular stereochemical structure which are based upon the measurement of molecular luminescence. In circularly polarized luminescence spectroscopy (CPL) one analyzes the luminescence for the normally very small difference in intensities between left and right circular polarization. In fluorescence detected circular dichroism (FDCD), the difference in absorption between left and right circularly polarized light is monitored through detection of the difference in total emission intensities associated with the different absorption polarizations. Although similar in experimental design, these techniques usually probe different aspects of molecular chirality, due to the fact that CPL is a probe of excited state structure, whereas FDCD is a probe of the molecular ground state. In this chapter we describe theoretical and experimental aspects of both of these spectroscopic procedures. Emphasis is placed on detailed discussion of a few applications which illustrate the kinds of unique information which may be obtained.

OUTLINE

1. INTRODUCTION

2. THEORETICAL PRINCIPLES
    2.1 Circularly Polarized Luminescence
        2.1.1 Time Resolved Circularly Polarized Luminescence
    2.2 Fluorescence Detected Circular Dichroism

3. INSTRUMENTATION
    3.1 CPL Instrumentation
        3.1.1 Measurements Statistics and Standards
    3.2 FDCD Instrumentation

1. INTRODUCTION

This chapter will be concerned with the description of experiments which probe the optical activity of molecular ground or *excited* states through detection of molecular luminescence. The principal techniques to be discussed will be circularly polarized luminescence (CPL), in which one analyzes the luminescence for the usually small difference between the intensity of right and left circular polarized emitted light, and fluorescence detected circular dichroism (FDCD), in which differences in the absorption of the two circular polarizations is detected through measurement of the difference in total emission intensities. As will be described in more detail below, these experiments, though related, probe quite different aspects of molecular chirality, and have very different experimental characteristics. Of primary importance is the fact that these experiments do *not* provide redundant information. FDCD is essentially a probe of ground state discrimination between incident circular polarizations, whereas CPL reflects differential emission probabilities of molecules in their excited (*emitting*) state. The discussion given here will be limited to applications of these (and other related) techniques to *naturally* optically active systems and, therefore, we will not consider those experiments in which external fields are applied in order to generate field-induced polarizations.

Measurement of the circular polarization in the luminescence of optically active molecules was first reported by Emeis and Oosterhof in 1967 [1]. Advancements in electronics, optics, and digital technology have led to the development of this area of research. Over the last 25 years, more than 150

published reports of CPL applications and theory have appeared in the literature [2-4]. This technique has at various times been referred to as circularly polarized emission, emission circular intensity differentials, circularly polarized luminescence, or, more specifically, as circularly polarized fluorescence or phosphorescence. In this chapter we will use only the CPL designation. For a more general treatment of CPL spectroscopy and applications, the reader is referred to one of the several review articles in this field [2-4]. Some effort will be given here to mention some of the most recent work in this area, since a review has not appeared since early in 1986.

FDCD measurements, and a basic theoretical formalism for this technique, were first reported by Turner, Tinoco and Maestre in 1974 [5]. In this experiment one uses the selectivity and sensitivity of luminescence measurements to probe the local chiral environment of fluorescent chromophores. The ultimate goal in many applications of FDCD is to relate the observed differential fluorescence signal to the conventional CD measurement. In certain multi-component absorbing systems this procedure may be difficult. This technique is sometimes applied to systems for which CD measurements are impossible or very difficult. FDCD, like CPL and other polarization sensitive techniques, is not immune to troublesome background and noise problems, and these will be discussed in Section 3. The only detailed discussion of the applicability of FDCD measurements, and other characteristics of the technique has been presented by Turner in 1978 [6]. In this chapter we will also list some of the more recent applications of FDCD.

2. THEORETICAL PRINCIPLES

2.1. Circularly Polarized Luminescence

In CPL spectroscopy, one analyzes the luminescence from a chiral sample and determines the differential emission intensity at wavelength λ, $\Delta I(\lambda)$. This quantity is related to the intensity of left (I_L) and right (I_R) circularly polarized light as follows [7,8]

$$\Delta I(\lambda) = I_L(\lambda) - I_R(\lambda) \tag{1}$$

Because of the difficulty in measuring absolute emission intensities, in CPL spectroscopy one commonly reports the ratio of $\Delta I(\lambda)$ to the total intensity $I(\lambda)$. This ratio, $g_{lum}(\lambda)$, is referred to as the luminescence (or emission) dissymmetry ratio, and is explicitly defined at wavelength, λ, as

$$g_{lum}(\lambda) = \frac{\Delta I(\lambda)}{\frac{1}{2}I(\lambda)} = \frac{I_L(\lambda) - I_R(\lambda)}{\frac{1}{2}(I_L(\lambda) + I_R(\lambda))} \tag{2}$$

The extra factor of 1/2 in this equation results from the fact that the equivalent expression for the absorption dissymmetry factor (or ratio), $g_{abs}(\lambda)$, employed in CD spectroscopy is defined in terms of the difference in extinction coefficients, $\Delta\varepsilon$, divided by the *average* extinction coefficient, ε.

$$g_{abs}(\lambda) = \frac{\Delta\varepsilon(\lambda)}{\frac{1}{2}\varepsilon(\lambda)} = \frac{\varepsilon_L(\lambda) - \varepsilon_R(\lambda)}{\frac{1}{2}(\varepsilon_L(\lambda) + \varepsilon_R(\lambda))} \tag{3}$$

The connection to molecular energy states and molecular geometry is through the appropriate expressions for quantum mechanical emission transition probabilities for circularly polarized light. The final formal relationships between the measurement of $\Delta I(\lambda)$ or $g_{lum}(\lambda)$ also contain geometrical factors due to the fact that different relative excitation/emission geometries will, in general, lead to different orientational distributions of emitting species contributing to the observed signal. These relationships must also include the possibility of geometry changes that may be associated with electronic absorption, and intermolecular and intramolecular reorientation processes that take place on the same time scale as emission. The dependence of the CPL signal on excitation and emission geometry and incident polarization is similar to that encountered, and often exploited, in linear depolarization measurements.

For the specific case of differential circularly polarized emission, starting with time-dependent perturbation theory, one obtains the following relationship between the time-dependent experimental observable, $\Delta I(\lambda,t)$, the excited state population, N_n, and the differential transition probability, $\Delta W = W_{Left} - W_{Right}$, following an excitation pulse of polarization, π, at time $t = 0$

$$\Delta I^\pi(\lambda,t) = f_{CPL}(\lambda)(hc/\lambda) \int <N_n^\pi(\Omega:\Omega_0,\gamma,t)\Delta W(\Omega,\gamma)> d\gamma \tag{4}$$

In this equation, the brackets, $< \cdots >$, denote an ensemble average over the orientational distribution of emitting molecules, denoted by Ω, and the integral denotes an average over molecular conformations, denoted by γ. $f_{CPL}(\lambda)$ is a normalized lineshape function, and the constants h and c have their usual meaning.

Even in situations in which the molecules of interest are randomly oriented (*e.g.* in solution) the orientational distribution of emitting molecules may not be isotropic, due to the fact that the incident (excitation) beam *photoselects* molecules based upon the relative orientation of the absorption transition dipoles, $\vec{\mu}_{abs}$, with respect to the incident polarization vector, $\vec{\pi}$ [7,9,10]. The probability of absorption is proportional to $| \vec{\mu}_{abs} \cdot \vec{\pi} |^2$; thus, for example, molecules oriented such that $\vec{\pi}$

is perpendicular to $\vec{\mu}_{abs}$ will not be excited, and will, as a result, not contribute to the subsequent emission. This is illustrated in Figure 1A in which we display molecules randomly oriented in a generalized laboratory coordinate system. The laboratory system is indicated by the labels (1, 2 and 3). In this figure, it has been assumed that excitation is along the $\vec{3}$ direction. As illustrated, $\vec{\pi}$ has been chosen to be parallel to the 1 axis.
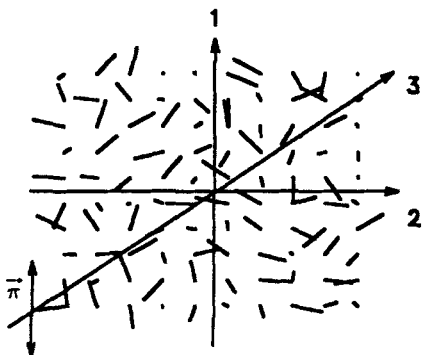
Figure 1A: Randomly oriented molecules in the laboratory (1,2,3) coordinate system.
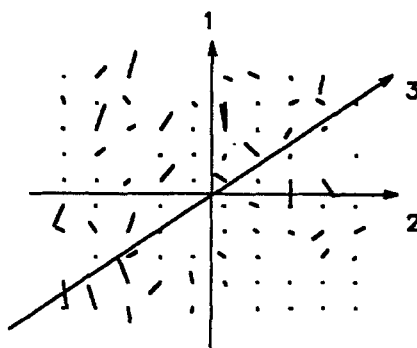
Figure 1B: Weighted distribution of photoselected molecules. (see text).

The effects of photoselection have been illustrated in Figure 1B by making the length of the vectors $\vec{\mu}_{abs}$ for the initially randomly oriented sample proportional to the excitation probability. Thus, molecules oriented such that $\vec{\mu}_{abs}$ is parallel to $\vec{\pi}$ are drawn as full length vectors, and those oriented perpendicular to $\vec{\pi}$ have zero length. In the limit that the excited molecules do not rotate during the excited state lifetime, the orientational distribution of molecules selected by the excitation beam is identical to the distribution seen in an emission experiment. If it is assumed that the emission transition dipole, $\vec{\mu}_{em}$, is parallel to $\vec{\mu}_{abs}$, and that the molecules are rigid, then the distribution given in Figure 1B corresponds exactly to the molecular orientational distribution of *emitting* states. The more generalized problem associated with non-parallel transition vectors and non-rigid systems has been treated elsewhere [7]. For detection along the 2 direction, the anisotropic, distribution given in Figure 1A is still appropriate. A different, albeit still anisotropic distribution will be generated for the case in which the excitation beam is unpolarized. It is important to recognize the fact that, in both cases, there is a preference for transition dipoles oriented along the laboratory 1 axis as compared to those oriented along the 3 axis.

As will be discussed in more detail below, there are several consequences to the previous discussion. As we and others have presented, the fact that the emitting state distribution can be anisotropic allows for the possibility of probing

molecular optical activity of oriented samples. Although to date no orientational dependence of the CPL signal has been seen, it should be possible to probe chirality along specific molecular directions even when the ground state is randomly oriented, as would exist in a solution. This information might be useful in comparing experimental results on CD and CPL to theoretical descriptions of the source of the optical activity. It is also evident that, in the experimental configuration represented by the distribution in Figure 1B, the luminescence will be partially linearly polarized. Of course, if the emitting molecules are optically active, the emission will also be circularly polarized, resulting in the luminescence being *elliptically* polarized. In principle, the presence of linear polarization has no effect on the measurement of circular polarization. In practice, however, as described below, it is very difficult to measure the usually very small circular polarization in the presence of significant linear polarization [11]. Thus, efforts are usually made to eliminate any linear polarization in CPL measurements by proper choice of experimental geometry. Finally, it should be noted than in the limit that the molecules of interest are sufficiently long lived so as to undergo substantial reorientational motion during the excited state lifetime, then the excited state distribution will be isotropic.

Returning to eq. (4), we identify $N_n^\pi(\Omega{:}\Omega_0,\gamma,t)$ as the number of species in the emitting state, n, with orientation Ω and conformation γ at time t, following an excitation beam of polarization π, given an initial orientation Ω_0; and $\Delta W(\Omega,\gamma)$ is the difference in emission transition probabilities of left minus right circularly polarized light for a species of orientation Ω and conformation γ. In a so-called "steady-state" experiment, where one employs continuous excitation and emission detection, the appropriate expression for the differential emission intensity is obtained by integrating eq. (4) over long times

$$\Delta I^\pi(\lambda) = \int_0^\infty \Delta I^\pi(\lambda,t)\mathrm{d}t \tag{5}$$

To date, most of the specific applications of eqs. (4) and (5) have involved considerable simplifications of the complex dependence on geometry and conformation implied in eq. (4), and described above. Some of these simplifications are due to the nature of the molecular system under study. For example, as we will discuss in more detail below, intraconfigurational f $\leftrightarrow$ f transitions are essentially spherical transitions, and, thus, complications due to photoselected orientational distributions are eliminated, and the emitting sample is essentially isotropic (*i.e.* independent of orientation). Other simplifications arise when one is concerned with $g_{lum}(\lambda)$. For example, Snir and Schellman have shown that when $\vec{\mu}_{abs}$ is parallel to $\vec{\mu}_{em}$, the geometry dependence in $I(\lambda)$ and $\Delta I(\lambda)$ is the same and can be factored out of the ratio [10].

Here we choose to develop the relationships for the observables, $\Delta I(\lambda)$, and $g_{lum}(\lambda)$ for a simple, but common, molecular system in which the orientational distribution is, in fact, isotropic. As mentioned above, this distribution arises if the transitions involved are spherical or if the system has undergone significant reorientation during the excited state lifetime. We also will assume that the conformation (molecular geometry) of the ground and emitting states are identical. For this system we may write the following expression for the population of the emitting state at time t

$$N_n^\pi(t) = N_n^\pi(0)\exp(-t/\tau_0) = A^2 f_n C_m I_0 \mid \vec{\pi} \cdot \vec{\mu}_{abs} \mid^2 \exp(-t/\tau_0) \tag{6}$$

where A^2 is a constant factor; f_n is the fraction of molecules that are initially excited that end up in the emitting state, n; C_m denotes the concentration of emitting species; and I_0 is the excitation beam intensity. In writing eq. (6) we have assumed that excited state relaxation processes that take the molecule from the final state in the excitation process to the initial state in the emission are fast compared to the emission state lifetime, τ. The differential transition rate may be written in the following form

$$\Delta W(\Omega) = K(\lambda^3) R^{gn}(\Omega) \tag{7}$$

where $K(\lambda^3)$ is a constant appropriate for spontaneous emission, and $R^{gn}(\Omega)$ denotes the *rotatory strength* for the emissive transition n $\rightarrow$ g. The dependence of ΔI on details of electronic and molecular structure (and molecular wavefunctions) is through $R^{gn}(\Omega)$.

Substituting eqs. (6) and (7) into eq. (4) we obtain the following expression

$$\Delta I^\pi(\lambda,t) = f_{CPL}(\lambda) K_R f_n C_m I_0 \mid \mu_{abs}^\pi \mid^2 R^{gn} \exp(-t/\tau_0) \tag{8}$$

where all of the constants have been included in the new constant K_R. In writing eq. (8) we have assumed that the averaging implied by the brackets in eq. (4) has been performed. Under the assumption that the system is isotropic, this simply results in a factor of 2/3. Eq. (8) displays the expected dependence of ΔI on excitation intensity, concentration, efficiency of populating the emitting state, and absorption strength. It is useful to compare this equation to the equivalent expression for the time-dependence of the total emission intensity under similar assumptions. This is given in eq. (9)

$$I^\pi(\lambda,t) = f_{TL}(\lambda) K_D f_n C_m I_0 \mid \mu_{abs}^\pi \mid^2 D^{gn} \exp(-t/\tau_0) \tag{9}$$

where $f_{TL}(\lambda)$ denotes the total luminescence line shape function; D^{gn} is the dipole strength for the emissive transition, and K_D is a constant. Since the leading terms in the dipole strength are $|\mu^{gn}|^2 + |m^{gn}|^2$, whereas optical activity results from the cross terms such as $2\mu^{gn}m^{gn}$, it can be shown that $K_R = 2K_D$.

Performing the simple time integrals in eqs. (8) and (9), one obtains

$$\Delta I^{\pi}(\lambda) = \tau_0 f_{CPL}(\lambda) K_R f_n C_m I_0 |\mu_{abs}^{\pi}|^2 R^{gn} \tag{10}$$

and from eq. (2)

$$g_{lum}(\lambda) = [f_{CPL}(\lambda)/f_{TL}(\lambda)] \frac{4R^{gn}}{D^{gn}} \tag{11}$$

The form of eq. (11) is similar to that encountered in CD spectroscopy. Finally, it should be noted that this equation has been derived for measurements at a particular wavelength, λ; expressions involving integrated (over the electronic band) rotatory and absorption strengths may also be developed [2].

It has been assumed in the above derivation that the system under study is composed of only one pure optically active emitting substance. If the sample of interest is only partially resolved, and both enantiomers (R and S) are present in unequal concentrations, then one may relate the measurement of $g_{lum}(\lambda)$ or $\Delta I(\lambda)$ to the enantiomeric excess, η, as follows [12]

$$g_{lum}(\lambda) = \eta_n g_{lum}^S(\lambda) \tag{12}$$

where η_n is defined in terms of the excited state (n) concentrations of the two enantiomers

$$\eta_n = \frac{C_n(S) - C_n(R)}{C_n(S) + C_n(R)} \tag{13}$$

and $g_{lum}^S(1)$ denotes the dissymmetry ratio for the pure S enantiomer. A relationship similar to eq. (12) may be written for the corresponding absorption process for measurements at wavelength λ'.

$$g_{abs}(\lambda') = \eta_g g_{abs}^S(\lambda') \tag{14}$$

where η_g refers to the *ground* state concentration of enantiomers. Obviously, if the sample of interest is racemic in the ground and excited state no CD or CPL will be detected.

As discussed below, it is possible in some cases to generate non-racemic excited state concentrations from racemic ground states by employing a circularly polarized excitation beam [12,13]. It is not difficult to show that, in this case, the measured dissymmetry ratio, measured when the excitation is right (r) circularly polarized is related to the dissymmetry ratios for the individual enantiomers as follows

$$g_{lum}^{r}(\lambda) = -\left(\frac{1}{2}\right) g_{abs}^{S}(\lambda') g_{lum}^{S}(\lambda) \tag{15}$$

where we have taken care to note the absorption and emission wavelengths. [Lower case letters, r and ℓ will be used here to indicate *excitation* polarization to distinguish them from emission polarizations for which we have used L and R] By symmetry

$$g_{lum}^{r}(\lambda) = -g_{lum}^{\ell}(\lambda) \tag{16}$$

where ℓ denotes left circularly polarized excitation. Comparison of eq. (15) with eq. (12) shows that the quantity $-g_{abs}^{S}(\lambda')/2$ is simply equal to the enantiomeric excess created in a racemic mixture by a right circularly polarized excitation beam.

It may also be useful to employ circularly polarized excitation in other situations in which the sample is composed of more than one emitting species with different chiral environments. In this case the different emitting species may interact with the excitation beam in different amounts and lead to some additional selectivity through polarization selective absorption (CD). Several examples of this type of double polarization experiment will be presented and described below.

2.1.1. Time-Resolved Circularly Polarized Luminescence

Very recently the research groups of Professor F. S. Richardson at the University of Virginia, and Dr. H. P. J. M. Dekkers of the University of Leiden have built instruments capable of measuring the time dependence of the CPL intensity [14-24]. As is evident from eqs. (8) and (9), for the simple system described in the previous section, in which we assumed no competing excited state processes, the time dependence of the CPL intensity would be exactly equal to that measured for the total luminescence intensity. Time-resolved CPL (TRCPL) is, therefore, an experiment suited for the study of excited state processes that result in optical activity *changes*. We will summarize here the theoretical formalism for two such processes, namely, excited state racemization, and excited state enantioselective quenching.

For excited state racemization that is fast enough to compete with emission, a simple kinetic model shows that the time-dependent difference in the excited

state concentrations of the two enantiomers can be expressed as [16]

$$[C_n(S) - C_n(R)]^t = [C_n(S) - C_n(R)]^0 e^{-(k_{rac} + k_0)t} \qquad (17)$$

where the superscripts t and 0 denote, respectively, the values at time t, and time $t = 0$; k_0 is equal to $(\tau_0)^{-1}$; and k_{rac} is the rate constant for racemization, which is equal to twice the rate of conversion of one enantiomer into the other. Similarly it is easily seen that

$$[C_n(S) + C_n(R)]^t = [C_n(S) + C_n(R)]^0 e^{-k_0 t} \qquad (18)$$

Thus, we can write an expression for the time dependence of the excited state enantiomeric excess, $\eta_n(t)$

$$\eta_n(t) = \eta_n(0) e^{-k_{rac} t} \qquad (19)$$

Identifying the enantiomeric excess at time 0 with $-g_{abs}^S(\lambda')/2$ (see above), we can express the time-dependent equivalent of eq. (15) as follows

$$g_{lum}^r(\lambda, t) = -\left(\frac{1}{2}\right) g_{abs}^S(\lambda') g_{lum}^S(\lambda) e^{-k_{rac} t} \qquad (20)$$

and thus, an analysis of the time-dependence of the measured dissymmetry ratio yields k_{rac}.

Later in this chapter we will describe a series of recent experiments in which non-racemic excited states were obtained from racemic mixtures by adding an optically active quencher molecule. The chiral quencher changes the excited state lifetimes of the enantiomers, and makes them unequal. We designate the new lifetimes as k^+ and k^-, and relate them to the concentration of chiral quencher, $[Q_\Delta]$, and bimolecular quenching constants, $k_q^{R\Delta}$ and $k_q^{S\Delta}$ as follows

$$k^- = k_0 + k_q^{S\Delta}[Q_\Delta] \qquad (21a)$$

$$k^+ = k_0 + k_q^{R\Delta}[Q_\Delta] \qquad (21b)$$

Both enantiomers, of course, contribute to $I(t)$ and $\Delta I(t)$. Summing up these terms, one obtains the following expressions

$$I(\lambda, t) = I_0[e^{k^- t} + e^{k^+ t}] \qquad (22)$$

$$g_{lum}(\lambda,t) = g_{lum}^{R}(\lambda) tanh\left(\frac{1}{2}k_d[Q_\Delta]t\right) \qquad (23)$$

where

$$k_d = k_q^{S\Delta} - k_q^{R\Delta} \qquad (24)$$

The individual chiral quenching rate constants may be determined either from analysis of the time-dependence of eq. (22) or eq. (23). Biexponential fitting of eq. (22) yields k^+ and k^- from which one can calculate $k_q^{R\Delta}$ and $k_q^{S\Delta}$ if the concentration of quencher and k_0 are known. Non-linear fitting of eq. (23) leads to the determination of k_d, and this coupled with a measurement of the average quenching rate constant, *i.e.* $(k_q^{R\Delta} + k_q^{S\Delta})/2$ also yields the chiral quenching rate constants. Precisely which method is used depends on personal choice, but also to some extent of the nature of the system under study. For example, fitting of the *tanh* function requires either previous knowledge of $g_{lum}^{R}(\lambda)$ or accurate asymptotic values to be successful. The biexponential fitting procedure required in analysis of the time dependence of I(t) is subject to instabilities if k^+ and k^- are not very different.

2.2. Fluorescence Detected Circular Dichroism

In FDCD spectroscopy one varies the polarization of the excitation (absorption) beam between right (r) and left (ℓ) circular polarization while measuring the *total* emission intensity. When the excitation is right circularly polarized we denote the measured fluorescence intensity by F_r, and by F_ℓ when the excitation is left circularly polarized. Once again, we will be concerned with the determination of the difference between these two quantities, which in this case we will denote as ΔF [6]. In a "steady state" experiment we may express this differential quantity as follows

$$\Delta F(\lambda) = F_\ell(\lambda) - F_r(\lambda) \qquad (25)$$

In order to simplify some of the formalism, we will assume here that the sample of interest is composed of only one optically active emitting chromophore, although there may exist more than one absorbing species. In addition, we will not consider here the interesting case in which energy may transfer from the non-fluorescent absorber to the fluorophore. These and other cases have been considered [5,6,25,26]. Within these assumptions, we may write the following expressions for the fluorescence intensities

$$F_\ell(\lambda) = B\phi I_0 \left(\frac{A_\ell^f(\lambda)}{A_\ell(\lambda)} \right) [1 - 10^{-A_\ell(\lambda)}] \tag{26}$$

$$F_r(\lambda) = B\phi I_0 \left(\frac{A_r^f(\lambda)}{A_r(\lambda)} \right) [1 - 10^{-A_r(\lambda)}] \tag{27}$$

In these equations, B is an instrumental constant; ϕ is the probability that an absorbed photon leads to fluorescence; and $A^f(\lambda)$ and $A_\ell^f(\lambda)$ are, respectively, the absorbance of the fluorophore only, and the total absorbance under left circularly polarized excitation at wavelength λ. Note that we have assumed that ϕ is independent of excitation polarization and wavelength. The form of eqs. (26) and (27) display one of the problems in simple interpretation of FDCD results in terms of ordinary CD spectroscopy. On the front surface of the sample cell the intensity of the alternating circular polarizations will be equal, but if A_r does not equal A_ℓ then the intensities will change due to differential absorption. Just as in CPL measurements, one is concerned in this case with measurement of the differential signal and the total fluorescence intensity, $F(\lambda)$

$$F(\lambda) = \frac{B I_0 \phi A^f(\lambda)}{A(\lambda)} [1 - 10^{-A(\lambda)}] \tag{28}$$

where $A(\lambda)$ denotes the total absorbance of the sample, and $A^f(\lambda)$ is the total absorbance of the fluorophore.

For instrumental reasons, it is again useful to consider the ratio of $\Delta F(\lambda)$ to the average fluorescence intensity $F(\lambda)/2$

$$g_F(\lambda) = \frac{\Delta F(\lambda)}{(\frac{1}{2}) F(\lambda)} \tag{29}$$

Substituting from above and after considerable rearranging we obtain the following expression

$$g_F(\lambda) = \frac{2[g_{abs}^f(\lambda) - 2R(\lambda)]}{2 - g_{abs}^f(\lambda)R(\lambda)} \tag{30}$$

where

$$R(\lambda) = \frac{A_\ell(\lambda)[1 - 10^{-A_r(\lambda)}] - A_r(\lambda)[1 - 10^{-A_\ell(\lambda)}]}{A_\ell(\lambda)[1 - 10^{-A_r(\lambda)}] + A_r(\lambda)[1 - 10^{-A_\ell(\lambda)}]} \qquad (31)$$

and $g_{abs}^f(\lambda)$ is the absorption dissymmetry ratio of the fluorescent species. Experimentally, $R(\lambda)$ may be determined from the absorption and CD of the sample. Obviously, from the form of eq. (30), the CD spectrum of the fluorophore may be obtained from measurements of $g_F(\lambda)$ and $R(\lambda)$.

3. INSTRUMENTATION

3.1 CPL Instrumentation

Commercial instruments capable of measuring circularly polarized emission are not available, and, therefore, research groups involved in this measurement have all constructed their own instruments following similar designs. A schematic diagram for such an instrument following the specific design used in the laboratory at the University of Missouri-St. Louis is illustrated in Figure 3. This instrument is capable of measuring "steady state" CPL. As can be seen in this figure, excitation may be accomplished either with a laser or with a focused arc lamp. In this experimental setup, the laser beam is situated below the sample and emission light path, and is reflected vertically through the sample cuvette with a polished glass bottom and top. In addition, the polarization of the laser beam is aligned along the direction of emission detection (laboratory 2-axis). This geometry is used so that the luminescence detected at 90° will not be linearly (1 or 3) polarized. This alignment is not important when the emission is isotropic as described in Section 2.2, but is extremely important for slowly rotating or oriented systems in which the emission could be linearly polarized. The nature of this artifact problem is presented below.

CPL instrumentation is identical to ordinary fluorescence spectrometers with the addition of a circular analyzer between the emitting sample and the emission monochromator. In all existing instruments the circular analyzer is composed of a photo-elastic (or elasto-optic) modulator (PEM) followed by a high quality linear polarizer. PEM's that operate around 50kHz are commercially available (Hinds Int.) and in this application act as dynamic quarter-wave modulators. During one half cycle of the modulation, left circularly polarized light is converted to linearly polarized light which then passes through the linear polarizer, and during the other half cycle, right circularly polarized light is passed on to the monochromator. In this setup the monochromator sees light with only one polarization throughout the

modulator cycle. This is a necessity due to the polarization sensitivity of monochromators. It is obviously necessary to minimize sources of depolarization. Thus, for example, one normally places no optical elements between the sample cuvette and the PEM. These precautions are especially important in CPL measurements, since, ordinarily, the difference in intensities between the left and right circularly polarized emitted light are 10 to 100 times less than that detected in linearly polarized luminescence measurements.
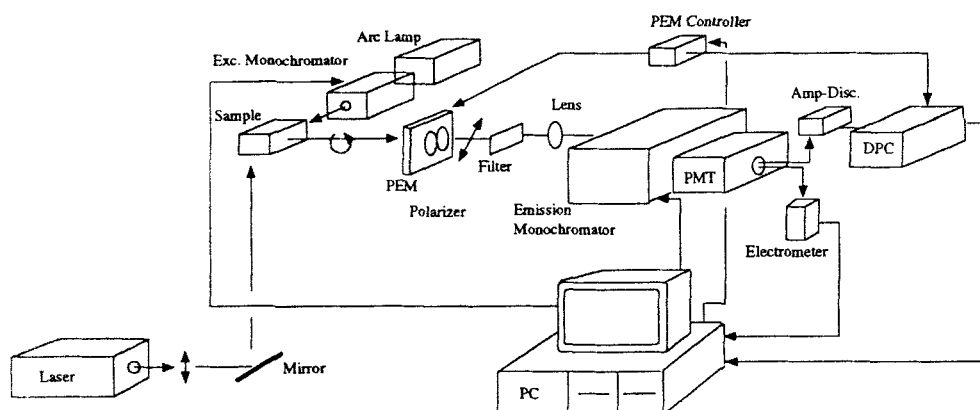
Figure 2: Schematic diagram of a CPL spectrometer. (See text)

The major source of artifacts in CPL measurements is the passing of linearly polarized light through the very slightly birefringent PEM [11]. Even though this effect is small, it may lead to a signal of comparable magnitude to many true CPL signals. Some success has been obtained in rotating the PEM and linear polarizer such that the birefringent axis of the PEM is parallel to the plane of polarization of the emitted light; however, it is our experience that one can only be sure of the accuracy of this measurement by ensuring that the emitted light is unpolarized. In order for the PEM to act as a quarter-wave device over the entire UV-visible spectral region, it must be driven at the appropriate amplitude corresponding to the detection wavelength. This may be accomplished either by coupling the wavelength drive of the emission monochromator to the PEM controller, or (as accomplished in our setup) by employing an inexpensive D/A interface board, and setting the appropriate voltage for the PEM controller. For the instrument described here, this voltage was determined by fitting the output voltages obtained from different settings of the front control dial of the PEM to a linear function of wavelength.

After passing through the PEM and linear polarizer, the emitted light travels through an appropriate filter to eliminate scattered excitation and other stray light, and a suitable lens is used to focus the beam onto the entrance slits of the emission monochromator. Detection is accomplished by a thermoelectrically cooled photomultiplier tube (PMT) operating in photon-counting mode. As shown in Figure 2, the output of the PMT can either be directed to an electrometer for a direct measurement of relative total luminescence in arbitrary units, or to an amplifier/discriminator which outputs photo-pulses to a custom-built differential photon counter (DPC). The DPC unit used in this setup was designed and constructed at the University of Leiden, The Netherlands, under the supervision of H. P. J. M. Dekkers [27]. In this device the leading edge of the 50 kHz reference signal from the PEM controller is used to define a time window centered on the peak of the modulation reference signal. During the "open" time of this variable time window, photopulses are directed into two separate counters. One of the counters counts every pulse that passes through the gate, and the other (up/down) counter adds the photopulses that enter the gate when left circularly polarized light is passing through the PEM and subtracts the pulses when right circularly polarized light intensity is being measured. Thus one counter contains a number proportional to I, and the other counter contains a number proportional to ΔI. These two quantities can be divided to yield $2g_{lum}$.

Perhaps the most difficult aspect of this gated-counter technique is the requirement that the time windows for left and right circular polarization detection must be positioned properly and must be exactly equal in width. The reader is referred to reference [27] for a more detailed discussion of this problem. In the experimental setup described here, the computer also steps the excitation and emission monochromator, monitors laser intensity, and stores and displays g_{lum} values and total emission signals as a function of wavelength. These functions are accomplished using commercially available digital and analog input/output boards. All of these activities are controlled by a computer program specifically written for this instrument.

3.1.1 Measurement Statistics and Standards

Prior to the development of high speed counters and associated electronics, CPL was routinely detected through lock-in detection of an analog PMT signal phase-referenced to the modulator frequency [28]. This measurement procedure suffers from two major drawbacks. First, for very low light levels, the lock-in detection system is not very stable due to ground-loop noise and related electronic problems. A second difficulty is that, using this method of detection, only a signal proportional to ΔI is obtained, and a more or less independent measurement must also be performed in order to obtain a signal proportional to the total emission intensity. A calibration or standard must then be run relating these two measurements in order to get the appropriate proportionality factor such that an

accurate value for g_{lum} can be determined. Both of these problems are addressed in the more recent digital differential photon-counting method. The photon counting detection system is very stable, and experiments lasting for several days have been performed in our laboratory with no noticeable drift or loss of precision or accuracy. Since both I and ΔI are determined simultaneously, g_{lum} is obtained directly without the need of a proportionality factor.

Even though this polarization sensitive spectrometer is, indeed, quite stable and reliable, it is still important to perform routine checks of the instrument. In our laboratory we accomplish this task by measuring g_{lum} using an *achiral* light source to ensure that a value of 0 is obtained, and by the use of a freshly prepared sample of the commercially available chiral shift reagent, Eu(3-trifluoroacetyl-d-camphorato = facam)$_3$, in dry DMSO. This species can be excited at 350 nm with arc-lamp excitation or by use of the 466 nm line of an Ar ion laser. The emission is reasonably intense in the spectral region from 575 - 635 nm, both positive and negative values of ΔI are observed, and g_{lum} varies from -0.78 at 595 nm to +0.072 at 613 nm [11]. Alternatively, Steinberg has described a procedure for calibrating a CPL spectrometer in which a quarter-wave plate and optical flat are used to generate continuous degrees of elliptical polarization [29]. We have found that the simpler procedure using Eu(facam)$_3$ as a standard is quite satisfactory. In the instrument described above, the only adjustment that we have found necessary is the positioning of the time windows. These have been observed to shift slightly when other electronic adjustments are made, such as in pulse shape, discrimination, *etc.*

Another advantage of the differential photon counting method of detection is that the measurement uncertainties can be estimated directly from photon statistics. Schippers [11] has demonstrated that the standard deviation, σ, of g_{lum} detected by the differential photon counting method can be related through Poisson statistics to the total number of photon counts, N, by the simple formula

$$\sigma = \sqrt{\frac{2}{N}} \tag{32}$$

Thus, in order to measure g_{lum} with a standard deviation of 1×10^{-4}, a total of 2×10^8 photon pulses must be counted. One can easily see that highly luminescent systems with transitions associated with large g_{lum} values can be studied quite rapidly with high precision. Low concentrations of weakly luminescent systems with small g_{lum} values require long collection times for precise measurements. In our instrument we record a CPL spectrum in which the standard deviation in the measurement of g_{lum} at any particular wavelength is proportional to the total emitted intensity. The procedure is essentially equivalent to scanning the excitation wavelength at a constant rate. This is accomplished by first recording and saving a total emission spectrum over the transition of interest, deciding upon

the standard deviation desired for the peak of maximum intensity, and scaling the remainder of the spectral readings by the total emission. Thus, at a wavelength where the intensity is one half the value of the maximum intensity, only one half as many photons are counted, and the error in g_{lum} is correspondingly higher. Alternatively, one could measure g_{lum} with equal uncertainty at all wavelengths by counting the same number of photons at each wavelength position, but this procedure is not practicable when recording an entire spectrum. This is because most of the acquisition time would be spent at wavelengths where the intensity is very low, e.g. in the wings of the transition.

3.2. FDCD Instrumentation

Instrumentation for the measurement of FDCD have been based upon modifications of CD spectrometers. The very first instruments simply placed a filter and detector at 90° to the absorption/transmission path, and directed the signal from the detector into the electronics of the CD instrument. This type of instrument gave reasonably good results for isotropic fluorescence systems, but, just as in CPL measurements, artifacts due to the presence of linearly polarized fluorescence in photoselected systems have led to a number of instrument modifications. A schematic diagram of an FDCD instrument following the basic design of Lamos and Turner [30] is presented in Figure 3.
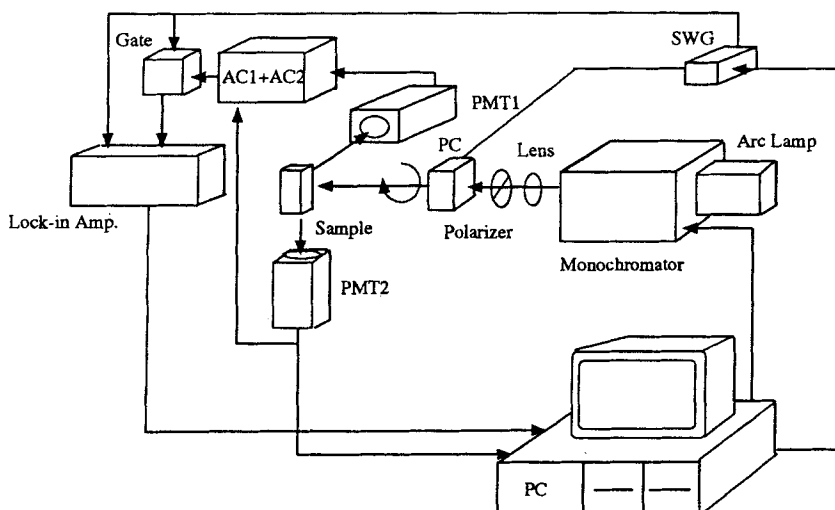
Figure 3: Schematic diagram of an FDCD instrument. (See text)

As displayed in this figure, the output of a xenon lamp is passed through a monochromator, focused, and sent though a high quality linear polarizer and Pockels cell (PC) before entering the sample cuvette. A computer controls the stepping of the monochromator and the square wave generator (SWG) for the Pockels cell. Two separate photomultiplier detectors (PMT1 and PMT2), oriented perpendicular to each other (along the **1** and **2** axis) and to the excitation beam direction (**3** axis), are used to minimize photoselection effects [31]. When the two AC voltages from the PMT's are added (AC1 + AC2) the dependence of the output on linear polarization (in particular, on artifacts due to imperfections in the PC) are significantly reduced. A reference signal from the SWG is used to control an electronic gate which is closed when the PC is switching incident circular polarizations. The final signal is input to a lock-in amplifier which is phase referenced to the SWG. Instrument control and data analysis are provided by a dedicated computer.

A calibration of an FDCD instrument has been described by Lobenstein *et al.* [32] in which a cell containing 10-*d*-camphorsulfonic acid (CSA) is placed in the excitation beam in front of a sample cell containing achiral sodium fluorescein. All incident photons not absorbed by the CSA are assumed to be absorbed by the fluorescein, and therefore, the fluorescein emission is a measure of the CD of CSA. These authors adjust their instrument to give the known ellipticity (304 mdeg at 291 nm for a 1 cm cell containing 1 mg/ml of CSA).

4. APPLICATIONS OF CIRCULARLY POLARIZED LUMINESCENCE

CPL measurements have been applied to a fairly wide range of optically active organic, inorganic and biochemical systems [2-4]. Although there has been a small number of CPL measurements from pure and doped solids, and frozen matrices, the vast majority of applications have involved liquid solutions. Applications of CPL to solids is limited by the requirement that the crystal structure must be at least uniaxial in order to avoid depolarization of the circularly polarized emitted light. CPL from chiral molecules imbedded in achiral frozen matrices are limited by artifacts due to linear polarization as described above. Some success has been reported by Blok *et al.* [33], but these experiments are very difficult due to the care one must take in controlling linear polarization, and in eliminating birefringence of cryostat windows *etc.* These problems are not insurmountable, and the advantages one gets with increased emission intensity at low temperatures warrant further efforts in this area. In this section we will be concerned almost exclusively with CPL from liquid solutions.

Before discussing some of specific uses of CPL spectroscopy, it is relevant to review some of the more important aspects of luminescence techniques, since it is the combination of the attributes of optical activity and luminescence

measurements that results in the special sensitivity and selectivity of CPL spectroscopy.

1. CPL is uniquely suited for the study of emissive transitions that do not terminate in a thermally accessible ground state. Obviously, these states cannot be studied by ordinary CD or absorption methods.

2. In many instances it is possible to observe CPL from excited states that are only weakly accessible via direct absorption processes from the ground electronic state, and, therefore, only weakly observable in CD. This is accomplished by populating the emitting state indirectly, either by intermolecular or intramolecular radiationless energy transfer, or by efficient radiationless decay from a higher excited state that has a larger absorption coefficient.

3. In liquid solutions it is usually the situation that emission, if present, is observed from only one excited state. This is in contrast to absorption experiments where overlapping bands are usually observed. In the development and application of correlations between observed spectra and molecular structure, this selectivity may be extremely important.

4. In large molecular systems, such as proteins, it is quite common to have a number of electronically similar chromophores. Thus, CD measurements involving these chromophores necessarily provide information about the average structure. In CPL studies, one is often concerned with only a very small number of emitting chromophores allowing for the opportunity of probing specific aspects of local molecular chiral structure.

5. Since, as discussed above, the orientational distribution of molecules that one observes in emission may be different than in absorption, CPL also provides information concerning the excited-state dynamics and energetics from the initial absorption event to emission of the circularly polarized photon.

For purposes of discussion, we divide applications of CPL spectroscopy into three categories; (1) efforts to develop reliable CPL "sector rules", (2) use of comparative CD and CPL studies to probe excited state geometry changes, and (3) the specific use of the selectivity and sensitivity of CPL to probe details of molecular and electronic structure, and dynamics. Since in this book we are primarily concerned with "analytical" applications of these chiroptical methods, we will emphasize here the last of these categories.

4.1. CPL Sector Rules

Just as in CD spectroscopy, one of the goals in CPL studies is the development of reliable so-called "sector rules" for selected chromophores. The objective of this work is the prediction of chiral structure from the sign and magnitude of the measured CPL. In the few cases that have been investigated, the primary interest has been in using these rules to determine specific geometry changes. For example, by measuring the CD of the $n \rightarrow \pi^*$ transitions for a number of rigid β,γ-enones, Schippers and Dekkers [34] developed a "chirality rule"

relating the angle between the C=O bond and the C_β=C_γ bond, to the position of the olefinic carbon atom and the angle between the magnetic dipole moment and the C=O bond. This rule was then applied to CPL studies of five rigid β,γ-enones for which significant differences g_{lum} and g_{abs} were measured [35]. The chirality rule was used to determine specific out-of-plane displacements of the carbonyl oxygen atom in the $^1n\pi^*$ excited state. Similar studies have been performed on substituted mono- and diketones [36,37].

There also has been one successful attempt at determining the absolute configuration through analysis of exciton coupling. This was reported by Barnett, Drake and Mason in a study of calycanthine in which CPL in the $\pi \to \pi^*$ spectral region was interpreted in terms of aniline dimers [38]. These authors compared their result to the previously published crystal structure.

4.2. Comparative CD and CPL studies

CPL and CD are based upon similar aspects of molecular structure. It is important to realize, however, that, even if the same states are involved, these measurements do not usually supply redundant information. From the Franck-Condon principle, CPL is a probe of excited state geometry, and CD is a probe of ground state geometry. CPL measurements have some advantages over the measurement of CD, as well as some inherent limitations. The most serious limitation is, quite obviously, that the optically active molecule under study must contain a luminescent chromophore with a reasonable quantum yield. Although this severely limits the range of possible applications of CPL, it does result in a *specificity* and *selectivity* that is not present in CD or absorption experiments.

As illustrated in a more quantitative way in the previous section, comparative CPL/CD studies can yield information concerning geometry differences between ground and excited states. In some cases this might be the major focus of a particular study; in other cases, the presence or lack of known geometry changes associated with well characterized chromophores may be used to probe aspects of molecular flexibility. A good example of this latter kind of study has been reported by Gafni [39] in a study of reduced nicotinamide adenine dinucleotide (NADH) in solution and bound to several dehydrogenase systems. In these experiments differences in the CPL from the various dehydrogenases were interpreted in terms of differences in the rigidity of the enzyme-coenzyme complexes.

4.3. CPL as a Selective Probe of Chiral Structure and Dynamics

Rather than presenting a review of all the possible applications of CPL spectroscopy as a selective probe of chiral structure, we will focus our discussion in this section on three specific experiments that, we believe, illustrate the kinds of unique information that may be obtained from this technique. These three studies will all be concerned with CPL from optically active lanthanide complexes of approximate D_3 symmetry. Almost all of these particular CPL measurements have

involved Tb(III) and Eu(III), since these are the most luminescent of the lanthanide series. Approximate energy level diagrams for the lowest energy states for Eu(III), Dy(III), and Tb(III) free ions are given in Figure 4 where each state has been
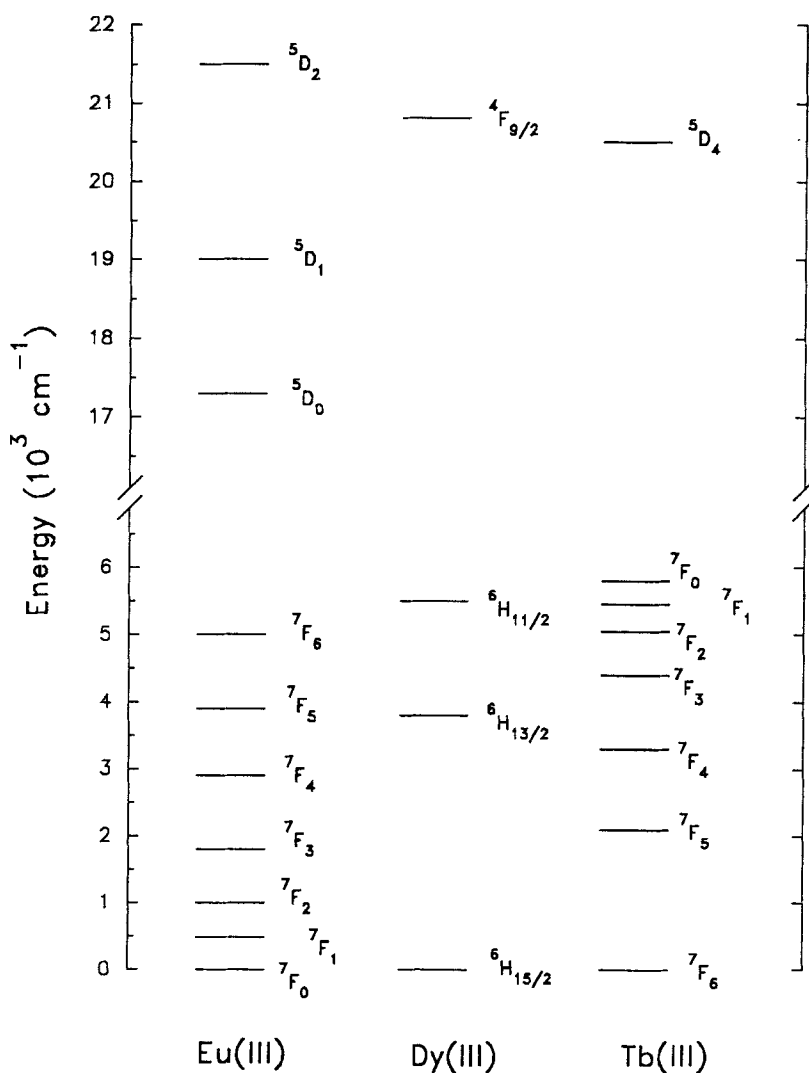
Figure 4: Schematic energy level diagram for Eu(III), Dy(III), and Tb(III).

labeled according to its dominant $^{2S+1}L_J$ Russel-Saunders component. Transitions between these states are intraconfigurational ($f \leftrightarrow f$), and, therefore, formally forbidden in the free ion. The emissive state for Tb(III) is the $^5D_4$ state, and for Eu(III) it is the $^5D_0$ level. For lanthanide (III) ions it has been shown that transitions that obey magnetic dipole selection rules, *i.e.* $\Delta J = \pm 1$ often possess quite large values for $|g_{lum}|$ (> 0.01) [40].

For the case of Tb(III) the most intense emission is the $^5D_4 \rightarrow {}^7F_5$ transition centered at approximately 543 nm. Since this transition satisfies the selection rule given above, it would also be expected to possess large g_{lum} values. Eu(III), in contrast to Tb(III), has a non-degenerate emitting state (J = 0). The most intense transition for this ion is usually at 612 nm and corresponds to a transition to the $^7F_2$ state, however $|g_{lum}|$ measured for this transition may be quite small (< 0.006). For CPL measurements, the transition located at approximately 594 nm ($^5D_0 \rightarrow {}^7F_1$) (which is normally much weaker) may be of more interest since this transition obeys magnetic dipole selection rules. Whereas for Tb(III) many different crystal field components may be observed in the CPL spectrum of the $^5D_4 \rightarrow {}^7F_5$ transition, the transitions of Eu(III) are much simpler due to the reduced degeneracy of the terms involved. Thus Tb(III) is often more useful for monitoring structural changes, and Eu(III) is a potential target for more quantitative attempts at comparing calculated, and experimental intensities and splittings.

Large g_{lum} values are indicative of large discrimination of these optically active species between left and right circularly polarized light. This can be seen, for example, by rearranging the definition of g_{abs} [see eq. (3)] to solve for the *relative* absorption of the two polarizations.

$$\frac{\varepsilon_L}{\varepsilon_R} = \frac{1 + (\frac{1}{2})g_{abs}}{1 - (\frac{1}{2})g_{abs}} \tag{33}$$

Using the value of 0.24 which has been measured for the absorptive transition $^7F_0 \rightarrow {}^5D_1$ of Eu(III) results in a relative absorption of 1.27 (approximately 5:4). This 25% preference for absorption of left circularly polarized versus right is large in comparison to any similar analysis for an optically active organic molecule, and illustrates the unique sensitivity of these transitions to chiral environment. Several values approaching 50% difference in absorption or emission selectivity have been determined in our laboratory for various optically active lanthanide complexes.

4.3.1. CPL as a Probe of Solution Structure

The increasing use of lanthanide complexes as luminescent probes and as NMR shift reagents has led to a number of studies aimed at the elucidation of the solution structure and dynamics of these species. Several of these studies have

been concerned with so-called *mixed-ligand* lanthanide systems, and especially with systems in which one or more of the ligands is optically active [41-43]. Results for one such system are presented in Figures 5A and 5B. We have chosen to plot I (lower curve) and ΔI (upper curve) in these (and subsequent) figures, even though, as described above, in our instrument we actually measure I and g_{lum}. The quantities are related through eq. (2). The spectra presented are for an aqueous solution of Eu(III) in which two equivalents of 2,6-pyridine-dicarboxylate (DPA) and 1 equivalent of L-malate (L-Mal) have been added [44]. Figure 5A corresponds to excitation with plane polarized light, and Figure 5B to a situation in which the excitation is circularly polarized. The spectral region displayed corresponds to the $^5D_0 \rightarrow {}^7F_{0,1,2}$ transitions of Eu(III).
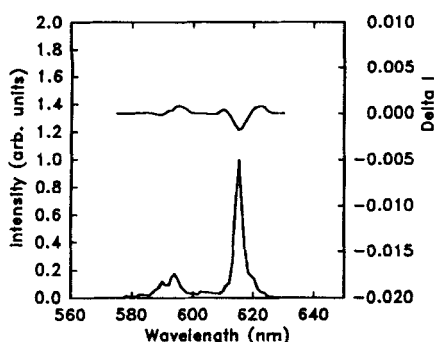
Figure 5A: CPL (upper curve) and TL (lower curve) for a solution of Eu(III), DPA, and L-Mal in the ratio of 1:2:1.5 using plane polarized 476.5 nm excitation.
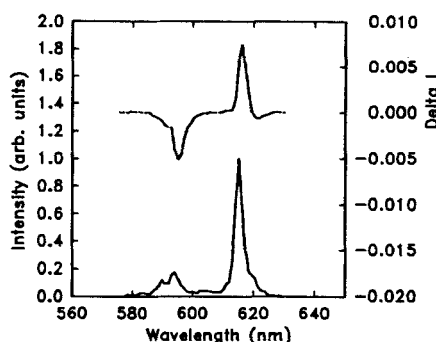
Figure 5B: CPL (upper curve) and TL (lower curve) for a solution of Eu(III), DPA, and L-Mal in the ratio of 1:2:1.5 using circularly polarized 476.5 nm excitation.

If only one emitting species contributed to the observed luminescence from this sample, then the lineshape of the total luminescence (TL) and the CPL should be independent of excitation polarization. That this is not the case for this system is most evident in examination of the CPL in the two figures. Obviously, in this system, preparation of solutions with a 1:2:1.5 ratio of metal: DPA:L-Mal do *not* yield complexes solely with this stoichiometry.

Further evidence of this conclusion may be obtained through examination of the data displayed in Figure 6. In this figure we plot the measured I and ΔI for a 1:3.1 solution of Eu(III):DPA. Comparison of the CPL data given in Figure 6 and Figure 5B show that they are virtually identical. This data clearly indicates that, in this system, most of the *total* emission originates from *racemic*-Eu(DPA)$_3^{3-}$, whereas the weak CPL seen in Figure 5A originates from an equilibrium distribution of chiral complexes, involving L-malate, of unknown geometry and stoichiometry. One major point of this work is that simply measuring I and ΔI for

solutions, in which the distribution of chiral species is undetermined, as in Figure 5A and 5B, is liable to misinterpretation.
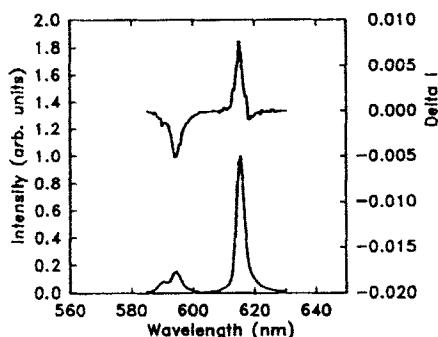
Figure 6: CPL (upper curve) and TL (lower curve) for *racemic*-Eu(DPA)$_3^{3-}$ using circularly polarized 476.5 nm excitation.

This analysis was made possible by our ability to measure CPL from *racemic* solutions of lanthanide complexes through use of circularly polarized excitation [12,45-47]. The varied lifetime of the lanthanide (III) ions allow for some insight concerning the lability of complexes of this type. For example, we have shown that although no CPL is detected in the luminescence from tris-terdentate complexes of Tb(III) and Eu(III) with oxydiacetate (ODA), CPL is observed from Dy(DPA)$_3^{3-}$, indicating that, indeed, this complex is D$_3$ in aqueous solution, but that only for the short lived Dy(III) ion ($\tau \approx 20$ μsec) is the photoprepared enantiomerically-enriched excited state maintained throughout the emission lifetime [45].

Measurements of this type are not restricted to the high-symmetry complexes discussed above. CPL has been observable in a fairly wide variety of solution complexes containing chiral ligands, although in most cases the structures of the emitting species are not well understood. The use of circularly polarized excitation, in concert with measurement of CPL, can yield information concerning the stability and structure of lower symmetry complexes with achiral ligands. For example, in Figure 7 we show spectra for a solution of Eu(III) with triethylenetetraaaminehexa-acetic acid (TTHA) [48]. The fact that we observe CPL from this system indicates that a chiral structure is formed, and that this structure is stable on the emission time-scale. Displayed in this figure is the spectral region corresponding to the $^5D_0$ $\to$ $^7F_1$ transition of Eu(III).
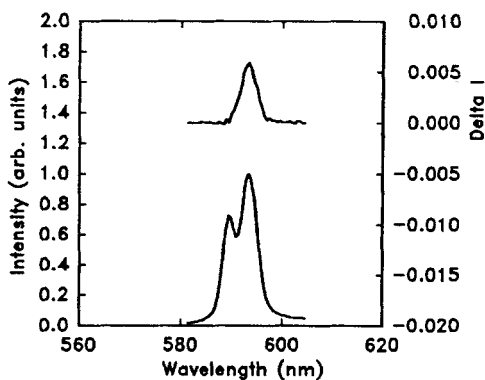
Figure 7: CPL (upper curve) and TL (lower curve) for a 1:1 complex of Eu(III) and TTHA at pH=7.0.

As one last example in this section, we plot in Figure 8 CPL and total emission spectra for Tb(III) as a substitutional replacement for Ca(II) in the protein trypsin [49]. The spectral region displayed in this figure corresponds to the $^5D_4 \rightarrow$ $^7F_5$ transition of Tb(III). CPL from Tb(III) and Eu(III) have been used to probe
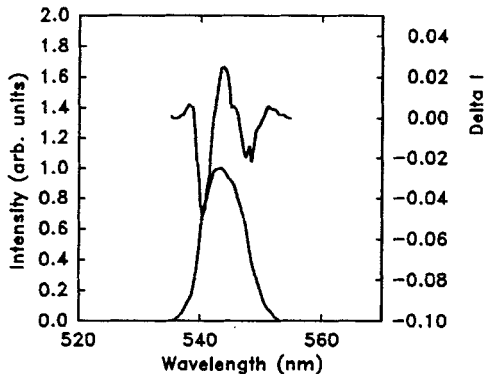
Figure 8: CPL (upper curve) and TL (lower curve) for a 10 µM solution of Tb(III) bound to trypsin.

conformational changes in calcium-binding and iron-binding proteins [50-52]. It has been shown, for example, that the CPL spectra for EF-hand proteins are all very similar, but that the sign and splitting pattern for other protein classes are

much different. These experiments have also been used to monitor structural changes as equivalents of metal ions are added to very dilute protein solutions.

4.3.2. Determination of Dissymmetry ratios

From eqs. (11), (13) and (14) from section 2.1, one can see that the use of CPL spectroscopy in combination with CD measurements, can lead to the determination of dissymmetry ratios for selected transitions of chiral species, even if the enantiomers can not be obtained enantiomerically pure. These three equations correspond to three separate measurements, and depend on the enantiomeric excess in the ground and excited states, $g_{lum}^S(\lambda)$, and $g_{lum}^S(\lambda')$. Under the assumption that the enantiomeric excess is the same in the ground and excited states, $\eta_g = \eta_n \equiv \eta$, the three equations contain only three unknowns, and, therefore, they may all be determined. To date, studies of this type have been focused on the tris-terdentate D_3 lanthanide (III) complexes described above. This work is based upon the disturbance of the racemic $\Delta \leftrightarrow \Lambda$ equilibrium through the addition of non-coordinating chiral "environment" compounds [53]. Thus, measurement of CPL from an unperturbed racemic solution, and measurement of CD and CPL from a solution in which the racemic equilibrium has been perturbed, yield not only the extent of perturbation, but also the dissymmetry ratios for the pure enantiomers, even though they have not been resolved. Obviously, it is important in this kind of study to ensure that the addition of a perturbing species does not change the nature of the emitting species, and simply results in a equilibrium perturbation. The fact that we can measure CPL from the racemic solution using circularly polarized excitation allows us to compare the spectra of the perturbed solution to that of the racemic solution. This is illustrated in Figures 9A and 9B for aqueous $Dy(DPA)_3^{3-}$.
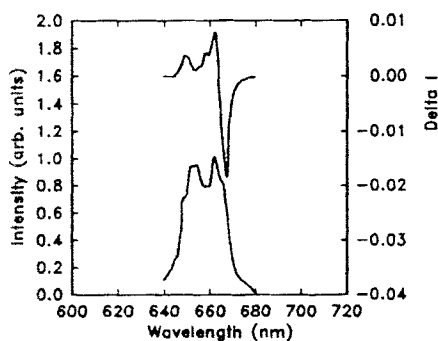
Figure 9A: CPL (upper curve) and TL (lower curve) for 0.015 M $Dy(DPA)_3^{3-}$ using circularly polarized 457.9 nm excitation.
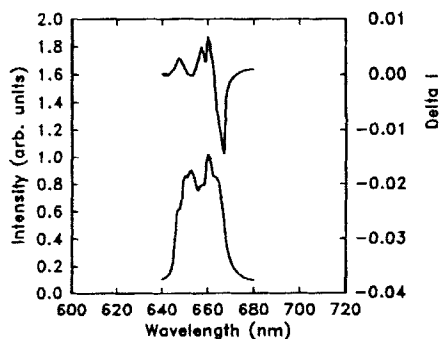
Figure 9B: CPL (upper curve) and TL (lower curve) for 0.015 M $Dy(DPA)_3^{3-}$ containing 0.075 M L-histidine using plane polarized 457.9 nm excitation.

Figure 9B corresponds to a solution which contains 0.075 M L-histidine. The spectral region shown in these figures corresponds to the $^4F_{9/2} \rightarrow {}^6H_{11/2}$ transition of Dy(III) As can be seen, these plots are almost identical, indicating that the addition of L-histidine has not significantly perturbed the structure of the $Dy(DPA)_3^{3-}$ complex [47]. Although not stated explicitly in the previous discussion, it should be noted that, in order to apply the analysis described above, g_{abs} must be measured at the same wavelength (λ') used for circularly polarized excitation of the racemic mixture. In Figure 10, we show the measured CD for this complex in the spectral region overlapping the excitation wavelength (457.9 nm) used to excite the samples given in Figure 9A and 9B. The spectral region shown corresponds to the $^4H_{15/2} \rightarrow {}^6F_{15/2}$ transition of Dy(III). From the values of the dissymmetry ratios obtained from these figures at the appropriate wavelengths, and using the three equations derived above, one obtains the result that, when 0.075 M L-Histidine is added to the initially racemic solution of $Dy(DPA)_3^{3-}$, the enantiomeric excess generated is approximately 4% [47].
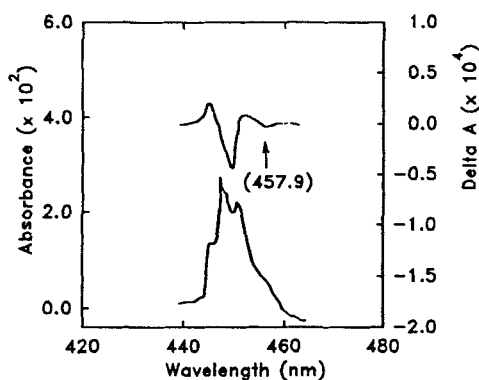
Figure 10: CD (upper curve) and absorption (lower curve) for a 0.015 M $Dy(DPA)_3^{3-}$ containing 0.075 M L-histidine.

Furthermore, using the procedure described above, one obtains the following results; $g_{abs}^{\Lambda}(457.9 \text{ nm}) = -0.086$, $g_{abs}^{\Lambda}(450.9 \text{ nm}) = -0.41$, and $g_{lum}^{\Lambda}(664.5 \text{ nm}) = -0.046$. The identity of the specific enantiomer in excess (in this case the Λ enantiomer) has been determined by comparison of CPL spectra for a similarly perturbed $Eu(DPA)_3^{3-}$ species and the solid state CPL and CD of Λ-$Eu(ODA)_3^{3-}$ [54,55]. The most difficult measurement of the three given above is the CD of the lanthanide complex at the excitation wavelength. This is due to the fact that the extinction

coefficients for these f ↔ f transitions are usually less than 10, and often less than 1. Under the reasonable assumption that the equilibrium perturbation caused by L-histidine (and other chiral agents) is the same for the different lanthanides, one can use the value of the enantiomeric excess obtained from the Dy(III) measurements for the other lanthanide complexes. In this way one may determine dissymmetry values for other lanthanide (III) transitions [56]. These experimental results, for these relatively high-symmetry lanthanide complexes, serve as useful models for the calculation or parameterization of rare-earth optical activity.

4.3.3. Enantioselective Quenching

In the previous section, we have described experiments involving racemic solutions in which a *non-racemic* emitting state was prepared by either enantioselective (circularly polarized) excitation or by disturbance of the racemic equilibrium by an added chiral substance. A third possibility, which has been exploited recently, is the generation of an optically enriched excited state through enantioselective quenching by an added chiral species [14,15,17-24,57]. The observation of chiral (or enantioselective) quenching was first observed in steady-state experiments [57], but the real proof that these systems involve chiral discrimination in quenching of the emitting state (and not a simple shift in the racemic equilibrium) are the lack of any measurable CD, and results from the time-dependent CPL experiments. In Figure 11 we show the time dependence of the total emission intensity and g_{lum}(543 nm) for a solution of Tb(DPA)$_3^{3-}$ in methanol quenched by Δ-(-)-Ru(phen)$_3^{2+}$. These data show that immediately following an excitation pulse ($t = 0$), g_{lum} equals 0, and then increases in magnitude during the time decay of the emission from Tb(DPA)$_3^{3-}$, confirming that one enantiomer is quenched more rapidly than the other. As seen in eq. (25) the time-dependence of g_{lum} should be described by a *tanh* function. The solid line in Figure 11 describes a fit to eq. (25) in which the unknown parameters are k_d and g_{lum}^{Δ}. It is also possible to fit the decay of the total luminescence to a biexponential function and determine the two diastereomeric decay constants.

The measurement of time-resolved CPL is a very recent advancement, and the number of systems which have been studied by this technique is relatively small. The research groups of Dekkers and Riehl have concentrated almost all of their published efforts on detailed examination of the Ln(DPA)$_3^{3-}$ complexes using Ru(phen)$_3^{2+}$ as the chiral quencher [17,19,21-23,53]. Richardson and coworkers have been applying the technique to a number of other interesting optically active quenchers [15,18,20,24]. The emphasis in their work has been on developing insight into the influences of ligand shape and configuration on the chiral discrimination. The degree of enantioselectivity in quenching is given by the quantity E_q which is defined in terms of the diastereomeric decay constants as follows
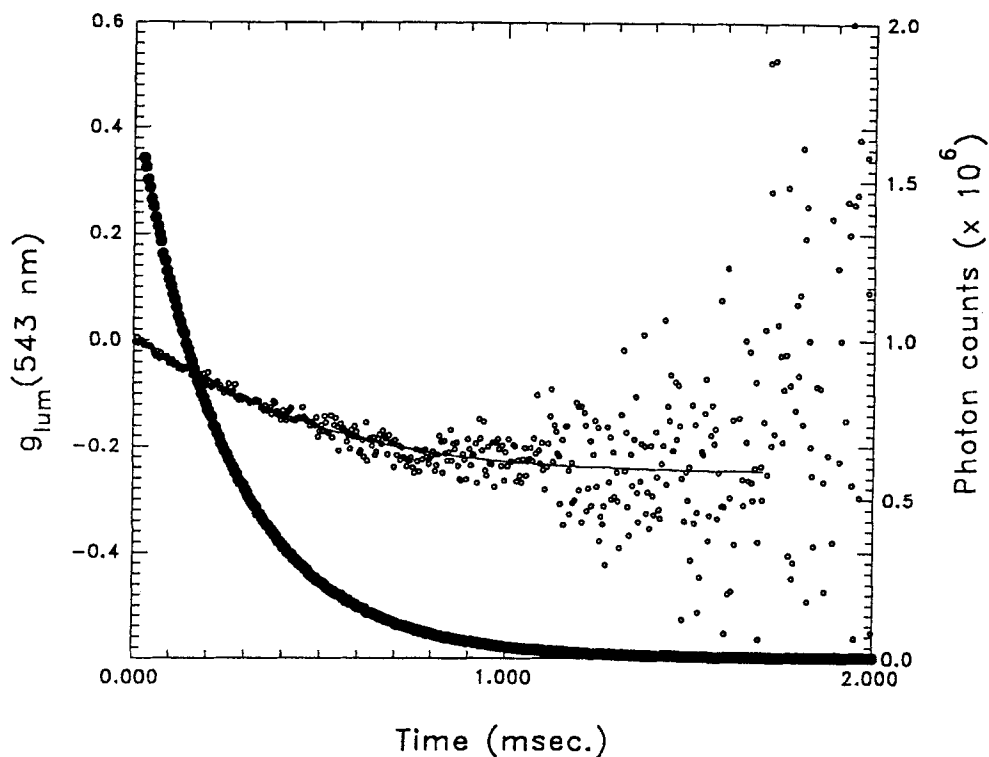
Figure 11: Time dependence of the intensity, measured in photon counts (filled circles), and $g_{lum}(543$ nm) (open circles) for a solution of 0.7 mM $Tb(DPA)_3{}^{3-}$ containing 5.2μM Δ-(-)-$Ru(phen)_3{}^{2+}$.

$$E_q = \frac{k_q^+ - k_q^-}{k_q^+ + k_q^-}$$

(34)

To date, the largest observed magnitude for E_q is -0.60. This has been reported by Metcalf *et al.* on the quenching of $Eu(DPA)_3{}^{3-}$ by Δ-Co(trans-1R,2R-1,2-diamino-cyclo-hexane)$_3{}^{3+}$ in water [24].

5. APPLICATIONS OF FLUORESCENCE DETECTED CIRCULAR DICHROISM

Most of the applications of FDCD that have been reported have been concerned with the use of this technique as a probe of specific aspects of the chiral environment of biochemical systems. Although, as indicated above, this technique is basically a probe of the molecular ground state, it uses the sensitivity and selectivity of luminescence measurements. FDCD has also been applied to highly scattering and optically dense samples for which polarized absorption measurements are not possible [58,59]. Some of the more recent applications of this technique include its use for on-column detection of chiral molecules in capillary electrophoresis [60], and in a modified phase-modulation spectrofluoremeter [61,62]. The purpose of the latter application is to develop a procedure to determine the distribution of chiral molecules in multicomponent samples [62].

To illustrate the kind of information that can be obtained from FDCD we will briefly describe here some published results on the binding of the fluorescent drug ethidium to synthetic and natural nucleic acid polymers [63-65]. Ethidium is known to bind to nucleic acids with an induced CD, as well as with an enhancement of fluorescence. Lobos, Lobenstein and Turner have shown that the FDCD spectrum of ethidium bound to polynucleotides (including tRNA and DNA) is composed of three bands at approximately 275, 320 and 380 nm, and that all three bands are sensitive to the base sequence at the ethidium binding site [63]. One of the advantages of FDCD over CPL in this kind of study is, in fact, that three bands are seen, allowing for more sensitive monitoring of structural modifications. In a typical luminescence measurement the emission spectra is often composed of only one band. By measurement of the FDCD [and calculated CD spectra, see eqs. (30) and (31)] from ethidium, these authors have been able to show that the pyrimidine-purine dimers are good models for pyrimidine-purine polymers. Furthermore, they have been able to apply their model study to DNA, and have even been able to measure FDCD from ethidium bound to DNA from complex *in vitro* and *in vivo* systems [64].

6. DISCUSSION

The increased stability and sensitivity of modern instrumentation for the measurement of CPL has opened the door for many future applications of this technique to probe local chiral structure. The improved stability of the instrumentation allows for much longer measurement times, and, consequently, weaker emitters may be studied. Additionally, the ability to work at very low concentrations of sample is an obviously important characteristic in studies of biomolecules that are only available in small quantities. With the availability of high quality strain-free objective lenses, it should even be possible to detect circular

polarization in the emission from microscopic samples. As mentioned above, FDCD has already been measured from *in vivo* samples, and there is no reason why CPL studies could not be carried out on similar systems.

The most exciting development in the last several years in the CPL field has been the work of F. S. Richardson and H. P. J. M. Dekkers and their students on the design and construction of instruments capable of measuring *time-resolved* CPL. The design of these instruments is such that a series of high-speed counters are used to accumulate values for I and ΔI as a function of time after an initial excitation pulse. The time scale that one is able to probe in time resolved CPL studies depends to a large extent on experimental design and on the nature of the emitting species. For example, the emitting state lifetime of Tb(III) is approximately 2 msec, and does not vary appreciably with coordination environment, and so processes that occur on this time scale may be studied. Eu(III), Sm(III), and Dy(III) have progressively shorter lifetimes, so that, in principle, molecular or energetic events occurring in the 20 μsec to 3 msec time region may be studied by simply changing the metal ion. It should be restated, however, that these different ions have quite different spectroscopic characteristics, and it may be that no suitable transition is available in the accessible spectral region. Time-resolved CPL experiments involving biochemical systems have not as yet been performed; however, these experiments have the potential of yielding interesting results concerning stereochemical changes within (or near) metal ion binding sites occurring around the millisecond time scale.

The most recent research efforts in FDCD have been concerned with developing analytical methods that are sensitive to fluorescent chiral systems. No doubt this will continue to be a driving force for experimental and conceptual advances in this field. One of the most interesting aspects of the technical improvements described in reference [21] for the measurement of time-resolved CPL is the fact that, by employing randomly spaced (in time) excitation pulses, the time scale for measurement has been decoupled from the 50 kHz PEM modulation cycle. In principle, this same approach could be used in FDCD measurements. Thus, it should be possible, for example, to measure time-resolved FDCD from fairly long-lived chromophores such as lanthanide (III) ions.

The fact that CPL and FDCD instruments are not commercially available, and, therefore must be constructed in individual research laboratories, has certainly affected the quantity of applications of these chiroptical techniques. Nevertheless, both have been shown to provide interesting, important, and often unique information concerning the structure and dynamics of optically active molecules. As needs develop for more selective and sensitive detection or imaging of chiral molecules or chiral molecular systems, the range of applications of CPL and FDCD will certainly increase, and these spectroscopic techniques should become even more important tools of molecular stereochemistry.

7. ACKNOWLEDGMENTS

8. REFERENCES

1. Emeis, E. H.; Oosterhof, L. J., Chem. Phys. Let. 54 (1971) 4809.
2. Richardson, F. S.; Riehl, J. P., Chem. Rev. 77 (1977) 1773.
3. Riehl, J. P.; Richardson, F. S., Chem. Rev. 86 (1986) 1.
4. Steinberg, I. Z., "Biochemical Fluorescence: Concepts" (R. F. Chen and H. Edelhoch eds.), Vol 1, Chapter 3, Marcel Dekker, New York, 1975.
5. Turner, D. H.; Tinoco, I., Jr.; Maestre, M., J. Am. Chem. Soc. 97 (1975) 4751-4753.
6. Turner, D. H., Methods Enzymol. 49G (1978) 199-214.
7. Riehl, J. P.; Richardson, F. S., J. Chem. Phys. 65 (1976) 1011.
8. Riehl, J. P., J. Phys. Chem. 84 (1980) 94.
9. Steinberg, I. Z.; Ehrenberg, B., J. Chem. Phys. 61 (1974) 3382.
10. Snir, J.; Schellman, J. A., J. Phys. Chem. 78 (1974) 387.
11. Dekkers, H. P. J. M.; Moraal, P.; Timper, J. M.; Riehl, J. P., Appl. Spectrosc. 39 (1985) 3203.
12. Hilmes, G. L.; Riehl, J. P., J. Phys. Chem. 87 (1983) 3300-04.
13. Dekkers, H. P. J. M.; Emeis, C. A.; Oosterhof, L. J., J. Am. Chem. Soc. 91 (1969) 4589-4590.
14. Metcalf, D. H.; Snyder, S. W.; Demas, J. N.; Richardson, F. S., J. Am. Chem. Soc. 112 (1990) 5681.
15. Metcalf, D. H.; Snyder, S. W.; Demas, J. N.; Wu, S.; Hilmes, G. L.; Riehl, J. P.; Richardson, F. S. , J. Am. Chem. Soc. 111 (1989) 3082.
16. Metcalf, D. H.; Snyder, S. W.; Demas, J. N.; Richardson, F. S., J. Phys. Chem. 94 (1990) 7143.
17. Rexwinkel, R. B.; Meskers, S. C. J.; Riehl, J. P.; Dekkers, H. P. J. M., J. Phys. Chem. 96 (1991) 1112.
18. Richardson, F. S.; Metcalf, D. H.; Glover, D. P., J. Phys. Chem. 95 (1991) 6249.
19. Rexwinkel, R. B.; Meskers, S. C. J.; Dekkers, H. P. J. M.; Riehl, J. P., J. Phys. Chem. 96 (1992) 5725.
20. Snyder, S. W., Ph. D. Thesis, University of Virginia, 1990.
21. Rexwinkel, R. B. Ph. D. Thesis, University of Leiden, The Netherlands, 1993.

22. Rexwinkel, R. B.; Schakel, P.; Meskers, S. C. J.; Dekkers, H. P. J. M., Appl. Spectrosc. (in press).
23. Rexwinkel, R. B.; Meskers, S. C. J.; Riehl, J. P.; Dekkers, H. P. J. M., J. Phys. Chem. 97 (1993) 3875-3884.
24. Metcalf, D. H.; Bolender, J. P.; Driver, M. S.; Richardson, F. S., J. Phys. Chem. 97 (1993) 553-564.
25. Sutherland, J. C.; Low, H., Proc. Natl. Acad. Sci. U.S.A. 73 (1976) 276.
26. White, T. H.; Pao, Y.; Tang, M. M., J. Am. Chem. Soc. 97 (1975) 4751.
27. Schippers, P. H., Ph. D. Thesis, University of Leiden, The Netherlands, Chapter 1, 1982.
28. Steinberg, I. Z.; Gafni, A., Rev. Sci. Instrum. 43 (1972) 409.
29. Steinberg, I. Z., Methods Enzymol. 49G (1978) 179-199.
30. Lamos, M. L.; Turner, D. H., Biochemistry 12 (1985) 2819-21.
31. Hug, W., Appl. Spectrosc. 35 (1981) 115.
32. Lobenstein, E. W.; Schaefer, W. C.; Turner, D. H., J. Am. Chem. Soc. 103 (1981) 4936-4940.
33. Blok, P. M. L.; Schakel P.; Dekkers, H. P. J. M., Meas. Sci. Technol. 1 (1990) 126.
34. Schippers, P. H.; Dekkers, H. P. J. M., J. Am. Chem. Soc. 105 (1983) 79-84.
35. Schippers, P. H.; Dekkers, H. P. J. M., J. Am. Chem. Soc. 105 (1983) 84-89.
36. Schippers, P. H.; Dekkers, H. P. J. M., Tetrahedron 38 (1982) 2089.
37. Schippers, P. H.; Dekkers, H. P. J. M., J. Chem. Soc., Perkin Trans. 2 (1982) 1429.
38. Barnett, C. J.; Drake, A. F.; Mason, S. F., Bull. Soc. Chim. Belg. 88 (1979) 853.
39. Gafni, A., Biochemistry 17 (1978) 1301.
40. Richardson, F. S., Inorg. Chem. 19 (1980) 2806.
41. Ransom, M.; Brittain, H. G., Inorg. Chem. 22 (1983) 2494.
42. Brittain, H. G., Inorg. Chim. Acta 70 (1983) 91.
43. Brittain, H. G.; Rispoli, L., Polyhedron 4 (1985) 39.
44. Hilmes, G. L.; Riehl, J. P., Inorg. Chim. Acta 129 (1987) 123-125.
45. Hilmes, G. L.; Riehl, J. P., Inorg. Chem. 25 (1986) 2617.
46. Hilmes, G. L.; Timper, J. M.; Riehl, J. P., Inorg. Chem. 24 (1985) 1721-23.
47. Hilmes, G. L.; Coruh, N.; Riehl, J. P., Inorg. Chem. 27 (1988) 1136-39.
48. Mondry, A.; Meskers, S. C. J.; Riehl, J. P., (to be published).
49. Çoruh, N.; Riehl, J. P., Biochemistry 13 (1992) 7970-7976.
50. Çoruh, N,; Hilmes, G. L.; Riehl, J. P., J. Luminescence 40-41 (1988) 227-8.
51. Çoruh, N.; Riehl, J. P., Eur. J. Solid State and Inorg. Chem. 28 (1991) 263.
52. Abdulhalli, S.; Harris, W. R.; Riehl, J. P., (to be published).
53. Wu, S; Bedard, T. C.; Riehl, J. P., Coll. Czech. Chem. Comm. 56 (1991) 3025-27.
54. Sen, A. C.; Chowdhury, M.; Schwartz, R. W., J. Chem. Soc., Faraday Trans. 2 77 (1981) 1293.
55. Morley, J. P.; Richardson, F. S., Mol. Phys. 47 (1982) 379.

240

56. Hilmes, G. L.; Çoruh, N.; Riehl, J. P., Inorg. Chem. 27 (1988) 3647.
57. Wu, S; Bedard, T. C.; Riehl, J. P., Coll. Czech. Chem. Comm. 56 (1991) 3025-27.
58. Tinoco, I., Jr.; Turner, D. H., J. Am. Chem. Soc. 98 (1976) 6453-6456.
59. Reich, C.; Maestre, M. F.; Edmondson, S.; Gray, D. M., Biochemistry 19 (1980) 5208-5213.
60. Christensen, P.; Yeung, E. S., Anal. Chem. 61 (1989) 1344-1347.
61. Wu, K.; McGown, L. B., Appl. Spectrosc. 45 (1991) 1-3.
62. Geng, L.; McGown, L. B., Anal. Chem. 64 (1992) 68-74.
63. Lamos, M. L.; Lobenstein, E. W.; Turner, D. H., J. Am. Chem. Soc. 108 (1986) 4278-4284.
64. Lamos, M. L.; Turner, D. H., Biochemistry 24 (1985) 2819-2824.
65. Lamos, M. L.; Walker, G. T.; Krugh, T. R.; Turner, D. H., Biochemistry 25 (1986) 687-691.

Chapter 8

Analytical applications of CD to the forensic, pharmaceutical, clinical, and food sciences.

Neil Purdie[a]

[a]Chemistry Department, Oklahoma State University, Stillwater, OK 74078-0447, USA.

ABSTRACT

1.   INTRODUCTION

2.   BASES BEHIND CHIROPTICAL DETECTORS

3.   COMPARISONS AMONG CHIROPTICAL DETECTORS

4.   CD VERSUS ABSORBANCE DETECTION

5.   CD VERSUS OTHER CONVENTIONAL DETECTORS

6.   CD (POLARIMETRY) AS AN ON-LINE DETECTOR FOR LIQUID
     CHROMATOGRAPHY
          6.1 Conventional systems
          6.2 Chiral phase systems

7.   CD AS A DIRECT CHIROPTICAL DETECTOR

8.   SPECTRA FOR STANDARD REFERENCE MATERIALS (SRM)

9.   APPLICATIONS
          9.1   Molecules with chiral chromophores
          9.1.1   Morphine alkaloids
          9.1.2   Phenethylamines and catecholamines
          9.1.3   Colored interferences
          9.1.4   Antibiotics
          9.1.5   Diastereomers
          9.1.6   Poisons
          9.1.7   Vitamins
          9.1.8   Plant extracts
          9.1.9   Steroids
          9.1.10   Carbohydrates
          9.1.11   Aminoacids, peptides, proteins

Abstract

The focus of this chapter is the application of CD as a detector in the analysis of natural products. For the most part the mixtures that are investigated are real samples and emphasis has been given to the development of methods that do not involve extensive separations. Analytes are divided among three subject groups according to how their structural properties meet the prerequisites of CD activity: those that are inherently chiral, those that absorb electromagnetic radiation but are not optically active, and those that are optically active but do not absorb. The measurement of optical purity, the determination of enantiomeric excess in partial racemic mixtures, and the molecular association of analytes with various auxiliary host molecules that enable or facilitate chiroptical detection, are discussed at some length. Where appropriate, critical comparisons are made with chromatographic methods of analysis.

1. INTRODUCTION

The unifying theme among the sciences that are covered by this chapter is that a great many of the prospective analytes are natural products for which a common structural property is optical activity or chirality. Synthetic analogs by comparison are, for the larger part, racemic unless stereospecific or stereoselective synthetic routes are used in their manufacture. In a recent survey [1] it was estimated that the world total for legally dispensed drugs is approximately 1,850, of which 523 are natural and semisynthetic (517 chiral), and 1,327 are synthetic (528 chiral). From a forensic viewpoint the number is even greater when the many natural and synthetic forms of illicit or controlled drug substances are added. These same drugs and their metabolic products are of great clinical significance too, as are the many pathologically important

compounds that are routinely measured in clinical assays. In the food sciences obvious chiral analytes are saccharides, proteins, glycosides, and some of the vitamins [2]. It is ironic therefore that relatively little attention has been given to the development and application of analytical methods that focus on the chirality property to either confirm a suspected molecular configuration, or to use it as an analytical probe for the identification of an anonymous stereomer. It is even more ironic that, although the original motivation behind the development of chiroptical methods was the determination of absolute configurations for natural products, implications were made very early that optical rotatory dispersion (ORD) and CD might well see development as analytical detectors [3]. Applications of the methods to structural studies are described in depth in Chapter XX and warrant no further discussion here. The production of optically or enantiomerically pure drugs is a technological area that is developing rather rapidly and as it does there will be a need for the development of routine analytical methods specific to chiral properties for use in product quality control [4].

Two general analytical options exist for the experimental determination of optical activity and/or optical purity. One relies solely upon the selectivity inherent to the detector to discriminate between enantiomers and/or diastereomers in the most direct manner. Such a method would almost certainly involve CD detection which has the greatest potential among the three available chiroptical detectors. How direct the method might be depends upon the nature of the sample. It may be necessary, for instance, to perform a quick sample clean-up step in order to remove the more obvious strong absorbing species. The second option, which happens to be the most prevalent in use at the present time, is to selectively separate the optical isomers by chiral chromatography allowing them to be detected using one of the more conventional non-selective detectors [5].

2. BASES BEHIND CHIROPTICAL DETECTORS

A beam of monochromatic linearly polarized light is the product of the coalition of two in-phase circularly polarized components whose electric vectors rotate in opposite angular directions. Passage of the beam through an achiral medium produces no angular deviation from the direction or plane of incidence. When the propagating medium is chiral one of the components is retarded with respect to the other, the beams are no longer in phase, and an angular rotation is observed [6]. This is the basis for polarimetry. The direction of the rotation from the plane of incidence is determined by the structural properties of the medium. Angles of rotation are wavelength dependent and when measured form the basis for optical rotatory dispersion (ORD) [7]. For a chiral medium that does not absorb energy from the incident beam the angle of rotation is observed to increase monotically with decreasing wavelength to produce a "plain" ORD curve, (see Chapter 1). If the chiral medium should also absorb energy within the wavelength range of investigation an "anomalous" ORD curve is produced. The anomaly is evident only over the wavelength range of the absorption band is sigmoidal in appearance, and is referred to as a Cotton effect or Cotton band. It is always superimposed over a plain curve.

Circular dichroism (CD), which also has its origins in the combined effects of chirality and absorbance, is established by absorbance differences. There is no CD equivalent of a plain ORD curve so outside the range of the absorption band the net CD signal is always zero, in other words the spectral baseline is flat. Wavelength ranges for CD and anomalous ORD effects coincide. A difference in absorbance produces unequal intensities for the out-of-phase beams that can be represented by vectors of unequal length. The combination of these unequal vectors at any given wavelength with the unequal angular rotations produces a transmitted beam that is elliptically polarized, Chapter 1. The magnitude of the CD signal can be determined by measuring either the ellipticity of the transmitted beam or the absorbance difference. The latter is exclusively used in modern instruments.

3. COMPARISONS AMONG CHIROPTICAL DETECTORS

All three chiroptical effects have been used as the basis for an analytical detector. Polarimetry and ORD are applicable to all chiral materials. ORD is in theory superior because it is a spectral method, but the advantage is observed for only anomalous ORD curves owing to their greater selectivity and greater sensitivity. Polarimetry has a definite edge when the method calls for single wavelength detection such as in liquid chromatographic applications, but excessive absorption can be a detriment to its use because of the low intensity of the transmitted beam. CD is limited to only those chiral analytes that absorb, and like anomalous ORD a high level of selectivity is introduced because both are spectral detectors. Of the two, the ultimate analytical advantage lies with CD because of the complications that arise in ORD detection which are associated first with the non-zero baseline outside the wavelength range of the Cotton effect, and second with the complexity of the spectra obtained whenever multiple Cotton effects are present and mutually interfere.

In making decisions about which analytes are CD active it is not always a simple matter to inspect a molecular formula and to know for certain that the chiral center and the chromophore are mutually located in a way that will produce observable activity. And furthermore, although the molecular structure might suggest that a chiral chromophore is present, the substance might only be available as a racemic mixture in which case it is not optically active and therefore undetectable by CD. Trial and error is often the only proven criterion that works.

The need for chirality and absorbance properties might imply that the potential analytical applications of CD are quite limited. The number can be significantly increased by reacting those molecules that meet only one of the criteria with derivatizing reagents that will induce or introduce the other. Inherently non-chiral molecules and racemic mixtures that absorb radiation can have chirality induced in very specific reactions with a chiral host, and preferably one that does not absorb, for example the cyclodextrin oligomers [2,5]. For racemates, the induced CD signal is the net result of differences in the binding parameters, meaning that there is either a difference in the individual complex formation constants, K_F, or in the induced rotatory powers, θ, or a combination of both. Color induction can be performed either

reversibly, for example by ligand substitution into the coordination sphere of a colored metal complex, (e.g. the Pfeiffer effect [8]), or irreversibly by producing unsaturation in the molecule in a way that selectively preserves the chirality. The latter approach has long been a strategy used in drug analysis and clinical analysis, and over the years a great many reagents have been discovered or developed that will combine quantitatively with a variety of organic functional groups [9]. Fluorescence and phosphorescence induction are naturally part of these general processes.

4. CD VERSUS ABSORBANCE DETECTION

Since the experimental manifestation of CD is by way of a measured difference in absorbance it might best be described as a modified form of absorption spectrophotometry. Its major advantage over absorbance detection is the high level of selectivity, and its major disadvantages are low signal intensities and the fact that, even in situations where it can be used, single wavelength detection is not really a viable option. All experimental variables that affect an absorption measurement, such as pH and solvent effects, also affect CD. Data analyses are no different. Beers' Law correlation curves can be non-linear for the same reasons, such as non zero intercepts, chemical equilibria, polychromatic radiation, stray light etc. It is rather easy therefore for anyone with experience in absorbance spectrophotometry to become acquainted with the experimental capabilities of CD. The many similarities end there and the differences are what make CD detection uniquely selective.

An equation that is analogous to the Beer Lambert Law ($A = a.c.d$) can be written for CD data, namely $\psi = \theta.c.d$, where A and ψ are the experimentally measured absorbance and ellipticity values, a and θ are the corresponding molar values respectively, c is the molar concentration, and d is the sample pathlength. There has been an apparent reluctance to adopt this familiar equation first because of some dubious loyalties to such terms as specific and molecular ellipticity that were defined in the original literature, and second because a great deal of the published reference works are expressed in the older form. Any values for θ included here will be in the units defined by the Beer-Lambert correlation equation. Historically the ordinate of a CD spectrum has been expressed as ellipticities in millidegrees, which is the parameter that is still displayed on most commercial instruments. But in keeping with the fact that an absorbance is measured, there is a growing tendency towards expressing the ordinate either as $\Delta A = A_L - A_R$ or as $\Delta a = (a_L - a_R)$. The conversion is easy. Molar ellipticities and molar absorbance differences are related by the simple relationship $\theta = 3300\Delta a$. The fact that a relationship exists between θ and the difference in molar absorptivities and not the absolute value of a means that it is possible to get strong CD signals from relatively weak electronic transitions, i.e. $n-\pi^*$, and vice versa.

The chromophores that are prevalent in the molecular structures of natural products are the aromatic ring and the carbonyl functional group. Symmetry elements associated with these functional groups means that they are achiral chromophores, so chirality has to be induced by their structural

association with a chiral center, such as an asymmetric carbon atom [6]. Photon absorption by the saturated bonding structure of the asymmetric carbon atom occurs only in the vacuum UV and is quite inaccessible to measurement. Wavelength maxima for the absorption bands of the unsaturated chromophores lie in the near to middle UV range; 200-290nm for the aromatic system $\pi-\pi^*$ transitions, and 280-340nm for the n-π^* transitions of the carbonyl group [10]. Conjugation will extend the range of absorption bands into the visible. Association of the chromophore with a chiral center can lead to the division of a typically broad and undistinguished absorption band into two narrower CD bands. These sub-bands are quite often of opposite sign and unequal intensity and are separated by a characteristic crossover wavelength where the CD signal is zero (see discussions of exciton coupling in the Chapter by Lightner elsewhere in this text). These data can be used for structural interpretations and for qualitative identifications [11]. The spectra do, however, lack the wealth of detail one normally associates with infrared fingerprinting.

A factor that affects the (S/N) quality of CD data is the total absorbance of the whole sample in the wavelength region of the CD band. Absorption may be by other non-chiral chromophores that are part of the structure of the CD-active analyte and/or by other chiral and achiral components in a mixture. The optimum wavelength range to use would be where the absorbance is least and the CD signal is greatest [12]. CD bands and absorption bands that maximize at wavelengths shorter than 230 nm are intense due to transitions of high probability. Although limits of detection on the order of 10nmol/L are possible the disadvantages to using CD detection are these: CD spectra in general mirror the absorption spectra in this range so all analytical selectivity is essentially lost, and interferences from strong absorbers are so great that total separation of the analyte from other components in the mixture is an absolute prerequisite to analysis. If separation is so essential, then the question of the value of CD as detector becomes moot. Is there any advantage to its use compared with absorbance or refractive index detection? Does it offer any advantage at all over polarimetric detection? On the other hand, electronic transitions that occur at wavelengths longer than 230 nm have lower molar absorptivities and are further removed from the potential interference from all strong absorbers. It happens that in this range CD is selective and signals are large enough that quantitative work can be done with relative ease. Limits of detection are proportionately higher but levels on the order of 0.1µmol/L are possible. The most favorable range is the visible but examples of analytical applications are still few in number.

5. CD VERSUS OTHER CONVENTIONAL DETECTORS

Similarities between CD and absorbance extend to CD and fluorescence (FDCD) and circularly polarized luminescence (CDL) detection as well [13,14]. Chiral fluorophores can be both natural and induced. The former are considerably fewer in number because of the fact that three prerequisites are necessary to create CD-fluorescence activity. Because CD signals are inherently small, and even smaller for induced forms, the higher emission signals normally associated with fluorescence are attractive to use for the

detection of chiral analytes. Induction is usually done by some molecular complexation mechanism, which besides creating CD activity, might sometimes serve as a fluorescence enhancer [15]. The obvious parallels between fluorescence and absorption and fluorescence and CD, make the advantages and disadvantages of FD-CD detection readily predictable. In cases of color induction combined with fluorescence induction, the combination of FD with CD detection can lead to even greater levels of selectivity among analytes that have been derivatized by the same color reagent.

Selectivity enhancement is in general a result of any of a number of circumstances, for example: (i) not all of the sub-bands in either the absorption or fluorescence spectrum of the derivative are necessarily CD-active, (ii) the chromophore must be located adjacent to an intact chiral center or the functional group is not CD-active, so any molecule, other than the analyte, that contains this group but fails to meet the requirement, is eliminated as a potential CD detectable interference (although it may still absorb or fluoresce strongly), (iii) if a chiral center in the molecule of a potential interfering compound is lost in the derivatization process that molecule will also be removed from the list of possible interferences.

Other more conventional detectors that might ostensibly outperform CD in selectivity are nmr and mass spectrometry, and in fact they do for the analysis of diastereomers, although quantitation is a much more difficult task. They cannot compete with chiroptical methods for the distinction between enantiomers. In nmr detection, derivatization to diastereomers is a prerequisite to enantiomer analysis, and chiral forms of lanthanide reagents can been used with good effect [16,17]. For the analysis of mixtures by either nmr or mass spectrometry, total chromatographic separation is a necessity, so the completeness of the baseline separation is the limiting step not the detector. In contrast CD can be applied to the analysis of enantiomers in mixtures in methods that require no prior separation.

6. CD (POLARIMETRY) AS AN ON-LINE DETECTOR FOR LIQUID CHROMATOGRAPHY

6.1. Conventional Systems:

Given the assumption that a mixture can be *completely separated* on an HPLC column packed with an achiral stationary phase, chiral components behave like any others, eluting at their characteristic retention times. So, in principle, conventional detectors should be just as easily used for their determination. In fact any detector that has a superior S/N ratio and therefore lower limits of detection is really preferred over chiroptical detectors for quantitative analyses. The only new information that a chiroptical detector will provide is the stereochemistry of the chiral analyte(s) which is confirmed by comparing signs of rotation or sense of CD with those for standard reference materials (SRM's). Of the two choices, polarimetry has two things to recommend it; first absorbance is not a prerequisite so *all* chiral molecules are detectable, and second it is operated at a *single* wavelength which simplifies on-the-fly detector technology. If CD detection is limited to measurements at a single wavelength, it is reduced to being no more than a very expensive polarimeter. On-the-fly CD spectral detectors have been described [18,19] but

as yet are not commercially available. Eventually these may be the starting point for the development of CD diode-array detectors. The only option for full spectrum CD detection is in the stopped-flow mode [20-22], a method that requires a focussed beam and rapid scanning capabilities.

To be effective, the light sources used for chiroptical detection systems must have an intensity that is much greater than those ordinarily used in polarimetry. This comes about because the angular rotations observed for the very low analyte concentrations and very short sample pathlengths typical of an analytical liquid chromatograph, are extremely small (mdeg. and less). Conventional light sources have been replaced with laser illumination but these are not without problems, a major one of which is the instability in the emission [23].

In circumstances where separations are *not* entirely complete there is an obvious selectivity advantage associated with chiroptical detection. For instance any achiral molecule that might co-elute, even partially, with a chiral component would be transparent and pass undetected unless it absorbed the observing wavelength. Retention times for enantiomers on conventional HPLC systems are identical, so their analytical distinction using a *single* HPLC detector is impossible unless they are first derivatized to diastereomers which would have different retention times. Baseline separation might be accomplished if column and solvent conditions are right, in which case both native diastereomers and derivatized enantiomers can be distinguished one from the other using only polarimetry or CD detection. Derivatizations are done by reacting the enantiomeric pair with a third chiral species, either pre-column or on-column. The problems with this particular method are that the number of suitable, 100% optically pure, chiral reagents that are available for pre-column derivatizations is limited and, even if derivatization is accomplished, baseline separation is not guaranteed. The effectiveness of the separation is also dependent upon the relative molar ratio of the isomers. For instance if one isomer is present in very large excess over the other, elution orders can be reversed from what is expected, and results can become quite ambiguous. Conditions should always be modified so that the minor component elutes first [24] and is not lost in the trailing edge of the band for the major component.

Distinction between enantiomers and their subsequent determinations can be made without derivatization when *two* detectors, one of which is chiroptical, are used in series [25,26]. Separation from all other components is a prerequisite to the analysis. The signal from the first detector (for example absorbance) would be proportional to the *sum* of the enantiomer concentrations and a polarimetric or CD signal would be proportional to the concentration *difference*. Concentrations of both isomers are easily determined by solving the two simultaneous Beers' law equations.

6.2. Chiral Phase Systems

Chiral chromatography methods are considered by many to be superior to conventional methods in that, besides analytical applications, they offer the greatest potential for the preparation of optically pure forms of the isomers [5,27,28]. In these examples the third chiral species is an integral part of the LC (or GC) system and may appear as a plain stationary phase (cyclodextrins),

as a modified stationary phase (ligand exchange [29] and Pirkle columns [30]), as a chiral mobile phase, or as some combination of both the mobile and stationary phase properties respectively. For the most part these on-column derivatizations are reversible equilibria and the eluting species are the enantiomers which is another very good reason why they are attractive as preparative methods. The greatest analytical errors are once again encountered when one of the isomers is in large excess, and at levels close to 98% or 52% the determination of the exact composition is so imprecise as to be completely meaningless [31]. On-column racemization is a further complication worthy of consideration in analytical applications [22,32]. In practical terms the ultimate expense of producing optically pure mobile phases which, realistically, can be used only once, and chiral stationary phases that are rugged enough to undergo several recycling processes and to withstand high hydrostatic pressures, can be very high. These factors are very important as they affect the development of routine analytical procedures.

7. CD AS A DIRECT CHIROPTICAL DETECTOR

In this context direct means that sophisticated or protracted separation procedures are not part of the analysis. Sample preparation is a simple solvent extraction step or, at the very most, extraction followed by a clean-up and pre-concentration step on a solid-state cartridge device. Only CD among the chiroptical detectors has the necessary selectivity. Chiral species that do not absorb except in the far UV (e.g. most simple sugars) are transparent in the wavelength range of concentration and are not to be counted among the possible interferences. Achiral molecules that absorb can affect the measurement by reducing the S/N ratio when their absorption bands lie in the wavelength range of the CD band. Some absorptions are very significant, for example from coloring agents that are present in pharmaceutical and clinical samples and pigments that occur in vegetable matter. A judicious choice of solvent helps to alleviate, and sometimes even eliminate, the problem.

More significant are the mutual interferences among chiral chromophores whose absorption bands overlap. There is less of a tendency for this to happen compared to absorbance spectrophotometry because CD bands are generally narrower and are often of opposite signs [11]. Spectra are of course additive; the experimental ellipticity $\psi = \Sigma(\theta_i c_i d)$. When the contribution from a component is less than 5% of the observed experimental ellipticity for the major component, its contribution is considered negligible. Curve fitting algorithms that use some acceptable best fit criteria are needed to resolve the spectrum among the components in the mixture. Those algorithms that are part of computer software packages for absorbance spectrophotometers will suffice if input of the CD data is convenient. Values for θ_i typically vary by only a factor of two or three in the preferred range, i.e. wavelengths longer than 230 nm. Concentrations ordinarily will vary by much more than this so the factor that really determines whether or not substances interfere is the concentration, rather than the rotatory strengths of the chiral chromophores. Prior knowledge of the relative amounts of each component in a sample is not generally available, except in specific applications such as product quality

control in the manufacture of pharmaceuticals and in the analyses of plant extracts [33], and less so in forensics.

Detection limits for transmission CD measurements on bulk samples are similar to those for absorbance, ca. 100nM for a 1-cm pathlength. Much lower levels are attainable with fluorescence probes. These lower limits pertain to the fluorescence mode of the observtion not the CD mode. By comparison in state-of-the-art detector development for UV absorbance based LC, picogram and even femtogram levels have been reported [23]. Such low levels are very impressive but are only significant when the specimens that are to be sampled are extremely small. This is not often the case in the areas of interest to this chapter with the possible exception of clinical samples.

8. SPECTRA FOR STANDARD REFERENCE MATERIALS (SRM)

There are no comprehensive data files for CD spectra for SRM's that compare with the many exhaustive files for absorbance data, either electronic or vibrational. Nor is there a plan in place to compile such a compendium. Analysts are required therefore to prepare their own reference files using whatever SRM's might be available from the usual manufacturers of fine chemicals. An obvious difficulty associated with this endeavor is the fact that although these materials are certified to be chemically pure few are ever certified to be 100% enantiomerically pure. More likely than not, these few materials have natural, rather than synthetic, origins. In actuality such materials probably do not exist. If they do, proof of their absolute enantiomeric purity is beyond the capabilities of currently available analytical methods [31]. In addition enantiomeric purity can be a time dependent transient state for materials that are prone to racemization, a process that is most likely for chiral liquids and chiral solutes in solution. It is not possible therefore to speak with conviction about exact molar ellipticity values.

CD spectra for pairs of enantiomers (or diastereomers) are mirror images of each other, yet the bands are equal in magnitude if, and only if, the isomers are available in equivalent enantiomeric purities. And the fact that they are equal is not evidence for absolute enantiomeric purity for both. The molar ellipticity for the purer isomer will be the larger number and presumably nearer to the "true" value. One has also to be aware that in the case of diastereomers there are a total of four enantiomers (R,R; S,S; R,S; and S,R) which produce two pairs of CD spectra that are mirror images of each other. Racemization, when it occurs, is between enantiomers and not diastereomers, so proof of absolute purity is a very difficult challenge. The practical answer to this problem is to run regular checks on the reproducibility of a "defined" enantiomeric purity for a chemically pure substance. This is done by adding the spectral data for every new issue of an SRM that is obtained from different product lots, and where possible from different manufacturers, to an ever increasing pool of data and periodically updating the files of Beers' Law correlation curves.

The importance of this experimental limitation is greatest when the analytical objective is to determine the enantiomeric purity of a drug that is but one component in a complex mixture. It must be understood that figures used to express an enantiomeric excess are relative to a defined enantiomeric purity

and not to the absolute enantiomeric purity, and that correspondence values therefore will vary from one substance to another. A number of difficult to answer questions come up if the chemically purest forms of the enantiomeric SRM's have different enantiomeric purities. Does one use the molar ellipticity value for just the purer isomer as the standard against which to measure the enantioexcess ? If one does, how is the contribution to the signal from the "impurity" in the other isomer accounted for? Are the effects of competing chiral interferences, incomplete separations, etc., of such a magnitude that the errors are so great and the determinations are entirely meaningless? These and many other questions take on considerably more significance as the need for the development of routine procedures to determine enantiomeric purities in quality control and quality assurance methods in drug analysis increases [4].

9. APPLICATIONS

Chiroptical methods have been and still are widely used as an aid in the elucidation of the structures of chiral molecules because of the extreme sensitivity of electronic excitations to the molecular dissymmetry that immediately surrounds the chromophore. Assignments of absolute molecular configurations to many of these compounds were made using the old empirical working models such as the octant and quadrant rules [3,34,35], and now using the more quantitative exciton coupling models [11] (see Chapter by Lightner elsewhere in this text). CD is also indispensable in deriving three dimensional structural information using vibrational CD spectral data gathered for macromolecules in solution; this represents information that is not easily obtained by any other way [36]. An experimental limitation that does affect the quality of these structural analyses is the fact that the far-UV (< 200nm) and the infrared spectral ranges are not conducive to easy data collection and interpretation. While these studies may be of special interest with regard to the historical development of CD as a viable analytical method, structure determination is not the objective of the work described in this chapter. It will not be entirely ignored, however, because there are instances where structural information is crucial to the interpretation of analytical data.

In spite of all the successes of this structural work, the extraordinary discriminatory potential that chiroptical methods would obviously have if applied to the rather mundane task of preliminary routine screening for drugs has never been exploited. One reason for this may be that the sensitivity to stereochemistry has not been fully explained in theoretical terms. The utter inadequacy of the aforementioned theoretical models is easier to understand and appreciate when one realizes that the spatial redirection of just one bond in a molecule, while not affecting the absorption spectra for the structural analogs, will produce changes in the CD spectra that are so dramatic that their individual distinction is elementary. Outstanding illustrations are plentiful in the CD literature of the steroids, for example testosterone and its dihydro-derivative, Figure 1.

So the basic question is this: if CD is so very effective for deriving absolute molecular configurations, why is it that analytical applications have been studied by surprisingly few investigators? The ubiquity of the aromatic
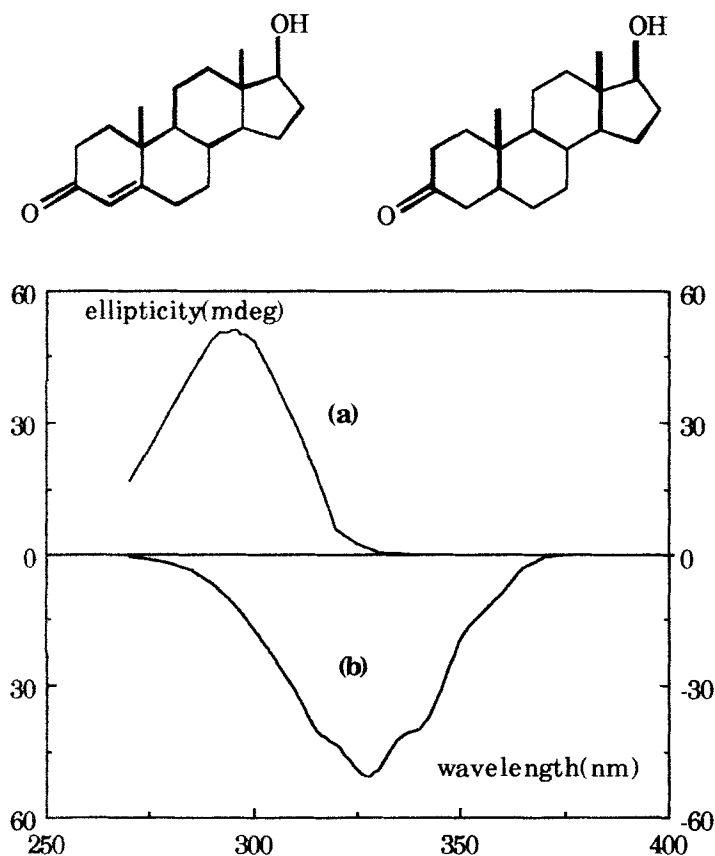
Figure 1: CD spectra for 2.5mM solutions of (a) dihydro-
testosterone and (b) testosterone in methylene chloride

ring and carbonyl functional groups in the molecular structures of natural
products means that the number of potential analytes is enormously large.
Djerassi pointed out the analytical potential of chiroptical methods as long ago
as 1960 [3], but even now (some thirty years later) the actual number that have
been investigated is very small.

It is obvious from the enormity of the literature on separation sciences
that these methods dominate over direct methods and, some would say, with
obviously good reasons because interferences are minimized. However it is
also fair to point out that, for a great many of these investigations, the samples
used to develop the experimental conditions and separation theories are
carefully tailored laboratory mixtures that are so elementary in composition
that they do not even begin to duplicate the many difficulties that are
encountered when the technology is transferred to the analysis of real
samples.

Direct analytical applications of chiroptical methods over the last 15 to 20 years, and most particularly with ORD and CD detection, have clearly demonstrated that *a priori* suspicions of serious problems from interferences are ill-founded, that sensitivities similar to those for absorption spectrophotometry are easily accessable, and, most important of all, that a much higher level of selectivity is obtained because of that very same property that makes CD a useful structural tool (namely the sensitivity of the chromophore to its stereochemical environment).

Since many of the analytes that will be included in the discussions are important in more than just one of the science disciplines that make up the title of this chapter, it is perhaps more efficient to group them according to their structural similarities and in that way to reduce the number of unnecessary duplications. A convenient division is to group them into three categories as molecules that:

- contain a chiral chromophore
- have an achiral chromophore but optical activity is induced by interaction with a chiral host molecule.
- are chiral but absorb only in the far and vacuum UV, which is very inconvenient for absorption detection.

Emphasis is given to direct methods of analysis. Comparisons with methods that do involve chromatography will be made where appropriate. For a fuller description of CD as a chromatographic detector the reader is referred to the Chapter by Gergely.

9.1. Molecules with Chiral Chromophores

Natural products that are amenable to analysis using CD detection would include individual molecules from many diverse categories such as: alicyclic compounds (alkaloids and terpenes); heterocyclic compounds (barbiturates, diazepams, indole alkaloids, quinolines, nucleic acids and nucleotides); aminoacids and peptides, oligopeptides, and proteins (globular, nucleo- and lipo-proteins); saccharides and polysaccharides; and not least of all the many molecules that are the metabolites and/or the naturally occurring condensation products of carbohydrates with the other categories of compounds, for instance glucuronides and glycosides of the alkaloids, proteins, lipids, etc.

So far, the analytical inroads that have been made into the investigation of this large inventory of compounds are very short. The initial major emphasis was given to the study of controlled drug substances [37]. In forensic and pharmaceutical applications the choice of real samples has been generally limited to solid and liquid drug forms [2,12,38]. Analysis of biological extracts is still relatively new, but is open to many interesting and novel analytical options that are fairly unique. In one of the more imaginative applications, fructose was measured *in situ* in vitreous humor [39], which suggests other rather interesting clinical and forensic uses for CD detection. Vitreous humor is a biofluid regularly examined in autopsies. Another illustration one can cite is the fascinating study in which the drug terfenadine was administered as a racemate but was shown by CD detection after HPLC separation on an

254

ovomucoid protein column to be enantiomerically enriched in the plasma of rats [40]. It is still however very difficult to successfully promote the relative value of a chiroptical detector, in spite of its virtues, in the face of the very rapid and very convenient hyphenated-detector systems that are used in conjunction with routine GC and HPLC procedures, yet there is no quicker or better way with which to confirm the identity of a natural product by way of its configurational stereochemistry as determined by a CD spectrum.

9.1.1. Morphine Alkaloids

One of the first applications of direct CD detection to the determination of chiral compounds in homogeneous solvent conditions was done on aqueous solutions of the morphine alkaloids [41]. Major maxima for the absorption bands occur at wavelengths shorter than 230 nm, but the CD bands that were best disposed for discrimination among the structural analogs maximized between 240 and 300 nm. Spectra for analogs with phenolic groups showed a pH dependence leading in some cases to a reversal in the sign of rotation. This was a distinct advantage in the application of CD detection to the analysis of mixtures. Ten opiates, a list that included the synthetic product heroin, were completely distinguishable one from the other by their individual CD spectra in aqueous media, and to lesser degrees in KBr pellets [42] and cholesteric liquid crystal solutions [43]. Heroin in real samples was identified and determined either directly, or as morphine after complete base hydrolysis [44]. Direct multicomponent analyses were easily done for morphine, codeine, thebaine, and noscapine in prepared laboratory mixtures and in extracts of opium [45]. Data for the analyses of plant extracts both here, and for others described throughout the chapter, can only be compared with tabulations of typical average values. But in a forensic science context it is reasonable to assume that the distribution of the components might be used to trace the origin of the specimen to a particular geographical region. This work on the opiate alkaloids set the stage for a series of investigations on other drug substances, as summarized in Table 1.

9.1.2. Phenethylamines and Catecholamines

Discrimination among analogs of these compounds is a very difficult problem, whether it is attempted by HPLC using a variety of detectors, or by direct CD [46] or ORD [47]. Chiroptical detectors are by far the better choices. CD spectra typically consist of four bands with maxima in the absorption range of the aromatic ring, Figure 2.

However signs do change with the "handedness" of the natural isomer so a higher level of distinction is achieved using CD or polarimetric detection. An enormous advantage is derived from the fact that achiral excipients, such as lidocaine, procaine, and benzocaine, often deliberately added to illicit drug preparations to complicate the chromatographic identifications of amphetamine and methamphetamine, present no interference problem whatsoever to CD detection. ORD detection was developed for the analysis of mixtures of pseudoephedrine and ephedrine [47], which because of the connection between anomalous ORD and CD, should be applicable to CD detection in the UV.
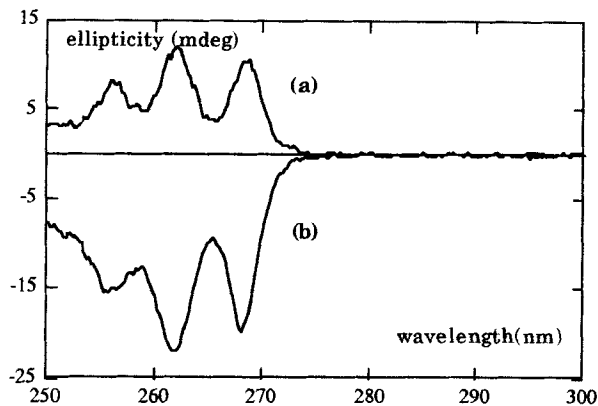
Figure 2: CD spectra for 0.02M solutions of (a) (D)-meth-amphetamine and (b) pseudoephedrine in strong base

TABLE 1. Chiral Analytes.

(A)	**Forensic Science**
	D-LSD; L-cocaine
	morphine, heroin
	cannabinoids (THC, CBD)
	amphetamine and analogs
	poisons: strychnine, colchicine
	plant extracts:
	    marihuana
	    opium
		(C)	**Clinical Science**
			sterones, sterols
			hormones
			proteins
			saccharides

(B)	**Pharmaceutical Science**
	morphine alkaloids
	antibiotics:
	    tetracyclines
	    penicillins, cephalosporins
	    aminoglycosides
	    polymixins
	indole alkaloids
	steroids
	vitamins: water and fat soluble
	plant extracts:
	    rauwolfia serpentina
	    digitalis
		(D)	**Food Science**
			plant extracts
			carbohydrates
			food glycosides
			vitamins

9.1.3. Colored Interferences

Another deliberate strategy that is used to foil the analysis of a forensic specimen is to add strongly absorbing dye materials. Also, but for quite different reasons, coloring materials and sweeteners are added in liberal amounts to pharmaceutical preparations, especially those for consumption by childrens. Quality assurance testing of drug formulations by LC is significantly complicated by the very unfavorable ratios of additives to drug. With regard to CD detection, only one chiral (and therefore only one CD-active) dye, O-benzyl-O-methoxydihydrofluorescein, has ever been reported in the literature [48]. The only real interference from colored additives to CD detection is the loss of S/N ratio for an already small CD signal caused by the enormous absorbance by the dye. In spite of this, the direct identification and quantitation by CD of D-LSD [49] distributed in the forms of intensely colored microdots and paper transfers turned out to be very straightforward. Viscous liquids of Brompton's cocktails (L-cocaine, morphine, and methadone mixed in solution with an intensely colored dyestuff) [50], and pseudoephedrine in children's Sudafed® [51] were analyzed with equal ease. Natural sweeteners present no difficulties in the near UV range, but one has to be aware of the interference from a chiral synthetic sweetener such as L-aspartame [51]. Applications of chiroptical detectors in the quality control analyses of pharmaceutical drug forms is a very attractive prospect because of their potential for development for routine, even robotic, use. This will become an even more important issue because of recent regulations prepared by the United States Food and Drug Administration (FDA), in which the onus of deciding on whether a new drug product will be developed as an enantiomer or as a racemate is given to the manufacturer. For FDA approval submissions must include analytical tests that confirm enantiomeric purity and/or enantiomeric excess and full material safety data sheet documentations for both enantiomers regardless of the choice.

9.1.4. Antibiotics

CD spectra have been measured for a number of SRM's of tetracycline [52], β-lactam [53], aminoglycoside [51], and the polymixin-B and bacitracin series of antibiotics [51]. The tetracyclines are bright yellow in color and have very broad and very intense molar ellipiticies in the visible spectral range. With the exception of the polymixins and bacitracin the CD selectivity among groups is excellent as with a number of other analytical methods. Penicillin-V and cephalothin were simultaneously determined in buffered solutions of prepared laboratory mixtures, and Pen-V was easily measured in pharmaceutical products and in a crude fermentation broth [53]. The level of selectivity among members within a given group varies from one series to the

penicillins and among the cephalosporins is entirely impossible unless a prior derivatization is done. For the penicillins the only molecular change among the congeners is the identity of the terminal R-functional group, and the reason for the lack of selectivity is most likely due to its relative isolation from the chiral centers that are adjacent to the two carbonyl chromophores.

Penicillin-V   Cephalothin
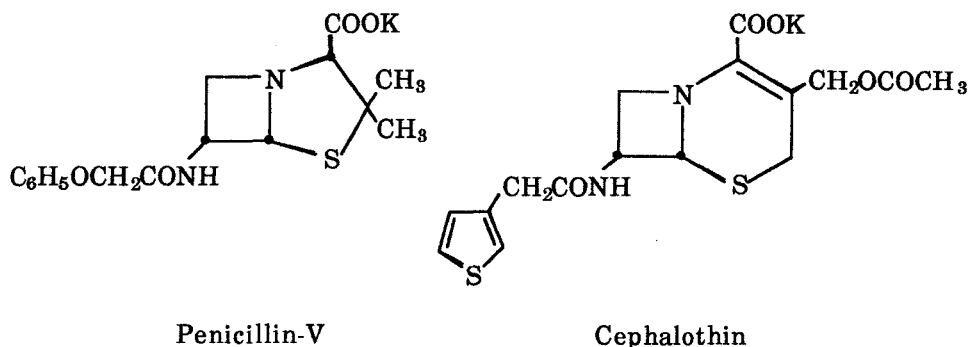
Discriminations might well be achieved using chemical derivatization, something we are in the process of investigating [51].

Selectivity between the aminoglycosides neomycin B and neomycin C using ORD detection [56] has been reported and is enough to determine both when they are present in a prepared mixture. Selectivity enhancement among the remaining aminoglycoside and polymixin analogs is an on-going study in our laboratory [51] but, like the penicillin study, derivatization is going to be a necessary prerequisite to the analyses. We will return to this topic in the section on color induction.

9.1.5. Diastereomers

Spectra for the diastereoisomeric pairs quinine-quinidine, cinchonine-cinchonidine alkaloids are mirror images of each other and mixtures have been determined using CD detection [57]. Spectra for the pilocarpine-isopilocarpine pair were such low quality that they could be used only for qualitative distinction. CD detection combined with UV detection was used to measure enantiomeric excesses in mixtures of L-hyoscyamine and atropine, *i.e.* racemic hyoscyamine. This subject is returned to in greater depth later.

9.1.6. Poisons

CD spectra for the major poisons colchicine, strychnine, brucine, and tubocurarine have been characterized in strong aqueous acid solutions [38] but none has, as yet, been used for direct analysis (not even on laboratory preparations). There seemed to be little additional value to continue to analyze laboratory prepared mixtures for these compounds because so many other illustrations of the effectiveness of direct CD detection in such simple circumstances have already been seen, and laboratory mixtures most likely are far removed from reality anyway. The successes obtained in other experiments where the analytes were extracted from complex matrices suggests that the presence of these substances could also be confirmed after a

simple solvent extraction of material ingested by a poison victim or by the examination of stomach contents. Their reference is included here as further evidence for the very broad range of applicability of direct CD detection.

9.1.7. Vitamins

The water soluble vitamins, B_2(riboflavin), B_{12}(cyanocobalamin), and C (ascorbic acid) provided a very interesting study. The spectra for B_{12} and some of its analogs were first reported by Williams et al., [58] and consist of very strong Cotton bands across almost the entire visible spectral range, Figure 3.
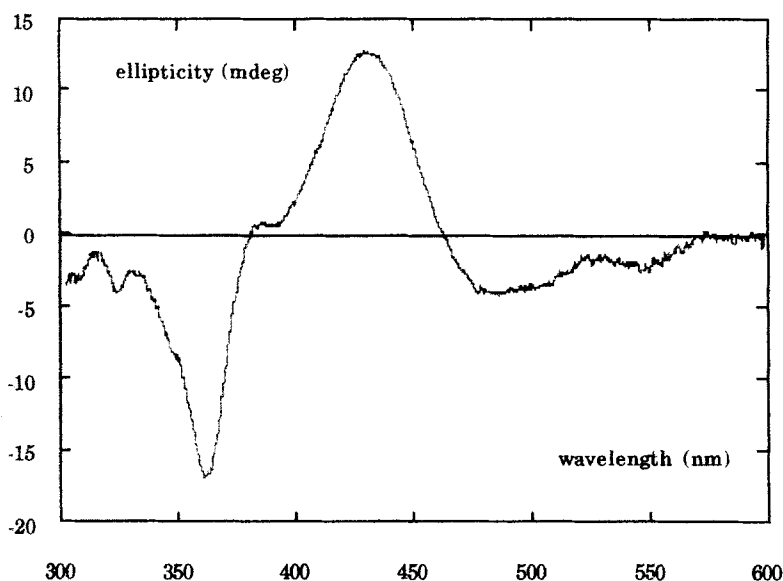
Figure 3: CD spectrum for vitamin B_{12} in aqueous solution.

Discrimination among all of these is a trivial exercise. Both B vitamins and C were easily quantitated in prepared mixtures as expected [59], but it was also relatively easy to measure each one after its simple extraction into aqueous buffer from pharmaceutical preparations, as well as (in the case of vitamin C) from extracts of fruit, fruit juices, and vegetables. A very thorough inventory of tests for possible interferences was run and the resultant analytical data for the vitamins compared extremely well with the labelled contents on the packages of pharmaceutical products and with the data in compendia that list the average compositions of vitamins and other essential products in plant food materials [33]. Analysis of the major fat soluble D_2 and D_3 vitamins (ergocalciferol and cholecalciferol) has not progressed with the

same degree of success [51]. Likewise, with digoxin and digitoxin. Vitamin D extracted from natural sources has a fixed stereochemistry which is equivalent to only one of several isomers found in synthetic preparations, not all of which perform the same biological functions as naturally occuring vitamin D. To certify that the natural form is in fact present in a synthetic pharmaceutical preparation, and to measure the relative amount, is a considerable analytical problem whose solution has both economic and ethical overtones. So far the problem has evaded an easy solution. We do know that it cannot be solved using direct CD detection on just the underivatized forms of the D vitamins, however a distinct possibility does exist that it can be done using a certain color derivatization reaction. Vitamins A and E (tocopherol) are not CD active in their native forms, but activity can be induced using the same color derivatization reaction.

9.1.8. Plant Extracts

The group of chiral drugs forms collected under plant extracts in Table 1 includes the opium alkaloids already mentioned, namely morphine, codeine, noscapine, and thebaine [41], S-(-)-nicotine from tobacco (both the indigenous plant and commercial products in the form of cigarets and smokeless tobacco) [60], Δ^9-tetrahydrocannabinol and cannabidiol from marihuana [61], reserpine alkaloids from Rauwolfia [62], pyrethroid insecticides [26], amaryllidacea alkaloids [21], atropine from digitalis [2], and humulone from hops [2], as well as the already mentioned examples of vitamin C from fruit and vegetables [59] and aureomycin from cattle feed [2]. The analyses in references [2,41,59,60-62] are the epitome of the meaning of direct analysis by CD detection because the only separation involved was a solvent extraction step into either a non-polar solvent or an aqueous buffer. The choice of solvent introduces a certain level of selectivity but the rest is due entirely to the selectivity of the CD detector. Stems, roots, leaves, or seeds were all used at one time or another. These were finely chopped and extractions were made under ambient conditions. If these analyses were to be repeated or if other systems were to be investigated in the future then the patented microwave extraction method would be recommended [63].

The four opium alkaloids were determined using a mathematical curve fitting algorithm. Although the data for tobacco were reported as S-(-)-nicotine, the truth is the CD spectra are actually unable to discriminate among it and its stereomers. However the other isomers are present in amounts that would contribute less than 5% to the total observed CD signal and were included as part of the major alkaloid. Spectra for the two major cannabinoids are sufficiently different that both can be also be fitted using the same algorithm that was used for the opiates. Reserpine is a substance that is not conveniently analysed by chromatographic methods, yet its determination by CD detection was relatively elementary. It might be anticipated that the co-extraction of green pigmentation material would present the major interference because of a significant decrease in the S/N ratio, but it turns out not to be a serious concern. If it ever does, then the recommendation would be to perform a quick sample clean-up on a solid state cartridge device.

9.1.9. Steroids

The seminal work on steroid analysis using chiroptical detection was performed by Djerassi [3] when he determined hecogenin acetate in the presence of tigonenin acetate. Although chiral centers are plentiful in steroids and they are therefore amenable to polarimetric detection after chromatographic separation, many present a difficult detection problem for either anomolous ORD or CD detection. This is due to the absence of an easily accessible chromophore, *i.e.* one whose absorption occurs in the near UV range. The only unsaturation in cholesterol, for instance, is the Δ^4-double bond which has an absorption maximum and CD activity around 205 nm. Color derivatization is always an option, and is commonly done in clinical analyses. This in itself is something of a surprise in the sense that other analytical sub-disciplines do not use color derivatization to an extent that even begins to approach that used by clinical chemists. Perhaps it is a consequence of clinical laboratory circumstances that analyses need to be fulfilled more urgently. Some of these color reactions as they pertain to chiroptical detection are referred to later.

Unsaturation, coupled with chirality in the steroids, lends itself to a certain level of selectivity that was ably demonstrated by Potapov et al. for analogs of progesterone [64]. But discriminations are probably even simpler than that, for instance, contrast the CD spectra for the underivatized testosterone and dihydrotestosterone molecules in methylene chloride, Figure 2. Gergely [65] and his colleagues have been particularly active in the development of ORD, and subsequently CD, detection methods for the determination of underivatized steroids, especially the Δ^4-3-ketosteroids, the 17-keto-, and the 17-ethynyl compounds. The last group are prepared from the corresponding keto- compounds and when used in pharmaceutical preparations the 17-keto analogs are often an impurity. The amount of keto in the product is readily determined using CD. The reader is referred to a subsequent Chapter where Gergely has described the work on steroids more fully.

Two general approaches to the analysis of underivatized steroids, either alone or in mixtures, have been described. One is the simple direct spectral analysis in which the spectrum for a mixture is resolved into the spectra for the components using an appropriate mathematical algorithm. Simple illustrations of the effectiveness of this method are the spectral distinctions between testosterone and its dihydro-derivative, Figure 2, and between cortisol and cortisone, Figure 4. The other approach, promoted by Gergely et al., is to enhance the selectivity of CD detection even more by measuring spectra for the analyte in two different solvent systems and to calculate and use the differences in the spectra for quantitative analysis. Solution modifications might involve a pH change if the steroid is water soluble, or a choice of two solvents that differ greatly in polarity, *e.g.* cyclohexane versus methanol. Corticosteroids and Δ^4-3-ketosteroids were determined in pharmaceutical products in this way [65]. Simple derivatization reactions, such as mild oxidations, will also affect the spectra in many ways. The extra selectivity is manifest by shifts in the wavelengths of band maxima, sign reversal, and the appearance or loss of Cotton bands. Binary mixtures therefore can be

quantitated from measurements made at only two wavelengths. The most convenient and most accurate results are obtained whenever one of the chosen wavelengths is at the crossover point of the difference spectrum of only one of the components, see for example Figure 4 around 350-400 nm.
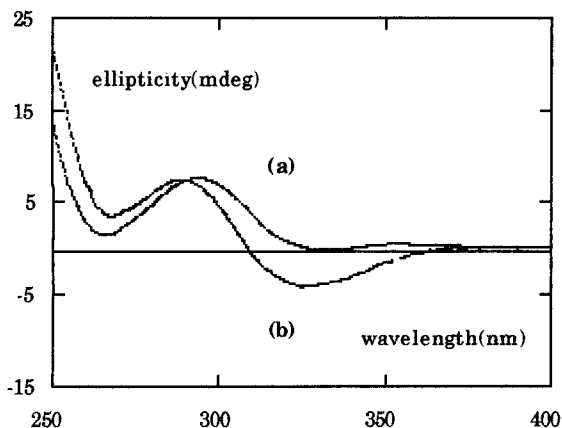
Figure 4: CD spectra for 0.1mM solutions of
(a) cortisone and (b) hydrocortisone in chloroform

9.1.10. Carbohydrates

Problems with chiroptical detection among the carbohydrates are exactly analogous to those for the steroids. Polarimetric detection can be used after total separation of all chiral species, and preferably at short wavelengths where its level of detection is greatest (for example in the analysis of urinary sugars [66]). ORD and CD detection in the near UV range are limited to the detection of saccharides that contain keto-, amide-, and carboxylate- functional groups [67]. CD detection has been successfully used for instance to determine ketoses [39,68,69], particularly D-fructose, and the N-acetyl content of chitosan from crustacean shells [70]. The review article by Johnson [67] on the application of CD to carbohydrates was devoted exclusively to how CD data can be used to derive structural information. In the absence of chromophores, data collection is limited to the far and vacuum UV and the infrared ranges. Measurements in these ranges are difficult to make and require custom built instrumentation because the wavelength range in commercial instruments is 180-820nm. In the far UV spectral bands are invariably incomplete and many do not reach a maximum in the range of measurement. Structural assignments are complicated even more by the fact that saccharides in solution exist in a multiplicity of stereochemical forms that are in equilibrium with one another. Each of these forms will contribute to the overall spectrum. Some of the spectral problems can be resolved in part by managing the equilibrium conditions to favor a particular stereochemistry, or by derivatizing the molecule to add a chromophore that absorbs in the near UV.

CD detection for colored derivatives might just as easily be used for structural information about the carbohydrates as well as for their analysis, but so far little attention has been given to either application. Cyclic oligomers of β-D-glucose have important supporting roles to play in analytical applications that are discussed in a later section. The union of chirality in the carbohydrate moiety of a glycoside metabolite with the unsaturation in the base in such compounds as nucleosides and nucleotides, saponins and flavones, etc., is another area that will ultimately be developed for applications of chiroptical detection methods. New and imaginative ideas are needed for the analysis of carbohydrates, and CD should be one of the favored methods.

Aldoses are determined by HPLC using absorbance detection around 300 nm. Polarimetry has also been used in this range and does add some discrimination to the analysis of mixtures based upon the signs of the measured rotations. Yeung combined absorbance and chiroptical detection for the analysis of several saccharides in both laboratory mixtures and urine extracts [66]. CD detection has also been used as an alternative to polarimetry. If it is operated at a single wavelength then in one sense it is just a very expensive polarimeter that is limited to only those chiral analytes that absorb. On the other hand it does have an extra selectivity advantage in the analysis of mixtures of chiral analytes where only some absorb in the wavelength range of the detector. Saccharides with unsaturated functional groups are detected at longer wavelengths. Most reports on the HPLC-CD determinations of monosaccharides have dealt with D-fructose and its congeners like D-tagatose, L-sorbose, and turanose [69], D-ribose, and vitamin C. One should mention again the reference to the determination of D-fructose in vitreous humor [39].

9.1.11. Aminoacids, Peptides, Proteins

The last subject in the discussion of inherently chiral compounds deals with the analysis of the aminoacids, peptides, and proteins. Most all of the remarks that were made about the steroids and carbohydrates regarding CD detection apply equally well to these. The enantiomeric purity of aminoacids is usually determined by their optical rotations at the sodium-D line. Rotations are normally so small that concentrated solutions and long pathlengths are needed. The detection is enhanced a little if laser illumination is used [66] or if ORD detection is done around 230 nm [71]. Without derivatization, only amino-acids with aromatic substituents are CD active in the near UV. Signals are generally weak and enantiomeric purity measurements are not quantitative.

Derivatization is the preferred option for aminoacids (making use of the anomalous ORD or CD effects introduced with the chromophore) to move the Cotton bands to longer wavelengths and to lower the limits of detection. Derivatizations might include N-acetylation as in the case of aminoglycosides [67], dansylation [72], or binding to metal complexes [73,74], see later. On the other hand aminoacids have an auxiliary role to play in the analysis of other substances, where advantage is taken of their chiroptical properties.

Peptides and proteins by comparison have stronger rotatory powers with obvious potentials in clinical analyses, either as the analyte or the auxiliary reagent. However, typical of the general trends in the study of oligomers and macromolecules, the major research interests were focussed on abstracting structural information [75], (and see the Chapter by Manning and Towell). The

intense CD bands are associated with electronic transitions in the peptide bond which absorb at wavelengths shorter than 230 nm. The literature on the interpretation of CD spectra in terms of tertiary and quaternary structure is immense. In stark contrast, the literature on analytical applications in which the peptides and proteins are the target analytes is very brief. More often these molecules have been used as auxiliary substrates with which other substances that bond with them in unique stereo-controlled ways can be analyzed, *e.g.* warfarin to human serum albumin [76] using FDCD detection. An occasional reference can also be located where quantitative information obtained by CD detection might be used in the investigation of metabolic disorders, *e.g.* for lipoprotein lipids [77].

10. DETERMINATION OF ENANTIOEXCESS IN PARTIAL RACEMIC MIXTURES

For all analytical methods the quality of the results ultimately relates back to the chemical purity of the very best available SRM and to the linearity of the correlation curve for the experimentally measured property vs. the SRM concentration. For substances that are naturally chiral there is the additional very serious concern about enantiomeric purity. The determination of an enantiomer whether for an enantiomeric purity test, or for an enantiomeric ratio or excess test in the study of a partial racemic mixture, is one of the more difficult analytical problems. To actually report the enantiomeric purity of an enantiomer as better than 99% is truly beyond the capability of current analytical methodology [31], for after all few substances ever have a chemical purity that is guaranteed to be greater than 99%. So, as mentioned earlier, one has to accept the fact that the results are measured relative to an enantiopurity of an SRM that is "defined" to be 100%. This limitation of course impacts on the true meaning of a calculated enantioexcess, and to a much lesser degree perhaps, in assays of chiral substances extracted from plant materials using calibration data that were obtained for synthetic SRM's.

Chemical purities aside, the measurement of enantiomeric purity and enantiomeric excess are, in many ways, technically the same thing, the difference being the extent of racemization. There are only two experimental options: the isomers are either separated and determined using a single detector, or left unseparated and the amounts calculated using data from two independent measurements made by either one or two detectors. The first approach requires either the intervention of chiral chromatographic methods (*vide supra*), or the very difficult task of crystallizing diastereomers. The second approach can be satisfied, in part, by using achiral chromatography and two detectors (*vide supra*). In a series of papers, Mannschreck [32,78,79] has described some innovative ways in which to use a non-racemic HPLC substrate (triacetylcellulose), and CD detection for the measurement of enantiomeric composition of partial racemic mixtures in spite of extensive peak overlap. Both stopped flow and on-the-fly detection methods were used. The third option of no separation and the use of only one detector involves two spectral measurements. First the CD spectrum of the mixture is measured, a chiral reagent is added and a second CD spectrum of the diastereomers is measured. The method calls for a convenient chiral agent that produces diastereomers instantly. One such agent that, in theory, has the potential, is β-

cyclodextrin. This was attempted for mixtures of S-(-)-nicotine spiked with R-(+)-nicotine [80]. The major problem associated with this reagent is that the spectral changes are often so small that they do not provide the necessary accuracy in the determination.

Other chiral hosts with considerably more potential are metal complexes where the ligands in the parent complex are chiral. Solutions of the complex will have a CD spectrum which, depending upon the choice of metal, might lie in the visible range and therefore remote from UV interferences. Diastereomers are formed when the isomers of a racemic or partially racemic mixture displace the chiral ligands in the first coordination sphere of the parent complex according to the equilibrium reaction:

$$ML_x + [y/2(+)L^* + y/2(-)L^*] \Longleftrightarrow ML_{(x-y/2)}(+)L^* + ML_{(x-y/2)}(-)L^* + yL \quad (1)$$
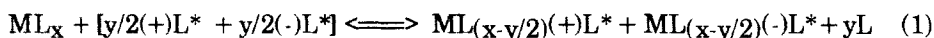
provided $[ML_x]$ is always much larger than [L] so that all of the analyte is complexed. The experimentally measured ellipticity in this case is given by:

$$\psi = \{\theta_u \cdot d \cdot [ML_x] + \theta_{(+)} \cdot d \cdot [ML_{(x-y/2)}(+)L^*] + \theta_{(-)} d \cdot [ML_{(x-y/2)}(-)L^*]\} \quad (2)$$

where ψ is the experimental ellipticity, d is the pathlength, and θ_u, $\theta_{(+)}$, and $\theta_{(-)}$ are the molar ellipticities of the unsubstituted and the mixed ligand metal complexes respectively.

The basis of the method is akin to the Pfeiffer effect [8] except that, in this instance, the roles of the ligands are reversed and reorganization of the inner sphere and not the outer sphere of the metal is intimately involved. The racemate originates in the solution environment and the enantiomer is part of the coordination compound (vide infra). Calculation of the enantioexcess is most easily done using spectral differences. Figure 5 shows the CD spectrum for the parent complex (lowest curve) where M is Cu(II) and L is L-tartrate in strong base together with a series of curves in which the L-pseudoephedrine concentration has been systematically increased. An isosbestic point at 538 nm is obvious [51].

In contrast the spectra for the substitution of L-tartrate by D-pseudoephedrine under identical concentration conditions show no isosbestic point, Figure 6. It should also be evident from this result that if the enantiomers are present together in a partial racemic mixture that the CD signal at 538 nm will be due to *just* the D-enantiomer. The correlation curve for ellipticity vs. the concentration of the D-enantiomer is linear throughout the full range. In the spectra of mixtures little change is seen in the value for the maximum signal at 620 nm as the ratio of the isomers is changed, provided the total enantiomer concentration is constant. In other words, a simple measurement at 620 nm will give the *sum* of the concentrations of the isomers. Consequently the enantioexcess is conveniently determined from measurements made at *two* wavelengths in just a *single* experiment. For a series of laboratory prepared mixtures where the ratios were varied from 1:1 to 99:1, the observed precisions were on the order of 0.5%. The effects are entirely opposite if L is changed to D-tartrate, in which case the D-form of L* will produce the isosbestic point. So if one prefers not to use the 620 nm data alone
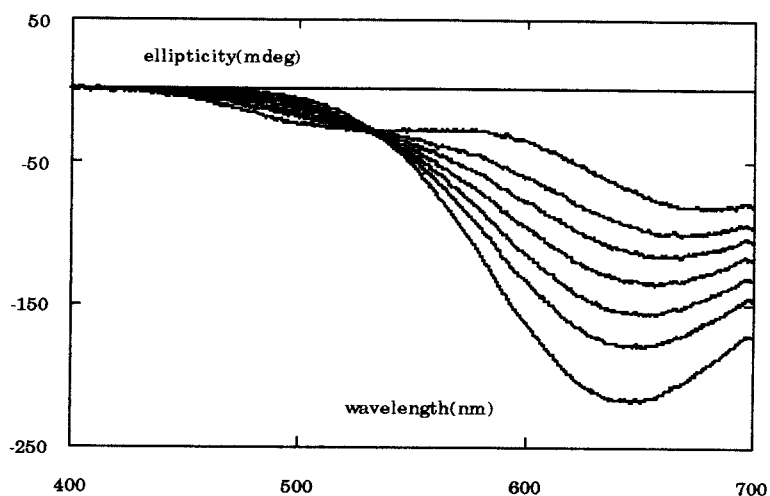
Figure 5: CD spectra for the parent Cu(II)-L-tartrate
(lowest curve) and a series of mixed complexes with
D-pseudoephedrine (0.30-1.60 mM)
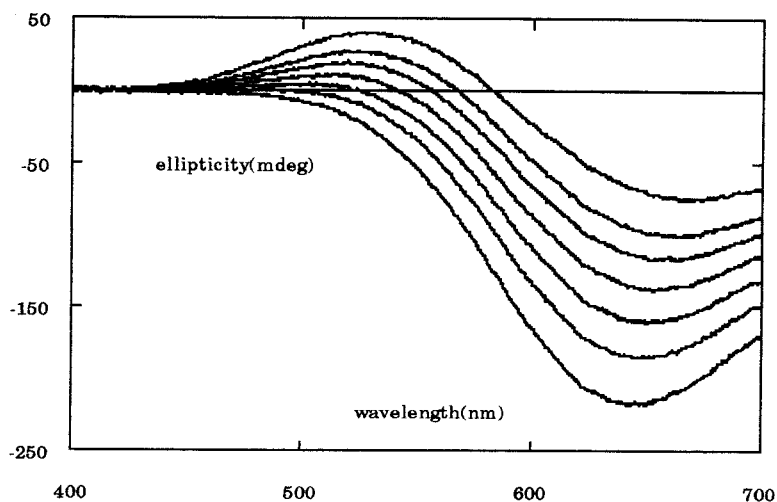
Figure 6: CD spectra for the parent Cu(II)-L-tartrate
(lowest curve) and a series of mixed complexes with
L-pseudoephedrine (0.3-1.6 mM)

to measure the total concentration, one can use instead the Cu-L-tartrate and the Cu-D-tartrate parent complexes to determine the L- and D-forms of L* directly with equivalent precision.

The method can be used effectively for the analysis of binary mixtures of chiral substances other than enantiomers provided the spectra for the mixed complexes of one of the components will produce an isosbestic point. Spectra for those ligands which substitute for L-tartrate without changing the sign of the original CD spectrum of the parent complex will invariably show an isosbestic point. The recommendation is not to try to use calculated metal complex formation constants in making the analyses, but rather to work with a reagent that is a stock solution of Cu(II)-tartrate with a fixed concentration in which the ligand to metal ratio is at least 4:1. Both are kept in large excess over the concentration of the entering ligand in order to reduce the chances of multiple substitution of L by L* on the same metal ion. Other uses of Cu(II)-L-tartrate where the selectivity of the substitution reaction are exploited are described later in the section on color induction.

11. MOLECULES WHERE CHIRALITY IS INDUCED

Molecules in this section fall into two general categories: those that are inherently achiral, and those that, in their most stable thermodynamic state, are racemic mixtures. All have at least one chromophore. The analytical approach is the same for both. They are made to form derivatives by reaction with a chiral host. In the case of racemates the derivatives are diastereomers and methods for their analytical applications have been referenced in earlier sections. Regardless of the distinction between racemic and non-racemic substances, the induced CD effects are uniformly smaller than the effects inherent to chiral molecules by one to two orders of magnitude.

11.1. Cyclodextrins as Host

To date the chiral host molecules most frequently used are the cyclic amylose oligomers or cyclodextrins (Cy), and the work in homogeneous solutions parallels the work done where they are used as chiral stationary phases [5,27]. Among the major reasons for the choice are the ready availability of the compounds in relatively high chemical and optical purity and the convenience of the complexation reactions:

$$Cy + L \iff Cy\text{-}L \qquad\qquad (3)$$

for inherently achiral molecules, and:

$$Cy + (\pm) L \iff Cy\text{-}(+)\text{-}L + Cy\text{-}(-)\text{-}L \qquad\qquad (4)$$
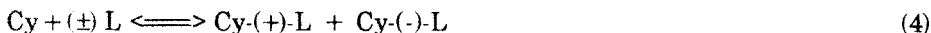
for racemates. On the down side, they do not exhibit a broad selectivity among analytes.

Structures for Cy and the molecular complexes have been described many times before [5] and require no repetition here. Suffice it to say that the hydrophobic center of the truncated conical shape of the host is the favored site for interaction with any non-polar group that is part of the guest on molecular association. Hydrophilic groups of the guest are left outside to interact with the

chiral hydrophilic collar of the Cy structure. The induced CD signals that are produced are weak for a number of reasons: formation constants K_F for the complexes are small (≤ 1000), rotatory powers for the complexes are very low ($\leq$ 100), and aqueous solubilities of the hosts are limited, ranging only from 10-100mM. Signals can be enhanced if host molecule solubilities can be increased. This has been accomplished by resorting to mixed solvents, by adding large excesses (6M) of urea to aqueous solutions [82], and by using the newer peripherally substituted Cy which are more water soluble [28]. Higher concentrations are desired in the conduct of an analysis in order to control the stoichiometry of the complex at 1:1 and is done by using at least a ten-fold excess of host over guest.

From one point of view, the Cy are excellent choices as host molecules because they absorb only in the far UV. As a result, the induced CD signal in the near UV is due only to the complex and its magnitude is, in principle, directly proportional to the concentration of the complex in solution, $\psi_i = \theta.d$ [Cy-L]. This is really true only in the cases where L is an inherently achiral molecule. For racemic mixtures the more exact Beers' law summation equation that relates the observed induced signal to the individual contributions is:

$$\psi_i = \theta_R.d\ [R] + \theta_S.d\ [S] + \theta_{CyR}.d\ [Cy-R] + \theta_{CyS}.d\ [Cy-S] \qquad (5)$$

where R and S are used to represent the two enantiomeric forms. θ_R must equal $-\theta_S$. If there is insufficient host to complex all the analyte the equilibrium concentrations [R] and [S] are less than the initial analytical concentrations, so the first two ellipticity terms on the right side of the equation are smaller than the values for the uncomplexed enantiomers. The decreases will only be equal when K_F values for both complexes are equal. As deduced from chiral chromatography studies, equal stabilities for the complexes are not to be expected. So, part of ψ_i is not related to the structures of the complexes at all. Current models that describe intermolecular binding propose a three point contact in order to produce stability. Because the stereochemistry of the host is fixed and the configurations of the enantiomers are mirror images of each other, the relative spatial orientations and binding energies for Cy-R and Cy-S complexes will differ in which case [Cy-R] $\neq$ [Cy-S], and therefore $\theta_{CyR} \neq \theta_{CyS}$. The relative importance of all the potential inequalities in establishing the magnitude of the induced signal has not been the subject of a major investigation, but the ultimate result is the same as it is for the achiral molecule. The observed signal does correlate linearly with the analytical concentration of the guest.

The linear concentration ranges are, however, fairly limited, being restricted on the low end by the low magnitude of the CD signal and on the high end by the strong UV absorption of the aromatic chromophores. The best compromise whenever possible is to work in the 230-340 nm wavelength range. For simplicity and greater precision, analyses should be done by fixing the solution conditions. For example, Cy at a concentration that is slightly undersaturated is prepared as a stock reagent in aqueous buffer. An aliquot of

268

this is added to a solution of the analyte (also in buffer) and the mixture made up to the mark. A "conditional" calibration curve is prepared using the SRM of the analyte. This procedure is so superior to the alternative in which the analysis is based upon a measured formation constant where errors in the ellipticity measurements can be unacceptably large.

If absorptions are limited to the UV range, interferences can become a considerable problem. The lack of selectivity of the Cy was also mentioned before. Future choices for chiral hosts will be based upon different association mechanisms and presumably will emphasize greater potential for selectivity. Virtually any material that has seen use as a stationary phase for chiral chromatography is a candidate, and others will eventually appear. Some of these have in fact been employed already, although not to the same degree that the Cy have, (*e.g.* cryptands, vesicles, micelles, metal complexes, and proteins). Their immediate most obvious advantage is a substantial increase in the magnitude of the induced ellipticity, which can be enhanced even further by fluorescence detection.

Barbiturates [83], phenethylamines [46], benzodiazepin-2-ones [84], PCP, some analogs, and a few miscellaneous compounds [85] are representative of the achiral substances that have been determined using β-Cy. The PCP's and β-phenethylamine are inherently achiral. Some members from the series of barbiturates and diazepams are racemic as is (±)-phenethylamine. At that juncture in time we were making the analyses using measured K_F values and all analytes were treated in the same way mathematically. The linearities of the correlation lines for achiral molecules and racemates are comparable, supporting the argument that the induced ellipticity is proportional to the analytical concentration whether or not part of it is due to a loss of signal from the uncomplexed form of the enantiomers. All analyses were done first on prepared laboratory mixtures and subsequently on real samples. Secobarbital was determined to within 0.8% of the labeled amount in seconal suppositories [83], and 98% recovery was reported obtained for meperidine in demerol dispensary products [85]. The analysis of PCP came at a time when there was no satisfactory method for its determination. The molecule is heat sensitive and could not be analyzed by GC. Nor was it stable under high vacuum so mass spectrometry could not be used. Diazepam and flurazepam were also analyzed in real samples.

11.2. Other Carbohydrates as Host

Cellulose, starch, and their derivatives are commonly used as chromatographic stationary phases. They are, in principle, potential hosts for inducing CD activity in small molecules and could be used with effect for analysis in homogeneous media with chiroptical detection. An example might be the starch (amylose)-iodide complex [86]. Low aqueous solubility however is an obstacle to their general use in homogeneous solutions. Linear oligomers of maltose are more soluble than starch and could theoretically be used as alternatives to Cy, however they do not really compete in terms of the stability of the association complexes.

The major historical interest in oligosaccharide-chromophore associations is as a source of information on the three dimensional structure of the oligosaccharide using the bi-chromophoric exciton coupling methods

[11]. Theories behind these methods were primarily developed for the determination of the absolute configurations of single molecules, especially steroids, and consist of derivatizing the molecule by substituting two identical chromophores at predetermined sites. Common substituents used as the molecular probes are para-substituted benzoates and polyacenes, *e.g.*
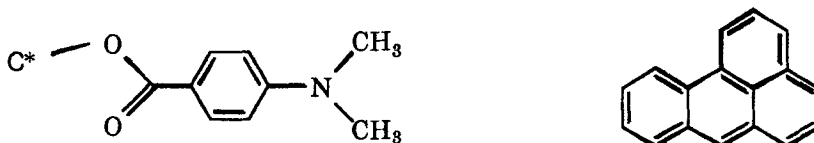
which are chosen because their principal polarization axes coincide with the long molecular axes. The resultant CD spectra typically consist of two adjacent identical Cotton effects that are opposite in sign and whose maximum wavelengths are roughly bisected by a crossover wavelength of zero signal. The order of the signs from long to short wavelength is used to define the relative rotational orientation of the long axes of the chromophores. For example if a positive sign precedes a negative sign, the orientation between the long axes is in a clockwise direction. A major part of the Chapter by Lightner is devoted to the discussion of exciton coupling.

In a totally analogous way CD data are used to elucidate linkages between monomers in oligosaccharides and the local stereochemistry in acyclic polyols [87]. Stereochemical assignments are derived for primary alcohol functional groups using 9-anthroate residues and for secondary alcohols substituents using p-hydroxycinnamate residues. A simpler derivatization reaction with considerable potential for gathering long range macromolecular structural information might be the association equilibrium reaction between a dye molecule and the oligosaccharide. Preliminary evidence appears to imply preferred conformations in solution even for short oligomers [88].

11.3. Proteins as Host

Macromolecule-dye interactions have been studied quite extensively in the proteins, with the emphasis being given to what could be learned from the CD data about the tertiary and quaternary protein structures and about the binding sites of small molecules. This is not the purpose of the present discussion. Analytically speaking, the proteins should be viewed as the host molecules that facilitate the determination of a variety of smaller molecules. Specificity will be great compared to Cy complexes because of the much more sophisticated nature of protein structures, and the subtle conformational changes that occur with solvent and pH. CD detection enhances the selectivity even more. A few references are mentioned only to illustrate the capabilities. One is the determination of drug molecules represented by the association of warfarin with human serum albumin (HSA) that was mentioned before [76], where the detection was by multidimensional FDCD. The article is interesting from the point of view of the chemistry as well as the demonstration of how sophisticated the CD detector can become. The other example is of practical

clinical significance and deals with the association of a wide selection of proteins and enzymes with the natural pigment bilirubin [76,89,90]. The extrinsic CD activity lies in the range of the strong bilirubin absorption bands in the visible, far removed from the range of the CD activity intrinsic to the protein moiety. The anticipated specificity in the binding is obvious from the differences in the CD spectra and especially for the bilirubin complexes with serum albumins from different mammalian species [91]. It is conceivable perhaps to imagine that, under the right solution conditions, bilirubin binding to human serum proteins might be selective enough to discriminate between HSA and gamma-globulins. Molecular complexation between bilirubin and cholesterol is also apparently the mechanism for the production of an extrinsic CD in chloroform extracts of human gallstones [2]. Bilirubin may be the pigment most often investigated but others, such as biliverdin [76], bile pigments [91], and even photosynthetic pigments, participate in associations equally well creating extrinsic CD effects that are just as strong.

Investigations of the structural details associated with protein-pigment equilibria apparently stimulated very few ideas for analytical applications. Complexation of bilirubin with HSA [89] was however used to determine just the unconjugated bilirubin fraction in blood plasma. A linear correlation was obtained up to 30mg/dL, and no interference was seen from hemolysis. A high bias was however reported at high levels of conjugated bilirubin. The obvious specificity of the dye-protein interactions coupled with CD detection, especially FDCD, might be worthy of serious consideration for the determination of urinary proteins that are present in very low concentration levels, for the determination of enzymes; for extra selectivity in immunoassay methods that use polyclonal antibodies; and for the analysis of oligopeptides and glyco-proteins.
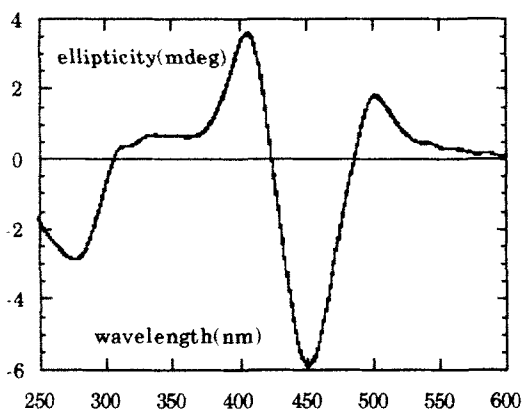
Figure 7: CD spectrum of chloroform solution of crushed cholesterol gallstone: absorbance is from complexed achiral bilirubin

11.4. Chiral Metal Complexes as Hosts

Metals and metal complexes have important roles in all of the sub-disciplines of analytical chemistry, where they are either the analyte or the

analytical reagent, and most especially in biological and environmental systems. As we have seen in every instance throughout this chapter, whenever chiroptical methods were applied to the study of complex systems, the major objective was to get structural information. The same is true for metal complexes where the metal-macroligand complexes are for instance metalloproteins, metalloenzymes, metal interactions with nucleic acids, metals in drug therapy, etc. [92]. In the present context of chirality induction as a means to induce CD activity by association, the focus is on chiral metal coordination compounds as host molecules or complex ions. The Pfeiffer effect [8] is defined to be the change in optical rotation of an optically active system (usually a solution of one enantiomer) upon the addition of a racemic mixture of a labile metal coordination compound. Even although it was applied to small ligand molecules, the motivation for its development was to obtain structural information. The Pfeiffer effect did play a very substantial role in the development of the theories of optical activity in the coordination spheres of metal complexes.

From an analytical viewpoint it was demonstrated that the magnitude of the experimentally observed Pfeiffer effect is proportional to the concentrations of both the complex and the exchanging ligand. It obviously has analytical potential. For greater analytical specificity one might consider replacing optical rotation detection with CD detection. Lability to substitution into the coordination compound is a prerequisite, and is conveniently met if the ligand exchange is confined to only the outer-sphere coordination layer. The easiest way to guarantee lability is to fill the inner coordination sphere with chelating ligands that are substitution inert (*e.g.* in $M.\{(\pm)(o\text{-phen})_3\}^{n+}$, where M most often is Co(III), and in $Ni(acac)_2$). No reference could be found for the use of these coordination compounds in analytical applications.

The selective binding of Cu(II)-L-tartrate to enantiomers of a partial racemic mixture in order to determine enantioexcesses was included in an earlier discussion. At that time, the reaction was compared to the Pfeiffer effect, except that the substitution takes place at the level of the inner-sphere coordination. Cu^{2+} is of course labile to ligand substitution in the inner-sphere because of the effect of the Jahn-Teller distortion. Use of this reagent for enantioexcess measurements is not an exclusive use for it because it is also the major component in the Biuret reagent that is used for the determination of total serum protein in clinical samples [93]. In that application, however, the detector is absorbance, so one would suspect that there can be no aspirations for ever achieving any degree of analytical selectivity. It turns out that selectivity is unobtainable even for CD detection whenever the incoming ligand L* is achiral (*e.g.* creatinine [38]). The only effect on the CD spectrum for the Biuret reagent on the substitution of L-tartrate by creatinine was a decrease in signal intensity that was proportional to the creatinine concentration and no change in the spectrum of the host complex. Creatinine could be measured directly in urine samples buffered to pH 12. On the other hand, if both ligands in the exchange are chiral, then the selectivity among analytes is increased considerably. The discussion of this topic is reserved for the next section on color induction for the creation of an extrinsic CD in non-absorbing chiral compounds.

12. MOLECULES WHERE COLOR IS INDUCED

As indicated in the introduction to the section on Applications, this last category covers those molecules that are chiral but have no chromophore and are therefore CD inactive. The chromophore would be introduced through some "color" derivatization reaction. Absorption in the visible would be the desirable end result, but in some instances absorption in the near UV may be the very best that can be accomplished. The category also includes those molecules that are already CD active but only at very short wavelengths where experimental data are hard to measure.

Color derivatization reactions can be broadly divided as being either reversible or irreversible. A number of examples of reversible reactions have already been described, such as equilibria that involve the association of macromolecules with drugs, pigments, and dye molecules, and substitutions into chiral metal complexes. These methods qualified for discussion prior to this section because they perform a binary function, depending on the circumstances, in that both molecules in the reaction can be either the auxiliary reagent or the analyte. Included under irreversible reactions are those reagents that are selective towards particular organic functional groups [9]. For the most part, reaction conditions are generally much more hostile than are the ambient conditions used for reversible reactions, because the function of the reagent is to produce a chromophoric system that will shift the absorption maxima to the visible range. Some loss of chirality can accompany the introduction of unsaturation. A great many of these reagents have been used in processes where the detector was absorption, *e.g.* concentrated sulfuric and nitric acids, Friedel Crafts reagents, etc. Specificity of the reagent is limited to its ability to react with certain functional groups only. No great degree of analytical selectivity would be predicted. From what we have learned, substituting absorbance with CD detection should enhance the specificity except in instances where all optical activity is lost. Major drawbacks to using most of these reagents routinely are that they are toxic and caustic, reaction conditions usually need to be anhydrous, and temperatures need to be elevated.

Short turn around times are an essential part of clinical analyses and the search for color reagents that are specific to the compounds of concern is supposedly a high priority item. Hostile conditions have been avoided in many instances by introducing enzymes and monoclonal antibodies which would imply that a high degree of specificity is achieved. It is not. To achieve greater selectivities in clinical, biological, immunochemical analyses, etc., CD detection might make a significant contribution. A serious question would be whether the detector is able to reach the low limits of detection. As a reply to that question, a strong argument can be made for FDCD detection.

The remainder of the chapter is devoted to the discussion of two color derivatizing reagents, one irreversible the other reversible, to explore the thesis that greater selectivity is always achieved with CD detection. Results turned out to be rather surprising because for one of the reagents, absorbance detection has defied its reputation as a non-selective detector and performs better than CD.

12.1. Irreversible Color Reaction

The reagent used in discussion of an irreversible reaction system is that originally described by Chugaev [94] as being a 2:1 mixture of 98% acetyl chloride and 35% w/v $ZnCl_2$ in glacial acetic acid. Its original function was that of an acylating and dehydrating agent in the study of reactions of steroids and terpenoids. Reaction conditions are anhydrous and the incubation temperatures used are anywhere from 55-67^{0}C. The mixture, in a somewhat modified form, was used by the author ostensibly to determine the distribution of cholesterol over the three major lipoprotein fractions in human serum, relying upon the selectivity of CD detection to make the discrimination [95]. It turned out that only total and HDL cholesterol levels could be measured, but the measurements were achieved simultaneously. Ironically all three fractions were subsequently measured in a simultaneous manner using the same reagent and the same reaction conditions without any intervening separation step, except the detector was absorbance [96]. The failure of CD detection relative to absorption detection was a definite disappointment but it does serve as a just reminder never to accept prior scientific lore without trial. Since the publication of the report on that first direct measurement of the full lipid panel, the reagent was modified yet again and the same analysis is now done at room temperature.

The same modified reagent has also been used with effect in the analysis of terpenoids and other steroids, and especially for the anabolic steroids. These applications are mentioned only as a passing reference because, like cholesterol, the analytes are more readily determined using zero and/or first order derivative spectrophotometry. If there is one distinct advantage associated with CD detection it is that the 17-ketosteroids, which are major interferences to absorbance detection in the analysis of urine for anabolic steroids, do react with the loss of all CD activity.

12.2. Reversible Color Reaction

For the example of a reversible color reaction we return once more to the equilibria that involve ligand substitution into the first coordination sphere of the Cu(II)-L-tartrate complex ion in aqueous base, namely the Biuret reagent. The tartrate ion is present in a 4:1 excess over Cu^{2+} and the stoichiometry of the complex is believed to be 1:2. The CD spectrum of the parent complex consists of a single, very broad, and fairly intense negative Cotton band maximizing around 620nm, Figure 4. The 620 nm band is localized on the Cu^{2+} ion and the CD would be due to a combination of ligand conformational and complex configurational effects. The incoming ligands L* will all be chiral and typically will absorb in the UV, so the electronic excitations in the mixed ligand complexes will still involve orbitals on the metal ion. New transitions will be possible. Many studies that have involved L* substitutions into aqueous cupric ion have used CD data to calculate stability constants, for example [73,74]. Data of this kind could also be used for analytical work but, as indicated earlier, results are much better if conditions are chosen that fix the stoichiometry of the complex by deliberately keeping its concentration in excess over the [L*]. If these conditions are maintained substitution will be one L* for one L. Within a working range of ratios for $[Cu^{2+}] : [L*] = 5:1$ and greater, good

linear correlation curves can be prepared for ellipticity vs. the concentration of a SRM from of L*.

The selectivity of the method for L* depends upon the changes that are observed between the spectrum for the parent complex, Cu-L$_2$ and the spectra for the Cu-L.L* derivatives. The chiroptical characteristics of the first coordination sphere will be altered after substitution because of the inherent chirality differences in the ligands, but the interactions between L and L*, which in certain cases might involve exciton coupling, are expected to take on a much more significant role in defining the changes in the CD spectra from that for the parent. Our initial study was made using SRM's for the series of aminoglycoside antibiotics, amikacin, gentamycin, kanamycin, neomycin, and streptomycin [51]. These compounds absorb in the far UV, and significant problems are associated with their analytical discrimination and determination. One procedure described in the literature for neomycin sulfate was exactly what is proposed here except that the detector was absorbance [97]. It was also reported earlier in this chapter that neomycin B and neomycin C are distinguishable on the basis of their ORD spectra [56], early testimony to the advantages of chiroptical detectors.

For analyses that use CD detection, either the spectrum for Cu-LL* by itself or the measured differences between the spectrum for Cu-L$_2$ and the spectra for Cu-LL* could be used for quantitation. All are intense enough to give good precision, and levels of detection are on the order of 50µM. Qualitative distinctions on the other hand are best made using the difference spectra which are shown in Figure 8 for the series of aminoglycosides.
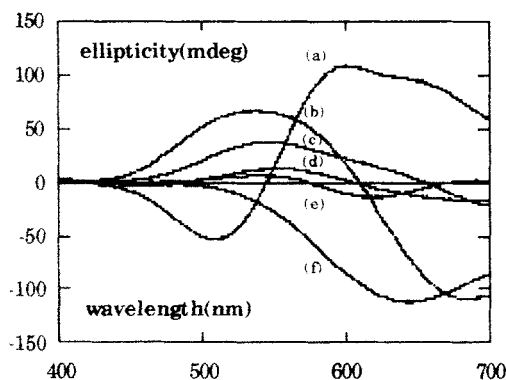
Figure 8: CD spectra for (a) streptomycin; (b) neomycin;
(c) amikacin; (d) gentamycin; and (e) kanamycin; plotted
the difference from the spectrum for the parent complex (f).

Beginning with this one example of a simple incursion into the realm of analytical applications of chiral ligand exchange in homogeneous media coupled with CD detection and the high level of selectivity observed, the prospects for even further enhancement appear to be very bright. Although

outer-sphere substitution into a chiral host, such as $Co(III)-(acac_2enL_2)^-$, by a chiral ligand and CD detection has been used to measure the enantiomeric purity of the incoming ligand [74], copper-L-tartrate is perhaps the first host complex where inner-sphere substitution combined with CD detection has been exploited for analytical purposes. The stability and kinetic lability of complex ions vary with the identities of the central metal ions and the primary ligands and whether the complex is inner-sphere or outer-sphere, so the choice of possible hosts is quite broad. It should be possible to combine the effects of these variables and organize the potential hosts in ways that analytical specificities can be calibrated. Add to these the extra effects on the CD spectra that will accompany the subtle ring-conformational changes that occur in a ligand on chelation, and it might become a very reasonable probability to actually design a host complex that will maximize its selectivity towards a particular analyte in a direct analysis and be of particular use in clinical chemistry.

13. SUMMARY

In this review an account has been given of the potential importance of chiroptical methods, especially CD, as a stand-alone analytical detector. The facility of CD to function in this way is a consequence of the high level of selectivity it has towards optically active analytes that absorb electromagnetic radiation. Derivatization reactions will extend the range of applicability of CD detection to include compounds that are either not optically active or do not contain an absorbing chromophore. So far the exploitation of chiroptical methods has attracted only a few entrepreneurs. Prospects for broader and more searching applications in the future are numerous and most especially applicable in the areas of pharmaceutical, biological, biotechnological, and clinical analysis. Important goals are the confirmation of molecular structures and the easy discrimination between a molecule and its chiral metabolites. Additional selectivity that might arise from first and second order derivative CD spectroscopy is an area that has not even begun to be explored. The discipline would benefit greatly from the involvement of additional practitioners.

14. REFERENCES

1   E.J. Ariens, quoted in Chiral Drug Analysis, C&EN, 68 (1990) 38.
2   N. Purdie and K.A. Swallows, Anal.Chem., 61 (1989) 77A.
3   C.Djerassi, in Optical Rotatory Dispersion and Circular Dichroism in Organic Chemistry, McGraw-Hill, New York, 1960.
4   W.H. DeCamp, Chirality, 1 (1989) 2.
5   T.J. Ward and D.W. Armstrong, Chromatographic Chiral Separations, M. Zief and L.J. Crane (eds.) Chromatographic Science Series, Vol 40, Marcel Dekker, New York, 1988.
6   T.M. Lowry, Optical Rotatory Power, Longmans, Green, London, 1935.
7   A. Cotton, Compt.rend., 120 (1895) 98.
8   P. Pfeiffer and K. Quehl, Ber., 64 (1932) 2667.
9   J. Bartos and M. Pesez, Colorimetric and Fluorimetric Analysis of Steroids, Academic Press, New York, 1976.

10   S.F. Mason, Q. Rev. Chem. Soc., 15 (1961) 287.

11   N. Harada and K. Nakanishi, Circular Dichroic Spectroscopy, Exciton Coupling in Organic Stereochemistry, University Science Books, Mill Valley, California, 1983.

12   N. Purdie, K.A. Swallows, L.H. Murphy, and R.B. Purdie, Trends Anal. Chem., 9 (1990) 136.

13   R.E. Synovec and E.S. Yeung, J. Chromatogr., 368 (1986) 85.

14   M.P. Thomas, G. Patonay, and I.M. Warner, Pract. Spectrosc., 12 (1991) 421.

15   I. M. Warner and L.B. McGown, Anal. Chem., 64 (1992) 343R.

16   H.G. Brittain, in Molecular Luminescence Spectroscopy: Methods and Applications, Chapt. 6, Part 1, (S.G. Schulman, ed.), Wiley, New York, 1985.

17   K.A. Kime and R.E. Seivers, Aldrichimica Acta, 10 (1977) 54.

18   M. Hatano, T. Nozawa, T. Murkami, T. Yamamoto, M. Shigehisa, S. Kimura, T. Kakakuwa, N. Sakayanagi, T. Yano, and A. Watanabe, Rev. Sci. Instrum., 52 (1981) 1311.

19   G. Brandl, F. Kastner, A. Mannschreck, B. Nolting, K. Andert, and R. Wetzel, J. Chromatogr., 586 (1991) 249.

20   T. Takakuwa, Y. Kurosu, N. Sakayanagi, F. Kaneuchi, N. Takeuchi, A. Wada, and M. Senda, J. Liq. Chromatogr., 10 (1987) 2759.

21   S.A. Westwood, D.E. Games, and L. Sheen, J. Chromatogr., 204 (1981) 103.

22   A. Mannschreck, Chirality, 4 (1992) 163.

23   E.S. Yeung and R.E. Synovec, Anal. Chem., 58 (1986) 1237A.

24   P. Salvadori, C. Bertucci, and C. Rosini, Chirality, 3 (1991) 376.

25   W. Boehme, Chromatogr. Newsletter, 8 (1980) 38.

26   C. Meinard, P. Bruneau, and J. Perronett. J. Chromatogr. 349 (1985) 109.

27   D.W. Armstrong, J. Liq. Chromatogr. 7 (1984) 353.

28   D.W. Armstrong, A.M. Stalcup, M.L. Hilton, J.D. Duncan, J.R. Faulkner, and S.C. Chang, Anal. Chem., 62 (1990) 1610.

29   V.A. Davankov, in Advances in Chromatography, Vol 18, (J.C. Giddings, ed.), Marcel Dekker, New York, 1980.

30   W.H. Pirkle and J.M. Finn, Asymmetric Synthesis, Vol.1 J.D. Morrison (ed). Academic Press, New York 1983.

31   J. Zukowski, Y. Tang, A. Berthod, and D.W. Armstrong, Anal. Chim Acta, 258 (1992) 83.

32   A. Mannschreck, D. Andert, A. Eiglsperger, E. Gmahl, and H. Buchner, Chromatographia, 25 (1988) 182.

33   S.W. Souci, W. Fachmann, and H. Kraut, Food Composition and Nutrition Tables 1982/82, 2nd. ed.,WissenschaftlicheVerlagsgesellschaft mbH, Stuttgart, 1981.

34   P. Crabbe, ORD and CD in Chemistry and Biochemistry; An Introduction, Academic Press, New York, 1972.

35   G. Schnatzke (ed.), Optical Rotatory Dispersion and Circular Dichroism in Organic Chemistry, Heyden, London, 1967.

36   L.A. Nafie, J.C. Cheng, and P.J. Stephens, J. Amer. Chem. Soc., 97 (1975) 3842.

37 N. Purdie, Prog. Anal. Spectroscopy., 10 (1987) 345.
38 N. Purdie, Forensic Sci. Rev., 3 (1991) 1.
39 N. Ueno and B. Chakrabarti, J. Biochem. Biophys. Methods, 15 (1988) 349.
40 K. Zamani, D.P. Conner, H. Weems, S.K. Yang, and L.R. Cantinela, Chirality, 3 (1991) 467.
41 T.A. Crone and N. Purdie, Anal. Chem., 53 (1981) 17.
42 J.M. Bowen and N. Purdie, Anal. Chem., 52 (1980) 573.
43 J.M. Bowen, T. A. Crone, A.O. Hermann, and N. Purdie, Anal. Chem., 52 (1980) 2436.
44 J.M Bowen, T.A. Crone, R.K. Kennedy, and N. Purdie, Anal. Chem., 54 (1982) 66.
45 S.M. Han and N. Purdie, Anal. Chem., 58 (1986) 113.
46 J.M. Bowen, T.A. Crone, V.L. Head, H.A. McMorrow, R.K. Kennedy, and N. Purdie, J. Forensic Sci., 53 (1981) 2237.
47 V.M. Potapov, V.M. Demianovich, and A.P. Terentiev, Zh. Anal. Khim., 19 (1964) 254.
48 A. Brossi and D, Tadic, quoted in Chiral Drug Analysis, C&EN, 68 (1990) 44.
49 J.M. Bowen, H.A. McMorrow, and N. Purdie, J. Forensic Sci., 27 (1982) 822.
50 W.M. Atkinson, J.M. Bowen, and N. Purdie, J. Pharm. Sci., 73 (1984) 1827.
51 A. R. Engle, PhD Dissertation, Oklahoma State University, 1993.
52 L.A. Mitscher, The Chemistry of the Tetracycline Antibiotics, Vol.13, Marcel Dekker, 1978.
53 N. Purdie and K.A. Swallows, Anal. Chem., 59 (1987) 1349.
54 R.F. Miller, T.D. Sokoloski, L.A. Mitscher, A.C. Bonacci, and B.A. Hoener, J. Pharm. Sci., 62 (1973) 1143.
55 J.M. Bowen and N. Purdie, J. Pharm. Sci., 71 (1982) 836.
56 A. Gergely, O. Papp, Gy. Szasz, J. Vamos, and Gy. Bacsa, Acta Pharm. Hung., 50 (1980) 98.
57 S.M. Han and N. Purdie, Anal. Chem., 58 (1986) 455.
58 R.A. Firth, H.A.O. Hill, J.M. Pratt, R.J.P. Williams, and W.R. Jackson, Biochemistry, 6 (1967) 2178.
59 N. Purdie and K.A. Swallows, J. Ag. Food Chem., 39 (1991) 2171.
60 W.M. Atkinson, S.M. Han, and N. Purdie, Anal. Chem., 56 (1984) 1947.
61 S.M. Han and N. Purdie, Anal. Chem., 57 (1985) 1068.
62 N. Purdie and K.A. Swallows, Anal. Chem.,
63 J.R.J. Pare, M, Sigonin, J. Lapointe, US Patent No. 5,002,784, (1991).
64 V.M. Potapov, V.M. Demianovich, and R.S. Rakovska, Zh. Anal. Khim., 39 (1984) 983.
65 A. Gergely, J. Pharm. Biomed. Anal., 7 (1989) 523.
66 J.C. Kuo and E.S. Yeung, J. Chromatogr., 223 (1981) 321.
67 W.C. Johnson, Jr., Adv. Carbohyd. Chem. and Biochem., 45 (1987) 73.
68 L.D. Hayward, S.J. Angyal, Carbohydr. Res., 53 (1977) 13.
69 A. Kimura, S. Chiba, and M. Yoneyama, Carbohydr. Res., 175 (1988) 17.
70 A. Domard, Int. J. Biol. Macromol., 9 (1987) 333.
71 S.S.M. Hassan, Microchim. Acta, 1 (1981) 9.

278

72   B.H. Reitsma and E.S. Yeung, Anal. Chem., 59 (9187) 1059.

73   V.A. Davankov and P.R. Mitchell, J.C.S. Dalton, (1972) 1012.

74   Y. Fujii, Bull. Chem. Soc. Japan, 47 (1974) 2865.

75   B. Jirgensons, Optical Activity of Proteins and Other Macromolecules, 2nd.Ed., Springer-Verlag, New York, 1973.

76   M.P. Thomas, G. Patonay, and I.M. Warner, Anal. Biochem., 164 (1987) 466.

77   G.C. Chen and J.P. Kane, Methods Enzymol. 128 (1986) 519.

78   A. Mannschreck, M. Mintas, G. Becher, G. Stuhler, Angew. Chem. Int. Ed. Engl., 19 (1980) 469.

79   A. Mannschreck, A. Eiglsperger, and G. Stuhler, Chem. Ber., 115 (1982) 1568.

80   N. Purdie and K.A. Swallows (unpublished work).

82   D.W. Armstrong and H.L. Jin, Anal. Chem., 59 (1987) 2237.

83   S.M. Han and N. Purdie, Anal. Chem., 56 (1984) 2825.

84   S.M. Han, N. Purdie, and K.A. Swallows, Anal. Chim. Acta 197 (1987) 57.

85   S.M. Han and N. Purdie, Anal. Chem.,56 (1984) 2822.

86   T. Nishimura, H. Yajima, S. Kubota, T. Ishii, R. Endo, Kobunshi Ronbunshu, 47 (1190) 717; Chem. Abstr., 113 (1990) 193806a.

87   W.T. Wiesler, K. Nakanishi, Croat. Chem. Acta, 62, (1989) 211.

88   A.R. Engle, J.A. Hyatt, and N. Purdie, (unpublished work).

89   A. Grahnen, I. Sjoholm, and M. Michaelsson, Clinica Chim. Acta, 52 (1974) 187.

90   G. Blauer, Biochim. Biophys. Acta, 884 (1986) 602.

91   G. Blauer, Israel J. Chem., 23 (1983) 201.

92   H. Sigel (Ed.) Metal Ions in Biological Systems, Vols.8,9,12,13,14. Marcel Dekker.

93   G.R. Kingsley, J. Lab. Clin. Med., 27 (1942) 840.

94   L. Chugaev and A. Gastev, Chem. Ber., 42 (1910) 4631.

95   N. Purdie, L.H. Murphy, and R.B. Purdie, Anal. Chem., 63, (1991) 2947.

96   N. Purdie, E.A. Lucas, and M.B, Talley, Clin. Chem., 38 (1992) 1645.

97   J.K Agrawal, S.G. Harmalkar, and R. Vijayavargiya, Microchem. J., 21 (1976) 202.

Chapter 9

The use of circular dichroism as a liquid chromatographic detector

Andras Gergely[a]

a Department of Pharmaceutical Chemistry, Semmelweis University of Medicine, H-1092 Budapest, Hogyes Endre U. 9 Hungary

Outline

1. **INTRODUCTION**

2. **APPLICATIONS**

3. **SUMMARY**

4. **REFERENCES**

Abstract
The article is a brief review of the applications of CD as a detector in both preparative and analytical liquid chromatography. The objectives are to identify elution orders for enantiomers, to measure enantiomeric purities and enantiomeric excesses, to analytically determine diastereoisomers, and to selectively determine chiral analytes when present as components in mixtures with achiral substances.

For specific details on the instrumental arrangements for LC detection, readers are referred to the chapter by Bobbitt.

1. INTRODUCTION

A great many naturally occurring compounds are optically active. Many others are prepared synthetically using stereoselective preparative methods. Altogether almost one-half of the 2050 pharmaceutical substances reported in the US Pharmacopoeial Dictionary of Drug Names [1] are chiral compounds. From a purely analytical point of view this is a very fundamental and important molecular property that must be characterized. Furthermore we are becoming increasingly aware of the fact that the stereospecificity of drug action is related to, even controlled by, the particular asymmetry of molecular receptors in various organs or fluid components of the human body. As a consequence, enantiomers of chiral drugs can have significantly different biological and pharmacological activities. Some of the side effects from metabolic processes that involve the distomer, or pharmacologically inactive form, are innocuous but for others relatively low toxicity levels and pathological reactions can produce tragic results. Such was the case with S(-) thalidomide. Differences of this kind are quite unexpected yet are very real. Not all are this serious. The enantiomers of propranolol, for instance, differ in biological activity by a factor of 100 in favor of the (S) enantiomer. For these reasons a complete stereochemical characterization (i.e. determination of absolute configuration and enantiomeric purity) should really be authorized for all chiral pharmaceutical substances before marketing the product. Legislation of this kind has already been written by the US FDA for new drug products that are chiral. Material safety data sheets and quality assurance testing protocols must be provided with the substances for both isomeric forms when a chiral drug is submitted for approval. At the present time chromatographic methods offer the best analytical alternatives for chirality characterizations.

2. APPLICATIONS

2.1 Stereoisomers

Distinction should be made at this time between diastereoisomers and enantiomers. The former are characterized by the presence of at least two closely associated asymmetric centers in the molecular structure, either of which can epimerize. Altogether then there are two pairs of enantiomers for a total of four stereochemically unique individuals. Diastereoisomers have different physical properties and as a result discriminations, and even separations, can be done relatively easily. Enantiomers on the other hand differ in only one physical property, i.e. the direction of rotation of polarized light. Reaction of an enantiomeric racemic mixture with a third chiral species will produce a mixture of diastereomers therefore facilitating their identification or their separation. Early examples of this were the separations done by fractional crystallization of salts produced by a derivatization reaction with, for example, the alkaloid (-)-brucine. Fractional crystallization would never seem to be an effective analytical method yet it was used with some success in a forensic sciences context to confirm the presence of (L)-cocaine by a carefully contrived microcrystalline test. The physical properties

of diastereoisomers that are of more value in modern analytical methods are the different chromatographic retention times and different NMR shifts. The prevailing thoughts behind methods development for the discrimination and quantitation of enantiomers in enantiomeric mixtures and the measurement of enantiomeric purity are still the same, namely that derivatization to diastereomers is a necessary pre-requisite. Compared with fractional crystallization, these methods are more reliable, more accurate, and more convenient.

2.2 HPLC separation methods

Apart from being able to distinguish between diastereomers the analytes must also be separated from all other potentially chiral interferences that either are endogenous to the mixture or are likely to be produced in the derivatization reaction. Accordingly interest has been directed towards the separation of drug enantiomers by high performance liquid chromatography (HPLC). The technique can provide a quick, reliable and sensitive method for chiral resolution and for the determination of the enantiomeric purity.

There are two general approaches to the separation of enantiomers by LC. In one the derivatizing agent is an integral part of a chiral stationary phase. Distribution equilibria differences determine the relative retardation of one diastereomer compared to the other and ultimately the analyte is eluted as the separated enantiomers after different retention times. In the other, the stationary phase is prepared from conventional achiral materials and the mobile phase is the chiral dertivatizing reagent. Chirality in the mobile phase is achieved by introducing chiral additives to an achiral solvent rather than by using chiral solvents which altogether are few in number, difficult to get at the required level of 100% enantiomeric purity, very expensive, and non-recyclable. Derivatizations occur either pre-column or on-column and the analyte is eluted as time separated diastereoisomers. Obviously the first option is the recommended one if the purpose of the separation is preparative and not analysis.

2.3 HPLC Detectors:

In its broadest terms the discussion of HPLC detection for chiral species must include the analysis of mixtures with achiral substances as well as the quality testing of, for example, the enantiomeric purity of a chemically pure drug form. The distinction between the definitions of chemical purity versus optical purity can not be overemphasized. In an efficient chiral HPLC system the latter problem is trivial, and if retention times are significantly different then any conventional detector such as RI, electrochemical, absorption, etc., could be used. Co-elutions are a major experimental concern in separations of mixtures and at this juncture it is not only prudent but absolutely necessary to involve a chiroptical detector to preferentially identify the chiral analyte.

The idea of two sequential detectors, one conventional the other chiroptical, is the basis of a third strategy for enantiomeric purity determinations using HPLC. It differs from the previous two by not involving a chiral separation. In it the enantiomers co-elute and the total amount is determined from an absorbance measurement. Subsequently a chiroptical

detector is used to measure a quantity that is proportional to the difference in the polarization properties of the enantiomers. Single wavelength detection will suffice for both detectors and simultaneous solution of the Beers' law type equations gives the concentrations for both enantiomers. With a more sophisticated mathematical model it is even possible to quantitate the enantiomeric ratio when only partial separation is achieved. This however will require detection at more than one wavelength. Once again only in the case of the determination of the optical purity for a chemically pure substance is the problem easy to solve.

In the study of mixtures, differentiation between enantiomers is a two level problem which is somewhat independent of whether the LC system is chiral or conventional. The problems common to both systems are the effects of overlapping bands on the performance of the detector(s). Overlap can be between chiral-achiral species on the one hand and co-eluted chiral-chiral with achiral on the other. On first thought the chiral-achiral distinction should be relatively easy if a chiroptical detector is used because the achiral compounds will not interfere with the detection measurement. In addition the ability of the chiroptical detector to measure both positive and negative signals makes the confirmation of the enantiomeric structure elementary [3,4]. As pointed out earlier, enantiomers co-elute from conventional columns and two detectors in sequence will provide the information to measure the enantiomeric ratio provided the mixture is not racemic. Partial or total overlap of the band for a non-chiral species with the chiral eluate band increases significantly the difficulty in measuring an enantiomeric ratio. In this instance the total absorbance that is measured may include a contribution from the non-chiral species which without correction will lead to an overestimation of the amount of chiral material and an erroneous value for the enantiomeric ratio. Under these circumstances there is no other LC option but to develop a separation that is based upon a chiral system.

These advantages inherent to chiroptical detectors are particularly useful in the analysis of physiological fluids. The unique selectivity of chirality detection for LC is often due to the fact that optical activity is frequently associated with biological activity, another form of a derivatization reaction.

Two types of chiroptical detectors can be designed; one is based on optical rotation (OR), i.e. polarimetry as a function of wavelength, and the other on CD. LC detectors based on optical activity (OA) measurements are potentially advantageous in a number of difficult areas of organic analysis. As most chromatographic eluants are not optically active, the analyst is not constrained by the choice of eluants or gradients. The dispersive nature of optical rotation, or ORD, means that rotations increase in magnitude at shorter wavelengths so rather than working in the range of the Na-D line, where direct polarimeteric measurements are typically made, OR detectors should be made that operate in the UV. Rotations that are coupled with absorbance create an anomalous dispersion known as a Cotton effect and are enhanced even more leading to even lower limits of detection. In LC, single wavelength detection is most often used so the Cotton effect curve is never developed. CD detectors on the other hand give a non-zero signal only in the region of the anomalous optically active absorption band. The range of a CD

detector therefore is more restricted but as a result it is more selective than an OR detector. This can be both an advantage and a disadvantage depending upon the system and the problem. The advantage is that with CD detection it becomes unnecessary to deliberately separate chiral species that do not absorb from those that do, provided, of course, the analyte of interest is CD active. On the other hand if one wishes to determine all sorts of chiral species then the OR detector has the edge. For saccharides the far UV is the only choice of wavelength and OR is much superior to CD detection.

2.4 Applications of polarimetric detection:

A variety of applications of polarimetric detection in HPLC have been reviewed in the literature [6-8]. The recent development of laser-based polarimeters with micro-degree sensitivity has substantially increased the applicability of OR detection in HPLC [4, 9-15]. Perhaps the most limiting features of LC detection using conventional light sources are the very low working concentrations of the analytes in the eluate in order to prevent overloading the column, and the very short sample pathlengths viewed, as they are, across the inner diameter of the eluate exit tubes. With the added sensitivity from laser illumination, Yeung and Reitsma were the first to demonstrate the enantiomeric purity determination of a series of amino acids by using UV and RI detection coupled with laser polarimetry [16].

Limits of detection for many amino acids were enhanced considerably by pre-column derivatization with the achiral reagent dansyl chloride whose function it was to increase their specific rotation [17]. Determinations of the enantiomeric purities for mixtures of D-and L-tryptophan [18] and of isomeric ratios for mixtures of pseudoephedrine and its diastereomer ephedrine [19], were effected using diode-laser polarimetry and using OR detection in series with UV absorbance detection respectively.

Bobbitt and Yeung [12-15] developed a novel variation to the method of OR detection by using an optically active eluant coupled with polarimetric detection to quantitate optically *inactive* components as they elute from an LC column. The time independent rotation signal of the eluant is changed when an achiral analyte is eluted. The amount of change in the angle of rotation from the solvent value is proportional to the concentration of the analyte and can be nulled by rotating the analyzer by an amount equivalent to the rotation from the "baseline" for the achiral eluate. This follows because as an optically inactive compounds elutes, it replaces an equal amount of the eluant in the detector cell which produces a decrease in the observed optical rotation. In such a manner the prospect exists for developing indirect polarimetry as a more universal detector for LC. Optically inactive analytes such as dibutyl phthalate and hydrocarbons could be detected at the 12µg level. The extent of its utility however is tempered by the availability and costs associated with optically pure solvents and it is not likely to become commonplace.

2.5 Applications of CD detection:
2.5.1 Dissymmetry ratios in (ee) measurement

A CD based LC detection system has been introduced by Mason and co-workers [20]. It has been shown to be capable of recording simultaneously

the concentration, as the absorbance (A), and the optical activity, on the basis of difference absorbance (ΔA) for left- and right-circularly polarized light of a given fraction with a single detection system, and also, of measuring the enantiomeric purity of that solute in the fraction.

The dissymmetry ratio or g-factor ($\Delta A/A$) is constant at a given wavelength with an optimum value for the optically-pure enantiomer (g_{max}). The g-factor is independent of the analyte concentration and is linearly related to the enantiomeric excess (ee), i.e. (ee) = [(g_{exp}/g_{max}) x 100]. The enantiomeric composition of the eluates can be determined directly during the chromatographic analysis. This is a convenient alternative to solving the pair of simultaneous equations that relate (A) and (ΔA) to the concentrations of both isomers.

The optical resolution of pavine (I) (obtained by synthesis from papaverine) and Tröger's base (II) on a microcrystalline triacetylcellulose (MCTC) column has been demonstrated [20].
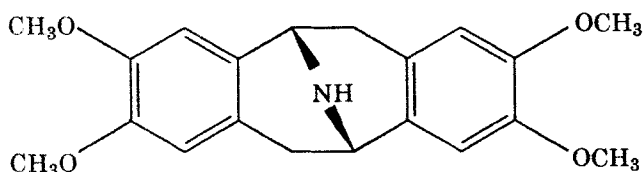
I
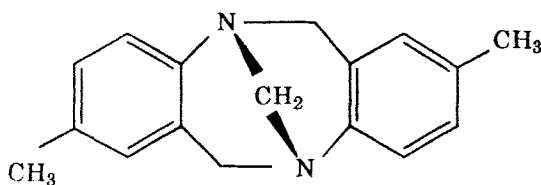
II

Chromatograms of the optical resolution of (I) and (II) are shown in Figure. 1. Compound (II) is completely resolved into its enantiomers chromatographically. The g-factor remains at its constant optimum value throughout the elution band of each enantiomer. Compound (I) in contrast is incompletely resolved, giving a single absorbance elution band, but a double bisignate difference absorbance band. The fractions of (I) eluted in the volume between the vertical dashed lines are incompletely resolved. Values for the g-max factors have been determined from the CD and absorption spectra of (I) and (II).

The chromatographic resolution of (R-S)-7-chloro-1,3-dihydro-3-methyl-5-phenyl-2H-1,4-benzodiazepin-2-one (III) is another example of the previous method that can be cited [21], Figure. 2.
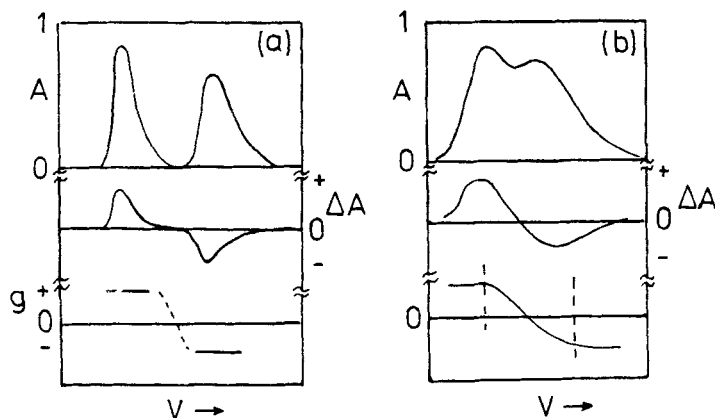
Figure 1. Chromatograms showing the optical resolution on micro- crystalline triacetylcellulose of (a) Troger's base, (II), and (b) pavine (I), with a mobile phase of ethanol-water (9:1). The chromatograms record the absorbance (A), the differential absorbance of LCP and RCP radiation, (ΔA), and the g-ratio (ΔA/A), as a function of the elution volume, (V). In (b) the fractions of pavine eluted in the volume between the vertical dashed lines are incompletely resolved, the volume being recycled to achieve a further separation. (Ref. 19).
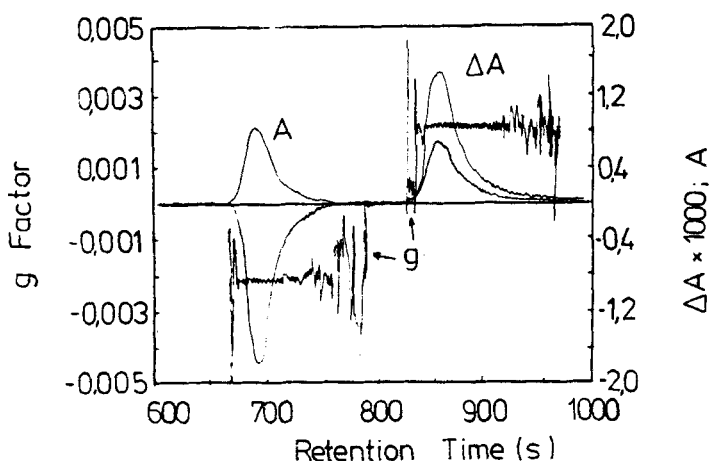
Figure 2. Chromatographic resolution of (III): chiral stationary phase is "SiSquinmai" (CSP I); eluant is hexane-2-propanol (90:10,v/v); flow rate is 1ml min^{-1}. UV, CD and g-ratio detection is at 254 nm. (Ref. 20).

The separation was confirmed using simultaneous detection by a CD detector, namely a Jasco, J-600 dichrograph equipped with a micro HPLC cell attachment with a volume of 8µl, and a UV detector operating at 254 nm. In this case, the values of the anisotropy factors are constant but reversed in sign for the two enantiomers. When baseline resolution is obtained, (ee) is 100% for each enantiomer, and the point at which the fractions should be collected becomes obvious.
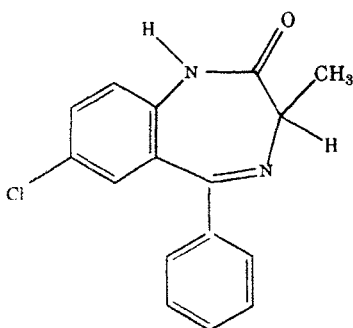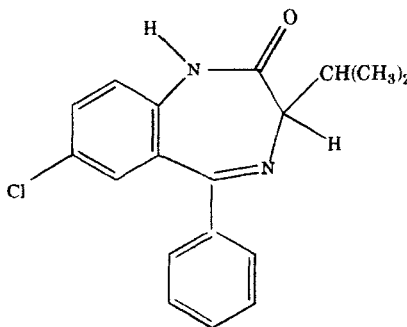
III   IV

2.5.2 Measurement of (ee) in preparative LC

The direct measurement of enantiomeric excess is important in the optimization of fraction collection in preparative LC because overlapping of the peaks that correspond with the two enantiomers often occurs. When partial resolution is reported, Figure. 3, the (ee) of the eluted fractions can be determined by the profiles of the g-factor [21]. It can be seen that the first eluted enantiomer can be collected at high optical purity (ee) $\geq$ 95%, while the second enantiomer can not (ee) around 60%).

If the g-factor is on the order of 10^{-3} or higher, this detection system can be used to determine the (ee) of chiral compounds using nonchiral HPLC columns. The absorbance gives the concentration of the eluate and the value of the CD gives its enantiomeric excess. The (ee) can be directly evaluated by the dissymmetry factor, because it does not depend upon concentration.

Another example of the chromatographic resolution of a starting mixture with relatively low chemical purity is shown in Figure 4, [21]. The chromatographic profile that is obtained with CD detection reveals only two peaks, allowing a safe identification of the antipodes of (R) and (S)-7-chloro-1,3-dihydro-3-i-propyl-5-phenyl-2H-1,4-benzodiazepin-2-one, (R,S)-(IV). But the profile obtained with the UV absorbance detector provides evidence for at least four different peaks, two of which are partially overlapped. Thus the enantiomeric composition is more correctly determined by CD detection.

CD detection can be used advantageously when the two peaks largely overlap. Only one peak is revealed by the UV detector, while two peaks are observed when CD is used for monitoring, Figure 5(a). The information that is obtained demonstrates the extent of the enantiomeric separation, and can
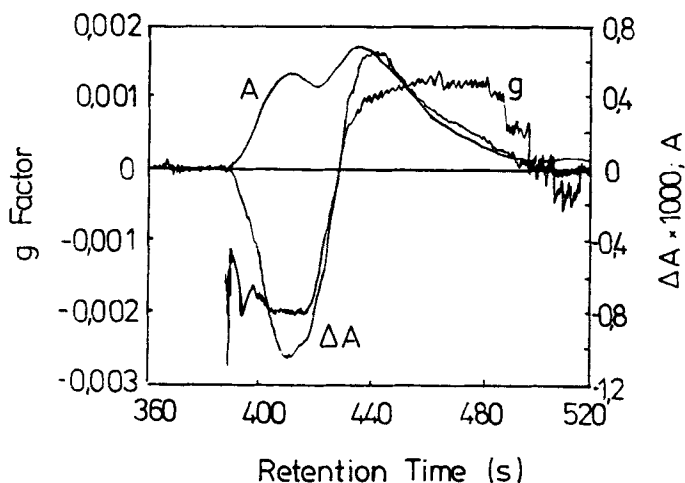
Figure 3. Chromatographic resolution of (III) on CSP I. Eluant is hexane-2-propanol-CH$_2$Cl$_2$ (88:2:10,v/v/v); flow rate is 1ml min^{-1}. UV, CD and g-ratio detection at 254 nm. (Ref. 20)
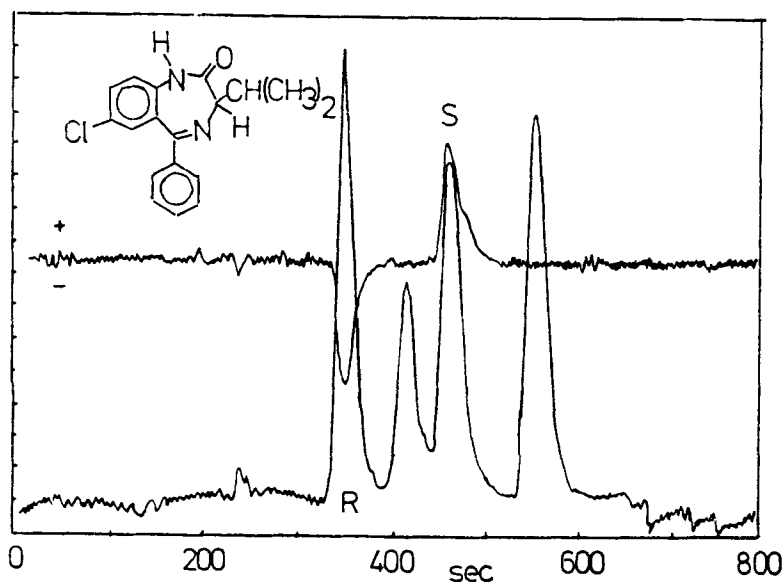
Figure 4. The chromatographic resolution of (R,S)-IV (of low chemical purity) monitored by absorption (lower trace) and CD detection (upper trace). (Ref. 21)

be used to suggest which changes in the chromatographic parameters might serve to improve the separation even more, e.g. see Figure 5(a)-5(c).

288
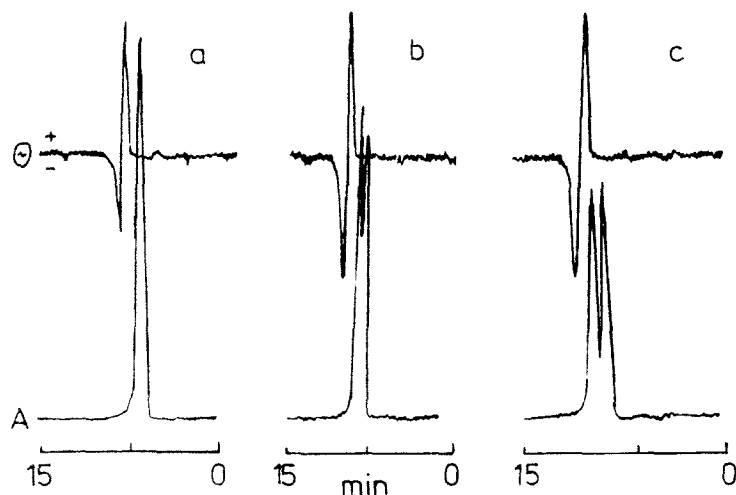
Figure 5. The chromatographic resolution of (R,S)-IV on an ionic Pirkle
column. Flow rate: 1 ml/min. Eluant hexane/2-propanol, 60/40 (a),
80/20 (b), and 90/10 (c). Absorption (A) and CD detection (~) at
254 nm. (From Ref. 21)

2.5.3 Determination of absolute stereochemistry of an eluate

Data from a CD detector can be used to successfully confirm the
absolute stereochemistries of the eluted enantiomers and the elution order.
This important application has been introduced by Salvadori and co-workers
[23]. More recently it was demonstrated that an on-line detection system can
be made which measures the CD spectrum of the eluate by trapping and
holding it in the HPLC cell. By comparing the spectrum with data in a CD
spectral library, absolute configurations can be confirmed. Where spectra are
unavailable, absolute configurations might be obtained by means of either
empirical and semiempirical approach or by using nonempirical methods
such as the exciton model or the DeVoe approach [22, 23].

2.5.4 Discrimination among enantiomers

Enantiomerically pure forms of 3-substituted-1,4-benzodiazepin-2-ones
show significant differences in their pharmacological activity. Compounds (V)
and (VIII) are the tranquilizers oxazepam and lorazepam while (VI) and (VII)
are structural analogs of oxazepam. Discriminations are possible using two
detectors in sequence after separation on a chiral column.

A variable wavelength UV detector and a CD detector were connected
in series. The chiral stationary phase (CSP) that effects the separation was
prepared by reacting N-methylquininium iodide with mercaptopropyl-
silanized silica (CSP I) [24]. For (V) and (VIII), where a free hydroxyl group
is present, an efficient separation was made using CSP I. By blocking this
functional group with an acetyl group, (VI), or by substituting it with an alkyl
group, (VII), the retention as well as the extent of resolution were greatly
decreased. Only a single peak is observable with the absorption detector for
(VI) and (VII); the actual separation of the enantiomers being confirmed only
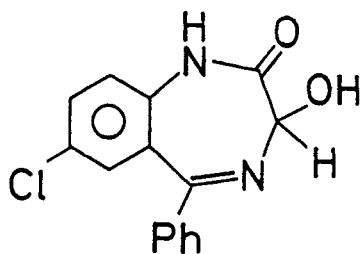
V
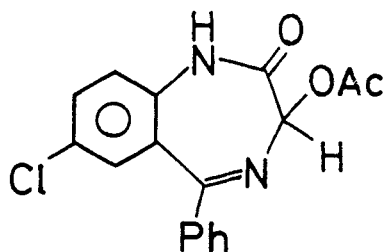
VI
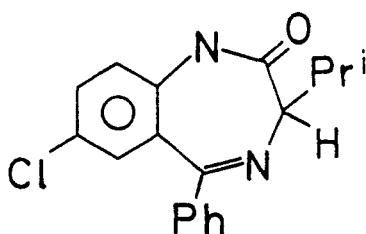
VII
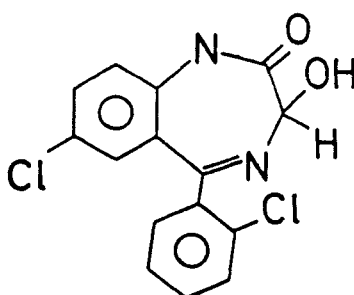
VIII

by the data from the CD detector. This observation points out the usefulness of the CD detector coupled with a spectrophotometric detector.

As reported earlier the sign of the CD signal for the (S)-(VII) enantiomer at the measuring wavelength is positive. The structures of compounds (V) and (VIII) are very similar and it can be assumed with reasonable assurance that a positive CD sign can be correlated with the structure that has the S-stereochemistry. The negative sign for the CD signal for the first eluted enantiomer from a mixture of (V), (VI), and (VIII) is a good indication that in this case the (R) enantiomer is the one that is retained to the least extent.

Biotransformations for the different 3-substituted-1,4-benzodiazepines during pharmacological testings have been monitored using CD and UV detectors connected in series and set at 254 nm [25]. Several CSP's have been used to obtain suitable amounts of pure enantiomers for the pharmacological tests. The enantiomeric purities of fractions were determined prior to their being administered. Chromatographic resolution was optimized in order to detect even a few per cent of the less abundant enantiomer. This can be achieved by choosing a CSP which will reverse the normal elution order for the enantiomers of the benzodiazepinones. With an appropriate choice the

less abundant enantiomer can be eluted first which illustrates very clearly another advantage that is associated with CD detection.

Three chiral stationary phases that were prepared by derivatizing γ-mercaptopropylsilanized silica gel with quinine (CSP II), quinidine (CSP III), and cinchonidine (CSP IV), have been used for the successful resolution of N-acyl derivatives of ß-hydroxyphenethylamines [25]. UV and CD detectors set at 270 nm were used in series. The effectiveness of the separation and the detection are illustrated in Figure 6 for the resolution of the N-(3,5-dinitrobenzoyl) derivative of phenylethanolamine on CSP III.
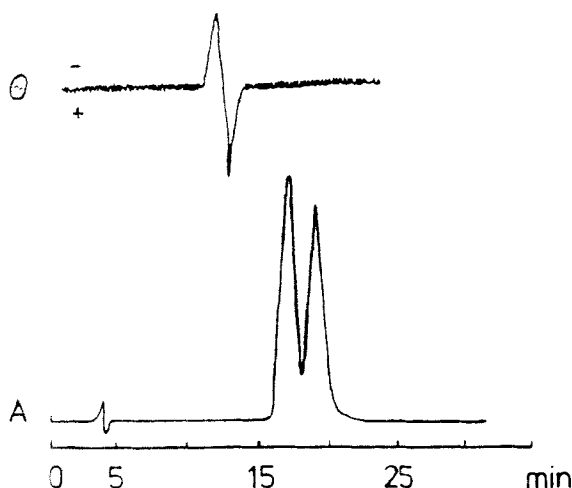
Figure 6. The resolution of N-(3,5-dinitrobenzoyl) derivative of phenylethan-
olamine on the CSP III. Eluant is hexane/2-propoanol/acetonitrile,
80/20/5 (v/v/v). Absorption (A) and CD (θ) detection at 270nm.
(From Ref. 24).

It is noteworthy that the elution order obtained on CSP II is the same as that provided by CSP IV, but CSP III reverses the elution order. It is well known that quinine and quinidine are diastereoisomeric compounds that, in practise, behave as though they were enantiomers. Actually with this system the less abundant enantiomer can always be eluted first making the determination of (ee) easy.

2.5.5 Applications to chiral-achiral mixtures

CD active compounds can be selectively detected when present in a complex matrix comprised of other, specifically achiral, compounds such as might normally be encountered in the extracts of either natural products or biological fluids. Pyrethrines, tryptophans, rotenoids, and amaryllidacae alkaloids have been used to evaluate the system [27]. Monitoring at selected wavelengths has enabled detection levels in the low microgram range to be realized. By using stopped-flow techniques, full CD spectra can be obtained.

2.5.6 Applications of LC-CD detection to the study of proteins

HPLC methods are well accepted for the rapid, selective, and highly efficient analytical scale separation and the semi-preparative recovery of proteins. CD spectral data measured in the UV have been instrumental in the interpretation of the secondary structure of the same macromolecules. Conceivably the coupling of these two techniques might provide extra specificity and structural sensitivity in the analysis of proteins [28, 29].

The biological activity of a protein is related to its three dimensional conformational structure. This activity however is often reduced or lost entirely during an HPLC separation process, for example by denaturation induced by the solvent mobile phase. Using gradient elution reversed phase LC the extent of denaturation should be measurable using an on-line CD detector and has in fact been accomplished on a micro sample in a flow cell arrangement. The influence of surfactants and packing materials on the extent of the loss of the α-helix content has been measured. Salts such as sodium chloride in the concentration range 0-300 mM have been seen not to cause the denaturation of proteins.

2.5.7 Miscellaneous systems

Synovec and Yeung developed a highly selective and sensitive laser-based CD detector for both conventional and microbore liquid chromatography [30] and applied it to the analysis of complex mixtures of optically active metal complexes. As expected limits of detection are very low. For example for the determination of (+) tris(ethylenenediamine) cobalt (III) using an Ar-ion laser source, a microbore column, and a CD detector operating at 488 nm, the measured limit of detection is 5.6 ng.

Riboflavin (vitamin B2) is an important chemical species that occurs in many complex biologically related samples. The substance is chiral and strongly fluorescent and the coupling of these molecular properties into the FDCD-HPLC detection system greatly enhances both the specificity and the limit of detection capabilities of the method. In the specific case of riboflavin an HPLC system using FDCD detection where excitation is done at 325nm with a HeCd-laser a detection limit of 170 pg of riboflavin [30] is attainable. This level is about 10 times better than what is possible with a laser excitation -transmission CD-HPLC system [29].

3. SUMMARY

This chapter is only a brief introduction to the science of HPLC with CD detection systems. The material that is included is not intended to be exhaustive and apologies are made to those whose work has been excluded. The area of research continues to offer exciting challenges for the future as the emphasis on the preparation of enantiomeric forms and the measurement of enantiomeric purities continue to tax our collective ingenuities.

4. REFERENCES

1   M.C. Griffith, in USAN and USP Dictionary of Drug Names, 1961-1980, Cumulative List, US Pharmacopoeial Convention Inc. Rockville, MD., 1980.

2   W. Boehme, H. Stenz, and O. Bonisgnori, Int. Lab. 13 (1983) 28.

3   E.S. Yeung, L.E. Steenhoek, S.D. Woodruff, and J.C. Kuo, Anal. Chem. 52 (1980) 1399.

4   J.L. DeCesare, L.S. Ettre,J. Chromatogr. 251 (1982) 1.

5   D.K. Lloyd, D.M. Goodall, Chirality 1 (1989) 251.

6   A. Gergely, J. Pharm. Biomed. Anal. 7 (1989) 523.

7   N. Purdie and K.A. Swallows, Anal. Chem. 61 (1989) 77A.

8   J.C. Kuo and E.S. Yeung, J. Chromatogr. 223 (1981) 321.

9   J.C. Kuo and E.S. Yeung, J. Chromatogr. 229 (1982) 293.

10   J.C. Kuo and E.S. Yeung, J. Chromatogr.253 (1982) 199.

11   D.R. Bobbitt and E.S. Yeung, Anal. Chem. 54 (1984) 1577.

12   D.R. Bobbitt and E.S. Yeung, Anal. Chem. 57 (1985) 271.

13   E.S. Yeung, J. Pharm. Biomed. Anal. 2 (1984) 255.

14   E.S. Yeung, Adv. Chromatogr. 23 (1984) 1.

15   B.H. Reitsma and E.S. Yeung, J. Chromatogr. 362 (1986) 353.

16   B.H. Reitsma and E.S. Yeung, Anal. Chem. 59 (1987) 1061.

17   D.K. Lloyd, D.M. Goodall, and H. Scrivener, Anal. Chem.61 (1989) 1238.

18   Z. Wu, D.M. Goodall, D.K. Lloyd, J. Pharm. Biomed. Anal. 8 (1990) 357.

19   A.F. Drake, J.M. Gould, and S.F. Mason, J. Chromatogr. 202 (1980) 239.

20   C. Bertucci, E. Domenic, and E. Salvadori, J. Pharm. Biomed. Anal. 8 (1990) 843.

21   P. Salvadori, C. Bertucci, and C. Rosini, Chirality 3 (1991) 376.

22   P. Salvadori, C. Rosini, and C. Bertucci, J. Org. Chem. 49 (1985) 5050.

23   C. Bertucci, C. Rosini, D. Pini, and P. Salvadori, J. Pharm. Biomed. Anal. 5 (1987) 171.

24   P. Salvadori, C. Bertucci, E. Domenici, and G. Giannaccini, J. Pharm. Biomed. Anal. 7 (1989) 1735.

25   P. Salvadori, C. Rosini, D. Pini, C. Bertucci, and G. Uccello-Barretta, Chirality 1 (1989) 161.

26   S.A. Westwood, D.E. Games, and L. Sheen, J. Chromatogr. 203 (1981) 103.

27   E. Castiglinoni, T. Takakuwa, Y. Kurosu, A. Wada, M. Saito, N. Sakayanagi, and H. Okahana, in. Proc. 2nd. Internat. Conf. on Circular Dichroism (M. Katjar, ed.), Eotvos University Press, Budapest (1987) 304.

28   Y. Kurosu, T. Sasaki, T. Takakuwa, N. Sakayanagi, K. Hibi, and M. Senda, J. Chromatogr. 515 (1990) 407.

29   R.E. Synovac and E.S. Yeung, Anal. Chem. 57 (1985) 2610.

30   R.E. Synovac and E.S. Yeung, J. Chromatogr. 368 (1986) 85.

Chapter 10

Application of circular dichroism spectropolarimetry to the determination of steroids

Andras Gergely[a]

[a] Department of Pharmaceutical Chemistry, Semmelweis University of
Medicine, H-1092 Budapest, Hogyes Endre U. 9. Hungary

Outline

1. INTRODUCTION

Abstract
    Analytical methods that use direct and difference CD detection which
have been developed for the determination of steroids, both as reference
standard materials and in pharmaceutical preparations, are critically
described.

1. INTRODUCTION

Chiroptical methods are widely used in the elucidation of the structure of steroid molecules [1-9]. Quantitative determination and control of the optical purity of drugs can also be solved by chiroptical methods, but they are rarely applied in pharmaceutical analysis. In pharmacopoeias, the only experimental measurements that are reported are optical rotations at the sodium D-line. These figures provide no specificity and relatively low analytical sensitivities. Nevertheless several papers have appeared in the literature where steroid determinations are based on the measurement of optical rotation [1,10-17]. The purpose of this chapter is to describe the applications of circular dichroism (CD) spectral measurements to the analysis of steroid molecules with particular emphasis to pharmaceutical preparations and drug forms.

2. DIRECT CD DETERMINATIONS OF STEROIDS

None of the steroid molecules is colored so direct electronic spectrophotometric analyses must be done in the near UV range. The major chromophores are, of course, the aromatic ring, ketone, conjugated ketones, and ethynyl groups. With some exceptions prior derivatization reactions are generally required for the determinations of sterols. These reactions can be either reversible or irreversible. Ketal formation, for instance, is an example of the latter type color induction reactions are examples of the second kind.

2.1 Ketal formation:

Ketal formation is a procedure used in steroid synthesis. For example the reaction of cholestan-3-one (I) in anhydrous methanol with a trace of concentrated hydrogen chloride was investigated by Zalkow and co-workers (18).

$$I \qquad\qquad II$$
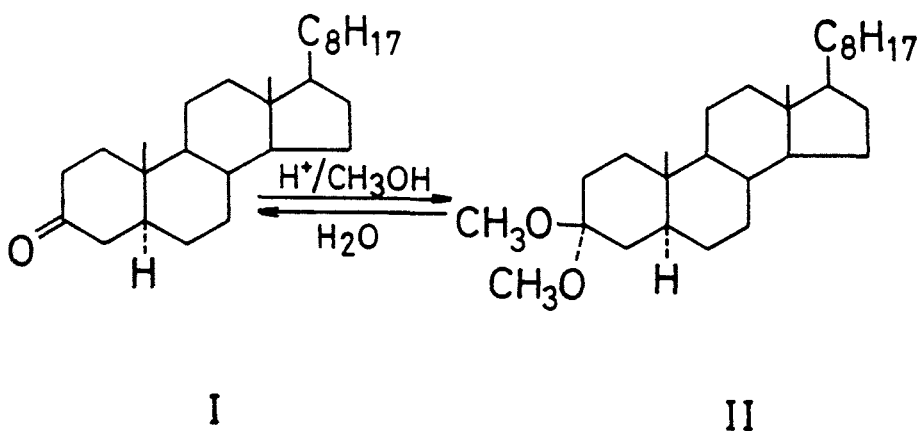
The course of the reaction can easily be followed by observing the decrease in the Cotton effect curve. The change in the CD curve for (I) indicates that

approximately 90% of the ketal (II) is formed after a few minutes. There is, however, an equilibrium between (I) and (II) that is dependent upon the amount of water present (Fig. 1).
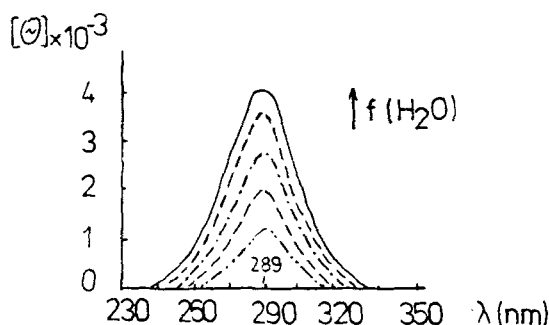
Figure 1. CD investigation of the ketone-ketal equilibrium for cholestan-3-one in acidified methanol. The Cotton effect due to free ketone increases with successive additions of water to the ketal. (From Ref. 18).

This figure also shows the potential for using CD as a tool for kinetic analysis. The Cotton effect at 289 nm is due to the concentration of free ketone present. The dimethyl ketal absorbs at much shorter wavelength. Repeated additions of small amounts of water shifts the ketone-ketal equilibrium toward the free ketone, which increases the value of the experimental molecular ellipticity. The formation of ketal also depends upon the structure of the alcohol, as well as on stereochemical factors. Thus cholestan-3-one gives 96% of dimethyl ketal, 84% of diethyl ketal and only 25% of the diisopropyl ketal. The proportion of ketal formed from the 3-keto-5β-steroids is higher than in the case of their 5 α isomer.

2.2 Specificity in chemical reactions:

Specificity in chemical reactions that form products which have CD Cotton effects at distinctly different wavelength ranges from the parent can be used for the direct analysis of steroids and even steroid mixtures. For instance a simple dilution of the reaction mixture after the enzymatic production of prednisolone from hydrocortisone was used by Bartos [19] in the determination of these two compounds. Hydrocortisone is measured selectively at 326 nm where prednisolone has no dichroism.

In the course of the production of medroxy-progesterone acetate (IV), a drug with a strong progestogenic effect, the isomer (V) is also formed from (III).

Discrimination between the isomers was possible because of an appreciable difference in their CD spectra, Potapov et al. [13]. At 308 nm, the molecular ellipticity of the β isomer is 5400° while that of the α isomer is zero. With a different chemistry one can also produce the 4,6-diene derivative, megastrol acetate (VI), by the isomerization of (III). At 292 nm, the molar ellipticity of (III) is 21000° while

$$\text{III} \qquad\qquad \text{IV} \qquad\qquad \text{V}$$
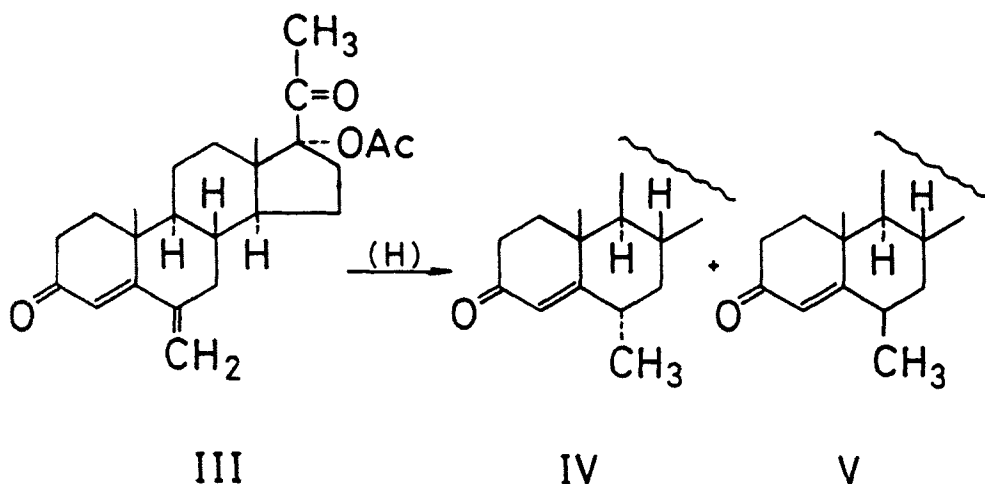
that of (VI) is 0°; while at 238 nm, the molar ellipticity of (VI) is 17000°, and that of (III) is 0°. Thus (III) and (VI) can both be determined directly in the presence of the other [20] without prior separation.

$$\text{VI}$$
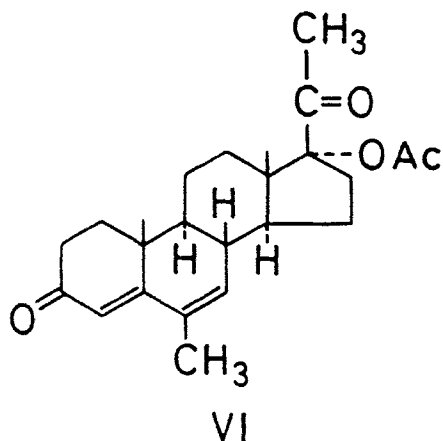
2.3 Ketosteroid impurities:

In a series of review papers Gergely et al. [21-23] reported the use of CD detection to solve various quantitative analytical problems. CD curves can, in some cases, be usefully applied to determine α, β-unsaturated ketosteroid impurities in basic drug materials [21]. For instance ethynodiol is manufactured from norethisterone, so norethisterone acetate might always remain as an impurity in

the product ethynodiol diacetate, in the same way that norethisterone may be present in ethynodiol. Norethynodrel, which contains the $\Delta^{5/10/}$-3-keto bonding system, is likewise always contaminated by a certain amount of Δ^4-3-keto compound, mainly norethisterone. Figure 2 shows the CD curves of norethisterone and norethynodrel in dioxan.
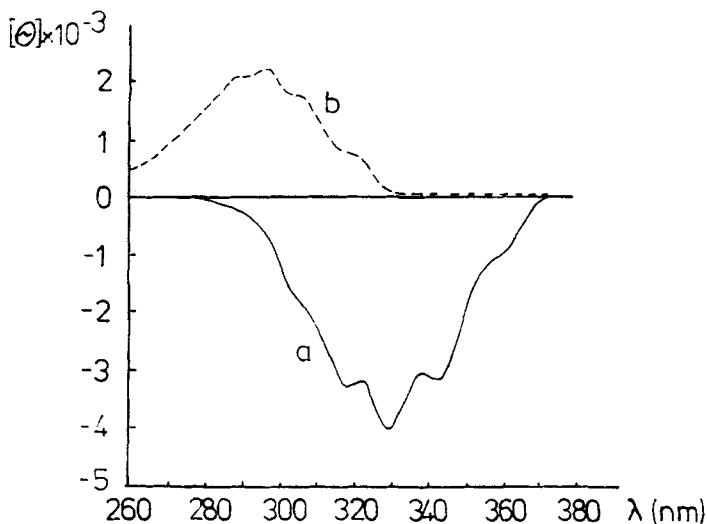
Figure 2. CD curves for (a) norethisterone and (b) norethinodrel in dioxane; c = 1 mg ml^{-1} (From Ref. 21).

At the negative maximum of 331 nm for norethisterone, the spectrum for norethynodrel still shows a slight positive ellipticity. Accordingly measurements were made at the other longer wavelength negative maximum in the spectrum of norethisterone, i.e. at 342.8 nm. At this wavelength, neither the base materials nor the common 3,5-diene impurities display any net ellipticity. Nor is the determination disturbed by the presence of contaminating oestrogenic compounds, making determination relatively easy.

From a quantitative study of model substances it was established that, for ethynodiol diacetate and norethynodrel contaminated with 0.05-5% norethisterone acetate and norethisterone respectively, the ellipticity varies linearly with the concentration and values that were found were in accordance with the results from the preceding difference spectrophotometric determination.

To summarize, it has been confirmed that the use of CD detection methods for the determination of Δ^4-3-ketosteroid impurities in the above substances is highly selective and the procedure is much shorter and less laborious than previous methods.

2.4 Analysis of steroids in oily injections:

Steroid hormones, especially those containing the Δ^4-3-keto-chromophore group, are frequently marketed in the form of oily injections. Direct determination of the active ingredient content using the CD method is conveniently done by measuring the ellipticity of an aliquot of the injection after the very simple process of dilution with an appropriate solvent [22]. Problems that might arise in these analyses and the recommended method of examination are discussed in the case of an oily injection that contains testosterone phenylpropionate.

In an earlier study [24], CD spectra for Δ^4-3-ketosteroids in different solvents were reported. Of the solvents studied, cyclohexane appeared to be the most suitable choice. However it was discovered that benzyl alcohol, present in the injection as a preservative at a concentration of 10% v/v, distorts the CD spectrum of testosterone phenylpropionate when cyclohexane is used as the solvent. Variations in the CD spectra of testosterone phenylpropionate in the presence of increasing concentrations on benzyl alcohol are shown in Fig. 3.
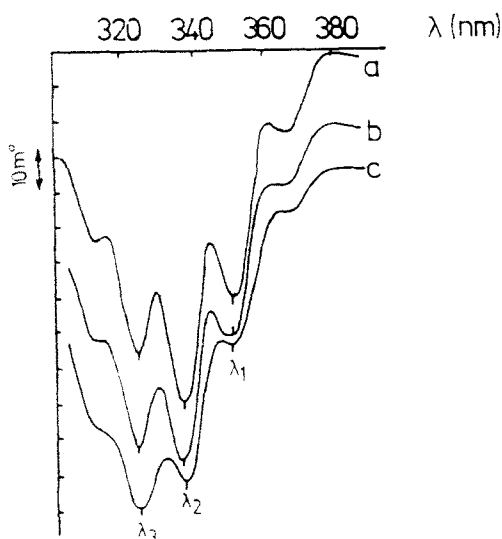
Figure 3. CD curves for testosterone phenylpropionate injections with various
concentrations of benzyl alcohol: a 1.0 ml injection was diluted to 25.0
ml with cyclohexane. (a) 50μl, (b) 200 μl, (c) 600μl benzyl alcohol per 1
ml oily solution. The descending ordinate represents increasing
negative ellipticity and the scale divisions are 0.01°. (From Ref. 22).

The seriousness of the extent of the distortions in the spectra are better represented in a plot of the ratio of ellipticities at the wavelengths of maximum negative ellipticity around 320 and 350 nm against the concentration of benzyl alcohol in the injection (Fig. 4a).

Obviously cyclohexane is an unsuitable solvent medium for this analysis. In further tests dioxan was determined to be the almost ideal choice of solvent as no

significant distortion of the CD spectra occurred in the presence of increasing concentrations of benzyl alcohol (Figs. 4b and 5). Ellipticities of oily injection solutions in dioxan vary linearly with the concentration of the steroid in the range 0.04-0.7 mg ml^{-1}.
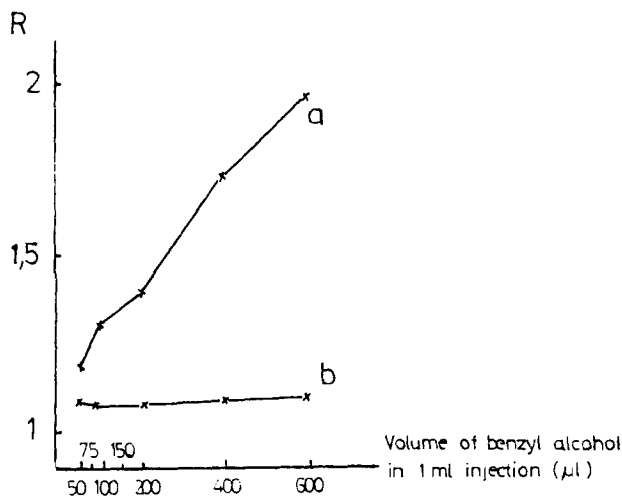
Figure 4. Dependence of the ellipticity ratio (R) of testosterone phenylpropionate on the benzyl alcohol content of injection after dilution with (a) cyclohexane and (b) dioxane. (From Ref. 22).
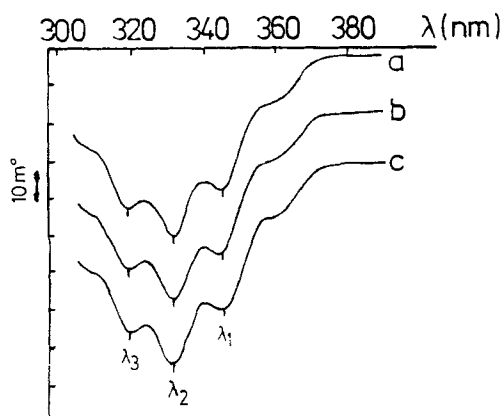
Figure 5. CD curves for testosterone phenylpropionate injections with various concentrations of benzyl alcohol: a 0.5 ml injection diluted to 25.0 ml with dioxane (a) 50µl, (b) 200µl, (c) 600µl benzyl alcohol per 1 ml oily solution. The descending ordinate represents increasing negative ellipticity and the scale divisions are 0.01°. (From Ref. 22).

Component(s) of sunflower oil, the carrier solvent in oily injection formulations, were found to produce a negative Cotton effect below 334 nm which will interfere with that for testosterone phenylpropionate at its wavelength of maximum negative ellipticity, 330 nm. Consequently, the wavelength selected for the direct measurement of ellipticity of the steroids was 342.8 nm, the long wavelength of maximum negative ellipticity of the steroids, where the sunflower oil exhibits no CD.

The procedure as described was successfully applied to the analyses of Retandrol[R] Injection (testosterone phenylpropionate), Nerobolil[R] Injection (nandrolone phenylpropionate), Glanducorpin[R] Injection (progesterone), and Limovanil[R] Injection (progesterone and oestradiol benzoate). The oestrogen component in Limovanil Injection was shown to have no effect on the ellipticity of progesterone and is not an interferent.

3. DIFFERENCE CD METHODS FOR DETERMINATIONS OF STEROIDS

The methods above are based on the direct measurement of the CD curves of the test compounds at one or more wavelengths. Now several difference CD (ΔCD) methods are described that are based upon the changes brought about in the CD curves by either physical or chemical effects. Difference chiroptical methods are generally introduced for the purpose of increasing analytical selectivity [25].

In the practise of difference CD methods, the compound to be determined must be present at the same concentration in both the test and reference solutions. The resultant ΔCD curve arises exclusively from the change in the spectrum of the compound in question in response to physical or chemical effects in one of the solutions. The technique is particularly important in cases where selectivity in the measurements are not possible.

3.1 Physical effects: solvent polarity

The lower intensity, long wavelength absorption bands of α, β-unsaturated ketones vary considerably with the polarity of the solvent. The same is also true for anomalous ORD spectra and CD spectra both of which have absorbance by a chromophore as a pre-requisite. The chiroptical spectra however are much more sensitive than absorbance spectra to the interaction between the solvent and the solute.

The fine structure of the absorption band associated with the n-π^* electronic transitions in Δ^4-3-ketosteroids is better resolved using chiroptical detection methods compared to absorbance spectrophotometry. Selectivity in the determination of these steroids, therefore, is increased using the solvent-dependent CD spectra of the compounds being investigated, and enhanced even more if difference CD procedures are developed [24].

CD curves for testosterone phenylpropionate in four different solvents are shown in Figure 6. Curves for the other compounds, testosterone, methyltestosterone, different testosterone esters, nandrolone phenylpropionate, norethisterone, and d-norgestrel, are essentially coincident with those in Fig. 6. The figure also demonstrates well how an increase in solvent polarity leads to a

characteristic hypsochromic shift of the peak related to the n-π^* electronic transition in the ketones.
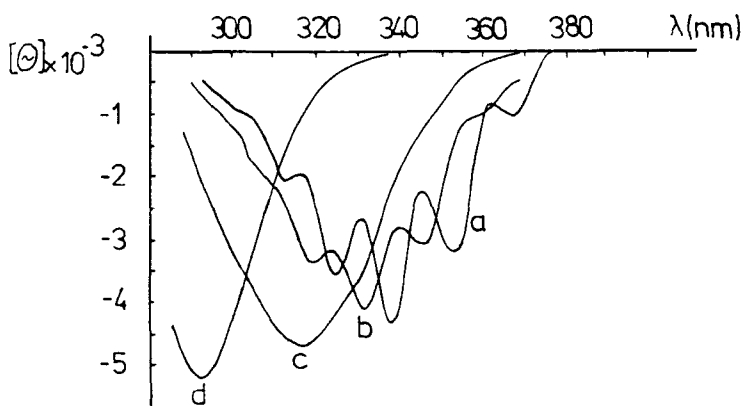
Figure 6. CD curves for testosterone phenylpropionate, c = 0.5 mg ml^{-1} (a) cyclohexane, (b) dioxane, (c) methanol, (d) hexafluoropropanol. (From Ref. 24).

This solvent effect is the basis for the development of a difference CD spectroscopic method for the determination of Δ^4-3-ketosteroids present in pharmaceutical formulations. Ellipticities for solutions of equal concentrations of these compounds in both cyclohexane and methanol are measured at 353.1 nm. A spectrum which is the difference between the CD curves obtained in this way for testosterone phenylpropionate is shown in Fig. 7.
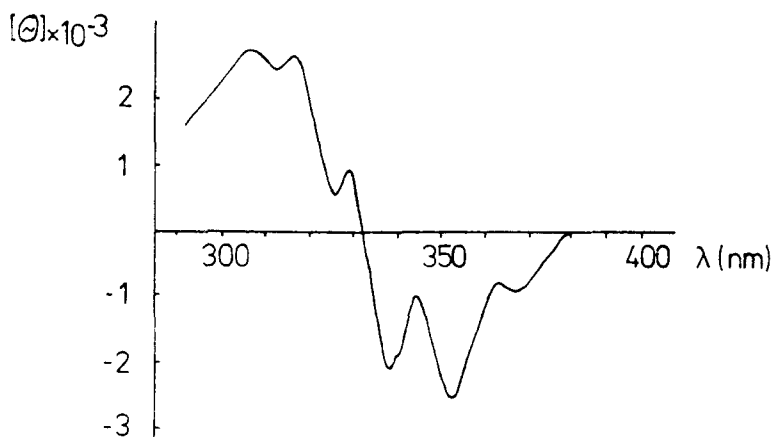
Figure 7. Difference CD curve for testosterone phenylpropionate (the cyclohexane solution was recorded against the methanol solution). (From Ref. 24).

The method has been applied successfully to the determination of the Δ^4-3-ketosteroid content of oily injections where the solvent pair were dioxane and isopropanol [26]. Likewise 21-hydroxy- and 21-acetoxycorticosteroids can be determined by means of ΔCD spectroscopy [27].

3.2 Chemical effects

3.2.1 Reactions with periodic acid:

Periodic acid is a selective reagent for the cleavage of 1,2-diols and related substances, such as 1-amino-2-hydroxy compounds, 1,2-diketones and α-hydroxyketones. With periodic acid, corticosteroid compounds (where R= H, OH), can be transformed into 17β-carboxylic acids and formaldehyde.

$$CH_2OH$$
$$C=O$$
$$\text{---R} \xrightarrow{\text{periodic acid}} COOH \text{---R} + HCHO$$
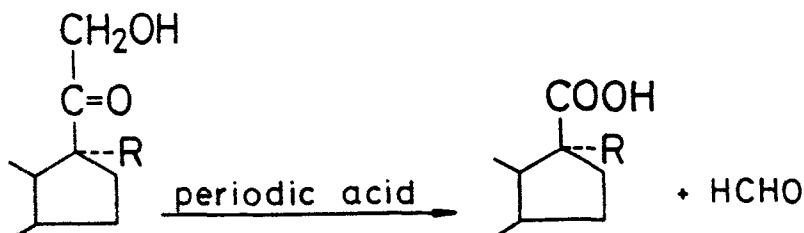
The C-17 side-chain of corticosteroids does not contain a chromophoric group suitable for spectrophotometric measurement, nor does oxidation of the chain lead directly to spectrophotometrically active derivatives. However, the 20-keto group of the 17 α-ketol side-chain, as a chirally perturbed chromophoric group, has an optically active absorbance band in the interval 270-300 nm that is characteristic of the n-π* electronic transition for saturated ketones. An intense positive Cotton effect is observed in the CD spectra; see the CD spectra for hydrocortisone and cortisone in Figures 8 and 9.
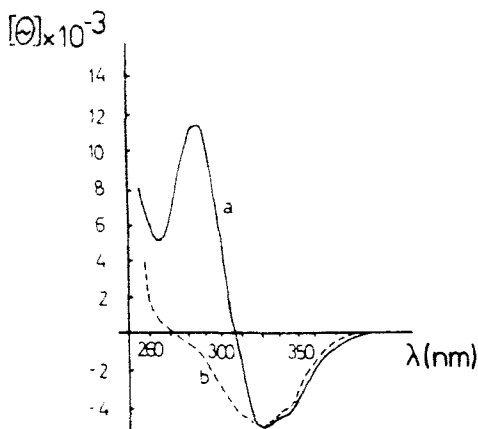
Figure 8. CD spectra of hydrocortisone. (a) before reaction; (b) after reaction; (c) 0.2 mg ml^{-1} (From Ref. 27).
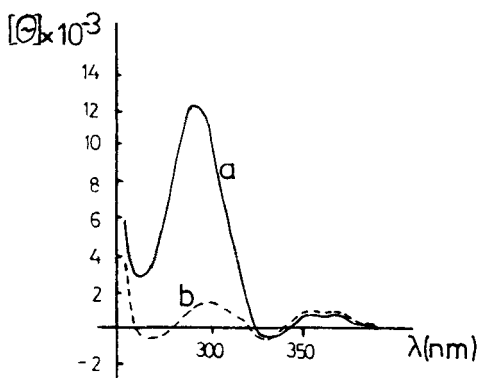
Figure 9. CD spectra for cortisone: (a) before reaction; (b) after reaction; (c) 0.2 mg ml^{-1} (From Ref. 27).

Under the conditions used, the periodic acid oxidation proceeds quantitatively in 20-25 min. The reaction is specific for the 17-ketol group. The oxidation is quantitative in either the presence or the absence of the 17-hydroxy group.

Progesterone, with a 17-COCH3 group, does not react with periodic acid. Neither do mestranol, ethynyloestradiol nor oestrone react with periodic acid during the given reaction time. However, over a period of 20-24h, ethynyloestradiol and oestrone solutions become pale yellow, the change also being discernible in the CD curve. This can presumably be explained by oxidation of the triple hydroxy- groups of aromatic ring A, and by the development of a chirally perturbed chromophoric group with a quinoidal structure.

Under the usual reaction conditions, the corticosteroid C$_{21}$-esters do not react at all with periodic acid but they do oxidize after alkaline hydrolysis. The possibility exists therefore of finding a selective difference CD method for the determination of this class of corticosteroid esters.

Generally speaking the classical alkaline hydrolysis reaction followed by back-titration could be used to determine steroid esters. The results for 21-acyloxycortico-steroids (where R = H, OH) are however quite unsatisfactory. The reason behind the unacceptable result is the auto-oxidation of the α-ketol side-chain in an alkaline medium. Because of the formation of acidic products in side reactions, there is an over consumption of base in the titration and a corresponding over determination of the amount of steroid.
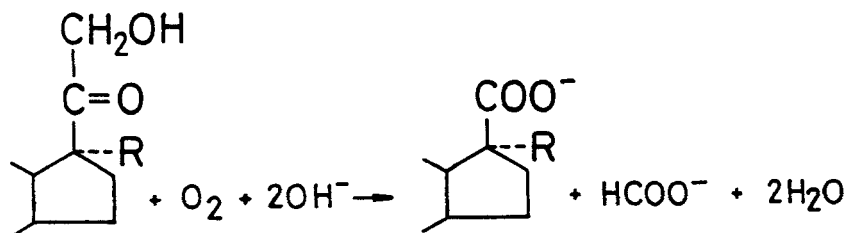
All is not lost however because the periodic acid method is found to be quantitative for the determination of corticosteroid esters, if these are first hydrolysed using a quaternary base, e.g. tetramethylammonium hydroxide. The acidic products formed in the above side-reaction do not perturb the determination, since the optically active product of the periodate oxidation following the hydrolysis is similar to the etianic acid.

The CD method selectively measures the quantity of corticosteroid ester in the presence of 21-hydroxycorticosteroids, as the latter are oxidized in both the unknown and the comparative solution.

3.2.2 Reactions that involve color induction

In the case of steroids that either lack a chromophore or contain just one isolated double bond that absorbs only in the far ultraviolet range of the spectrum, the application of CD is limited unless the detection is preceded by a color derivatization reaction. The best derivatizing reagents introduce extensive conjugation by combinations of dehydration and dehydrogenation reactions that moves absorption bands into the visible range where, if the reagents are steroid selective, there is a minimum of interference from other components in the mixture. The extended chromophore when coupled with the remaining optically active centers makes the electronic transitions chiral leading to anomalous chiroptical behavior and therefore ORD and CD activity. These reagents for the most part are anhydrous and caustic making handling rather difficult, e.g. the Liebermann-Burchard, Zak, and Chugaev reagents. On the other hand they do possess a high degree of specificity.

Of these possibilities only a few can be used where CD is the detector. Sterols, sterones and water insoluble vitamins e.g. vitamin D_2 and D_3 have been investigated by colour induction [28]. Purdie et al. have successfully applied these selective CD methods in the chemical analysis e.g. by the determination of serum cholesterol [29].

4. REFERENCES

1   C. Djerassi, in Optical Rotatory Dispersion and Circular Dichroism in
    Organic Chemistry, McGraw-Hill, New York, 1960.
2   P. Crabbe, in Optical Rotatory Dispersion and Circular Dichroism in Organic
    Chemistry, Holden-Day, San Francisco, 1965.
3   P. Crabbe, in An Introduction to the Chiroptical Methods in Chemistry,
    Syntex, S. A., Mexico, 1971.
4   L. Velluz, M Legrand, in Optical Circular Dichroism. Principles,
    Measurements and Applications, Verlag Chemie-Academic Press, New York,
    1965.
5   G. Snatzke, in Optical Rotatory Dispersion and Circular Dichroism in
    Organic Chemistry, Heyden, London, 1967.
6   W. Klyne, in Optical Rotatory Dispersion and the Study of Organic
    Structures, Advances in Organic Chemistry, Vol. 1, R.A. Raphael, E.C.
    Taylor, and H. Wynberg (eds), Interscience, New York, 1960.
7   F. Ciardelli, S. Salvadori, in Fundamental Aspects and Recent Development
    in Optical Rotatory Dispersion and Circular Dichroism, Heyden, London,
    1973.

8   J.B. Lambert, H.F. Shurvell, L. Verbit, R.G. Cooks, and G.H. Stout, in
     Organic Structural Analysis. Macmillan, New York, 1976.
9   N. Harada, K. Nakanishi, in Circular Dichroic Spectroscopy, Exciton
     Coupling in Organic Stereochemistry, University Science Books, Mill Valley,
     CA, 1983.
10   C. Djerassi, Bull. Soc. Chim. France (1957) 741.
11   V. Avico, R. Guaitolini, P. Zuccaro, Boll. Chim. Farm. 116 (1977) 341.
12   S.S.M. Hassan, Z. Anal. Chem., 269 (1974) 363.
13   V.M. Potapov, V.M. Demyanovich, R.S. Rakovska, Zh. Anal. Chim. 39 (1984)
     983.
14   A. Gergely, Gy. Szasz, J. Nagy, (nee): Magyar Kemiai Folyoirat 82 (1976)
     363.
15   A. Gergely, Gy. Milch, V.K. Papp, (nee), Gy. Szasz, Acta Pharm. Hung.
     51(1981) 168.
16   A. Gergely, Gy. Szasz, Acta Pharm. Hung. 53 (1973) 1, and Z. Anal. Chem.
     309 (1981) 126.
17   A. Gergely, Gy. Szasz, in Advances in Steroid Analysis, S. Gorog (ed)
     Akademiai Kiado, Budapest, Elsevier, Amsterdam, 1982, 527.
18   L. Zalkow, R. Hale, K. French, P. Crabbe, Tetrahedron , 26 (1970) 4947.
19   J. Bartos, Prod. Pharm. 2 (1972) 79.
20   V.M. Potapov, V.M. Demyanovich, R.S. Rakowska, G.S. Grinenco, Zh. Analyt.
     Khim. 33 (1978) 534.
21   A. Gergely, Gy. Szasz, J.Z. Soos, Z. Analyt. Chem. 318 (1984) 528.
22   A. Gergely, Gy. Szasz, J. Soos, J. Pharm. Biomed. Anal. 4 (1986) 517.
23   A. Gergely, Gy. Szasz, Proc. Symp. on the Analysis of Steroids, Szeged,
     Hungary, in Advances in Steroid Analysis Ser., S. Gorog (ed), Akademiai
     Kiado, Budapest, 1985, 581.
24   A. Gergely, Gy. Szasz, Acta Pharm. Hung. 53 (1983) 280.
25   A. Gergely, J. Pharm. Biomed. Anal. 7 (1989) 523.
26   A. Gergely, Dissertation (Candidate of Sciences), Budapest, Hungary, 1988,
     102.
27   A. Gergely, Gy. Szasz, J. Soos, Z. Analyt. Chem. 323 (1986) 157.
28   N. Purdie, K.A. Swallows, Anal. Chem. 61 (1989) 77A.
29   N. Purdie, K.A. Swallows, L.H. Murphy, R.B. Purdie, J. Pharm. Biomed.
     Anal. 7 (1989) 1519.

This Page Intentionally Left Blank

Chapter 11

Circular Dichroism Studies of the Optical Activity Induced in Achiral Molecules Through Association with Chiral Substances

Harry G. Brittain

Bristol-Myers Squibb Pharmaceutical Research Institute,
 P.O. Box 191,
New Brunswick, NJ 08903, USA

Abstract
    The circular dichroism induced in achiral compounds upon complexation with a chiral material can be used to characterize the nature of the interaction responsible for the association. Studies of this type may be conveniently classified as being the optical activity induced upon dissolution of a solute in a chiral solvent, through association of the species of interest with a co-dissolved chiral solute, or through association of the solute with chiral polymers.

Contents

1. INTRODUCTION

The power of circular dichroism (CD) spectroscopy is unfortunately limited to the study of chiral molecules having accessible chromophores, and cannot be applied to the study of achiral compounds. However, a great many compounds of interest are not intrinsically dissymmetric, so the induction of chirality into such species is a fundamental requirement for the performance of CD studies. In the present work, investigations into the CD induced in achiral molecules by the action of chiral agents is reviewed.

Strict analytical applications of induced CD have been limited, and the methodology has primarily been used to study the modes of interaction between the solute and the chiral environmental substance. Nevertheless, this information can be extremely valuable in support of alternate analytical methodology. For example, the enantiomeric composition of a compound can be measured using chiral solvating agents and NMR spectroscopy. It is not difficult to see how the mechanism of interaction could be probed in additional detail through the CD induced in the solute absorption bands.

Although chirality may be induced in any compound through the use of longitudinal magnetic fields [1], these effects are normally too weak to be useful in the study of organic compounds. Such Faraday effects have been effectively used to deduce significant information about the energy levels in inorganic complexes [2]. Magnetically induced optical activity will not be covered in the present review.

2. OPTICAL ACTIVITY INDUCED UPON DISSOLUTION OF AN ACHIRAL SOLUTE IN A CHIRAL SOLVENT

In many cases, optical activity can be induced in achiral molecules through the imposition of dissymmetric environmental effects. The simplest situation of this type would represent the dissolution of an achiral solute into a chiral solvent system. Negatively signed CD was obtained in the n→π* transitions of benzil and benzophenone when these compounds were dissolved in $(2R,3R)$-2,3-butanediol [3]. No such induced optical activity could be detected when planar and rigid compounds (such as fluorenone or bis-N-methylacridinium) were dissolved in the same solvent. These findings suggest that the solutes were stabilized into a dissymmetric configuration upon dissolution in the chiral solvent, probably through a hydrogen-bonding mechanism. Were the solvent capable of solvating the aromatic rings to an appreciable extent, CD should have been observable in the region of the long-axis-polarized transitions.

In subsequent work, the CD induced in the n→π* transition of benzophenone was confirmed and studied in a variety of chiral solvent systems [4]. Representative examples of the CD induced by chiral several solvents in the benzophenone n→π* band system are shown in Figure 1. In the same study, CD

within the $\pi\to\pi^*$ transition of fluorenone was detected and found to be an order of magnitude weaker than the effects noted for benzophenone. It was concluded from these studies that the CD induced in electric dipole allowed transitions would be inherently stronger than CD induced in magnetic dipole-allowed transitions.
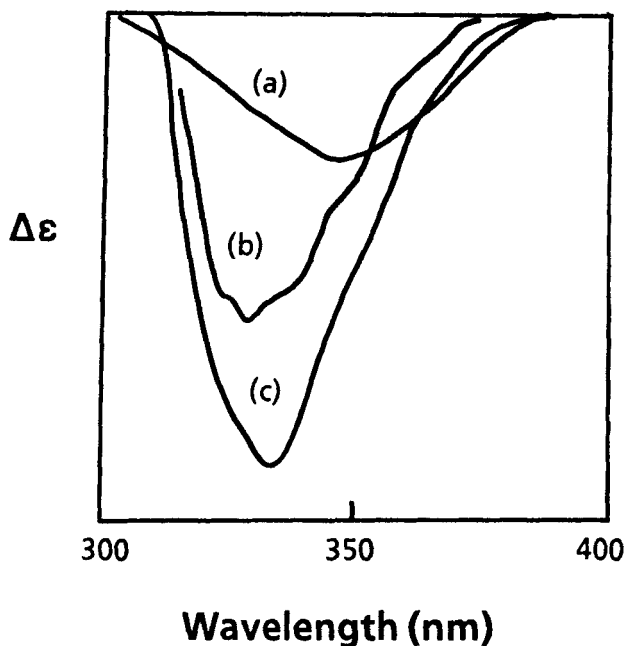
Figure 1. CD spectra obtained within the n$\to\pi^*$ band system of benzophenone upon dissolution in (a) methyl-(S)-2-chloropropionate, (b) (R)-α-phenylglycinol, and (c) (2R,3R)-2,3-butanediol (data adapted from reference [4]).

A variety of studies have been performed in which the chirality induced in ketone chromophores has been characterized by CD spectroscopy. CD has been induced in the n$\to\pi^*$ transition of cyclohexanone upon its dissolution into several alcoholic and ester-functionalized solvent systems [5]. In this work it was established that hydrogen bonding between solute and solvent was not required for the generation of solvent-induced CD. In a more comprehensive work, the CD induced in 20 compounds containing a ketone chromophore was studied in approximately 15 chiral solvent systems [6]. It proved difficult to develop general rules for the observation (or lack thereof) of solvent-induced CD, with the rotational strengths being found to be solvent, temperature, and

concentration dependent. The absolute stereochemistry of the dissymmetric centers in the chiral solvents correlated only partially with the signs of the induced CD spectra.
One interesting effect noted was that halogenated solvents tended to yield larger degrees of CD intensity, and could even reverse the sign of the CD bands.

Schipper and coworkers conducted an extensive investigation of the effect of substituents on the CD induced in the n→π* transition of the carbonyl chromophore [7]. Using the simple solutes represented as R_1R_2CO (where R_1 = $-CH_3$, $-OH$, and $-NH_2$), it was possible to use both the CD intensities and energies of the spectral features to evaluate the forces responsible for the observed effects. The results suggested that there was resonance (through space) coupling between the chiral solvent and the carbonyl π-system. Examples of the induced CD spectra obtained for acetone, acetic acid, acetamide, and urea dissolved in (2R,3R)-2,3-butanediol are shown in Figure 2, where it may be noted that the maxima in the CD bands shift to lower energies following the substituent order $-CH_3$, $-OH$, $-NH_2$.

3. OPTICAL ACTIVITY INDUCED UPON ASSOCIATION OF AN ACHIRAL SOLUTE WITH A CHIRAL SOLUTE

An extremely large body of work exists in which CD spectroscopy has been used to study the optical activity generated in achiral compounds when these are co-dissolved in a solvent with a chiral resolving agent. Many of these investigations have involved inorganic compounds of various types, and the range of chiral agents used to produce chirality in these species is extensive. The manifestation of this induced optical activity is often termed the "Pfeiffer effect", and reviews of this field are available [8-10].

The resolution of racemic compounds through the formation of reversible diastereomer complexes is certainly an example of the generation of chirality upon association of an achiral solute (the racemate to be resolved) and a chiral solute (the resolving agent). Such interactions are normally considered solely from the separations point of view [11], and only rarely is CD used to follow the association mechanism. It is evident, however, that the spectroscopic method would be of great value to characterize the associated species.

3.1 Chirality Induced by Simple Associating Agents

It was noted that *l*-menthol could induce CD in the n→π* transition of a large number of saturated, achiral, compounds containing a ketone group when these were co-dissolved in a suitable solvent [12,13]. It was concluded in these works that 1:1 association complexes were formed in the solutions, primarily owing to hydrogen-bonding forces between the two
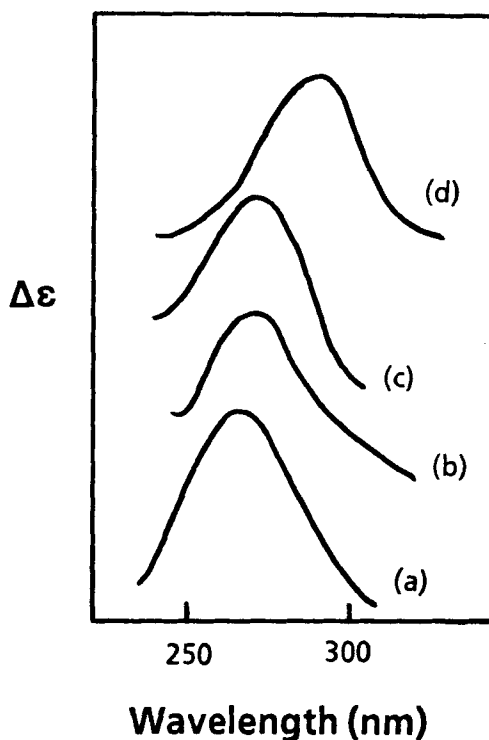
Figure 2. CD spectra obtained within the n→π* band system of
the carbonyl chromophore upon dissolution of (a)
acetone, (b) acetic acid, (c) acetamide, and (d)
urea in (2R,3R)-2,3-butanediol (data adapted from
reference [7]).

solutes. As would be expected, the degree of complex
formation was determined by the steric requirements of the
ketone entity.

In a series of works, Tokura and coworkers have
systematically studied the CD induced in a number of
carboxylic acids through their association with optically
active amines [14-17]. Salts of 1:1 stoichiometry were formed
as contact ion pairs, with limiting values normally being
obtained for the observed ellipticities at equivalent molar
amounts. The degree of salt formation could be related to the
polarity of the solvent medium, as has been summarized in
Table 1. The data in the table illustrate that, as the degree
of solvent polarity increases, the limiting ellipticity
induced in the carboxylate carbonyl band decreases.

Table 1

**Solvent Effects on the Induced CD of the
2-Benzoylbenzoic Acid:(R)-Amphetamine System [14]**

Solvent System	CD Band Maximum	Molar Ellipticity
carbon tetrachloride	324 nm	+1320
toluene	324	+1239
benzene	322	+1010
chlorobenzene	324	+830
chloroform	322	+477
dichloromethane	318	+434
t-butanol	320	+329
1,4-dioxane	326	+324
acetonitrile	320	+229
tetrahydrofuran	325	+224
2-propanol	318	+191
1-propanol	318	+124
ethanol	318	+76
methanol	–	0

The induced CD effects were found to be strongly dependent on the salt concentration, an effect in turn directly related to the dissociation state of the complex. As would be anticipated, the solvent was found to play a strong role in the concentration dependence of the induced CD. This has been illustrated in Figure 3.

Several efforts have been made to develop general rules for the induction of CD in the absorption bands of achiral compounds. Hayward was able to correlate the CD induced in the n→π* transition of a series of 30 oxyketones and thioketones (when these were dissolved in (S)-propylene carbonate) with the structures of these solutes [18]. Schipper has developed a theory for the induction of optical activity in achiral molecules, first by treating the van der Waals coupling phenomena [19], and then in a more abstract sense through the use of point chirality functions [20].

3.2 Chirality Induced Upon Formation of Cyclodextrin Inclusion Complexes

However, the largest number of studies performed where chirality is induced upon dissolution of two solutes in a solvent system concerns the particular instance where the chiral solute is one of the cyclodextrins. These compounds are torus shaped, cyclic oligosaccharides consisting of six (denoted as α-cyclodextrin), seven (ß-cyclodextrin), or eight (γ-cyclodextrin) glucose units. Owing to their hydrophobic
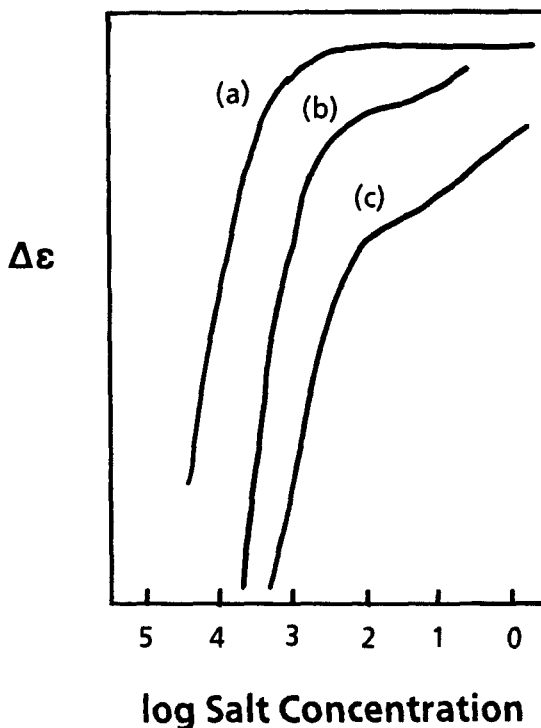
Figure 3. Effect of concentration on the induced CD of the 1:1
ion pair formed by 2-benzoylbenzoic acid and (R)-
amphetamine in (a) toluene, (b) anisole, and (c)
chloroform (data adapted from reference [16]).

interior, the different cyclodextrins are capable of including
a variety of solutes within the inner cavity. These
association complexes are normally of 1:1 stoichiometry, but
other ratios of host and guest are known [21-23]. The
predominant forces responsible for the formation of the host-
guest complexes are hydrogen bonding [24] and van der Waals
forces [25]. CD may be induced in the absorption bands of the
included solute since the cavity of the cyclodextrin host is
inherently chiral.

A theoretical explanation for the chirality induced upon
formation of inclusion or intercalation complexes was given by
Schipper and Rodger, who developed symmetry rules based on a
coupled-oscillator model [26]. These workers were able to
obtain a correlation of the sign of the induced CD with

details of the intercalation geometry. Kodaka used the same
basic model to conclude that the outside of a cyclodextrin
cavity would induce CD opposite in sign to that which would be
induced inside the cavity [27]. He concluded that outside of
the cavity an electric-dipole transition polarized along the
axis of the cavity would yield negatively-signed CD, while a
transition polarized orthogonal to the direction of the would
lead to the observation of positive CD. Kodaka has also
developed a general model for the induced CD based on the
Kirkwood-Tinoco equation [28]. This model also predicts that
the sign of the CD inside a cyclodextrin cavity would be
opposite in sign to the CD induced outside of the cavity. One
interesting finding in this work was the prediction that the
absolute value of CD induced in a transition polarized
parallel to the cyclodextrin cavity axis should be
approximately twice as intense as the CD induced in a
transition polarized perpendicular to the cavity axis.
Additional experimental verifications of these predictions
have been obtained, with the CD induced in the absorption
bands of various arenes being used to study the polarization
of transitions and the signs of the CD bands [29].
     From a study of the complexation between benzoylbenzoic
acids and ß-cyclodextrin [30], it was shown that the phenyl
portion of the compounds was included within the cyclodextrin
cavity, and that the induced CD originated from the carboxyl
group. Insight into the nature of the interaction was
obtained through the pH dependence of the magnitude of the
induced CD, where it was noted that full ionization of the
carboxyl group totally eliminated the induced CD through
dissociation of the complex.
     Vibrational fine structure within the induced CD bands of
several monosubstituted benzenes has been discerned when these
were included in ß-cyclodextrin [31]. From prior knowledge of
the vibrational energies, it was possible to identify the
modes which coupled into the CD bands.
     In another study involving substituted benzene solutes, it
was shown that association took place with the long axis of
the solute being included parallel to the axis of the
cyclodextrin cavity [32]. Representative examples of the
various induced CD band patterns are found in Figure 4.
The predictions reached on the basis of the induced CD data
were verified through calculations conducted using the
Kirkwood-Tinoco equations. In a related work, CD induced
through complexation with ß-cyclodextrin in a series of *ortho*,
meta, and *para*-substituted benzenes was compared [33]. The
magnitude of the induced CD effects revealed that strong
complexation took place only for *para* substitution, and that
the presence of substituents at the *ortho* or *meta* positions
interfered with the inclusion process.
     A novel mode of complexation across the "lid" of the
cyclodextrin cavity was proposed for the interaction of *p*-
dimethylaminobenzoic acid with 2,6-dimethyl-ß-cyclodextrin
[34]. Although the induced CD was weaker than that normally
encountered for axial inclusion in the cyclodextrin cavity, it
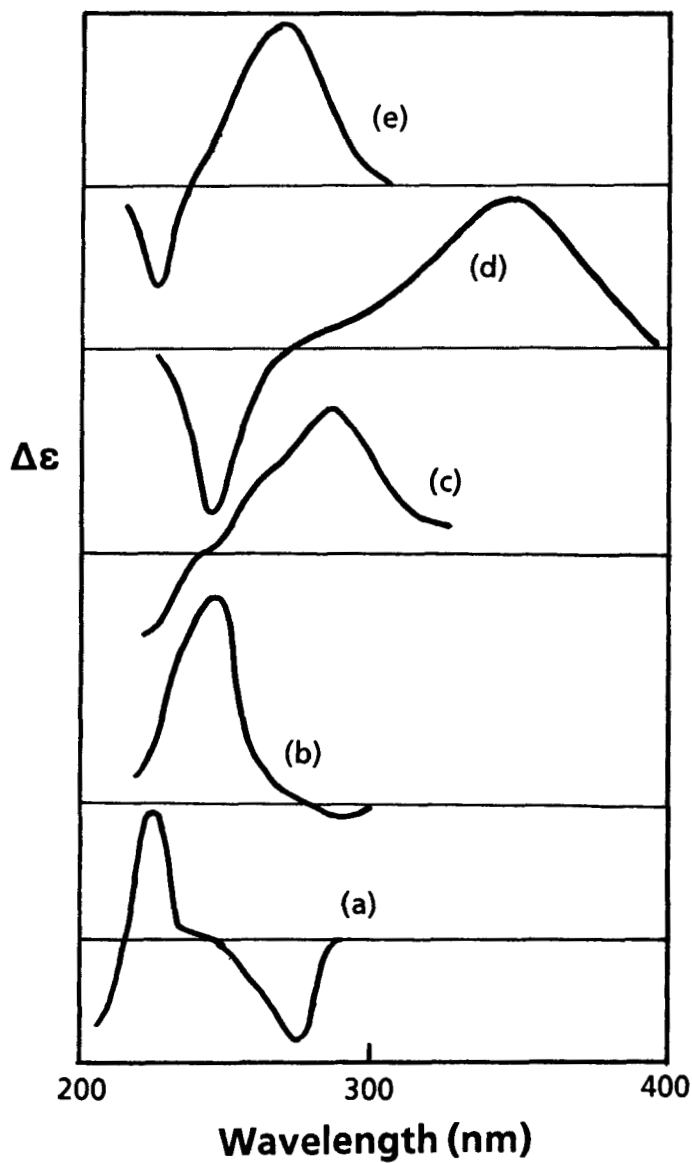
Figure 4. CD of various substituted benzenes after their inclusion in ß-cyclodextrin. Spectra are shown for (a) phenol, (b) benzoic acid, (c) nitrobenzene, (d) p-nitrophenol, and (e) p-hydroxybenzoic acid (data adapted from reference [32]).

was still measurable.

The inclusion of a large number of benzophenone derivatives into ß-cyclodextrin has been studied through characterization of the induced CD [35]. It was concluded that all CD activity originates within the carbonyl chromophore, with the degree of complexation being affected by the nature of the substituents on the included solutes. Derivatives containing hydrophobic groups were found to include more efficiently than those containing hydrophilic groups, confirming the hydrophobic nature of the cyclodextrin cavity. The steric arrangement of the substituent groups was found to exert a secondary influence on the complexation phenomena, since groups located *ortho* to the carbonyl group were found to lead to significantly reduced induced CD effects.

The CD induced in several naphthalene derivatives upon their inclusion into the cavity of ß-cyclodextrin has been used to investigate the complexational mode [36]. The induced data for the 2-naphthyl derivatives was found to agree well with predictions made on the basis of the Kirkwood-Tinoco model, indicating that well-defined complexes of axial substitution were formed. However, a much poorer fit with theory was obtained for the 1-naphthyl derivatives, and this was interpreted to indicate that both axial and equatorial complex types could be formed in the same solution. This work was taken forward in a detailed study of three 2-naphthyl derivatives, with the temperature dependence of the induced CD being used to deduce additional details of the association mechanisms. The complex formed between ß-cyclodextrin and 2-naphthol was found to exhibit an analogous temperature dependence for the observed CD spectra, which signified that changes in complex geometry could take place.

The CD obtained after mono-, di-, and triazanaphthalenes were complexed with ß-cyclodextrin has been correlated with theoretical results obtained using the CNDO-S-CI approximation [38]. As shown in Figure 5, the induced CD associated with the lowest energy $\pi \rightarrow \pi^*$ band system of various azanaphthalenes is very sensitive to the position and number of aza nitrogens contained in the ring system. Correlation with the theoretical results permitted deductions to be made regarding the orbital character of the bands involved in the observed CD, and several LCAO-MO selection rules for the signs of the induced CD bands were obtained.

Inclusion complexes between the 2-naphthyl derivatives and γ-cyclodextrin have been studied as well [39]. In this cyclodextrin system, it is possible to include two solute molecules within a single cavity. This association mode leads to the observation of exciton CD bands in the absorption spectrum, and excimer bands in the fluorescence spectrum. Both types of dimer spectroscopy revert to monomer-type features when dimethyl sulfoxide is added to the medium. This latter observation is probably due to the expulsion of one of the included solutes by an organic solvent molecule. When the dinaphthalene solutes are linked (as in the case of
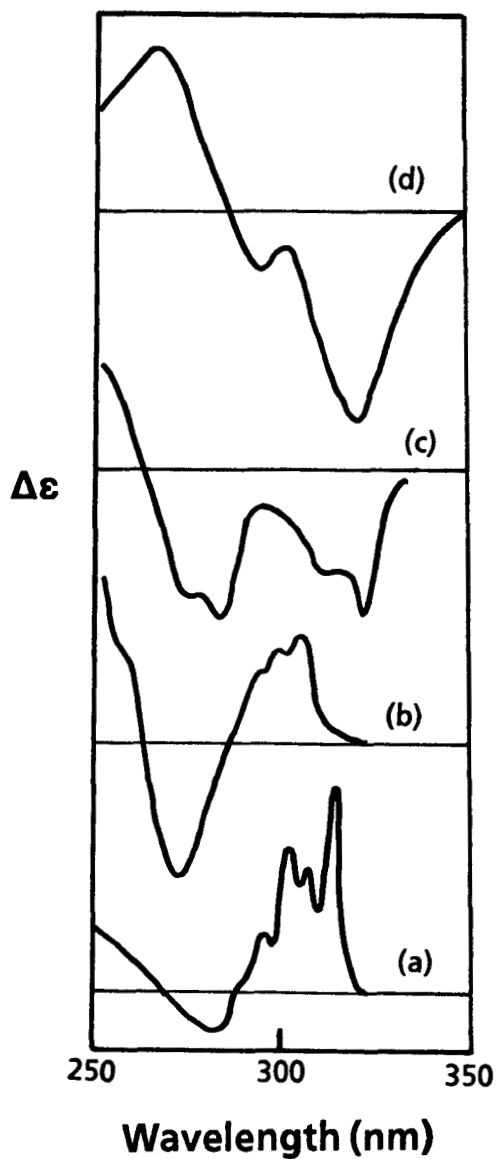
Figure 5. CD within the near-UV region of azanaphthalenes after formation of inclusion complexes with ß-cyclodextrin. Spectra are shown for (a) quinoline, (b) phthalazine, (c) isoquinoline, and (d) cinnoline (data adapted from reference [38]).

dinaphthylmethanes), a very interesting adduct is formed with γ-cyclodextrin [40]. One of the naphthalene arms is included within the cyclodextrin cavity in the usual sense, while the other associates with the hydroxyl groups at the rim of the cavity. This phenomenon results in a partial self-resolution of the potentially chiral dinaphthylmethane solute, and an additional contribution to the observed optical activity.

2,3-anthracenedicarboxylate has been shown to form a 1:1 complex with ß-cyclodextrin in water, and a 2:1 complex with γ-cyclodextrin [41]. The addition of organic co-solvents was found to weaken the association complex, and the greater the hydrophobicity of the solvent the greater the weakening effect. In the case of the 2:1 complexes with γ-cyclodextrin, addition of the organic co-solvent was found to expel only one of the included solutes.

It has been estimated that the internal cavity of ß-cyclodextrin is optimal for the inclusion of unsubstituted pyrene [42]. The axis of the included solute is located parallel to that of the cyclodextrin cavity. In the case of benzo(a)pyrene, no complex can be formed with either α- or ß-cyclodextrin [43]. However, a strong complex can be prepared using γ-cyclodextrin, with the long axis of the included solute lying along the direction of the cavity axis.

Owing to the selection rules associated with the generation of induced optical activity in included solute bands, the polarization of solute absorption bands can be established through suitably designed studies. This method has been calibrated in the instance of azulene, where the predictions reached on the basis of cyclodextrin induced CD were compared with those already reached by alternate methods [44]. In all instances, the predictions made on the basis of induced CD work were in accord with the accepted energy level sequence of azulene. The method has been used to obtain the polarization directions associated with the transition moments of 2-hydroxytropone [45], as well as fluorene, carbazole, dibenzofuran, and dibenzothiophene [46] when each of these was included in ß-cyclodextrin. The most stringent test of the method was the investigation conducted into the energy levels of 9-fluorenone [47]. In this case, only two out of four observed absorption bands had been completely assigned. Even though a multitude of alternate methods had been used to study the system, only the cyclodextrin induced CD method could provide the necessary discrimination needed to complete the band assignments.

Different modes of solute inclusion were deduced for three N-alkyl-dihydronicotinamides when these were complexed with (2,6-di-O-methyl)-ß-cyclodextrin [48]. The CD was found to originate from the $\pi \rightarrow \pi^*$ transition of the conjugated enone system of the dihydronicotinamide group, and consideration of the selection rules led to the postulation of different inclusion geometries for the three solutes. These are schematically illustrated in Figure 6. The trends noted in the data indicated different degrees of insertion for the carbonyl group in the various solutes. It was also found that
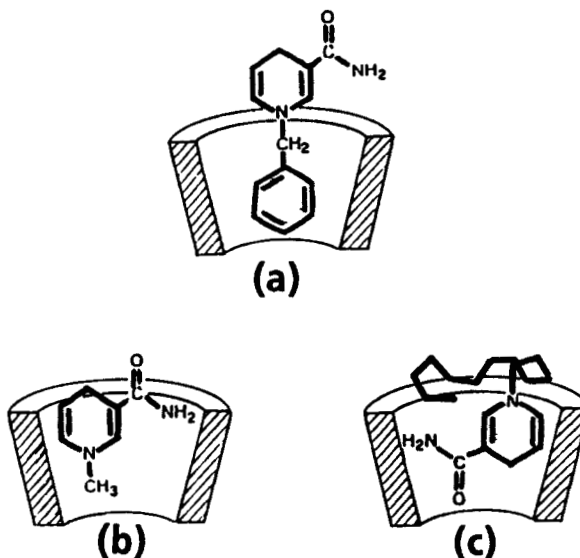
Figure 6. Modes of inclusion deduced for the ß-cyclodextrin
        complexes of (a) *N*-benzyl-1,4-dihydronicotinamide,
        (b) *N*-dodecyl-1,4-dihydronicotinamide, and (c) *N*-
        methyl-1,4-dihydronicotinamide (data adapted from
        reference [48]).

the induced CD was not greatly affected by changing the
solvent from pure methanol to 1:1 methanol/water.
    The CD induced in 2-(2,4,6-cycloheptatrien-1-ylidine)-4-
cyclopentene-1,3-dione upon its inclusion in ß-cyclodextrin
was used to obtain full assignment of the observed absorption
bands [49]. It was concluded that the low energy band system
was composed of three electronic transitions, two of which
were polarized perpendicular, and one parallel, with respect
to the long molecular axis of the solute. The higher energy
band system was found to also consist of three allowed
electronic transitions, but two of these were polarized
parallel, and one perpendicular, to the long axis of the
solute molecule. These deductions were supported by a series
of CNDO/S-CI calculations performed on the system. A similar
approach was taken to assign the polarizations of the various
transitions associated with 2-thioxo-1,3-benzodithiole and 2-
selenoxo-1,3-benzodithiole [50].
    Phlorizin is known as a glucose transport inhibitor in the
kidney, and contains two aromatic ring systems. It was found
that this compound was capable of forming complexes with both
ß- and γ-cyclodextrin, but that the complexation modes were
not equivalent in the two systems [51]. No evidence for

complexation could be obtained for α-cyclodextrin. The
induced CD was used to estimate the orientation of the
aromatic rings in the hydrophobic cavity of the cyclodextrin
hosts. In the case of ß-cyclodextrin, the long axis of one
ring was almost perpendicular to the molecular axis of the
cyclodextrin with its plane being parallel to the cyclodextrin
axis, while the short axis of the other ring was perpendicular
to the cyclodextrin axis. For γ-cyclodextrin, it was deduced
that the two rings of phlorizin were included by two different
host molecules. The long axis of one ring was oriented
perpendicular to the molecular axis of the cyclodextrin host
(with its plane being considered perpendicular to the
cyclodextrin axis), and the short axis of the other ring being
parallel to the axis of its cyclodextrin host. The magnitude
of the induced CD was also used to obtain the apparent complex
formation constants, and it was concluded that phlorizin
formed stronger inclusion complexes with ß-cyclodextrin than
it did with γ-cyclodextrin.

The organometallic compound, ferrocene, has also been
shown to form different types of complexes with either ß- or
γ-cyclodextrin [52]. In ß-cyclodextrin, ferrocene is included
in an axial complexational mode, while it adopts an equatorial
mode when binding to γ-cyclodextrin. The perturbations caused
by ß-cyclodextrin and 2-hydroxypropyl-ß-cyclodextrin on the CD
spectra of purine nucleosides have been investigated [53].
The data suggest that the microenvironment about the N-7 site
of adenine nucleosides is dramatically altered after
complexation. It was concluded from this work that in
complexes with ß-cyclodextrins, the purine residue was
oriented in the complex with its short axis nearly parallel to
the long axis of the cyclodextrin cavity.

Since the cyclodextrins are inherently chiral, there
always exists the possibility that stereoselectivity might
accompany the inclusion of chiral solute molecules. The
dinitrophenyl (DNP) derivatives of valine, leucine, and
methionine complexed with ß-cyclodextrin [54]. In these
complexes, the DNP group is included within the cyclodextrin
cavity, thus placing the other functional groups of the solute
at the edge of the cavity. These groups tend to interact with
the hydroxyl groups at the edge of the cavity, thus providing
a mechanism for chiral recognition. In the case of DNP-(L)-
amino acids, the protruding alkyl groups form a secondary
inclusion complex with a second cyclodextrin molecule.
However, for DNP-(D)-amino acids, the alkyl groups are
repulsed by the hydroxyl groups and a second cyclodextrin
molecule cannot bind. Both two types of complex binding are
illustrated in Figure 7. These findings may be taken to imply
that chiral recognition in complex formation is a requirement
for the types of chromatographic chiral separations being
practiced with soluble or immobilized cyclodextrins.
Sufficient chiral recognition also requires interaction of
other functional groups around the chiral center with the lip
of the cyclodextrin cavity, and possibly even with secondary
cyclodextrin molecules.
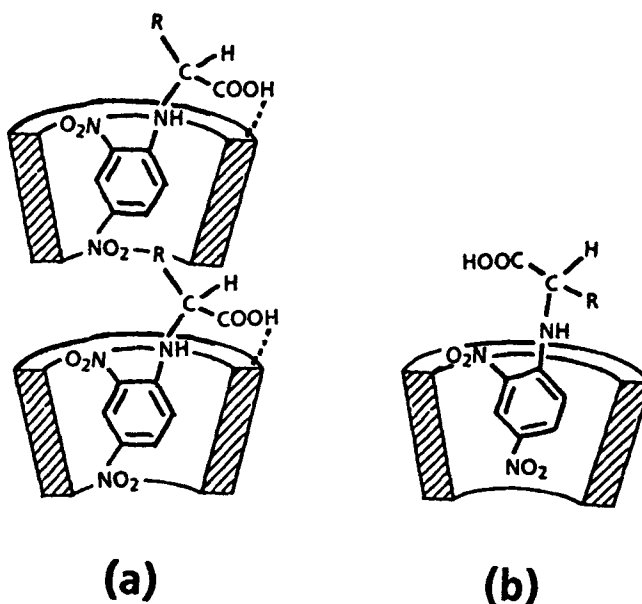
Figure 7. Postulated structures for the ß-cyclodextrin complexes of (a) *DNP*-(L)-amino acids, and (b) *DNP*-(D)-amino acids (data adapted from reference [54]).

3.3 Chirality Induced Upon Inclusion of Pharmaceutically Active Compounds Into Cyclodextrins

A variety of studies have been conducted in which the CD induced in pharmaceutically active compounds was used to characterize the nature of the inclusion complexes. The interaction of four barbiturates with ß-cyclodextrin was studied by solubility and chiroptical methods [55]. It was found that the solubility of the barbiturates increased significantly upon formation of the inclusion complexes, and this enhancement was used to deduce the formation constants for the associated species. The induced CD data were also used to evaluate the strength of the complexes, with the relative strength of interaction with ß-cyclodextrin being phenobarbital > pentobarbital > amobarbital > barbital.

It was found that ß-cyclodextrin will form 1:1 complexes with the entire series of anti-inflammatory fanamates, with the exception of the parent compound anthranilic acid [56]. Inclusion complexes could not be formed with α-cyclodextrin, indicating that the cavity of this host was too small to permit complexation. Formation of the inclusion complexes

resulted in a slight shift of the absorption maxima to lower energies, and the observation of induced CD within the shifted bands. The wavelength maxima of the absorption bands could be more easily evaluated in the CD spectra, owing to the greater degree of band resolution noted in the chiroptical data. Quantitative analysis of the induced CD data permitted the calculation of complex formation constants, with the trend consisting of flufenamic acid > mefenamic acid > meclofenamic acid.

The interaction of β-cyclodextrin with several coumarin anticoagulants has been studied by solubility analysis, UV and fluorescence spectroscopies, microcalorimetry, and through the induced CD [57]. It was noted that 4-hydroxy-coumarin, phenprocoumon, and warfarin did not yield measurable induced CD, even though it was deduced from the fluorescence and microcalorimetry studies that complexation did indeed take place. As may be seen in Figure 8, relatively weak CD was induced in coumetarol and acenocoumarin upon formation of the β-cyclodextrin inclusion complex, while stronger CD was obtained when dicumarol and ethylbiscoumacetate were reacted with the same host system. The complex association constants of these latter systems were evaluated, and found to be significantly higher than those obtained for the other coumarin systems. On this basis, it was hypothesized that the dicumarol and ethylbiscoumacetate molecules penetrated most deeply into the cavity of the cyclodextrin host, and thus yielding the largest degree of induced CD.

Purdie and coworkers have conducted a series of studies in which drug compounds were included in cyclodextrin hosts, and the induced CD was then used to evaluate the properties of the complexes. They first noted that structural dissymmetry could be induced in L-cocaine and phencyclidine upon complexation with β-cyclodextrin [58]. The aromatic ring of L-cocaine represents the principal chromophore in the molecule, and CD can be measured within this absorption for resolved material. Upon formation of the inclusion complex, the CD spectra were found to undergo a total inversion while the absorption intensity of this band increased only slightly, as shown in Figure 9. These findings would imply that the spatial relationship of the spectroscopically observable phenyl group with respect to its intrinsic source of chirality (the alkaloid group) must be substantially changed upon formation of the inclusion complex. It was suggested that the specificity associated with the CD of the association complex would present an analytical utility in the discrimination of L-cocaine in the presence of other ecgonine alkaloids.

Subsequently, Purdie and coworkers studied the CD induced in phencyclidine (and its pyrrolidine and morpholine analogues), β-phenethylamine, phenobarbital, meperidine HCl, diazepam, and dilantin by β-cyclodextrin [59]. In this work, a method was described for the assay of meperidine in commercially available Demerol tablets. The complexation between β-cyclodextrin and eight 5,5-disubstituted derivatives of barbituric acid was characterized on the basis of the
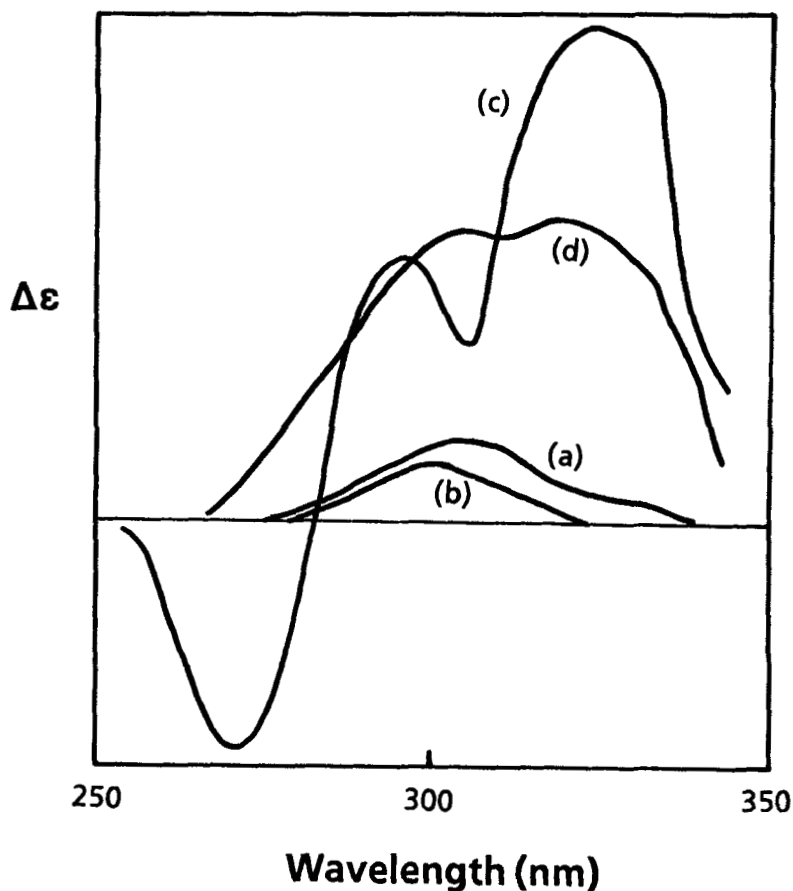
Figure 8. CD of various coumarin anticoagulants after their inclusion in ß-cyclodextrin. Spectra are shown for (a) coumetarol, (b) acenocoumarin, (c) dicumarol, and (d) ethylbiscoumacetate (data adapted from reference [57]).

induced CD [60]. The values obtained for the various formation constants were found to vary over an order of magnitude, with the strength of the complexation being relatable to the structural details of the solutes. The formation constants calculated from the induced CD data would then be of use in the development of quantitative assays of achiral analytes without separation procedures. Finally, in another work, the same group surveyed seventeen drug compounds for their ability to form inclusion complexes with ß-cyclodextrin [61]. Less than one-third of the solutes were

Wavelength (nm)
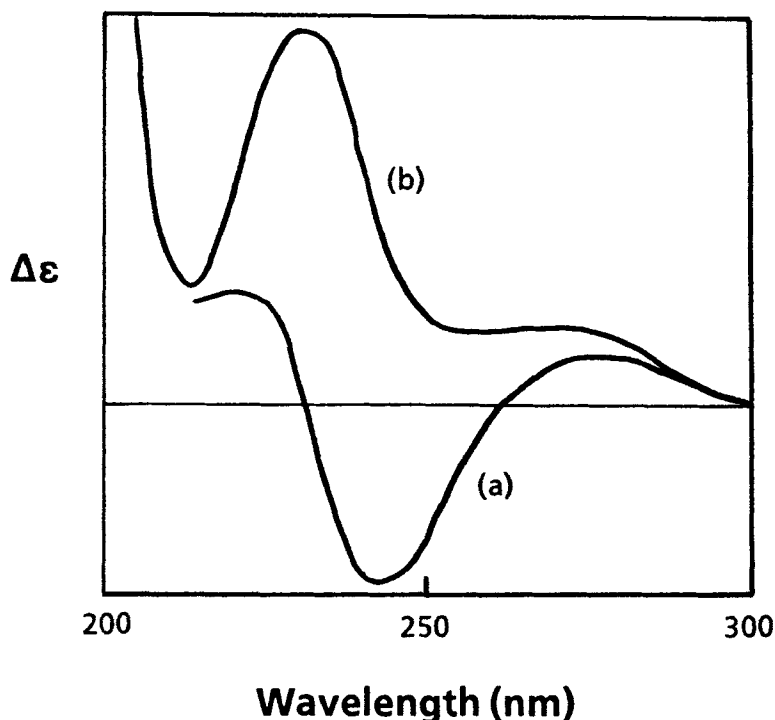
Figure 9. CD spectra obtained for the aqueous solutions of
(a) L-cocaine, and (b) L-cocaine after addition of a
large excess of ß-cyclodextrin (data adapted from
reference [58]).

actually found to yield suitable CD after complexation, thus
enabling a clever analyst to design suitable experimental
parameters that would permit the design of assays not
requiring a separation step. A similar series of studies were
carried out in which CD was induced in a number of
benzodiazepin-2-ones upon complexation with ß-cyclodextrin
[62]. Based upon their results, these authors were able to
develop methods for the direct determination of diazepam and
flurazepam in dosage forms.

The complexation of bilirubin by ß-cyclodextrin leads to
the observation of remarkably intense induced CD, which has
been attributed to the preferential stabilization of chiral
molecular conformations [63]. In addition, the bilirubin
solute may be sufficiently solubilized in alternate solvents
so that new analytical methods can be developed for its
determination. This latter feature of the complexation
phenomenon is of analytical significance, since quantitation

of bilirubin levels is required during the treatment of jaundice.

The interaction of α-, β-, and γ-cyclodextrins with doxorubicin and daunorubicin was studied through the induced CD [64]. It was found that these anthracycline antibiotics would only form inclusion complexes with γ-cyclodextrin, undoubtably owing to the large steric requirements of the fused ring system. These antibiotics are known to be chemically unstable in aqueous solutions, but upon complexation with γ-cyclodextrin in acidic media, significant increases in stability can be obtained. Through the use of the induced CD method, the formation constants of the association complexes were found to be of comparable magnitude over a wide range of pH values. This information was taken to imply that the mode of complexation was equivalent for both anthracycline solutes in the pH range of 1.5 - 10.

Retinoic acid is actively used as a dermatologic agent, but its use is limited by its insolubility in aqueous media. It was found that formation of the β-cyclodextrin inclusion complex improved the compound solubility from less than 0.5 mg/mL to 160 mg/mL, eliminating the formulation problems associated with solubility concerns [65]. Although retinoic acid does exhibit intrinsic CD when dissolved in dimethyl sulfoxide, the CD spectrum is drastically upon formation of the cyclodextrin inclusion complex (see Figure 10). That CD can be measured in the absorption bands located at 350 and 400 nm can be taken as evidence that it is the conjugated sidechain of the retinoic acid solute which becomes included in the cavity of the cyclodextrin host system.

4. OPTICAL ACTIVITY INDUCED UPON ASSOCIATION OF AN ACHIRAL SOLUTE WITH A CHIRAL POLYMER

An extremely large body of literature exists in which the CD induced in achiral solutes upon association with a chiral polymer system has been used to characterize the nature of the interaction [66]. A complete review of this field is beyond the scope of the present article, but the type of work which has been done will be illustrated through the discussion of selected and representative examples.

4.1 Chirality Induced Through Association with Polypeptide Systems

Many pharmaceutical compounds are known to bind to serum proteins during their interval of action, and these effects are often related to the duration of action for the drug. It is generally assumed that only the unbound portion of the drug possesses biological activity, and consequently the investigation of drug-protein interactions is of importance to the full understanding of these systems. The drug-protein
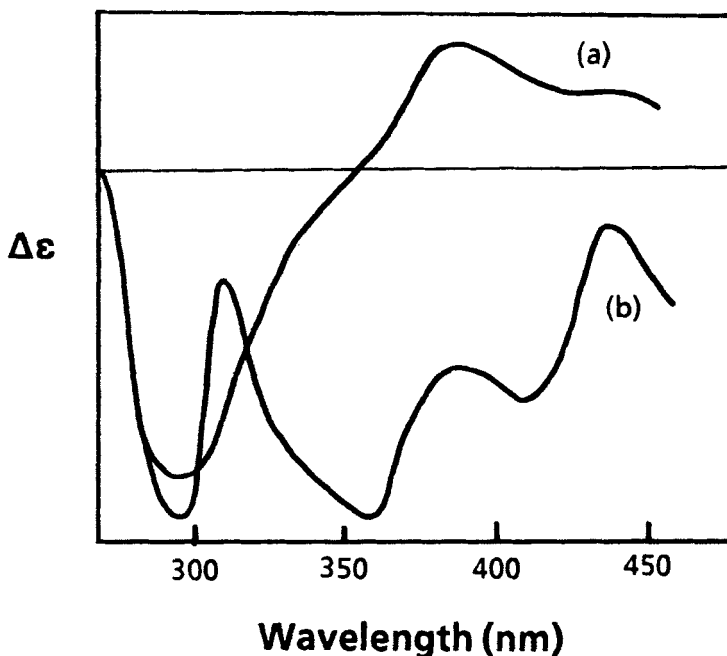
Figure 10.   CD spectra of (a) retinoic acid dissolved in
              dimethyl sulfoxide, and of (b) retinoic acid
              included in β-cyclodextrin (data adapted from
              reference [65]).

equilibrium is normally interpreted through characterization
of the number of binding sites per protein molecule, and in
the associated binding constants.

Since the polymeric serum proteins are inherently
optically active, it follows that chiroptical behavior can be
observed if the solute interacts with the protein in a
stereoselective manner. A variety of studies have been
performed in which the induced CD has been used to evaluate
critical details of drug-protein interaction, and the early
applications of these have been reviewed by Perrin and Hart
[67]. When the chiroptical effects are sufficiently intense,
the method may even be used to study the competitive binding
of two drugs to a given protein system, thus providing data
pertaining to the concurrent administration of these agents.

It has been observed that acidic drugs exhibit strong
binding affinities for the serum albumins. Strong CD is
induced in sulfaethidole when this compound binds to either
crystalline or fraction V bovine serum albumin [68]. The data

indicated that the α-helical structure of the protein was not affected by the association of the drug. In a subsequent study, it was established that induced CD was only obtained when sulfaethidole was allowed to bind at the primary binding site of bovine serum albumin [69]. A variety of other drug compounds were investigated as to their ability to compete with sulfaethidole for the primary binding site, and a number of acidic compounds were shown to be capable of such competition.

The single tryptophan residue of human serum albumin is thought to contribute to the microenvironment essential for the binding of substrate molecules, and this possibility was evaluated through the chemical modification of this group and a subsequent study of the protein binding capacity [70]. The tryptophan residue was alkylated with 2-hydroxy-5-nitrobenzyl bromide, and these modified proteins were then allowed to interact with four acidic drug compounds. Through comparison of the induced CD with that obtained in unaltered albumin, it was demonstrated that the primary binding site of the acidic drug compounds did indeed involve the tryptophan region. As has been illustrated in Figure 11, quite different induced CD spectra were obtained from the different bound drugs.

The binding of sulfonamides to serum albumin is thought to strongly affect the pharmacokinetics of drug action, and therefore CD spectroscopy has been used to deduce the nature of the association mechanism [71]. It was found in this study that most of the drug compounds would exhibit induced CD upon binding to either human, bovine, or rabbit serum albumin, and that the particular lineshape of the chiroptical spectrum was determined by the structural details of the bound solute. Only binding at the primary site of the proteins led to the observation of induced CD, and the degree of induced optical activity generally decreased with pH. This latter effect was attributed to protonation of the solutes and the albumins, and the accompanying conformational changes of the polymer system. Some species variability was noted, with the rabbit serum albumin generally leading to the largest degree of interaction for a given drug compound.

Bishydroxycoumarin has been found to be totally bound to serum proteins after administration, and the ensuing CD spectra were used to study the interaction [72]. A well-defined 1:1 complex was formed at equimolar amounts of bovine serum albumin and solute, but alterations in the induced CD spectra noted at higher solute/protein ratios indicated the existence of other binding sites. These other sites were judged to be less specific in their interaction, since the CD spectra were found to undergo continuous changes as the solute/protein ratios were increased up to 10:1. These trends stand in sharp contrast to analogous data obtained for the interaction of bishydroxycoumarin with human serum albumin [73]. In this latter work, it was found that no change in CD lineshapes or magnitudes occurred at solute/protein ratios exceeding 3:1.
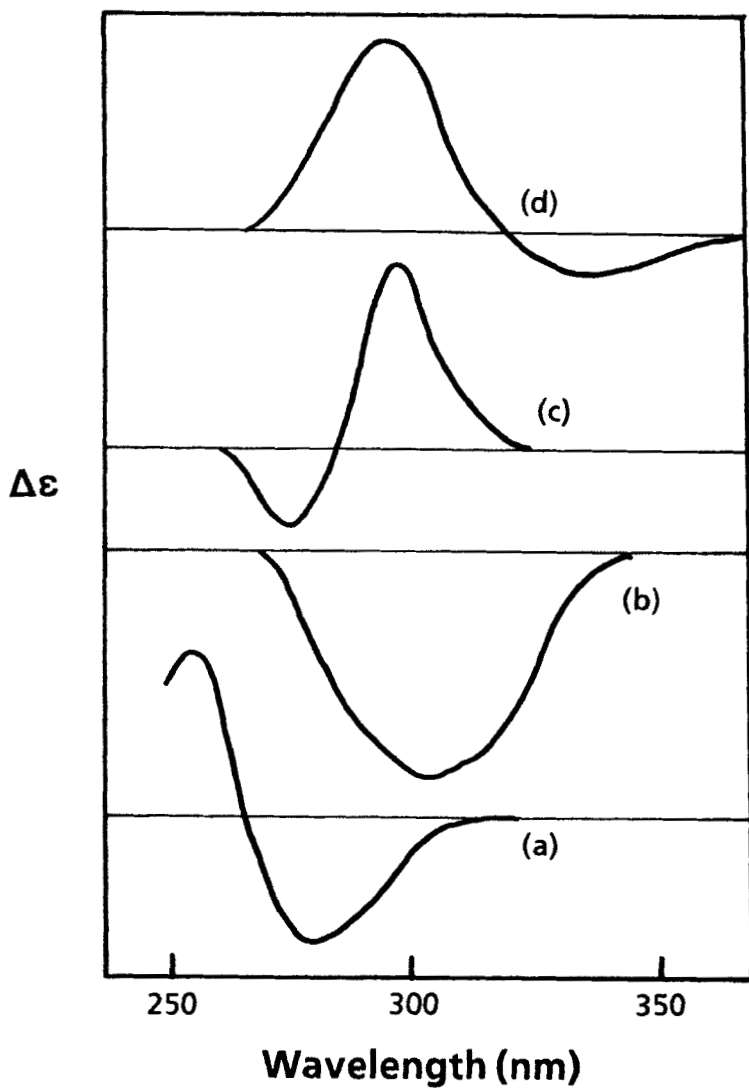
Figure 11.   CD spectra of (a) sulfaethidole, (b) dicumarol,
(c) phenylbutazone, and (d) flufenamic acid upon
complexation with human serum albumin (data
adapted from reference [70]).

While the compounds just described generally bind to one particular site on the albumin protein, other compounds prefer to bind at an alternate site. A variety of anti-inflammatory drug compounds have been shown to bind to human serum albumin at this other site, and the interactions can be followed by means of the induced CD spectra. For instance, 2-(3-phenoxy-phenyl)-propionic acid (fenoprofen) and some of its analogues have been shown to bind hydrophobically to albumin via the phenyl rings, and after dipole interactions of the carbonyl group and ether oxygen [74]. These conclusions were reached through a systematic correlation of induced CD (when observed) with the compositional details of a series of 16 structurally related compounds. It was determined that it was necessary to have two aromatic rings hydrophobically bound to the albumin protein in order to achieve the structural rigidity necessary for the observation of induced chirality in the solute absorption bands.

The interaction of benoxaprofen with human serum albumin was extensively investigated through induced CD studies. It was shown that this compound has a very high affinity for human serum albumin, but that this compound does not compete with warfarin for the same site [75]. It was determined that when human serum albumin is in its B-conformation, the protein has a greater affinity for benoxaprofen than when it is in its N-conformation. The effect of benoxaprofen on the N→B transition of human serum albumin was studied in greater detail through a combination of induced CD and dialysis measurements [76]. Strong counterion effects were noted upon addition of either chloride or calcium to solutions containing the benoxaprofen-albumin complex, with these observations being interpreted to mean that both ions were capable of competing for the same protein binding site. The effect of counterions on the degree of induced optical activity in the benoxaprofen-albumin complex is illustrated in Figure 12. It is evident from the data that a much larger effect from binding site competition is possible with calcium than was observed with chloride.

The interaction of two homologous series of bilary contrast agents with human (both natural and modified) and bovine serum albumins has been studied through characterization of the induced CD [77]. Strong chirality was induced in most of the agents upon binding to the polymer systems, with slight variations in the solute structures leading to large differences in the observed CD spectra. The CD data were therefore useful in deducing trends associated with the binding site selectivity known for some of these agents. For instance, it was noted that while iopodate normally binds only at the warfarin site of human serum albumin, modification of the propionate side chain results in a reduction in the affinity for this site and strongly increases the affinity for binding at the diazepam site.

The effects upon the secondary structure of poly(L-lysine) upon binding of volatile anesthetics (chloroform, halothane, and enflurane) have been studied through perturbations induced
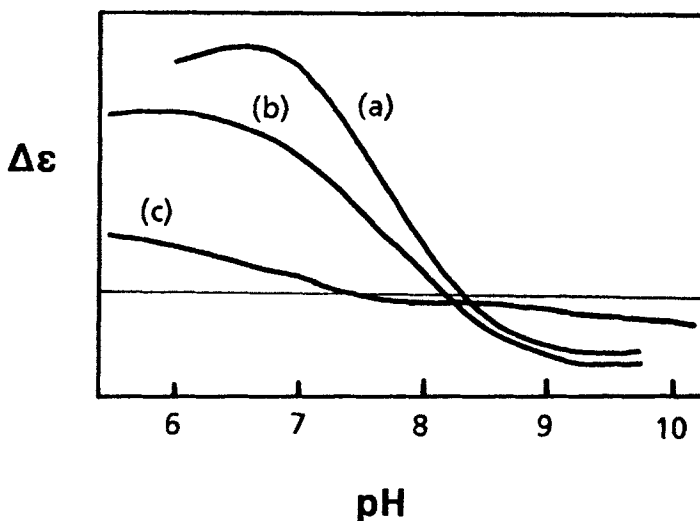
Figure 12.   pH dependence of the counterion effect on the CD
              spectrum of the benoxaprofen-albumin complex.
              The magnitude of induced CD was measured at 305
              nm for (a) the complex in phosphate buffer
              (reference), (b) upon addition of a 2000-fold
              excess of NaCl, and (c) upon addition of a
              50-fold excess of $CaCl_2$, (data adapted from
              reference [76]).

in the polymer CD spectra [78]. It was found that the agents
were all capable of transforming the normal conformation of
poly(L-lysine) (α-helical) into a ß-sheet structure. No
evidence was found in the CD data to indicate the induction of
significant random coil structure. It was also found that the
ability of a given compound to transform the secondary
structure of poly(L-lysine) (as determined by the complex
association constant) was directly related to the anesthetic
potency of the agent. The structural effects induced by the
agents were found to be completely reversible upon
volatilization of the compounds, suggesting that these
compounds rearranged the hydrogen bonding patterns which had
generated the particular α-helical structure noted for the
original protein. It was proposed that the structural changes
were effected through the enhancement of hydrophobic
interactions among protein site-chains, and by the
rearrangement of hydrogen bonds in the peptide backbone.

4.2   Chirality Induced Through Association with Oligo-
nucleotide Systems

A second major area in which the CD observed in a solute-
polymer system has proven to be very useful in studies of the
interactions has been for the particular instance where the
polymer was an oligonucleotide. This area is also
characterized by an extremely large literature, so in the
present work we will restrict our focus on the CD induced in
planar aromatic molecules which may or may not intercalate in
the oligonucleotide structure. Perrin and Hart have reviewed
the work performed prior to 1970 [67], and the focus of the
current review will be on later works.

It has been demonstrated that the binding geometry of
solute adducts with DNA can be determined through detailed
analyses of the induced CD [80]. This method involves
predictions of the degree of alignment relative to DNA fixed
axes made from determinations of the sign of the induced CD in
an adduct transition of known polarization. Validation of the
theoretical approach was obtained by observing induced CD data
for a series of acridine analogues upon their binding to DNA,
and comparing the bandshape data with that predicted using the
theoretical model.

The induced CD of an electric dipole transition of a
solute intercalated in DNA has been calculated using a matrix
method and wavefunctions proposed for the $\pi \rightarrow \pi*$ transitions of
oligonucleotides [80]. The induced CD was found to be
strongly dependent on the angular orientation of the
intercalated solute with respect to the polymer, and only
moderately dependent on the particular details of its
coordinative environment. Subsequently, an algorithm based on
an idealized coupled-oscillator model was used to calculate
the CD induced in an achiral solute upon its binding to DNA,
and to deduce sector rules for non-intercalated complex
species [81]. A compound bound in either of the grooves of
DNA is predicted to exhibit positive induced CD for electric
dipole-allowed transitions whose transition moments are
aligned parallel to the groove axis. Negative induced CD
would be observed for transitions whose moments were aligned
perpendicular to the groove axis. Verification of the rules
was sought through the study of several non-intercalators, and
reasonably good agreement of experimental results with the
theoretical predictions was obtained.

A number of studies have been conducted in which the
interaction of acridine and its derivatives with
oligonucleotides has been studied through measurement of the
induced CD. The binding of 1-, 2-, 3-, and 9-aminoacridine,
as well as that of proflavine (3,6-diaminoacridine), with
native calf thymus DNA has been studied through evaluation of
the CD induced in the absorption bands of the dye solutes
[82]. It was concluded in this work that the dye molecules
are situated between adjacent bases on the same polynucleotide
chain, thus allowing the positively charged ring nitrogen of
the acridine to interact with the negatively charged phosphate

of the polymer. The different types of CD bandshapes which
result are thus explained on the basis of structurally induced
variations in the binding, and through the addition of other
bound solutes to the site. Examples of the types of CD
bandshape which have been obtained for the various substituted
acridines are found in Figure 13.
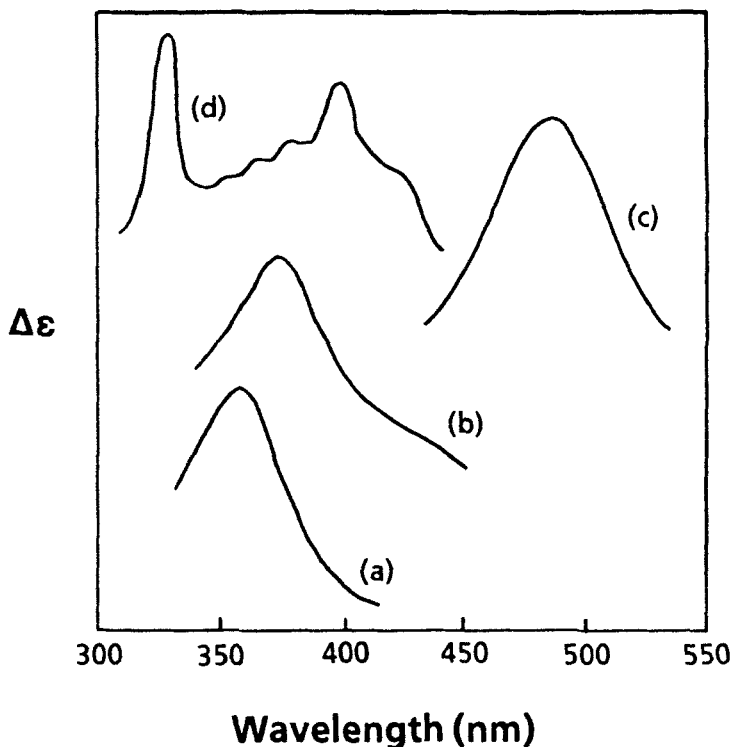
Figure 13.   CD spectra of various substituted acridines upon
              binding to calf thymus DNA. Data are shown for
              (a) 1-aminoacridine, (b) 2-aminoacridine,
              (c) 3-aminoacridine, and (d) 9-aminoacridine
              (data adapted from reference [82]).

In a subsequent work, the interaction of proflavine, 9-
aminoacridine, and 4-ethyl-9-aminoacridine with calf thymus
DNA was investigated in greater detail [83]. Taken together,
these works permitted the classification of acridine analogues
into two groups, based on the trends in the induced CD data.
For compounds containing a 3-amino group, the degree of
induced optical activity increased rapidly and cooperatively
with increasing amounts of bound solute. For compounds

lacking a 3-amino group, the degree of induced CD varied only slightly with the solute concentration.

The CD induced in the visible absorption bands of proflavine cation intercalated to DNA was characterized in terms of the dye-DNA base pair exciton interactions [84]. In this work, the data were obtained at very low amounts of intercalated solute relative to the amount of oligonucleotide, with the goal of observing the CD spectra of isolated and monomeric dye systems. Substantial ionic strength effects were noted, indicating the electrostatic nature of the interaction. Comparison of the data with the results obtained after theoretical modeling indicated that the proflavine molecules insert in the DNA helix with the molecular plane parallel to the stacking plane of the DNA base pairs.

Linear response polarizability theory of spectral bandshapes was applied to the numerical analysis of the chiroptical spectra obtained for DNA-acridine orange complexes [85]. After analysis of various models of conformation, it was concluded that a dimer-pairs repeating sequence model was best able to account for the observed spectral trends. In another work, the CD induced in the same band system was studied at several ionic strengths [86]. The spectra were able to be interpreted in terms of the long-axis-polarized electronic transitions of the dyes, with the induced CD being attributed to intercalated and non-intercalated dye species superimposed by degenerate vibronic exciton interactions between these.

The binding of 9-aminoacridine to calf thymus DNA has been studied at low ratios of dye/polymer [87]. Once the dye concentration levels were increased to the point where bound dye molecules could interact with each other, the spectra could be interpreted in terms of exciton coupling. In another system involving the same intercalation system [88], the observed spectra were deconvoluted into contributions from three $\pi \rightarrow \pi *$ transitions and the dipole and rotatory strengths of one long-axis and one short-axis polarized transition were determined for each intercalating species. Through comparison of the experimental results with those of theoretical calculations on the induced CD, it proved to be possible to draw several conclusions about the nature of the intercalated species:

1. The geometries of the intercalated 9-aminoacridine group differ for the mono- and bisfunctional forms.
2. The intercalated solutes were situated off the center of the DNA helix.
3. The long axis of the intercalated 9-aminoacridine moiety is parallel to the axis formed by the base pairs.

It has been shown that methylene blue binds to DNA in a manner similar to that of acridine orange, with the intercalated solute being coplanar with the base pairs at low dye/polymer ratios and low ionic strengths [89]. The induced CD data indicated the existence of two origins for the observed chirality. At low ratios of dye/polymer, the CD is

dominated by the transition at lowest energy (which is polarized parallel to the long axis of the solute). The sign of this type of CD can be completely reversed at successively higher ionic strength conditions, which may be related to conformational changes of the oligonucleotide structure. At higher dye/polymer ratios, a strong exciton CD (associated with interactions between adjoining methylene blue units) dominates the observed spectra. The particular interaction responsible for the exciton band appears to be that taking place between an intercalated and non-intercalated methylene blue pair, located in the minor groove of the DNA polymer.

Ethidium bromide has been used as a probe of oligonucleotide structure, being known to intercalate between base pairs but being restricted in its interactions due to its particular steric requirements [90]. These studies are of particular importance since the compound is also a therapeutic agent capable of interfering with the synthesis of nucleic acids. When ethidium bromide is allowed to interact with DNA, a series of diagnostic bands at 510, 380, 340, and 310 nm are observed in the induced CD spectra [83]. Owing to their intrinsic intensity, the CD bands at 310 and 340 nm are particularly useful for characterization studies. These two bands appear to originate from a red-shift of the bands which are located at 285 and 325 nm in the free solute. The binding nature of this solute greatly resembles that of the 3-aminoacridines in that the induced CD bands indicate the presence of cooperative binding.

A very detailed study into the interaction of ethidium bromide with oligonucleotides was reported by Aktipis and coworkers [91]. The primary binding effect is the strong interaction associated with the intercalation process, but a secondary contribution is made by the electrostatic interactions between phosphate residues and ethidium bromide molecules attached to the outside of the oligonucleotide helix. When interacted with calf thymus DNA, ethidium bromide exhibited CD bands at 290 and 360 nm which were strongly dependent on the dye/polymer ratio. Examples of the induced CD bands are found in Figure 14, where the distinction between monomer and exciton lineshapes is evident.

Additional insight into the association phenomena was obtained by using CD spectroscopy to probe the interaction between ethidium bromide and synthetic oligonucleotides, such as poly(dA-dT)/(dA-dT) or poly(A-U) [92]. The interaction modes noted for these systems were found to be similar to those observed for native DNA polymers. In more unusual double-stranded oligonucleotide structures such as poly(A-I) or poly(I-C), the solute intercalates between stacked base pairs with an orientation which permits interaction between the oligonucleotide backbone and the ring nitrogen. Single stranded polymers, such as poly(C) or poly(U), appear to form similar complexes as noted with poly(A-I) or poly(I-C), but poly(A) appears to interact with the solute in a nonspecific manner.
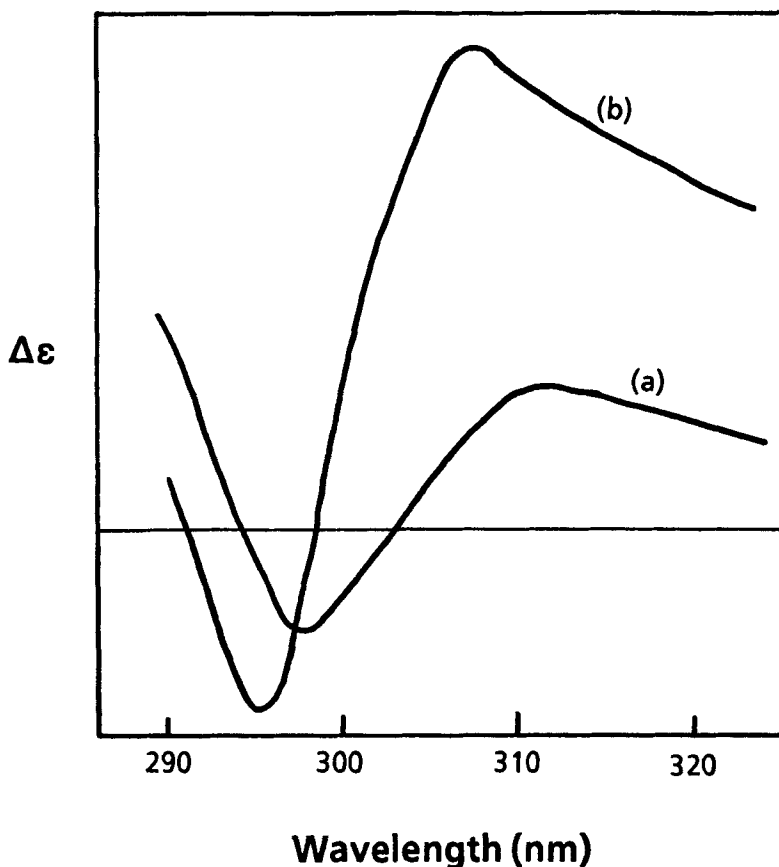
Figure 14.   CD spectra of ethidium bromide complexed with
              calf thymus DNA at pH 7.9, for dye/polymer ratios
              of (a) 0.086, and (b) 0.16 (data adapted from
              reference [91]).

     The solution complexes of ethidium bromide with nine
different deoxydinucleotides and the four self-complementary
ribodinucleoside monophosphates, as well as mixtures of
complementary and non-complementary deoxydinucleotides have
been studied as models for binding of the solute to DNA and
RNA [93].   Ethidium bromide was found to form the strongest
complexes with pdC-dG and CpG, and showed a definite
preference for interaction with pyrimidine-purine sequence
isomers.   Cooperative effects in the interaction of ethidium
bromide with a number of oligonucleotides weres observed
through studies of the induced CD, which was interpreted as

indicating the formation of a minihelix about the solute. The
results also indicated that the binding of ethidium bromide to
various sequences on DNA and RNA took place with significantly
different binding constants, an observation related to the
intimate stereochemical and electrostatic details of the
binding site.

In another study, the binding of ethidium bromide to eight
dinucleoside phosphates of different complementary base
sequences, to trinucleoside diphosphates with mismatched
bases, and to calf thymus DNA was studied through the induced
CD spectra, and through the induced fluorescence-detected
circular dichroism (FDCD) spectra [94]. A series of
correlations relating polymer details and the magnitude of
interaction with the solute were deduced on the basis of the
chiroptical data. Monomer and exciton CD bands were confirmed
in this work at varying dye/polymer ratios, and the FDCD
spectra were used to obtain additional details of the polymer
chirality in many cases. Through the use of minihelix
complexes (two dinucleoside phosphates per molecule of
ethidium bromide), it proved possible to model the DNA-
ethidium complex.

The interaction of other drug compounds with oligo-
nucleotides has been used to study the modes of interaction
for these compounds with DNA. Differential binding of the
enantiomers of chloroquine and quinacrine to the synthetic
poly(dA-dT)·poly(dA-dT) and poly(dG-dC)·(dG-dC) oligo-
nucleotides was followed through the CD induced in the solute
absorption bands [95]. As would be anticipated, mirror image
CD bands were observed for the enantiomers of each compound
after intercalation with the chiral polymers. However, the
association constants for the enantiomers were found to differ
significantly, and this information is summarized in Table 2.
One generalization made was that the binding affinity of the
(-)-enantiomer of each drug compound for a given oligo-
nucleotide system was less than that of its enantiomer. In
general, chloroquine exhibited less affinity for the oligo-
nucleotides than did quinacrine, a finding which was
attributed to differing numbers of fused rings in the two
solute systems.

The interactions of epinephrine, norepinephrine, and
isoproterenol with poly(A) have been studied through
characterization of the induced CD [96]. These catechol-
amines were all found to intercalate with the oligonucleotide
in the conventional manner, and the results were interpreted
in terms of the possible role played by these agents as
control mechanisms for the poly(A)-regulated translation of
the mRNA genetic code. It was found that these compounds were
capable of causing the native coil conformation of poly(A) to
convert into the helical conformation upon formation of the
intercalated complex. The kinetics of the transformation
could be followed by monitoring the evolution within the CD
spectra, and the activation energy associated with the
coil→helix transition was deduced through study of the
temperature dependence of the rate constant data.

Table 2

**Association Constants for the Interaction
of Quinacrine and Chloroquine [95]**

Drug	Oligonucleotide	Formation Constant (M^{-1})
(+)-Quinacrine	poly(dA-dT)·poly(dA-dT)	97,000
	poly(dG-dC)·(dG-dC)	42,000
(-)-Quinacrine	poly(dA-dT)·poly(dA-dT)	127,000
	poly(dG-dC)·(dG-dC)	121,000
(+)-Chloroquine	poly(dA-dT)·poly(dA-dT)	3,600
	poly(dG-dC)·(dG-dC)	6,800
(-)-Chloroquine	poly(dA-dT)·poly(dA-dT)	4,600
	poly(dG-dC)·(dG-dC)	8,800

5. SUMMARY

The CD induced in the absorption bands of an achiral
solutes can be an extremely powerful tool for the
characterization of the adduct species, and often represents
the primary means to characterize the nature of the
interaction phenomena. It is possible to induce chirality
through the application of numerous mechanisms, and the
observation of induced CD provides indisputable evidence for
the formation of well-defined complexation. Through the use
of suitably designed experiments, it is possible to deduce
both thermodynamic and kinetic information pertaining to the
associated solute. Such information has proven to be
extremely valuable when investigators have attempted to
understand the binding of pharmaceutically active agents by
biomolecules under physiological conditions. Workers in these
areas would be prudent to include chiroptical investigations
in the arsenal of techniques used to probe such interactions.

338

6. REFERENCES

1. A.D. Buckingham and P.J. Stephens, *Ann. Rev. Phys. Chem.*, 71 (1966) 399.
2. S.B Piepho and P.N. Schatz, *Group Theory in Spectroscopy: With Applications to Magnetic Circular Dichroism*, John-Wiley & Sons, New York, 1983.
3. B. Bosnich, *J. Am. Chem. Soc.*, 89 (1967) 6143.
4. P.E. Schipper, J.M. O'Brien, and D.D. Ridley, *J. Phys. Chem.*, 89 (1985) 5805.
5. E. Axelrod, G. Barth, and E. Bunnenberg, *Tetrahedron Lett.*, 57 (1969) 5031.
6. L.D. Hayward and R.N. Totty, *Can. J. Chem.*, 49 (1971) 624.
7. P.E. Schipper and A. Rodger, *Spectrochim. Acta*, 89 (1985) 5805.
8. S. Kirschner, N. Ahmad, and K. Magnell, *Coord. Chem. Rev.*, 3 (1968) 201.
9. P.E. Schipper, *Inorg. Chim. Acta*, 12 (1975) 199.
10. S. Kirschner and I. Bakkar, *Coord. Chem. Rev.*, 43 (1982) 325.
11. J. Jacques, A. Collet, and S.H. Wilen, *Enantiomers, Racemates, and Resolutions*, John-Wiley & Sons, New York, 1981.
12. K. Noack, *Helv. Chim. Acta*, 52 (1969) 2501.
13. J. Bolard, *J. Chim. Phys.*, 66 (1969) 389; 67 (1970) 550.
14. N. Tokura, T. Nagai, S. Takenaka, and T. Oshima, *J. Chem. Soc. Perkin Trans. I*, (1974) 337.
15. S. Takenaka, K. Kondo, and N. Tokura, *J. Chem. Soc. Perkin Trans. I*, (1974) 1749.
16. S. Takenaka, K. Kondo, and N. Tokura, *J. Chem. Soc. Perkin Trans. I*, (1975) 1520.
17. S. Takenaka, M. Sugiyama, and N. Tokura, *J. Chem. Soc. Perkin Trans. I*, (1976) 555.
18. L.D. Hayward, *Chem. Phys. Lett.*, 33 (1975) 53.
19. P.E. Schipper, *Mol. Phys.*, 29 (1975) 1705.
20. P.E. Schipper, *Chem. Phys.*, 57 (1981) 105.
21. M.L. Bender and M. Komiyama, *Cyclodextrin Chemistry*, Springer-Verlag, New York, 1978.
22. J. Szejtli, *Cyclodextrins and Their Inclusion Complexes*, Akademiai Kiado, Budapest, 1982.
23. J. Szejtli, *Cyclodextrin Technology*, Kluwer Academic Publisher, Dordrecht, 1988.
24. F. Cramer, *Rev. Pure Appl. Chem.*, 5 (1975) 143.
25. R.L. VanEtten, J.F. Sabastian, G.A. Clowes, and M.L. Bender, *J. Am. Chem. Soc.*, 89 (1967) 3253.
26. P.E. Schipper and A. Rodger, *J. Am. Chem. Soc.*, 105 (1983) 4541.
27. M. Kodaka, *J. Phys. Chem.*, 95 (1991) 2110.
28. M. Kodaka, *J. Am. Chem. Soc.*, 115 (1993) 3702.
29. N. Kobayashi, S. Minato, and T. Osa, *Makrol. Chem.*, 184 (1983) 2123.

30. S. Takenaka, N. Matsuura, and N. Tokura, *Tetrahedron Lett.*, (1974) 2325.
31. H. Yamaguchi and S. Abe, *J. Phys. Chem.*, 85 (1981) 1640.
32. H. Shimizu, A. Kaito, and M. Hatano, *Bull. Chem. Soc., Jap.*, 52 (1979) 2678.
33. H. Shimizu, A. Kaito, and M. Hatano, *Bull. Chem. Soc., Jap.*, 54 (1981) 513.
34. N. Kobayashi, *J. Chem. Soc. Chem. Comm.*, (1989) 1126.
35. N. Matsuura, S. Takenaka, and N. Tokura, *J. Chem. Soc. Perkin Trans. II*, (1977) 1419.
36. K. Harata and H. Uedaira, *Bull. Chem. Soc., Jap.*, 48 (1975) 375.
37. K. Harata, *Bull. Chem. Soc., Jap.*, 52 (1979) 1807.
38. H. Shimizu, A. Kaito, and M. Hatano, *J. Am. Chem. Soc.*, 104 (1982) 7059.
39. A. Ueno, F. Moriwaki, T. Osa, F. Hamada, and K. Murai, *Bull. Chem. Soc., Jap.*, 59 (1986) 465.
40. K. Kano, M. Tatsumi, and S. Hashimoto, *J. Org. Chem.*, 56 (1991) 6579.
41. M. Opallo, N. Kobayashi, and T. Osa, *J. Incl. Phen. Mol. Recogn. Chem.*, 6 (1989) 413.
42. N. Kobayashi, R. Saito, H. Hino, A. Ueno, and T. Osa, *J. Chem. Soc. Perkin Trans. II*, (1983) 1031.
43. G. Patonay and I.W. Warner, *J. Incl. Phen. Mol. Recogn. Chem.*, 11 (1991) 313.
44. N. Ikeda and H. Yamaguchi, *Chem. Phys. Lett.*, 56 (1978) 167.
45. H. Yamaguchi, N. Ikeda, F. Hirayama, and K. Uekama, *Chem. Phys. Lett.*, 55 (1978) 75.
46. H. Yamaguchi and K. Ninomiya, *Spectrochim. Acta*, 37A (1981) 119.
47. H. Yamaguchi, K. Ninomiya, and M. Ogata, *Chem. Phys. Lett.*, 75 (1980) 593.
48. R. Fornasier, M. Parmagnani, and U. Tonellato, *J. Incl. Phen. Mol. Recogn. Chem.*, 11 (1991) 225.
49. M. Higashi, H. Yamaguchi, and M. Oda, *J. Incl. Phen. Mol. Recogn. Chem.*, 6 (1988) 249.
50. H. Yamaguchi, M. Higashi, J. Nakayama, and M. Hoshino, *J. Incl. Phen. Mol. Recogn. Chem.*, 9 (1990) 253.
51. Y. Ishizuka, Y. Nagawa, H. Nakanishi, and A. Kuboyama, *J. Incl. Phen. Mol. Recogn. Chem.*, 9 (1990) 219.
52. N. Kobayashi and M. Opallo, *J. Chem. Soc. Chem. Comm.*, (1990) 477.
53. T.-X. Xiang and B.D. Anderson, *Int. J. Pharm.*, 59 (1990) 45.
54. S. Li and W.C. Purdy, *Anal. Chem.*, 64 (1992) 1405.
55. A.L. Thakkar, P.B. Kuehn, J.H. Perrin, and W.L. Wilham, *J. Pharm. Sci.*, 61 (1972) 1841.
56. K. Ikeda, K. Uekama, M. Otagiri, and M. Hatano, *J. Pharm. Sci.*, 63 (1974) 1168.
57. M. Otagiri, J.G. Fokkens, G.E. Hardee, and J.H. Perrin, *Pharm. Acta Helv.*, 53 (1978) 241.
58. J.M. Bowen and N. Purdie, *Anal. Chem.*, 53 (1981) 2239.

59.   S.M. Han and N. Purdie, *Anal. Chem.*, 56 (1984) 2822.
60.   S.M. Han and N. Purdie, *Anal. Chem.*, 56 (1984) 2825.
61.   S.M. Han, W.M. Atkinson, and N. Purdie, *Anal. Chem.*, 56 (1984) 2827.
62.   S.M. Han, N. Purdie, and K.A. Swallows, *Anal. Chim. Acta*, 197 (1987) 57.
63.   G. Tsoucaris, G. Le Bas, N. Rysanek, and F. Villain, *J. Incl. Phen. Mol. Recogn. Chem.*, 5 (1987) 77.
64.   O. Bekers, J.H. Beijnen, M. Otagiri, A. Bult, and W.J.M. Underberg, *J. Pharm. Biomed. Anal.*, 8 (1990) 671.
65.   D. Amdidouche, H. Darrouzet, D. Duchene, and M.-C. Poelman, *Int. J. Pharm.*, 54 (1989) 175.
66.   M. Hatano, *Induced Circular Dichroism in Biopolymer-Dye Systems*, Springer-Verlag, Berlin Heidelberg, 1986.
67.   J.H. Perrin and P.A. Hart, *J. Pharm. Sci.*, 59 (1970) 431.
68.   H.B. Kostenbauder, M.J. Jawad, J.H. Perrin, and V. Averhart, *J. Pharm. Sci.*, 69 (1971) 1658.
69.   J.H. Perrin and D.A. Nelson, *J. Pharm. Pharmacol.*, 25 (1972) 125.
70.   J.J. Vallner and J.H. Perrin, *J. Pharm. Pharmacol.*, 33 (1981) 697.
71.   M. Otagiri, H. Nakamura, Y. Imamura, and U. Matsumoto, *Pharm. Weekbl.*, 11 (1989) 207.
72.   J.H. Perrin and P. Idsvoog, *J. Pharm. Sci.*, 60 (1971) 602.
73.   C.F. Chignell, *Mol. Pharmacol.*, 6 (1970) 1.
74.   J.H. Perrin, *J. Pharm. Pharmacol.*, 25 (1972) 208.
75.   J. Fleitman and J.H. Perrin, *Int. J. Pharm.*, 11 (1982) 215.
76.   J. Fleitman and J.H. Perrin, *Int. J. Pharm.*, 11 (1982) 227.
77.   K.J. Fehske and W.E. Muller, *J. Pharm. Sci.*, 70 (1981) 549.
78.   A. Shibata, K. Morita, T. Yamashita, H. Kamaya, and I. Ueda, *J. Pharm. Sci.*, 80 (1991) 1037.
79.   P.E. Schipper, B. Norden, and F. Tjerneld, *Chem. Phys. Lett.*, 70 (1980) 17.
80.   R. Lyng, T. Hard, and B. Norden, *Biopolymers*, 26 (1987) 1327.
81.   M. Kubista, B. Akerman, and B. Norden, *J. Phys. Chem.*, 92 (1988) 2352.
82.   D.G. Dalgleish, H. Fujita, and A.R. Peacocke, *Biopolymers*, 8 (1969) 633.
83.   D.G. Dalgleish, A.R. Peacocke, G. Fey, and C. Harvey, *Biopolymers*, 10 (1971) 1853.
84.   M. Kamiya, *Biochim. Biophys. Acta*, 562 (1979) 70.
85.   H. Ito and Y.J. I'Haya, *Bull. Chem. Soc., Jap.*, 52 (1979) 2823.
86.   D. Fornasiero and T. Kurucsev, *J. Phys. Chem.*, 85 (1981) 613.
87.   D. Fornasiero and T. Kurucsev, *Biophys. Chem.*, 23 (1985) 31.

88. D. Fornasiero, T. Kurucsev, R. Lyng, and B. Norden, *Croat. Chem. Acta*, 62 (1989) 339.
89. B. Norden and F. Tjerneld, *Biopolymers*, 21 (1982) 1713.
90. M.J. Waring, *J. Mol. Biol.*, 13 (1965) 269.
91. S. Aktipis and A. Kindelis, *Biochem.*, 12 (1973) 1213.
92. S. Aktipis and W.W. Martz, *Biochem.*, 13 (1974) 112.
93. T.R. Krugh, F.N. Wittlin, and S.P. Cramer, *Biopolymers*, 14 (1975) 197.
94. K.S. Dahl, A. Pardi, and I. Tinoco, Jr., *Biochem.*, 21 (1982) 2730.
95. P.V. Scaria, J.C. Craig, and R.H. Shafer, *Biopolymers*, 33 (1993) 887.
96. H.N. Borazan and S.N. Koumriqian, *J. Pharm. Sci.*, 72 (1983) 1450.

This Page Intentionally Left Blank

Subject Index

A

absolute configuration, 135,160,294,302
-, diols, 165,166,168
absorption
-, differential, 9,16,19,245
-, dissymmetry factor, 210,219,300
ac component, 22
adamantone, 138
-, derivatives, 138,140,154
alkaloids, 253,304
-, indole, 253
-, marihuana, 259
-, morphine, 254
-, quinine, 253,257,304
aminoacids, 74,93,253,262,320
p-aminobenzoates, 160,165
amphetamine. 254
-, meth-, 254
anisotropic materials, 25
anisotropy ratio, 30,55,300
antibiotics, 256,262,274,325
antibodies, 272
arc lamps, 18
-, high pressure Hg, 32
-, high watt deuterium, 23
-, mercury-Xe, 23
-, Xe, 22,32
anticoagulants, 322,327,329

B

Babinet-Soleil compensator, 38
background limited, 17
barbiturates, 253,268,320
benzodiazepines, 253,268,299,302,322,324
Beers law, 245,250,267
bicyclic ketones, 146
-, derivatives, 146
bilirubin, 324
birefringence, 16,225
-, intrinsic, 16
bis-anthracene, 165
Bruhat, 20

C

calcite, 24
capillary electrophoresis, CD, 37,237
carbohydrates, 171,243,253,261,268,297
-, derivatives, 261
-, fructose, 253,261
-, ketoses, 261,262
-, pyranosides, 171
chiral quencher, 217
chiral shift reagent, 222,247
cholesterol, 17,260,270,273
chromatography, 247
-, achiral, 248
-, capillary electrophoresis, 37,237
-, CD detection, 33,253
-, chiral, 248,263,266,268,320
-, GC, 33
-, HPLC, 34,35
-, microbore HPLC, 34,305
-, thermal lens, 43
chromophores,
-, amide, 11
-, aromatic ring, 245
-, carbonyl, 245,310
-, extra perturbation, 135
-, extrinsic, 194,244
-, peptide-amide I and III, 94,100,106
Chugaev reaction, 273
circular birefringence, 4,20
circularly polarized light, 3,25,133,225
- ,ammonium dideuterium phosphate, 9
-, Babinet-Soleil compensator, 38,75
-, calcium fluoride, 33
-, electrooptic modulator (EOM), 60,74,97
-, Fresnel rhomb, 19,25,42
-, half wave plate, 77,84
-, left, 9,16,22,55,133
-, photoelastic modulator (PEM), 9,18,26,
                29,31,33,58,97,219
-, Pockels cell, 9,18,22,26,35,42,49,225
-, quarter wave plate, 9,19,20,23,25,60,
                75,83,219
-, right, 9,16,22,55,133
clinical science, 12,249
Co(en)3, 43,44,45
L-cocaine, 256,294,322
collagen, 181
complexes, 17,308